A Variable-Capacity Heat Pump for Renewable Energy Recovery

Robert E. Low

Doctor of Philosophy

University of Edinburgh

1991

Declaration

The work described in this Thesis is the original work of the author and was carried out without the assistance of others, except where explicit credit is given in the text. It has not been submitted, in whole or in part, for any other degree at any University.

Robert Elliott Low

Edinburgh
June 24, 1991

Acknowledgements

The eventual production of this thesis will have come as a surprise to many, not least the author. It was produced on the departmental Sun workstations, using the LaTeX document formatting program. This *magnum opus* could never have been achieved without the help and assistance of many people, for which I shall be eternally indebted (well,...) The following deserve special mention for their donations of advice, aid, succour, comfort and encouragement through the long dark years:

- *Dr Colin Pritchard,* for presiding over the whole project.
- *Alan and Anne Crerar,* for putting up with the paranoia, bullying me into finishing and generally making life worth living.
- *My relatives,* for all their kindnesses.
- *Rab Kilgour, Kenny Fee and Bobby Hogg,* for translating my crazed designs into reality.
- *Matthew Rea,* for his electronic wizardry.
- *Neil Skilling,* for his selfless assistance with the preparation of the printed text and his instruction in the arcana of the LaTeX cult.
- *Andy Doig, Karen Ferguson, John Burns and other postgraduates too numerous to mention,* for their provision of wit, wisdom and companionship.
- *The Electricity Research and Development Centre,* for their financial lifeline which rescued me in my hour of need.
- *Cal-Gavin Limited of Birmingham,* for supplying the evaporator which gave so much useful data.

Abstract

This thesis describes research carried out by the author between 1986 and 1990 at the Department of Chemical Engineering, University of Edinburgh, under the supervision of Dr Colin Pritchard. The aim of the research was to devise and evaluate a novel compression heat pump cycle as a potential technology for the utilisation of work and heat from environmental sources in industrial applications. The principal requirement of such a heat pump is that it can accept time-varying inputs of work and heat whilst supplying a controlled heat load at constant delivery temperature to an external load. This requires a cycle with the ability to "self-regulate" its capacity to match external variations in *either* energy input *or* energy takeoff. The use of a nonazeotropic mixture as working fluid offers the potential to vary the composition of circulating fluid in a heat pump cycle, thereby varying the capacity, and this was chosen as the basis for research.

The design, construction and operation of a "self-regulating heat pump" pilot plant is described. The basis for plant design is that a progressive shift in the active refrigerant composition in the heat pump cycle may be achieved through a combination of partial condensation and working fluid storage. The design philosophy is explained in detail; a review of the knowledge on this technology is included. A comprehensive analysis of experimental measurements is used to highlight the advantages and disadvantages of a mixed working fluid which the author observed in the course of the work. It is demonstrated that the principle of self-regulating capacity control by split condensation is valid, and that the results obtained on the pilot plant justify further research to optimise design of the cycle.

The prediction of thermodynamic properties of halogenated hydrocarbon refrigerants is reviewed with special emphasis on: acquisition of sufficient data for preliminary plant design from minimum information, and on the prediction of binary vapour-liquid equilibrium data (VLE) in the absence of experimental measurement. The Cubic Chain-Of-Rotators (CCOR) equation of state is assessed as a route to these properties; it is shown that this equation offers improved liquid-phase property prediction compared to other cubic equations of state. The CCOR equation is also shown (by comparison with experimental measurements from the literature) to predict binary VLE to the same degree of accuracy as the Redlich-Kwong-Soave, Lee-Kesler and Carnahan-Starling-DeSantis equations in the absence of any parameter optimisation. Procedures are decribed for the optimisation of the CCOR equation's performance as a predictor of both pure-fluid and mixture properties by the fitting of empirical parameters to experimental data. It is demonstrated that this optimisation procedure allows quantitative description of the liquid phase of pure fluids and of mixtures.

—But if one were to repent?

—Repent of what?

—Oh, one wouldn't need to go into detail...

...*Waiting for Godot*, **Samuel Beckett**

Contents

List of Figures

List of Tables

Chapter 1

Introduction

1.1 Energy Sources and the Environment

1.1.1 Introductory Remarks

The global environment abounds in sources of energy, which are essentially limitless, yet today remain–for the most part–untapped. These "renewable" resources are in stark contrast to the main sources of energy used in the industrial economies of the world: coal, oil, gas (the "fossil" fuels) and nuclear fuels. Supplies of *these* resources, while large, are certainly not infinite. Nuclear energy offers the potential of extremely high energy densities in the fuel (and hence durable fuel stocks) but the costs associated with nuclear plant, especially in the spheres of waste disposal and decommissioning, make justification of its use increasingly hard. Furthermore, a considerable degree of refinement is required before energy may be extracted from fossil fuel sources, while

the preparation of nuclear fuel has enforced the development of several complex technologies. This is often conveniently overlooked by those opponents of renewable energy development, whose argument is that the technology required to harness the energy would be too complex. It is hard to envisage a wind energy collector of the same complexity as the Advanced Gas-Cooled Reactor. It is not too optimistic to state that the design of efficient devices for abstraction of energy from the environment should be perfectly feasible on technical grounds, if nothing else. The eventual assessment of the relative merits of such technologies should really be made on the final cost of each option; by cost is meant some notional concept representing not only the monetary costs of plant and fuel but also the environmental effects of the technology. It is becoming increasingly obvious that all industrial activities must be carefully and continually scrutinised for any potential damage to our environment. The possibility that our ecology could be tipped into a chaotic but hostile state by our polluting activities now seems very real We do not fully understand the complex mechanisms of our planetary ecosystem, yet the rapid and measurable increase in the average global temperature has been brought about through scarcely 150 years of modern industrial civilisation. The role of energy technology in the future well-being of the industrial society is crucial, although marginalised in recent times by the politicians of most countries in favour of cheap votes through cheap fuels. The environmental impact of a society may be related to the amount of energy it consumes to produce its necessary goods and services, therefore the efficient and wise generation of energy is bound to have a favourable effect on the environment and on the economy. It is instructive in such a discussion to consider the effects on the environment of different methods of energy production.

1.1.2 Non-Renewable Energy Sources

1.1.2.1 Power Generation Using Fossil Fuels

The oil and gas used for power generation represent the end products of a complex refining process, which in its turn uses energy to effect the separations and purifications required to yield a good fuel. Gas requires fewer refinement steps than oil; the chief purpose of gas refinement is to remove acid gases (*e.g.* hydrogen sulphide) . In both cases there is an inevitable production of waste streams, which must be rejected into the environment. Coal does not in general require the same degree of refinement before combustion but is a "dirtier" fuel, as it may still contain impurities no longer present in

refined fuels. When any fossil fuel is burnt, moreover, large quantities of carbon dioxide must be rejected to the atmosphere, with a consequent increase in the ability of the atmosphere to trap solar energy, causing global warming. The production of acid gases in the combustion process is another environmental hazard associated with use of fossil fuels in power stations. These gases are chiefly oxides of nitrogen, with a proportion of sulphur oxides dependent on the sulphur content of the fuel. The effects of acid flue gas are far-reaching; it is now thought that some, if not all, of the defoliation observed in European forests is a result of acidified rainwater, whose acidity comes from power station flue gas. (Another suspect is the pollution caused by car exhaust fumes, which also contain acid gases.) Steps are being taken to reduce this problem; use of low-NO_x burners and fitting of flue-gas desulphurisation (FGD) equipment are two examples. In a sense, however, these steps can only ever be palliative treatments. Indeed it may be argued that FGD is an inappropriate and expensive palliative: it reduces the efficiency of the power station, has high capital costs, requires large amounts of basic absorbent and produces large quantities of waste. The best way to reduce emissions must inevitably be to reduce fuel consumption, and this means: either improve the conversion efficiency of the power generation process, or reduce the industrial energy requirement.

The conversion efficiency of a heat engine is restricted by the temperature difference between heat source and heat sink: this is a fundamental constraint of thermodynamics. The heat engines used in power stations—Rankine cycles using steam as working fluid—have an upper temperature constraint imposed by the materials of construction (between 650 °C and 700 °C), while the heat sink temperature can be no lower than that of the environment, *e.g.* 20 °C. This gives a Carnot efficiency of 68-70%. When the irreversible losses of a real Rankine cycle are accounted for, the best thermal power stations are found to have an efficiency of approximately 40%. The greater part of the fuel's energy must be discarded to the environment. Improvements in the overall efficiency are always being sought, as even a fractional percentage improvement may yield big savings, given the massive scale of power generating equipment. Nonetheless, the cycle will always reject large quantities of useful energy as heat. There is, then, only limited scope for improvement of the basic cycle until the upper temperature restriction is eased: while any increase in efficiency is welcome, more fundamental modifications should also be considered.

Various schemes have been proposed to improve the efficiency of power generation, notably the Combined Heat and Power (CHP) processes. These systems use a proportion of the heat generated during the conversion process to satisfy an existing demand for heat by an external client. In some cases the development of CHP schemes has not

been found economic: for example, district heating schemes, in which residential heating requirements act as part of the heat sink of the power station, never really lived up to expectations. The reason for this, in essence, is that such heating requirements are seasonal in nature and cyclic over a period of hours in demand. For a power station to function efficiently, by contrast, it must generally be run continually, with output controlled by the station operators to meet energy demand. As a consequence, heat must be rejected by the station *whether the residential customers require it or not.* This implies a parallel set of heat exchangers, a parallel heat sink, and nearly double the capital cost of a single heat sink scheme. Likewise, power stations are generally part of a grid setup, and are switched in and out by the grid operators as national, not local, power demand dictates. If the local power station were tripped out, its ability to supply heat to the locality would be lost, implying further capital cost to the customer. The chemical industries can lay claim to better experience of CHP cycles: the pattern of heat demand in a large-scale plant with internal electricity generation is liable to be more closely suited to the operation of a local power station. Operating efficiencies of 60% have been claimed for CHP units within the context of a large plant; clearly then, there is great benefit to be obtained from use of such cycles where possible.

1.1.2.2 Power Generation from Nuclear Energy

The use of nuclear energy has been surrounded with controversy almost from its inception; much of the controversy being more political than technical. No other technology (with the possible exception of chemical weapons manufacture) seems to cause so much public disquiet. This disquiet is perfectly legitimate, if it concerns the radiological hazards inherent in the technology (of which more below) , or the murky waters separating civil applications from military and/or para-military uses. Often, however, one receives the impression that the public perceives *all* parts of the nuclear generation cycle as intrinsically unsafe: this is not so. It may be argued that the apparent reluctance of the nuclear industry to "come clean" about its operating procedures and reliability record is more a result of a fear of misinterpretation. What may be regarded by all inside an industry as a harmless mishap may readily be interpreted by the inquiring media as a potential catastrophe. Of course, this is not to say that complacency should ever be acceptable as an operating policy: the Chernobyl explosion of 1985 demonstrated the ability of a non-nuclear explosion to contaminate a very wide land-mass, with unknown long-term consequences. Likewise, it is not implied here that the nuclear industry has a track record of exceptional probity in its dealings with the public. The intention is instead briefly to discuss the environmental impact of nuclear power generation, with the generous assumptions regarding reliability which are made by its developers.

The process by which nuclear energy is converted to electricity is basically identical to that used to convert the energy of fuels: a heat engine, normally a Rankine cycle, driving turbines connected to generators. Instead of a chemical reaction (combustion) , heat is generated at elevated temperature through a controlled fission reaction. Owing to the intense levels of radioactivity associated with the fission reaction, one or more sets of cooling circuits (using liquid metal as coolant) must be used to remove heat from the reactor core, then transfer it to the working fluid of the Rankine cycle; in most other respects the process is indistinguishable from a conventional power generation cycle. The capital cost of a nuclear plant is many times that of an equivalent conventional plant, though; this is a result of the (literally) massive shielding and containment required to keep radioactive material inside those parts of the plant designed to handle it. Furthermore, the quality of manufacturing and assembly required of nuclear plant is exceedingly high: this too has its effect on cost. This has always been acknowledged by its proponents: after all, it is hard to conceal the order of magnitude of expenditure on any plant built in the public eye, with public money. (Not impossible, though.) The justifications given by the supporters of nuclear power for such large initial outlay have traditionally been those of low operating cost, high load factor, and slight effect on the environment: increasingly these tenets of the nuclear creed are being called into question. Operating cost and load factor are inter-related: if a poor load factor is obtained for a power station attached to a grid, then other stations must be switched in to compensate for it. These stations are likely to burn fossil fuels, so that the environmental cost of an inoperative nuclear plant is an increase in emissions from conventional plants. The loss of load factor in nuclear plant is often associated with a need for running maintenance or repair: as mentioned above, costs of fabrication and assembly in nuclear installations are high, and working procedures may be slow through consideration of safety. This contributes to running costs and load factors which may be quite different from those projected when the plant was conceived and planned for in the national energy strategy.

The true environmental cost of operating a nuclear power station is hard to assess. Certainly a nuclear station produces no carbon dioxide or acid flue gases: this is a big advantage over fossil fuels, and one much trumpeted by a recent Prime Minister of the United Kingdom. Likewise, it is not really fair to single out the discharge of warmed cooling water to the sea under normal operating conditions, since all thermally-based power stations must do this. The possible discharge of cooling water contaminated by radioactive material is, however, a fair cause for concern: such an accident could devastate marine ecology or lead to an increase in the levels of radioactivity in the human food chain. It has been observed above that nuclear plant may be responsible for the combustion of fossil fuels by its unexpected *absence* from the grid; some of its critics would argue that it is indirectly responsible for such polluting activities by

its *presence*! The reasoning is that by making energy available at low unit cost, one allows a decrease in production costs of most goods, with corresponding increase in consumption and global pollution. It must be said that this argument should really be considered as a spur to a general reduction in the consumption of energy, irrespective of its source. In the final analysis, the major concern over the environmental impact of nuclear power must lie in the field of waste disposal.

Waste produced by nuclear power stations falls into three broad categories: high level waste, lethally radioactive; low-level waste, only slightly radioactive but still a health hazard under some circumstances, and intermediate waste- a fuzzy middle ground. High-level waste is typically material from the reactor or surroundings inside the containment, and must be stored in high-integrity chambers with constant removal of heat and absorption of radiation, until its activity is acceptably low. This may mean storage times of several thousand years, or longer than the current existence of civilisation in Europe! The major flow of such waste during the operational life of a plant will be spent fuel elements. As these may still contain significant quantities of fissile material, there is a strong incentive to invest in re-processing technology, in order that this fuel might be recycled to the reactor. Such reprocessing technology will itself produce high-level liquid wastes, which must then be stored, and so on. Low-level waste produced during operation is generally composed of consumable items which have been in brief contact with a radiological source, for example tools and overalls used by operational staff in areas of potential radioactivity. The majority of waste produced by a plant will only come at the end of its life, when it is scrapped. In that case the entire reactor, coolant and containment sections of the plant must be regarded as waste: this is a considerable volume of material which will require safe disposal. The likely cost of safe decommissioning has in the past been assumed "reasonable" in calculation of the economics of nuclear power. In recent months, however, prompted by the drive of the Thatcher privatisation juggernaut, the true costs of decommissioning have been admitted with reluctance by the nuclear industry. These figures bear essentially no relation to those used in the original costings, and make nuclear electricity far less economic than generation by conventional methods. Even so it is reckoned that these latest costs may be far too low. The simple truth is that nobody really knows: although certain British reactors (notably those used by the military for manufacture of weapons-grade plutonium) are long past their original design lifetimes, none have yet been closed down in this country. The official reason given is that performance is still competitive; if so, why must new technology, such as the Advanced Gas-Cooled Reactor or Pressurised Water Reactor be developed? Political expediency must be suspected to have played a part in such decisions.

To summarise the nuclear option, then: the high capital costs and unknown decommissioning costs make the use of nuclear power an expensive option, and one which can only really be pursued as part of an integrated and diversified power production scheme. The potential benefits of nuclear power should not be underestimated, and neither should the advantages accruing to a system of power generation which produces no waste gas streams. The radiological hazards of nuclear power, however, make it far from ideal as a panacea for meeting energy requirements within a "green" energy strategy.

1.1.3 Renewable Energies: an Overview

1.1.3.1 Introductory Remarks

There follows a very brief summary of the principal attributes of the main sources of renewable energy, with emphasis on the advantages and difficulties associated with utilisation of these sources on an industrial scale. This is *not* intended to be a complete discussion of what is a wide and interesting topic; for this the reader is referred to the general literature. The aim is to highlight those key factors which may make or break the viability of such energy sources, both in the present and in future economic climates.

1.1.3.2 Solar Energy

In a sense, solar energy is already the most widely-used source of all on the Earth today: the only available energy on our planet which does not originate from the Sun is that locked in the nucleii of fissile elements. Coal, for example, may be thought of as crystallised sunlight, since its energy content originates from the covalent bonds created by photosynthesis of prehistoric plant matter. Solar energy is normally thought of as a renewable source only in the context of direct usage of sunlight, and this is the context used here.

Sunlight is a diffuse and widely variable energy source, one which may never be useful

in large areas of the globe for these reasons. Technology for harnessing sunlight on the large scale has hitherto been confined to those areas of the world where there is both a high intensity and a high proportion of sunny days in every month (a high "insolation") . Recent advances have been made in the development of collectors which use indirect sunlight, of the intensities prevalent in North Europe for example; the best sites for collectors on the industrial scale will not be in Europe, though. There are two basic approaches to utilisation of solar energy: either direct use of the energy as a heat source, or conversion to electricity, by whatever means. Although the former approach might seem the more attractive, as having fewer steps between source and final supply, this is not necessarily so. The capture and focussing of large quantities (*i.e.* of the order of megawatts) into a load would present great practical problems, and so an intermediate conversion into a compact energy supply is attractive even for heating applications.

Examples of the use of sunlight as a direct heat source include "solar panels" for production of hot water and sun-driven small-scale evaporation plants for the purification of water. A common refinement is to place a heat store between the solar collector and the eventual load: in this way the heat may be recovered during periods when there is little or no direct sunlight. The development of suitable storage devices has been widely researched: Cooke (1987) [15] has reviewed the "state of the art". The economic viability of such schemes is dependent on the initial capital cost of the store, which is traded off against the improvement in annual load factor to be gained.

Conversion of solar energy to electricity is achieved chiefly through utilisation of the photo-voltaic effect of certain materials; a spectacular example of this technology is the power plant for the NASA Hubble space telescope, which consists of a bank of such converters linked to high capacity storage cells. The extension of this technology to production of electricity on the large scale is still some way off, however: the collection areas required for operation on a large scale are still too large to be economic in comparison with other methods. (The cost of the collectors themselves is not so important as the cost of the tracking equipment required to maintain the optimum incidence of sunlight on the panels by moving the panels to follow the sun's path.) It has been suggested that use of geo-stationary satellites carrying large photo-voltaic arrays could be a future power source, since the energy density of sunlight outside the atmosphere is much greater than that at the Earth's surface. Such a satellite would transmit its garnered power to Earth via a coherent beam of radiation; a laser. This proposal is really not practical for the near future: the cost of the technology required, and the possible consequences of a stray energy beam playing over the Earth, make this no more than an intriguing fiction.

There is another method of electricity generation from solar power, which is still the subject of keen research. This is to use a Rankine cycle, as used in ordinary thermal power stations. The sunlight is used to create a heat source, which then evaporates a working fluid in the normal way. As the attainable temperatures are much lower than those of a conventional thermal cycle, water is not the working fluid. Organic fluids, *e.g.* chlorofluorocarbon refrigerants, are the favoured working fluids for these processes. The development of these "Organic Rankine Cycles" has been pursued vigorously in Israel with some success. Of course, the maximum theoretical efficiency of such a cycle will be far lower than that of a conventional cycle, since the temperature of the heat source is lower. This need not be a worry, though, because the heat supplied is free and creates no pollution. Furthermore, the power generation equipment itself is existing, mature technology and so is of relatively low incremental cost. The heat source used in these systems is normally a stream of hot brine, at or near 100 °C. The brine is produced from an ingenious reservoir known as a "solar pond": in essence this is a large pond, aligned to receive maximum insolation, and filled with a concentrated brine. The pond water stratifies and a large portion of the energy incident on the surface is trapped by the top layer. This energy heats up the bottom layers of the pond and so a thermal gradient is established from surface to bottom. Hot brine may then be extracted from the bottom, cooled in an exchanger against the organic working fluid, then diluted and returned to the top of the pond. Once the thermal gradient is established in the pond it should act not only as receiver but also as buffer storage of heat. The engineering of solar ponds is well covered in the American Society of Mechanical Engineers' "Journal of Solar Energy Engineering", to which the interested reader is referred for further information.

In summary, then, solar energy is the subject of active research and development but its diffuse nature and variable supply lessen its attraction as a major energy source until more efficient collection technology is developed. The very existence of a dedicated ASME journal is proof enough, however, that it is still taken seriously as a potential energy source in the future.

1.1.3.3 Wind Energy

Wind energy has been used by Man since ancient times: working windmills were features of ancient Greek and Egyptian civilisations. The two most attractive features of wind power are its ready availability in most locations and the ease of its conversion into mechanical work. Thus it is possible to convert wind energy to electricity by use of

a turbine generator without incurring the large losses inherent in use of an intermediate thermal cycle between energy source and turbine. The major drawbacks to use of wind energy are connected with its variable nature: although many locations may have a reasonably constant average wind climate, sudden, fierce gusts can never be discounted. In a similar way periods of flat calm must also be assumed. If a wind energy device is to be used as a power source, then, it must be of sufficiently robust design to cope with sudden overload and requires a backup power supply for the periods when it is becalmed.

Traditional applications of wind energy have been on a small scale: one windmill, providing direct mechanical drive for *e.g.* water pumping or corn grinding. Attempts at capture of wind energy for industrial use have been based around electricity generation technology, and have been targetted to achieve far greater power outputs than simple windmills. It has been found that there is an upper economic limit on the size on any individual wind turbine: currently the largest in the U.K. is a 3 MWe turbo-generator, run by the English electricity boards as a test unit. This device is a twin-blade design, much like the child's toy windmill. Unlike the child's device, the 3 MWe turbine blade span is some 87 metres! The existence of this upper limit has led to the "wind farm" concept, where a set of turbo-generators are built in a common site and connected individually to a link with the national electricity grid. The use of wind farms offers the twin advantages of multiple redundancy and low unit manufacturing costs. The drawbacks are: visual and aural pollution caused by the presence of many windmills may lead to restriction of available sites; furthermore the average efficiency of a single unit in a wind farm may be less than its equivalent stand-alone efficiency because of the effect on wind-flow of its neighbours.

Operational experience of wind farming has been gained in several countries, notably the Netherlands, Denmark and the United States: the results of such ventures have been mixed. In California several large wind farms were established during the 1980s, helped in part by generous tax concessions from the State administration. These farms were supplied with a British design of wind turbine, a 3-blade, 370 kWe device designed and built by Howdens of Glasgow. A design flaw led to large numbers of these units suffering failure, through shearing of the blades near the root. This was unforeseen and came about through an imperfect understanding of the forces exerted on the blades by the wind. The resultant cost of redesign and compensation nearly bankrupted the manufacturers, and forced their withdrawal from the wind energy market. By contrast, the experience in the Dutch and Danish wind farms has been rather better: these farms benefitted from good coastal locations and steady unidirectional winds off the North Sea, which enabled the attainment of higher load factors and outputs than

the comparable Californian farms. in Britain, meanwhile, wind energy is now being researched by the English generating boards, after some years of apparent indifference, although it is not yet clear whether the moves afoot are anything more than token gestures to met the impending regulations of privatisation. In defence of the power generators, it must be said that their attitudes do seem to be changing to a more favourable assessment of wind power. It may be that it has finally been accepted that any technology will only develop if there is a realistic amount of R&D resource and time invested in it: the development targets set for wind energy by the Department of Energy have often seemed ludicrously tight in budget and timescale, especially when compared to the amount of time and money spent in the nuclear industry on such *extremely* long-term areas as fast breeder reactor technology. It is to be hoped that the future will bring a further development of the use of wind energy in the U.K. but it should always be appreciated that the land areas required for wind farms may simply not be available in much of England. There are large expanses of Highland Scotland which could however be used as wind farm sites without untowardly affecting the local environment. Sheep and deer rapidly become accustomed to poles in the ground; and if they can live under the sound of low-flying RAF fighters, the sussurations of a wind turbine will not cause livestock undue trauma.

In contrast to the large-scale electricity generation projects, there are also research projects which are targetted at the use of the wind energy directly as shaft work. This is reminiscent of the traditional uses of wind power; the aim must be to find industrial applications which can benefit from the cheap, multiple unit approach of the wind farm. A good example of this is desalination by reverse osmosis (R.O.) . In this process, pure water is extracted from brine at ambient temperature by literally squeezing it through a semi-permeable membrane, which does not pass dissolved solids. The process requires generation of considerable pressures: the higher the recovery rate required the greater must be the pressure difference between the salt and pure streams. Use of wind energy to drive the pumps required in such a process could greatly improve the yield of fresh water per unit cost. This process is ideally suited to use of wind power, since desalination is always carried out using product reservoirs, which could compensate for any fluctuation in wind speed (and hence production rate) by acting as buffers. The current market for desalination is dominated by the petrodollar, since a high proportion of the global demand for water comes from the oil-rich Gulf states. As a consequence, the favoured processes used in these areas are thermal in nature: either vapour compression desalination or multi-stage flash desalination are the most common types of desalination plant sold on the large scale. There is nonetheless a large potential market outside this region, which has no special concessions on the fuel oil required to drive such thermal processes. One only need to reflect on the now annual panic over water shortages in much of Southern England to realise just how close to home this

market could be. While it is true that the English situation has come about largely through chronic mismanagement and neglect of the national water infrastructure, the anticipated increases in average summer temperatures in coming years will probably increase the need for water purification technology in the South.

Finally, the future for wind energy may cautiously be described as promising. The development of systems which utilise high quality shaft work directly may result in a greatly increased acceptance of the wind as a power source for sectors of industry, particularly those which are constrained to work near coastlines, where winds are in general constant and dependable in nature.

1.1.3.4 Wave Power

State of the Art A good recent review is contained in Whittaker's paper [124]. The exploitation of wave energy on the commercial scale has lagged behind that wind and solar energies. This is surprising in some respects, since wave energy is far more concentrated an energy than either wind power or wave power; moreover, the fluctuations in an ocean swell are much more slow to develop than those in wind power. It may also be reasoned, of course, that the best sites for wave energy collectors are offshore: this will necessitate a robust means of channelling the harvested energy back to its users on land, which will be an additional and considerable cost.

The British government instigated a wave energy research program in the mid 1970s, in response to the OPEC oil crisis of 1973: the bulk of research was eventually concentrated on a device developed at Edinburgh University, under the guidance of Professor Steven Salter [99, 100]. This device, christened a "Duck" by Salter, was reckoned to offer the greatest potential for offshore extraction of energy. In 1982 funding for the Duck was cut off, on the basis of evidence submitted by the Energy Technology Support Unit (ETSU) , the Government's overseeing body for energy research in the U.K. The alleged reasons for abrupt termination of the project- which was regarded as making good progress by the team- were unreliability and high projected generating costs. The decision was contested at the time, and continued pressure by the proponents of wave power has brought to light a strange tale of misinformation and questionable decisions regarding the direction of alternative energy research in the U.K. It is now known that the cost which was claimed by ETSU for wave powered electricity generation, at 5.4 p/kWh, is *less* than the latest best estimates for electricity generation from British nuclear plant, for which 7 p/kWh is now accepted as a reasonable figure. Yet in 1982

the cost of wave-power-generated electricity was deemed too high! The whole affair is currently under Parliamentary scrutiny, although the outcome is far from certain to be a vindication of the Edinburgh team's claims of a conspiracy directed against their work. Whatever the final judgement, it seems safe to make two general statements: firstly, that the economics of electricity generation from wave energy are likely to be more favourable than was officially maintained until the recent embarrassing disclosures, and secondly, that Britain has lost the edge in development of a viable, large-scale wave energy conversion system.

Technical constraints The technology required to harness wave power must meet certain special restrictions; principally that it must deal with the extremely high forces experienced in storm conditions. An important aspect of the system must also be its conversion/transmission mechanism, responsible for accepting a "raw" mechanical energy input and producing a smooth power output, either directly as work or as electricity. Two different approaches to wave energy conversion are used: either a land-based, fixed device, which may be sited to obtain maximum benefit of coastal geometry; or a floating, ocean-going device, moored offshore and connected to mainland through an umbilical system. The Norwegian wavepower programme uses the first approach, while the Edinburgh duck is a floating device. Both approaches have their merits and demerits; while use of land-based energy converters restricts the scope of wave climates available to the device, it makes maintenance and power take-off relatively simple. In addition, the coastline around the site may discreetly be engineered to focus and enhance the incident waves on the collector, without any great adverse effect on the local ecology. On the other hand, while use of a duck or similar device requires the construction of a power transmission link from sea to shore, the ducks may be placed in a region of near-constant swell, even in cases where the local coastline sees a variable or small swell. Use of ocean-going schools of ducks would also enable modular construction and expansion of the wave power station to suit demand: the capacity of any coastal site is fixed and represents an upper limit on the power recovery. For the very large scale application, then, the use of multiple duck modules would seem appropriate, while smaller power needs could be met by land-based devices. In this way the benefits of multiple redundancy should offset the increased cost and time of maintenance associated with a duck project.

OWC Devices The fixed installations favoured by Norwegian researchers are described as "Oscillating Water Column" (OWC) devices. (*NB* a prototype device of this class has also been constructed by a British research team on the Scottish island

of Islay.) This technology is based on the naturally occurring, "spouting" caves which are to be found on many cliff-bound coastal shores: these are sea-caves whose roofs contain holes which permit the venting of air and water in times of high swells. The heart of the system is a man-made sea-cave, in which the level of water rises and falls in time with the incident waves. A vent in the cave roof is connected *via* a ducting to a bi-directional turbine and thence to atmosphere. The turbine provides a resistance to air flow; as the water level in the cave rises so does the pressure, forcing air through the turbine and thereby doing work. When the level falls, the pressure in the cave drops below atmospheric and so air is sucked back through the ducting into the cave. The cunning piece of design is the turbine: fitted with blades of a profile developed by Wells and co-workers at Queens' University in Belfast, it rotates in the same direction irrespective of the direction of air-flow. The incoming air therefore also does work and a reasonably smooth power take-off is achieved. The system may be thought of as a large, slow-moving, double-acting piston compressor, with the water column in the cave acting as the piston. Them mechanical difficulties lie chiefly in the turbine manufacture and in the construction of a sufficiently robust structure.

Edinburgh Ducks By contrast, the duck device designed by Professor Salter's team is a far more complex engineering project, although the principle of operation is extremely straightforward. Figure 1.1 shows a cross-sectional schematic of a duck wave absorber. The device is shaped like a cam, with the "beak" aligned towards incoming waves. It is moored by linkages to the axis of the cam, so that it is free to rotate about this axis but not to slew around (and hence out of the path of the waves) . When a wave is incident upon the duck the beak will rise, then fall again as the trough reaches the device. Work may be abstracted from such a motion by providing an opposing force for the duck to act against. The mechanism chosen by Salter's team was intended for use with a whole series of ducks, mounted on a common spine with flexible linkages. Each duck was to contain four gyroscopes to provide the opposing force: mounted in the nose of the duck, these would experience precession as a result of the duck motion. This precession would then be used to drive a hydraulic "ring-cam" pump, producing a stream of high-pressure oil. The oil would then be passed through a variable-power hydraulic motor, connected to the gyroscope flywheel. This would serve to maintain the gyroscopic motion, act as a short term energy store and smooth the power output. From there it would drive a second motor connected to a generator, producing an averaged electrical current. This current would then be sent *via* appropriate linkages to the common spine and thence to shore. The Edinburgh team spent considerable time on research into the many novel aspects of this proposed design: design and construction of an advanced wave tank for simulation of real sea states; optimisation of the duck shape by wave tank experimentation; design and testing of the hydraulic technology

required; dynamics of linked duck systems in real sea conditions, and so on. Although the system is far more complicated than the OWC device, Salter argues that this does not make it more difficult or impractical: all the moving parts are contained in the hermetic duck environment, and the behaviour of all the components may accurately be predicted. The OWC, being an open system whose prime mover is connected directly to the environment, is inherently more unpredictable, as it must then assume some of the characteristics of the chaotic local sea states. In any event, work was halted by the U.K. government on the grounds of complexity, but this has not prevented Salter from maintaining some research activity in some of the key areas of the design.

Magnus-Budal Devices As a result of Norwegian researchers' investigations of the fluid mechanics of wave power systems, it is possible to postulate another class of wave energy devices, utilising the so-called "Magnus-Budal" effect. This is a type of lift force experienced by cylinders submerged near the surface of a water wave field. It arises as a result of the near-circular streamlines found in the water below waves; any cylinder placed in such a position will experience a net circulation of fluid and hence a transverse force. Budal's discovery was that by rotating a cylinder in such a situation, it was possible to enhance or decrease the net force, depending on the direction of rotation of the cylinder. The power required to rotate the cylinder would be small compared with the potential of the resultant enhanced force to do work. Experimentation in Norway and in Salter's Edinburgh wave tank has confirmed the existence of the effect, and it has been quantified to some extent. The Magnus-Budal effect is particularly promising because it offers the ability to regulate the power take-off according to the wave climate; in addition devices of useful power rating could be very much smaller than either ducks or OWC installations. Figure 1.2 shows a schematic visualisation of a conceptual pump or compressor design, using the Magnus-Budal effect to drive the device.

1.1.3.5 Other Renewable Energies

Some other renewable sources are worthy of brief mention, although they are of only tangential relevance to the research described in this thesis.

Geothermal Energy This is another energy source which has been recognised and used by Man in the past; the chief usage being as a source of free hot water. New

technologies aimed at exploiting the heat of the Earth's core have the aim of steam generation: in this way the steam may be used to drive a turbine hooked to an electricity generator. Work has been carried out in several countries, notably Mexico, but the capital cost is still high, as deep boreholes must be drilled to enable supply and takeoff of feed water and steam.

Tidal Energy This energy source is extremely restricted in the locations suitable for situation of collectors; where a large tiderace does exist, however, the potential for extraction of mechanical energy is very great. A barrage across the estuary of the Severn River in England, for example, has long been advocated as a means of tapping the "Severn Bore". Power would be extracted by funneling a portion of the tiderace through large turbines situated on the barrage. The effect on the river estuary of such a project is not known exactly, though: some fear it could lead to extensive silting upstream. The capital cost of such a scheme may prevent its adoption in the near future.

OTEC Devices This is the class of floating heat engines whose purpose is to produce work by utilisation of the temperature difference between the surface of the ocean and its seabed. In suitable locations (*e.g.* off the Florida coast) this temperature difference may be in the range 10 °C–20 °C. While these devices display great ingenuity, they are not likely to be economically attractive in Britain unless there is a sharp rise in other energy prices: at the moment most British power stations return sea-water used as coolant at *ca.* 30 °C–35 °C. This represents an equivalent temperature difference (relative to the bulk sea temperature) to that used by the OTEC devices, yet it is regarded as useless for practical (economic) purposes. This is a good example of how different perceptions of "useful" energy are created by energy pricing structures.

1.1.4 Summary

At the time of writing the Western energy economy is heavily dependent on fossil fuels, and to a lesser extent on nuclear energy, as primary sources of heat and power. These are now regarded as mature technologies, suitable for trade to developing nations with urgent needs for cheap energy to aid in creation of industrial infrastructures. The

wisdom of maintaining this policy of energy supply is increasingly being called into question, as more and more compelling arguments for change come to light. The proven detrimental effects of the combustion of fossil fuels on the global ecology suggest that at the very least, future use of these resources should be not much more than current rates of consumption. The world's largest oil reserves are situated in the politically volatile Middle East; at the time of writing the actions of Saddam Hussein's Iraq are clear reminders of the folly of over-dependence on one source of supply, especially given the recessive effect that increased oil prices can have on even well-developed national economies. It is also doubtful whether an emerging nation should be saddled with the level of debt implied by an extensive nuclear power plant construction problem. This would seem to make a compelling case for the adoption of renewable energy as a main source to meet future power requirements.

Research into renewable energy usage has so far been relatively low-key and low-budget, aimed at demonstrating basic feasibility for the most part. What is now needed is research, whose aim is to identify and quantify those applications in industry whose demands mesh neatly with the special characteristics of renewable energy sources. In this way the potential of renewable energy may be maximised, demonstrating that it is more than an ecologist's fantasy but rather is of immediate relevance to traditional industrial processes.

1.2 Process Energy Requirements

1.2.1 The Value of Energy: Exergy

In this Section the aim is to assess some of the more common processes in the chemical and related industries, on the basis of their energy costs. The intention is to show that many current processes use energy of a far greater quality than is actually required to "do the job". This represents a wasteful use of what is essentially a non-renewable resource. It will be shown that the most thermally intensive processes operate for the most part well at temperatures attainable by heat pumping from *ca.* 100 °C or lower. Heat is abundantly available at this range on most chemical complexes, in the

form of low-pressure steam, yet is not much used. The reasons for this are purely economic: there has been little monetary gain in the development and installation of new thermal energy technology. This situation cannot last, however, so some way is needed to quantify the benefits and costs of alternative energy supply strategies on the overall energy efficiency of a plant. The cost of fuel is the most obvious criterion, and the one which is used by the accountants to determine financial weakness: this is not always a satisfactory criterion for long-term comparison or analysis of processes. Fuel prices may be subject to rapid, short-term fluctuations, such as those caused by a nervous stock market, or may be artificially depressed for political reasons. A better tool, and one which turns out to give the answers the accountants like too, is provided by application of the fundamentals of thermodynamics. The quantity and quality of energy consumed by a process may accurately be analysed; the most costly steps in a process may also be identified and targetted for improvement. The tool is the "exergy" concept, and its application is described as "exergy analysis".

Exergy may be thought of as the maximum proportion of a substance's energy which is accessible in practical terms, if a Carnot heat engine whose sink is the environment is used to abstract energy from the substance. Conversely, the exergy of separation of a mixture defines the minimum work requirement for the separation. It is not a new concept but its application to process analysis has only become widespread in recent years. In its development it has variously been referred to as "availability", "useful work", "maximum work" and "absolute work". The term most commonly used in European analysis is exergy, and this will be used henceforth.

The formal definition of exergy is:

$$Ex = H(T,P) - H_o(T_o,P_o) - T_o\,[S(T,P) - S_o(T_o,P_o] \qquad (1.1)$$

in which the conditions (T_o, P_o) refer to the standard temperature and pressure of a chosen ambient or "dead" reference state.

The choice of dead state is not absolute, and as a consequence some people do not feel comfortable with the treatment of exergy as a thermodynamic state function, since the magnitude of changes from the datum state may depend on the datum state. In practice this should not be treated as a problem, since most calculations involving exergy are only concerned with the exergy change of a stream that is never actually at the datum. In this case, the exergy is a straightforward linear combination of state function differences, whose absolute values are independent of any datum states. The exergy must therefore also be a state function in this respect.

In any process where there is a finite change in the state of a stream, there is an associated change in exergy. So, for a heat exchanger, having two streams, there are two changes in exergy which may be calculated. The exergy gained by the cold stream will always be less than the exergy lost by the hot stream; this is a consequence of the Second Law of thermodynamics. The loss of exergy may be attributed to the existence of a finite ΔT between the streams, and any pressure drops experienced by each stream in the unit. Likewise, in any separation process, the actual work of separation will be greater than the exergy of separation; the reason being the existence of finite gradients of temperature, pressure and/or concentration in or between streams. The quantity of exergy degraded will depend on the design and process conditions of the unit, so by defining suitable dimensionless quantities it is possible to make a rigorous analysis of the design of individual units in a plant, or assess a unit's effect on the overall exergy balance. In this way it is possible to identify the potential for addition of energy conservation technology to existing equipment, or to screen possible designs for new equipment. Even a qualitative assessment of a particular method of energy supply is possible: for example, in burning oil to supply heat to a domestic water tank, the exergy supplied to the process is equivalent to the heat of combustion of the fuel. Although the domestic boiler may have a First Law efficiency of *ca.* 90%, its exergetic efficiency ("Second Law efficiency") is bound to be far lower than this, as the delivery temperature of the product is so low compared to the combustion temperature. The use of oil in this way is then fairly described as very inefficient. Use of electric heating to accomplish the same duty must be even worse: for if the electricity comes from a conventional power station, there are additional losses resulting from the processes of converting heat to work, work to electricity and electricity to heat.

1.2.2 Heat Recovery In Thermally Intensive Processes

The chemical process industry abounds in operations which require far more energy in practice than the minimum exergy predicted by thermodynamics. Typically these processes involve both heat transfer and separation of mixtures: the excess exergy consumption serves to reduce the size of the plant and hence the capital cost, at the expense of increased running costs. These processes are the obvious targets for development of new heat pump technology: the goal is to achieve a system whose running costs are so low that the additional capital cost may be amortised within acceptable periods. Previous attempts to incorporate heat pump technology into industrial thermal processes have foundered between the Scylla of cheap fuel oil and the Charybdis of

high investment costs for retrofitted heat pump systems. It has been found, however, that if a process is designed *from the start* with heat recovery and heat pumping in mind, then the performance of the system may greatly be improved. The use of active heat recovery—heat pumping—is *not* incompatible with the techniques of passive heat recovery, despite the protestations of the Linnhoff school of thought (whose position is that there is little or no place for heat pumps in a plant with a near-optimum degree of heat integration) . This bold statement is readily justified if one considers the additional flexibility offered by the presence of a heat pump in a heat-integrated process. Such processes tend to have "stiff" control systems, with the incoming feeds being heated by product streams and consequent problems on startup or under part load. If a heat pump is used, abstracting heat from the environment or another , ever-present source, the additional heat required in such situations may be supplied in a painless manner.

The processes of most interest may be classified broadly as separation processes and drying processes. These are extremely intensive in their specific energy consumption. Drying is also a separation, but we will extend it to include dehumidification operations. A brief examination of the main processes in each category follows.

1.2.2.1 Separation Processes

The most common thermal separation processes are: distillation; absorption; stripping; evaporation, and crystallisation. Of these, distillation, stripping and evaporation require a major heat input: all processes require the removal of heat, *i.e.* a source of cold. Varying degrees of heat recovery technology have been implemented in most of these unit operations but there is still significant potential for increasing the sophistication of the technology.

The thermal inefficiency of the techniques used in each operation depend to a great extent on the nature of the products and the degree of impact the running cost will have on the final plant product. For example, cryogenic separation of gases is accomplished using refined distillation flowsheets incorporating a high degree of heat recovery, because the amount of energy required to work so far away from the ambient conditions is very high. The economies of scale therefore dictate that any gain in efficiency will be valuable. Everyday distillation is however far less efficient, as it is not subject to the same exigencies.

1.2.2.2 Distillative Separation

The thermal inefficiency of conventional isobaric distillation columns is as obvious as it is high: heat is supplied to the reboiler of the tower and degraded to the temperature of the cooling water used in the condenser. in many cases this may mean a temperature difference of over 100 °C between supply and sink. If the column produces sidestream products these must also be cooled (ultimately) to ambient temperature, which represents an additional inefficiency.

Most distillation columns are found in groups together on a site, for example as a separation train on a refinery site. In this case the application of the "pinch" methodology may be used to integrate the heat loads and cooling loads of the columns' boilers and condensers. Such a strategy is relatively inexpensive if long periods of steady operation with no great change in loads may be assured. Another, related, approach is to perform an exergy analysis on each component of the plant, as described in Section 1.2.1. In both cases, the gain in energy savings must be offset by a loss of operability.

The application of heat pumps to distillation has been investigated, notably in connexion with extremely costly separations, which require many equilibrium stages and a high energy input. Notable examples are: ethanol/water; propane/propene; ethane/ethene, or xylenes/benzene/toluenes. The most simple-minded approach is to "bolt on" a ready-built heat pump to an existing distillation column. The schematic flowsheet for such an application is shown in Figure 1.3. The heat pump uses an internal working fluid circuit and operates by vapour compression. The method is generally termed a "Closed-Cycle Heat-Pump-Assisted Column". This arrangement has both advantages and disadvantages: the chief advantages are that the working fluid of the heat pump may be chosen to suit available low-cost compressors, and that the process streams need experience no disturbance in conditions from the plain column design. This type of heat pump application is therefore of interest as a retrofit, where minimal disturbance to the process stream exit states is desired.

The disadvantage of using an external working fluid become apparent, however, when one considers the scheme shown in Figure 1.4. In this scheme, the vapour leaving the top of the column is compressed directly, then condensed against the bottoms in the reboiler. This scheme requires only one main heat exchanger, performing the functions of the separate reboiler and condenser of the first scheme. Further, the temperature lift over which the cycle operates are necessarily lower, because the need for temper-

ature driving forces in one of the exchangers has been eliminated. The anticipated Coefficients of Performance (COP) will therefore be better. The disadvantages of this scheme, the so-called "Mechanical Vapour Recompression" (MVR) scheme, are that the compressor must handle process streams, and that the efficiency is a strong function of the temperature lift. A hidden restriction on the use of MVR is the operating column pressure: a low operating pressure implies a low vapour density at the compressor suction and hence a high investment cost. The industry has adopted MVR in conventional plant, notably to perform the separations described above, yet the penetration of heat pumps to columns with large lifts is still slight.

There would seem to be a distinct niche, therefore, for heat supply technology which retains flexiblity of operation, yet maintains a good performance over temperature lifts of more than 20°–30°, this being the maximum Δ T over the columns described above.

1.2.2.3 Evaporative Separations

This class of separation includes the thickening and concentrating operations such as those found in sugar refining, or production of a salt. (in the latter case, a crystallisation step is also involved.) The general problem is the same: removal of a portion of water from a liquid stream. One of the major examples of this operation is sea-water desalination to produce potable water. This technology has a substantial world market, especially in the arid but fuel-rich regions of the Arabian Gulf. As pollution control regulations will tighten in the future, the use of this technology by the "mainstream" chemical industry will increase, with the aim being to separate more pollutants from waste process water. A less obvious future market may be provided by the need for fresh water in the South of England, stemming from the inadequacy of existing reservoirs and supply piping rather than from any especial aridity of climate. The now-privatised English water supply utilities may well decide that a desalination technology can offer a cheaper option than the massive repair and upgrading programme required as a result of years of Governmental neglect.

There are four main methods used in desalination technology today: reverse osmosis (RO); mechanical vapour recompression (MVR); multi-effect boiling (MEB) , and multi-stage flash (MSF) . The RO process is a non-thermal process but requires significant amounts of shaft work. The other three are all thermal processes, using differing amounts of energy per kilogramme of product. They are all carried out at temperatures near 100°C: higher temperatures may not be used, as sea-water forms increasing

amounts of "scale" as its temperature is increased. This scale (principally calcium and magnesium salts) severely increases the thermal resistance of heat transfer surfaces if allowed to build up, with corresponding deterioration in fuel economy. MVR has the potential to yield a highly efficient separation, given that the pressure ratio required to effect the heat transfer is very low for this system. However, the use of low, near-ambient pressures, corresponding to saturation temperatures of *ca.* 100 °C, restricts the use of MVR to small-to-medium plant. The vapour density of saturated steam is very low under these conditions, leading to high compressor capital cost.

Multi-effect boiling and MSF are two similar processes, each using a high degree of heat recovery between feed and product streams. In each process the separation is carried out in a number of different heat-transfer stages, with heat being supplied by internal heat transfer where possible. The more important of the two, and the most popular method for really large-scale desalination plant, is MSF. A schematic of an MSF plant is shown in Figure 1.5. The essence of operation is that hot seawater, initially under some pressure, is throttled into a chamber and undergoes partial evaporation as a consequence. The vapour produced by the throttle is condensed against a feed stream, and the remaining hot liquid may then be throttled into the next stage of the process. The heat to drive the whole process is put in at the "top end" of the thermal cascade, normally by condensing steam. (In MEB, the feed stream is partially evaporated in each of several stages. MSF is the limiting case, where no boiling takes place and the maximum amount of sensible temperature rise in the feed occurs.) Typical thermal economies, expressed as the ratio of (kg product) /(kg steam used) fall in the range 10–20. This implies a specific energy consumption of *ca.* 120–240 kJ/kg. This is to be contrasted with the exergy of separation of seawater into a pure stream and a double-strength brine solution, of 35–40 kJ/kg (see Crerar *et al.* [19, 18, 17]) . Greater efficiency can be achieved by using more stages but the limit imposed by fuel economics is such that economies of 20 kg/kg are typical maxima.

1.2.2.4 Drying and Dehumidification

In contrast to the partial evaporation of liquids discussed in Section 1.2.2.3 are the drying operations. These normally involve the total, or near-total, removal of water from solids, whether particulate or bulky in nature. Examples include: final crystalline/powder product drying; grain or corn drying, and timber conditioning. The first applications of heat pumping to these areas were based on compression cycle technology; these were rendered marginally economic by the compressor cost, for this

problem also typically involves large volumetric vapour flows. The problem in the case of drying is that a large diluent stream at low pressure is involved, so that direct vapour recompression is not very attractive. Significant steps have been taken, however, using the technology of absorption heat pumping, in this field. The absorption heat pump offers the ability to deliver heat over a significant range of loads without marked deterioration in performance, and does not require compression equipment. The cycle used may be either closed-cycle, where the working fluid is quite distinct from the process side, or open cycle, where the working fluid is the process fluid itself.

1.3 Aims of Research

1.3.1 Motivation: Possible Applications of Renewable Energy

The foregoing text outlined the state of energy technology today: in particular it should be apparent that there is considerable uncertainty over future costs of "traditional" energy sources. This would imply a greater role for the renewable energy sources in the future. but there is still a great deal of research which must be carried out, in order to enable use of renewable energies by the process industries. The most concentrated renewable energy sources are wind and wave power: furthermore, the technology required to capture these sources is further advanced than that of other renewable energies.

The most attractive areas of usage will be those where the inevitable variation of available power associated with wind or wave energy is not a problem. This makes the existence desirable of some kind of intermediate storage, be it of energy or of matter. By the same token, any process which exhibits regular variations of heat requirement will be best served by heat pumps designed to accommodate such a variation. This opens up a range of applications, such as batch processing, where the load conditions previously rendered conventional heat pumps inefficient.

A good example of a process whose instantaneous output need not be held constant is desalination: this always is operated with several days' consumption in storage as

a product buffer. Greenhouse or other space heating is another example: the heating requirements of such buildings tend to follow the weather conditions, and the thermal mass is usually so great that variation in input power has only slight effect on the temperature. This means that the heat lost from a building is highest when the external wind is strongest, which is a happy match of load and supply!

The development of heat pumps accepting a variable amount of work from the environment depends crucially on the ability of the system to cope with changes in the load pattern without a corresponding change in the quality of heat output. The heat sources used by such heat pumps may be environmental (humid air, the sea, the ground,...) in nature, in which case the supply temperature is effectively constant. They may alternatively be process streams, in which case the source may be non-isothermal. In the majority of applications the sink of the heat pump will be non-isothermal. The heat pump must make best use of these process characteristics, in order to maximise efficiency and reduce capital cost. The running costs of a heat pump whose energy comes entirely from the environment will only be those costs associated with control and maintenance; therefore the pump should be able to regulate and control its own behaviour in response to the load and available power.

1.3.2 Basis of Experimental Research

The principal aim of the research described in this Thesis was to investigate the suitability of a modified vapour compression cycle as the basis of a "self-regulating" heat pump for use with wave or wind energy sources. in order to do this, it would be necessary to design and build a pilot plant capable of simulating a realistic load, source and variable work input. By operating the pilot plant it was hoped that enough information would be garnered to give a definite indication of the feasibility of such an inherently self-controlling heat pump. The nature of the modified cycle to be explored is outlined in the following paragraphs.

A compression heat pump cycle will normally use a positive–displacement compressor, as the pressure ratios encountered are rather higher than those attainable with single-stage centrifugal units of the same capacity. A heat pump compressor will therefore exhibit a nearly linear relationship between the rotational speed and the throughput of gas at the suction over a large part of its operational speed range. There will

of course be some variation in volumetric efficiency over a range of speeds but this may be neglected in this qualitative analysis. One way of regulating the capacity of the heat pump cycle is therefore to change the speed of the compressor. This is not entirely satisfactory; there will be a size of compressor below which the cost of the apparatus required to control the speed will cost more than the compressor. There will be an even larger size of compressor below which the additional incremental cost of the control system will negate the energy savings resulting from the introduction of the heat pump system. A crude approximation may be made to speed control by cycling the compressor on and off; this is even less desirable, as every time the compressor trips, the equilibrium of the heat pump is destroyed and refrigerant migrates around the pipework. On restart energy must be consumed to drive the working fluid back to steady-state levels throughout the plant. This very control strategy has contributed greatly to the low achieved COPs of the first generation of heat pumps, introduced in the 1970s (see Cooke [15]).

Even if breakthroughs in engineering technology, or the tooth fairy, presented us with utterly reliable and inexpensive control hardware, capable of providing 0–100% of any compressor speed without destroying the energy economics of our heat pump, this would *still* not suffice for use in most renewable energy applications. These applications, as discussed above, may exhibit a very wide range of potential energy availabilities. A single compressor, designed to cope with the full range of available power inputs over a year's operation from a windmill, would be grossly oversized for the mean power input; this would destroy the economics of the project. The desired strategy in compressor choice is therefore to choose the size of unit which is best suited to the expected mean power input range, then to devise a means of altering its capacity away from that mean by the desired amount when necessary.

The key to this solution is in the nature of the compressor itself; as a positive-displacement device operating at constant speed inducts a constant volumetric flowrate of suction gas, *independent of line pressures on either side of the unit.* A change in the density of the suction gas will therefore change the mass flowrate of gas through the compressor. This in turn affects the capacity of the heat pump cycle. The problem now is: how to change the gas density without changing the evaporation temperature of the cycle, since this is presumed as part of the design specification. With a pure working fluid, this would be impossible: some small density change could be introduced by tinkering with the amount of superheat on the suction gas side, either by heating or throttling the suction gas . This could never provide the wide variations in capacity required, and is in any case a bad idea; it would introduce thermodynamic inefficiency to the cycle. Some better solution must therefore be found, or the project abandoned.

With a nonazeotropic binary (or greater) mixture as working fluid, the problem may be solved. At a specified evaporation temperature, such a mixture has a range of possible vapour pressures, between the vapour pressures of the pure components. This in turn implies a range of gas densities and a range of heat pump capacities. If some means were available to change the circulating composition of working fluid it would be possible to change the performance of the cycle. The heat pump cycle to be investigated was based on just this principle, with a binary mixture as working fluid. A binary mixture was preferred as it gave the necessary additional degree of freedom, yet the working fluid composition could be calculated from experimental measurements of temperature and pressure. This would allow demonstration of the basic principle, even if the chosen working fluid mixture did not have all the characteristics of an optimum fluid for the design specification.

The chosen means of working fluid separation was partial condensation: by using two or more condensers in series as the output heat exchangers it would be possible to collect condensates of differing composition. If these streams were then taken to storage, rather than returned directly to the evaporator of the heat pump, the overall composition of circulating working fluid could be rectified. By selective use of fluid from particular tanks, it would be possible to achieve a progressive shift in composition. The beauty of such a system was its simplicity; at high loadings the condensation process would require the surface in both condensers; at low loadings, only the surface in the first condenser would be necessary. The unit would therefore run with feed from both storage tanks at high powers, taking however feed from only the storage tank connected to the first tank at very low inputs. At intermediate powers the components of the working fluid could be shifted around the storage by manipulation of the condensation rates and evaporator feed rates in each half of the plant.

The ability of such a split condenser system to operate under widely differing loadings was to be investigated: central to the success of such a system would be the ability to maintain a desired degree of separation, irrespective of the magnitude of power available to drive the heat pump.

The use of non-azeotropic mixtures as working fluids was known to give improved COPs if non-isothermal source and sink streams were used: this was to be another topic of the research. The intention was to determine the relationship between COP and capacity for the chosen fluid pair. The improvement in COP would come about through closer matching of the temperature profiles in the heat exchangers of the heat pump, which would improve the thermodynamic efficiency of the heat pump. (See Bett *et al.* [9] for quantitative explanation of availability loss in heat exchangers.) To this end, provision

would be made for the independent control of each condenser's operating pressure; this could in theory give even better matching of the profiles. The use of nonazeotropic working fluids in heat pumps has received much attention in recent years; it is covered in the literature review contained in Chapter 2.

1.3.3 Subsidiary Research Aims

As stated above, the main aim of the experimental work was to investigate the ability of a split-condensation system to provide self-regulating capacity control in a heat pump pilot plant. There were several subsidiary aims of the experimental programme, imposed by cruel necessity rather than a desire for a more arduous project.

The plant would be commissioned with a pure fluid, in order to assess the performance of the components of the heat pump under relatively unambiguous conditions. The performance of the compressor in particular would require to be examined carefully, as this would be a major source of any thermodynamic inefficiencies in the plant.

At the start of the project, it was decided to seek all possible sources of external funding; the proposed pilot plant was (correctly) envisaged as being very costly in time and money. One such source of aid was provided by Messrs Cal-Gavin Ltd. of Birmingham, who supplied free of charge a prototype evaporator. The sole condition of supply was an evaluation of the performance of the unit by the author as part of the research work. This was therefore incorporated into the planning for the experimental programme.

1.3.4 Thermodynamics Research

As the project progressed, it became necessary to obtain thermodynamic data for nonazeotropic, binary mixtures of CFC refrigerants, in order to proceed with the design of plant. These properties would also be required in the analysis of any experimental data. The author started an investigation of this subject and embarked on a quest

for a good method of obtaining such data. This expanded into a major component of the research, allied to and running parallel with the experimental programme. The objectives were: to predict properties of CFC fluids and in particular the properties of those fluids mooted as replacements for the traditional refrigerants. The work is decribed in full in Chapter 6.

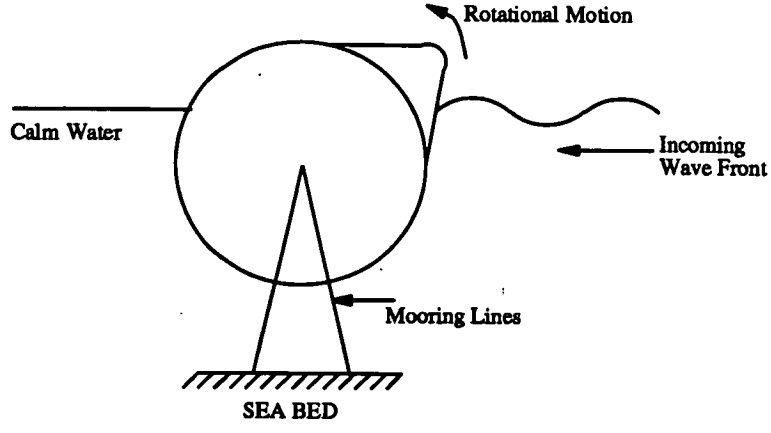

Figure 1.1: Cross-Section of Edinburgh Duck

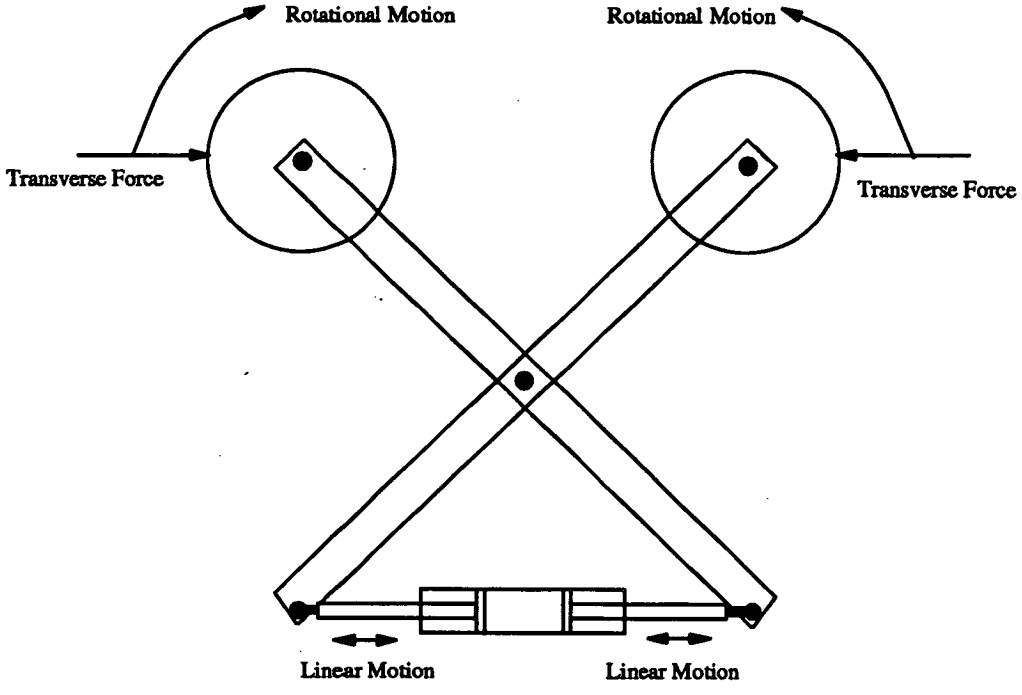

Figure 1.2: Conceptual Pump Driven by Magnus-Budal Effect

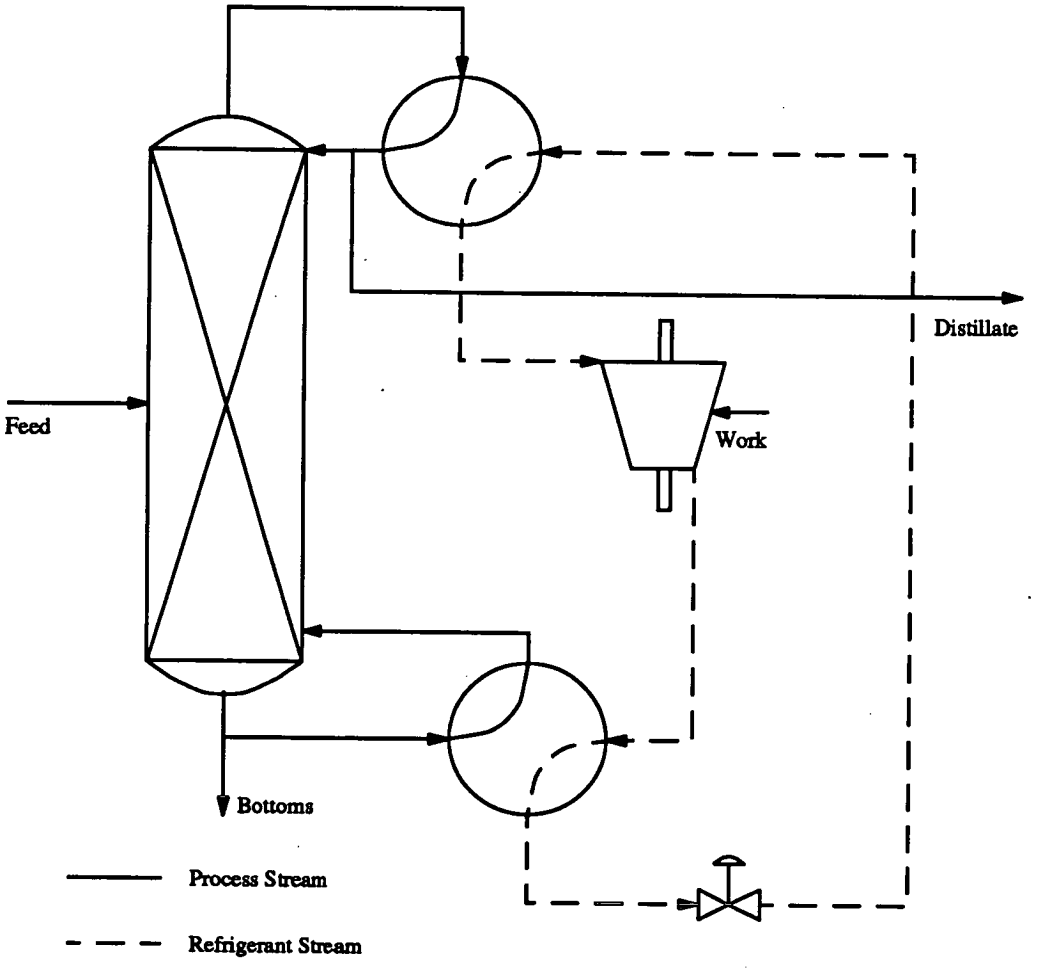

Figure 1.3: Distillation with External Heat Pump

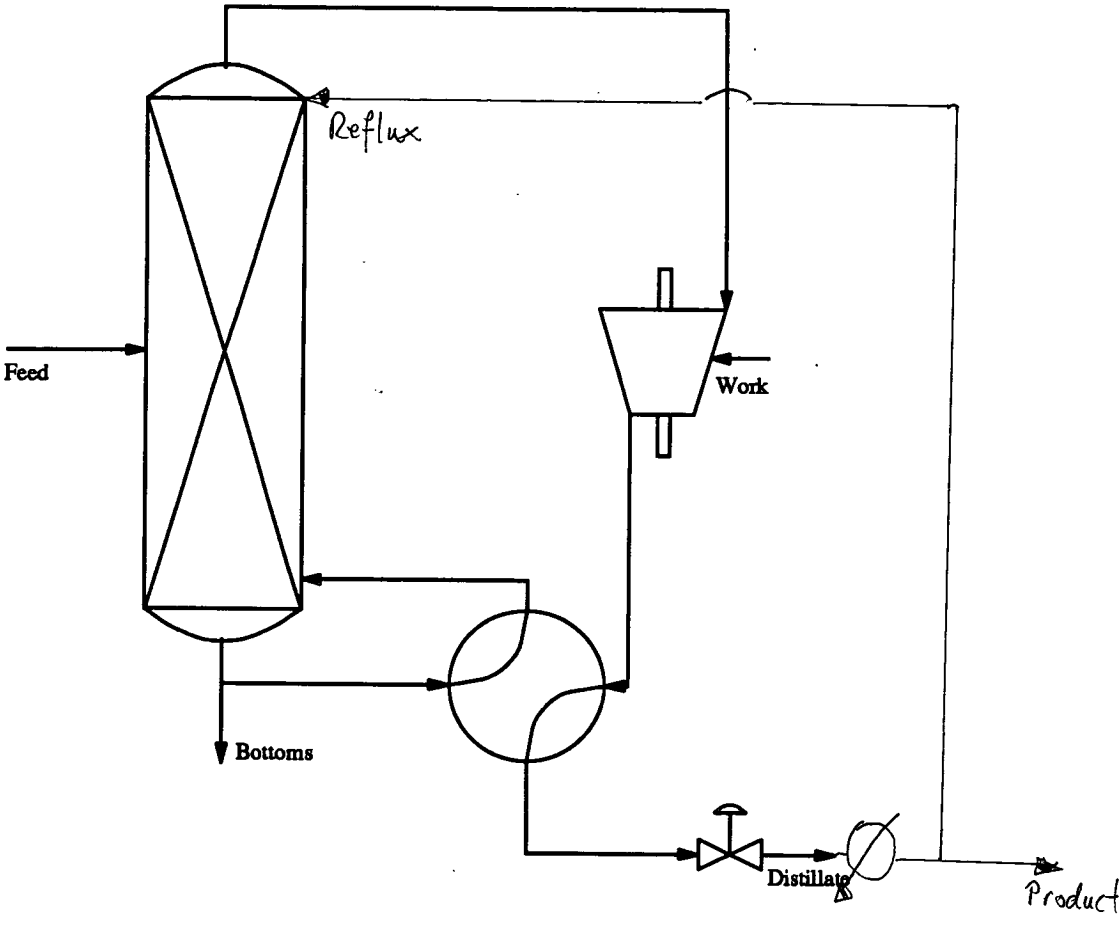

Figure 1.4: Distillation with Vapour Recompression

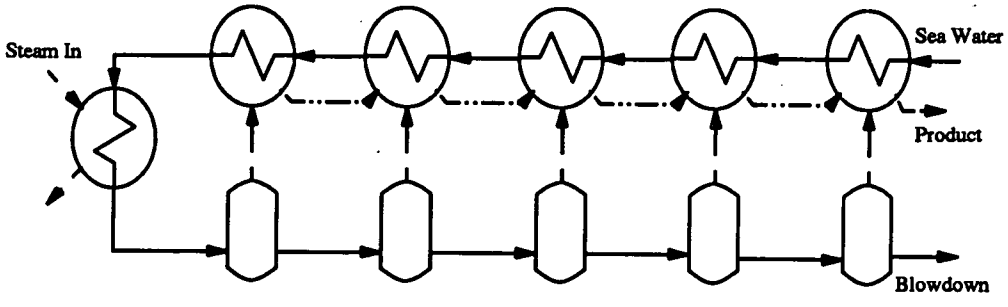

Figure 1.5: Multi-Stage Flash Desalination Process

Chapter 2

Theory and Review of Literature

2.1 Capacity Control of Compression Heat Pumps

2.1.1 Introduction to Vapour Compression

Many heat pump and refrigeration devices are based on a reversed heat engine cycle, the *vapour compression* (VC) ôr *Reversed Rankine* cycle, which is essentially a Rankine power cycle run backwards. In such cycles the working fluid is conventionally termed *refrigerant*, irrespective of the nature of the cycle. Details of such cycles are given in the standard thermodynamic texts *e.g.* Bett, Rowlinson and Savile [9] or in the classic work on heat pump devices by McMullan and Morgan [65]. The implementation of the VC cycle which is normally quoted for flowsheeting or educational purposes is depicted in the schematic Figure 2.1, and has four components. These are: evaporator, compressor, condenser, and expansion device. In practice all practical implementations include an

accumulator vessel between the expansion device and evaporator: this is needed to hold spare refrigerant charge until needed. The cycle extracts heat at a rate Q_{ev} from a source at T_{so} and discharges it at a rate Q_{co} to a heat sink at T_{si}. This upgrading of energy is accomplished by consumption of mechanical energy at a rate W in the compressor. The operations which make up the ideal VC cycle are:

- Refrigerant is vapourised in the evaporator by the heat source.
- Vapour undergoes adiabatic, reversible compression in the compressor.
- The compressed vapour is condensed against the heat sink.
- The condensate produced by the condenser is throttled across the expansion device, passing eventually to the evaporator to complete the cycle.

This cycle performs well enough to be the standard for nearly all modern domestic refrigerators; it is also used as the basis of many industrial refrigeration systems. The first generation of compression heat pumps, based on this refrigeration technology, failed however to make any real impact on either the domestic or industrial heating markets. Why should this be so?

2.1.2 Control of the VC Cycle

A principal reason for poor market penetration of heat pumps is the poor response of the basic VC cycle to fluctuations in process conditions. The only means of matching the capacity of this cycle to heating (or refrigeration) demand is to change the mean throughput of working fluid. The flow/pressure ratio characteristics of most heat pump cycles require use of a positive-displacement machine. At constant stroking frequency such a machine exhibits a near-constant volumetric throughput, irrespective of suction gas density or pressure ratio. The efficiency of such a unit may however depend quite strongly on these process parameters. The only ways, therefore, to change the mass throughput of working fluid are to alter the suction density or change the compressor's operating speed. The former method is essentially impossible with a fixed evaporator temperature and pure working fluid; although some small variation in gas density may be achieved by superheating of the vapour entering the compressor suction, the density

is essentially fixed by the vapour pressure of the working fluid at the evaporation temperature. The second option—variation of the compressor speed—is a possibility but in practice there are drawbacks.

The cheapest method of capacity control is to cycle the compressor motor on and off, providing intermittent refrigeration capacity. This is expensive if the cycling needs to be frequent, as working fluid will migrate round the apparatus on every shutdown. Energy must then be consumed to restore pressure levels and liquid holdups to their design values. The other option is to provide a means of continuous variation of the compressor speed, using for example an electrical variable-speed drive unit. This is commonly done but is not economic for small (domestic and light commercial) units, as the cost of the drive exceeds that of the compressor. Most compressors are furthermore designed for optimum efficiency over only part of the possible speed spectrum. Finally, variation of compressor speed by itself can only give a turndown of 0–100% of maximum rated compressor throughput. This may lead to problems with compressor sizing if the anticipated range of frequently-occurring capacities is very large. In the case of heat pump devices for abstraction of work and heat from the environment, the mean energy inputs may be specified with some certainty from meteorological data; there will always exist however large variations from this mean, and so a simple VC cycle would evidently be inadequate for this duty. The modification of the simple VC cycle to allow good capacity control is discussed in the following sections.

2.1.3 More Complex Cycles

Many modifications have been made to the basic VC cycle for use with pure fluids; these are dealt with by McMullan *(op. cit.)* They have been aimed primarily at the improvement of cycle efficiency by internal heat exchange; their economic worth is dependent on a careful optimisation of heat exchanger areas. A gain of a few percent in thermodynamic efficiency may often only be bought at considerable incremental increase in capital cost. The use of elaborate heat interchange is precedented; cryogenic cycles are the best-known example. In that case, however, different circumstances prevail, making the design of more efficient cycles both desirable and economical. There are no real alternatives to the technologies used in gas liquefaction at low temperature, whereas there are myriad alternative sources of low-grade heat to displace the heat pump.

A very important cycle modification which is aimed at using the properties of non-azeotropic mixtures is the *compression-absorption* cycle, shown in Figure 2.2. This incorporates a liquid solution pump and liquid return line, linking the evaporator and compressor of the basic VC cycle. In this cycle the working fluid is only partially vapourised in the evaporator; the remaining liquid is pumped into the condenser, where the compressed vapour condenses (is absorbed) into the liquid stream. Such an arrangement offers no advantage if the working fluid is a pure substance; if however the working fluid is a mixture then this arrangement offers many advantages. These will be discussed below; the chief of them is the potential reduction in cycle compression ratio, which implies lower compressor running costs.

2.2 Mixtures as Working Fluids

2.2.1 Introduction

The use of mixtures of fluids in a vapour compression cycle is here examined; it is demonstrated that a nonazeotropic mixture (or a mixture which exhibits azeotropy but whose overall inventory is not at the azeotropic composition) offers potential for smooth capacity control of a VC cycle over a greater range than would be possible using a variable-speed compressor. The use of binary *azeotropic* mixtures as refrigerants has long been part of standard refrigeration practice; this offers a fluid which behaves like a pure fluid but has superior characteristics to either of its constituents. The refrigerant R502 is extremely common in existing equipment; it is an azeotropic mixture of R12 (difluorodichloromethane) and R152a (1,1-difluoroethane). Other azeotropes have also been used in various specialist applications.

The range of fluids suitable for use in vapour compression heat pump devices is also examined; the fluids which have until now been used in VC plant must be replaced by fluids whose effect on the environment is less malign. Some considerable thought has been given to this, and the major suppliers of current refrigerant fluids are locked in a grim race to successful mass-production of the next generation of refrigerant fluids. At the time of writing, Imperial Chemical Industries plc seem to be in the lead, thanks

in no small part to their single-minded establishment of a high-powered process design team. It is still too early however to say for certain whose name will adorn the world's refrigerant storage tanks in years to come.

2.2.2 Working Fluids in Compression Cycles

2.2.2.1 CFC Fluids

The fluids most commonly used in vapour compression refrigeration or heat pump cycles until recently have been (almost without exception) members of the chlorofluorocarbon (CFC) family of fluids. The first major (and still one of the most widely used) CFC refrigerant, dichlorodifluoromethane, was made by Midgley [69] in 1930. These fluids are conventionally referred to as "Freons" or "Arctons", depending on the supplier's brand name. Individual fluids are normally described by the (rather cryptic) refrigerant codes introduced by the American Society of Mechanical Engineers in 1957 as a systematic shorthand nomenclature for refrigerants. Midgley's pioneering fluid is better known as R12; other common refrigerants are R22 (chlorodifluoromethane), R11 (chlorotrifluoromethane, used in foam blowing) and R113 (1,1,2 trichlorotrifluoroethane, used as an industrial solvent). At the time of their introduction, these fluids were regarded as near-perfect for these duties; they are mostly non-toxic, non-flammable and extremely unreactive. The controversy over depletion of atmospheric ozone, which was first detected in the 1970s, has focussed on the CFC fluids as the probable cause of this worrying phenomenon. The very unreactivity of the CFC fluids, which makes them so attractive for use at surface level, ensures that the atmospheric lifetimes of gaseous CFCs are extremely long—long enough for gases emitted at ground level to diffuse into the upper layers of the Earth's atmosphere. It is now believed that, once there, molecules of chlorine-containing compounds are decomposed by the action of ultra-violet radiation, producing free radical chlorine atoms. These radicals then attack and destroy ozone molecules, producing oxychloride radicals and diatomic oxygen. The radicals formed by these reactions continue to attack ozone until "mopped up" by self-recombination. It is still not certain that CFC fluids are entirely to blame for the undeniable depletion of ozone; it is nonetheless accepted by many countries and most of the major CFC producers that the existing fluids may no longer be used in quantity; an historic accord was reached with the agreement of the Montreal Protocol in 1986; this sets out an internationally-agreed timetable for cessation of production of all existing

CFC fluids with a known potential for the depletion of ozone. In engineers' terms, this means that chlorine-containing refrigerant fluids have no future.

The replacement fluids which are under current consideration are either HCFC (hydrochlorofluorocarbon) or HFC (hydrofluorocarbon) substances. The reasons for choosing these fluids have been excellently summarised by McLinden and Didion [64]; the move towards partially hydrogenated substances will decrease the atmospheric life of the compounds, while any reduction in chlorine content (by replacement of chlorine with fluorine) will reduce the ozone depletion potential.

2.2.2.2 Other fluids

Other fluids have been considered as potential working fluids in vapour compression cycles. One of the most attractive (and one of the few to gain commercial application) is water. This is not however suitable for use in the applications where there have been attempts to develop commercial heat pumps, that is in low-temperature heat supply. For obvious reasons water could not be used at temperatures close to 0 °C; in fact below 100 °C its low specific volume makes the compressor component cost prohibitive. Ammonia, and mixtures of ammonia with water, have been used in several installations (some of which will be described below); this fluid has good latent heats and heat transfer properties but its high vapour pressure, toxicity, flammability and corrosivity make it a non-starter for use outside industry. Mixtures of R22 with a double ether, diethylene glycol dimethyl ether (DEGDME) were studied by several workers (see *e.g.* Pourreza-Djourshari [88]) for use in both compression and absorption applications; this was perceived as potentially more attractive than the toxic, corrosive electrolyte solutions commonly used in absorption technology. This binary system uses relatively benign fluids yet exhibits a heat of mixing of about 5000 kJ/kmol, substantially more than the heats of mixing of most CFC binaries.

Ethyl chloride ($CHClCH_3$) has recently been proposed as a working fluid for compression heat pumps by Austrian and Swedish heat pump research teams [77, 76, 121]. It has several attractive features: it is essentially non-toxic; it is compatible with refrigeration oils and common metals used in refrigeration or heat pump plant, and its thermodynamic properties give superior results when compared against those of R114 (1,2 dichloro- 1,1,2,2 tetrafluoroethane), the CFC whose volatility it most closely matches. It is however flammable. Narodoslawsky found that use of ethyl chloride in a heat pump pilot plant consistently gave superior coefficients of performance and

specific heating capacites compared to R114 under the same conditions. Vamling performed a computer-based analysis of several HCFC, HFC and other fluids, including ethyl chloride. He concluded that ethyl chloride would give better COPs than any of the other fluids he tested, and suggested that a mixture of R123 with ethyl chloride might give a good working fluid with low or zero flammability. He was unable however to estimate the flammability limits of this mixture.

There are two disadvantages associated with ethyl chloride: its flammability and its chlorine content (low though it is). These are in fact greater blocks to its adoption than might be expected: there is a tremendous emotional barrier against the adoption of flammable working fluids in refrigeration equipment entrusted to the public, the ready availability and vending of petroleum spirit notwithstanding. Recent measurements of atmospheric ozone depletion over the North Pole, which indicate a greater depletion of ozone than expected, suggest to the intuitive observer that ultimately no chlorine-containing compound will be acceptable as a bulk refrigerant.

2.2.3 Discussion and Simulation of Mixed-Fluid Cycles

2.2.3.1 Cycle Efficiency: The Lorenz Process

The performance of any heat engine or heat pump is constrained to a maximum by the laws of thermodynamics: the ultimate attainable performance is fixed by the temperature limits between which the cycle must operate. The performance of VC heat pump cycles is conventionally gauged by the *Coefficient of Performance, COP*, defined as the ratio of heat output to work input. (Refrigeration cycle COP is ratio of refrigeration duty to work input.) The ultimate COP for a heat pump using a constant-boiling refrigerant is defined by a Carnot cycle, as shown in Figure 2.3. The Carnot COP, COP_c is given by:

$$\mathrm{COP}_c = \frac{T_{co}}{T_c - T_{ev}} \tag{2.1}$$

where T_{co} is the condensing (absolute) temperature and T_{ev} is the evaporation temperature.

The effectiveness of a real heat pump is often gauged by the ratio of attained COP

(COP_a) to the Carnot COP: this quantity is denoted the Carnot efficiency or *heat pump effectiveness factor.* It is conventionally denoted by ε:

$$\varepsilon = \frac{COP_a}{COP_c} \tag{2.2}$$

The reasons for deviation from the Carnot COP are manifold yet strangely inevitable: frictional losses in equipment; the need for finite temperature and pressure differences to drive heat transfer and fluid flow; compression of a gas in an irreversible manner, and the thermodynamic properties of the working fluid itself. Typical Carnot efficiencies for installed heat pumps using pure CFC refrigerant are on the range 55–65%. Higher efficiencies may of course be attained but there is an ugly tradeoff between efficiency and economic return. A high cycle efficiency saves on running cost but is usually obtained at an additional installation cost: for example, lowering the minimum acceptable temperature difference for heat transfer will boost the efficiency but requires more heat-transfer area. A more complex cycle topology may also increase steady-state efficiency without an additional plant item penalty; this path however usually involves internal heat integration within the cycle. The implication of this is that startup of the cycle may take longer than a simple cycle; so the "on-off" control methods in conventional use as capacity trimmers may cause operation in a near-permanent transient state, leading to a *lower* efficiency than would be obtained by a simple cycle under the same conditions.

If a vapour-compression cycle is operated using a working fluid which exhibits a distinct boiling range, for example a nonazeotropic binary mixture, then the Carnot cycle no longer is the appropriate measure of efficiency of that cycle. The ideal cycle which should instead by used as a reference is the *Lorenz Cycle*, proposed in 1894 by the German thermodynamicist Hans Lorenz. This is discussed by Altenkirch [3] in some detail; he includes a bibliography of Lorenz' publications on this cycle. The Lorenz cycle is shown schematically in Figure 2.4: in temperature-entropy co-ordinates it is a parallelogram. The assumption made by Lorenz was that the heat transfer processes in his cycle were characterised by a quantity analagous to the specific heat capacity; in other words, the change in specific enthalpy of the fluid per unit change in temperature was constant. Under this assumption it is straightforward to show that the COP of a Lorenz cycle (using the same definition as above) is given by:

$$COP_l = \frac{\overline{T}_{co}}{\overline{T}_{ev}} \tag{2.3}$$

in which the quantities $\overline{T}_{co}$ and $\overline{T}_{ev}$ are the *thermodynamic mean temperatures* in the condenser and evaporator (heat output and heat input units). These mean temperatures are defined as the logarithmic means of the temperatures at the start and finish

of the heat transfer process. The form of the Lorenz COP is thus externally similar to the Carnot COP; the temperature variation is described by a mean temperature which represents the equivalent state change by an isothermal path.

The advantage of using the Lorenz cycle lies in the study of cycles which transfer heat to and from non-isothermal sources. In this case the nature of the external process streams may influence adversely the performance of a heat pump running with pure fluid. Such conditions are not typical of domestic heat pumps or refrigerators, which often transfer heat from air source to air sink; in this case both sink and source are well-mixed and essentially isothermal. An external evaporative or condensative duty will also occur isothermally, if the external stream is constant-boiling. Transfer of heat to and from liquid streams will normally take place with sensible change of temperature; such duties are also common in industrial (process) applications. The loss of exergy incurred in the heat transfer between the working fluid and external streams is a function of the mean temperature difference between the streams; this is a consequence of the Second Law of thermodynamics. If the working fluid gives up heat in the condenser in a near-isothermal manner, and the heat sink stream undergoes a large temperature change in accepting this heat, then the loss of exergy will be quite large, even though a small temperature driving force may prevail at one end of the exchanger. A parallel situation exists in the evaporator. If on the other hand the working fluid gives up its heat in such a manner that it changes in temperature, and the rate of temperature change matches that of the sink stream, then the temperature profiles will run parallel and the rate of loss of exergy will be minimised. Such temperature profiles are commonly described as "gliding" temperature profiles. This is shown pictorially in Figure 2.5, which is a plot of temperature against heat transferred in a notional heat exchanger. The loss of exergy is related to the area enclosed between the temperature profile of the hot and cold streams; it is apparent that this area is reduced by use of a non-isothermal hot stream for the same end temperature difference. This topic is covered in detail by Vakil [117].

The Lorenz cycle should therefore exhibit a greater efficiency than the Carnot cycle between the same limits of temperature: if a Carnot cycle to perform a required duty may be visualised as a rectangle in temperature-entropy co-ordinates, the equivalent Lorenz cycle will be a parallelogram fitting snugly inside the rectangle. The enclosed area of the Lorenz cycle will therefore be less than that of the Carnot cycle; this implies a higher COP. (The visualisation of such cycles in these co-ordinates means the enclosed area represents an exergy difference.) The greater the temperature change in each transfer of heat, the larger the difference between Carnot and Lorenz COP.

The reason for use of the Lorenz cycle as a measure of the performance of a heat pump charged with a nonazeotropic mixture should now be apparent. Such a fluid may not exhibit a linear variation of enthalpy with temperature as it undergoes phase change; in practice it has been found that (for conventional refrigerants) the use of log-mean temperatures, using the dew and bubble points as the start and end-points of heat transfer, gives satisfactory results. (A rigorous approach to evaluation of COP would derive an expression for the true thermodynamic mean temperature by numerical integration of the temperature-enthalpy curve associated with the phase-change.) In fact, for reasonable differences in start and end temperature the simple arithmetic mean temperature may be used without significant error. An analagous efficiency factor to the Carnot efficiency may be defined for such heat pumps as the ratio of the achieved COP to the Lorenz COP; most researchers have found that the Lorenz efficiency of real plant is of the same order as the Carnot efficiency would be for an equivalent pure fluid system. This reflects the similarities in equipment used for both cycles: the major sources of irreversibility are unchanged.

To summarise: the use of a nonazeotropic working fluid in a VC cycle offers the potential for improvement of COP by approximation to a Lorenz cycle rather than a Carnot cycle. The magnitude of such improvement will depend on the degree of temperature matching between the internal and external streams in the heat exchangers. It is also possible to conceive of an improvement in COP brought about through the physical properties of a nonazeotropic mixture: the size of any such improvement can only be quantified by experiment or simulation using accurate physical property correlation functions. The cycle configuration itself will play a part in determining the scope for gain in COP.

2.2.3.2 Performance Enhancement: Cycle Analysis

Lorenz [56] analysed the potential for application of a binary refrigerant mixture in a refrigeration plant. He covered the use of both azeotropic and zeotropic mixtures, identifying potential applications of mixture of both classes where performance would be enhanced over that obtainable by a pure fluid. He also identified some of the problems assicated with use of mixtures, in particular heat transfer; oil solubility and miscibility, and differential leakage.

Kruse has published several papers dealing mostly with experimental work; these are covered later. He has also published discoursive articles on the application of zeotropic

refrigerant mixtures [50, 48]. In these he demonstrated the potential for improvement in heat pump performance, and backed up his assertions by calculation of cycle performance, including the effects of heat transfer resistances in the analysis. A maximum in COP for mixtures of R22 and R114 was predicted for a typical cycle; this was later verified by experiment.

Hansen [31] studied the performance of the R22/R114 mixture by a detailed cycle simulation, using the RKS equation of state to predict all thermodynamic properties of the mixture. He included heat transfer and pressure drop effects in his simulation. He observed quite complex variation of COP with composition, according to the external fluid conditions; in most cases studied the COP exhibited at least one maximum and minimum between that of pure R114 and that of pure R22. Gains of 5–7% in COP at the maximum were typical. The addition of a *recuperator*, exchanging heat between the hot condensate and vapour leaving the evaporator, was shown to yield significant gains in thermodynamic efficiency: the improvement in COP was more than doubled on average, and the COP was greater than that of pure R22 over nearly all of the composition range.

In 1979 Vakil [118] was granted a United States patent for a proposed heat pump cycle using a nonazeotropic mixture as working fluid. The patent gives an analysis of the benefits to be gained by capacity modulation of refrigeration, air conditioning and heat pumping equipment. His proposal used two liquid accumulators, one connected to the condenser and one to the evaporator, to effect a partial separation of refrigerant. The proposal is ingenious, relying on the components to distribute themselves between the accumulators, with the more volatile accumulating at the high-pressure side of the system. The principle of operation is that changing evaporator temperature causes a change in the pressure difference between the high and low pressure sides of the circuit (the discharge temperature is assumed to be controlled to a constant value). This change in pressure changes the liquid flow returning to the evaporator and thus changes the capacity of the cycle by changing the proportion of more volatile in active circulation. The system also has the advantage that it may be run in reverse, a common configuration in the USA, where summer cooling and winter heating are often performed by single units.

Cooper [16] proposed a similar concept of capacity levelling in an application for a European patent. The specific claim of his patent was the working fluid—a 60% (w/w) mixture of R13B1 in R152a—but he gives details of a simple method of capacity control using a low-pressure accumulator. In his scheme the low-pressure accumulator is attached to the evaporator exit; this provides one equilibrium stage of separation and

enables a progressive shift in composition as the evaporator temperature changes.

Stoecker and co-workers [52, 110, 109] developed a simulation program for the analysis of performance of heat pumps charged with refrigerant mixtures. They too discovered the characteristic maxima in COP and strong dependence of capacity on composition, although they identified many parts of their model which required further refinement, notably the description of the heat transfer and pressure drop losses. Domanski [21] developed a model of a heat pump system which was considerably more sophisticated in its treatment of the losses in a real plant: it used the CSD equation of state to generate all thermodynamic properties of the refrigerant mixtures used, permitted analysis of differing cycle geometries and topologies, and incorporated sophisticated correlations of heat transfer coefficients and friction factors in each unit of the plant. The computing overhead was reduced by pre-generating all thermodynamic data, then fitting them to simple correlation polynomials or splined functions. His final report contains extensive details of the moethods used and the complete FORTRAN source for the program. It was found that the predictions of the program regarding heat fluxes and COP matched actual pilot plant data to within 5%, which was within the accuracy of the experimental measurements. The broad conclusions drawn by Domanski were that in most cases studied the COP of the heat pump would exhibit a maximum, but that the size of this maximum would generally be less than 12%, although simpler calculations might indicate a greater benefit. The potential for capacity control was recognised and demonstrated to be viable.

Schnitzer and Moser of the Technical University of Graz in Austria have published several analyses of the effects of using nonazeotropic mixtures in heat pump cycles [8, 103, 73, 102]. They have shown that there should exist maxima in COP arising from the use of a mixed working fluid for a wide range of cycle conditions and mixtures. The variation of COP with composition was again found to be a complex function of composition: twin peaks in COP were observed under certain cases. This behaviour calls into some question the wisdom of choosing a mixture as working fluid in the hope of attainging higher COP alone: variation in active working fluid composition could force the operating point into a trough rather than up a peak.

2.2.3.3 Control *versus* Performance: the Solution Circuit

It has already been shown that the capacity of a VC cycle may be altered by progressive alteration of the refrigerant density; this may simply be done using a nonazeotropic

mixture of variable composition. The wider the boiling range of the mixture, the greater will be the potential for capacity regulation by composition shift. It has also been shown that the use of nonazeotropic mixtures as working fluids offers potential for enhancement of performance by approximation to a Lorenz rather than a Carnot cycle. The intuitive reader will already have spotted a potential clash between these two desirable concepts: if the application requires only modest changes in temperature yet large changes in capacity, then there will be an imbalance between the optimum mixture for capacity control and the optimum mixture for gliding temperature matching. It was shown by Ofner [78] that most industrial applications require temperature changes of 10–20° at most. If one examines common CFC fluid mixtures, a rule of thumb is that the maximum difference between dew and bubble points falls between 50 and 60 mol% more volatile: by taking this as 20° and examining different fluid mixtures for an application, one normally finds this to imply a potential capacity shift of not more than 300% between less volatile and more volatile. In other words, the turndown attainable will be 3:1 (roughly), if complete evaporation of the working fluid is assumed.

The requirement of complete evaporation of working fluid is removed by the shift to the compression-absorption (CA) cycle, or compression cycle with solution circuit, mentioned briefly above. This was observed by Altenkirch [3, 4], who first pointed out that a very wide-boiling mixture as working fluid would bring the technologies of compression and absorption together. He presented an analysis of the Lorenz cycle and an economic model of its potential benefits in the example case of brine chilling. He proposed the use of a solution circuit as a means of improving the performance above that of a VC cycle.

In the simple CA cycle of Figure 2.2 the refrigerant is actually only that fraction of the working fluid which is vapourised and passes through the compressor. The remainder of the working fluid acts only as an absorbent, whose function is twofold: to transport the volatile refrigerant from heat sink to heat source, and to reduce the pressure ratio over the compressor by introduction of less volatile component to the condenser. This enables the generation of higher temperatures in the condenser than would be attainable by a simple VC cycle operating with the same fluid and compressor, at the cost of additional capital cost and a slight incremental work cost (the cost of operating the solution pump).

This circuit may be modifed to incorporate capacity control by addition of intermediate storage of working fluid at some point in the cycle. The partial evaporation effects a separation; so this could be coupled with suitable storage to add or remove more volatile from the active circuit as required.

Professor Georg Alefeld of Munich Technical University has published numerous articles dealing with all aspects of absorption heat pumping. In 1982 he published an exhaustive analysis [2] of the different potential combinations of units to form compression heat pumps with solution circuits in many topologies. He showed that for a system operating with t levels of temperature and p levels of pressure, the number of possible heat pump or heat engine cycles N_{cyc} is given by:

$$N_{cyc} = 2^{(t-1)(p-1)} \tag{2.4}$$

of which of course many will be redundant or senseless. His paper presents analysis of all possible cycles for units of two, three and four temperature levels. In the analysis the effect of differing proportions of refrigerant being sent round the internal loops of the cycles is discussed; the consequent COP and heat fluxes are represented in graphical form. The paper is instructive because of its detailed consideration of the underlying mathematics and physics of the combinatorial and engineering problems in the same breath.

Another interesting publication by Alefeld's team is the work by Ziegler [126], which is an experimental study of a two-stage solution-circuit heat pump. The unit studied is a so-called *double-lift* cycle: it is essentially a CA plant with internal cascading of heat fluxes to boost the temperature lift over that achievable using a single-stage CA cycle. Ziegler's plant permitted simultaneous refrigeration effect at -20 °C and heat supply at over 100 °C, with a COP of about one for each case, using a standard single-stage compressor. This could not be achieved using a straightforward VC cycle with pure refrigerant. The working fluid used was ammonia in water: Ziegler concluded that a redesign of the plant using his acquired knowledge would lead to improved COPs for both heating and cooling. The paper includes an analysis of this cycle, including an economic comparison with conventional technologies which could meet the same simultaneous demands. He showed that, even assuming performance no better than his prototype plant, the double-lift CA cycle would consume 20% less primary energy than the best solution which used separate refrigeration and heating technology.

The double-lift cycle has also been studied by Pourreza-Djourshari [88], Radermacher [94] and Åhlby [1]. Porreza-Djourshari studied both a single-stage and a double-lift cycle using R22/DEGDME as the working fluid mixture, by means of a simulation program written specifically for this task by him. He used two evaporator temperatures: -5 °C and -25 °C, with a gliding temperature interval of 50 °C–60 °C for each case. The cycles he used both incorporated internal heat exchange between the liquid stream fed to the condenser and that being returned to the evaporator: this would give a better efficiency than the simple cycle with no internal heat exchange. He found that in both

cases both CA cycles gave higher COPs than the equivalent pure-fluid cycle using R22. The improvement was 12–20% for the higher evaporator temperature and 27% at the lower temperature, and the single-stage cycle gave higher COP than the double-stage cycle. The best composition of working fluid (the one giving the largest COP) was found to be the highest possible mol fraction of R22 which permitted matching of the gliding temperature intervals of internal and external streams. In the cases studied the amount of less volatile (DEGDME) used at optimum concentration was very low: the liquid entering the evaporator was 98 mol% R22 but this still gave the required temperature glide of 10°. He also found the thermal capacity of both cycles to be strong functions of mixture composition: the capacity could be increased for the single-stage cycle by a factor of 8, for the double-stage cycle by a factor of 6, simply by adjustment of the composition. The adjustment of composition could be accomplished by control of the solution circuit flowrate (recirculation rate).

Radermacher studied both a single-stage and double-stage CA cycle, using R22/R114 as the working fluid pair. The thermodynamic properties of the system were calculated using the CSD equation of state, of which more later. The justification given by the author for use of this mixture was that sufficient experimental data existed to enable fitting of interaction constants for the equation of state: this implies that the work was carried out more as a test of the equation of state software than of the fluid mixture's potential. The results are nonethelss similar to those found by Pourreza-Djourshari. He studied three cases: use of a zeotropic mixture in a simple VC cycle; use of a single-stage CA cycle, and use of a double-lift CA cycle. It was found that the COPs for the cycles with solution circuits were in all cases greater than those of the straightforward VC cycle; further, the COPs of the solution circuit cycles were only weakly dependent on composition, whereas those of the VC cycle exhinited strong dependence on composition. The potential for capacity control was again identified, although the mixture used in this study would not permit change over the same turndown as R22/DEGDME.

Åhlby carried out extensive simulation of both pure absorption and compression-absorption cycles. She identified the same benefits of use of solution circuit technology as other workers, mamely: capacity variation, improved COP and reduction in pressure ratio for a given temperature lift. She also pointed out the likely extra capital cost of CA technology: additional heat-transfer surface and a solution pump. She found that the efficiency of all CA cycles was quite strongly dependent on the amount of internal heat exchange between the liquid streams flowing between condenser and evaporator. The effect of the recirculation rate on gliding temperature difference was also noted.

2.2.4 Experimental Work on Mixed-Fluid Cycles

McHarness and Chapman [63] produced in 1961 some of the first measurements of performance of mixed refrigerants in real refrigeration plant. They undertook a comprehensive test of CFC fluids and their mixtures, using a standard R22 refrigeration set with modified heat transfer units to permit accurate calorimetry. Both azeotropic and nonazeotropic mixtures were studied; it was conclusively demonstrated that the use of nonazeotropic mixtures of varying composition afforded the refrigeration engineer considerable scope in tuning the properties of a working fluid to suit restrictions imposed by limitations of hardware or temperature levels. For example, they showed that the degree of suction superheat in a refrigeration cycle could be altered by alteration of the composition. They also measured the relative cycle inefficiencies as functions of composition and found that, under some circumstances, the use of a nonazeotropic mixture would result in a more efficient cycle than any obtained using a constant-boiling mixture. At this time the prediction of thermodynamic properties of mixtures was not an advanced art; the authors foresaw that this would change and were optimistic in their conclusion about the future use of mixtures, while highlighting potential problems such as differential leakage of the components.

Lorenz [57] investigated the use of the mixture R12/R11 as the working fluid in a conventional refrigeration application, for which the condenser (heat sink) temperature was 35 °C and the evaporation temperatures varied from -25 °C to 0 °C. He found a steady variation in refrigerating capacity with capacity between the capacities of the pure components; unsurprisingly the best results were those for which the temperature lift of the cycle was smallest. A flat maximum in COP was observed, at about 80% (w/w) R12; the maximum was most pronounced for the highest evaporation temperature.

Work was carried out over a period of several years by workers at the University of Hannover in Germany; Jakobs [41] described results from operation of a straightforward heat pump cycle, discharge temperature 55 °C, source temperature varying from -10 °C to 5 °C, using R22/R114 as the working fluid. He found pronounced maxima in all his plots of COP, over the composition range 50–55% (molar) R22. The exact location of the point of maximum COP varied with evaporation temperature; the proportion of R22 in the mixture at the maximum increased as the source temperature decreased. Jakobs also observed maxima in the family of heating capacity curves and minima in the work requirement and compressor discharge superheat temperature. It is interesting to note that these extrema did *not* coincide with those in the COP plots: the composition giving maximum heat capacity was in the region of 75% R22, while the minimum

superheat was observed at about 20% R22.

Kruse [47, 49] has published details of work carried out under his direction at Hannover; he emphasises the importance of the nature of the temperature profiles in condenser and evaporator to the efficiency of a mixed-refrigerant heat pump cycle. The properties of nonazeotropic mixtures may generally of themselves offer a slight improvement in COP over those of the pure components but the best way to gain a large increase in COP when using a mixture is to ensure that the temperature profiles of the working fluid in the heat exchangers run parallel to those of the external (source and sink) fluids. This latter point was also demonstrated by Vakil [117] in an analysis of the thermodynamics of heat exchange in mixed-refrigerant heat pump cycles. The reason for this is simple; the loss of exergy is reduced by bringing the temperature profiles of hot and cold fluids closer together in the heat exchangers. The extent of the improvement and the sensitivity to change in composition will of course depend not only on the mixture but on the exact nature of the compression cycle hardware and the process temperature levels. Kruse backed up his analysis with determination of the phase envelopes of the R12/R114 and R22/R114 mixtures; he found the R12/R114 system to be nearly ideal, whereas the R22/R114 system in his view was non-ideal. (See Chapter 6 for comparison with other workers' data.)

Kruse's experimentation with the R12/R114 system revealed that this too exhibited maxima in the variation of heat pump COP with performance: the maxima were both flatter than those displayed by R22/R114 and less significant in terms of improvement over the COP of the pure more volatile. The R22/R114 system gave an increase of 25% in maximum COP, while the R12/R114 system gave an increase of only 15%. This may have been a result of the closer volatilities of R12 and R114 as against R22 and R114: the reduction in pressure ratio obtained by adding R114 to R12 would be less pronounced than that obtained by addition of R114 to R22. The corresponding reduction in compressor work would have been less profound for the R12/R114 system.

The potential for capacity regulation by composition control was explored as a thought experiment by Schwind [104], who suggested use of an inline rectifier. He quantified his proposal by calculating the properties of a mixture of R12 and R13, assuming ideal-mixture behaviour. (His paper is one of the first serious attempts at derivation of enthalpy-pressure charts and other useful thermodynamic datasets for a mixed working fluid.) . His analysis was amplified by Kruse: the favoured approach involved the control of the rectification column, to add or remove differing proportions of the mixture components according to the external conditions so as to yield the desired heat output rate. This idea would probably not stand stringent economic analysis if implemented

in a pilot plant; the cost of the column plus control hardware would be too great. Nonetheless it is important to recognise that the problem here lies, not in the principle of capacity regulation by composition shift, but rather in the method chosen to achieve the desired shift in composition. A better scheme would use less hardware and be intrinsically self-controlling, removing the cost and difficulty associated with distillation column operation.

Rojey and co-workers [97, 98, 95] have published several articles and reports on work performed by *l'Institut Français du Pétrole* in the field of nonazeotropic working fluids for heat pumps. They performed both a simulation exercise (using the RKS equation of state to predict properties of refrigerant mixtures) and an experimental programme. Their experimental programme was split into two parts: an investigation of the performance of a single-condenser VC cycle using R22/R11 as the working fluid, and a study of the variation of evaporative and condensing heat transfer coefficients with composition for a binary mixture undergoing phase change. The chosen experimental work indicated an increase in COP of up to 50% could be attained: this was caused by the nature of the source and sink flow-temperature characteristics. The heat source and heat sink streams were both characterised by a large change in temperature through the exchangers of the heat pump; this meant that approximation to a Lorenz cycle by use of a nonazeotropic mixture was almost guaranteed to give better results than those from a pure-fluid heat pump plant. Typical process conditions quoted by Rojey were: source stream cooling from 44 °C to 15 °C; sink heating from 25 °C to 55 °C. The COP obtained for these conditions with pure R22 was 6.84; a 70% mixture of R22 in R11 under the same conditions gave a COP of 13.5, indicating a doubling of efficiency in this case. The temperatures quoted were the external levels; thus the actual lift of this pump is only 11 °, (55 °–44 °). Under these conditions the Carnot and Lorenz COPs (based on external temperature) are both 29.8; therefore the mixture gives a much better thermodynamic efficiency than the pure fluid: 45% as opposed to 23%. These efficiencies however indicate the unusual nature of the application; typical Carnot efficiencies for well-designed, single-fluid heat pumps are in the range 55–65%. This must be borne in mind when considering Rojey's results.

In the second part of Rojey's study, alkanes rather than CFCs were used to make up the mixtures under investigation. The results are therefore of only academic interest for this thesis: they bear out the common observation of a reduction in heat transfer coefficient as the composition shifts from either pure component towards a 50% mixture. The reasons for this effect have been broadly discussed in the literature; the chief of these is thought to be the diffusion resistance put up by the less volatile near the heat transfer surface. Existence of such effects implies a possible need for non-equilibrium

heat and mass transfer models as part of a rigorous phase change model in heat pump simulation; such material is outside the scope of this thesis.

Mučić and Scheuermann [74, 75] studied the compression-absorption cycle (compression cycle with solution circuit). Their final report contains detailed thermodynamic analysis of the units of their plant design, which demonstrates the advantages and disadvantages of each of their chosen units. For example, the thermodynamic efficiency of the main heat exchangers is derived and presented. The technical and economic justification of their chosen plant design is also informative as a source of information on the design choices which the engineer keen to build a compression-absorption plant must resolve.

Their chosen system used ammonia/water as the working fluid; the plant consisted of an evaporator, solution pump, desuperheater, compressor, condenser and throttle valve, configured in the most common single-stage arrangement discussed earlier. A refinement was the preheat of the heavy solution in the condenser before its entry to the gas desuperheater. This was a flowsheet modification intended to improve the internal efficiency of the cycle and help match the temperature profiles of internal and external fluid in the condenser/absorber. They demonstrated conclusively that in certain circumstances the addition of water and a solution circuit could yield large improvements in COP over that obtained using a pure working fluid with no solution circuit. Typical quoted operating conditions were: heat source cooling from 60 °C to 45 °C; heat sink heating from 25 °C to 78 °C. For these cases, experimental COP values were 11.3 for the mixed fluid, 5.8 for a pure ammonia circuit with condensate subcooling as a refinement. The use of a nonazeotropic mixture in this case therefore effectively doubled the attainable COP of the heat pump. It is of course questionable whether the conditions quoted were really suitable for installation of pure ammonia as working fluid; this may present the mixture in a rather rosy light. Their work is nonetheless useful; it is certainly possible to envisage combinations of source and sink temperatures corresponding to those used. The capacity of their plant, at 380kW (th), was large enough to be of use in assessing placement of such systems in commercial usage with a high degree of confidence in performance prediction.

The conclusions drawn by Mučić and Scheuermann were in agreement with those found by previous workers: the main benefits in their view to use of a compression/absorption configuration were the reduction in pressure levels, boost in COP and improvement in capacity control. They made the valid point that in this case, the large increase in COP was probably caused—in part at least—by careful matching of the internal and external temperature profiles in the main heat exchangers.

Stokar and Trepp [111, 112] worked on the compression-absorption cycle, using ammonia/water as the working fluid. Their plant extracted heat from a water source, cooling it from 4- °C to 15 °C, discharging the heat into a water sink, thereby raising the water temperature from 40 °C to 70 °C. Their papers present a thorough, meticulous discussion of the design methodology of their plant, including complete sensitivity analysis and description of practical problems encountered in construction and operation. Thier test plant could operate with heating capacities of 5–15 kW; the capacity was easily varied by adjustment of the solution composition, and this was performed as part of the experimental programme. One facet of their work which is of particular interest is their theoretical and practical study of the influence of the relative rates of liquid and vapour feed to the condenser (absorber) on the cycle efficiency. It is demonstrated in their articles that the temperature profiles in the absorber and generator are sensitive to the fraction of total circulating refrigerant which is transferred by the solution pump. This was verified by experiment, and a good scheme for control of the temperature intervals by variation of the pump rate was developed. The extent to which the internal and external temperature profiles in evaporator and condenser ran parallel was quantified by Stokar as a dimensionless parameter ϕ, the ratio of the temperature change of the internal fluid to that of the external fluid. It was found, both analytically and by experiment, that the optimum operating conditions would occur when ϕ was near (but not exactly equal to) unity; the eact location of the optimum would depend on the cycle operating conditions and fluid properties. The improvement over a single-fluid was demonstrated by comparison of the measured average COP (4.3) against the best attainable COP from a single-fluid cycle having the same heat-exchange areas; the single-fluid COP was 3.3, indicating an energy saving of 23% by use of the mixture.

2.3 Equations of State

A thermodynamic equation of state is a mathematical relation which purports to describe the interdependence of the pressure, density, temperature and composition of a fluid. Such equations can only ever approximate to the behaviour of a real fluid but are nonetheless commonplace aids to engineers requiring thermodynamic data on either pure fluids or mixtures. In this section is presented a review of the application of equations of state to the correlation and prediction of the properties of pure fluids and mixtures. Special emphasis is laid on the suitability of these equations to correlation of properties of mixtures of CFC and HCFC fluids. The material contained in this chapter is intended to be complimentary to that in Chapter 6; in an ideal world

the reader would assimilate these chapters in parallel. This is of course prevented by basic anatomical shortcomings, but it should be remembered that any apparent gaps in the text of one chapter will probably be covered in the other. Most of the basic thermodynamic relations and manipulations required to apply equations of state to practical problems are covered in the introductory sections of Chapter 6, where they are of immediate relevance.

2.3.1 Common Equations of State

2.3.1.1 Perfect and Imperfect Gases: the Virial Equation

The simplest of all equations of state is that which describes the perfect gas:

$$Z = Pv/RT = PV/n_T RT = P/RT\rho = 1 \tag{2.5}$$

in which Z represents the compression factor (compressibility), P the pressure, T the temperature, V the total volume, v the specific (intensive) volume, ρ the density and n_T the total number of moles of gas in the system.

The behaviour of all fluids approaches that of a perfect gas in the limit of zero pressure; this equation may be used for non-zero pressures of about 1 atmosphere without significant error for many substances. The imperfections of reality render this increasingly inaccurate at higher pressures; this is the fundamental reason for development of all other equations! The perfect gas equation is also the only equation which may easily be written in either a pressure-explicit or volume-explicit form. For most process engineering problems the known quantities are temperature and pressure, and so a volume-explicit equation would be the more useful form. Nearly all other equations of state are however explicit in pressure, requiring inversion by whatever means possible to yield volume as a function of temperature and pressure.

The next simplest equation of state is also one of the few to have any sound basis in theory. This is the virial equation, which can be shown to relate the behaviour of a real gas to the number and type of interactions between molecules. It is normally written in the form:

$$Z = 1 + \sum_{i=2}^{\infty} \frac{K_i}{v^i} \tag{2.6}$$

The equation is normally truncated after the first or second term of the polynomial expansion, yielding a simple quadratic or cubic equation. This is computationally convenient, as analytical formulae exist for the solution of such equations. The early coefficients K_i of the virial equation have been tabulated for many compounds, and good references exist in Perry [82] for sources of such data. An important publication in this area was that of Tsonopoulos (1974) [115] which presented correlations of the second virial coefficient with the basic (constant) properties of a molecule: critical temperature; critical pressure; acentric factor, and reduced dipole moment for polar molecules.

2.3.1.2 Common Cubic Equations of State

The virial equation can only describe the properties of a gas; the only significant volume roots of the equation are all of vapour phase magnitude. In order to describe the liquid phase behaviour of a fluid as well as the vapour phase, it is necessary to develop an equation with at least three real roots; one representing the liquid phase, one the vapour phase, and a third, meaningless root at some intermediate position. The reason for this is shown in Figure 2.6, which depicts the path of an isotherm in pressure-volume coordinates for a pure fluid. The behaviour of a real fluid is truly depicted by the solid line; there is a discontinuity in the path of the isotherm at the vapour-liquid equilibrium point. In order for a smooth analytic function to approximate this behaviour, it must take the notional path represented by the dashed line. In this path, real roots exist at either phase volume but in order to portray the correct isotherm behaviour on either side of the phase equilibrium point, the function must go through both a minimum and maximum between the two phase volumes. The first derivative of the function must therefore be at least quadratic in form, indicating that a cubic equation is the simplest analytic function capable of predicting liquid and vapour phase behaviour.

Van der Waals The first worker to recognise the potential application of cubic equations was van der Waals, who in 1873, as part of his doctoral dissertation, produced his eponymous equation of state, Equation 2.7, which has featured in nearly all subsequent texts on thermodynamics ever written. Alas, such lasting fame does not come readily to latter-day postgraduates!

$$P = \frac{RT}{v-b} - \frac{a}{v^2} \tag{2.7}$$

In the van der Waals equation, the variables P, v, T take their usual meaning; the constants a and b are dependent on the fluid to which the equation refers but are

invariant for a pure fluid. They may be evaluated by application of the *van der Waals Relations*, which are given in full in Chapter 6, Equation 6.41–Equation 6.43. These equations express the known behaviour of a real fluid in terms of the gradient of the critical isotherm curve, which passes through a horizontal point of inflection in the pressure-volume plane at the critical point.

The great significance of the van der Waals equation is twofold: it gives a qualitatively correct prediction of the shape of the phase envelope for vapour-liquid equilibrium in pressure-volume coordinates, and the pressure is described by two separate terms (commonly described as *pressure contributions*) approximating the repulsive and attractive forces exerted by the molecules of a fluid on one another. As implied in the preceding paragraph, it also predicts the existence of a critical point for a fluid, although the point predicted by this equation is not very realistic for most fluids.

A major improvement to the van der Waals equation was made by Redlich and Kwong in 1949 [96]. They published their equation, subsequently used as a predictive tool for many years, in the following form:

$$P = \frac{RT}{v-b} - \frac{a/T^{0.5}}{v(v+b)} \tag{2.8}$$

The Redlich-Kwong (RK) equation is clearly sired by van der Waals; the important developments are the introduction of a temperature-dependent parameter $a/T^{0.5}$ in the attractive force term, and the slight alteration of the volume dependency of this latter term. These apparently minor changes yielded a great improvement in the quantitative accuracy of the equation's volumetric predictions for the vapour phase. Description of the liquid phase behaviour by this equation is still poor.

The improvement in volumetric predictions of the RK equation was not matched by an improvement in the prediction of the VLE of mixtures, and in 1972 Soave [107] published a modification to the RK equation (by then 23 years young!) which aimed to ameliorate this inaccuracy. The subsequent equation is still one of the most widely used of all equations of state, especially in flowsheeting packages used for "what-if" exploratory calculations. It is referred to as either the Redlich-Kwong-Soave or Soave-Redlich-Kwong equation: in this thesis it will be described in brief as the RKS equation. Its form is given by Equation 2.9:

$$P = \frac{RT}{v-b} - \frac{a(T)}{v(v+b)} \tag{2.9}$$

$$a(T) = 0.42747\alpha(T_r)(RT_c)^2/P_c \tag{2.10}$$

$$\alpha(T_r) = (1+\kappa(1-T_r^{0.5}))^2 \tag{2.11}$$

$$\kappa = 0.48 + 1.574\omega - 0.176\omega^2 \quad (2.12)$$

$$b = 0.08664(RT_c)/P_c \quad (2.13)$$

in which ω represents the acentric factor, T_c, P_c the critical temperature and pressure, and T_r the reduced temperature.

The significance of the Soave modification is the introduction of a strong temperature dependency in the attractive-force pressure contribution; this sits well with intuitive pictures of the way in which molecules behave as their average kinetic energy (temperature) changes. The practical effect of the RKS modification was to improve the VLE predictions of the equation to the point where it could be used with reasonable success for multicomponent mixtures of industrially important fluids, such as natural gases or oils. The value of this speaks for itself.

The usage and application of both the RK and RKS equations has been so widespread that there is little point in attempting to produce here an exhaustive bibliography on these equations. New work is published in all the standard chemical engineering journals even today, almost twenty years after Soave's crucial modification to the RK equation. Instead the application of the RKS equation to refrigerant mixtures will be discussed in a later section.

One recent modification to the RKS equation worthy nonetheless of brief mention was discussed by Sandarusi and co-workers [101]. The modification itself was the idea of Soave himself, and was studied in detail by Sandarusi's team. The standard form of the RKS equation requires knowledge of three parameters: the critical temperature, critical pressure and acentric factor. The proposed modification to Equation 2.9 entailed a further change to the α function in the attractive-force pressure contribution term. The explicit dependence on acentric factor was removed, as this quantity is of dubious significance for polar molecules. It was replaced by two empirical constants, in a relation of the form:

$$\alpha(T_r) = 1 + (1 - T_r)(m + n/T_r) \quad (2.14)$$

in which m and n are the two parameters. The procedure used by the authors to determine values of these constants was a least-squares fit of the α function to vapour pressure data for the fluid in question. Their paper indicates that use of this technique substantially improves the predictions of the RKS equation for polar fluids, and values of m and n are tabulated for 286 compounds, both organic and inorganic compounds. This paper is an illustration of typical research performed on the basic equation in recent years, aimed at improving specific aspects of the equation performance without inventing a new equation of state.

The RKS family of equations still represents a major portion of usage of equations of state; there have however been developed a raft of other cubic equations of state aimed at bettering the basic RKS performance. The importance of the other cubic equations may be judged on their takeup by industry; this may not necessarily indicate the *best* equations, rather the most convenient to use! It is again stressed that the field is too large for comprehensive coverage within the scope of this thesis, and only a sampler of the subject is here presented for inspection.

The Peng-Robinson Equation One of the main rivals to the RKS in commercial software products has been the Peng-Robinson (PR) equation of state [80], whose basic form is given by Equation 2.15.

$$P = \frac{RT}{v-b} - \frac{a(T)}{v(v+b)+b(v-b)} \tag{2.15}$$

$$a(T) = 0.45724\alpha(T_r)(RT_c)^2/P_c \tag{2.16}$$

$$\alpha(T_r) = (1+\kappa(1-T_r^{0.5}))^2 \tag{2.17}$$

$$b = 0.0778RT_c/P_c \tag{2.18}$$

The similarity in functional form between the a and b parameters of the RKS and PR equations is evident. The attraction of this equation is easy to see; it has an extremely simple form, making the manipulation of the equation very straightforward in terms of computational effort. The PR equation in this form requires knowledge of the critical temperature, critical pressure and acentric factor; it is therefore termed a *three-parameter* equation. Much work has been done on improving the performance of the PR equation by tampering with the definitions of the equation's parameters a and b; a useful source of information is the paper by Xu and Sandler [125]. This details the results of the authors' fitting of both parameters to rather complex spline functions of temperature. Their modification required determination of two sets of three empirical constants for each equation parameter, making a total of twelve numbers to be determined by regression on saturation property prediction for each fluid of interest. The resulting improvement in accuracy seems impressive, especially for the prediction of liquid phase volume; the complicated nature of the resulting parameter calculations and the amount of data reduction required, however, make this technique of little use in the production of data for little-studied substances.

Martin's Equation In 1979 Martin [61] published his cubic equation of state (not to be confused with the *Martin-Hou* equation, of which more later). This equation

uses three parameters and takes the form:

$$P = \frac{RT}{v-b} - \frac{a}{(v+c)^2} \tag{2.19}$$

in which a is a function of temperature and b, c are constants for any given pure fluid.

It was argued by Martin that this equation should be the best cubic equation for prediction of mixture properties. Joffe (1987) [42] showed that the temperature dependence of the a function in the Martin equation should use the same functional form as that of the corresponding functions in the RKS and PR equations, if best results for mixture VLE prediction were desired. His paper detailed work on mixtures of polar compounds under high pressure, and demonstrated that the Martin equation could predict the liquid volume and both phase compositions of a binary, polar mixture well except in the critical region.

2.3.1.3 Cubic Chain-Of-Rotators Equation

This is dealt with in detail in Chapter 6; for completeness' sake the original source references are described here. It is a three-constant equation, requiring knowledge of the critical temperature, critical pressure and acentric factor. It differs from the wholly empirical cubic equations such as RKS or PR in that it is based on results from a theory of molecular dynamics, which uses the techniques of statistical thermodynamics to extrapolate the properties of a macrofluid from the behaviour of individual molecules. (Recall that the virial equation is the most fundamental of such equations.) The equation was described by Lin *et al* in 1983 [55], in a paper which outlines the basis for derivation of the equation as a cubic approximation to the more complex Chain-Of-Rotators equation. Significant differences from the simple cubic equations are: the use of five named equation parameters (as opposed to two for RKS and PR), two of which were made functions of temperature; and the use of two empirical interaction constants as aids to improving the fit of mixture VLE data. (Other cubic equations use only one interaction constant.) The *raison d'être* of the CCOR equation was the perceived poorness in prediction of liquid phase volumetric properties by other cubic equations; the parent Chain-Of-Rotators equation was known to be excellent in its description of high-density fluid states, and so a good cubic approximation might be expected to show the same characteristics.

In the 1983 paper was presented a comparison of the predictions of the CCOR equation with the RKS and PR equations for saturated liquid density and vapour pressure of 15

pure substances. The test fluids were mostly alkanes, with the remainder being argon, nitrogen, carbon dioxide, benzene, toluene and meta-xylene. The RKS equation and the CCOR equation were both slightly superior to the PR equation for prediction of vapour pressure; each gave relative errors in pressure of 0.7–3.5%. The CCOR equation was however clearly superior in the prediction of saturated liquid volume: the RKS equation was up to 25% in error for longer-chain alkanes' liquid volumes, compared to errors of 12% for the PR and 1.5% for the CCOR equation.

Also presented were some results found by fitting of the CCOR equation to reasonably difficult mixture data: solutions of hydrogen, nitrogen, carbon dioxide and methane in non-paraffinic solvents (tetralin, m-cresol, quinoline and n-methyl naphthalene). The CCOR equation predicted K values (equilibrium composition ratios) for the mixture which were in good agreement with the measured data: typical deviations in K value were of the order of 3–6%.

In 1985 the same team produced two papers dealing with the application of the CCOR equation to polar substances and their mixtures [29, 30]. In these papers was illustrated the authors' chosen technique of coping with polar fluids; regression to fit an additional two parameters for the scaling temperature function a, which may be thought of as the analagous function to the a function in other cubic equations. Optimised parameters were given for 45 pure fluids and 30 polar mixture properties. The performance of the CCOR equation in low-pressure VLE calculations was compared against the Wilson equation for activity coefficients, using literature data for the latter equation. The CCOR equation was consistently as good, or better than, the activity-coefficient model in the prediction both of vapour mol fraction and vapour pressure. Typical average absolute deviations on pressure were of the order of 1–2%; those on vapour mol fraction were in the range 0.003 mol fraction to 0.018 mol fraction in the worst case (ethanol/nitromethane). The mixtures tested included: ammonia/water; ethanol/water, and acetone/chloroform. At higher pressures tested systems included hydrogen sulphide/water (for which there exists no known critical point). In the high pressure systems the worst errors in pressure deviation were for the carbon dioxide/methanol system (9%) but more typical deviations were in the range 1-4%. The prediction of vapour composition was in all cases to an accuracy of better than 0.012 mol fraction.

In 1986 there appeared two further papers on the CCOR equation [45, 54], which served as summaries of the previous work. Further comparisons were given with the RKS and PR equations for heavy, non-paraffinic substances; these demonstrated the superior liquid-phase predictions of the CCOR equation over the two other equations of state.

2.3.1.4 More Complexity: Benedict-Webb-Rubin Equation

The Benedict-Webb-Rubin (BWR) equation was originally proposed in 1940 [6] for hydrocarbon fluids; it has since been extended to a wider range of substances. The equation is wholly empirical in derivation and can have up to six real roots; its common formulation is pressure-explicit in terms of density, as given in Equation 2.20.

$$\begin{aligned} P &= RT\rho + \left(B_oRT - A_o - C_o/T^2\right)\rho^2 + (bRT - a)\rho^3 + a\alpha\rho^6 \\ &+ \left(c\rho^3/T^2\right)\left(1 + \gamma\rho^2\right)\exp\left(-\gamma\rho^2\right) \end{aligned} \tag{2.20}$$

The original BWR equation has eight parameters which require to be determined for each fluid of interest; a good source of further information on tabulations of these constants is Perry Section 3 *op. cit.* It gives good results for both liquid and vapour phase properties up to a density of about 1.5 times the critical density, beyond which further correction terms are required. It is extended to mixtures in the usual way, using whatever mixing rules suit the particular task. It has been used as the basis for several other equations of state, the two most significant of which are the Lee-Kesler and Bender equations, described below.

The Lee-Kesler Equation In 1975 Lee and Kesler [53] published details of a generalised, three-parameter equation of state; this required knowledge of the critical temperature, critical pressure and acentric factor to be applicable to a fluid. The equation made use of the principle of corresponding states to derive an expression for the compressibility of a real fluid in terms of the compressibility of a "simple" fluid (a noble gas) and that of a real, "reference" fluid. (This required *a priori* knowledge of the properties of some arbitrary pair of such fluids.) The authors used argon and n-octane as the simple and reference fluids. The form of the equation is represented below by Equation 2.21, in which the superscripts denote the simple fluid (Z^o) or the real reference fluid (Z^*).

$$Z = Z^{(o)} + \frac{\omega}{\omega^{(*)}} \times \left(Z^{(*)} - Z^{(o)}\right) \tag{2.21}$$

The values of $Z^{(o)}$ and $Z^{(*)}$ are found by substitution of appropriate universal constants into the following equation:

$$Z = \left(\frac{P_rV_r}{T_r}\right) = 1 + \frac{B}{V_r} + \frac{C}{V_r^2} + \frac{D}{V_r^5} + \frac{c_4}{T_r^3V_r^2} \times \left(\beta + \frac{\gamma}{V_r^2}\right) \times \exp\left(-\frac{\gamma}{V_r^2}\right) \tag{2.22}$$

where

$$B = b_1 - b_2/T_r - b_3/T_r^2 - b_4/T_r^3 \tag{2.23}$$

$$C = c_1 - c_2/T_r + c_3/T_r^3 \quad (2.24)$$

$$D = d_1 + d_2/T_r \quad (2.25)$$

The subscript 'r' in the above equations denotes use of a reduced property; this makes the universal equation constants independent of the units system employed.

The equation of Lee and Kesler has subsequently been used in many applications, although there are drawbacks, principally associated with spurious volume roots, which make coding of routines to use this equation a non-trivial task. The equation gives good accuracy on prediction of saturation properties of both non-polar and some polar compounds.

In an attempt to improve the performance of the Lee-Kesler equation for mixture VLE prediction, Plöcker [84] proposed a set of mixing rules to be used in calculation of the equation parameters for mixtures. These rules were used specifically to calculate pseudo-critical properties of the mixture and were reckoned to be an improvement on the simple rules proposed by Lee and Kesler. The combination of the LK equation with Plöcker's rules is normally denoted (unsurprisingly) the Lee-Kesler-Plöcker (LKP) equation of state. An example of its application to refrigerant mixture VLE by Ström [113] is discussed later in the text.

Bender's Equation Bender's equation was originally developed for use in cryogenics but has been applied with success to the prediction of properties of refrigerant fluids [86]. The equation requires twenty empirical constants for each fluid of interest. It is therefore of interest as a correlator rather than a predictor. The form of the equation is similar to that of the BWR or LK equations:

$$P = T\rho\left[R + B\rho + C\rho^2 + D\rho^3 + E\rho^4 + F\rho^5 + \left[G + H\rho^2\right]\rho^2 \exp\left(-a_{20}\rho^2\right)\right] \quad (2.26)$$

in which ρ denotes the density $1/V$ and R the universal gas constant.

The main equation parameters are defined as temperature functions by the set of relations:

$$B = a_1 - a_2/T - a_3/T^2 - a_4/T^3 - a_5/T^4 \quad (2.27)$$

$$C = a_6 + a_7/T + a_8/T^2 \quad (2.28)$$

$$D = a_9 + a_{10}/T \quad (2.29)$$

$$E = a_{11} + a_{12}/T \quad (2.30)$$

$$F = a_{13}/T \quad (2.31)$$

$$G = a_{14}/T^3 + a_{15}/T^4 + a_{16}/T^5 \quad (2.32)$$

$$H = a_{17}/T^3 + a_{18}/T^4 + a_{19}/T^5 \quad (2.33)$$

Polt's paper contains a useful discussion on the application of this paper as well as a comprehensive bibiliography of other literature on the application of the Bender equation to other fluid systems.

2.3.1.5 Equations Based on Molecular Dynamics

The development of equations of state from a molecular standpoint is in total contrast to the traditional, empirical approach which gave the world the RKS, PR and BWR equations of state. The molecular dynamicist tries to generate properties *a priori*; while the empirical thermodynamicist measures properties and attempts to infer a mathematical relationship which will interlink the experimental data in a satisfactory manner. The development of molecular dynamics was hastened by the availability of powerful computing facilities to the researcher; such hardware is a key component in the testing of modern theories of molecular behaviour. It should not however be forgotten that the two simplest equations of state, the perfect gas equation and the two-term virial equation, may be derived exactly, using only pencil, paper and raw logic, from the "billiard-ball" kinetic theory of gas behaviour taught in schools to this day.

The great, overriding advantage of equations of state arising from molecular dynamic simulations is that they describe the behaviour of a known fluid in a wholly exact and rigorous manner. The fluid is not necessarily a real fluid, but its every nuance of behaviour is specified by the designer of the mathematical model of the molecular behaviour. Thus several models may be evaluated for desired approximations to the behaviour of real fluids, with the best features of each model being incorporated into later versions. By analogy with the pressure contributions of the earlier equations of state, models may be constructed which separately describe the contribution to system pressure of the effects of molecular rotation, vibration stretching, collision *etc.* The normal method of evaluation is stochastic, using for example the Monte Carlo technique to determine the probable behaviour of a miniature molecular system of 1, 10, 50...molecules. These results, simulations of a microfluid, may then be extrapolated to the macro-thermodynamic reality and tested against known data.

One of the most significant contributions in the field was made by Carnahan and Starling in 1969 [12]. They derived an expression for the compressibility of a so-called *hard-sphere* fluid, which is essentially a hypothetical fluid in which there exist no attractive forces; repulsive forces are zero beyond a critical radius from the notional centre of the molecule's mass and infinitely great at radii less than this distance. This relation, written as Equation 2.34, has been thoroughly checked and tested by molecular simulation and is now accepted as a sound approximation to at least part of the truth.

$$Z_{hs} = \frac{1 + y + y^2 - y^3}{(1-y)^3} \quad (y = K/v) \tag{2.34}$$

where the quantity y is a reduced volume, the ratio of the close-packed specific volume of the fluid to the actual specific volume v.

The hard-sphere compressibility has been used as the basis of a number of equations of state: some of the most interesting will now be described.

Carnahan-Starling-DeSantis Equation DeSantis [20] substituted the hard-sphere compressibility model into the Redlich-Kwong equation (keeping the RK attractive contribution), to yield the original version of what is now described as the Carnahan-Starling-DeSantis (CSD) equation.

$$Z_{CSD} = Z_{hs} - Z_a = \frac{1 + y + y^2 - y^3}{(1-y)^3} - \frac{a}{RT(v+b)} \tag{2.35}$$

The temperature dependency of compressiblity in this equation is implicit in the parameters a and b. These temperature functions were defined by DeSantis in such a way as to force a fit to the critical point, using van der Waals' relations to accomplish this. The equation was tested on a variety of non-polar or slightly polar hydrocarbons and was found to give an accurate description of fluid behaviour for these substances over a wide range of densities (perfect gas to saturated subcritical liquid).

In 1985-6 a series of articles were published by McLinden and Morrison of the American NBS research division, culminating in a comprehensive technical monograph [70, 71, 72]; the subject of these notes was the modification of the CSD equation of state for specific application to mixtures of refrigerant fluids. This latter topic will be covered in more detail later in Chapter 6: here it is sufficient to describe the modifications which were made to the CSD equation, as it is now almost universally used in the McLinden/Morrison format.

The requirement that the CSD equation fit the true critical point of the fluid was removed, as this affected the accuracy of volumetric property prediction at significant distances from the critical point. The loss of applicability in the near-critical region was outweighed by the gain in accuracy, especially for mixtures containing supercritical components at low pressure. The temperature dependency of the two equation parameters was also rationalised; the logarithmic functions used by DeSantis were replaced by two quadratic expressions, requiring a total of only six constants to be determined for each fluid of interest.

Perturbed Chain Equations In 1975 Beret [7] proposed an equation of state which was based on treatment of a molecule as a rigid, chain-like structure, moving in an even, *isotropic* field of force; this is the Perturbed Hard-Chain Theory (PHCT) equation. The equation is complex (see Equation 2.36) but it requires determination of only three constants per fluid; the source gives these constants for twenty-two substances.

$$Z = Z_{hs} - \frac{a}{RTv} \tag{2.36}$$

$$Z_{hs} = 1 + c\frac{4(\tau/\overline{v}) - 2(\tau/\overline{v})^2}{(1-\tau/\overline{v})^3} \tag{2.37}$$

$$a = -R\left(\frac{\varepsilon q}{k}\right)(rv^o)\sum_{n=1}^{4}\sum_{m=1}^{M}\left(\frac{mA_{nm}}{\overline{v}^{m-1}}\right)\left(\frac{1}{T^{n-1}}\right) \tag{2.38}$$

$$\overline{v} = \frac{v}{Nrv^o} \tag{2.39}$$

in which the coefficients A_{nm} are universal (listed in the source), the number of molecules in the system is denoted by N (Avogadro's number multiplied by the number of moles present), and τ denotes a numerical constant, $\pi\sqrt{2}/6 = 0.7405$. The adjustable parameters for a pure fluid are: rv^o, $(\varepsilon q/k)$ and c, where k is Boltzmann's constant. In order to use the equation for mixtures it would be necessary to split the products, then determine separately the parameters r and q. The application of the equation to mixtures was described by Donohue [23].

The utility of the PCHT theory was stated by its originators as the potential applicability to mixtures of molecules of substantially different sizes. The PHCT equation was found to perform well for the fluids tested, except in the critical region. Vapour pressure and liquid density were both very well correlated for non-polar or slightly polar fluids; the vapour pressure of water was correlated to within 5% maximum error. The poor performance in the critical region was ascribed to the then limits on computing power which restricted the initial molecular-dynamic simulation work, used to find the constants A_{nm}. Donohue's extension to mixtures of the PHCT equation also gave good results, including excellent prediction of Henry's constants for several hydrocarbon sys-

tems; it was again found that the equation performed well on asymmetric mixtures of molecules.

Equations for Associating Systems The PHCT theory was modified by Gmehling *et al.* [27] to include the effect of hydrogen bonding in the equation's description of a fluid's properties. The approach taken described a system which exhibited dimerisation in both liquid and vapour phases; the dimerisation process was described by the classical thermodynamic equilibrium conditions:

$$M + M \rightleftharpoons D \tag{2.40}$$

$$y_D = 1 - y_M \tag{2.41}$$

$$K = \frac{y_D}{y_M^2} \times \frac{\phi_D}{\phi_M^2} \times \frac{1}{P} \tag{2.42}$$

$$\log K = \frac{\Delta S^\circ}{R} - \frac{\Delta H^\circ}{RT} \tag{2.43}$$

where M represents monomer, D dimer, y mol fraction and ϕ the fugacity coefficient.

Gmehling's work included a reduction in the number of universal constants proposed by Beret for the PHCT equation; this compensated in part for the additional computational effort required to determine the energies of association ΔS° and ΔH°, and reduced the overall execution time of the equation-solving routines. It was found that this modification permitted prediction of the properties of substances such as water, acetic acid and acetone; vapour pressure was correlated to about 1% accuracy, liquid volume to better than 2% accuracy. The same principle was extended to mixtures by consideration of cross dimers, formed between unlike molecules. It was found that several difficult systems (pinched phase envelopes or azeotropy) were well described by this modified PHCT equation over a substantial temperature range. The ethanol-water phase envelope was described quantitatively in the temperature range 70–350 °C. The ethane-methanol system exhibits two liquid phases at 25 °C; this was correctly predicted by the equation, although the description of the composition boundaries was only semi-quantitative. This paper clearly showed that the treatment of associated systems in this manner was valid.

The PHCT theory assumed that all molecules in a system existed in an homogenous, isotropic force field; this assumption was removed in a development by Vimalchand [122]. He produced a new equation, the Perturbed Anisotropic Chain Theory (PACT) equation whose form resembles the PHCT, only more complex and with further parameters. This equation should have been adequate to describe mixtures of

polar and/or nonpolar molecules; it was found that its predictions were in fact superior to the PHCT equation (and many of the cubic equations) for difficult systems. It was further altered by Ikonomou [37], who combined the PACT equation with oligomerisation equilibria constants: as in Gmehling's work, a simple monomer-dimer approach was assumed, but a more complex model including higher oligomers was also used. This proved yet more successful in the quantitative prediction of the properties of all phases for systems exhibiting complex behaviour, such as liquid phase separation and heterogenous azeotropy.

Chain-Of-Rotators Equation The final equation covered here is the Chain-Of-Rotators (COR) equation, described above as the basis for the CCOR equation. This model, published by Chien *et al.* in 1983 [13], uses the Carnahan-Starling model of a hard-sphere fluid for the description of the repulsive intermolecular forces. The attractive forces are described by a reasonably complex expression incorporating rotation, translation and attraction of molecules, envisaged as chains of dumb-bell rotators. The complex expression for pressure which falls out of the mathematics is more daunting than the reality, which is that the COR equation requires fitting of only three parameters by regression on experimental data for each fluid to which iit is to be applied. The source paper gives these parameters for 23 substances, including alkanes, aromatics and inorganics polar compounds (CO_2, H_2S). The resulting fits to saturation properties of the test fluids gave average absolute deviations of better than 3% on vapour volume; better than 1.6% on vapour pressure, and better than 1.5% on liquid volume in all cases.

Data were also presented on the predictions of the COR for several binary mixtures of polar and nonpolar fluids. It was found that, using only one empirical interaction constant, the typical deviation between predicted and calculated K values for the systems was less than 4%.

2.3.2 Algorithms and Problems

In this section is given a brief description of the main literature sources used by the author as aids during the development of software for the application of the CCOR equation. The sources quoted are good starting points for an exhaustive exploration

of the vast body of literature which deals with computational aspects of equations of state.

A review of the available methods for *a priori* prediction of interaction constants to be used with equations of state was presented by Pesuit [83]. A wide variety of recipes for calculation of interaction constants from known characteristics of pure-component molecules was surveyed; the conclusion drawn was that there was no one rule which would be guaranteed to give good results for a wide range of mixtures, and that empirical determination of these constants would probably still be necessary for high-accuracy prediction of mixture VLE. This was made obvious by the application of some of the suggested recipes to systems whose interaction constants for accurate equations of state had previously been determined. There were often significant differences between the predicted and regressed constants.

The behaviour of the RKS equation of state was studied by Poling *et al.* (1981) [85]. They discovered that, for mixtures of a given pressure and total composition, there would exist a temperature range over which the RKS equation would exhibit three real compressibility (volume) roots. Inside this region there would be no difficulty in obtaining properties for either liquid or vapour phases. Outside this region however they identified a very real problem: only one real root to the equation of state would imply that the given composition were no longer stable in one of the two phases. The stable phase may be identified by comparison of the magnitude of the volume root against the pseudocritical volume $V_{pc} = R(\sum_i T_{ci}/P_{ci})/3$. A volume greater than the pseudocritical volume implies a vapour-like phase, below the pseudo-critical volume implies a liquid-like phase.

A further, more subtle problem, was also identified; it was possible to be within the temperature range which gave three volume roots and still obtain spurious roots. This situation would arise near the edges of the three-root region, where derivative properties could exhibit zeros or discontinuities. Poling proposed heuristics to identify spurious roots and flase derivatives by the examination of the isothermal compressibility function $\beta = -(\partial V/\partial P)_T/V$. The heuristics were:

- A volume root is satisfactory for liquid-phase behaviour if $\beta < 0.005$ atm^{-1}
- A vapour root is satisfactory if $0.9/P < \beta < 3/P$
- To bring a spurious point into the desired region of validity for vapour phase work, the pressure should be adjusted downwards until a vapour phase appears.

- To generate a valid liquid phase root, the composition should be adjusted by increase in the heaviest component at the expense of the lightest component.

Gundersen [28] published a paper dealing with similar subject matter; the behaviour of the RKS and PR equations at increasing (near-critical) pressures when used in flash calculations. He suggested perturbation of the system pressure and/or composition as necessary to generate valid compressibility roots.

In 1988 Topliss *et al.* [114] presented an efficient algorithm for use with non-cubic equations of state, which was intended as an aid to avoidance of infeasible regions of the state space. They observed that the algorithm could be used with equal success for cubic equations of state, if the conventional analytic solution technique were replaced by an iterative solution algorithm. The reasoning for this suggestion was based on the demonstration by Mathias [62] that the most time-consuming stages in use of an equation of state were not those involved in iterative solution but rather the evaluation of mixture parameters and their property derivatives.

McLinden and Morrison [72] give complete FORTRAN77 source code for an implementation of the CSD equation of state capable of predicting properties of binary mixtures. Their work includes derivation of the basic thermodynamic relations and a discussion of the necessary additional features which must be incorporated into any computer programs for use of equations of state. This proved especially useful in the author's work. The reader should refer to Perry or journals such as *Computers and Chemical Engineering* and *Fluid Phase Equilibria* for further information on programming techniques and tricks.

2.3.3 Application of Equations of State to Refrigerants

A brief summary of some applications of the equations decribed above to refrigerants and their mixtures is given here: more details are given later in the chapter and in Chapter 6. The purpose of these paragraphs is to tidy up a few references whose primary content was not experimental data correlation.

Kandlikar (1975) published a paper detailing the application of the Martin-Hou equation to the R22/R12 system. The form of the Martin-Hou equation which was used by this author was a truncated, four-term version of the equation, requiring 10 parameters per fluid. Special mixture mixing rules for calculation of the equation parameters for mixtures were presented: these were more complex than the simple van der Waals' rules used by many other workers. The dew and bubble curves of the R22/R12 system were fitted to equations of the same form as the familiar Antoine vapour-pressure correlation for a pure fluid; composition-dependent parameters were incorporated into the equilibrium pressure correlations to account for the shape of the phase envelope. Kandlikar also presented detailed correlations of the liquid phase behaviour, using polynomial expansions to represent the density and enthalpy of saturated liquids. He used activity coefficients calculated from literature data on the heat of mixing of the system to attempt a correction of the shapes of the enthalpy-concentration and volume-concentration curves. The work yielded good accuracy: better than 1% on liquid properties and better than 3% on all vapour properties, except in the critical region. The number of polynomial-expansion coefficients used by the equations in this work however militate against the application of this technique to less widely-tabulated mixtures.

In 1978 was published work by Asselineau and co-workers [5], which dealt with the use of the RKS equation of state for refrigerant property prediction. Their paper presented details of the errors in vapour pressure, liquid and vapour volumes, and latent heat of vapourisation when predicted using the RKS with three slightly differing α functions, obtained from regression by the authors on experimental data. The vapour pressure was correlated to better than 2%; the vapour volume and latent heat to better than 6%. The liquid volume was not however well predicted; errors of up to 25% were found. The VLE of several refrigerant systems, both azeotropic and nonazeotropic was also studied; interaction constants were regressed for each mixture at each temperature of interst, using a least-squares minimisation on the error in equilibrium pressure prediction. It was found that for most systems the RKS equation could correlate the pressure to better than 2% accuracy: the detection of azeotrope behaviour was also good, and the error in calculated vapour compositions was typically less than 3% in mol fraction of the worst cases studied.

In 1983 Brousse [10] published a useful paper showing that even the virial equation of state could be applied with success to the problem of refrigerant mixture property prediction. The application studied was heat-pump assisted distillation, in which the modest pressure levels (maximum 4 bar) rendered applicable the two-term virial equation of state. The technique used by Brouse was to subject the virial equation to the usual manipulations for gas-phase properties, then infer liquid phase properties from

the vapour-liquid equilibrium constraints on the pure fluids. Thus the method was not wholly self-contained; knowledge of the variation of vapour pressure of each component with temperature was required. Nonetheless the results predicted by the equation agreed well with the measurements made on a pilot plant by Brousse, which must be a validation of the simplifications made in this case.

Domanski and Didion [22] applied the CSD equation of state as part of a software package for the generation of thermodynamic property charts. Their paper contains details of the algorithms they employed in their work for solution of the binary VLE problem, and specimen property charts for the mixture R13B1/R152a. The bulk of their paper is however a straight reproduction of the original work by Morrison and McLinden.

2.4 Experimental Studies of Refrigerant Mixtures

In this section is presented a review of recent work on the measurement and prediction of the thermodynamic properties of refrigerant mixtures. In this context *refrigerant* is used to denote a wholly or partially substituted chlorofluorocarbon compound. The predictive and correlative techniques are also covered in Chapter 6 but the scope of this chapter is to supply further details of the techniques used by other workers to obtain and correlate thermodynamic data for these fluids.

2.4.1 Overview

Measured properties of refrigerant mixtures were published as long ago as 1950, when Pennington and Reed [81] studied the R12/R152a system. They recorded isothermal VLE measurements at 0 °C, discovering an azeotrope whose composition was 39.8 mol% R152a. There remained little publication of studies on mixtures for some time: the refrigeration industry was convinced that the problems of differential leakage and the uncertainty regarding thermodynamic properties were too difficult to justify research into mixtures of fluids. At this time, of course, the CFC refrigerants were still regarded

as some of the most "user-friendly" of industrial chemicals; there was no impetus for change or improvement. Thereafter some work was done in the 1960s, mostly on mixtures of R12 and R22, for which there already existed extensive tabulations of data. Publications appeared thereafter at sporadic intervals; until towards the end of the 1970s there began a wave of serious interest in the application of mixtures both in refrigeration and in heat pumping. The bulk of the papers reviewed here were published between 1977 and 1990; the author restricted his search for reference data to the most recent publications (which in any case refer to the few articles published prior to this time). The reason for this was that the earlier papers concerned fluids such as R14 (tetrafluoromethane) which were of no use as heat pump working fluids. The reader is referred to the paper by Meskel-LeSavre *et al.* [66], which contains a bibliography of the best data published before 1982.

The material covered has been grouped into several sections; the most commonly studied systems have been allocated separate sections. Many of the published articles deal with the properties of more than one system; the reader may therefore experience a certain *déja vu* but should not be unduly deterred! Reference is made to several methods of data correlation or prediction; these are clarified in Section 2.3 below.

2.4.2 Sampling Techniques

The reader is referred to the source literature for details of the methods used to measure thermodynamic properties of mixtures. Nonetheless it is useful to supply a sketch of the main methods used to avoid repetition later.

There are two main ways to measure properties of a mixture which is at vapour-liquid equilibrium: one way uses a sealed sample vessel, charged with a known mass and composition of fluid; the other uses a recirculating device, of similar principle to the well-known Othmer still, containing a mixture of arbitrary composition. In the former case, the sample cell is subjected to a range of temperatures and pressures, enabling the calculation of densities at given composition. The dew and bubble points may be determined by plotting the measured isochore: a sudden change in slope indicates a two-phase region boundary. Such sample cells are often fitted with transparent windows; the onset of dewing or bubbling may then be observed and recorded.

The recirculation devices offer the advantage of simultaneous determination of both phase compositions at a given temperature and pressure. They are more difficult to bring to true equilibrium: material must be withdrawn for analysis and returned many times, and there may exist stagnant zones in the unit which prevent adequate contacting of the two phases. Typical accuracies on composition measured in these devices are 1–2 mol%.

2.4.3 The R12/R22 System

This is one of the most widely studied of all binary refrigerant systems; the motivation for this intensive work has been partly investigative and partly as a calibration system for experimental apparatus. The volumetric properties of both components are well known and may be used to check the measurement system and technique used before venturing into the unknown.

Eiseman [25] recorded isobaric measurements of the vapour-liquid equilibrium at 1.0 bar absolute, over the temperature range 231.74–243.35 K in 1957. He did not detect an azeotrope for the system. Kriebel (1967) [46] produced a much-cited paper detailing isothermal VLE measurements, performed over a range of temperatures between 40 and 80 °C. He found an azeotrope; the azeotropic composition was measured at 10° intervals over the given temperature range; it was found to increase with increasing temperature, until the azeotrope became pure R22 at 85.5 °C.

Kagawa *et al.* (1983) [43] prepared a comprehensive map of the thermodynamic state surface of the R22/R12 system, including the critical locus of the mixture. Their data were obtained by use of a constant-volume sample cell, giving measurements of temperature, pressure and composition along a set of isochores. They fitted the state surface to a modified twenty-constant Benedict-Webb-Rubin equation of state, using forty numerical parameters for each pure fluid: these were two sets of twenty parameters, corresponding to two different portions of the state surface. The paper cited does not contain the complete details of their work, but it references the related publications by the same authors, notably Uematsu *et al.* (1984) [116], which contains more detail of the sampling technique and an updated bibliography of the work by this research team on the R22/R12 system.

Morrison and McLinden (1985–6) [70, 71] produced several articles and a full technical report on the use of the CSD equation of state as a correlator of thermodynamic properties. They used the R22/R12 system as a test of the equation's predictive powers; their final report to the American National Bureau of Standards (NBS) contains experimental measurements of the system VLE and thermophysical properties over a large portion of the two-phase space. They found azeotropic behaviour roughly in agreement with that measured by Kriebel. They also found that the equation could predict the total heat of vapourisation of the nonazeotropic mixture of R22 and R12 with good qualitative and quantitative accuracy. The accurate prediction of such second-order thermodynamic properties was taken as an indicator of a good correlation method.

In 1989, Ström [113] published an article detailing isobaric measurements of VLE of the systems R22/R12, R22/R114 and R12/R114. The method of measurement was the Jones recirculation cell, *i.e.* an equilibrium still. The data presented for R22/R12 were measured at 9.85 and 13.95 bar, over the whole composition range. The existence of an azeotrope was detected under 9.85 bar: its composition was roughly 0.985 mol fraction R22 at 25.7 °C, in rough agreement with other workers. Ström fitted three equations of state to his data: the Lee-Kesler, Soave-Redlich-Kwong (SRK) and CSD equations of state. Interaction parameters were found for each equation by numerical optimisation: the objective function was the least-squares deviation between calculated and measured equilibrium K values for each component. It was found that the Lee-Kesler and SRK equations represented the data better than did the CSD equation, contrary to the findings of Morrison and McLinden, who developed the CSD equation for use with refrigerants. It is significant that the interaction constants found for each equation by Ström had similar magnitudes; this led the author to his experimentations with interaction constants, whose outcomes are described in Chapter 6.

2.4.4 The R12/R114 System

Papers on this system have been published by Ström *et al.* (1989) and Kubota *et al.* (1990). The data taken by Ström were measured under isobaric conditions, using a Jones recirculation cell. The data quoted in the reference are: temperature and both phase mol fractions over the complete two-phase region, for pressures of 3.5, 8.85 and 14.5 bar. Experimental uncertainties in direct measurement were given as ±10 mK on temperature and 0.05 bar on pressure. Composition was measured using a six-figure accuracy densitometer, calibrated with mixtures of known composition. The data were

fitted well by the Lee-Kesler, RKS and CSD equations of state to within the quoted experimental incertainty of 0.01 mol fraction; the authors found that the interaction constants required to optimise data fitting for this system were almost zero (0.01) for each equation. Their conclusion was that this system could be considered near-ideal under the pressures examined in their study.

Kubota's work was carried out in an isothermal, constant-recirculation apparatus, for which the system temperature was controlled to better than 30 mK, with an uncertainty of 50 mK on the overall temperature measurement. Pressures below 5 bar were thought to have an uncertainty of 0.01 bar; above 5 bar the uncertainty was thought to be 0.03 bar. (Two pressure transducers, of differing range, were used in this work.) Composition of each phase was obtained using an on-line gas chromatograph; the maximum uncertainty on composition was thought to be 0.009 mol fraction near 50% R12, falling to 0.003 mol fraction at either 10% or 90% R12. The data were checked for thermodynamic consistency using a plot of the quantity $y_2 P/p_2^*$ *versus* $(P - p_2^*)$, where y_2 is the mol fraction of less volatile, P is the system pressure and p_2^* is the vapour pressure of less volatile at the system temperature. Data plotted in thes co-ordinates should lie on a smooth curve whose extrapolated ordinate is unity. The data met this simple criterion.

Measurements were taken of the phase compositions and pressures for temperatures of -20 °C, 10 °C and 40 °C. The data were then fitted to two cubic equations, the Peng-Robinson (PR) and RKS equations. Separate interaction constants were evaluated for each temperature and each equation; the objective function used in the optimisation procedure was a standard sum of squared deviations between predicted and calculated phase compositions. The optimised interaction constants found for the PR equation at the three temperatures used were: 0.0176, 0.0112 and 0.0150 respectively. Those found for the RKS equation were 0.0217, 0.0087 and 0.0099, under the same criteria. Both equations gave similar deviations in phase compositions—0.006 to 0.012 mol% for either phase—when the optimised interaction constants were used.

2.4.5 The R22/R114 System

Data on this system have been published by Kagawa [43] (1983); Hasegawa [32] (1985); Valtz [119] (1986); Ström [113] (1989) and Kubota [51] (1990). Of these publications,

those of Kagawa and Hasegawa are of little direct interest, as they give nunerical correlations of data rather than "raw" figures.

Valtz' data were measured under isothermal conditions in a variable-volume sample cell; this allowed the simultaneous determination of bubble pressures and saturated liquid molar volumes for mixtures of known (specified) composition. The quoted accuracies were: 0.1 K on temperature and maximum of 0.08 bar on pressure (for pressures above 10 bar). The quoted data were measured at temperatures of 25, 50, 75 and 98 °C, the last temperature being above the critical temperature of R22. The Peng-Robinson equation was used to correlate the data; an optimum interaction constant was determined at 0.044 for the complete set of recorded data. It was found that the PR equation could correlate the bubble pressures of the system well at all temperatures, but that the prediction of liquid volume was not good. At the highest temperature the equation of state predicted a rapid increase in molar volume at high mol fractions of R22 where in fact only a modest increase was observed. This behaviour was explained as an effect of the proximity to the mixture critical point.

The data of Kubota and Ström were taken using the apparatus described in the previous section for R12/R114. Ström recorded temperatures and compositions for two pressures, 9.85 and 13.5 bar, while Kubota recorded pressures and phase compositions for temperatures of -20, 10, 40 and 65 °C. This system was also classed by Ström as exhibiting near-ideality; this was borne out by the excellent fits to data which he obtained for the LK, RKS and CSD equations of state. Stated accuracy on prediction of composition was 1 mol% for either phase.

Ström's optimised interaction constants for these three equations were 0.03, 0.025 and 0.04 respectively. Kubota fitted his data to the PR and RKS equations, finding mean interaction constants of 0.0545 and 0.0541 for these equations. The resulting uncertainties on phase composition were 0.009 mol fraction for each equation. These results suggest that consistent methods of interaction constant determination yield similar results, irrespective of the equation of state used. Furthermore, there appears little difference between the PR and RKS equations for prediction of the VLE of this system.

2.4.6 Systems Containing R13B1

Several workers have published papers on mixtures of fluids with R13B1 (bromotrifluoromethane), which was seen as a possible substitute for chlorine-containing refrigerants. The author had no interest in mixtures containing R13B1; its volatility was rather too high for the high-temperature application modelled by the experimental plant described in Chapter 3 and Chapter 4. A brief review is nonetheless presented here of recent work on mixtures containing R13B1.

Connon and Drew (1983) [14] presented some data on a mixture of R13B1 with R152a (1,1-difluoroethane). They used the RKS equation of state to produce a pressure-enthalpy chart for the system, based on experimental measurements of liquid density and bubble pressure.

Morrison and McLinden *op. cit.* carried out a more detailed examination of the R13B1/R152a system, reporting VLE and density measurements over a wide range of temperatures. They found the CSD equation was capable of reproducing to good accuracy the unusual shape of the phase envelope of this system near the critical temperature of R152a. Tables of the volumetric (PVTx) behaviour of this system are contained in their publications.

Hosotani *et al.* (1988) [36] studied the R13B1/R114 system, determining the variation of pressure, volume and temperature at a series of compositions. They used a constant-volume sample cell and explored a wide range of temperature, pressure and density (303–443 K; 5–103 bar; 150–1200 kg/m^3). Data were published for four different compositions: 25, 50, 70 and 80 weight percent R13B1. The dew and bubble points were obtained by plotting the resulting isochores and noting sudden changes in gradient as edges of the two-phase region. Higashi *et al.* (1988) [34] also studied R13B1/R114, this time in the critical region. They studied the vapour-liquid coexistence behaviour in an optical cell by visual observation of the presence or absence of a liquid meniscus, for the same compositions used by Hosotani. Hosotani fitted his data to the Peng-Robinson, RKS and Patel-Téja equations (the latter being another generalised cubic equation of state). He concluded that all these equations gave roughly similar accuracy of prediction of VLE behaviour, but that their density prediction was poor for liquid or supercritical phases. In the critical region there were significant deviations from the qualitatively correct variation of liquid volume with composition.

Kubota (cited above in connection with R22/R12, R12/R114 and R22/R114) also studied the R13B1/R12 system, taking measurements of pressure and phase compositions at temperatures of -20, 10 and 40 °C. He fitted the PR and RKS equations to his data and found a consistent pattern of prediction with each equation: typically the equations' predictions of composition were accurate to better than 0.009 mol fraction for either phase. The interaction constants which Kubota obtained were slightly unusual in that they took small negative values (-0.013) rather than the more usual positive values taken by the constants when fitted to other systems.

2.4.7 Work Performed at the Ecole Supérieur des Mines, Paris

Several papers on the thermodynamic properties of CFC fluid mixtures have been published by research workers at the *Centre Réacteurs et Processus* attached to the *Ecole Supérieur des Mines* in Paris. The experimental apparatus and procedures detailed in the papers are broadly similar, and so the results will be described together in this section.

2.4.7.1 Apparatus and Procedures

The French workers used a variable-volume, isothermal sample cell apparatus: this was charged at the start of an experiment with a known quantity of mixed fluids, of known composition. A pressure transducer and thermocouples were attached to the cell and gave readings to 0.1 bar and 0.1 K accuracy. The cell temperature was maintained by total immersion in a thermostat-controlled oil bath; continuous mixing inside the cell was achieved by use of a magnetic stirrer. The cell volume could be altered by movement of a snugly-fitting piston acting on the fluid.

The experimental procedure was straightforward: the cell pressure was steadily increased by reduction of the sample cell volume. A record of total pressure against cell volume was kept and plotted: the plot of pressure against volume exhibited a discontinuity at the bubble point.

2.4.7.2 The System R22/R11

Data on this system were published by Meskel-LeSavre *et al.* [66] (1982). Four temperatures were used: 25, 50, 75 and 100 °C; this last temperature is greater than the critical temperature of R22. The experimental apparatus was used to measure saturated liquid volumes and vapour pressures for each of the pure components at the given temperatures (excepting 100 °C for R22). The measured pressures agreed with literature data to within the experimental accuracy of 0.1 bar: the liquid volumes were slightly higher than literature data but were reproducible to within 1% of the published figures for either R22 or R11.

The data on R22/R11 mixtures published in the reference consists of tabulations of measured pressures and liquid volumes at the four studied temperatures, for a range of 6 or 7 compositions in each case. In addition are included calculated vapour phase compositions; these were obtained by fitting the Peng-Robinson equation of state to the measured datasets. The objective function used to find an interaction constant for the system was a sum of squared errors in pressure prediction; this function was used to find an average value of the interaction constant over the range 25–100 °C. The interaction constant for this system was found to be 0.0466 over the specified temperature range.

The predictions of the PR equation using the optimised interaction constant were illustrated in the literature by graphical plots showing experimental and calculated bubble pressures and liquid volumes. These showed that the prediction of bubble pressure was excellent (better than the experimental accuracy of 0.1 bar) but that the prediction of liquid volume was only fair—a mean accuracy of 5% at best was obtained. In particular the PR equation did not predict correctly the observed minima in the plots of volume *versus* composition at 75 °C or 100 °C. The equation of state predicted a monotonic increase in liquid volume at these temperatures. In a sense this is no surprise: the objective function did not include liquid volume.

The data contained in Meskel-LeSavre's paper have been used at some length in Chapter 6 as input to optimisation programs for the CCOR equation of state, and there the reader will find graphical illustration of these measured data.

2.4.7.3 The R13/R113 System

This system was studied by Meskel-LeSavre, Richon and Renon; a paper was published in 1982 [67]. The properties determined were bubble pressure and saturated liquid volume as functions of composition at five temperatures: 25, 30, 50, 75 and 100 °C. The liquid volume results showed that the system exhibited a significant volume contraction of mixing even at 25 °C. The composition corresponding to minimum liquid volume decreased with temperature, from about 0.73 mol fraction R13 at 25 °C to about 0.35 mol fraction at 100 °C.

The Peng-Robinson equation was fitted to the experimental data, using the same methods as those described for the R22/R11 system. It was found that the equation gave very good predictions of the bubble pressures and could represent qualitatively the liquid volume contraction of mixing. The accuracy of liquid volume prediction was however no better than 5%on average. The interaction constant found for the PR equation and this system took the value 0.0191: this was found using an objective function based on the fractional error in bubble pressure prediction.

2.4.7.4 R22/R113 and R22/R142b

Data on these systems were published by Valtz and co-workers in 1986 [119]. Experimental measurements of bubble pressure and saturated liquid volume were quoted over a range of compositions for temperatures of 25, 50, 75 and 99 °C. The composition range used depended on the temperature of the system; obviously at temperatures higher than the critical temperature of the more volatile the two-phase region would not span the whole composition rqnge. (Critical temperature of R22 is 93.6 °C; critical temperature of R142b, difluoromonochloroethane, is 137.2 °C.) The Peng-Robinson equation of state was fitted to the data for each system; the objective function used for this fitting was in each case the sum of squared fractional errors in bubble pressure. The fitting of non-zero interaction constants for the PR equation gave an accuracy of bubble pressure prediction of approximately 1%; the prediction of liquid volume was however poor, with an accuracy of about 8% over the composition range chosen for each fluid system. The interaction constants found for these mixtures were: 0.042 for the R22/R113 system, and 0.0043 for the R22/R142b system.

2.4.7.5 R23/R113, R152a/R113 and R152a/R12/R113

In 1987 Valtz [120] published a paper dealing with the thermodynamic properties of these mixtures, notable for the rare inclusion of measurements on a ternary system. The reason for study of the latter system becomes easier to understand if one appreciates that the binary R12/R152a is azeotropic and marketed under the code R502, a common refrigeration working fluid. Addition of a markedly less volatile component (R113) might therefore be expected to give a pseudo-binary mixture with a large potential for capacity modulation by rectification of composition in a refrigeration or heat pump cycle. The data presented were bubble pressures and saturated liquid volumes over the possible composition range, at temperatures of 25, 50, 75 and 100 °C.

The experimental measurements on the two binary systems were used to fit interaction constants for the Peng-Robinson equation of state; with the use of the optimised interaction constants the equation represented the experimental bubble pressures within an accuracy of 2%. It was found that the equation could not represent the experimental bubble pressures for either system well if the interaction constant were set to zero. The authors used the volume translation method of Péneloux [79] to improve the prediction of saturated liquid volume; it was found that the use of this technique allowed prediction of liquid volume to within 2% without affecting the prediction of the vapour-liquid equilibrium of the system.

2.4.8 Other Systems

Stein and Proust (1971) [108] studied the system R23/R13. This was not of immediate interest to the author, as both components were too volatile to be considered for high-temperature heat pump applications. Their paper is however worthy of review, as it is an exemplar in the analysis of refrigerant-mixture data. The R23/R13 system exhibits azeotropy and has been marketed as R503; Stein and Proust investigated not only the azeotropic mix but also the VLE over the entire composition range. The system was studied in a recirculation still, run under isothermal conditions. Temperature was measured to 0.02 °F; pressure to 0.1 psia, and liquid and vapour phase compositions were determined by gas chromatography to better than 0.3% on mol fraction. Results were presented at four representative temperatures: -100.05 °F; -55.1 °F; -0.1 °F, and 31.9 °F. The exact position of the azeotrope at each temperature was obtained by

careful graphical construction from the measured data on either side of the azeotropic point, and the azeotropic pressure and composition were tabulated as functions of temperature. The Redlich-Kwong equation of state was used to represent the vapour phase of the mixture; activity coefficients for the liquid phase were calculated using the pure component liquid states at the same temperature as reference data. These activity coefficients were then fitted to the Wilson equation. The resulting formulae allowed prediction of the equilibrium pressures to 0.44% and vapour compositions to better than 0.005 mol fraction.

In 1984 Watanabe and Uematsu [123] published a review of continuing work performed by their team on the properties of some perfluorocarbon fluids. These fully fluorinated alkanes were thought to hold attractions as working fluids for organic Rankine Cycle power plant, operating in the temperature range 450–650 K. Their paper provided a description of their experimental apparatus and procedures, as well as considerable data on the properties of a number of these fluids. The molecular weight, critical properties, melting and freezing points for a number of fluids (up to C_{11} chain length) were tabulated. Extensive measurements of volumetric properties had been carried out for two of these fluids, namely perfluoro–iso–hexane and perfluoro–n–octane. These data were summarised by the authors in the form of a 5-constant Antoine-type vapour pressure–temperature relation and a 15-constant modified Benedict-Webb-Rubin equation of state. The same forms of function were used by these workers to describe the R22/R12 and R22/R114 systems discussed above.

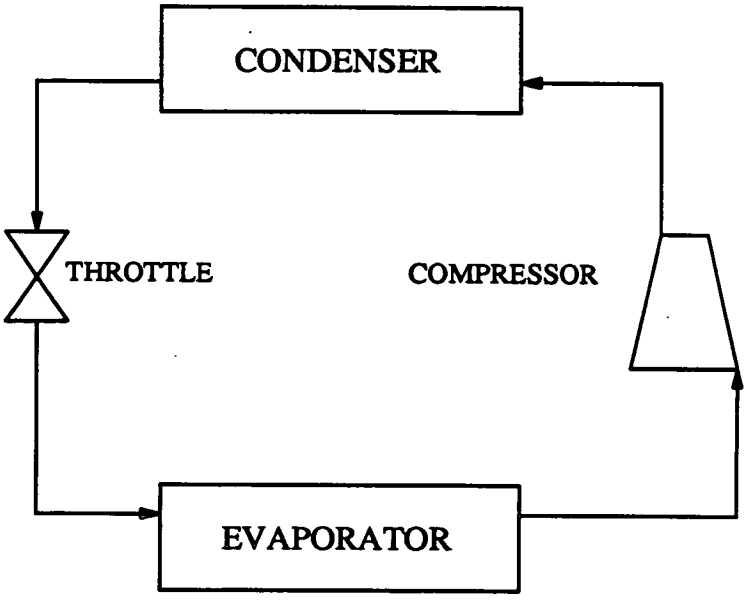

Figure 2.1: Idealised Vapour-Compression Cycle

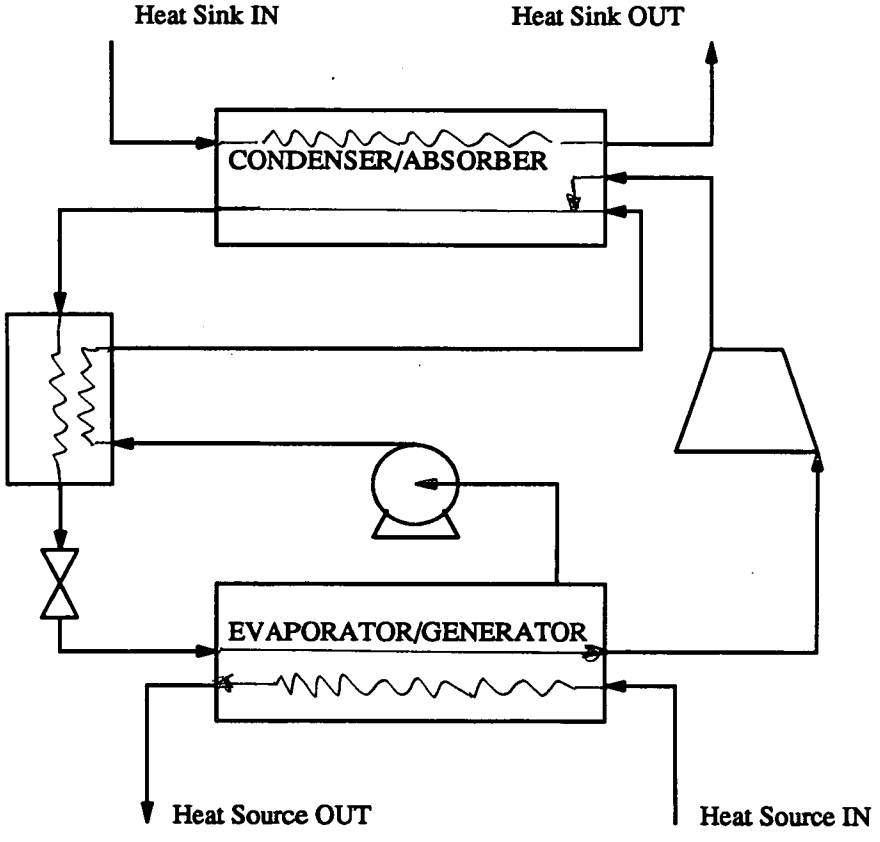

Figure 2.2: Idealised Compression Absorption Cycle

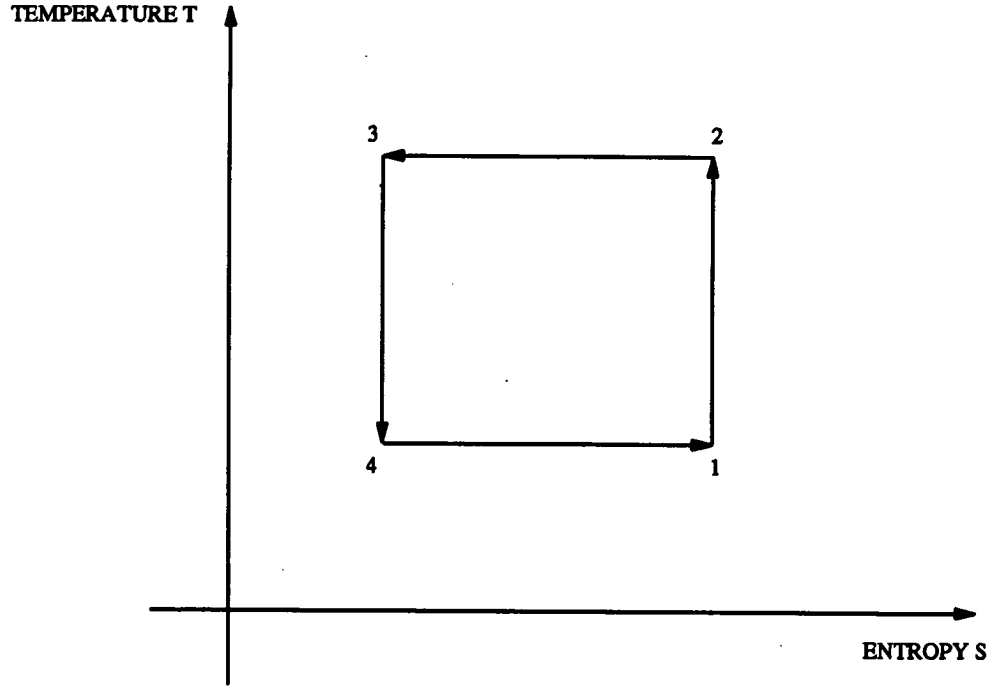

Figure 2.3: Carnot Cycle in Temperature-Entropy Plane

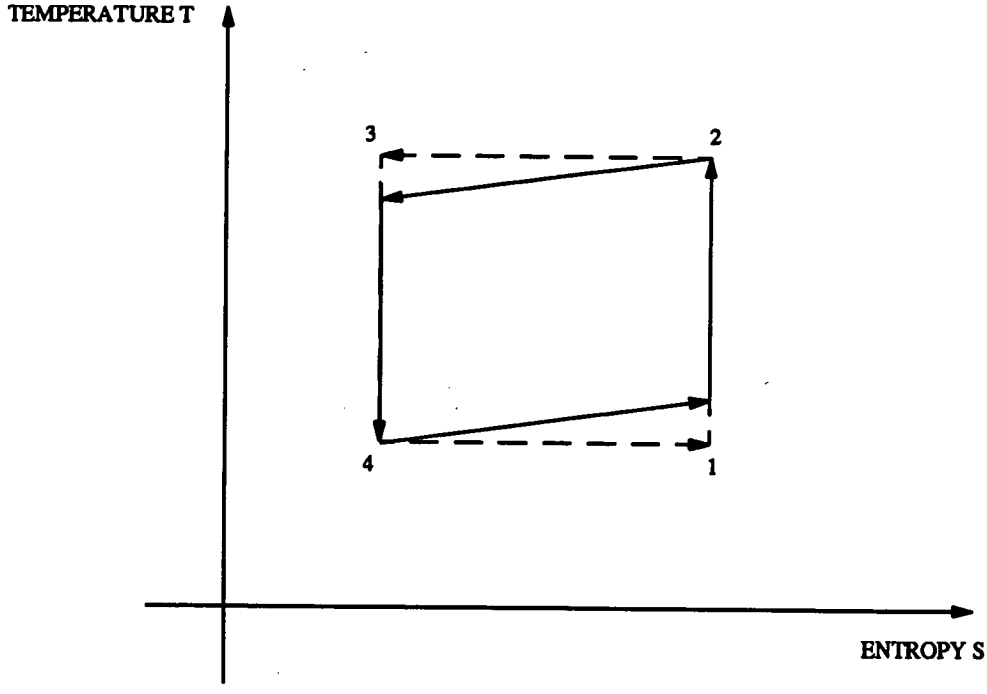

Figure 2.4: Lorentz Cycle in Temperature-Entropy Plane

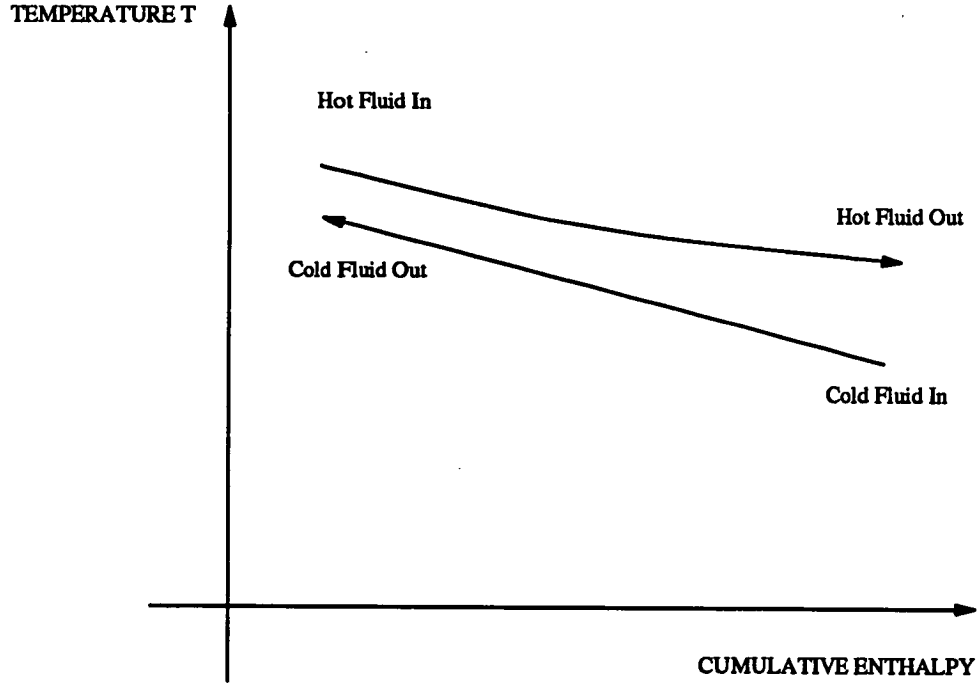

Figure 2.5: Temperature Profiles in a Heat Exchanger

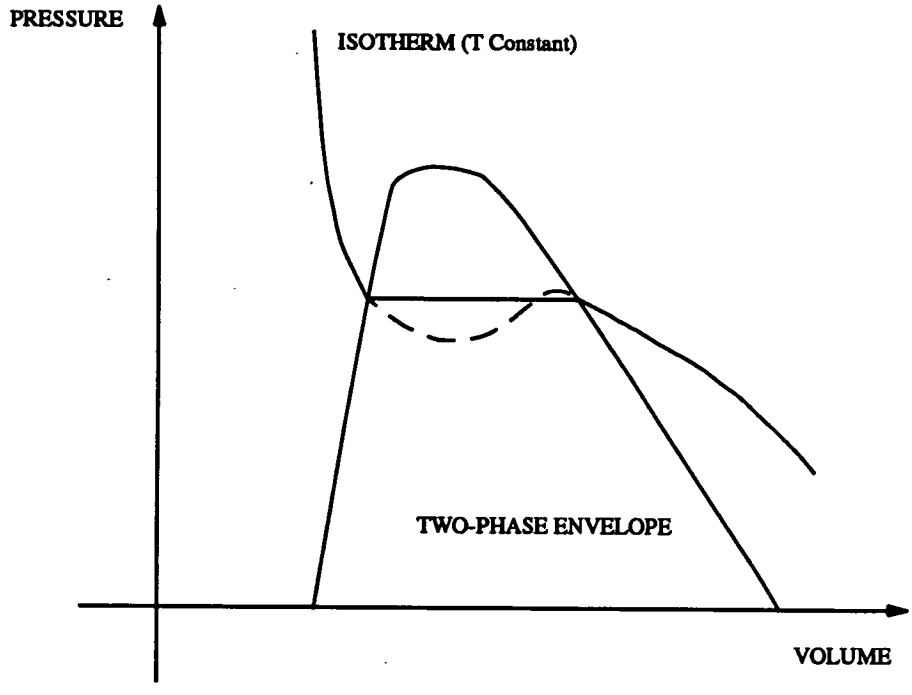

Figure 2.6: Pure Fluid Isotherm in Pressure-Volume Plane

Chapter 3

Design and Construction of Experimental Plant

3.1 Process Design Constraints and Requirements

3.1.1 Introductory Remarks

As described in Chapter 1, the motivation for this research was the need for a compression heat pump, capable of accepting widely varying work inputs, as part of a wave-powered desalination process. The load of such a heat pump would follow the work input (as the total throughput of the desalination process would vary as the power available in the waves) but the quality of heat delivered would be required to remain constant. This duty could not be performed by a conventional, single-fluid heat pump,

without expensive control of the compressor speed. The turndown ratios required for successful application to a renewable energy stream would in any case be too great for a linear compressor speed control system; such systems can only cope with modest turndown ratios. It was decided to design and build a pilot plant heat pump, using a non-azeotropic (zeotropic) mixture as working fluid, in order to regulate more widely the capacity of the heat pump cycle. The design of the pilot plant was affected by considerations of the following:

- The nature of the proposed application (preheat for a desalination process) constrained the choice of heat sink and heat source streams.
- The range of power inputs had to reflect the variable nature of a typical renewable energy (wave or wind power) source.
- Areas of interest for research work. A set of target subjects for investigation was chosen and the requirements of each subject kept in mind throughout the design process.
- The choice of working fluid was affected by:
  - Safety considerations (flammability, toxicity, etc)
  - Availability of hardware (compressors, etc)
  - Availability and cost of fluids
  - Environmental effect of fluids
  - Thermodynamic considerations (relative volatility, shape of the boiling-point diagram, *etc.*)

The following subsections expand on these constraints to give a final set of constraints used in the design.

3.1.2 Choice of heat sink and heat source

The heat source and heat sink streams were both chosen to be water streams; in an actual desalination plant these would be, respectively, the product streams (after passive feed-product heat exchange) and the feed to the still. The temperature of

the products would typically be 10–15° higher than the cold feed to the process, as a consequence of the finite temperature difference in any passive heat recovery net. An alternative source of heat would be the sea itself. In the latter case, the temperature profile of the heat source in the evaporator of the heat pump would be very flat, as the sea is a good approximation to an isothermal source. The sink temperature would be lower than the boiling point in the still by a similar amount. Another, practical observation which affected the design was that, as the plant was intended for experimentation, it should be capable of handling lower yet evaporation temperatures, down to ca. 0 °C, as typical wintertime ambient temperature source quality.

For these reasons it was decided to specify the heat source as a stream of water, temperature controlled to a setpoint in the range 25–35 °C, flow regulated to give a Δ T for the heat source of approximately 5° in the heat pump evaporator, as this gave a source which was a good approximation to the "real-life" situation. The consequences for design and performance of these decisions are:

- The exergetic efficiency of the evaporator will not be maximised, as the temperature difference between the source stream and evaporating working fluid will not, in general, be constant.
- Both flow and temperature will require some means of regulation, be it automatic or manual; furthermore a buffer tank will be required to smooth out any fluctuations in temperature.
- The source stream should be a closed system, so that anti-freeze solution may be used for lower evaporator temperature levels in winter.

Specification of the heat sink stream was straightforward: a water stream, with its temperature regulated to some arbitrary setpoint in the range 60–80 °C, with Δ T for the heat sink stream in the heat pump condensers to be in the range 10–20°. The sink stream condenser exit temperature was to be controlled to some other arbitrary setpoint, in the range 80–95 °C. The Δ T quoted above was chosen in an attempt to optimise the exergetic efficiency of the condensation process. It has been found by other workers that the optimum Δ T for a zeotropic working fluid's temperature profile will normally lie in the range 10–20°: for the best exergetic efficiency the sink temperature profile should be parallel to that of the working fluid. A closed-loop system with buffer tank was chosen, to enable close control of the inlet temperature.

3.1.3 Process load and power input ranges

Both wave and wind power may exhibit significant changes on amplitude of the available power about the mean value for the particular location chosen. With wave power, however, the changes in amplitude take place relatively slowly, as the inertia of an ocean wave system is considerable. A timescale of hours is not inappropriate; whereas the changes in wind power may occur more rapidly and more often. In order to study the effects of both characteristic changes in available work, some means of achieving significant work input change was required. The most obvious method was to regulate the speed of the heat pump compressor. This meant that the compressor had to be of a type which could perform acceptably well over a wide range of turndown (see later), with a rapid and easily-controllable, variable speed drive unit.

3.1.4 Areas of Planned Investigation

Several areas of interest were identified in advance of any detailed pilot plant design work. These were principally related to the effect of various cycle modifications on: the degree of separation achievable in the condensers; the Coefficient of Performance and exergetic (2nd Law) efficiency; the transient response of the system, and the quality and quantity of output heat. The plan of operations was as follows:

1. Operation of the heat pump with a pure fluid (to obtain a set of reference data). This operation was to include measurements of the transient response of the system and sets of steady-state performance data obtained with differing lifts and discharge temperatures.
2. Steady-state operation of the basic circuit with a zeotropic mixture, over a range of lifts and discharge conditions.
3. Transient response measurements of the system with a mixture as working fluid.
4. Effect of subcooling the condensate streams on COP and response.
5. Effect of control of condensing pressure on COP.
6. Effect of flash vapour return on the degree of separation.

7. Ability to regulate the composition of the working fluid in response to changes in work input (manifested by varying compressor speed.)

8. Effect of using a partial evaporator in conjunction with liquid injection to the condenser inlet on performance. (This is the "compression-absorption" cycle discussed in Chapter 2)

3.1.5 Choice of Working Fluid

3.1.5.1 Safety Considerations

As the proposed pilot plant was for experimental use in a University laboratory, there were several constraints on the choice of working fluid which might not apply so rigorously in an industrial usage. These were identified by the following observations:

- The fluid chosen should be non-flammable in all concentrations with air.
- The toxicity of the fluid should be as low as possible; it should also be harmless to the skin or eyes in the event of leakage.
- There should be little or no thermal decomposition of the fluid in the temperature ranges of interest, nor should it undergo any significant chemical decomposition reaction during the programme of research as a consequence of contact with the materials of construction.
- The fluid should be readily available and relatively inexpensive, as the experimental nature of the facility makes losses a real possibility.

Halogenated hydrocarbons, such as the chlorofluorocarbon (CFC) fluids, were obvious candidates, as these are commonly used in conventional compression heat pumps. While they do not represent ideal candidates for working fluids—their latent heats are low and transport properties are poor—they fulfil all the safety criteria outlined above. (Other workers have used NH_3/H_2O as a mixture but this gives rise to concern on grounds of corrosivity, toxicity and flammability of ammonia.) It was therefore decided to choose two halogenated hydrocarbon compounds as the working fluid mixture components.

3.1.5.2 Practical Considerations

Pressure levels For line pressures below about 25 bar, it is possible to use compression fittings and couplings on pipework without significant leakage problems or risk of failure. Such couplings are cheap and easy to fabricate: they also facilitate modification of pipework, should this be desired. At higher pressures, it becomes necessary to use brazed, welded or flanged fittings, which represent a considerable increase in cost and inconvenience. The maximum allowable pressure was therefore taken as 25 bar: this would occur at the highest permissible temperature in the condenser, using pure more volatile. Given that the maximum possible water temperature in the condenser is 100 °C, this constrained the more volatile to have a vapour pressure at 100 °C of less than 25 bar.

A minimum vapour pressure of ca. 0.5 bar at 25 °C was specified for the less volatile: this was an arbitrary constraint to reduce the possibility of air ingress to the refrigerant circuit. A better constraint would have been a vapour pressure of at least 1 bar at 25 °C; as it was intended to use QVF glassware for storage vessels, however (see below), this was relaxed. A minimum vapour pressure for the less volatile of 1 bar, coupled with a maximum vapour pressure of 3.5 bar for the more volatile, would have restricted the choice of pairs and limited the amount of capacity shift achievable in the system.

Compatibility The materials of construction favoured for the plant were: copper (where possible) or mild steel for pipework; mild steel, stainless steel, or glass for vessels; brass or duralumin for flanges, fittings and headpieces, and PTFE for packing and gasket materials. The halogenated hydrocarbons are compatible with all the above materials but duralumin should not be used at high temperature, as there is a slight risk of reaction with the working fluid to give hydrochloric acid amongst other decomposition products.

The use of glass would restrict the permissible pressure in the circuit at that point and necessitate pressure relief devices to guard against overpressure. As glass vessels would only be used on the low-pressure side of the heat pump cycle, this gave a low-pressure constraint on the working fluid: the vapour pressure of the more volatile at the design temperature of any glass component should be no higher than the design pressure of the component quoted in the manufacturers' product guide. The quoted working pressure ratings for QVF sections are: 35 psig for 4" section and 25 psig for 6" section. The temperature levels on the low pressure side of the cycle were to be in the

range 15–30 °C (see Section 3.1.2): this was therefore taken as the design temperature range for any glassware in the system.

3.1.5.3 Environmental Considerations

Existing refrigerant CFC fluids are not satisfactory for long-term usage, because their potential for ozone depletion in the upper atmosphere has caused the international community to outlaw or gravely restrict their future use. The possible replacements for them include perfluorinated hydrocarbons and partially substituted hydrofluorocarbons (HFCs). In order that such fluids might be charged into the plant as and when available, the range of possible fluids was extended to include these families of compounds. The intention was to select a suitable "ozone-friendly" pair, design the plant around this pair, then use a more readily available pair of fluids for initial investigations pending production of the original choice.

3.1.5.4 Thermodynamic Criteria

The principal thermodynamic criteria for working fluid selection, given the aforementioned safety and practical constraints, are the relative volatilities of the components and the shape of the boiling-point diagrams. The larger the difference in relative volatilities, the greater the change in potential capacity change and the larger the gliding temperature difference associated with phase change of the mixture. The shape of the boiling-point diagram affects the degree of separation achieved by condensing a fixed split fraction of a vapour feed and hence the ease of separation of the working fluid by the proposed method of partial condensation. If too large a gliding temperature difference is used, however, it becomes difficult to match the temperature profiles of the heat sink and working fluid in the condenser without departing from realistic temperature differences and flows. The final criterion used was that the difference between dew and bubble point temperatures should be no greater than 50 ° at a composition of 50 mol% more volatile: this is arbitrary but corresponds fairly closely to the composition giving maximum gliding temperature interval for most refrigerant mixtures.

3.2 Development of Basic Flowsheet

3.2.1 Proposed Principles of Operation

The principle of capacity control proposed in Chapter 2 was the regulation of working fluid composition by separation and storage of the less volatile and more volatile, according to the load requirement. The separation was to be accomplished by use of a twin-condenser arrangement, yielding two condensates of differing compositions. This arangement avoids the need for any external control of the comosition shift and is inherently simple in concept. A basic block flow diagram for the heat pump process is shown in Figure 3.1

The order of operations is:

1. Liquid refrigerant is passed to the evaporator, where it undergoes a non-isothermal change of phase to saturated vapour, absorbing heat from a non-isothermal source.
2. The vapour from the evaporator is compressed to and passed to the first condenser, where it undegoes a partial condensation, the heavy component condenses preferentially.
3. At the condenser exit, the liquid and vapour streams are separated: the vapour is passed to the second condenser and there condensed.
4. Both condensate streams are throttled into storage tanks maintained at ambient temperature.
5. Liquid is drawn off from the storage to feed the evaporator and complete the cycle.

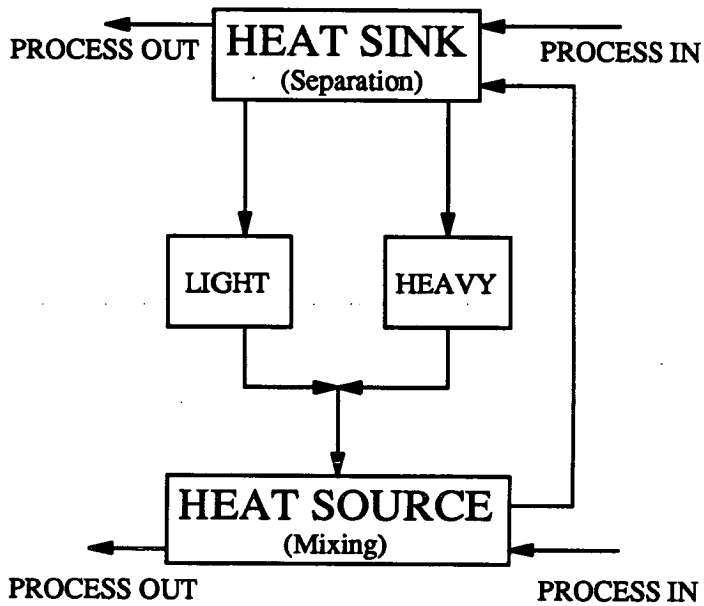

Figure 3.1: Block Flow Diagram for Two-Fluid Heat Pump

The above does not yet constitute a flowsheet, merely a summary of the necessary units involved. Nonetheless, it contains enough information to specify a "minimum-unit" flowsheet, by which is meant a flowsheet which may be used to get approximate mass flows, temperatures, pressures etc. for design of a yet more complex pilot plant. The rationale here is that, in an experimental plant, with conditions varying over a wide range of operating states, close design to a complex flowsheet is neither necessary nor desirable. The line sizes to be used and the main plant items may be sized from a skeleton flowsheet without any untoward effect, as the additional units to be used will not affect the key streams to a great extent; their inclusion in a heat and mass balance would, however, make the calculation more difficult.

3.2.2 Minimum-Unit Flowsheet

3.2.2.1 Calculation scheme for flowsheet

On the basis of the block flow diagram shown above, a skeleton flowsheet was drawn up for the pilot plant, shown below in Figure 3.2.

The notation in this figure is straightforward: CV for control valve; P for pump; C for condenser; E for evaporator; T for tank; and J for compressor. There are four points where streams mix, denoted A,B,C,D for further reference. The scheme of operation is basically the same as that outlined above, except that partial condensation is assumed to occur in the second condenser as well as in the first unit. No control loops are shown, but the use of the indicated control valves permits the control of pressure in each condenser and of level in each condensate receiver. The use of pumps P1 and P2 permits regulation of the liquid feed at any composition intermediate between those of the tanks. The steady-state heat and mass balances for this flowsheet may be calculated without iteration if the following assumptions are made:

Assumptions used:

- All pressure drops may be ignored.
- The composition of the vapour at the inlet to the condenser C–1 is fixed.
- The split fractions (*i.e* fraction of feed uncondensed at exit) in the two condensers are fixed.
- The dewpoint temperatures in both condenser and in the evaporator are fixed.
- The streams leaving the receivers T–1 and T–2 are in equilibrium.
- The condensate streams undergo adiabatic throttling into T–3 and T–4, such that the streams leaving these tanks are likewise in equilibrium.
- The isentropic efficiency of compression is specified.

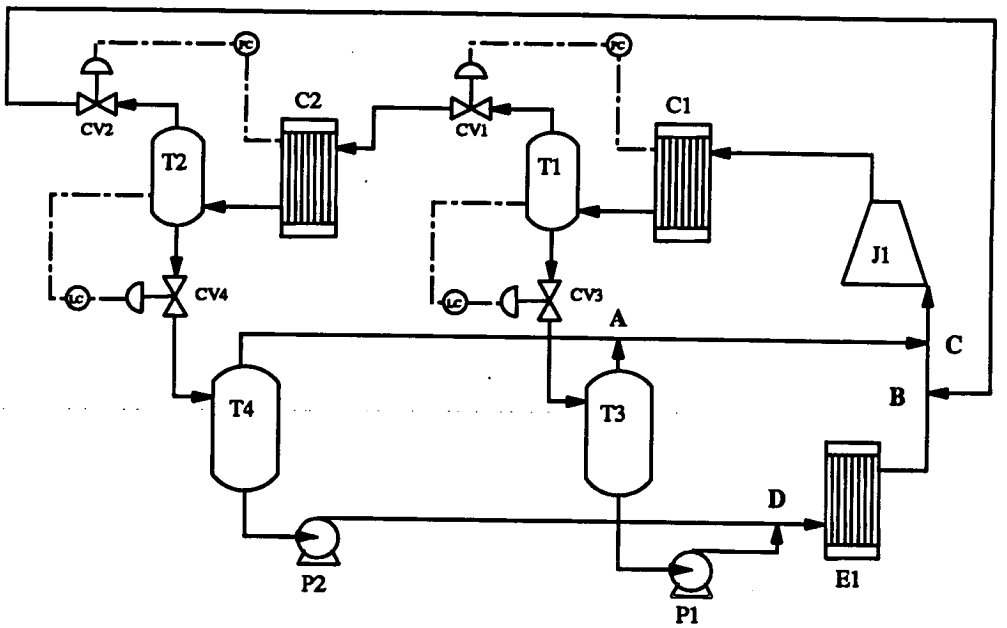

Figure 3.2: Skeleton Flowsheet for Twin-Condenser Heat Pump

The method of calculation used is best described as a list of steps. These were initially performed by hand for the chosen pair of R123a/RC318, using thermodynamic properties predicted by the Cubic Chain-Of-Rotators equation of state for the pure components, with the assumptions of ideal-mixture properties. At a later stage a computer program was written to perform the calculations for the substitute pair of R114/R113, using accurate thermodynamic properties predicted by the Carnahan-Starling-DeSantis equation of state. For further discussion of the prediction of thermodynamic properties by these equations of state, and more full discussion of the programs used in the calculations, see Chapter 6.

Calculation Procedure

1. The basis of calculation was 1 kmol entering the condenser C–1
2. The fixed process parameters were chosen: typical values are given below:
    - C–1 inlet vapour composition: 0.500
    - C–1 dew temperature: 85.0 ° C
    - C–2 dew temperature: 75.0 ° C
    - C–1 split fraction: 0.500
    - C–2 split fraction: 0.050
    - E–1 dew temperature: 25.0 ° C
    - Compression efficiency: 0.700
3. The dew pressure in C–1 was calculated.
4. For the given C–1 split fraction the exit temperature, specific enthalpy change and exit stream compositions were obtained.
5. If the exit temperature from C–1 was lower than or equal to the set dew temperature in C–2, then the pressure of C–2 was taken as that of C–1. Otherwise, the pressure in C–2 was obtained by a dewpoint calculation on the vapour leaving T–1.
6. For the given C–2 split fraction the exit temperature, specific enthalpy change and exit stream compositions were obtained.
7. A pseudostream of the same size and composition as a combination of the two condensate streams was calculated: the evaporator pressure was set by a dewpoint calculation on this pseudostream for the given dew temperature.
8. An adiabatic flash calculation was then peformed on each condensate stream to obtain the temperatures in T–3 and T–4, with the compositions and flows of each stream leaving these vessels.
9. The liquid evaporator feeds were mixed at point D and the specific enthalpy change over the evaporator calculated by heat balance.
10. An adiabatic throttle was calculated for the vapour stream leaving T–2 to the evaporator pressure.
11. The vapour streams were mixed at points A, B and C and the vapour stream feed to the compressor determined.
12. The enthalpy change for adiabatic, reversible compression of this vapour stream was calculated and used in conjunction with the given isentropic efficicency to calculate the shaft work requirement.

13. The Coefficient of Performance and exergetic efficiency for the cycle were calculated.

3.2.2.2 Equations For Thermodynamic Properties of a Mixture

At the time of design, computer programs had been written to calculate the thermodynamic properties of pure fluids using the CCOR equation of state: these had not, however, been extended to mixture property calculation. In order that manual calculation of the heat and mass balance could be performed, simple equations relating the volume, enthalpy and entropy of a mixture to the pure component properties were developed. The following assumptions were made:

- The vapour phase is an ideal mixture of perfect gases, for which:
  - Raoult's Law describes vapour-liquid equilibrium (VLE)
  - There is no volume change of mixing
  - There is no enthalpy change of mixing, and enthalpy is independent of pressure.
  - The entropy change of mixing is $\Delta S = -R\Sigma\, y.\log\, y$
- The vapour density is given by the CCOR equation, with both interaction constants set to zero.
- The liquid phase is an ideal mixture.
- All liquid properties are independent of pressure and may be found using the pure-component liquid properties at the system temperature.

These assumptions lead to the following equations, which were used throughout the heat and mass balance. The use of the CCOR equation is described in detail in Chapter 6.

VLE Relations Raoult's Law was assumed to hold in the following form:

$$P.y = p_1^*.x \tag{3.1}$$

$$P.(1-y) \;=\; p_2^*.(1-x) \qquad (3.1a)$$

where P is the system pressure, y the mol fraction mvc in the vapour, p* the vapour pressure of either component and x the mol fraction in the liquid phase. This was a reasonable assumption since most refrigerant mixtures' deviations from ideality are slight. Rearrangement of Equation 3.2 gives dew pressure from the specified vapour composition:

$$P_{dew} = \frac{p_2^*}{1 + y.\left(\frac{p_2^*}{p_1^*} - 1\right)} \qquad (3.2)$$

The bubblepoint pressure is given by:

$$P_{bubble} = x.p_1^* + (1-x).p_2^* \qquad (3.3)$$

Vapour Heat Capacity This was found for each component using a cubic polynomial in temperature:

$$C_{p_i} = A + B.T + C.T^2 + D.T^3 \qquad (3.4)$$

where C_{p_i} is in kJ/kmolK and T is in K.

Vapour Enthalpy The enthalpy of a pure component at a given temperature T and pressure P is related to its enthalpy at saturation under the same pressure by:

$$H_i(T,P) = H_i(T_{sat},P) + \int_{Tsat}^{T} C_{p_i}^{\circ}\, dT \qquad (3.5)$$

where T_{sat} represents the saturation temperature under the system pressure and $C_{p_i}^{\circ}$ is the perfect-gas heat capacity of pure i.

The difference in enthalpy between saturated vapour at T_{sat} °C and the component enthalpy at T °C is found by integrating Equation 3.4:

$$\begin{aligned} \Delta H &= \int_{T_{sat}}^{T} C_p^{\circ} dT \\ &= A(T - T_{sat}) + \frac{B}{2}(T^2 - T_{sat}^2) + \frac{C}{3}(T^3 - T_{sat}^3) + \frac{D}{4}(T^4 - T_{sat}^4) \end{aligned} \tag{3.6}$$

The enthalpy of the mixed vapour is then given by:

$$H_{mixture} = y.H_1 + (1 - y).H_2 \tag{3.7}$$

where H_1 and H_2 refer to the component enthalpies calculated using Equation 3.5.

Vapour Entropy The entropy of a pure component at a given temperature T and pressure P is related to its entropy at the saturation temperature by:

$$S_i(T, P) = S_i(T_{sat}, P) + \int_{T_{sat}}^{T} \frac{C_{pi}^{\circ}}{T} dT \tag{3.8}$$

The difference in entropy between saturated vapour at T_{sat} °C and the component entropy at T °C is found by integrating Equation 3.8:

$$\begin{aligned} \Delta S &= \int_{T_{sat}}^{T} \frac{C_p^{\circ}}{T} dT \\ &= A \log\left[\frac{T}{T_{sat}}\right] + B(T - T_{sat}) + \frac{C}{2}(T^2 - T_{sat}^2) + \frac{D}{3}(T^3 - T_{sat}^3) \end{aligned} \tag{3.9}$$

The entropy of a mixture is then given by:

$$S_{mixture} = y.S_1 + (1 - y).S_2 - R.(y.\log y + (1 - y).\log(1 - y)) \tag{3.10}$$

Liquid phase properties

$$v_{mixture} = x.v_1 + (1-x).v_2 \quad (3.11)$$

$$H_{mixture} = x.H_1 + (1-x).H_2 \quad (3.12)$$

$$S_{mixture} = x.S_1 + (1-x).S_2 - R.(y.\log y + (1-y).\log(1-y)) \quad (3.13)$$

where the component properties are those of saturated liquid at the system temperature.

3.2.2.3 Sources of Data

The perfect gas heat capacity parameters for each component were calculated using a group-contribution method, described fully in Sinnott [106] and in Chapter 6. The use of the CCOR equation of state requires knowledge of the critical temperature, critical pressure and acentric factor: these were obtained from the Physical Properties Data Service (PPDS) databank for the two components. (This is a commercial, computerised properties database maintained by the Institution of Chemical Engineers, which contains information on many of the CFC fluids.) These data are presented in Table 3.1 and Table 3.2 below. These data were then used to calculate the parameters of the CCOR equation for each component. The equivalent data for R114 and R113 are widely available in the literature (see *e.g.* Sinnott *op. cit.*)

Component	A	B	C	D
R123	-85.717	0.90674	-7.227×10^{-4}	21.143×10^{-8}
RC318	4.5744	0.39064	-3.1814×10^{-4}	8.834×10^{-8}

Table 3.1: Heat Capacity Parameters of R123a and RC318

3.2.2.4 Calculation of Flowsheet Heat and Mass Balance

Rather than bore the gentle reader with pages of arithmetic, only the results of calculation of the heat and mass balance for the simplified flowsheet are given here. It is assumed that the reader understands the basic calculation procedures described in Section 3.2.2.1. The only points worthy of further explanation are described in the following paragraphs.

Component	T_c	P_c	v_c	ω	MW
	K	bar	$m^3/kmol$	–	–
R123	456.3	36.07	0.284	0.285	152.93
RC318	388.5	27.83	0.323	0.352	200.04

Table 3.2: Basic Properties of R123a and RC318

Calculation of VLE Problems In the hand calculation the simplified procedure decribed above was used; in the computer program version the real VLE problem was solved, using fugacity coefficients obtained from the CSD equation of state. As far as design knowledge went the difference in the final answers was negligible; the most important VLE parameters for component design were the maximum vapour pressures to be expected, which were predicted accurately using either method.

Solution of Adiabatic Flash The method chosen in both cases to solve the adiabatic flash problem was one due to Ponton [87], which converges rapidly for mixtures of fluids such as R114/R113 or R123a/RC318. It is suitable for non-iterative hand calculation or may be coded for iterative solution in a program, should higher accuracy be required. In the test calculations performed by the author as part of the debugging process, this method invariably converged to a tolerance of better than 1% on vapour fraction within three iterations.

Specification of parameters The predefined parameters (dewpoints, phase splits, etc.) used in this calculation have the following values:

- **C–1 Dewpoint:** 85 °C
- **C–2 Dewpoint:** 75 °C
- **C–1 Exit Vapour Fraction:** *ca.* 50%
- **C–2 Exit Vapour Fraction:** *ca.* 5%
- **Compressed Vapour mol fraction:** 0.500
- **Evaporator Dewpoint:** *ca.* 20 °C
- **Degree of Condensate Subcooling:** ZERO
- **Degree of Suction Superheat:** ZERO

- **Flash Vapour Returned?** YES
- **Compression Work:** 3 kW

Hand Calculation for R123a/RC318 The results of the calculation for the R123a/RC318 pair are given in Table 3.3, in which the stream numbers correspond to those in Figure 3.2.

Stream	T	P	v	$\dot{m}$	z	h	State
	K	bar	l/kg	kg/s	—	kJ/kg	—
1	372.2	8.17	17.05	0.0687	0.500	235.8	VAPOUR
2	358.2	8.17	16.59	0.0687	0.500	216.8	VAPOUR
3	353.4	8.17	0.738	0.0324	0.373	115.1	LIQUID
4	353.4	8.17	15.82	0.0363	0.621	205.2	VAPOUR
5	350.5	7.23	18.05	0.0363	0.621	205.2	VAPOUR
6	338.7	7.23	0.717	0.0344	0.609	90.1	LIQUID
7	338.7	7.23	15.60	0.0019	0.817	184.0	VAPOUR
8	321.2	1.19	11.17	0.0019	0.817	184.0	VAPOUR
9a	283.2	1.19	0.613	0.0200	0.504	37.3	LIQUID
9b	283.2	1.19	9.70	0.0144	0.765	161.7	VAPOUR
10a	292.5	1.19	0.647	0.0161	0.237	48.0	LIQUID
10b	292.5	1.19	10.73	0.0163	0.518	111.1	VAPOUR
11a	292.5	1.19	0.647	0.0161	0.237	48.0	LIQUID
11b	292.5	1.19	10.73	0.0163	0.518	111.1	VAPOUR
12a	283.2	1.19	0.613	0.0200	0.504	37.3	LIQUID
12b	283.2	1.19	9.70	0.0144	0.765	161.7	VAPOUR
13a	286.6	1.19	0.632	0.0361	0.380	42.1	LIQUID
13b	288.0	1.19	10.25	0.0307	0.630	134.8	VAPOUR
14	295.2	1.19	11.12	0.0668	0.425	191.4	VAPOUR
15	295.9	1.19	10.93	0.0687	0.500	191.2	VAPOUR
16	295.2	1.19	11.12	0.0668	0.425	191.4	VAPOUR

Table 3.3: Heat and Mass Balance for R123a/RC318

Comments on Table 3.3 The important points to pick up from Table 3.3 are as follows:

- The consequence of operating with both storage vessels connected to the evaporator and compressor suction, in conjunction with no subcooling, is that roughly 44% of the working fluid is not vapourised in the evaporator but is flashed directly to the suction. This means that much of the more volatile will remain in circulation, and that the cycle efficiency will suffer.

- The heat pump will not be a good choice in this configuration for a twin-duty heat pump-chiller.
- The consequence of nearly equal condensate loadings in each condenser is that the heat duties are nearly equal, representing the optimum duty split for conservation of availability, providing the load stream is matched to the gliding temperature profile.
- The COP to be expected is 3.0

3.3 Development of Plant from Flowsheet

This section briefly explains the function of each of the additions to the basic flowsheet which were made: the relevant design details and dimensions are quoted in the following Section.

3.3.1 Condensate Receivers

These were necessary for several reasons:

- To separate condensate from vapour and so prevent transfer of liquid between the condensers.
- To provide a vessel in which a vapour-liquid equilibrium could be assumed: this was needed to give an estimate of the composition of refrigerant.
- To provide a few minutes holdup of liquid before the throttle down into the glass storage, acting as a safety measure against pressure letdown into these fragile vessels.

3.3.2 Condensate Subcoolers

The use of subcooling as a means of cycle enhancement in compression cycle heat pumps is well-known; however the subcoolers in this design were not principally intended as such a modification. Their function was to enable the analysis of the effect of subcooling on the efficiency of composition shift within the cycle, and so they were specified as externally-cooled devices, which could be regulated by the external cold sink without affecting the rest of the refrigerant circuit. An added benefit of these devices was that they would result in a low flash vapour production rate and thus reduce the size of any cooling equipment required in the storage tanks.

3.3.3 Evaporator and Liquid Injection Line

The evaporator feed line was specified as a union of two lines, one from each storage tank. In addition, the pipework was laid out with a line from the heavy pump outlet through a hand valve to the heavy condenser inlet. The reason for this was to enable pumping of heavy liquid to the condenser, where it would act as an absorbent stream. This type of cycle modification has been used with some success (see Chapter 2): it was decided to make provision for this, although it would not be used in the initial experimental programme.

3.3.4 Refrigerant Charging Pipework

The plant had to be equipped with a means of transferring refrigerant to and from the storage, so pipework and valvegear were added to enable this. The heavy storage tank was fitted with plumbing to enable pumping of liquid into the tank, while the light tank was equipped with both liquid and vapour connections, as the pure more volatile would be supplied in a gas bottle.

3.3.5 Water Heat Interchanger

In order to reduce the total energy requirement of the plant under full load, it was decided to transfer heat between the source and sink streams. The effect of this would be to reduce the amount of energy supplied to the heat source header tank: under ideal operating conditions there would in fact be no need to supply any heat to the system. A heat exchanger was therefore added to the flowsheet, the hot fluid being the total sink stream and the cold fluid a stream of water from the source circuit.

3.3.6 Vapour-Liquid Separator

This modification was installed after the initial commisioning period, when it had been found that the evaporator had a tendency to flood. This in turn led to the admission of a two-phase mixture to the compressor, which caused problems of oil carryover. A vapour-liquid separator on the evaporator outlet was required to remedy this problem.

3.3.7 Suction Gas Superheater

This modification was also made as a consequence of commissioning experience. The problem of oil carryover was severe, and after consultation with Rotocold technical staff it was realised that between 15–20° of suction gas superheat were required. A heat exchanger was placed between the vapour-liquid separator and the compressor to accomplish this duty: the heat was supplied from the heat sink stream after its exit from the condenser C-1.

3.4 Equipment Specification and Selection

3.4.1 Compressor and Ancillary Fittings

Requirements The compressor was the first main plant item to be sized and the most important; its capacity and operating range would determine the specification for all other plant items. The requirements used in the process of compressor selection were: compatibility with refrigerant fluids; ability to produce pressure ratios in the range 5:1 to 6:1 (these being the anticipated ranges of pressure ratio for the duty and working fluid chosen); suitability for high temperature use; ability to vary the compressor shaft speed (and hence work input), and reasonable cost. Two options were open:

(a) Use of a centrifugal compressor, driven by an air turbine: such a unit was available from the Research wing of the French company Elf, where it was being used in heat pump studies.

(b) Purchase of a conventional refrigeration compressor, with specification suitably robust to withstand temperatures of 100 °C or more at the discharge.

Both options had their merits and demerits: the centrifugal turbine was however in many ways the more attractive. It offered oil-free compression, coupled with an inexpensive final control element (an air throttle valve): a refrigeration compressor would be a positive-displacement machine, requiring lubricating oil pipework and an expensive electronic variable-speed drive unit. The use of an oil circuit was undesirable because of the potential effect of such a non-volatile absorbent on the VLE of the working fluid: presence of oil would affect separation of the components and render difficult the calculation of mixture compositions. Nonetheless, it was eventually decided to purchase a refigeration compressor, for the following reasons:

- The air turbine drive for the centrifugal compressor required a large throughput of clean, dry air from a buffered supply: the Chemical Engineering Department's air supply could not meet the demand specified in Elf's performance data sheets. A suitable supply was available in the Department of Mechanical Engineering but was being used: this would cause problems of scheduling.

- The Elf performance data indicated that, using ambient-temperature air as the feed to the turbine would result in an exit stream whose temperature was ca. -57 °C: this would require to be safely vented to atmosphere. A large air heater on the outlet would almost certainly be required to prevent extensive icing round the vent pipe.
- The timescale for delivery and proposed price of the Elf plant were not favourable.

Compressor The compressor chosen for use in the plant was a model manufactured by Rotocold Limited, a British manufacturer. This was selected after discussion with representatives of the Electricity Council Research Centre, who had experience of such units in heat pump installations. Rotocold compressors are rotary, sliding-vane designs: this was advantageous, as such designs can tolerate wet compression. Liquid injection to the suction would therefore be possible as a means of improving the isentropic compression efficiency. After consultation with Rotocold, a model R3 'HIVI' unit with 3.7 kW, 3-phase (415V, 50 Hz) electric motor drive was selected. The nominal throughput of this unit was 12.6 m^3/hr at 1500 rpm, over a design pressure ratio of 5.5:1, with a maximum shaft work rating of 3.3 kW. On the advice of Rotocold, an IMO Jaguar electronic variable-speed drive, whose principle of operation was modulation of the drive current frequency, was purchased to drive the compressor. This could supply drive currents in the range 0–100 Hz, giving a nominal maximum displacement of 25+ m^3/hr.

Oil circuit After further consultation with ECRC and with Mobil sales staff, Mobil Gargoyle Arctic 224 synthetic hydrocarbon lubricating oil was selected for use with the proposed fluid mixture of R114/R113. In order to prevent soakout of the oil, a high-efficiency, coalescing oil separator was purchased with the compressor. The compressor and separator were supplied on a common mounting by Rotocold. In accordance with the piping diagrams supplied in the Installation Manual, the separator was plumbed to the compressor with two oil return lines: the primary return from the base of the separator to the oil port on the compressor case, and a secondary return from the top of the separator to the compressor suction. Each line was fitted with a sight glass and check valves: in addition an oil filter strainer unit was put in the primary return. The valves and fittings used were supplied by Messrs Dean & Wood of Glasgow, and were manufactured by Danfoss for use in refrigeration applications.

Other hardware It was necessary to put a non-return valve in either the discharge or suction lines, to prevent the compressor reverse-rotating, with consequent pressure blowdown from discharge to suction side, on shutdown. As the use of inexpensive Danfoss NRVs was confined to temperatures less than 60 °C, the valve, a Danfoss 15mm bore right-angle NRV, was placed in the suction line. The nominal pressure drop caused by this valve of 0.07 bar was deemed acceptable. A suction gas filter was also necessary: this was placed in the suction line immediately before the NRV. The filter chosen, on recommendation from Messrs Dean & Wood, was a separate case/cartridge type, the cartridge being manufactured by Mueller. To permit easy charging of refrigerant and oil directly into the circuit (rather than into the storage), a Yellow Jacket charging manifold was plumbed into the compressor manifold. (The compressor was fitted with service ports and valves.) This unit, ready fitted with pressure gauges and isolation valves on either side of the manifold, was equipped with a $\frac{1}{4}$" NPT connection to the external world, enabling either charge to the suction or purge from the discharge side. A Mueller pressure relief valve, set to blow at 350 psig, was plumbed into the discharge after the oil separator and vented to outside the building *via* the common plant vent line. This valve could easily handle the full throughput of the compressor at the discharge pressure and was selected from the Dean & Wood catalogue.

Trips and Controls A Danfoss combined high pressure-low pressure trip switch was plumbed in, to protect the compressor from overpressure. The high pressure switch was set to trip at 24 barg, which was the maximum recommended working pressure of the unit. The low pressure trip was connected but disabled, as it was designed to trip should the suction pressure fall below a set value; this was not a problem for the proposed modes of operation. A Danfoss high-temperature trip was also fitted to the compressor discharge, set to trip at 120 °C, *i.e.* 5° below the maximum permissible working temperature specified in the Rotocold manual. These cutout devices were wired into the Jaguar control box as recommended by the manufacturers' literature.

3.4.2 Condensers

The original intention was to design and build the condensers in the department; after performing some rough calculations, however, it was decided to use a proprietary design of heat exchanger. It became apparent that the design of a compact unit capable of performing the required duty under pressures of up to 24 barg would not be

straightforward, indeed would be less cost-effective than a purchase of a proven commercial design. Messrs Alfa-Laval were consulted: they recommended the use of their Type CBH25 brazed-steel plate heat exchangers. This type of unit would offer high heat transfer coefficients with adequate mechanical strength. The condensers were subsequently purchased from Alfa-Laval, who were asked to supply units capable of meeting the specification shown in Table 3.4. As accurate transport property data on R123/RC318 mixtures were not available, a mixture of R114/R11 was specified but in all other respects the duties corresponded to the original flowsheet. The specified water flowrate through the condensers was 332 kg/hr, entering the lights condenser (C-2) at 60 °C, leaving C-2 at 70 °C and leaving C-1 at 80 °C.

Unit	Feed Rate	Condensate Rate	Feed Temperature	Exit Temperature
	kg/hr	kg/hr	°C	°C
C-1	247	130	99.0	80.4
C-2	117	111	77.4	67.7

Table 3.4: Final Condenser Specifications.

3.4.3 Condensate Receivers

These were designed by the author and built in the Department workshop. The receivers were sized on a basis of a holdup of approximately 2 minutes at design condensate rate: this would give adequate time to shut down in the case of failure of the control system. The condensate rate for each unit was to be 110–130 kg/hr, so a holdup of 4 kg was used: the density of the proposed liquids was roughly 1400 kg/m^3, giving a total volume of *ca.* 1.5 litres per pot. The separation pot would not normally be more than half full, so a capacity of at least 3 litres would be required. The final size chosen was in fact rather greater than this. The reason for the use of a larger vessel arose from the method of level measurement used in the level control loop: a long, thin pot gave a larger differential head between the inlet and outlet of the unit.(See Section 3.5 for explanation of the control loop.) The internal diameter was chosen using the criteria given in Sinnott [106] for the dimensions of a vapour-liquid separation device: 3 inches was an appropriate standard pipe size close to the calculated optimum diameter. The body of each unit was made from a length of steel pipe, wall thickness $\frac{1}{4}$", with threaded steel endcaps of similar thickness. The inlet was through a 1" BSP female connection, welded into the side of the pipe. Liquid outlet was through a $\frac{1}{2}$" bore line. The vapour outlet from each receiver was the same diameter as the liquid outlet and was situated in the top centre of the pot. The top was also penetrated to permit insertion of a thermocouple pocket, *via* a $\frac{1}{4}$" BSP plug, and a pressure transducer *via* a $\frac{1}{2}$" BSP

connection. The differential pressure transducer for level measurement was connected as shown, *via* $\frac{1}{4}$" BSP tappings at the top and bottom of the vessel.

3.4.4 Storage Tanks

The storage tanks were made from QVF glassware: this permitted observation of the rates of condensate accumulation. The use of glass would also permit rapid detection of refrigerant contamination, whether by water, lubricating oil or solid detritus. The use of glass imposed a maximum pressure restriction on this part of the plant; this was not felt to be a limitation for the proposed working fluids of R113, R114, RC318 and R123a. The two tanks were of identical design: the body was a 1 metre length of standard QVF pipe, nominal bore 4". QVF domed ends with a single neck were used to make bottom pieces for the vessels, while flat metal flanges were used to form the tops of the tanks. The metal used was dural alloy. The joints between the glassware and endpieces were sealed using standard QVF integral 'O'-ring gaskets, made from PTFE. The joints were secured using QVF tension bolts and sprung washers; this method of fastening gave a good seal without any risk of over-stressing the glass.

The capacity of each tank was estimated to be 8.5 litres: as the maximum dosing flow was 100 l/hr, this gave a holding time of approximately 6 minutes at maximum throughput.

The headplate of each tank was fitted with the following:

1. Throttled refrigerant inlet: $\frac{3}{4}$" BSP connector
2. Flash vapour outlet: $\frac{3}{4}$" BSP connector
3. Inlet and outlet for C/W coil: $\frac{1}{4}$" BSP connectors
4. Thermocouple pocket, in a $\frac{1}{4}$" BSP nipple.
5. Pressure gauge, mounted through a $\frac{1}{8}$" BSP fitting

The vapour outlet lines were used, not only to return vapour to the compressor suction

but also to mount pressure transducers and pressure relief valves. The relief valves used were brass-bodied Hattersley SG322 models: the original brass seats were replaced with machined PTFE seats, made in the department. This was necessary to give a good gas-tight seal. Both relief valves vented *via* $\frac{1}{2}$" copper pipe to a common vent, led outside the building. Liquid takeoff was from the 1" outlet on the domed base, *via* a brass flange and reducer to a $\frac{1}{2}$" copper line. Each tank was fitted with 2mm square steel mesh cages, as a safety precaution: the cages were stiffened with dural battens and bolted to the main frame of the plant.

The cooling coils in the tanks were sized to condense residual flash vapour, assuming that subcooling would be in effect for normal operation. The physical dimension of each coil was: 3" coil diameter, pipe size 9mm OD, 7.5mm ID. This pipe size was chosen to ease the task of bending it to shape.

The design specification for the coil was: 0.04 kg/s R114 (full design flow for one half of the plant), entering the throttle at 35 °C and flashing to saturation conditions at 25 °C. Cooling water was to be taken at a flow of 1 litre/minute (the required cold water makeup rate for the hot tank) and at a temperature of 15 °C. The data on R114 in Perry [82] were used to calculate the duty and the heat transfer coefficient of the condensing vapour. The duty was found to be 0.4 kW; the flash caused 8% of the incoming R114 (0.0032 kg/s) to vapourise.

The number of turns was found by trial and error: a number of coils was picked, the refrigerant heat transfer coefficient was calculated and the area required to perform the duty with the resulting overall heat transfer coefficient was compared with the actual area of that size of coil. The heat transfer coefficients for condensing refrigerant were calculated from the correlations given in Kern [44]. The heat transfer coefficient on the water side was found from the Sieder-Tate relation, with the MacAdams modification for coil flow, which is given in Perry, Section 10. The final size chosen was 5 turns per coil, with a length of connecting pipe equivalent to about one turn connecting the coil to the head flange.

3.4.5 Metering Pump Selection

The feed to the evaporator was to be supplied by a metering pump, for two reasons. Firstly, it was important for analysis of the final results that both the total feed and the composition of the evaporator feed be quantified; use of a high-precision pump should enable accurate feed rates from each tank to be specified and delivered. Secondly, it was desired to run the plant as a hybrid compression/absorption unit, with a solution circuit to permit the pumping of involatile refrigerant liquid to the condenser pressure as an absorbent stream. This was to be accomplished by direct pumping from the heavy storage tank with the evaporator feed pump, and so it was necessary to use a device capable of delivering a low flow to a pressure of up to *ca.* 10 bar or so. A reciprocating-action metering pump would be far better suited to this than other, less costly options.

The unit chosen was manufactured by MPL Ltd. The pump was purchased in three sections: the pumpheads, type SS-40C, rated at 100 litre/hr nominal discharge into a 7 bara delivery pressure; the pump itself, fitted with a 240v, 50Hz a.c. fixed-speed electric motor, geared to operate at 96 strokes per minute, and a pair of electrically-driven stroke positioners. The stroke positioners required a 240 V mains supply; this was taken from the drive motor supply. The control circuitry required to drive the pump was designed and built by Matthew Rea, and is described in Section 3.5.

Installation of the pump was straightforward: the only special requirement was the fitting of shut-off valves on the suction lines and loading valves on the discharge from each pumphead. The loading valves were required to ensure that the pump would always be working against a positive discharge head, regardless of downstream pressure. This would then enable metered delivery irrespective of the operating state of the evaporator.

3.4.6 Evaporator Design

The process specificaation required an evaporator capable of producing the full refrigerant flowrate as vapour, from a heat source of water at *ca.* 30 °C, with an approach of 5 °. The construction of an evaporator from smooth tubes was not favoured, as the

refrigerant side film heat transfer coefficients would not be large: as a consequence the required heat transfer area would be incompatible with the required flowrates. The design flow of 0.08 kg/s refrigerant meant that liquid phase Reynolds numbers in the evaporator would be in the laminar-transition reason for most pipe sizes compatible with the equivalent vapour flow. The effect of this would be to render the prediction of the refrigerant heat transfer coefficient subject to great uncertainty. The conclusion drawn was that some combination of extended and/or enhanced heat transfer surface would be required in order to meet the design specification.

A possible material was the "Hi-Flux" tubing, produced by Union Carbide. This special tubing, layered with sintered metal to provide a greatly increased number of nucleation sites, was reported to give excellent boiling heat transfer coefficients. A major drawback was the difficulty in obtaining the tubing, or design data pertaining to it, as it was not then manufactured in the U.K. The use of "Hi-Flux" was ruled out for these reasons.

Another option became available after discussion with representatives of Cal-Gavin Ltd. This Birmingham-based company specialises in enhanced heat transfer materials and equipment, and were already involved in research projects in the Department. An agreement was reached, whereby Cal-Gavin would design and build a prototype film evaporator, to be supplied to the project for no charge. In return it was agreed that they would be given an analysis of the performance of the unit, operating both with pure fluids and with mixtures. This was an agreeable arrangement for all parties. The internal structure of the evaporator is not discussed in this thesis, for obvious reasons of commercial discretion. It may be broadly described as a combination of extended and enhanced heat transfer material, with an extremely high exposed area (in the region of 50 times the equivalent plain-tube area).

The external structure of the Cal-Gavin evaporator is shown in schematic form in Figure 3.3. It has three 'shells', with liquid refrigerant fed in parallel to the base of these shells and vapour taken off into a common manifold. The heat source is pumped through the tube side in one pass: thus if the source enters at the top there are two counter-current and one co-current passes. The tube side pipes were fitted with Cal-Gavin's standard-mesh "Heatex" turbulence promotion inserts. This is reckoned to give an enhancement factor of *ca.* 2.0 to the tube side heat transfer coefficient, at the expense of a correspondingly increased pressure drop. As the manufacturers felt that there was more than enough heat transfer surface, a valve was provided to shut off one of the shells. It is possible to derive an effective temperature difference for this geometry, after the methods outlined by Kern [44]. In practice, the performance of the unit as a combined evaporator/superheater would make calculation of an overall

heat transfer coefficient difficult, though not impossible. It would be simpler to report values of heat transfer product ($UA = Q/\Delta T_{LM}$), as opposed to pure heat transfer coefficients.

The evaporator was mounted vertically, with 1/2" liquid feed lines. The initial vapour take-off was into 22mm Kuterlite tubing (ID 20mm); this was increased to 28mm Kuterlite (ID 25.5mm) with soldered connections, to improve the seals and to reduce vapour velocities. The tube side connections were made to standard 22mm Kuterlite. Thermocouples were fitted to all of the points indicated on Figure 3.3, although only the four thermocouples on the inlets and outlets were returned to the computer. (The remaining thermocouples could be read using a "Comark" electronic thermometer.

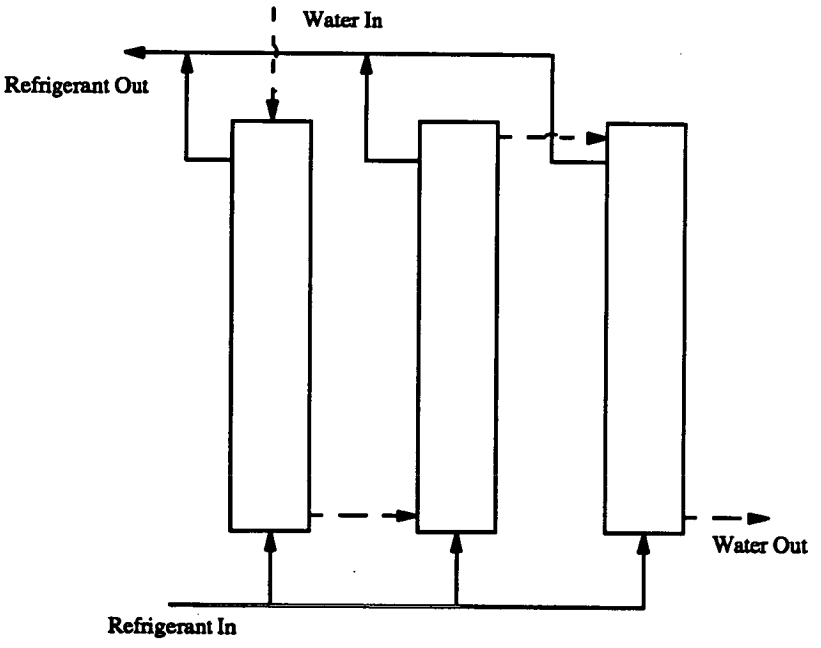

Figure 3.3: Cal-Gavin Evaporator Schematic

3.4.7 Ancillary Pipework

The liquid pipework around the base of the tanks and the metering pump has already been discussed: it remains to point out that there are several "spurs" of pipework on the plant, intended chiefly as charging and take-off points for refrigerant and/or oil. There is also the pipework which accepts the vents from the three relief valves fitted to the system. This pipe, 15mm bore, leads by the shortest route to the external wall of the laboratory, at some 7 feet above ground level. This is a safe discharge, given the nature of the inventory.

3.4.8 Subcoolers

The purpose of the subcoolers was twofold: first, to enable study of the effect of flash vapour return on the degree of separation; and second, to reduce the load on the storage tank cooling coils. The subcoolers were designed and built in the Department, as the size and duty of the units was not large.

The design chosen was a double-pipe, "trombone" arrangement, with the refrigerant liquid on the tube side. This was desirable, as it made design of a unit to the maximum possible condenser pressure very much more straightforward. The cooling source was water from the mains, flowing through with no regulation from the plant operating system. The liquids were to flow in a counter-current arrangement. Cal-Gavin "Heatex" turbulence promoters were placed in the refrigerant tubes to compensate for the poor heat transfer properties of liquid refrigerants. The likely effect of these promoters was assessed by analysis of the results obtained by undergraduates in experimental studies of the effect of "Heatex" on measured heat transfer coefficients of a water/glycol system. It was found that the film heat transfer coefficient obtained in pipes fitted with Heatex would be approximately 2.5 times that predicted by the usual heat transfer correlations (*e.g.* the Sieder-Tate relation).

The physical dimension of the unit were: Tube side to be $\frac{3}{8}$" copper refrigeration pipe (actual dimension 9.5mm ID, 11mm OD). The jacket of the exchanger was chosen to be "Kuterlite" copper water pipe, nominal size $\frac{3}{4}$". This has actual dimensions of 17.5mm ID, 19.0mm OD.

The two subcoolers were identical in construction and were sized on the following basis: cooling of half the design flow, from 75 °C to 25 °C. Assuming the feed is R114 simplifies the calculation and does not result in a significant error in sizing, as the heat capacity of similar to that of either R113 or the RC318/R123 mixture. The water flowrate was taken as 12.0 l/min: this flow would not in fact be metered or controlled in any way but bench tests with bucket and stopwatch indicated that the mains could deliver this flow. In any event, the controlling resistance to heat transfer would be the refrigerant film heat transfer coefficient, so the size of water coefficient would not be very important here.

Heat Duty The heat duty was:

$$\begin{aligned} \dot{Q} &= \dot{m}_R \times C_p \times \Delta T \\ &= 0.04 \times 1.0 \times 50.0 \\ &= 2.0\text{kW} \end{aligned} \tag{3.14}$$

(3.15)

where the mean heat capacity of R114 is 1.0 kJ/kgK (Perry).

The physical properties used were taken from Perry [82] and are as follows:

Fluid	ρ	μ	C_p	k	Pr
	kg/m^3	kg/m s	kJ/kg K	W/m K	-
Water	1000	0.0009	4.18	0.611	6.16
R114	1385	0.00027	1.06	0.059	4.84

Table 3.5: Transport Properties of Water and R114

Refrigerant Side HTC The Reynolds Number Re for the refrigerant was given by the relation

$$Re = \frac{4\,\dot{m}_R}{\pi\,\mu\,d_i} \tag{3.16}$$

where d_i represented the inner diameter of the central tube. Thus,

$$\begin{aligned} Re &= \frac{4 \times 0.04}{3.142 \times 2.69 \times 10^{-4} \times 0.0095} \\ &= \underline{19900} \end{aligned}$$

(3.17)

The well-known Sieder–Tate relation, Equation 3.18 was applicable to this flow regime, giving the Nusselt Number Nu in terms of the Reynolds Number Re and the Prandtl Number Pr:

$$\begin{aligned} Nu &= 0.023 \times Re^{0.8} \times Pr^{0.33} \\ &= 0.023 \times \left(19900^{0.8}\right) \times \left(4.84^{0.33}\right) \\ &= \underline{107.1} \end{aligned} \tag{3.18}$$

The actual Nusselt number obtained by using the Heatex turbulence promoter was 2.5

times this figure, giving Nu = 267.8. The refrigerant film heat transfer coefficient was therefore:

$$h_R = Nu \times (k/d_i) = 267.8 \times (0.059/0.0095) = 1660 \text{ W/m}^2 \text{ K} \tag{3.19}$$

Water Side HTC The water flows through a non-circular duct, so the equivalent hydraulic diameter d_e of the duct was used. In this case,

$$d_e = D_i - d_o = 17.5 - 11 = 6.5 \text{ mm} \tag{3.20}$$

Without repeating the relations stated in the previous paragraph, it may be shown that this gave a water-side film heat transfer coefficient $h_W = 6250 \text{ W/m}^2\text{K}$.

Overall Heat Transfer Coefficient Allowing a small fouling heat transfer coefficient $h_F = 5000 \text{ W/m}^2\text{K}$, the overall heat transfer coefficient U was given by:

$$\frac{1}{U} = \frac{1}{h_R} + \frac{1}{h_W} + \frac{1}{h_F} \tag{3.21}$$

This gave an overall heat transfer coefficient $U = 1040 \text{ W/m}^2\text{K}$.

Sizing of the Unit The final size of exchanger to use was now be found, using the heat transfer relation:

$$\dot{Q} = UA\Delta T_{LM} \tag{3.22}$$

It was found that an active length of 1.6–2.0 metres would suffice: accordingly the final length chosen was 1.8 metres, in two equal sections.

3.4.9 Vapour-Liquid Separator

This was made from available QVF glassware in the department store: a 6" bore section, two feet long, with corresponding domed base, formed the body of the unit. The top of the unit was a brass flange, $\frac{3}{8}$" thick. Feed to the unit was through a side-arm, 3" in diameter reducing to a 25mm pipe. The liquid return line was $\frac{3}{8}$" copper tube, while the vapour takeoff was 22mm OD copper tube.

The maximum safe working pressure of this type of glassware is 25 psig (from the QVF specification); the properties of saturated R114 vapour under this pressure were used to check the suitability of the design under maximum design throughput.

From Sinnott [106], a simple V/L separator should have one vessel diameter at least of disengagement space above the liquid level. In order to achieve good separation, the vapour velocity in the vessel should not exceed the velocity given by:

$$v_{max} = 0.035\sqrt{\rho_L/\rho_V} \tag{3.23}$$

A pressure of 25 psig corresponds to a boiling temperature of 32.5 °C for R114; at these conditions the densities of liquid and of vapour are 1430 and 19.8 kg/m^3 respectively. Thus:

$$v_{max} = 0.035 \times \sqrt{1430/19.8} = \underline{0.30 \text{ m/s}} \tag{3.24}$$

The maximum mass flow of refrigerant was taken as 0.09 kg/s, in accordance with the calculations on the vapour superheater, which are detailed below. This gave a vapour velocity in the 6" section of 0.25 m/s.

3.4.10 Vapour Superheater

This was designed as a straight double-pipe heat exchanger, with the fluids in true counter-flow, water on the shell side and refrigerant vapour on the tube side. The design flowrates were taken as 90% of the maximum possible flows on each side of the unit: the nominal displacement of the compressor was 25 m^3/hr, the measured maximum throughput of the water pump was 9 litre/min. Pipe sizes were chosen from the "Kuterlite" range of copper piping: inner tube 22mm OD, 19.5mm ID; outer pipe 28mm OD, 25.5mm ID. This combination would lead to quite high pressure drop on the water side but this was not envisaged as a problem.

The thermal requirement was to provide at least 15° of superheat to the vapour, which would enter as saturated vapour at 25°C. The water supplying the heat would be the hot water stream leaving the condensers, at a temperature of at least 80°C. The use of this stream as a heat source would provide a large driving force to compensate for the anticipated low heat transfer coefficient on the refrigerant side of the exchanger. In this case it was decided *not* to use Heatex turbulence promoter inserts, as this would cause unwanted pressure drop between the evaporator and compressor.

The physical properties of R114 vapour may be found in Perry: the vapour pressure of R114 is 2.13 bar at 25°C. Under this pressure, the change in vapour enthalpy between 25°C and 40°C is 11.6 kJ/kg. The mean vapour density over this range of temperature is 15.2 kg/m^3 and the change in density with temperature is less than 8%, so that for design purposes the density may be taken as constant.

Flowrates and Velocities The refrigerant volumetric flowrate is $0.9 \times 25/3600 = 0.00625 m^3/s$. Using the average density given above, this gives a refrigerant mass flowrate:

$$\dot{m}_R = \dot{V}_R \times \rho_R = 0.00625 \times \ 15.2 = \underline{0.095} \text{ kg/s} \tag{3.25}$$

The water flowrate is:

$$\dot{m}_W = 0.9 \times 9/60 = \underline{0.135} \text{ kg/s} \tag{3.26}$$

For the pipe sizes given above, the corresponding velocities v are:

$$\begin{aligned} v_R &= \underline{20.9}\ \text{m/s} \\ v_W &= \underline{1.15}\ \text{m/s} \end{aligned} \tag{3.27}$$

The physical properties of the fluids are contained in the following table:

Fluid	ρ	μ	C_p	k	Pr
	kg/m^3	kg/m s	kJ/kg K	W/m K	–
Water	1000	3.65E-4	4.18	0.668	2.29
R114	15.2	1.2E-5	0.77	0.0112	0.83

Table 3.6: Transport Properties of Water and R114 in Superheater

Heat Transfer Coefficients The Sieder-Tate relation, Equation 3.18 in the form applicable to plain tubes, was used to obtain film heat transfer coefficients for water and refrigerant sides. The calculations have been illustrated in previous paragraphs; only the results, and the property data used, have been presented here.

Refrigerant HTC:

$$h_R = \underline{460}\ \text{W/m}^2\,\text{K} \tag{3.28}$$

Water HTC:

$$h_W = \underline{9900}\ \text{W/m}^2\,\text{K} \tag{3.29}$$

The presence of fouling on both sides of the exchanger was assumed to allow for any possible contamination by lubricant oil or corrosion products. Sinnott was consulted and fouling coefficients of 4000 W/m^{2}K on the water side, 2500 W/m^{2}K on the refrigerant side were chosen. The overall heat transfer coefficient was then found by the usual method of summing resistances (neglecting the conductive resistance of the pipe wall).

$$U_{sh} = \underline{340}\ \text{W/m}^2\,\text{K} \tag{3.30}$$

Exchanger Sizing The actual heat duty of this unit is found from:

$$\dot{Q} = \dot{m}_R \times \Delta h_R = 0.095 \times 11.6 = \underline{1.1}\ \text{kW} \tag{3.31}$$

The corresponding water temperature drop by heat balance is 2°. This gives a log-mean temperature differenece $\Delta T_{LM} = 46.2°$. The required heat transfer area is then found to be:

$$A_{sh} = \frac{Q_{sh}}{U_{sh}\Delta T_{LM}} = \frac{1100}{340 \times 46.2} = \underline{0.07}\ \text{m}^2 \tag{3.32}$$

The length of pipe required was found by assuming the area to be approximately that of the outer surface of the central tube. With the dimensions quoted above, this gave a required length of 1.0 m. This was considered acceptable. Further, although the calculations are not repeated here, it may be shown that the performance of the superheater is not significantly affected by reductions in either flowrate. (The water side film resistance is negligible, and the load drops proportionately more than the heat transfer coefficient on the vapour side.)

Pressure Drop The pressure drop through the exchanger was only of interest on the refrigerant side: it would be easy to substitute a more powerful water pump to overcome the added flow resistance presented by the superheater in the hot water circuit. The refrigerant side pressure drop was calculated by use of the friction factor f, which is defined in Perry in terms of Reynolds Number for incompressible flows by the relation

$$1/\sqrt{f} = 3.60 \log(Re/7) \tag{3.33}$$

The pressure drop per unit length of pipe was then found from the relation:

$$\frac{\Delta P}{L} = \frac{4\rho f v^2}{2d} \tag{3.34}$$

The pressure drop calculated from the information in previous paragraphs was $\Delta P/L$ = 2220 Pa/m, which was sufficiently low to rule out use of a larger internal diameter of refrigerant pipe.

3.4.11 Final Flowsheet

The experimental plant underwent considerable modification in its transition from the skeleton flowsheet of Figure 3.2 to the final, operational plant used by the author. In

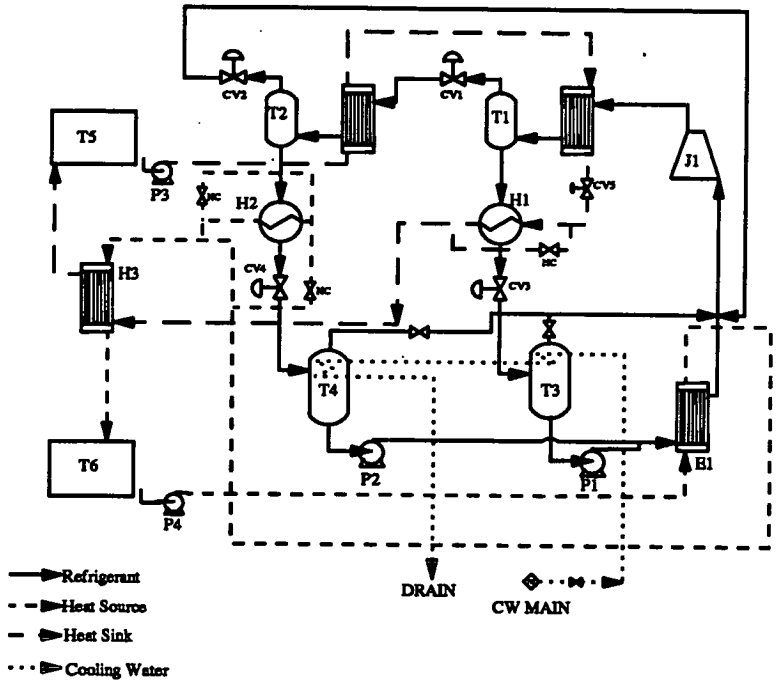

Figure 3.4: First Operational Flowsheet (May 1990)

order to clarify the different modifications, the three operational equipment configurations are sketched as schematic flowsheets in Figure 3.4, Figure 3.5 and Figure 3.6. In all of these diagrams the lubricant oil pipework is omitted for reasons of clarity.

Figure 3.4 depicts the pilot plant as it was in the first experimental work. The notable points are the absence of any phase separation facility on the outlet of the evaporator, and the lack of a suction gas superheater.

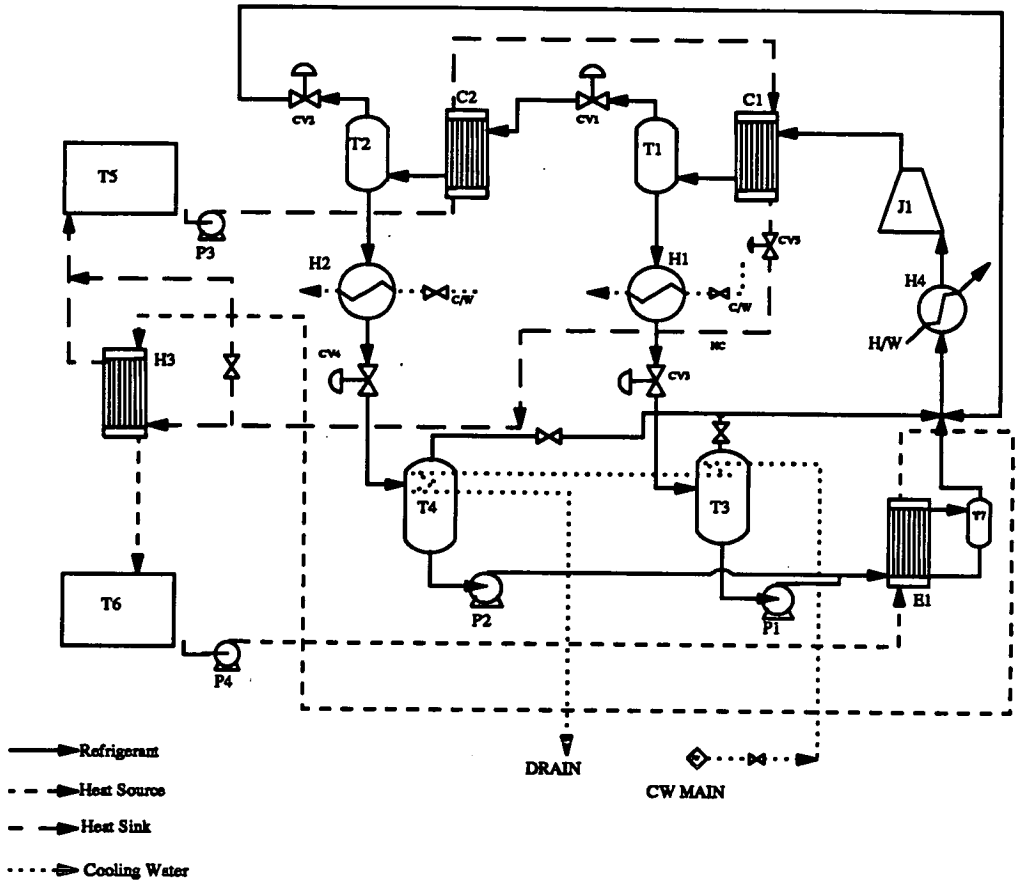

Figure 3.5: Second Operational Flowsheet (June-July 1990)

Figure 3.5 shows the effects of the first major rebuild. A vapour-liquid separator and gas superheater have been added to the suction pipework.

Figure 3.6 shows the final version of the pilot plant flowsheet. This is actually a piping and instrumentation (P&I) diagram; it shows the locations of each thermocouple, pressure transducer and other instrument located on the apparatus. These are identified in Appendix D. In this diagram, all the remaining modifications carried out to the plant are incorporated together. The important details are:

1. Elimination of the suction side pressure drop by bypassing of the suction filter and redesign of the suction pipework.
2. Alteration of the evaporator water flow configuration from a series-parallel to a parallel configuration. The new configuration used parallel, co-current flow of water and evaporating refrigerant.
3. Total separation of the auxiliary cold water supplies to the subcoolers from the heat source and heat sink streams.

3.5 Instrumentation & Control

3.5.1 Requirements

In the earlier stages of the design, the P & I diagram for the pilot plant was established: this set out requirements to be met by the instrumentation. It was necessary to base this system around a microcomputer, as the complexity of the plant would mean too great a quantity of data to be logged well by one operator. The essential requirements of the instrumentation were as follows:

1. Monitor and control the process variables specified in the flowsheet, scanning the instruments at a rate adequate for automatic control.
2. Take preventive action should an excursion of process conditions from the regions of required or safe operation occur. (*e.g.* in the event of an over-pressure in a glass vessel.)

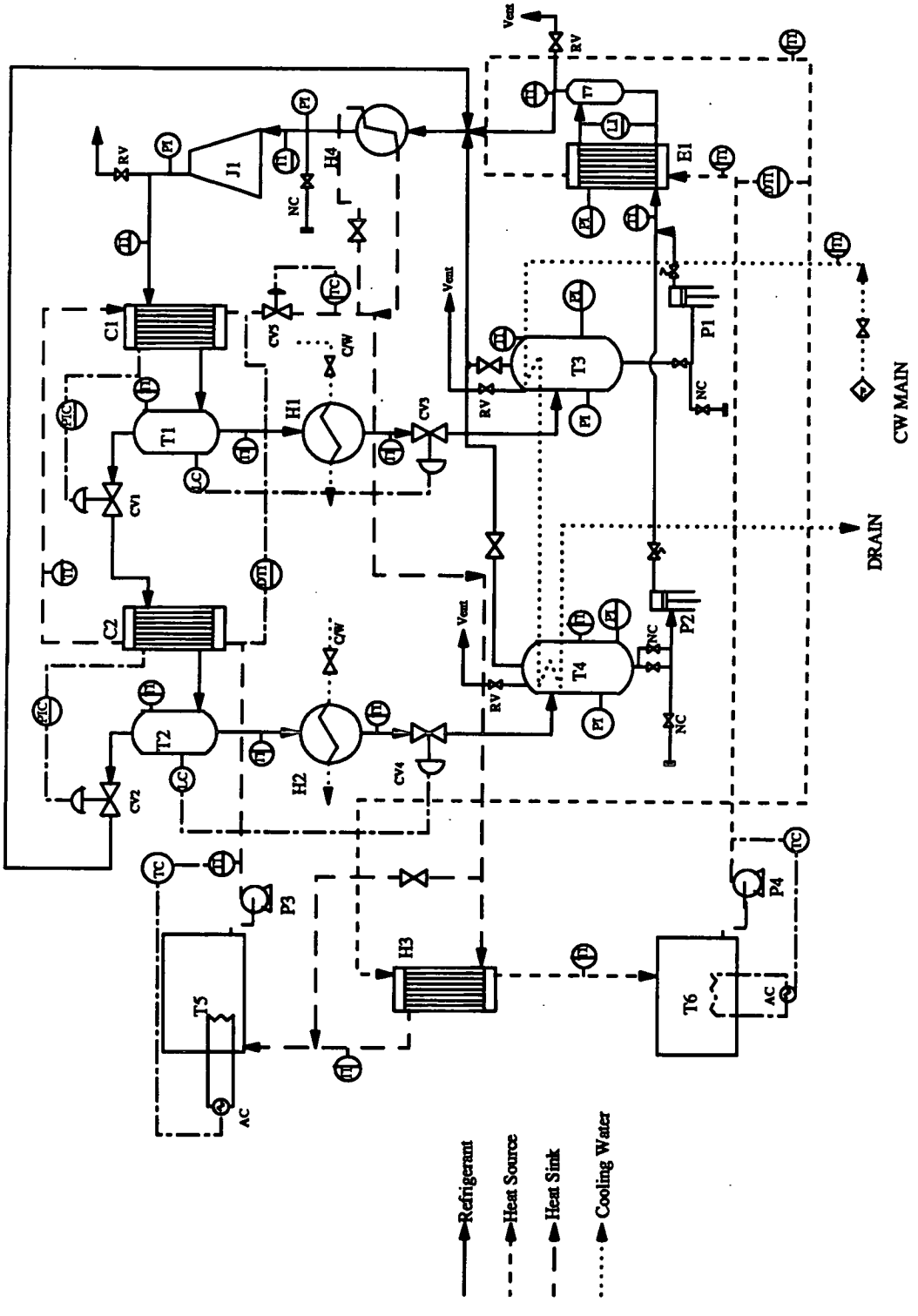

Figure 3.6: Third Operational Flowsheet (July–December 1990)

3. Record all process variables at regular intervals, storing data in disc files for future reference

4. Display selected measurements in an unambiguous and comprehensible manner on the computer console, to inform the operator of the behaviour of the plant.

5. Enable the operator to switch or set any piece of hardware from the console.

The following subsections expand on the details of the equipment chosen to perform these tasks.

3.5.2 Microcomputer and Interface

An IBM-XT compatible PC was available at no cost and was adopted as the basis of the instrumentation system. This machine, manufactured by DCS Ltd of Leith, had previously been purchased for another laboratory project, and was already fitted with two expansion cards for interfacing with instrumentation hardware.

One card provided an IEEE–488 parallel interface communication port; this would enable communication with two thermocouple amplifier units, which were also available at no extra cost. This card was manufactured by IBM and supplied with software to enable programming of the card in BASIC or IBM FORTRAN. The thermocouple amplifiers, manufactured by CIL Microsystems, were PCI 1002 units, each capable of accepting 12 Type K thermocouple inputs and two analogue voltage inputs.

The other card was an Amplicon PC-30 interface, capable of dealing with both analogue and digital voltage signals. The card provided 16 analogue inputs, 4 analogue outputs, and a 24-pin digital interface which could accept both inputs and outputs. The potential capacity of this system was therefore: twenty-four specialised thermocouple inputs; 20 analogue voltage inputs, to be used for other instruments; four analogue voltage outputs for control, and up to 24 digital signals, either input or output, for switching relays or providing alarm signals.

In fact, the flowsheet required more than four control loops to be implemented and so it would be necessary to use hardware controller units in addition to software control.

Furthermore, signal conditioning hardware would be required to link the Amplicon card to the instrumentation hardware. The details of these items of equipment follow below.

In summary: the instrumentation and control requirements of the plant may be itemised in the following manner.

Control Loops

- Compressor speed
- Pressure in first condenser (C–1)
- Pressure in second condenser (C–2)
- Load output temperature
- Load input temperature
- Source delivery temperature
- Level in V/L separator T–1
- Level in V/L separator T–2
- Set points on metering pump heads
- Positions of vapour return solenoid valves

Measurements

- Compressor speed
- Compressor torque
- 5 pressures:
  - Evaporator

  - First condenser
  - Second condenser
  - Heavy storage tank T–3
  - Light storage tank T–4
- 24 temperatures (see table in Appendix D)
- 2 water flowrates: heat sink and heat source
- 3 liquid levels: Evaporator, T–1 and T–2
- 2 temperature differences: over C–1 and C–2, and over evaporator.
- positions of the metering pump heads.

3.5.3 Instrument Hardware

3.5.3.1 Signal Conditioning

The Amplicon interface card would accept voltage inputs in the range ±5 Volts: it would be necessary to build additional circuitry to bring most of the transducers' output signals into this range. In addition, there would need to be provision for filtering of mains "hum" and electromagnetic noise. It was decided to run the control outputs and certain of the instrument inputs as 4–20 mA current signals rather than voltages, to avoid problems of induced voltages and ground-loop errors. (The plant would use two water pumps, a metering pump and a 3-phase compressor motor: each of these units would contribute to an etheric din.)

After discussion with the department services manager, the form of the additional instrumentation hardware was decided: a modular racking system. This comprised a 64-track backplane fitted with a mains supply and transformer, from which would be supplied mains voltage and ±15 V d.c. The rack case accommodated up to six plug-in circuits, or "cards", each performing a specific function. The use of a backplane meant that utility supplies, and all instrument readings, would be available to every circuit board if required. Furthermore, it permitted testing or replacement of one part of the system need not compromise the remaining sections. The amount of cabling would be kept to a minimum, which would reduce likelihood of poor connections causing failure.

The final arrangement of connections to the rack backplane is listed in Appendix D: a brief description of each card used follows.

Card 1: Inputs This provided eight 2-wire current inputs, accepting 4–20 mA. External conmnections were provided via BNC plugs, with the drive line on the core and the return on the shield. The inputs were connected to channels 0–7 of the PC–30 card. (Channel 7 was later disconnected to be freed for use in another circuit.)

Card 2: Metripump This card controlled the MPL metering pump. Five of the digital outputs of the PC–30 were used: one to switch the pump motor, the remainder to actuate forward or reverse motion of the electric stroke positioner motors on each pump head. Feedback of the stroke position was given by voltages from potentiometers inside each pump head: these positions were connected to channels 8 and 9 of the PC–30 card. The front plate of this card was fitted with coloured LEDs to indicate the status of the pump motor and of each positioner motor.

Card 3: Control Outputs This card provided the PC–30's four analogue control outputs in the form of 4–20 mA driver circuits. In addition, digital switching was provided via two DIN plugs for control of water tank heater elements and of the solenoid valves fitted to the plant.

Card 4: Temperatures This card provided an independent thermocouple amplifier for rapid measurement of the load output temperature. The same card held the amplifier circuits for the two thermopiles used in the water circuits. The thermocouple connection was made on a standard RS thermocouple plug, while the thermopile signals were connected using 3-way DIN plugs.

Card 5: Pressures This card held four independent instrumentation amplifier circuits, to match with the pressure transducers connected to the two high-pressure separation vessels and the two glass storage tanks. These signals were left as voltages, as the wires for the transducers were high-quality shielded cable. Connections were made using 6-way DIN plugs.

Card 6: Level controls This card provided proportional control of the liquid level in each high-pressure separation vessel. The control action was independent of the computer, and was tuned by adjustment of potentiometers in the circuitry. The input to the card from the level measuring device was via a BNC plug; output action was transmitted as 4–20 mA through a 3-way DIN plug.

3.5.3.2 Pressure

Five pressure transducers were connected to the plant: one on the separation pot attached to each condenser; one on each of the main storage vessels, and one on the evaporator at the vapour exit. The two transducers on the separator pots were Druck PDCR510 gauge pressure transducers, with a maximum working pressure of 35 barg. The heavy storage vessel was fitted with a Druck PDCR510 gauge transducer, maximum working pressure 15 barg; the other storage vessel was fitted with a SHAPE absolute transducer, maximum pressure 15 bar. The evaporator pressure was measured by a Landis & Gyr gauge transducer, range 0–10 barg.

3.5.3.3 Temperature

The temperature measurement element used throughout was the K type thermocouple. These were made by department technicians, by spot-welding of proprietary thermocouple wires. The amplifiers mentioned above accepted inputs from these thermocouples without any pre-conditioning. The manufacturer's literature suggested that an accuracy of $\pm 0.1°$ could be achieved in the range 0–100 °C.

The thermocouples were not placed directly into pipework, as it was felt that this would lead to sealing difficulties. The thermocouples were rather placed in pockets, made from small-bore stainless steel tube soldered into brass nipples. These could be attached to matching couplings and brazed into pipework wherever required. Most of the thermocouple pockets were eventually fitted to elbows or tee-pieces; this resulted in a simple brass-brass connection and gave a useful thickness of metal on both sides of the joint. These properties of the joint greatly improved the ease of fabrication of a gas-tight seal.

3.5.3.4 Differential Temperature

It was decided to measure the temperature differences on the water side of the evaporator and of the condenser bank, in order to obtain accurate values of the most important heat fluxes in the plant. The temperature differences on the water side would in some operating conditions be so small that straightforward subtraction of two thermocouple measurements would give a difference with a high fractional error. The measuring element employed on both locations was a 5-junction thermopile: this device removes any need for cold-junction compensation and produces a voltage five times greater than the equivalent single-thermocouple measurement. The signals from these devices were led into two channels on the PC–30 board: special amplifier and filter circuits were built to condition the thermopile signals. These were based around a high-stability operational amplifier, with strongly-damped filtering to remove electromagnetic interference. The final circuit had a gain equivalent to a maximum temperature difference of 37 °, ample for the proposed operating conditions.

3.5.3.5 Water Flowrate

Both hot and cold water flowrates were measured using orifice plates in conjunction with differential pressure measurement. This method was cheap and reasonably effective. Industrial differential pressure transmitters driving 4–20 mA into two wires, over the range 0–150 mbard were used. The orifice plate sizing was based on the following calculation:

Design water flows were taken as 75% of the maximum metered flow for each stream. In other words, the full-scale pressure drop was to correspond to four-thirds of design flow. Equation 3.35 was then used to estimate the size of orifice necessary to meet this condition. The orifice discharge coefficients were estimated from the correlations given in Section 5 of Perry.

$$\frac{\Delta P}{\rho} = \frac{u_2^2 (1 - \beta^4)}{2} \tag{3.35}$$

where

$$u_2 = C_D \sqrt{\frac{2 \Delta P}{\rho (1 - \beta^4)}} \tag{3.36}$$

(β is the ratio of orifice diameter to pipe diameter.)

The discharge coefficient C_D was estimated as 0.65 for both orifices, while the design flowrates for hot and cold side respectively were 0.1075 and 0.287 kg/s. The plates were to be mounted in 22mm Kuterlite copper pipe, which has approximate dimensions of 22mm O.D., 19.5mm I.D. The resulting orifice diameters were 8mm (hot) and 11mm (cold).

For details of the calibration of these orifices, see Chapter 4

3.5.3.6 Level

Three liquid levels were to be measured: the same type of device was used in each case. Level was measured by connection of a differential pressure transducer between the bottom and top of the vessel to measure the head of liquid. The transducers used were Druck PDCR120 units, range 0–150 mbard. The transducers on the separator pots were connected with a reference leg of uninsulated pipe to the top of each pot: this side was used as the positive connection. Initially empty, as the heat pump was run these lengths of pipe would fill with condensed refrigerant and act as a (reasonably) constant reference pressure. The negative connection of the transducer was linked to the base of the vessel, as the level in the pot would normally be lower than the level in the reference leg. The connection of the transducer on the evaporator was more straightforward: the positive side was linked to the base of the unit and the negative side to the vapour exit pipework a convenient distance away from the evaporator itself. This meant that there would be little or no condensation in the negative connection pipe run.

3.5.4 Control Loops

The following control loops were identified and dealt with.

Load temperature This was to be controlled by feedback control on water flow, with setpoint cascaded off a thermocouple measuring the condenser water outlet temperature. The final control element was a Platon 1/2" Type M control valve, driven by a 4–20 mA output from the PC via the rack interface. The only available trim for this valve was size A, which was really oversized for the duty. However, Platon could not guarantee delivery of a replacement trim at short notice, so the trim was left in place.

Pressure in Condenser C–1 This was to be controlled by throttling an exit vapour stream from the top of separator T–1. The final control element was a second Platon 1/2" valve with an A trim. This would also be driven from one of the PC's analogue output signals, with the control action implemented in software.

Pressure in Condenser C–2 This had to be controlled to ensure control of the pressure in C–1. The control was to be achieved by throttling of a vapour return to the compressor suction. The final control element was a small control valve manufactured by Badger Ltd. This occupied a third analogue output of the PC.

Compressor Speed It was not strictly necessary to use feedback on control of this quantity: the speed of the compressor was linearly dependent on a 4–20 mA drive input signal over most of the operational range. This signal was provided by the fourth analogue output available on the rack interface. A tachometer was added to the setup towards the end of the work: this would enable implementation of feedback on the speed.

Water Tank Temperatures The water tank temperatures were controlled by on-off control, using 3 kW electric heating elements switched in software to implement the control. As each tank had a holdup of several minutes water flow, a periodic fluctuation of tank temperature was inevitable and accepted for these variables.

Condensate Receiver Levels These were controlled in hardware using a proportional algorithm. The final control elements were 1/4" Platon control valves, with type H trims. These worked well once a reference leg of liquid had been established.

3.5.5 Operating Software

3.5.5.1 Choice of Language

The choice of programming language was constrained by the need to write software capable of addressing both of the interface cards at sufficient speed to enable software-driven feedback control. The IBM-supplied IEEE interface could only be programmed in BASIC, IBM FORTRAN v2.0 or Lattice C v2.0. The Amplicon card on the other hand could not be programmed directly in IBM FORTRAN. In order to address both cards in the same language, it would have been necessary to use either BASIC or Lattice C. BASIC would be too slow and cumbersome for the task; Lattice C would cost upwards of £250. A compromise was reached: Borland's Turbo C v2.0 was purchased (£65). This compiler was more powerful than the Lattice product and was highly compatible with the dialect of C used by the department's Sun workstations. The language difficulty was overcome by writing a small program in FORTRAN, which scanned the temperature amplifiers and stored the readings in a disc file. The main program, written in Turbo C, could run this program at any time and read the temperature data from disc. While this was not entirely satisfactory, it was far simpler than obtaining sufficient information from IBM on the workings of their IEEE interface to write a device driver for the IEEE card in Turbo C. This latter technique would be a recommended step in any future work with less pressing deadlines.

3.5.5.2 Design of Main Program

The core routine `main()` of the source code for the main monitoring program is contained in Appendix C. The structure is simple, as may be seen by inspection of the `main()` calling function at the end of the code. The program operates a continuous loop: at the start of each loop the current time is recorded. The instruments monitoring the controlled process variables are then scanned and any necessary changes to the control outputs are made. At regular time intervals, the complete set of process instruments is scanned, including all the temperature signals. As reading of the temperature signals requires suspension of the control loop and launching of a second "child" program, this is not performed at every pass through the loop: this operation requires several seconds. The log files are updated when the difference between the current time and the previous update exceeds the preset recording interval. The last operation in any loop is to check for a keypress, which may be the signal to terminate

all operations or to change one of the control parameters. Should this be the case, the necessary action is taken and will affect the next loop's output and input signals.

3.5.5.3 Auxiliary Software

In addition to the thermodynamic property subroutines described in Chapter 6, several other programs were used in operation of the pilot plant. These were: a program to scan the thermocouple boxes; a program to display one input channel as a real-time plot, and a program to sample any given channel a number of times, then produce a file of statistics on the sample set for calibration purposes.

3.6 Physical Layout

This is best described by a series of pictures showing the plant from both sides of the main framework. The picture captions indicate the points of interest in each case.

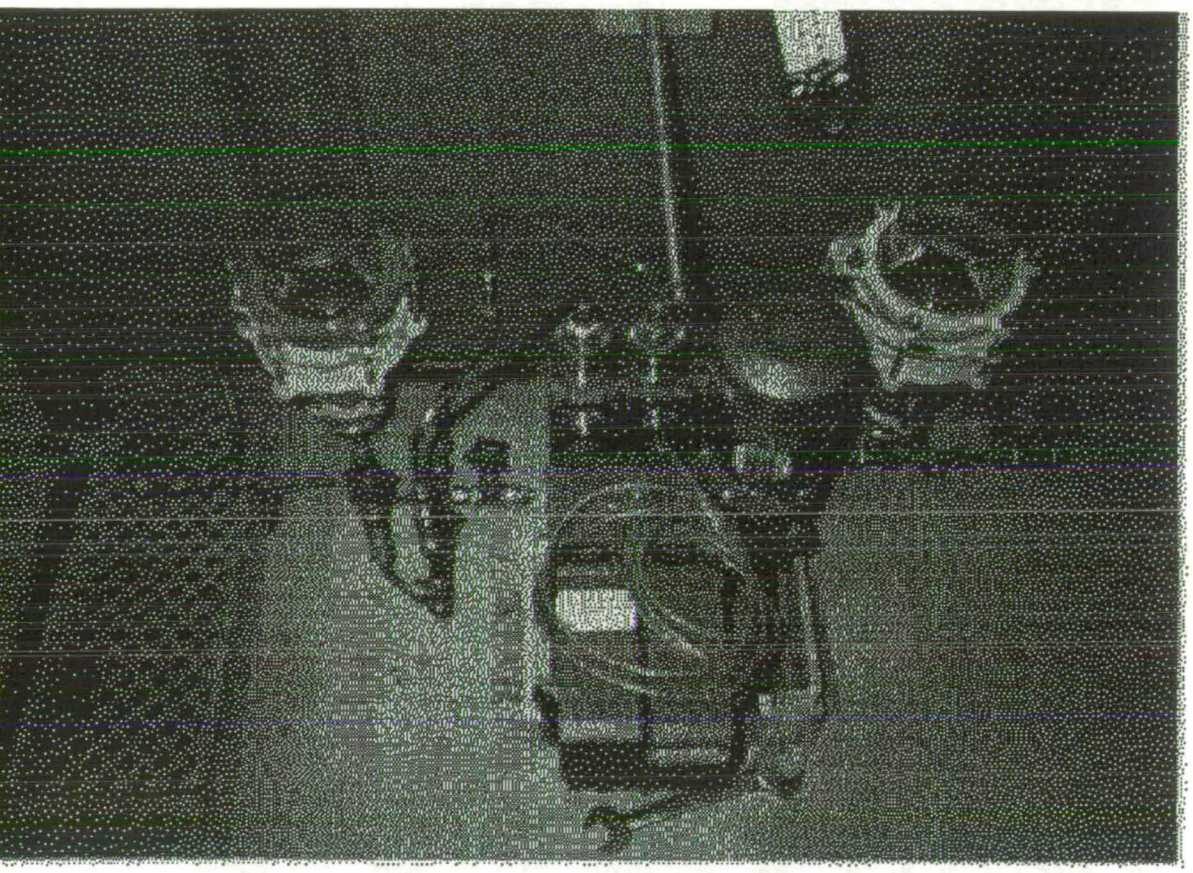

Figure 3.7: Metering Pump, Showing Valve Gear and Storage Vessels

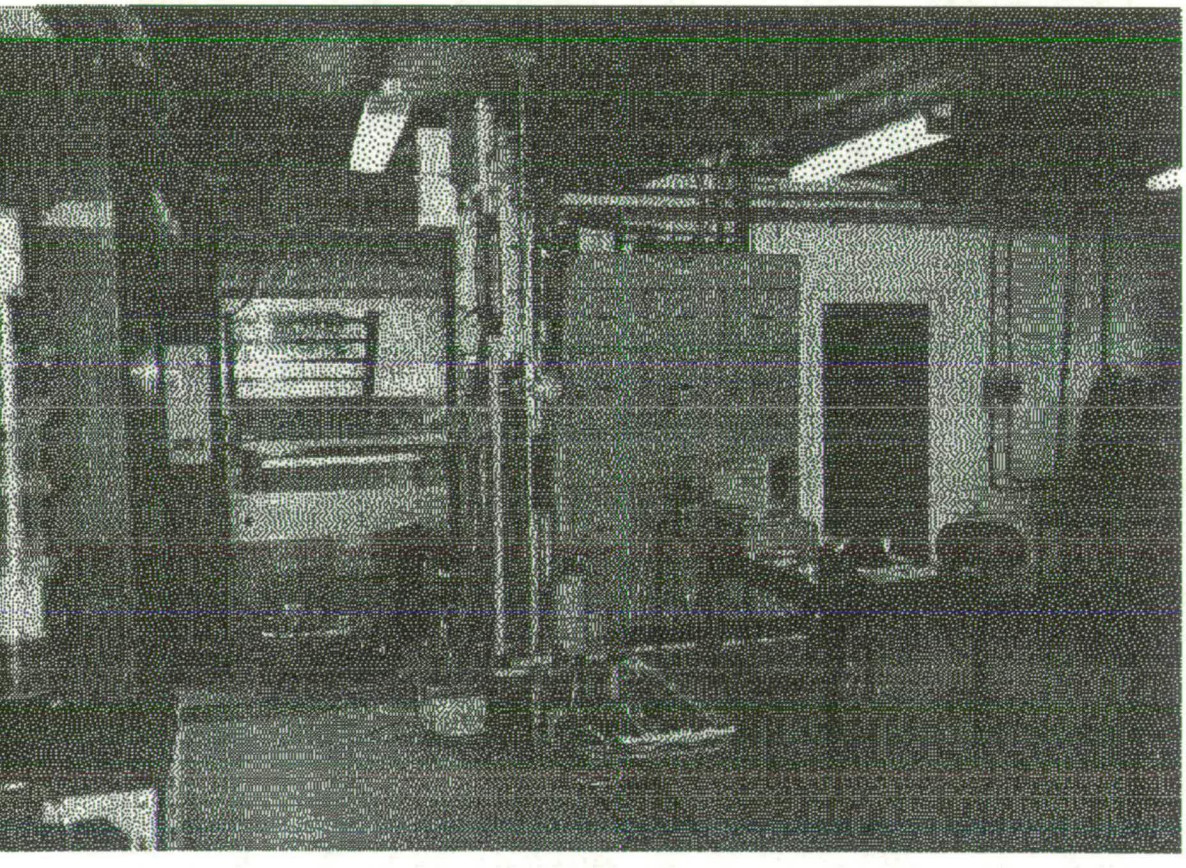

Figure 3.8: View of Plant From Side, Showing Control Desk

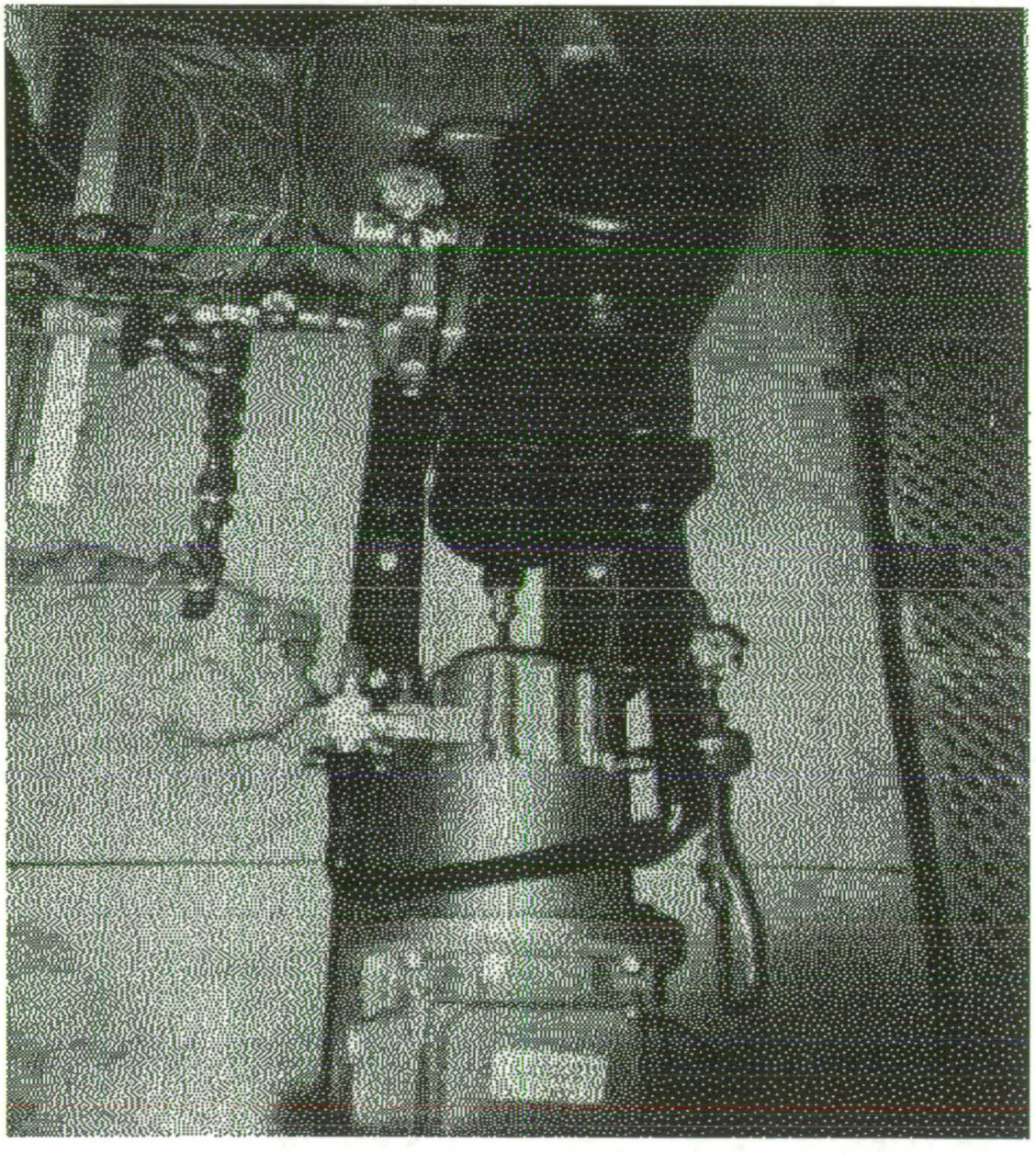

Figure 3.9: Compressor During Rebuild, Showing Oil Pipework and Separator

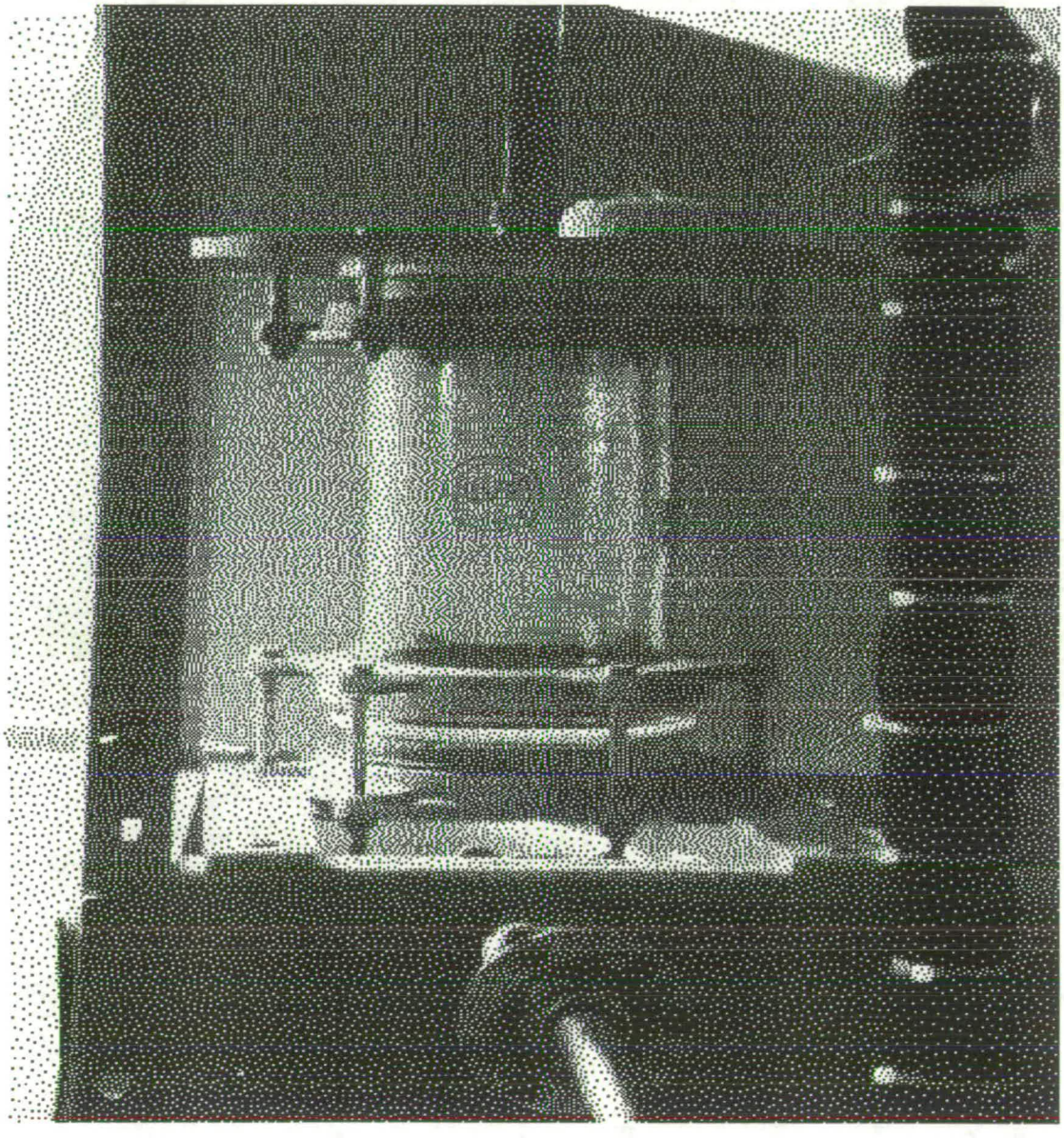

Figure 3.10: Vapour-Liquid Separator from Side, Showing 3–D bend on Inlet

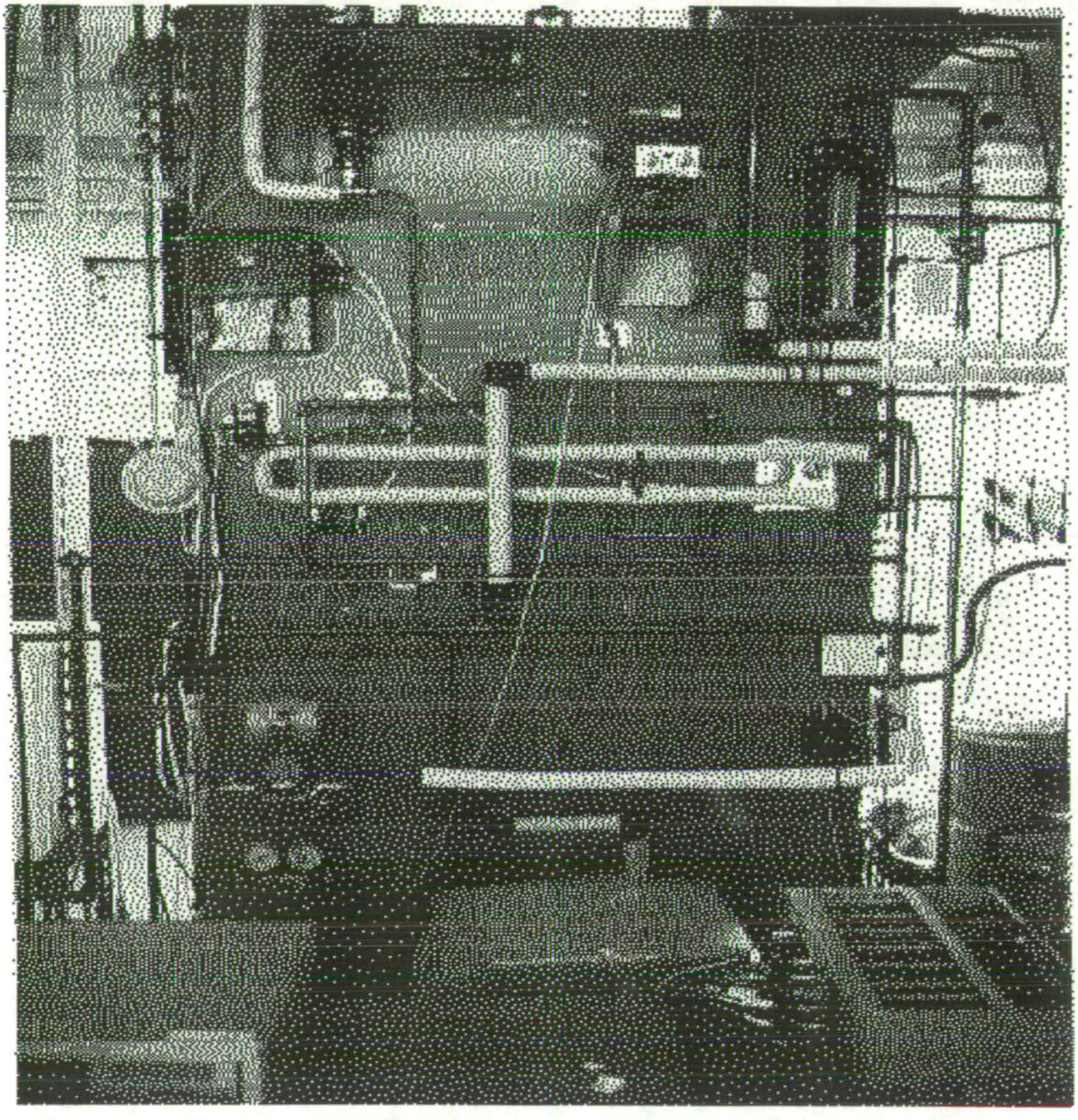

Figure 3.11: Plant from Control Desk, Showing Subcooler and Water Pipework

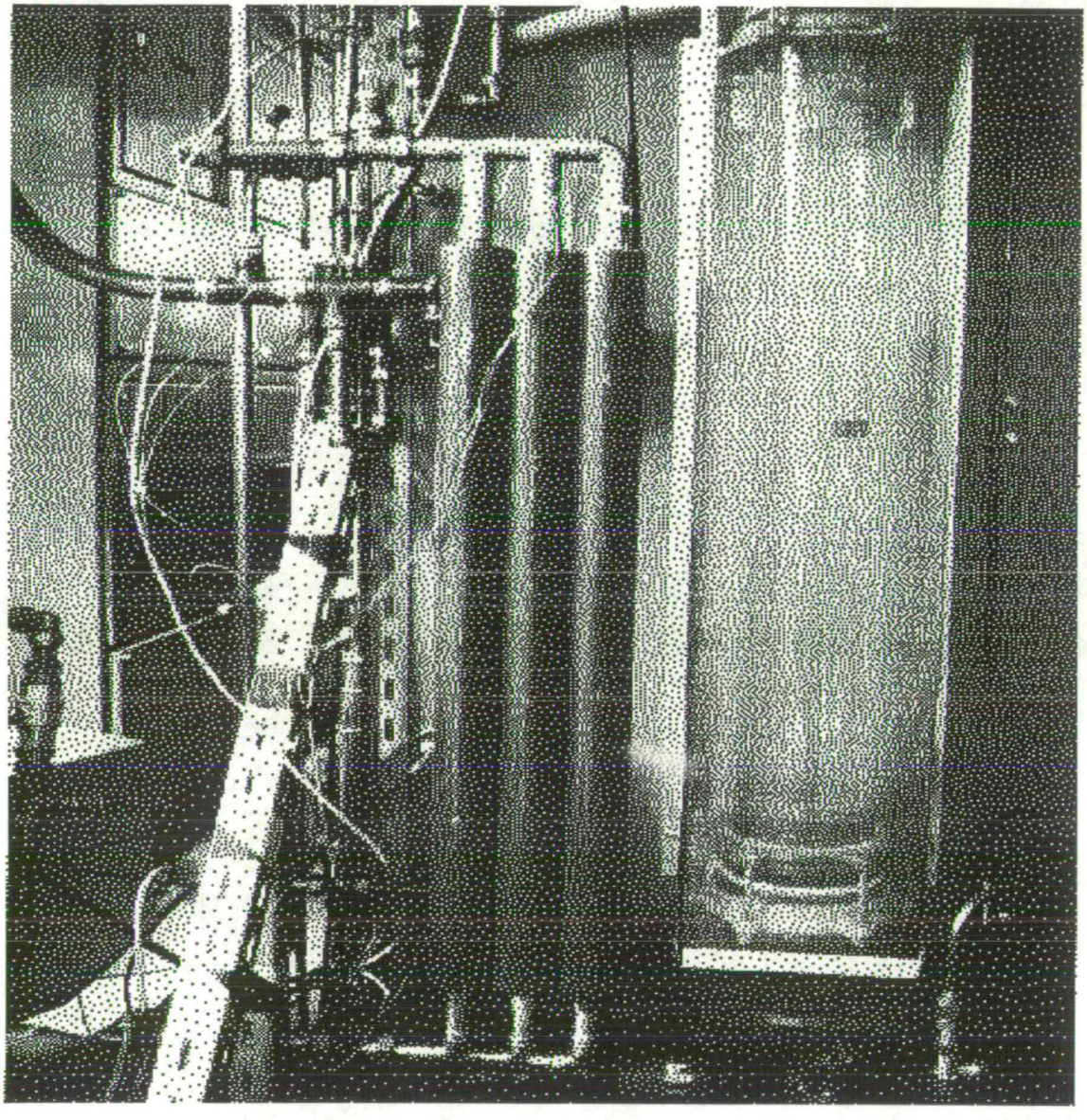

Figure 3.12: Cal-Gavin Evaporator in Final Flow Arrangement

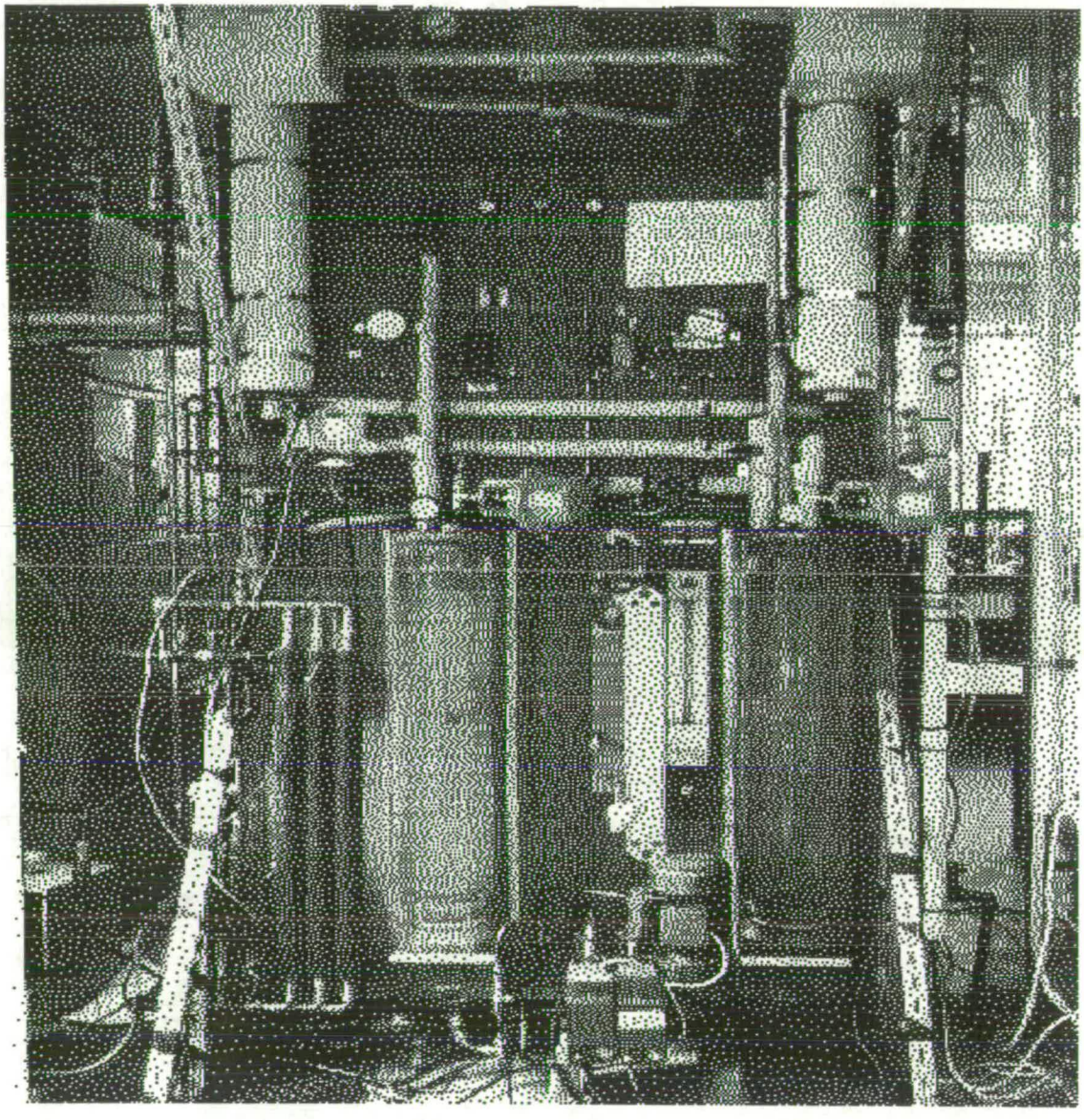

Figure 3.13: View of Plant, Showing Condensers, Receivers and Storage

Chapter 4

Experimental Work

4.1 Introduction

In this chapter the experimental work carried out on the pilot plant is described. The plant was commissioned over a period of about two months, in which time the instruments were tested; equipment was put into operation; the plant was rendered leak-tight, and sufficient operational experience was gained to enable the development of procedures for the safe startup, shutdown and normal operation of the plant. In this time, several major pipework modifications were carried out, and the reasons for these changes are described in the appropriate sequence in the text.

4.2 Commissioning

4.2.1 Water Circuits

The water circuits used were the first parts of the plant to be commissioned, as the refrigerant circuit depended on the presence of controllable sink and source streams. The basic procedures required to commission each stream were as follows:

1. Leak detection and elimination.
2. Thermocouple placement and testing.
3. Installation and calibration of the orifice plate flowmeter.
4. Testing of the temperature control subroutine and hardware.
5. Calibration of the thermopiles and independent thermocouple.

The first two tasks were perfectly straightforward: the only problem lay in containment of the thermocouple wires to protect them from damage. This was eventually accomplished by passing them in groups of six through sections of PVC tubing, 2–3 feet in length.

The orifice used in the hot water circuit for the first set of experiments was of 8mm diameter (in a tube diameter of 20mm). This was calibrated at a temperature of 60 °C, against the rotameter (a size 18, steel float) which had been placed in the circuit. The rotameter reading was converted to flow by use of a chart prepared by the author for water at 60 °C, according to the information given in the manufacturers' literature. The orifice used in the cold water circuit was larger (11mm) because of the higher flowrates used in that circuit. The cold water calibrations were performed at room temperature, using a chart supplied by the manufacturers for the appropriate rotameter (size 24, steel float). The calibration procedure was identical in both cases.

The relation between the measured signal at the computer I/O port and the flowrate of water was expressed as a function of the form:

$$Q = A \times (S)^{\frac{1}{2}} + B \tag{4.1}$$

where Q represents the flowrate in litre/min and S represents the signal, an integer in the range 0–4095 (*i.e.* 12-bit accuracy). The signal from the differential pressure transmitter was rather rough: this was probably caused by fluctuations in the local pressure around the orifice, rather than by RF interference. To reduce the effect of this variation in signal, an average of 20 readings, taken at one second intervals, was used for the calibration measurement. In order to simplify the task of data collection, the calibration data were logged using the programs **CALIBS.EXE**. This simple program logged data for a given channel at a specified frequency and stored the mean signal, with variance and standard deviation, to a text output file. The procedure for each calibration was:

1. The water was heated to calibration temperature, with the pump circulating water to warm up the pipework.
2. The pressure transmitter was flushed through to eliminate air bubbles, by means of the bypass line.
3. A flowrate was set by use of a hand valve, reading the setpoint off the rotameter.
4. After 5 minutes (to allow stabilisation of the water flow) the sample was initiated.
5. Steps 3 and 4 were repeated over a range of flows, including several repeat measurements as a check on the repeatability of the measurement.

4.2.2 Compressor and Ancillary Equipment

The compressor commissioning procedure was taken in the main from the manufacturers' literature, and is described very briefly here.

Before charging of the plant for the first time, oil was charged into the separator until the visible level had passed the bottom sight port on the separator casing. The electronic control unit and electrical power connections were tested by Matthew Rea,

and the functioning of the trip switches fitted to the unit was checked. The operation of both manual and remote drive signals was verified, and the direction of rotation of the motor was confirmed to be correct. At this stage it was found that the manufacturers had supplied the unit with the discharge pipe connected to the suction of the unit: consequently it was necessary to cut the pipework, fabricate new sections and reconnect to the plant. The charging manifold connected to the compressor was checked for leaks and malfunctioning gauges but no problems were found.

4.2.3 Leak Detection and Refrigerant Charging

The refrigerant pipework had to be made as leak-tight as possible, to minimise costly losses. Most of the joints in the plant were threaded connectors; this was a major task, requiring over two weeks before satisfactory sealing was obtained in all parts of the apparatus. The first leak detection method was to pressurize the refrigerant pipework with compressed air from the ring main to the vapour pressure of R114 at room temperature (about 1 barg). A soap solution was then dribbled over the joints to be tested: any leak of air from the joint would blow a fine froth of bubbles. As a result of this first step, it was necessary to remachine the dural header plates used in the refrigerant storage vessels: these had to be demounted from the plant and separately pressurised before satisfactory sealing was obtained.

The second stage in the process, carried out after all obvious leaks had been detected and eliminated, was to pressurise the plant to a given pressure, leave it overnight, then observe the pressure readings on the gauges the following morning. This showed that leaks were still present: the major leak was found in the machining of a penetration face on one of the separation pots. This entailed stripping down and removal of one condenser from the offending pot, followed by fabrication of a special PTFE gasket to cure the problem.

Eventually it became obvious that small leaks were evading detection, and it was decided to invest in a refrigerant detection gun, capable of tracing tiny leaks of refrigerant from pipework. This tool is sensitive yet inexpensive. In order to use it, of course it was necessary to charge refrigerant into the plant.

The first step in the charging procedure was to open all isolation and control valves, so that no section of the plant was shut off. A vacuum pump and gauge were then fitted to the vent line at the top of the plant, and the vacuum pump was run until the gauge reading steadied. The final vacuum reached was rather lower than 28 inches mercury, which represented an acceptably low holdup of air in the plant. The vent line was then shut, the pump disconnected and a cap placed on the end connection of the line.

Following evacuation of the plant, refrigerant was drawn into the plant using the compressor, which had already been commissioned. Cold water was circulated through the condensers and the compressor was started at low speed (about 300 rpm). The control valves separating the high pressure pipework from the low pressure pipework were shut, as was the compressor auxiliary oil return line. Thus any vapour inducted to the compressor would remain in the high pressure section. This would eventually be condensed and returned to the storage tanks. The largest quantity of refrigerant held in the plant at any one time was about 8 litres of liquid (the contents of a standard 12kg bottle). Although the plant could be run with a much smaller holdup, it was easier to operate with a reserve refrigerant capacity until steady control of evaporator feed rate and condensate level could be achieved.

Once the charge had been completed and all refrigerant condensed, as much as possible was transferred into the low-pressure storage. After some time the high and low pressure sides of the plant were isolated using the relevant valve gear. The vent line was then uncapped and cracked open for several seconds: this was to allow the residual air in the system to escape. The rationale was that air would tend to accumulate in the topmost pipework and vessels, those closest to the vent line. As a precaution, the low-pressure storage vessels were also vented, by cracking open the pressure gauge connecting fittings. It was possible to check for the presence of trapped air in these vessels by comparing the pressure transducer readings with the measured temperatures and vapour pressure tables.

On completion of the charge and purge, after the laboratory had been ventilated, a second check of all jointing using the detector torch was required. This took several days but was successful in finding previously undetectable leaks. At the end of the work it was concluded that the plant was as gas-tight as possible given the number and nature of the fittings used.

4.2.4 Instrumentation

The commissioning procedure for the electronic hardware and PC software which together comprised the instrumentation system in essence consisted of testing signals against known measurements. Most of the circuitry described in the previous chapter had been bench-tested at the construction stage. In particular the pressure transducer amplifier circuitry had been set up using the plant's transducers connected to a Druck calibration tool which permitted fine tuning of amplifier gains. There were nonetheless numerous minor faults which could only be detected on installation of the equipment onto the plant, and these took some weeks of work to eliminate. This timescale was considered fast in view of the size and complexity of the system—considerably more advanced than the instrumentation hitherto used in the department. At the end of the commissioning period the only unsatisfactory outstanding problem lay with the thermocouple amplifier units, which were in need of professional recalibration.

4.3 Experiments With Pure Working Fluid

4.3.1 Justification

The pilot plant was initially operated with a charge of pure R114: this made data analysis relatively straightforward and allowed attempts at determination of heat transfer coefficients in the evaporator. The aims of these initial experiments were: to gain operational experience; to check the function of the instruments; to measure the efficiency of the compressor as a function of speed, and to identify any parts of the plant which would require to be changed. The procedure followed in all these experiments was similar to that described in Appendix B, dealing with startup and operation of the plant. Variations from the standard procedures are described where necessary.

4.3.2 Initial Experimentation: May

The first runs on which data were recorded took place in May 1990. The data from these experiments were logged but are not included here for reasons which will be made clear in the following paragraphs.

4.3.2.1 Procedure in brief

The experimentation was intended to investigate the performance of the heat pump at steady state. The compressor speed, water tank temperatures and water flowrates were fixed. Refrigerant was drawn from either or both of the storage tanks using the metering pump, whose stroke settings were empirically chosen to achieve steady levels in the vessels. The startup and operational procedures were as described in Appendix B. The plant was run for several hours at a time in an attempt to achieve true steady states. During each run, data were logged using the control program described in Chapter 3. These were stored in disc files for later analysis; this was never done, however, as there were profound difficulties of operation which rendered the datasets useless. These were caused by a number of factors, chiefly relating to the compressor and its ancillary oil circuit.

4.3.2.2 Operational problems: Oil Carryover

The chief problem encountered in this period of operation was the carryover of lubricating oil beyond the oil separator and into the condensers. This resulted in the complete distribution of oil throughout the system; in turn this implied fouling of the heat transfer surfaces with oil. A further problem caused by oil carryover was the entrainment of liquid refrigerant from the evaporator. The result of this was a feed to the compressor, not of superheated vapour but rather a three-phase mixture of oil, liquid refrigerant and saturated vapour. The skewed phase envelope of R114 meant the state of the refrigerant during the compression process never left the saturation region. In effect, the compressor acted as a pump: this did not damage the unit as sliding vane compressors can tolerate a high liquid content in the material to be compressed.

The circulation of this mess of fluids resulted in very low observed heat fluxes: it appeared that only 25% of the liquid pumped to the evaporator was eventually condensed from the vapour phase. Attempts were made to improve this by careful adjustment of feed rates, compressor speed and use of the oil separator's secondary return line as a bypass on the compressor. None of these were successful, indicating that the problem lay in the hardware rather than the control scheme. It was therefore necessary to analyse the plant in an attempt to identify the physical modifications which would be required to achieve operation without oil carryover.

The projected mechanism of oil carryover was initiated by entrainment of liquid refrigerant in the vapour feed to the compressor. This was felt to be the key factor: on startup from a tank of clean refrigerant a period of clean running could be obtained, in which some small degree of suction superheat was observed. From an initial feed of two-phase refrigerant, carryover of oil was however inevitable: the nature of R114 meant that any such feed would increase in liquid content during compression, and this liquid would then entrain oil. The oil separator would not be able to perform adequately under these conditions and hence the stream leaving the separator would contain oil in significant quantity.

The mechanism for oil carryover proposed above was confirmed in the course of discussion with representatives of Rotocold Ltd, the suppliers of the compressor. It was suggested that at least 10–15 degrees superheat on the suction side of the compressor were required with fluids like R114, in order that the oil separator might remove all traces of liquid from the vapour stream. The implications of this were obvious:

1. *Remove all possibility of liquid refrigerant being fed to the compressor.*
2. *Provide adequate superheating capability to achieve the specified degree of superheat on the suction no matter the operating state being used.*
3. *Instigate a thorough cleansing of all the parts of the plant which had been contaminated with oil, chiefly the evaporator.*

A vapour-liquid separator and vapour superheater were designed, fabricated and installed in the plant (see Chapter 3 for description of these units). The evaporator was demounted and emptied of accumulated oil: almost 250cc had gathered in the unit, which must have rendered most of the heat transfer surface practically useless.

4.3.2.3 Other Operational Problems

Pressure Drop It became apparent that there was a significant loss of pressure between the evaporator and compressor suction, as indicated by the pressure transducer on evaporator and the manifold vacuum gauge. A typical pressure drop was over 0.5 bar. The design suction pressure was the vapour pressure of R114 at 25 °C, *i.e. ca.* 1 bar gauge: in practice the suction pressure was between 0 and 0.5 bar gauge. The accumulated resistances caused a choking of flow: above a certain flowrate, increasing the compressor speed merely decreased the suction pressure without any increase in the mass flow of vapour.

There were two main reasons for this pressure drop: poor choice of suction side pipework, and the need to meet manufacturers' requirements by installation of a suction-side vapour line filter element. The available recommended units were designed for use in refrigeration sets, whose gas densities are in general several times those expected in the heat pump plant. Consequently the connections to the filter case were of very small bore, causing high entrance and exit losses to the device.

In this first round of modifications, the suction side pipework was expanded and straightened out: the diameter was more than doubled and the number of bends reduced. The filter element was left in the circuit but the cartridge elements were butchered to reduce the pressure drop. The original vapour inlet was sealed and a new, larger bore inlet was drilled in the face of the unit. This reduced the observed pressure drop but did not eliminate it, and this was to remain a problem throughout most of the operational period.

Metering Pump The metering pump failed to stroke during this period of operation and was stripped down for repair while the evaporator was being cleaned. During this operation, the loading valves on the metering pump were found to be faulty: they should have been factory-set but in fact were fully open. This was probably a significant factor in the flooding of the evaporator which in turn led to oil carryover. The function of the loading valves was to present a positive head for the metering pump heads to discharge into: in the absence of a positive discharge head flow would no longer be accurately metered, as liquid would be drawn through the pump without hindrance. The valves were set to open at 15 psig before the pump was replaced, and gave no trouble thereafter.

Condenser Pressure Control The initial aim of operation was to use both condensers and both heads of the metering pump. Had everything operated at its design state, this should have been perfectly feasible, and would have yielded a heat output of about 10kW at full compressor speed. However, it was soon found that it was very difficult to control the proportion of condensation in each condenser. The tendency was for one condenser to do the bulk of the duty; this made it exceedingly difficult to obtain a steady state throughout the entire plant. This may have been due to the oil carryover problems described above: in any case it was decided that future experiments with pure fluid be restricted to using the first condenser only. The observed suction pressure drop in any case meant that the maximum throughput of refrigerant would be limited to less than the design flow of 0.08 kg/s.

4.3.3 Data Reduction

4.3.3.1 Aims of the Analysis

Analysis of experimental data would take two forms: qualitative description of the operational behaviour of parts of the plant; and quantitative data reduction, yielding parameters to characterise different features of the equipment in operation. The qualitative observations made in the following sections are chiefly concerned with matters such as the hydrodynamics of the evaporator, the time required to achieve a stable operational states, and so on. These are chiefly of interest as evidence to support the explanations of any perceived shortcoming of the equipment or the operational philosophy implemented by the author.

There were three key areas of interest in the quantitative analysis of data obtained running with pure R114 as the working fluid of the heat pump: heat pump performance; compressor performance, and evaporator performance. The aims of the data analysis to be attempted for each of these topics are described below.

Heat Pump Performance The performance of a compression heat pump cycle is known to be a function of: the equipment configuration; working fluid; temperature lift, and discharge temperature. Of these quantities, the lift and discharge temperature

were the two which could be varied given the nature of the plant; quantitative analysis of the experimental data would therefore be directed at establishing the effect of these variables on the Coefficient Of Performance (COP) of the plant. The use of a pure working fluid would permit direct comparison with a Carnot process operating between the same conditions. For such a process the COP is simply given by:

$$COP_c = \frac{\text{Heat Output}}{\text{Work Input}} = \frac{T_{si}}{T_{si} - T_{so}} \tag{4.2}$$

where T_{si} is the sink temperature and T_{so} is the source temperature, under the assumption that there is zero temperature difference between the working fluid of the Carnot process and the heat source and sink.

A useful index of heat pump performance is the "Carnot Efficiency", designated by ϵ in this Thesis. It is defined by:

$$\epsilon = \frac{\text{Actual COP}}{\text{Carnot COP}} \tag{4.3}$$

The Carnot efficiency (also known as the "heat pump effectiveness factor") will be used in the analysis of the results obtained using a pure working fluid. Deviation below unity implies irreversible losses in the actual heat pump performance, which may be identified more closely (if desired) by entropy balances and/or exergetic analysis. For the purposes of this work the analysis will be restricted to derivation of the Carnot efficiency and its variation under differing process conditions.

Compressor Performance It was intended to attempt a reasonably detailed exploration of the performance of the compressor under operational pressure ratios and running speeds. The intention was to obtain characteristic data describing the effect of speed and pressure ratio on the volumetric throughput and isentropic compression efficiency. The displacement and compression efficiency would directly affect the heat pump performance, in terms of output capacity and thermodynamic efficiency. It was hoped to obtain numerical parameters characterising these effects, which could then be used to project the compressor performance into datasets taken using a mixture as a working fluid.

Evaporator Performance The evaporator performance was to be characterised in terms of its capacity and the heat transfer rates achieved in stable operational modes. It was not possible directly to calculate the heat transfer coefficients for evaporation

and superheat (see Chapter 5) and the heat transfer processes taking place were to be described in terms of heat transfer *products*, defined by:

$$(UA) = \frac{\text{Heat Flux}}{\text{Mean Temperature Difference}} \tag{4.4}$$

The geometry of the evaporator, and the available temperature measurements, further meant that even these products could not be obtained by simple calculation. It would be necessary to employ a computer-based numerical model to estimate these heat transfer products from the known measurements of temperature and flowrate. The derivation and compilation of such programs is described in more detail in Chapter 5

The complete data sets recorded in these experiments are not given in the thesis for reasons of space. Instead the important derived data are presented in tabular and graphical form. The derivation of data was performed in several ways with the first results (taken on June 7th 1990), in order to assess the accuracy of different property calculation techniques. The initial aim of this assessment was to choose a technique for implementation in the real-time control program; this was however frustrated by hardware limitations and a lack of time for the programming effort.

The different techniques used to obtain derived data were: manual calculation of all properties by interpolation from manufacturers' property tables for R114; use of a computer program incorporating high-accuracy correlations of the thermodynamic properties of R114, and use of computer implementations of the CCOR and CSD equations of state. The results obtained from the manufacturers' data were taken as the reference for comparison of the techniques. The use of equations of state is discussed elsewhere in this thesis and is not described here in any detail. The programs used to produce the properties are listed in Appendix C.

4.3.3.2 Heat Pump Analysis Program: "HPUMP"

The property correlations for R114 were taken from the paper by Downing [24], which is accepted as a seminal source of such information for CFC refrigerant fluids. The correlations were then incorporated into a program which was designed to accept input of the experimental pressures and temperatures relevant to the plant in single-condenser mode. In this configuration the plant may be represented by the flowsheet in Figure 4.1. There are eight streams of refrigerant fluid. The units they connect are: feed tank; evaporator; superheater; compressor; condenser; subcooler, and throttle valve. For the

purposes of data analysis it is possible to ignore the compressor lubricating oil circuit, since no oil should be present in any part of the plant which is of interest in analysis.

The program used the experimental measurements to calculate densities, enthalpies and entropies in each part of the plant. From these data could be derived the heat pump performance, as well as an analysis of the compressor performance in terms of pressure ratio, isentropic efficiency and polytropic indices. The output from the program was written to three files: one detailing the stream properties in the plant; one listing the compressor performance parameters, and one listing the specific energy fluxes, COP and Carnot efficiencies of the heat pump. The program, called **"HPUMP"**, was written in C for use on either a PC or Sun workstation. A sample of the output is given later in this section. Some explanation of the quantities derived by the program follows.

Stream properties The properties calculated from each set of temperature and pressure readings were: specific volume; enthalpy; entropy, and vapour fraction (where appropriate). The output generated from each dataset was a tabular representation of these properties at each point in the plant. The volume, entropy and enthalpy were written as intensive (specific) quantities.

Compressor Performance The compressor was to be analysed to determine several characteristics: the volumetric displacement at a series of speeds; the isentropic compression efficiency and its variation with speed and pressure ratio, and the polytropic indices characterising the behaviour of the compressor. As these quantities may be defined in several ways, the definitions used by the author are given here.

The volumetric displacement was taken as the volumetric flowrate of gas on the suction side of the compressor. This was obtained from the mass flow of refrigerant fed to the evaporator by the metering pump, given that the suction gas density could be calculated from the inlet manifold temperature and pressure.

The isentropic efficiency was defined as:

$$\eta_S = \frac{h_d^* - h_s}{h_d - h_s} \tag{4.5}$$

where the suction gas enthalpy is h_s, the actual discharge enthalpy is h_d, and h_d^*

represents the enthalpy of fluid at the discharge pressure which has the same entropy as the suction gas. (*NB:* this does not exclude a two-phase fluid at the compressor exit, which is a hazard of operation with R114 and so must be allowed for.)

Two polytropic indices, K and N, were calculated for the compression path. These were defined by the relations:

$$\left(\frac{T_d}{T_s}\right) = \left(\frac{P_d}{P_s}\right)^{\frac{K-1}{K}} \tag{4.6}$$

$$\left(\frac{P_d}{P_s}\right) = \left(\frac{v_s}{v_d}\right)^{N} \tag{4.7}$$

The significance of these indices is: K permits direct calculation of the discharge temperature from the pressure ratio and inlet conditions, while N may be used to estimate the frictional heat loss in the compression process.

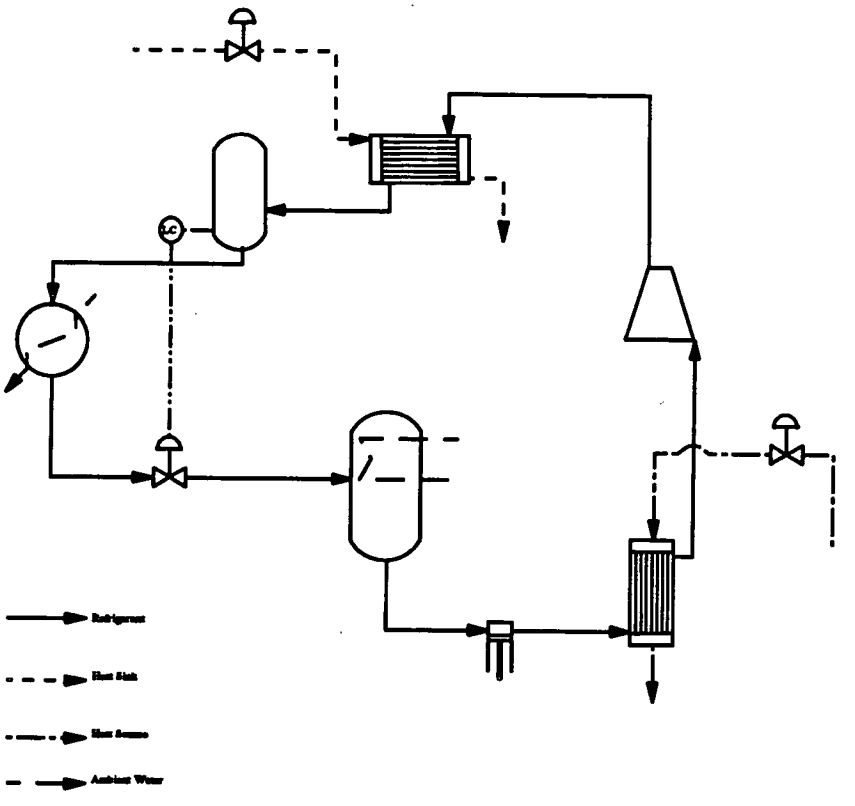

Figure 4.1: Single-Condenser Flowsheet for Data Analysis

4.3.4 Operation in June and July

4.3.4.1 Procedure

After completion of the modifications and repairs described above, the next set of experiments was carried out in June-July 1990. Steady state operation was again the desired working condition: it was hoped to succeed where the initial attempts had

failed. Only the first condenser was used. The addition of the vapour-liquid separator and superheater meant that the effective flowsheet of the pilot plant for these runs was as given in Figure 3.5.

Operational procedure was broadly similar to the previous work: no attempt was made to control the condenser pressure in an explicit manner. The controlled variables were: compressor speed; evaporator feed rate; water flowrates; condenser water inlet temperature, and evaporator water inlet temperature. The degree of suction superheat was not controlled; if anything the superheater performed too well, giving over 20 degrees of superheat in most cases.

It was the intention to run the evaporator with only partial flooding, so that there would be some superheat performed by the unit as well as the evaporation duty. There were insufficient thermocouple channels available to permit explicit calculation of the heat transfer products for evaporation and for superheat, so a simple numerical model of the unit was developed as an aid to estimating these data from experimental measurements of temperature and flow. (See Chapter 5 for description of this model.)

In the initial days of operation, data were logged both by the computer and by hand; the continuing presence of *gremlins* in the instrumentation, particularly the thermocouple amplifiers, made this a necessity. In the following discussion, any data recorded before June 14th may be taken as coming from the data sheets completed by the author. In these data sheets, certain variables are not recorded directly; instead they are represented by analog measurements of some other quantity. Thus the compressor speed is not quoted in terms of frequency or rotational speed, but in the indicated voltage signal produced by its electronic drive unit. The metering pump setting is given as an indicated percentage of full stroke (100%=100 litre/hr). The evaporator level is quoted as an indicated height in centimetres. (In fact, this was not the true level, since the primary measurement was of pressure drop between the base of the evaporator and the vapour pipework connected to its outlet. The evaporator contents were vigorously-boiling liquid, hence the apparent density would at all times be much less than that of quiescent liquid and so the calculated level would be too low.) The signal seemed reproducible; under the same conditions at steady state the indicated level would be contained within a few cm range.

4.3.4.2 Qualitative Results

At this point it is pertinent to record some other qualitative observations about the behaviour of the plant in response to changes in process conditions; these were made during these experiments and held good in subsequent operation.

Compressor Behaviour The system was sensitive to changes in compressor speed: this could be adjusted from zero to full scale in a matter of seconds, thanks to the electronic drive. The manifold pressures would adjust in the same timescale. Adjustment of the compressor speed much above 50% would not result in a corresponding higher boilup rate in the evaporator, however: the presence of a large resistance to flow between the evaporator and the compressor inlet was to blame. This meant that the system could never be operated at design heat outputs without increasing the evaporator pressure to compensate for the larger pressure drop. Scope for this was limited by the maximum safe working pressure of the glass-bodied vapour-liquid separator to 25 psi gauge (2.72 bar absolute).

Dynamics of the Evaporator The evaporator had a tendency to flood, with a holdup of liquid appearing in the separator *above* the level of the inlet; this was obviously held there by pressure exerted by the incoming fluid. This appeared to be a stable operational state but it was one which could cause problems of operation: in order to guarantee a metered flow to the evaporator it was necessary to maintain a level of liquid in the feed tank. A large-scale transfer of liquid from the feed tank to the separator tank had to be avoided, or the level in the feed tank would become too low for convenient operation.

The flooding of the evaporator was observed to exhibit a kind of hysteresis: the conditions for flooding could take some time to appear, with only slow changes in process conditions downstream. When the flooding was counteracted by switching off the evaporator feed, however, the effects on both the flooding and the compressor suction conditions were rapid. The liquid level and suction pressure would both drop rapidly in response to a cessation of feed flow, causing a transient which would upset the stable state of the whole heat pump. Recovery of suction conditions to a state close to the original steady state would then be a slow process in comparison to the loss of level. The typical timescale observed in such a transient flood was:

- From a known steady state, a small increase in feed rate to the evaporator starts the flood off.
- After 5–10 minutes of slowly increasing level in the evaporator (in which time the superheat performed in the evaporator decreases steadily) the first liquid appears in the separator.
- In the space of 30–60 seconds the evaporator exit fluid turns from a spray of mostly vapour to a jet of frothing liquid; exit and inlet temperatures are now equal.
- The feed pump is turned off. Immediately the pressure in the evaporator falls, as does the level. After no more than 60 seconds the evaporator is essentially empty, and the compressor suction gas has lost both pressure and temperature.
- The feed pump is turned back on at the original setting. At least 5, and more probably over 10 minutes are required to restore a stable state of operation to the evaporator and compressor.

Thermal Inertia in the Oil Separator The oil separator acted as a heat sink during the initial period of operation; some considerable time was required in order to warm the plant up to steady operating temperatures. The oil separator acted in effect as a crude absorber; the compressed vapour would condense into the oil, thereby warming it up. Even after condensation had broken through to the condensers and a reasonably steady condensation temperature had been achieved, the gas temperature at the separator exit would continue to climb for some time. The implication is that, although the conditions in the condenser and evaporator might have stabilised (near constant mass and heat fluxes, *etc.*) the system might not be at a true steady state. The compression efficiency as calculated from the exit temperatures could therefore be in error, as the exit temperature was measured at the separator exit rather than the compressor exit; this had to be borne in mind when performing the quantitative analysis of data.

Instrumentation Performance The first days of operation revealed several difficulties with thermocouples giving false readings as a result of damage to the wire or the junction itself; these were duly repaired. It then became obvious that the amplifiers themselves were in need of recalibration; this was not done until July, as time and money were in short supply. The effect of the inaccuracies will be discussed in Section 4.3.4.3.

The pressure transducers were found to be reliable and agreed (within the limits of measurement accuracy) with the vapour pressures to be expected from the thermocouple readings. The main drawback encountered with the transducers used was that four of the five in total were gauge pressure transducers. As a consequence, if the evaporator pressure or the heavy storage tank pressure dropped below atmospheric, then there was no way of recording the actual pressure using the PC. This had not been envisaged as a problem at the design stage but the presence of additional pressure drops between the evaporator and compressor suction exacerbated the problem.

The measurement of water flowrate by the orifice plate assemblies was found to be very good for the cold water circuit, but less stable for the hot water flowrate. The hot water flowrate signal was subject to a great deal of fluctuation, especially at the low end of the flow range. This made time-averaging a necessity but even with this enforced there was still a degree of uncertainty associated with the measurement. Accordingly the rotameter readings were logged at regular intervals as a backup measurement. Use of a turbine meter could have solved this problem; although such a meter was available it was found to be non-functional. As no additional funds were available there was no alternative to the orifice plate assembly.

4.3.4.3 June 7th Part 1: Procedure, Summary of Run

On June 7th, the rig was operated for a period of over 3 hours at steady state, in which time the compressor speed was kept constant. The feed rate to the evaporator was progressively increased in an attempt to determine the capacity of the unit for evaporation under constant heat source conditions. The invariant process parameter settings were as follows:

- **Compressor speed:** *ca.* 45% *i.e.* 1350 rpm.
- **Heat source flow:** 15.6 l/min *i.e.* 0.26 kg/s
- **Heat source temperature:** 26-29 °C
- **Heat sink flow:** 4.8 l/min *i.e.* 0.08 kg/s
- **Heat sink temperature:** 60 °C
- **Metering pump setting:** 3 settings: 45%, 56%, 60%

Data were recorded manually at intervals of approximately 10 minutes: it was found that once the plant had been "warmed up" this was ample time for adjustments to the evaporator feed rate to work through the system. As explained in Section 4.3.3 the raw data from this day's operation were processed in several ways, and the results of each analysis are clearly indicated in the following text.

Temperature Variations Table 4.1 lists the time histories for some of the key temperatures in the heat pump. The temperatures are: refrigerant at the evaporator inlet and outlet; compressor suction; compressor discharge; refrigerant condensation temperature; heat source inlet; heat sink inlet, and heat sink outlet (product) temperature. In studying this table it is important to note that the feed rates to the evaporator were: 0.0185 kg/s until 14:45; 0.023 kg/s until 15:30, then 0.024 kg/s until shutdown. The three sets of data are divided by horizontal lines in the table.

Time hr	$T_{ev,i}$ °C	$T_{ev,o}$ °C	T_{suct} °C	T_{dis} °C	T_{co} °C	T_{so} °C	T_{si} °C	T_{load} °C
13:40	11.8	22.5	41.8	88.1	69.4	28.1	61.5	68.0
13:52	11.1	24.0	42.4	90.0	67.8	29.9	58.7	67.4
14:00	11.0	23.3	43.8	90.8	67.6	35.0	60.1	66.4
14:10	8.5	23.4	43.1	90.6	67.8	27.7	60.4	66.6
14:22	8.7	20.4	42.6	91.2	68.1	26.3	60.6	66.9
14:30	10.7	21.1	42.4	91.8	68.8	27.7	60.9	67.4
14:40	11.0	20.9	42.9	92.3	69.5	27.2	61.3	68.0
15:03	14.8	18.8	42.1	92.6	70.9	26.4	61.4	69.0
15:10	15.2	18.4	42.2	92.6	70.6	26.5	61.4	68.8
15:20	11.9	16.8	41.6	92.2	69.5	26.6	60.9	67.8
15:30	14.8	18.7	42.2	92.3	69.4	26.6	59.6	67.8
15:46	13.9	22.8	40.4	91.6	69.3	26.5	59.2	68.7
16:00	16.9	25.0	42.0	92.0	71.6	26.7	61.6	69.9
16:10	13.3	22.7	42.0	91.7	69.8	29.7	59.2	68.2
16:20	14.0	23.5	43.9	91.3	69.8	29.0	61.2	68.1

Table 4.1: Temperature Histories for June 7th 1990

It may be seen from Table 4.1 that the set temperatures of the heat source and heat sink were subject to variation; these led to slight alterations in the phase–change temperatures and product temperature. The mean product temperature was 67.9 °C ± 0.9 °C. The mean heat sink temperature was 60.5 °C ± 1.0 °C. The mean heat source temperature was 28.8 °C until 14:40 hr, when there was a step change to a new mean of 26.6 °C.

Thus the mean external lift was approximately 40 degrees over the whole period.

In the same period, there were three distinct variations in mean evaporation temperature, corresponding to the three evaporator feed rates used. Within each set of constant feed conditions, there were local variations corresponding to the heat source temperature. The refrigerant exit temperature followed the boiling temperature, with each feed rate characterised by a roughly constant degree of superheat in the evaporator. The variation of temperatures in the evaporator is shown in Figure 4.2. The differences in superheat are probably explained by variations in level of liquid held up in the evaporator; the variations in gas throughput were probably too small to affect the heat transfer coefficient for superheating, implying a change in the proportion of area available for superheat.

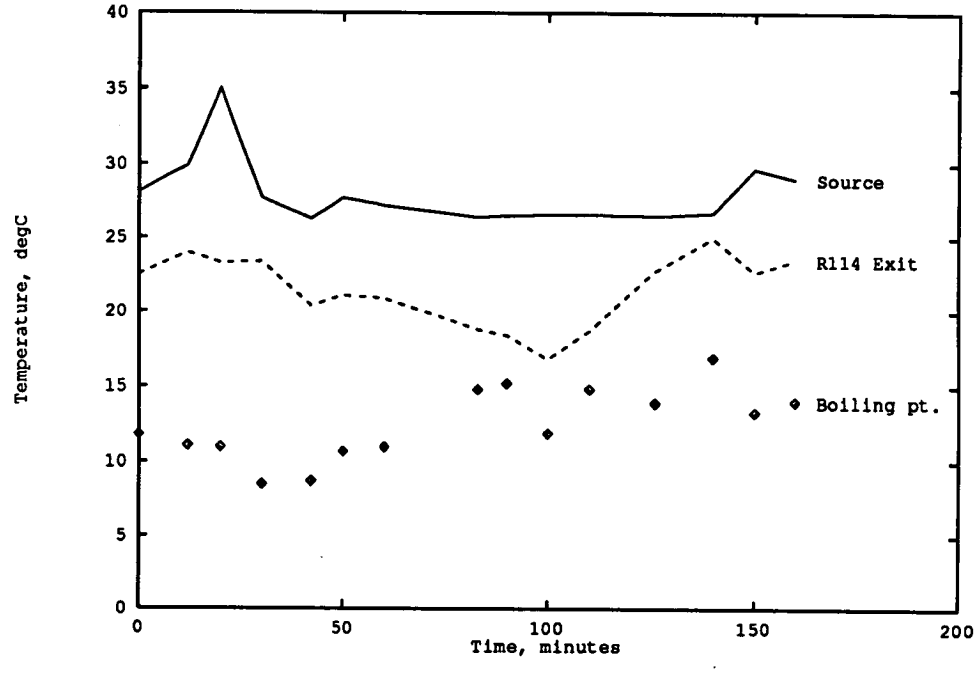

Figure 4.2: Temperatures in Evaporator, June 7th 1990

The condensation temperature, compressor suction and discharge temperatures, heat sink and product temperatures are shown in Figure 4.3. In this figure the effect of varying heat sink temperature is clearly illustrated; the condensation temperature and the compressor discharge temperature vary to follow the varying sink temperature.

This is to be expected; the condensation temperature will vary to enable complete condensation of the (constant) refrigerant flow, thus the condensing pressure must also vary. As there is a relationship between the pressure ratio of the compressor and the discharge temperature, one would expect this variation in pressure to cause a corresponding variation in temperature. (As the suction conditions were not rigidly controlled the correspondence is not perfect.) It should also be noted that the product temperature and the condensation temperature are consistently close to one another; the exchanger is oversized for this duty.

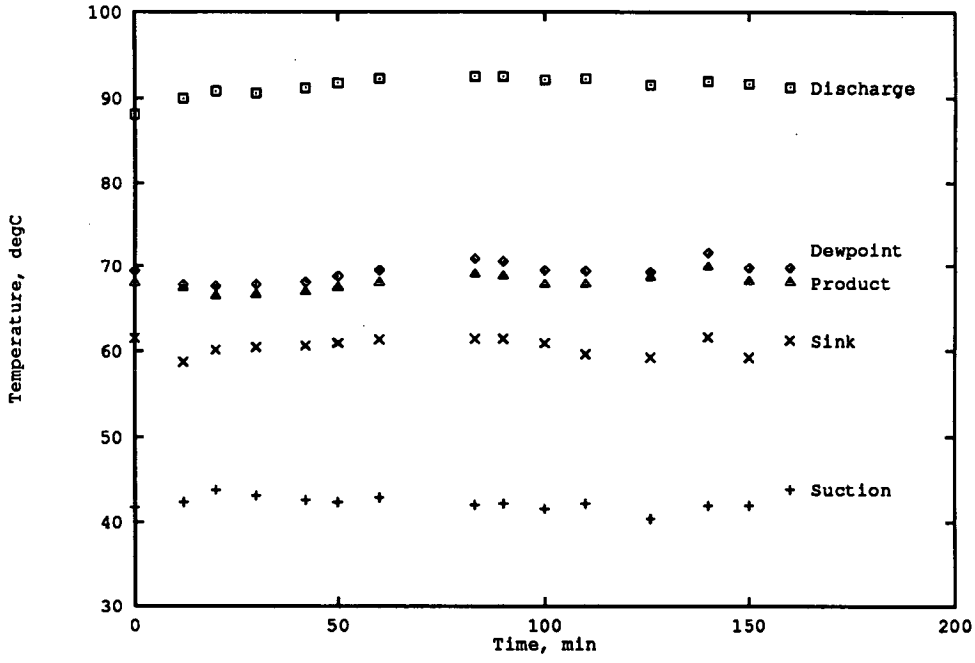

Figure 4.3: Temperatures in Condenser, June 7th 1990

Estimated Reading Error The estimated inaccuracy in each thermocouple signal was nominally $\pm 0.1\,^{\circ}C$. As the amplifiers were in need of recalibration, the actual error in some channels was found to be considerably greater. The maximum error found before recalibration was found to be 1.5 degrees. It was not possible to isolate the errors precisely without preparing calibration polynomials for each channel, *using the actual thermocouples mounted on the rig, in their correct position.* As this would have been extremely time–consuming and difficult to perform this was not attempted.

Pressure Variations The pressures in the evaporator, condenser, compressor suction and compressor discharge are shown in Figure 4.4 as functions of time. The original gauge readings have been converted to absolute pressures in bar.

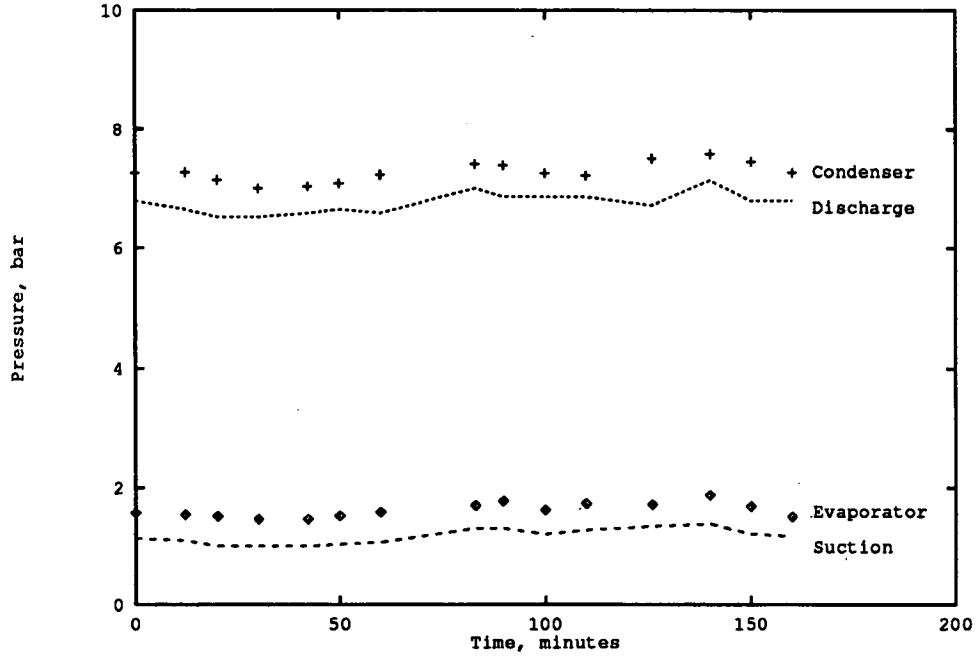

Figure 4.4: Recorded Pressures: June 7th 1990

It is obvious that the variation in pressures follows the variation in condensing and evaporating temperatures. This is to be expected, given the direct relationship between vapour pressure and temperature. The graph also illustrates the pressure drop between the evaporator and compressor suction quite clearly. Of especial interest is the discrepancy between the compressor discharge pressure and the condensing pressure. The discharge pressure was read from a gauge mounted directly onto the compressor manifold, while the condensing pressure was read by a transducer connected to the outlet of the condenser. As the transducer was calibrated and checked before installation, and given that the transducer pressure reading agreed with the known vapour pressure at the measured condensing temperature (within the accuracy of the thermocouple), there are four possible conclusions to be drawn.

The first is a faulty manifold gauge; however the gauge agreed with the suction gauge when the two sides of the compressor were at the same pressure, so this is not likely. The second is that the reading of the gauge was inaccurate; the subdivisions on the gauge in this range were at 5psi intervals. Assuming a "worst-case" error of half a division (*i.e.* 2.5psi) yields a reading error of 0.17 bar, which does not explain the difference in reading by itself. The third possibility is that the thermocouple *and* the transducer are both in error, in such a way that the transducer reading coincides with the vapour pressure indicated by the thermocouple. This does not seem very probable, but should be acknowledged. The last option is that the gauge does not measure the final exhaust pressure of the compressor.

Error Estimation The estimated reading error on the compressor suction gauge was 0.5psi (0.03 bar). The error on the discharge gauge was 0.17 bar. The error on the pressure transducers was 0.05 bar (found by use of a calibration meter).

4.3.4.4 June 7th Part 2: Heat Pump Performance

The heat fluxes in the evaporator and condenser were calculated from measurements on the water streams in each unit. This calculation was performed in two ways; by use of a thermopile to measure the temperature difference in the water stream, and by subtraction of the independent thermocouple readings at inlet and outlet to recalculate this difference. The first method incurs less error, as there is no cold-junction and no subtraction of similar values. Table 4.2 shows the heat fluxes in evaporator and condenser, calculated using both methods.

The heat fluxes in the evaporator and condenser were also calculated on the basis of the metered pump feed rate to the evaporator. This method used the measured refrigerant states at the inlet and outlet of the evaporator and condenser to derive specific enthalpies of the refrigerant. These data were then combined to give predictions of the heat fluxes; the results are shown in Table 4.2 on the right-hand side of the entries. The values shown were calculated using the enthalpies from the manufacturers' tables of thermodynamic data.

Time	$\dot{Q}_{ev}$ T/C	$\dot{Q}_{ev}$ T/PILE	$\dot{Q}_{co}$ T/C	$\dot{Q}_{co}$ T/PILE	$\dot{Q}_{ev}$ (PREDICTED)	$\dot{Q}_{co}$ (PREDICTED)
hr	kW	kW	kW	kW	kW	kW
13:40	2.50	2.42	2.17	2.65	2.33	2.34
13:52	4.14	2.46	2.91	3.14	2.35	2.38
14:00	—	2.17	2.11	2.57	2.34	2.42
14:10	1.74	1.97	2.04	2.36	2.36	2.43
14:22	1.52	1.93	2.11	2.38	2.43	2.49
14:30	1.74	2.16	2.18	2.56	2.41	2.49
14:40	1.85	2.22	2.24	2.67	2.40	2.47
15:03	2.07	2.54	2.55	3.01	2.88	2.98
15:10	2.72	2.54	2.48	2.97	2.88	2.98
15:20	3.91	2.32	2.31	2.75	2.88	3.00
15:30	3.04	2.56	2.75	2.96	2.88	2.97
15:46	3.59	2.40	3.18	3.56	3.10	3.13
16:00	2.39	2.68	2.78	3.20	3.09	3.11
16:10	2.83	2.29	3.01	3.35	3.10	3.12
16:20	2.50	2.21	2.31	2.73	3.17	3.16

Table 4.2: Heat Fluxes: June 7th 1990

There is considerable variation between the instantaneous heat fluxes measured directly from the water stream temperatures and those calculated indirectly from measurements of temperature and pressure. The problem is more evident in the evaporator, where the temperature difference on the water side was typically less than 2.5 degrees. This made the calculation of heat flux extremely sensitive both to measurement error and to small local fluctuations of temperature at the time of sampling. The heat fluxes as calculated by the thermopile signals are closer to the expected values; the condenser fluxes as calculated from the thermopile are on average greater than expected, while those in the evaporator are less than expected. It is possible that some of this deviation at least is due to small differences in the thermopile amplifier gain from the measured gain at the time of construction; since these amplifiers had to take a signal of millivolt magnitude and produce an output of volt magnitude, a relatively minor deviation in gain could produce a measurable difference of several percent. Another possible explanation for the low measured heat fluxes in the evaporator is that of inward heat leakage; the evaporator was unlagged and was situated over an open drain containing hot, running water. Condensation was observed on the surface of the evaporator during operation and could have supplied some of the "missing" heat.

A quantitative assessment of the deviations between measured and calculated heat fluxes is provided by Table 4.3, which is a list of the differences between the calculated

and measured heat fluxes (found from the thermopile readings) at each sample time. The table also contains mean heat fluxes for each metering pump setting; these mean values are listed after the last dataset taken for each setting.

Time	$\dot{Q}_{ev}$ (PREDICTED)	$\Delta\dot{Q}_{ev}$	$\Delta\dot{Q}_{ev}$ %	$\dot{Q}_{co}$ (PREDICTED)	$\Delta\dot{Q}_{co}$	$\Delta\dot{Q}_{co}$ %
hr	kW	kW	—	kW	kW	—
13:40	2.33	+0.09	+4	2.34	+0.31	+13
13:52	2.35	+0.11	+5	2.38	+0.76	+32
14:00	2.34	-0.17	-4	2.42	+0.15	+6
14:10	2.36	-0.39	-16	2.43	-0.07	-3
14:22	2.43	-0.50	-20	2.49	-0.11	-4
14:30	2.41	-0.25	-10	2.49	+0.07	+3
14:40	2.40	-0.18	-8	2.47	+0.20	+8
MEAN:	2.37	-0.18	-7	2.43	+0.18	+8
15:03	2.88	-0.34	-12	2.98	+0.03	+1
15:10	2.88	-0.34	-12	2.98	-0.01	0
15:20	2.88	-0.56	-19	3.00	-0.25	-8
15:30	2.88	-0.32	-11	2.97	-0.01	0
MEAN:	2.88	-0.39	-14	2.98	+0.06	2
15:46	3.10	-0.70	-23	3.13	+0.43	+14
16:00	3.09	-0.41	-13	3.11	+0.09	+3
16:10	3.10	-0.81	-26	3.12	+0.23	+7
16:20	3.17	-0.96	-30	3.16	-0.43	-14
MEAN:	3.12	-0.72	-23	3.13	+0.08	+3

Table 4.3: Heat Flux Statistics: June 7th 1990

Calculation of Enthalpies In Section 4.3.3 it was explained that the data of June 7th would be analysed in several different ways as a means of assessing the accuracy of different property calculation techniques. These techniques have been detailed in that section, and only the key results will be presented here. The specific enthalpy and entropy changes will *not* be tabulated; the COP and Carnot efficiency have been calculated from these quantities for each method and are listed in Table 4.4.

Data from Tables The reference technique for this analysis was manual interpolation of thermodynamic properties from the manufacturers' tables for R114 [38]. In these calculations the following assumptions were made:

- Liquid phase properties a function of temperature only.
- Presence of lubricating oil in vapour has negligible effect on the thermodynamic properties.
- All throttles are adiabatic; thus the enthalpy of liquid entering the evaporator is that of liquid refrigerant in the feed tank, if the evaporator pressure is less than that of the feed tank.

The results of the calculation are summarized in Table 4.4. The COP varies from 3.8 to 4.4; the Carnot efficiency varies from 0.63 to 0.75. The Carnot efficiency is noticeably higher for the set of data taken at the lowest feed pump setting. This appears to be a consequence of the compressor's performance. It will be shown in following paragraphs that at this speed, over the range of manifold pressures recorded, the compressor's isentropic efficiency correlates with the pressure ratio. The first set of data were also those with the highest pressure ratios, and this may explain the higher values of ϵ.

Time hr	COP_c CARNOT	COP ICI	ϵ	COP CSD	ϵ	COP CCOR	ϵ	COP HPUMP	ϵ
13:40	5.95	4.40	0.74	4.50	0.76	4.17	0.70	4.27	0.71
13:52	6.01	4.28	0.71	4.42	0.74	4.74	0.79	4.21	0.70
14:00	6.02	4.40	0.73	4.51	0.75	4.85	0.80	4.29	0.71
14:10	5.75	4.34	0.75	4.44	0.77	4.77	0.83	4.23	0.73
14:22	5.74	4.23	0.75	4.33	0.75	4.64	0.81	4.13	0.71
14:30	5.89	3.81	0.65	4.23	0.72	4.50	0.76	4.04	0.68
14:40	5.86	4.14	0.71	4.20	0.72	4.46	0.76	4.01	0.68
15:03	6.13	3.98	0.65	4.05	0.66	4.29	0.70	3.87	0.63
15:10	6.20	3.98	0.64	4.05	0.65	4.28	0.69	3.88	0.62
15:20	5.95	4.00	0.67	4.09	0.69	4.33	0.73	3.91	0.65
15:30	6.27	3.98	0.63	4.13	0.66	4.37	0.70	3.96	0.63
15:46	6.18	3.97	0.64	3.98	0.64	4.19	0.68	3.82	0.61
16:00	6.30	3.99	0.63	4.07	0.65	4.32	0.68	3.89	0.61
16:10	6.07	4.05	0.67	4.15	0.68	4.40	0.73	3.96	0.65
16:20	6.15	4.32	0.70	4.39	0.71	4.71	0.76	4.18	0.68

Table 4.4: Calculated Heat Pump Performance Parameters

Data from CSD Equation of State The CSD equation of state was used to calculate the change in refrigerant enthalpy over the evaporator, compressor and condenser, using the experimental measurements of temperature and pressure to indicate the state of the refrigerant. The COP values predicted by the equation's property calculations

are slightly higher (by 3–4%) than those yielded by the manufacturers' data. This may be attributed to a slight underprediction of the work of compression by the CSD equation of state. The results are still acceptable, as interpolation of properties by hand is a lengthy process, subject to human error.

Data from CCOR Equation of State The CCOR equation of state was used *in its generalised form.* The equation of state leads to an overprediction of COP. This is chiefly through the underprediction of the vapour phase volume, which is discussed in Chapter 6. Otherwise the prediction of phase-change enthalpies is in good agreement with the other calculation methods. The COP predictions, though too high, follow the same trend as those of the other calculation techniques.

Data from HPUMP Analysis Program These data are those in best agreement with the data interpolated from tables; this is not surprising, as these tables were probably generated from the same (or very similar) data correlations. The difference in results is probably due to the interpolation process; in the light of possible temperature errors of 1–2 degrees in the key measurements, the results from the program **HPUMP** are good enough to justify the use of this program to perform all analysis of future datasets (providing the working fluid is pure R114).

Summary of Data Prediction Techniques The closest approximations to the results yielded by ICI data tables [38] were those produced by the program **HPUMP.** This gave Carnot efficiencies and COP values which were within 3% of the values obtained by interpolation from tables. The use of the CSD equation gave slightly worse results: with this equation the COP values were consistently rather higher, by about 5%. The CCOR equation of state was the worst method tested: deviations of up to 12% were found in the prediction of COP. This can be attributed chiefly to its inferior performance in the superheated vapour region, a characteristic of the equation which had previously been identified by the author (see Chapter 6). It is important to stress that this equation of state was *not* used with the optimised parameters which would have reduced this error; the aim was to assess the likely error resultant from use of the CCOR equation to calculate cycle behaviour for heat pumps using possible CFC

replacement fluids. The error in COP obtained through use of the CCOR equation is not so large that it becomes a useless method, but it would be important in using this equation to remember that the calculated compression work would be too low, and compensate accordingly in any design based on this data.

Summary of Heat Pump Performance The plant transferred heat over a near–constant lift of 40 degrees throughout the period of operation. In this time the recorded condensation temperature did not vary by more than 2 degrees; the evaporation temperature was however subject to considerable variation. The *internal* lift of the heat pump, that is, the difference between evaporation and condensation temperatures, was on average 57.8 °C, ± 1.5 °C. The Carnot efficiency of the heat pump varied between 0.61 and 0.73 (using the data from **HPUMP**.) This variation is clearly wider than the variation in internal lift (which might be expected to affect the efficiency). Some explanation should be found for this variation in efficiency; the main irreversible losses in the plant must therefore be identified.

The bulk of heat transferred in the condenser is that heat transferred by condensation; the desuperheating duty is a fraction of the total heat duty. Any significant irreversibility in the condensation heat transfer process must therefore be related to the driving force for condensation; that is, the mean temperature difference between the condensing fluid and the water stream. It has already been observed that the recorded condensation temperature was very close (*ca.* 1 degree) to the water exit temperature; this would imply that the condenser was operating with a *low* driving force and hence a low degree of irreversibility.

By contrast, the evaporator, although performing as a superheater which brought the temperature approach at the vapour exit to within 5 °C of the water temperature, exhibited much greater differences between the boiling temperature and the heat source. This unit was therefore operating with an avoidable irreversibility; a more efficient mode of operation would have reduced the degree of superheat performed in the evaporator. The stable operation of the evaporator was very difficult to achieve, as a result of the flooding problem discussed earlier. Nonetheless, it is possible to conceive of a cunning control plan, whereby feedback would be used to set the feed pump rate. The controlled variable would be the temperature difference between inlet and outlet of the evaporator

on the refrigerant side. Thus the proportion of surface in the evaporator devoted to evaporation would be increased as necessary to achieve a closer approach between the heat source and boiling fluid. (NB: adaption of this technique to a binary working fluid would involve intermediate computation of composition and dewpoints to determine the actual superheat involved.)

The third major potential source of irreversibility in this plant was the compressor. This will operate with varying efficiency under different operating conditions of speed and pressure ratio. The data of June 7th have been analysed, using the program **HPUMP**, to identify the compressor performance and relate it to the known process variables. These results will be discussed in the following paragraphs

There were other losses of exergy related to the hardware; notably the throttling of the feed to the evaporator, and the pressure drop between the evaporator and the compressor suction. In these items, the working fluid does not lose or gain enthalpy but there is an increase in entropy. The effect of throttling the evaporator feed is to increase the driving force (and hence the irreversibility) in the evaporator. Of course, this was not deliberate, rather it stemmed from the self-adjustment of the pressure in the evaporator to meet the volumetric flowrate demanded by the compressor. Better heat-transfer coefficients, more area, or an increased feed rate (with less superheat in the evaporator) would reduce this loss. The pressure drop between the evaporator and compressor, by contrast, was caused entirely by flow resistance from filter elements and poorly-sized pipework. Hardware modification could reduce or even eliminate this loss, and this was in fact carried out (see later).

The final cause of deviation from the Carnot process was the working fluid itself; the shape of the phase envelope, and the variation of the enthalpy and entropy of the fluid with temperature and pressure, will cause losses of exergy even if the heat transfer processes and compression take place with little or no exergy loss. This cannot be helped; such is life.

A graphic illustration of the causes of deviation from Carnot behaviour is provided by plotting some measured state points on thermodynamic charts. The path of a typical dataset is plotted in Figure 4.5 and Figure 4.6, which are pressure-enthalpy and

temperature-entropy plots for R114. The gain in entropy through the superheater and compressor is clearly seen. So also is the effect of the pressure drop between evaporator and compressor.

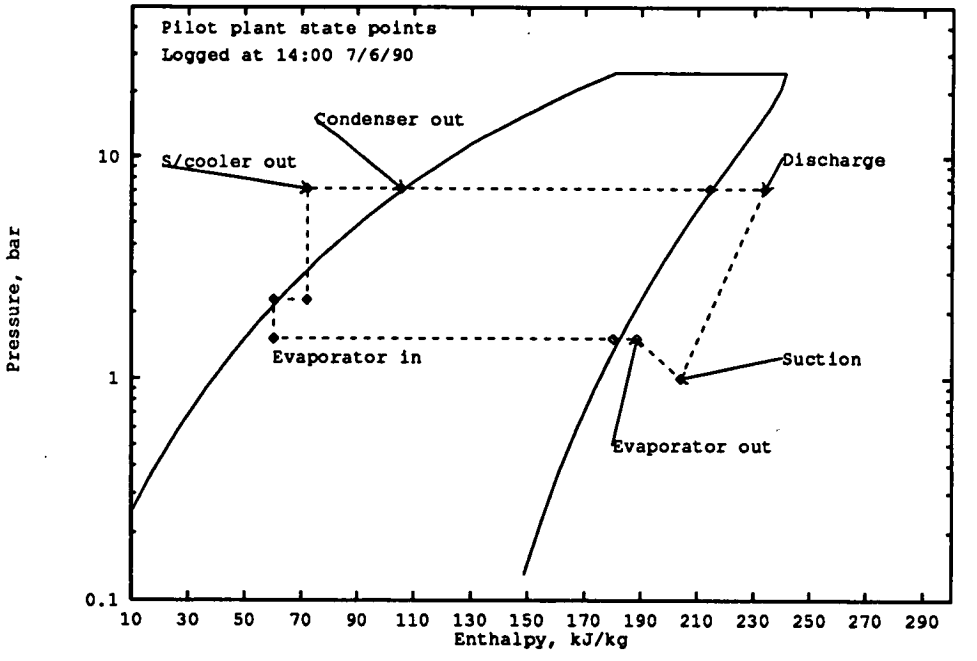

Figure 4.5: Cycle on Pressure–Enthalpy Chart

In conclusion, the range of Carnot efficiencies exhibited by the plant in this series of data is rather better than the normal values attained by compression heat pumps, which typically are in the range 50–60%. The reasons for deviation of the real plant COP from the Carnot COP have been identified and discussed at some length. This discussion will be continued and concluded in Chapter 7.

4.3.4.5 June 7th Part 3: Compressor and Evaporator Performance

In this section, the performance of the compressor and evaporator is examined at some length. By necessity, much of the data quoted in the analysis has been generated by computer programming; the programs used have been described elsewhere (Section 4.3.3, Chapter 5, Chapter 6).

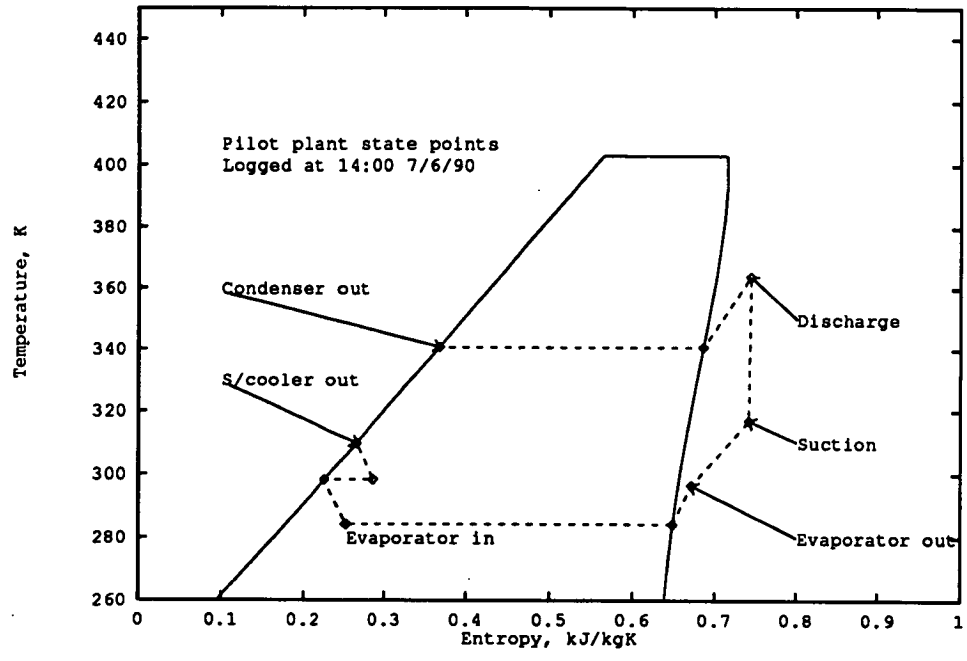

Figure 4.6: Cycle on Temperature–Entropy Chart

Compressor Performance The program **HPUMP** was used to determine the isentropic efficiency of the compressor, using the data of June 7th detailed above. As these data were all taken at constant compressor speed, any variation in efficiency must be correlated with other factors, such as pressure ratio, or degree of superheat. The results of this analysis are presented in Table 4.5. This shows: pressure ratio Π; specific suction volume; degree of superheat (DOSH); specific work of compression W_{comp}; isentropic compression efficiency η, and the two polytropic indices K and N.

The isentropic compression efficiency varied from 0.72 to 0.97; the efficiency is shown as a function of pressure ratio in Figure 4.7. This figure also shows a straight line fitted to these data points by linear regression. The fit is acceptable, although the data are rather more scattered towards the high end of the plot. The fitted line was:

$$\eta = 0.041 + 0.14 \times \Pi \tag{4.8}$$

for which the regression coefficient r was computed as +0.94, indicating a reasonable fit.

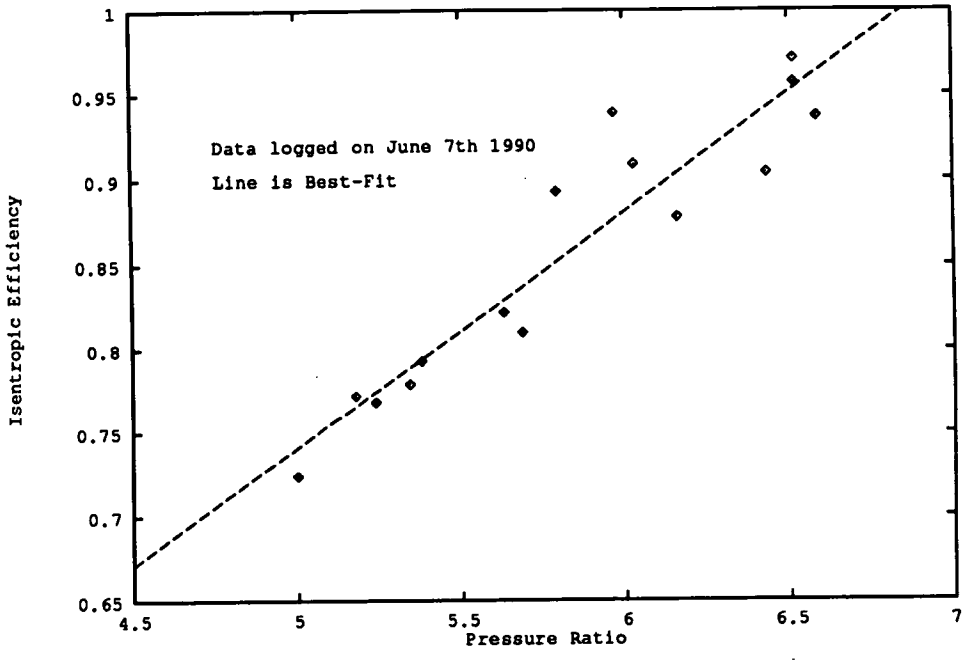

Figure 4.7: Isentropic Efficiency *vs.* Pressure Ratio

The compression efficiencies found during this session of operation are quite high compared to typical efficiencies found by other heat pump researchers; also remarkable is the nature of the relationship between efficiency and pressure ratio, which seems to be monotonically increasing. The Rotocold R3 "HIVI" compressor used in the plant had a nominal design pressure ratio of 5.5:1; it was expected that the isentropic efficiency would have exhibited a maximum in this region of the plot. One possible explanation for this behaviour could lie with the density of the suction gas (and hence the mass flow of refrigerant). As the discharge pressure was subject to a much lesser fractional change with time than the suction pressure, the observed changes in pressure ratio were chiefly caused by variation in the suction pressure. The suction gas temperature was also nearly invariant (a range of 41.8–43.9°C); so any change in suction gas density would be almost proportional to a change in suction pressure (and hence related to pressure ratio). The work of compression, calculated from the averaged data referring to the lowest metering pump setting, was 0.5 kW, compared to a rated power of 3.3 kW for the device. The apparently wonderful performance at high pressure ratios may not translate to a heat pump running with similar evaporator conditions but higher output temperatures. This point is borne out by Figure 4.8, which is a plot of the

isentropic efficiency as a function of the suction gas density. This clearly indicates an inverse relationship between the compression efficiency and the density of the gas being compressed.

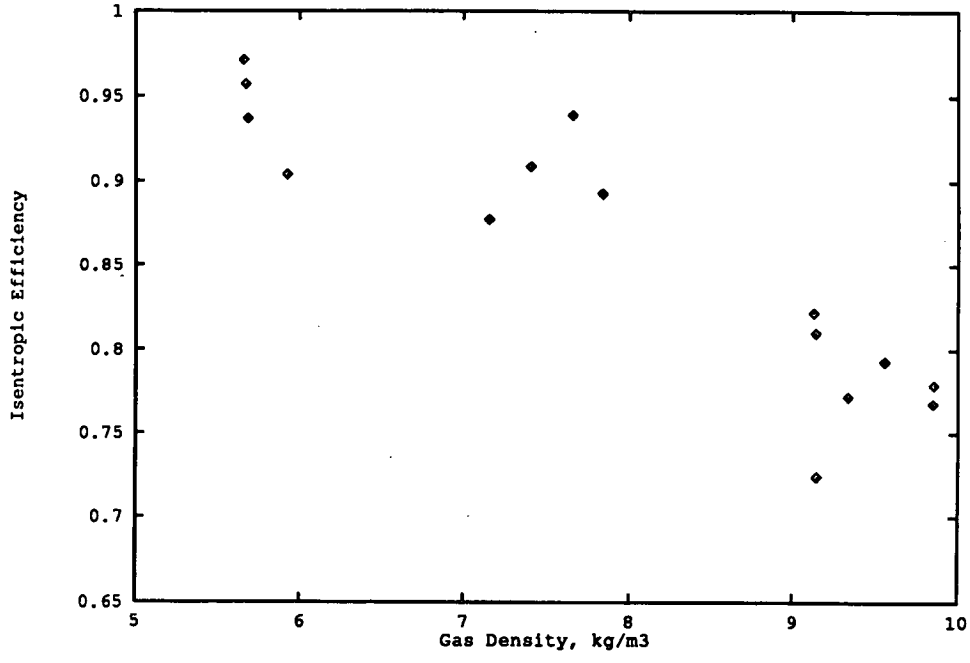

Figure 4.8: Variation of Isentropic Efficiency with Gas Density

The two polytropic indices which were computed were both almost invariant; the conclusion is that these values could safely be used to predict the performance of the compressor using R114, providing the range of inlet conditions used was similar to that used to derive the indices. The frictional heat loss may also predicted using the polytropic index N, by application of the First Law of Thermodynamics to the compressor:

$$\Delta h = q + w \tag{4.9}$$

For a polytropic path described by Equation 4.7, the work required to compress a real gas is given by:

$$w = P_s v_s \times \frac{N}{N-1} \times \left[\left(\frac{P_d}{P_s} \right)^{\frac{N-1}{N}} - 1 \right] \tag{4.10}$$

where P_s, v_s are the pressure and specific volume at the suction and P_d is the pressure at the discharge of the compressor. Once the specific work w has been calculated the

shown is the level indicated by the differential pressure transducer connected across the evaporator. The level is shown as the equivalent height of quiescent liquid; the real level could not be detected by simple measurement of the head, as the liquid holdup in the evaporator would be bubbling liquid. These level signals were used to construct the plot shown in Figure 4.9, which is a plot of the calculated evaporative heat transfer product $(UA)_e$ *versus* the indicated level. Both quantities have been plotted in dimensionless form: the data were divided by the values recorded at 14:10 hrs (the lowest indicated level). These data were regressed to a straight line fit, including the zero co-ordinate. The correlation coefficient r was +0.98, so this fit is good. Although the zero was included in the regression, the correlation yielded by the regression takes the form $y = m\,x + c$ rather than $y = m\,x$. This offset could be reduced by weighting the zero or by inclusion of additional data at lower measured levels, had these been available. The equation of the straight line was:

$$\frac{(UA)_e}{(UA)_{e,base}} = -0.047 + 1.17 \times \left[\frac{h}{h_{base}}\right] \tag{4.11}$$

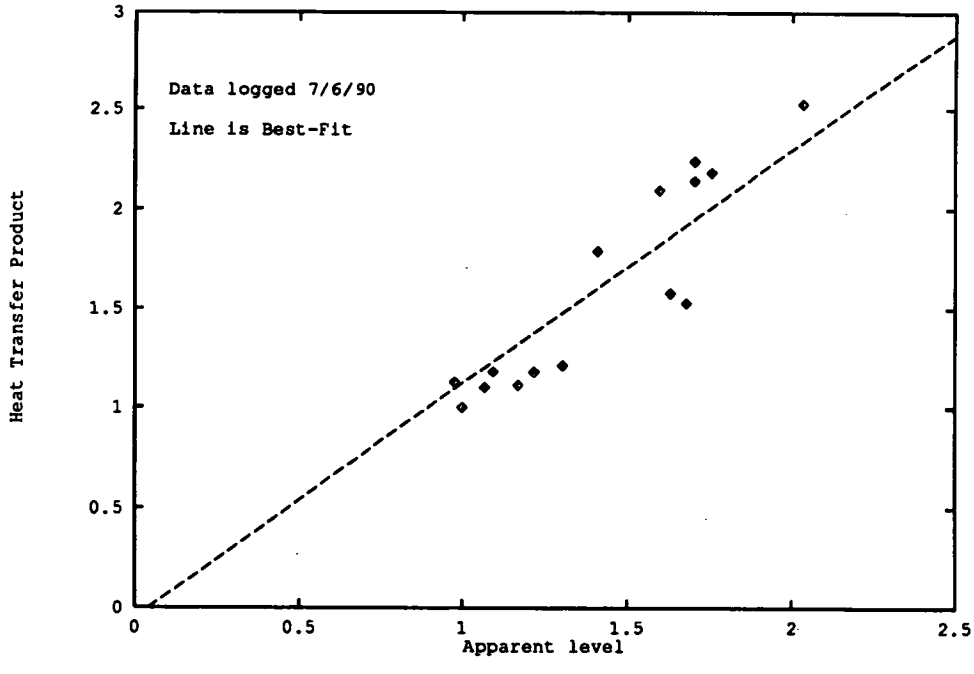

Figure 4.9: Evaporative UA vs Apparent Level

The relationship between the apparent level of liquid in the evaporator and the overall evaporator duty will be further explored in a later section, as part of an analysis based

Time	Level	$(UA)_e$	$(UA)_{sh}$	$\frac{(UA)_{sh}}{(UA)_e}$
hr	cm	kW/K	kW/K	—
13:40	15.5	0.0521	0.0047	0.089
13:52	13.0	0.0508	0.0056	0.111
14:00	11.5	0.0485	0.0049	0.101
14:10	11.9	0.0430	0.0056	0.130
14:22	12.7	0.0473	0.0043	0.091
14:30	13.9	0.0478	0.0039	0.082
14:40	14.5	0.0507	0.0039	0.078
15:03	19.0	0.0900	0.0023	0.026
15:10	20.3	0.0920	0.0020	0.022
15:20	16.8	0.0769	0.0026	0.034
15:30	20.3	0.0962	0.0025	0.026
15:46	20.9	0.0938	0.0098	0.083
16:00	24.2	0.1087	0.0091	0.084
16:10	20.0	0.0657	0.0049	0.075
16:20	19.4	0.0679	0.0053	0.078

Table 4.6: Evaporator Performance from **RIGEVAP** Program

on *all* the data gathered in these experimental runs.

4.3.4.6 June 9th Part 1: Summary of Run

On June 9th the plant was run for a period of several hours at three different compressor speeds. In this experiment, the evaporator feed rate was altered to maintain a near-constant evaporator pressure (and hence near-constant evaporation temperature). The flowrates of both water streams were not altered throughout this experiment. The aim of the experiment was to determine the performance of the plant as a function of compressor speed, under broadly similar conditions to those used in the first experiment on June 7th. The set points and main controlled variables are summarised below:

- **Compressor speed:** 3 speeds: 53%, 66%, 40% (1590 rpm, 1980 rpm, 1200 rpm)
- **Heat source flow:** 15.0 l/min *i.e.* 0.25 kg/s
- **Heat source temperature:** 30 °C
- **Heat sink flow:** 5.6 l/min *i.e.* 0.093 kg/s

- **Heat sink temperature:** 60 °C
- **Metering pump setting:** 3 settings: 72%, 88%, 57%
- **Evaporator pressure:** 1.8 bar (Saturation temperature = 18 °C)

Procedure The procedure was as used on June 7th; after each alteration of compressor speed, the metering pump setpoint was slowly changed until the evaporator pressure was restored to the desired value. Both water flowrates were left at constant settings throughout the experiment.

Temperature Variation The temperature history is shown in Table 4.7, which has the same format as that used in Section 4.3.4.3. The datasets corresponding to different compressor speeds have been separated by horizontal lines; the other tables in this section will follow the same pattern where necessary. The temperature profiles in the evaporator and condenser are plotted in Figure 4.10 and Figure 4.11.

During this experiment the thermocouple used to record the temperature of water leaving the evaporator developed a fault; this affected the readings taken at the last compressor speed used (from 18:25 to 19:00). The temperature difference indicated by the evaporator thermopile has been used to estimate the water exit temperature where this is required in analysis.

The control of the heat source and heat sink temperatures was much improved for this experimental run; this was caused by modification of the monitor program to implement on-off automatic control on the water tank temperatures. The control of evaporation temperature was also reasonably good, given that this was done manually by the author in the breaks between reading gauges and checking the satisfactory operation of the plant. To summarise these temperature data:

- **Mean heat source temperature:** 29.6 °C ± 1.0 °C
- **Mean evaporation temperature:** 17.5 °C ± 0.8 °C
- **Mean heat sink temperature:** 59.6 °C ± 0.6 °C

Time hr	$T_{ev,i}$ °C	$T_{ev,o}$ °C	T_{suct} °C	T_{dis} °C	T_{co} °C	T_{so} °C	T_{si} °C	T_{load} °C
16:10	17.3	29.6	43.8	95.5	69.7	30.4	59.6	68.1
16:20	17.9	30.3	44.2	96.4	70.9	31.3	60.2	69.9
16:30	17.2	29.9	43.8	96.6	70.7	30.1	59.3	70.2
16:40	17.8	29.8	43.8	96.9	70.1	30.9	60.0	69.5
16:50	16.9	28.8	44.0	96.9	69.4	29.4	58.5	69.8
17:00	17.4	29.4	43.7	97.0	70.6	30.4	59.7	69.6
17:15	17.5	30.5	44.2	97.1	70.9	31.5	59.9	69.9
17:30	18.1	27.5	43.6	100.8	72.0	29.4	58.9	71.0
17:40	18.1	28.0	43.8	102.1	72.5	29.9	58.4	71.4
17:50	18.2	28.4	43.5	102.3	73.1	29.9	60.5	71.8
18:00	17.4	28.9	43.7	102.3	72.5	30.1	59.8	70.7
18:10	18.5	29.0	43.9	102.6	73.4	30.3	59.0	72.3
18:25	17.6	27.6	43.8	96.1	69.4	29.1	59.7	67.5
18:35	14.9	25.8	43.4	93.1	68.7	26.5	59.9	67.1
18:45	17.1	25.0	42.8	92.0	68.7	26.7	59.6	66.7
18:55	18.2	25.7	42.9	91.0	69.4	27.5	59.8	67.3
19:00	17.0	23.9	42.3	90.4	69.0	30.3	59.7	67.2

Table 4.7: Temperature Histories for June 9th 1990

- **Mean condensation temperatures:**
  - *Compressor Speed 1:* $70.3\,°C \pm 0.6\,°C$
  - *Compressor Speed 2:* $72.7\,°C \pm 0.6\,°C$
  - *Compressor Speed 3:* $69.0\,°C \pm 0.4\,°C$
- *Mean product temperatures:*
  - *Compressor Speed 1:* $69.6\,°C \pm 0.7\,°C$
  - *Compressor Speed 2:* $71.4\,°C \pm 0.6\,°C$
  - *Compressor Speed 3:* $67.2\,°C \pm 0.3\,°C$

It is obvious from these data that, despite a near-constant set of pressure ratios and suction conditions, there was a correlation between compressor speed and discharge temperature. The degree of superheat on the compressed vapour increased with increasing speed. This implies that the compression efficiency is a decreasing function of compressor speed; an observation that agrees with intuition. The analysis of compressor performance will bear this out.

A further important point to be gleaned from Table 4.7 is that the temperature approach at the evaporator outlet was consistently very low, *even at the highest pump rate.*

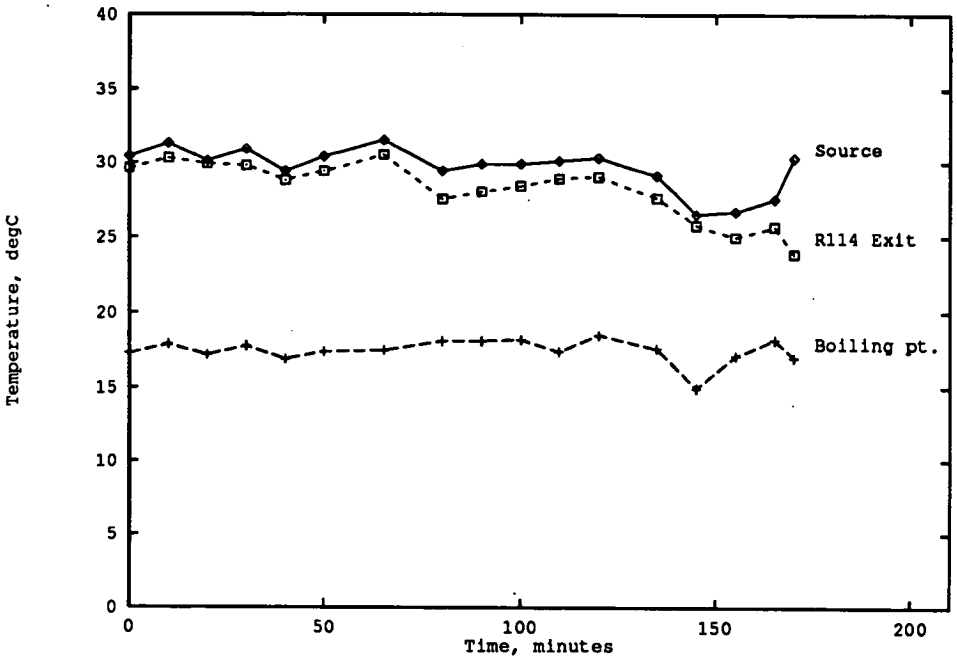

Figure 4.10: Temperatures in Evaporator, June 9th 1990

The implication is that the special surface inside the evaporator gave high (UA) values for gas heating, as the evaporator was operating rather close to its known flooding limit under these conditions. This could imply that controlling the feed rate on the observed degree of superheating performed by the evaporator (as proposed in Section 4.3.4.3) may not be a good idea; the sensitivity and rate of response of the pump might lead to frequent incursions into the flooded region of operation, with the problems that could entail.

Comparison of the temperature approaches attained on June 9th with those obtained on June 7th revealed that the attainable approaches on June 9th were closer on average than on June 7th. This may be in some way related to the mass flow of refrigerant; the highest mass flow used on June 7th was the same as the lowest used on June 9th.

Pressure Variation The variation of pressures in the plant with time is shown in Figure 4.12. The discrepancy between the recorded discharge pressure at the compres-

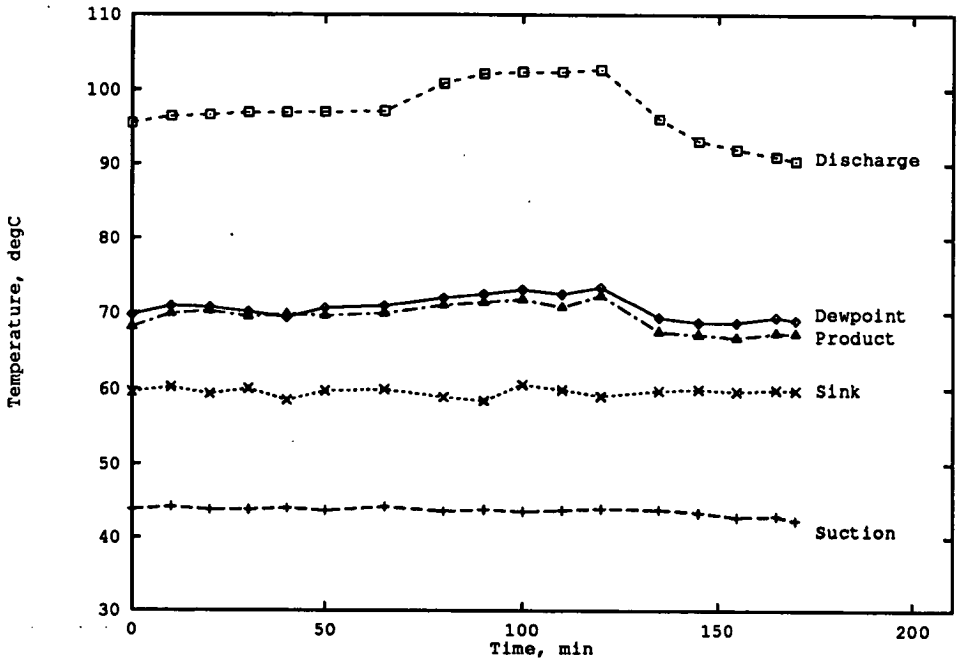

Figure 4.11: Temperatures in Condenser, June 9th 1990

sor manifold and the registered condensation pressure was more marked during this run. This must be an effect of the increases in compressor speed.

4.3.4.7 June 9th Part 2: Heat Pump Performance

The temperature records shown in Table 4.7 show that the heat pump operated over an external lift of *ca.* 40 degrees throughout the experiment. The internal lift was approximately 53 degrees; most of the difference in these lifts was caused by the evaporator. Although the exit approach in the evaporator was very low, this unit was performing 10-12 degrees of superheat; the bulk of the heat transferred in the evaporator was used to evaporate the refrigerant, and *this* heat transfer process took place with a much larger exit approach than the superheat.

The heat duties, calculated from the experimental measurements of water flowrate and

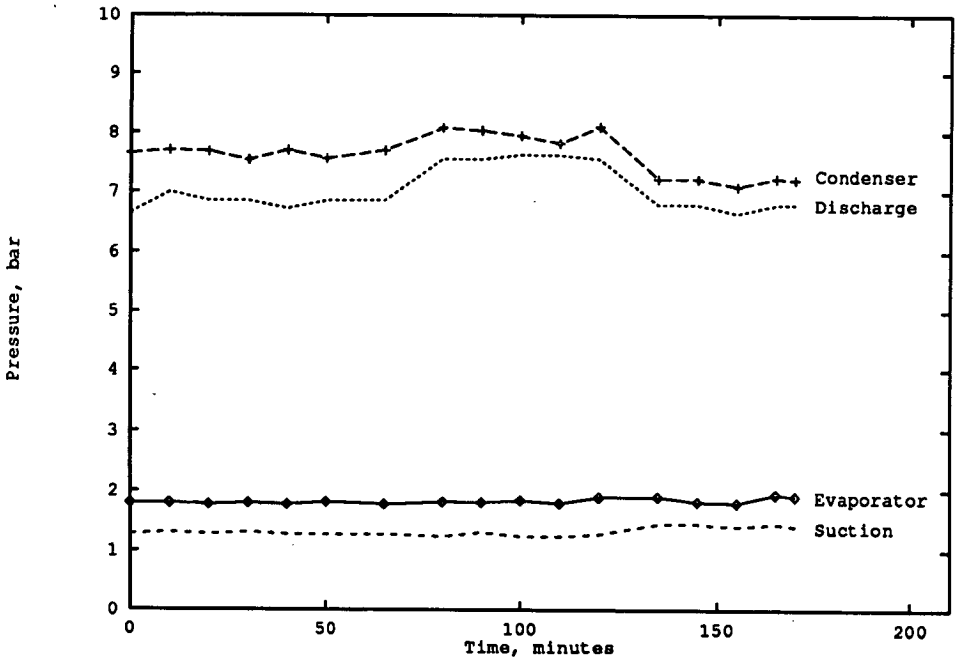

Figure 4.12: Recorded Pressures, June 9th 1990

temperature difference, are shown in Table 4.8. This table also shows the apparent level of liquid in the evaporator, for future reference. The heat duties are plotted in Figure 4.13 and Figure 4.14, which show the condenser and evaporator heat fluxes calculated by each route.

These figures illustrate that, while the measured heat fluxes followed the same trends as the heat flux calculated from the average refrigerant circulation, there was some variation between the instantaneous signals and the predicted fluxes. The condenser fluxes were more consistently close to the calculated heat output than the evaporator fluxes were to the calculated heat input. This suggests inward heat leakage as a possible occurrence in the evaporator. Furthermore, the measured fluxes in the condenser seemed to oscillate about the mean flux as calculated from the feed rate. This is probably caused by the way in which the monitor program read the thermocouples and thermopiles: the signals were only scanned once before display (and/or storage). Averaging the input signals over a period of time would have smoothed the readings from both thermocouples and thermopiles but was not performed by the control pro-

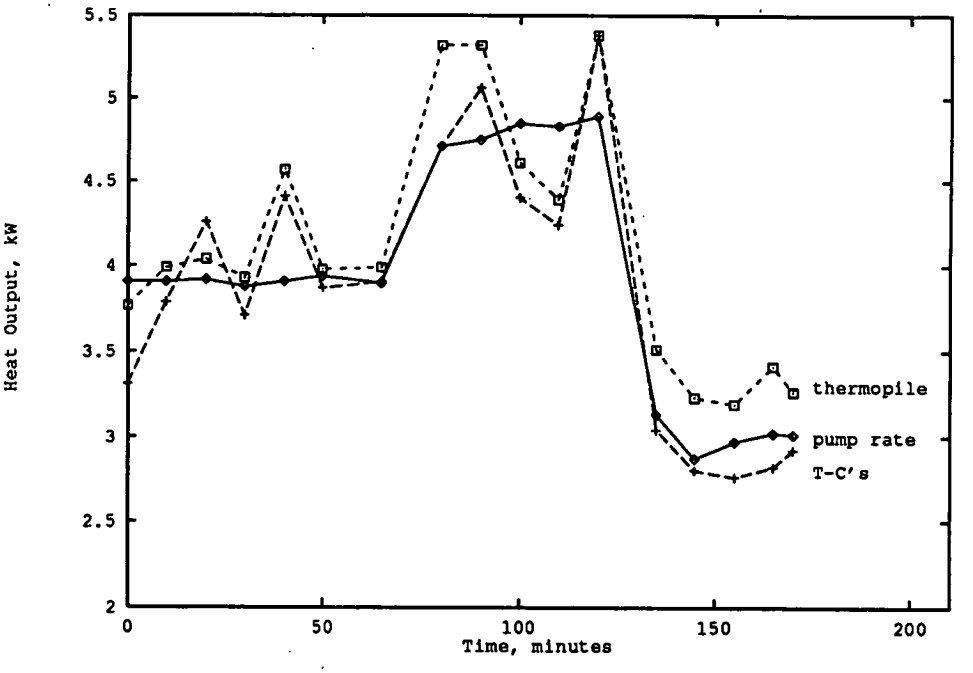

Figure 4.13: Condenser Heat Outputs: June 9th 1990

gram; it would have required too much CPU time from the PC. Figure 4.13 shows that averaging of the recorded heat fluxes in the condenser would give mean heat fluxes close to those calculated from the feed rate; so the analysis of the heat pump may proceed using the flux values calculated from the pump rate.

Efficiency of Heat Pump The program **HPUMP** was again used to calculate the specific enthalpy changes of the refrigerant in the evaporator, condenser and compressor. The output from **HPUMP** is summarised in Table 4.9. The COPs attained by the heat pump in this experiment show a dependence on the compressor speed (and hence throughput of refrigerant). At the lowest feed rate used, which was almost identical to the highest feed rate used in the experiment of June 7th, the COPs and heat fluxes obtained are comparable to the results of June 7th. This is a satisfactory indication of consistency. It is also evident that under these conditions the effect of gas density and pressure ratio on the heat pump efficiency is not so marked; the analysis of the compressor in Section 4.3.4.8 bears this out.

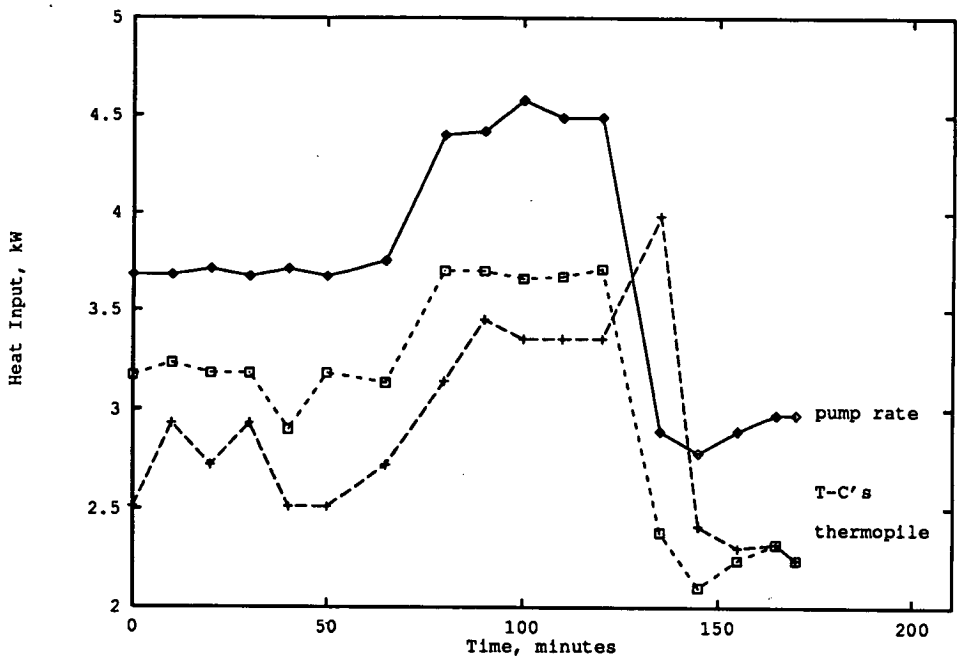

Figure 4.14: Evaporator Heat Inputs: June 9th 1990

4.3.4.8 June 9th Part 3: Compressor and Evaporator Performance

The analysis presented in this section follows the pattern used in Section 4.3.4.5, to which the reader is referred for further detail.

Compressor Performance The compressor's isentropic efficiency was calculated for each data point using the **HPUMP** program, resulting in the data shown in Table 4.10. The efficiencies recorded in this experiment varied from 0.67 to 0.76; the pressure ratio varied from 4.7 to 6.1. Both these ranges are narrower than those recorded on June 7th. The variation of efficiency with pressure ratio is shown in Figure 4.15. There appears to be only a slight dependence on pressure ratio: in contrast to the previous experiment. This figure also shows the straight-line fit to the data, which has the equation:

$$\eta = 0.788 - 0.0116 \times \Pi \tag{4.12}$$

for which the regression coefficient r was computed as -0.25, indicating a mediocre fit.

Time	Level	$\dot{Q}_{ev}$ T/C	$\dot{Q}_{ev}$ T/PILE	$\dot{Q}_{co}$ T/C	$\dot{Q}_{co}$ T/PILE	$\dot{Q}_{ev}$ (PREDICTED)	$\dot{Q}_{co}$ (PREDICTED)
hr	cm	kW	kW	kW	kW	kW	kW
16:10	26.9	2.51	3.17	3.31	3.77	3.68	3.91
16:20	25.8	2.93	3.23	3.79	3.99	3.68	3.91
16:30	24.2	2.72	3.18	4.26	4.04	3.71	3.92
16:40	27.1	2.93	3.18	3.71	3.93	3.67	3.88
16:50	27.2	2.51	2.90	4.41	4.57	3.71	3.91
17:00	26.8	2.51	3.18	3.87	3.98	3.67	3.94
17:15	26.0	2.72	3.13	3.91	3.99	3.75	3.90
17:30	35.5	3.14	3.70	4.71	5.32	4.40	4.71
17:40	35.8	3.45	3.70	5.06	5.32	4.42	4.75
17:50	37.8	3.35	3.66	4.40	4.61	4.58	4.85
18:00	35.2	3.35	3.67	4.24	4.39	4.49	4.83
18:10	37.3	3.35	3.71	5.38	5.38	4.49	4.89
18:25	20.4	3.98	2.38	3.04	3.51	2.89	3.13
18:35	17.6	2.41	2.10	2.80	3.23	2.78	2.87
18:45	23.6	2.30	2.24	2.76	3.19	2.89	2.97
18:55	22.8	—	2.32	2.82	3.41	2.97	3.02
19:00	23.5	—	2.24	2.92	3.26	2.97	3.01

Table 4.8: Heat Fluxes: June 9th 1990

Figure 4.16is a plot of isentropic efficiency *versus* suction gas density. This indicates that for this experiment the isentropic efficiency was almost independent of suction gas density.

The conclusion drawn from these figures is that the significant variation in compression efficiency was caused by variation in the compressor speed: the highest speed setting used gave the highest pressure ratios and hence the lowest efficiencies. The analysis of the variation in compressor efficiency as a function of speed will be left for later; by using data from *all* the pure-fluid runs it should be possible to identify any correlation with *either* speed *or* mass flowrate.

Evaporator Performance The gross deviations between the calculated and measured heat fluxes in the evaporator made any attempts to derive quantitative heat-transfer product data seem rather pointless. Furthermore, in this experiment trouble was experienced with *both* water-side thermocouples; neither measured temperature may be considered to be accurate. This would lead to difficulties in preparing input for the calculation program **RIGEVAP**. The major observations on the evaporator

Time hr	Δh_{ev} kJ/kg	Δh_{co} kJ/kg	Δh_{comp} kJ/kg	COP_a —	COP_c —	ϵ —
16:10	123.99	129.62	33.92	3.82	6.54	0.584
16:20	124.50	128.64	34.02	3.78	6.49	0.583
16:30	125.17	129.74	34.59	3.75	6.48	0.579
16:40	125.07	130.10	34.88	3.73	6.56	0.568
16:50	124.47	131.03	34.84	3.76	6.52	0.576
17:00	125.36	129.63	34.99	3.70	6.46	0.573
17:10	125.71	129.38	34.71	3.73	6.44	0.579
17:30	123.37	130.45	37.40	3.49	6.40	0.545
17:40	123.65	130.97	38.43	3.41	6.35	0.536
17:50	123.58	130.39	38.65	3.37	6.31	0.535
18:00	124.12	131.06	38.50	3.40	6.27	0.543
18:10	123.74	130.38	38.73	3.37	6.31	0.533
18:25	127.02	130.29	34.47	3.78	6.61	0.572
18:35	126.66	128.60	32.30	3.98	6.35	0.627
18:45	126.93	127.85	31.95	4.00	6.63	0.604
18:55	126.61	126.09	30.94	4.08	6.69	0.609
19:00	125.87	126.04	30.84	4.09	6.58	0.621

Table 4.9: Heat Pump Performance: June 9th 1990

performance are restricted to the effect of the variation in feed rate on the amount of heat-transfer surface required to maintain the constant evaporator pressure used in this experiment. It is evident from reference to Table 4.8 that there is a definite link between the apparent level measurement and the overall duty: this is to be expected, since most of the evaporator's duty will be the latent heat transferred to liquid in contact with the surface. Comparison of the indicated levels in Table 4.8 with those in Table 4.6 further indicates that this relationship may be applicable to all the data obtained in the course of experimentation. Therefore the derivation of a correlation between heat transferred in the evaporator and the level will be delayed until the remaining experiments using pure R114 have been described.

The analysis presented through Section 4.3.4.3 to Section 4.3.4.8 has been fairly exhaustive. The remaining experimental work performed using pure R114 in June 1990 will be more briefly described; the intention is to summarise all the findings of this phase of work.

Time hr	P_d:P_s —	V_s m^3/kg	$DOSH$ °C	Δh_{comp} kJ/kg	η —	Polytropic K	Indices N
16:10	5.216	0.1169	33.8	33.92	0.732	1.10	1.04
16:20	5.342	0.1138	33.5	34.02	0.747	1.10	1.04
16:30	5.378	0.1169	33.8	34.59	0.738	1.10	1.04
16:40	5.237	0.1137	33.1	34.88	0.718	1.10	1.04
16:50	5.270	0.1169	34.0	34.84	0.724	1.10	1.04
17:00	5.378	0.1168	33.7	34.99	0.729	1.10	1.04
17:15	5.378	0.1170	34.2	34.71	0.736	1.10	1.04
17:30	6.083	0.1201	34.4	37.40	0.733	1.10	1.04
17:40	5.763	0.1137	33.1	38.43	0.689	1.11	1.04
17:50	6.139	0.1201	34.3	38.65	0.712	1.10	1.04
18:00	6.139	0.1202	34.5	38.50	0.715	1.10	1.04
18:10	5.919	0.1169	33.9	38.73	0.696	1.11	1.04
18:25	4.690	0.1024	30.3	34.47	0.673	1.11	1.04
18:35	4.690	0.1023	29.9	32.30	0.717	1.10	1.04
18:45	4.707	0.1047	30.0	31.95	0.727	1.10	1.04
18:55	4.690	0.1021	29.4	30.94	0.748	1.10	1.03
19:00	4.805	0.1045	29.5	30.84	0.763	1.10	1.03

Table 4.10: Compressor performance on June 9th 1990

4.3.4.9 June 10th: High-Speed Run

Description of Run On June 10th the heat pump was run with the following operational setpoints:

- **Compressor speed:** 100% (3000 rpm)
- **Heat source flow:** 13.4 l/min *i.e.* 0.223 kg/s
- **Heat source temperature:** 36 °C
- **Heat sink flow:** 4.75 l/min *i.e.* 0.079 kg/s
- **Heat sink temperature:** 60 °C
- **Metering pump setting:** 100% *i.e.* 0.041 kg/s
- **Evaporator pressure:** *ca.* 1.8 bar (Saturation temperature = 18 °C)

These conditions were chosen to illustrate the effect of compressor speed on the heat pump performance for a given set of source and sink conditions. The heat source

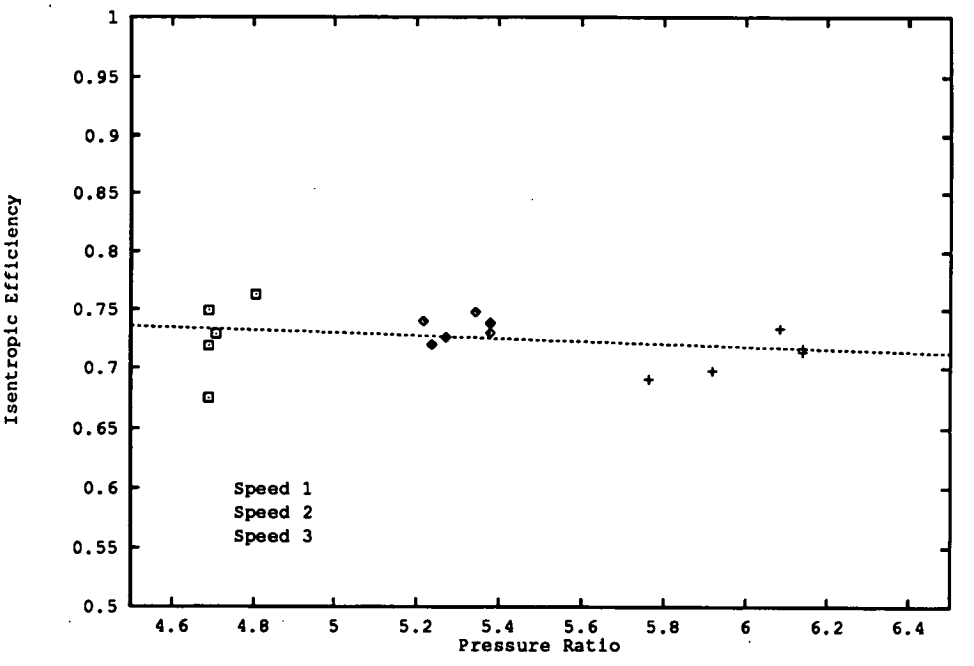

Figure 4.15: Isentropic Efficiency *versus* Pressure Ratio

temperature was raised to enable use of the higher compressor speed; if it had been left at 30 °C (cf. the earlier runs) then the evaporation temperature would have dropped below the desired setpoint. This was established at the time and the new source temperature chosen by trial and error.

The detailed temperature and pressure histories have not been included for reasons of space; they were only included in previous sections to illustrate the kind of variations which could occur throughout the course of an experiment.

Heat Pump Performance In this experiment the mean product temperature was 76 °C; the external lift of the heat pump was therefore approximately 40 degrees, as in the other runs. The mean condensation temperature was 76 °C (in line with previous observations of close approach in the condenser). The mean evaporation temperature was 19 °C, yielding an overall internal lift of 57 degrees. This is roughly equivalent to the lifts attained in the previous work (58 degrees on June 7th, 53 degrees on June 9th),

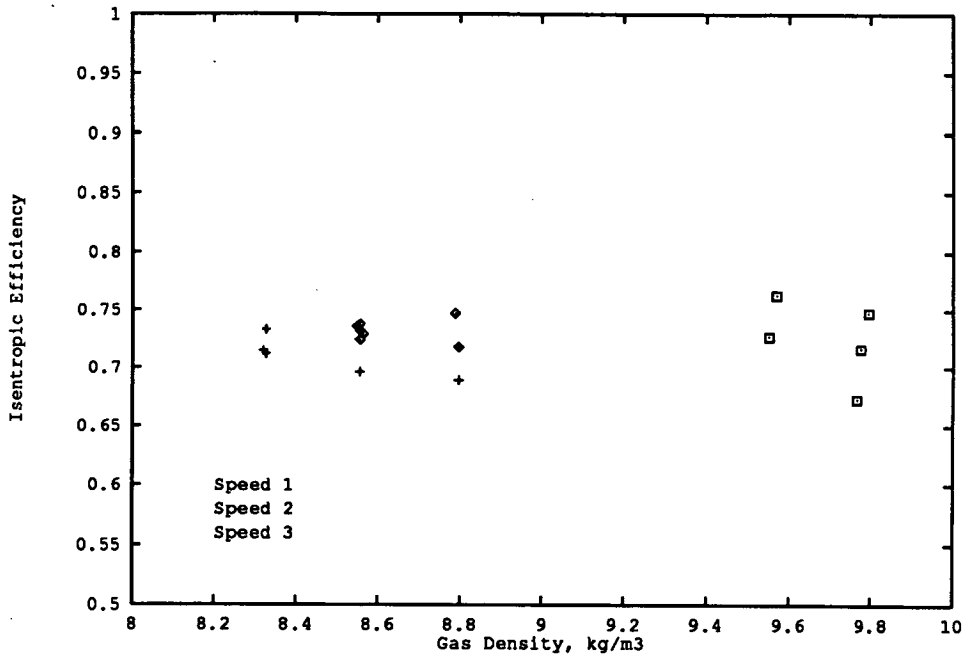

Figure 4.16: Isentropic Efficiency *versus* Suction Gas Density

and the effect on Carnot efficiency may be small compared to the effect of increased compressor speed.

The performance of the heat pump is summarised in Table 4.11. This follows the format of the tables used in previous sections but the heat fluxes are lumped in with the COP data. The apparent evaporator level is also shown in this table. The heat fluxes were calculated from the feed pump rate. The heat fluxes as calculated from the water thermocouple and thermopile measurements exhibited the same patterns of behaviour as those gathered on June 7th and 9th; underprediction of evaporator heat flux and agreement between the measured and calculated condenser heat fluxes to within 10%.

It is evident that the Carnot efficiency and attained COP are both significantly lower than those found previously; the explanation is a decrease in the isentropic efficiency of compression. This was manifest in an increase in the adiabatic discharge temperature (not tabulated here).

Time hr	Level cm	$\dot{Q}_{ev}$ kW	$\dot{Q}_{co}$ kW	$\dot{W}_{comp}$ W	COP_a —	COP_c —	ϵ —
16:00	40.9	5.16	5.51	1.79	3.07	5.99	0.513
16:10	43.9	5.13	5.55	1.81	3.06	6.11	0.501
16:20	43.3	5.15	5.65	1.84	3.08	6.35	0.484
16:30	44.5	5.13	5.44	1.80	3.02	5.98	0.505
16:40	38.4	5.16	5.61	1.83	3.06	6.10	0.502
16:50	43.3	5.15	5.52	1.82	3.03	6.14	0.494

Table 4.11: Heat Pump Performance: June 10th 1990

Compressor Performance The performance of the compressor is summarised in Table 4.12. The compressor worked over a higher pressure ratio in this experiment than in most of the other runs because of a combination of higher condenser temperature and suction-side pressure drop. This may explain some of the deterioration in isentropic compression efficiency. The isentropic efficiencies obtained in this experiment are closely grouped around a mean of 66%, where the efficiencies obtained previously were in the range 70–95%. The polytropic indices calculated for this experiment were constant; there is a slight increase in both indices compared to previous values. The significance of this is slight; the smallest value of K was recorded as 1.09, compared to the value of 1.11 obtained here. This translates to a 2.5% error in prediction of discharge temperature using the standard pressure ratio of 5.5:1.

Time hr	$P_d : P_s$ —	V_s m^3/kg	$DOSH$ °C	$\dot{W}_{comp}$ kJ/kg	η —	Polytropic K	Indices N
16:00	6.853	0.1290	39.5	43.78	0.670	1.11	1.05
16:10	6.600	0.1253	39.0	44.25	0.657	1.11	1.05
16:20	6.543	0.1251	38.6	44.79	0.646	1.11	1.05
16:30	6.694	0.1219	38.6	43.89	0.667	1.11	1.05
16:40	6.853	0.1289	39.2	44.68	0.664	1.11	1.05
16:50	6.829	0.1250	38.3	44.40	0.665	1.11	1.05

Table 4.12: Compressor Performance, June 10th 1990

Evaporator Performance The evaporator operated very close to the flooding region in this experiment; flooding was known to start with indicated levels in the range 40–50 cm. The mean refrigerant vapour exit temperature was 33.5 °C ± 0.4 °C. Thus on average the unit performed 14.5 degrees of superheat– superior to the figures obtained on June 9th. The approach between refrigerant vapour and water inlet was typically between 2–3 degrees. The performance as a superheater therefore seems to be rather better at the higher compressor speed. This may indicate a sensitivity of the vapour-

side film heat transfer coefficient for superheat to the vapour velocity, which could be expected. The increased source temperature may also play a part in the improved heat transfer.

4.3.4.10 June 14th: Transient Response Run

The experiment performed on June 14th was intended both to supply further information on the compressor performance and to illustrate the transient response of the plant to a number of deviations from steady state. The aims of the experiment were:

- To collect performance data for a new compressor speed.
- To record the approach to true steady-state operation by the plant.
- To test the ability of the PC to maintain control of the product temperature by feedback control of the product flowrate.
- To demonstrate the effect of a shift in evaporator feed rate on the system (all other variables held constant).

Procedure The plant was started in the normal way and allowed to come close to a steady state. The initial control settings were:

- **Compressor speed:** 75% (2250 rpm)
- **Heat source flow:** 14.2 l/min *i.e.* 0.237 kg/s
- **Heat source temperature:** 28 °C
- **Heat sink flow:** varied to control load temperature.
- **Product temperature:** 70 °C
- **Heat sink temperature:** 60 °C
- **Metering pump setting:** 86.5% *i.e.* 0.0354 kg/s

- **Evaporator pressure:** *ca.* 1.7 bar (Saturation temperature = 17 °C)

The first data were logged at 15:54 hr, then at 2 minute intervals until 16:04, when the feed pump rate was increased to 92%. At 16:18 the product temperature setpoint was changed to 80 °C. At 16:26 the feed pump rate was further increased to 96% in order to compensate for an observed fall in evaporator pressure. The experiment had to be aborted after 16:31, as a vapour lock developed in the heat sink stream, preventing flow of water and thereby destroying the equilibrium of the plant. It was not possible to recover the operational state from this setback in a reasonable timescale.

Transient Responses The plant was already delivering heat under controlled circumstances when data logging began; however, a true steady state had still not been attained at that time. The behaviour of the plant is clearly shown in Figure 4.17 and Figure 4.18, which show the variation of temperatures throughout the plant with time.

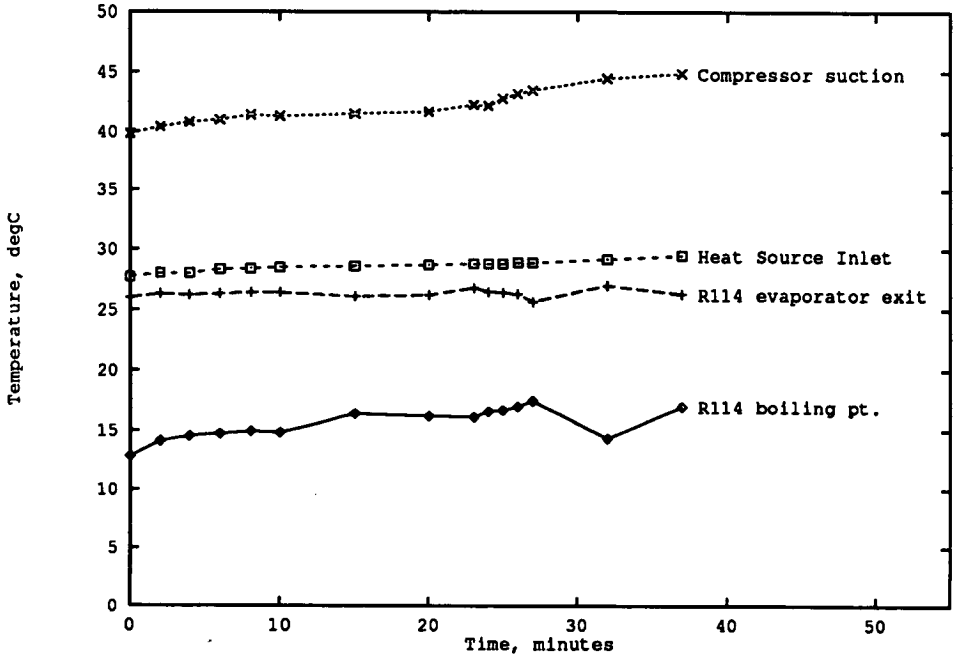

Figure 4.17: Temperatures in Evaporator, 14th June 1990

The temperatures in the evaporator remained substantially constant for most of the

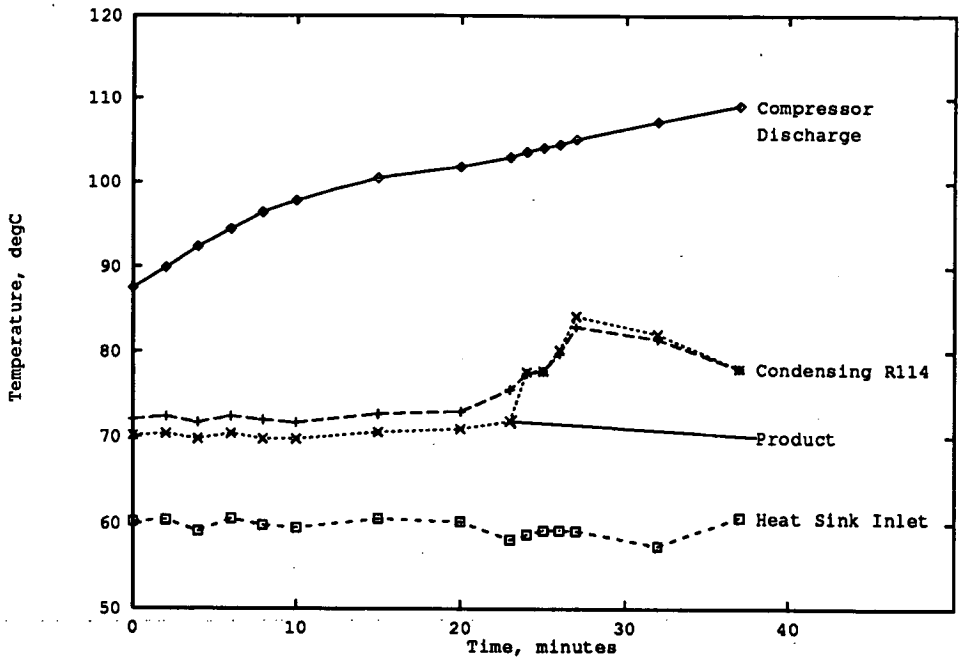

Figure 4.18: Temperatures in Condenser, 14th June 1990

experiment, save for the dip in pressure which necessitated the second increase in feed rate. This was probably a consequence of an increase in the required condensing temperature which accompanied the change of product temperature setpoint. The compressor suction temperature showed a slow increase after the point at which the product setpoint was changed; this was because the suction superheater used the product stream as a heat source. Any increase in product temperature could therefore be expected to cause an increase in suction gas temperature.

In contrast to the temperatures on the low-pressure side of the plant, there was considerable variation of the high-pressure stream temperatures. Figure 4.18 shows that the compressor discharge temperature had not stabilised at the start of data recording, but was levelling off when the product water temperature setpoint was altered. This caused a renewal of the rate of increase in the discharge temperature. This behaviour indicates the effect of the oil separator on the thermal inertia of the system; the compression efficiency in the early readings would be improved by heat transfer from the gas *via* the lubricant. The effect of changing the set point for the product temperature was of

course to increase the saturation temperature (and hence condenser pressure) required to meet the duty. It may therefore be inferred that the resultant increase in pressure ratio caused a decrease in compression efficiency, manifest by an increasing degree of superheat at the discharge. It was not possible to quantify this as the manifold pressure gauge readings were not taken in this experiment: the author had insufficient time to perform this task while overseeing the necessary alterations to the rest of the control setpoints.

Figure 4.18 also shows a classical overshoot and recovery of a controlled variable in response to a step change in setpoint. The product water temperature was stable at 70 °C when the change in setpoint to 80 °C was initiated: the plot shows the temperature overshooting the setpoint from below, dropping to a (smaller) negative overshoot from above, then heading back up towards the new setpoint. It was unfortunate that the plant should fail at this point: this prevented determination of the time constant of the product control loop. The time constant was evidently on the scale of a few minutes, however, which suggests the equipment could cope with the kind of fluctuation timescales envisaged with wave or wind energy sources.

Heat Pump Performance The lack of compressor manifold readings made calculation of actual COP and compression efficiency impossible, as the pressure ratio over the compressor was not known. It was still possible to calculate the heat transferred in the evaporator and condenser from the available measurements. These have been plotted as functions of elapsed time in Figure 4.19 and Figure 4.20, in order to illustrate the effect of the transients on instantaneous heat fluxes as opposed to the fluxes predicted by the constant feed rate.

Figure 4.19 shows the heat fluxes in the evaporator, calculated from: the feed pump rate; the thermocouple signals, and the thermopile signals. Both thermocouple and thermopile signals yield a heat flux lower than the predicted value from the feed pump setting. Furthermore, the similarities in the shape of the flux graphs from the measurements indicates that these provide reliable information about trends in the instantaneous heat flux in the evaporator; the calculation of heat flux from the evaporator feed rate fails to account for the possible variation in holdup of liquid inside the evaporator.

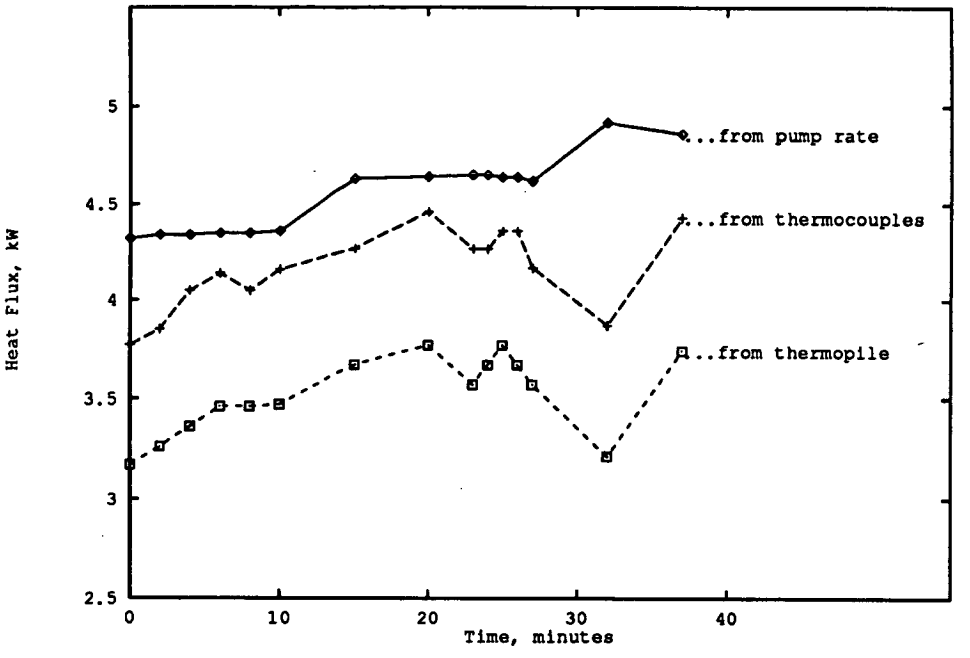

Figure 4.19: Evaporator Heat Flux, June 14th 1990

Figure 4.19 is a plot of the calculated heat fluxes in the condenser; it shows a similar correspondence between the heat fluxes predicted by the thermocouples and the thermopile. The plot also indicates a sharp dip in heat output; cross-reference to Figure 4.18 shows this to occur after the alteration of the product temperature setpoint. This is probably explained by diversion of refrigerant to the vapour phase to raise the pressure throughout the high-pressure side; the thermal requirement of the fabric of the heat pump would also have played a major part in this dip in performance. This is an example of one of the drawbacks of a heat pump operating with a pure working fluid.

Evaporator Performance The problems with evaporator thermocouples had been solved by the time of this experiment; consequently the program **RIGEVAP** was used to obtain heat transfer product data from the experimental measurements of temperature and flowrate. The storage tank temperature in this experiment was stable at 32 °C and 2.5 bar; an adiabatic flash to the mean evaporator pressure (1.7 bar) would cause vapourisation of 12% of the feed. This figure would therefore be the expected *minimum*

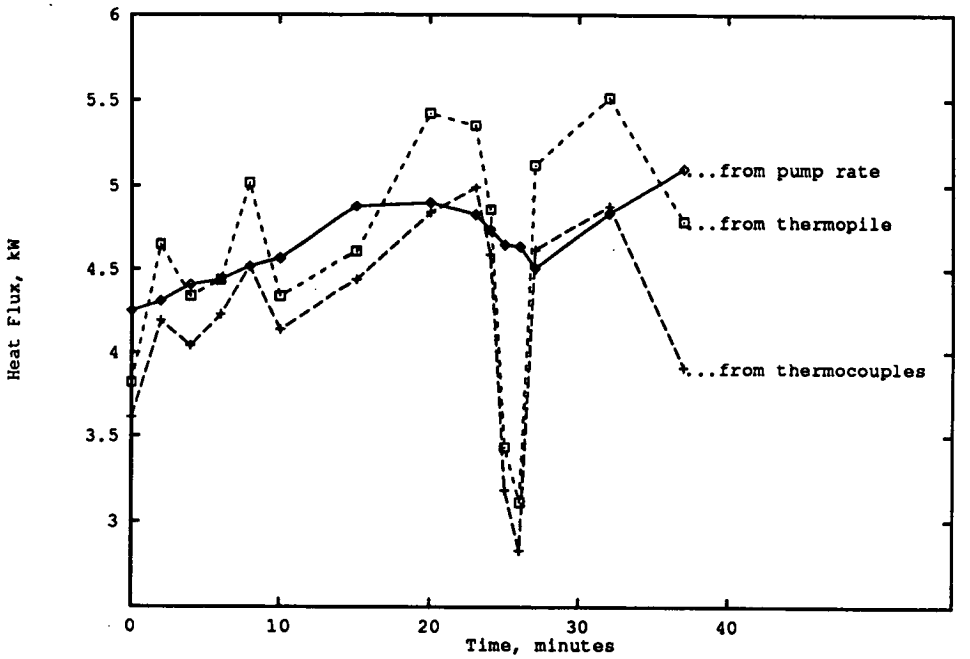

Figure 4.20: Condenser Heat Flux, June 14th 1990

feed vapour fraction; inward heat leakage would cause some additional vapourisation. The loading valve on the metering pump, which would raise the pressure in the line above the suction (storage tank) pressure, would cause some additional flashing of vapour. The results of the analysis are summarised in Table 4.13.

The vapour fraction of feed (shown as x_{vap}) required to satisfy the heat balance varied around a mean of 19%; as the minimum expected vapour fraction was 12% this indicated a believable vapour fraction. The repeatability of the indicated level as an index of evaporative heat duty is shown by this table; this prompted construction of Figure 4.21 and Figure 4.22.

Figure 4.21 shows the correlation between the evaporative heat duty (calculated by **RIGEVAP**) and the measured level signal. A regression was performed, yielding the relation:

$$\dot{Q}_e = 0.65 + 0.084 \times h \tag{4.13}$$

where the evaporative heat duty $\dot{Q}_e$ is in kW and the apparent level h in cm. The

Time	Level	$(UA)_e$	$(UA)_h$	$\frac{(UA)_h}{(UA)_e}$	X_{vap}	$\dot{Q}_e$	$\dot{Q}_h$
hr	cm	kW/K	kW/K	—	—	kW	kW
15:54	33.8	0.089	0.0167	0.188	0.27	3.43	0.33
15:56	35.8	0.100	0.0169	0.169	0.24	3.55	0.30
15:58	37.4	0.111	0.0169	0.153	0.20	3.77	0.29
16:00	38.0	0.113	0.0165	0.146	0.18	3.86	0.29
16:02	38.2	0.111	0.0164	0.148	0.20	3.76	0.29
16:04	38.9	0.113	0.0162	0.144	0.17	3.88	0.29
16:09	40.5	0.135	0.0162	0.120	0.19	4.01	0.26
16:14	41.6	0.139	0.0165	0.119	0.15	4.20	0.27
16:17	40.1	0.128	0.0178	0.140	0.20	3.98	0.28
16:18	39.8	0.135	0.0168	0.125	0.19	4.00	0.26
16:19	40.7	0.141	0.0167	0.118	0.17	4.11	0.26
16:20	43.2	0.144	0.0160	0.111	0.17	4.12	0.25
16:21	39.2	0.144	0.0137	0.095	0.20	3.95	0.22
16:26	33.4	0.091	0.0174	0.191	0.33	3.52	0.35
16:31	39.9	0.139	0.0159	0.109	0.19	4.21	0.26

Table 4.13: Evaporator Performance Data for June 14th 1990

correlation coefficient r for this regression was +0.93, indicating a good fit.

Figure 4.22 shows the correlation between the evaporative heat transfer product (calculated by **RIGEVAP**) and the apparent level. A second regression was performed on these data, which gave a correlation coefficient r of +0.92 and a relation:

$$(UA)_e = -0.13 + 0.0065 \times h \tag{4.14}$$

where the heat transfer product $(UA)_e$ is in kW/K and the level signal h is in cm.

The significance of these figures is that for this run the evaporative heat transfer coefficient was very nearly constant; thus the heat duty performed was directly proportional to the area of submerged surface. The variation in corrected driving force was probably not significant, as the temperatures of the boiling R114 and the heat source were nearly invariant (see Figure 4.17). This is an important validation of the calculation of the evaporator performance using the program **RIGEVAP**; the level signals quoted were independent measurements and were not used in the calculation process.

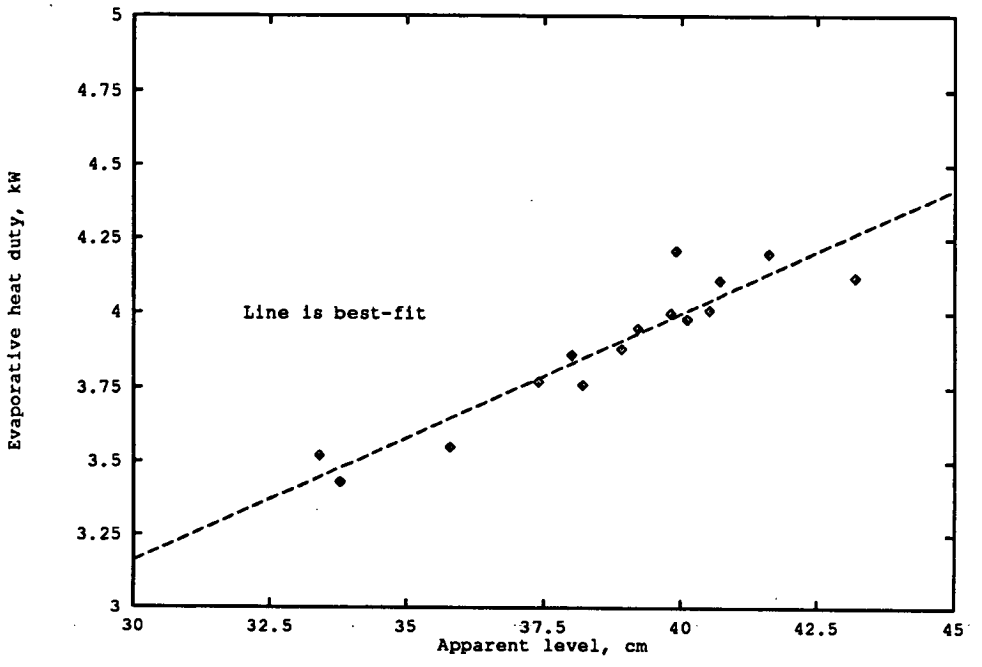

Figure 4.21: Calculated Evaporative Duty *vs.* Measured Level, June 14th

4.3.4.11 Summary of Evaporator Performance, June-July

The work performed in June and July established the ability of the plant to pump heat over an external temperature lift of up to 50 degrees, without forcing the compressor to operate outside its safe working region. Some data were also collected on the performance of the prototype evaporator; although problems with the instrumentation system prevented a comprehensive analysis. It was decided to examine the available data on the evaporator for any evidence of correlation between the duty performed and the indicated level of fluid un the unit. This was by analogy with the work described in Section 4.3.4.10 and illustrated in Figure 4.21 and Figure 4.22.

The mean heat fluxes in the evaporator, as calculated from the pump rate, were plotted against the mean observed level signal for each setting of the feed pump used on June 7th, June 9th and June 10th. In this fit the *total* heat flux predicted by the pump rate was used. By way of contrast the data are plotted in Figure 4.23, which also shows

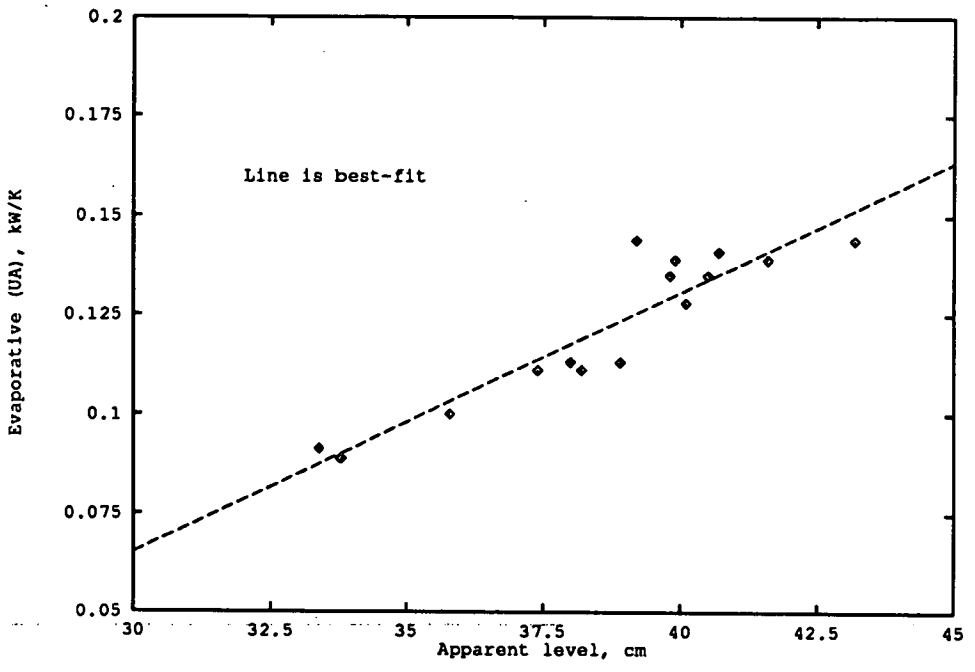

Figure 4.22: Calculated $(UA)_e$ *vs.* Measured Level, June 14th

the heat flux *due only to evaporation* calculated from the data on June 14th. It may be seen that the two best-fit lines are of similar slope: the equation of the fit to the averaged points was:

$$\dot{Q}_e = 0.95 + 0.10 \times h \tag{4.15}$$

for which the correlation coefficient $r = 0.99$. Comparing this to Equation 4.13, the difference in offset is 0.95-0.65 = 0.3 kW. This was the mean superheat duty on June 14th (see Table 4.13) which is another indication that the data are consistent with a constant straight-line relationship between capacity and level of fluid in the unit.

It was not possible to assess the effect of varying heat source flowrate on the evaporator performance from these data. This was no in fact investigated, as it was felt the major heat transfer resistance would lie on the evaporating (shell) side of the unit. Nor was it possible to explore the effect of temperature difference and gas flowrate on the performance; time constraints and the difficulty of guaranteeing that all other variables be held constant ruled this out.

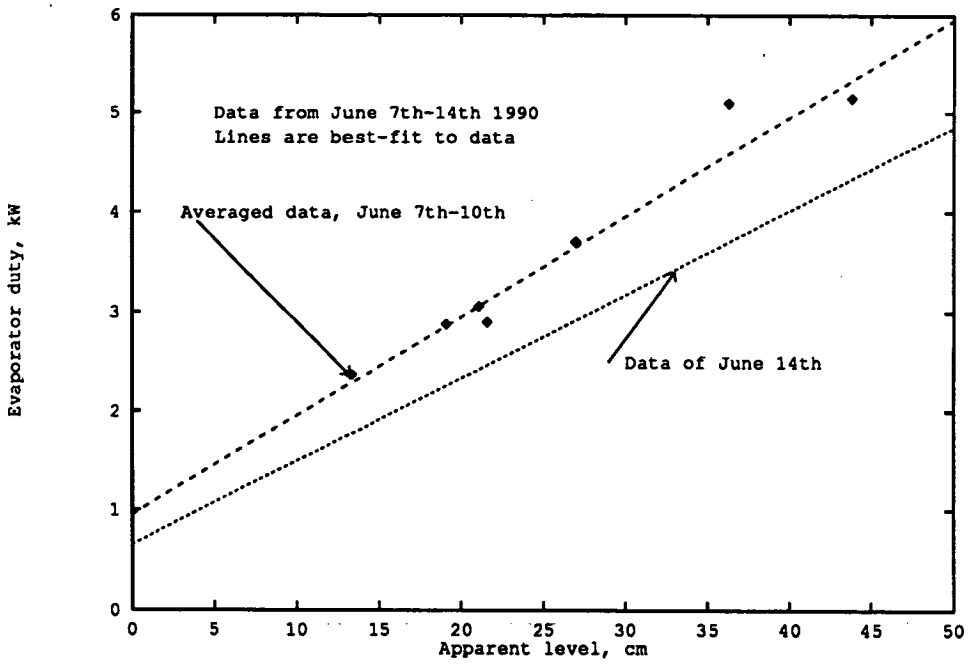

Figure 4.23: Evaporator Heat Duty *vs.* Apparent Level Signal

4.3.4.12 Summary of Compressor Performance

The compressor was found to perform well: a range of isentropic efficiencies from 70 to 90% was discovered. The nature of the compression process could be characterised for each experiment by a common polytropic path; the polytropic indices calculated from the experimental data gathered in each experiment were in good agreement. Insufficient experimental data were gathered to enable complete characterisation of the variation of isentropic efficiency with speed, throughput and pressure ratio; the available data indicated the following:

- The isentropic efficiency was a decreasing function of compressor speed.
- One set of data indicated a variation of efficiency with pressure ratio, whereas other datasets indicated only a very weak variation of the efficiency with pressure ratio. The density of the gas at the suction seemed to play a part in this; at low densities the variation in efficiency was more noticeable.

The main characteristic of the compressor which has not so far been addressed is the flow characteristic: as the compressor used was a positive-displacement device, a direct relationship between the compressor speed and the volumetric throughput was to be expected. In order to illustrate the relationship between the volumetric throughput and speed, the average throughput for each speed used was plotted in Figure 4.24. This shows the calculated volumetric flow at the suction as a function of the voltage signal produced by the compressor drive unit. The relationship is near-linear over the range 3–6 Volts but the average throughput at the highest speed used (full speed) was only 18.6 m^3/hr, against the expected figure of 25 m^3/hr. This must indicate an increase in back-flow of vapour at the highest speed used; a possible explanation is that the high-speed run (June 10th) was performed over a greater pressure ratio than most of the other data. This was caused by a large increase in flow resistance on both suction and discharge sides of the compressor. A more plausible explanation is that the output from the electronic driver unit exhibits non-linearity; the accompanying literature hinted that this might be the case. In that case, the apparent top speed might not be 3000 rpm: this could only be checked by direct calibration with a tachometer (impossible at the time).

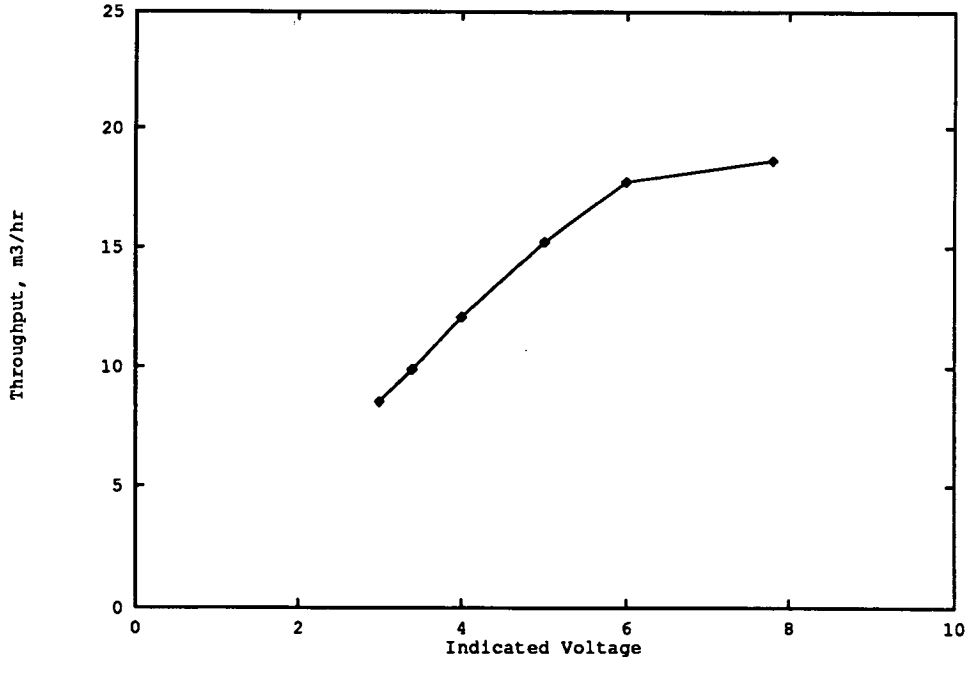

Figure 4.24: Average Compressor Throughput *vs.* Speed Indication

4.3.5 Final Experiments: December 1990

4.3.5.1 Final Rebuild

After the original experimental work had been terminated, further modifications to the hardware of the plant were carried out. There were two motivating factors behind this further rebuild: the desire to eliminate the pressure drop between the evaporator and the compressor, and a wish to reconfigure the evaporator to permit calculation of heat transfer products without resort to use of the **RIGEVAP** program.

Compressor Pipework The pipework on the compressor suction was drastically modified; the inlet manifold was replaced by a straight-through connector block. The number of bends in the pipework was further reduced and a bypass line was placed across the line filter element. The flow of gas to the compressor could be diverted through the filter if required by use of hand-operated isolation valves in the line. The effect of these modifications was to ensure that the pressure indicated by the compressor manifold gauge agreed with the evaporator pressure transducer; this was verified in operation.

Evaporator The evaporator was demounted; the original flow arrangement was altered from a single tube-side pass to three once-through streams, with a manifold arrangement at each end of the evaporator. The direction of flow was altered so that water entered at the base (along with the refrigerant) and exited at the top; this was done to prevent "waterfalling" of flow. New thermocouples were mounted in pockets at the ends of each length of water pipework; it was possible to incorporate these into the instrumentation scheme as some of the original thermocouples were no longer required. The presence of these additional thermocouples was meant to allow calculation of log-mean temperature differences in each shell of the evaporator, thereby enabling calculation of heat transfer products in each shell.

Heat Sink Hardware The original pump used in the hot water circuit was replaced with a Stuart-Turner N10 centrifugal pump, identical to that used in the cold water circuit. This was necessary in order to overcome the vapour-locking problems encountered in the initial experimentation (see Section 4.3.4.10). The orifice plate assembly had given trouble at low flowrates and so a second orifice, diameter 5mm, was machined and calibrated for use at low flowrates.

Other Modifications A tachometer was fitted to the compressor control circuitry, initially to feed back directly to the hardware, but with the eventual aim of providing an accurate indication of compressor speed to the computer. The control program was modified slightly to cope with the alterations in the instrumentation scheme. The original PC-30 interface card was replaced by an identical card, freely available, pending replacement of an integrated circuit which had malfunctioned during the summer.

4.3.5.2 Aims of the Work

This work was carried out with three main aims: firstly, to recommission the plant after the rebuild; secondly, to demonstrate the safe operational procedures to other members of the research team, and thirdly, to gather more and better data on the performance of the evaporator. The modifications to the evaporator temperatrue measurement system would enable direct calculation of heat transfer products and so experimental data analysis would proceed with this very much in mind.

4.3.5.3 December 7th: First Run

Summary of Experiment This was conducted with a constant compressor speed and metering pump feed rate; the objective was to obtain sufficient data points to ensure attainment of a true steady state in all parts of the plant. The plant was run in the same single-condenser configuration used with success in the earlier experiments, as desribed in *e.g.* Section 4.3.4.3.

The control setpoints were:

- **Compressor Speed:** 50%, 1500 rpm (4.5 Volts indicated)
- **Feed Pump Rate:** 64%, 0.0265 kg/s
- **Heat Source Temperature:** 30 °C
- **Heat Sink Temperature:** 70 °C
- **Product Temperature:** 80 °C
- **Heat Source Flowrate:** 13.1 l/min (0.218 kg/s)
- **Heat Sink Flowrate:** 3.1 l/min (0.052 kg/s)

The experiment was terminated abruptly by a power failure but sufficient data had been gathered by then to satisfy the objectives of the work.

The pressure drop between evaporator and compressor had been eliminated by the pipework modification: the average suction pressure reading from the manifold was 4.0 $\pm$1.0 psi gauge, which agreed with the evaporator pressure within the limits of reading error. The discharge manifold reading of 115 psi was in good agreement with the condenser pressure, so the transducers' readings were used in computation of pressure ratios for the analysis.

There were two real drawbacks with the instrumentation system during this experiment. The first was a failure in the circuitry of the evaporator level measurement transducer, which prevented cross-referencing of the data with the results of previous experiments. The second was an unreliable flow measurement produced by the orifice plate assembly in the hot water circuit; this was caused by the low flowrate used but could be solved by using the rotameter as a manually-logged flow measurement to read the average flowrate. As feedback was used to control the water product temperature, however, this led to a degree of uncertainty about the true flowrate as logged by the PC.

Experimental Data The key refrigerant temperatures are shown in Table 4.14, which lists: the evaporator inlet and exit; the compressor suction and discharge, and condensate temperatures. Not shown is the storage tank temperature, which was essentially constant at 20.5 °C throughout the period of operation. This table also contains the evaporator and condenser pressures as logged by the instrumentation system.

Time hr	$T_{ev,i}$ °C	$T_{ev,o}$ °C	T_{suct} °C	T_{dis} °C	T_{co} °C	P_{ev} bar	P_{co} bar
10:21	11.6	22.9	36.6	100.5	78.2	1.13	8.58
10:26	12.2	19.7	37.5	103.1	79.3	1.16	8.71
10:31	12.3	18.9	37.6	104.5	79.4	1.17	8.81
10:36	12.7	17.9	37.3	105.1	78.6	1.16	8.73
10:41	12.0	17.5	37.5	105.4	78.0	1.14	8.60
10:46	12.0	17.4	37.7	105.6	77.9	1.14	8.83
10:51	12.7	21.7	37.9	105.8	77.8	1.17	8.48
10:56	12.5	25.7	38.7	106.2	79.4	1.17	8.73
11:01	11.8	26.4	39.2	106.6	77.8	1.14	8.56

Table 4.14: Refrigerant Data: Morning, December 7th

The important water stream temperatures are shown in Table 4.15, which shows: evaporator inlet and outlet; outlets from each evaporator shell; condenser inlet and outlet temperatures.

Time hr	$T_{ev,i}$ °C	$T_{A,o}$ °C	$T_{B,o}$ °C	$T_{C,o}$ °C	$T_{co,i}$ °C	$T_{co,o}$ °C
10:21	27.5	24.6	24.3	24.1	69.5	80.5
10:26	26.9	23.9	23.7	23.6	70.2	81.2
10:31	26.6	23.7	23.5	23.4	70.2	80.7
10:36	26.2	23.3	23.1	23.0	70.3	79.7
10:41	25.9	23.0	22.8	22.8	70.2	79.1
10:46	26.0	23.0	22.9	22.8	70.1	78.9
10:51	28.6	25.1	24.9	24.8	70.2	78.6
10:56	30.5	27.1	26.8	26.7	70.1	81.3
11:01	30.1	27.0	26.7	26.5	70.4	78.8

Table 4.15: Water Temperatures: Morning, December 7th

Heat Pump Performance The plant operated over an external lift of 50 degrees: the control system maintained the product temperature within 1 degree of the set-point. The internal lift of the heat pump was approximately 66 degrees from the mean evaporation temperature to the mean condensing temperature. The analysis of the performance data by use of the program **HPUMP** led to the data shown in Table 4.16. The energy fluxes were calculated on the basis of the mean feed pump rate listed above.

Time hr	$\dot{Q}_{ev}$ kW	$\dot{Q}_{co}$ kW	$\dot{W}_{cmp}$ kW	COP_a —	COP_c —	ϵ —
10:21	3.52	3.21	1.08	2.98	5.28	0.565
10:26	3.44	3.23	1.11	2.90	5.25	0.552
10:31	3.43	3.26	1.14	2.85	5.25	0.543
10:36	3.41	3.30	1.16	2.84	5.30	0.535
10:41	3.40	3.33	1.17	2.85	5.32	0.535
10:46	3.40	3.33	1.17	2.85	5.33	0.536
10:51	3.47	3.34	1.17	2.85	5.39	0.528
10:56	3.55	3.30	1.16	2.84	5.27	0.539
11:01	3.56	3.35	1.16	2.89	5.32	0.544

Table 4.16: Performance of Plant on December 7th, from **HPUMP**

The heat fluxes recorded from the measurements of the water streams are given in Table 4.17. In common with the previous experimental analysis, the heat fluxes calculated from the thermocouple and thermopile signals are given.

Time hr	$\dot{Q}_{ev}$ T/PILE kW	$\dot{Q}_{ev}$ T/C kW	$\dot{Q}_{co}$ T/PILE kW	$\dot{Q}_{co}$ T/C kW
10:21	2.62	2.92	3.79	3.82
10:26	2.63	2.92	4.10	3.79
10:31	2.63	2.92	2.43	2.12
10:36	2.65	2.83	2.11	1.77
10:41	2.52	2.94	1.23	1.04
10:46	2.68	3.05	1.85	1.55
10:51	2.98	3.47	3.49	3.06
10:56	3.00	3.36	4.59	4.24
11:01	2.91	3.20	2.08	1.76

Table 4.17: Measured Heat Fluxes, Morning of December 7th

It is evident from Table 4.17 that the heat flux in the evaporator was essentially stable; while that in the condenser was subject to considerable variation. This may be explained by the use of feedback control to regulate the product water temperature by alteration of the flowrate of water through the condenser. If this is the reason, then the control settings used for the (proportional) control algorithm were not ideal; the rest of the plant was stable, so the response of the product stream should not have been such a large oscillation in flow. The conclusion is that this oscillation in flow may be less desirable than a swing of a few degrees in output temperature.

The heat fluxes measured in the evaporator were consistently about 20% below those

calculated from the feed rate; this may be explained, as before, by the effects of heat leakage and the action of the pump loading valve. The discrepancies between the fluxes resulting from use of the thermopile measurements and those calculated from the thermocouple measurements may be explained by a combination of thermocouple error and slight error in estimation of the gains of the thermopile amplifiers. As the thermocouple amplifiers had been recalibrated by the manufacturers, it was felt that the likely errors in the measurement of temperatures with thermocouples was much smaller than in the experiments performed in June and July. The total of four thermocouples placed in the outlet of the evaporator all agreed with each other and suggested that the gain of the evaporator was slightly too low; as only one reliable thermocouple was located in the outlet of the condenser it was not possible to make the same kind of judgement on the condenser thermopile.

Reference to thermodynamic tables shows that, from a suction feed of saturated liquid at 20.5 °C (the tank condition), a flash to a vapour fraction of 20% at 12 °C (the evaporation temperature) would require an initial pressure increase of 1.35 bar from the vapour pressure of the feed stream. The metering pump loading valve was rated at 15–30psi, so this would seem plausible. The consequence for analysis is that the vapour fraction of the evaporator feed should be calculated to satisfy the heat balance over the unit. In other words, if the total heat duty in the evaporator is:

$$\dot{Q}_T = \dot{m}_w \times C_{p,w} \times (T_{w,i} - T_{w,o}) \tag{4.16}$$

$$= \dot{m}_r \times [(1 - x) \times \lambda + C_{p,r} \times (T_{r,i} - T_{r,o})] \tag{4.17}$$

then the vapour fraction x to be used is given by:

$$x = \frac{\dot{Q}_T - \dot{m}_r \times C_{p,r} \times (T_{r,i} - T_{r,o})}{\dot{m}_r \times \lambda} \tag{4.18}$$

where λ represents the latent heat of vapourisation and C_p denotes a constant-pressure heat capacity. This will be important in the detailed analysis of the evaporator given below.

Compressor Performance The compressor performance was analysed using the program **HPUMP**; the results are summarised in Table 4.18. The mean volumetric displacement for this steady-state run was calculated at 12.1 m^3/hr. This compares well with a nominal displacement of 12.6 m^3/hr at 50% speed over the design pressure ratio of 5.5:1. The isentropic efficiency deteriorated slightly over the period of sampling: examination of the temperature log (Table 4.14) shows that this was a result of the thermal inertia of the oil separation system, as in previous runs. The steady-state efficiency was 68%: this was lower than the efficiencies found at similar speeds in the earlier work. The high pressure ratio used in this experiment may be a factor here, as the suction densities and temperatures are roughly comparable with those used in previous runs.

Comparison of the polytropic indices N and K with those calculated in previous analyses shows that the compressor performance obeyed the same polytropic paths as in the previous work. If nothing else, this indicates that the machine suffered no significant harm as a result of the use of a mixture as working fluid during the summer.

Time	$P_d : P_s$	V_s	$DOSH$	Δh_{comp}	η	Polytropic	Indices
hr	—	m^3/kg	°C	kJ/kg	—	K	N
10:21	7.604	0.1292	30.0	40.93	0.726	1.10	1.03
10:26	7.510	0.1261	30.1	42.36	0.707	1.10	1.03
10:31	7.551	0.1255	30.1	43.38	0.692	1.11	1.04
10:36	7.533	0.1261	29.9	44.18	0.678	1.11	1.04
10:41	7.544	0.1284	30.6	44.41	0.677	1.11	1.04
10:46	7.568	0.1280	30.7	44.37	0.679	1.11	1.04
10:51	7.227	0.1248	30.2	44.64	0.659	1.11	1.04
10:56	7.452	0.1254	31.1	44.11	0.679	1.11	1.04
11:01	7.512	0.1292	32.2	44.05	0.686	1.11	1.04

Table 4.18: Compressor Performance: December 7th Run 1

Evaporator Performance The evaporator performance is summarised in Table 4.19. This lists: the calculated feed vapour fraction; evaporative and superheat duties; degree of superheat performed; heat transfer product for evaporation, and heat transfer product for superheat. The overall heat balance on the evaporator required use of the thermocouples to calculate the heat lost by the water stream, rather than the thermopile.

The main conclusion to be drawn from Table 4.15, Table 4.17 and Table 4.19 is that the

Time hr	x_{feed} —	$\dot{Q}_{ev}$ kW	$\dot{Q}_{sh}$ kW	DOSH °C	$(UA)_{ev}$ kW/K	$(UA)_{sh}$ kW/K
10:21	0.23	2.70	0.22	11.3	0.188	0.0428
10:26	0.21	2.77	0.15	7.5	0.211	0.0211
10:31	0.21	2.78	0.14	6.6	0.219	0.0189
10:36	0.22	2.73	0.10	5.2	0.229	0.0133
10:41	0.20	2.83	0.11	5.5	0.230	0.0143
10:46	0.16	2.94	0.11	5.4	0.239	0.0143
10:51	0.06	3.31	0.18	9.1	0.236	0.0273
10:56	0.09	3.19	0.17	13.2	0.197	0.0327
11:01	0.17	2.92	0.28	14.6	0.176	0.0700

Table 4.19: Evaporator Performance Data: December 7th Run 1

evaporative capacity of the unit remained essentially constant over this run. The ability of the unit to perform superheat seemed sensitive only to the heat source inlet temperature. The lowest calculated heat transfer products for superheating correspond to those data points where the degree of superheat was highest. This is probably explained by fluctuations in the evaporator holdup affecting the area available for superheat: the heat transfer coefficients obtained in the evaporator were probably constant, as the mass flows of both streams were constant.

4.3.5.4 December 7th: Second Run

Summary of Run In the afternoon of December 7th, a second experiment was performed, the aim of which was to demonstrate the effect of changing heat source flow on the performance of the evaporator. The intention was to establish a steady state close to that of the morning, then progressively to reduce the heat source flowrate and allow the plant to come to new quasi-steady operating conditions. Any reduction in flowrate which affected the heat transfer coefficients in the evaporator would firstly reduce the degree of superheat performed, secondly reduce the total capacity of the unit. As the compressor speed would be kept constant, this would be accompanied by a drop in pressure and subsequent drop in boiling temperature to compensate for the increased resistance to heat transfer.

The control setpoints used were as for the experiment described in Section 4.3.5.3, save that feedback control of the product temperature was abandoned. The product

flowrate was set manually and left untouched; the independent thermocouple circuit had failed, making automatic temperature control impossible.

Five source flows were used; it was necessary to alter the metering pump rate from its initial setting of 65% to 60% after the first change in source flow was made, in order to overcome a flood of the evaporator. Manual adjustments were made to the product flowrate, using the hand-operated gate valve in the circuit, in order to maintain a semblance of control over the condensing pressure of the heat pump.

The response of the evaporator to a reduction in the source flowrate was characterised by a loss of evaporator pressure, caused by depression of the evaporation temperature. This is seen clearly in Figure 4.25, which is a plot of the inlet and exit temperatures of both R114 and water in the evaporator during the run. The water flowrate changes took place at the times marked "Change" on the time axis; the evaporator flood which occurred shortly after the first water flow change is also marked.

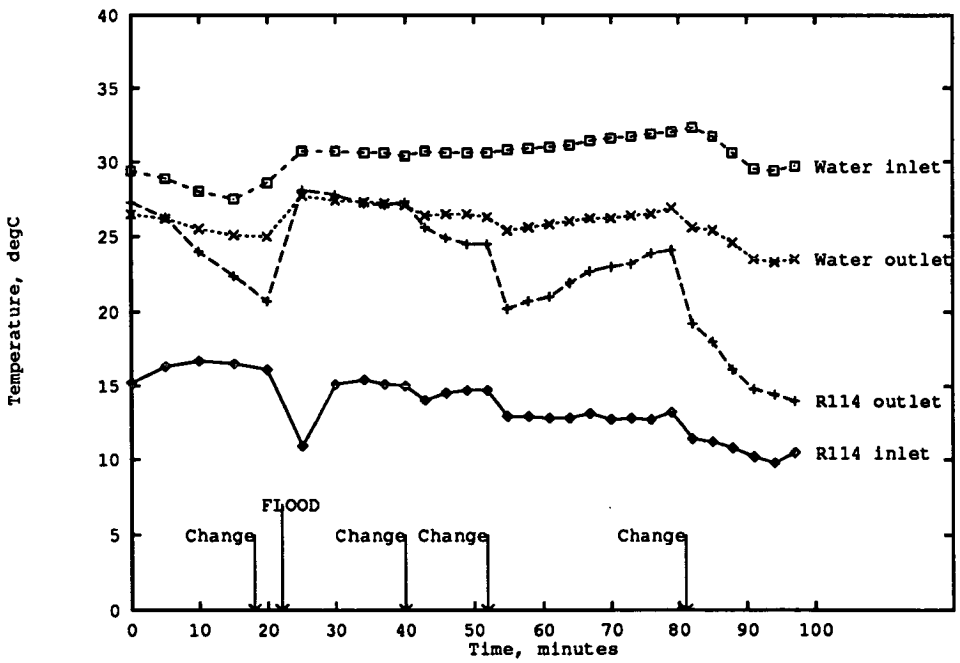

Figure 4.25: Evaporator Temperatures: December 7th Run 2

The important temperatures in the rest of the plant were essentially invariant through-

out this experiment: they are plotted in Figure 4.26. This shows: compressor suction and discharge; heat sink inlet; product outlet, and condensation temperatures. The initial period of operation was characterised by a steady climb in the compressor discharge temperature, corresponding to higher isentropic efficiencies in the compressor. The "rule of thumb", found in earlier work, that the condensation temperature is very close to the product temperature, is borne out once more by this figure.

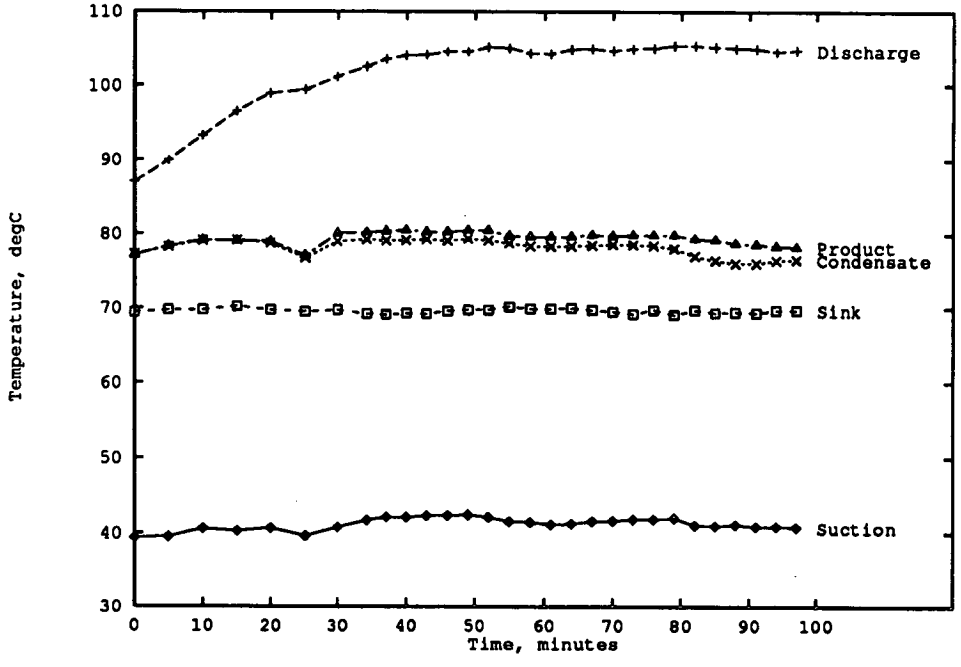

Figure 4.26: Other Temperatures: December 7th Run 2

Heat Pump Performance The plant's performance as a heat pump in this experiment was broadly comparable to that attained in the morning's work and is summarised in Table 4.20. This shows: the Rankine (actual) COP; Carnot COP; Carnot efficiency, and isentropic compression efficiency.

The initial higher Carnot efficiencies are explained by non-equilibration of the temperatures in the high-pressure part of the plant, as in previous work. Thereafter the performance of the plant was unaffected by the changes in evaporator exit conditions, despite the change in evaporation temperature. The average COP was 3.06 ± 0.02; the average Carnot efficiency was 57%,± 0.6%. The external lift was, as before, approxi-

Time hr	COP_a —	COP_c —	ϵ —	η_S —
15:33	3.97	5.64	0.704	0.941
15:38	3.74	5.67	0.659	0.871
15:43	3.56	5.65	0.631	0.822
15:48	3.34	5.62	0.594	0.756
15:53	3.24	5.61	0.578	0.724
15:58	3.21	5.31	0.604	0.755
16:03	3.15	5.51	0.571	0.711
16:07	3.13	5.52	0.567	0.697
16:10	3.11	5.50	0.566	0.692
16:13	3.09	5.49	0.564	0.696
16:16	3.09	5.40	0.573	0.699
16:19	3.08	5.45	0.566	0.693
16:22	3.08	5.45	0.566	0.694
16:25	3.05	5.46	0.558	0.685
16:28	3.03	5.34	0.568	0.696
16:31	3.07	5.37	0.571	0.703
16:34	3.03	5.36	0.566	0.693
16:37	3.03	5.36	0.565	0.691
16:40	3.04	5.38	0.565	0.692
16:43	3.06	5.34	0.574	0.704
16:46	3.06	5.35	0.572	0.702
16:49	3.05	5.34	0.572	0.700
16:52	3.07	5.41	0.567	0.699
16:55	3.04	5.33	0.570	0.699
16:58	3.06	5.35	0.571	0.695
17:01	3.09	5.35	0.577	0.713
17:04	3.07	5.30	0.579	0.714
17:07	3.07	5.24	0.586	0.719
17:10	3.06	5.29	0.577	0.712

Table 4.20: Heat Pump Performance: December 7th Run 2

mately 50 degrees.

The relation between the compression efficiency and the heat pump's Carnot efficiency is demonstrated in Figure 4.27, which is a plot of Carnot efficiency and isentropic efficiency as functions of time.

Compressor Performance The performance of the compressor has already been illustrated in the preceding paragraphs: the polytropic compression indices K and N were on average 1.11 and 1.04 respectively, in agreement with the morning's work. The

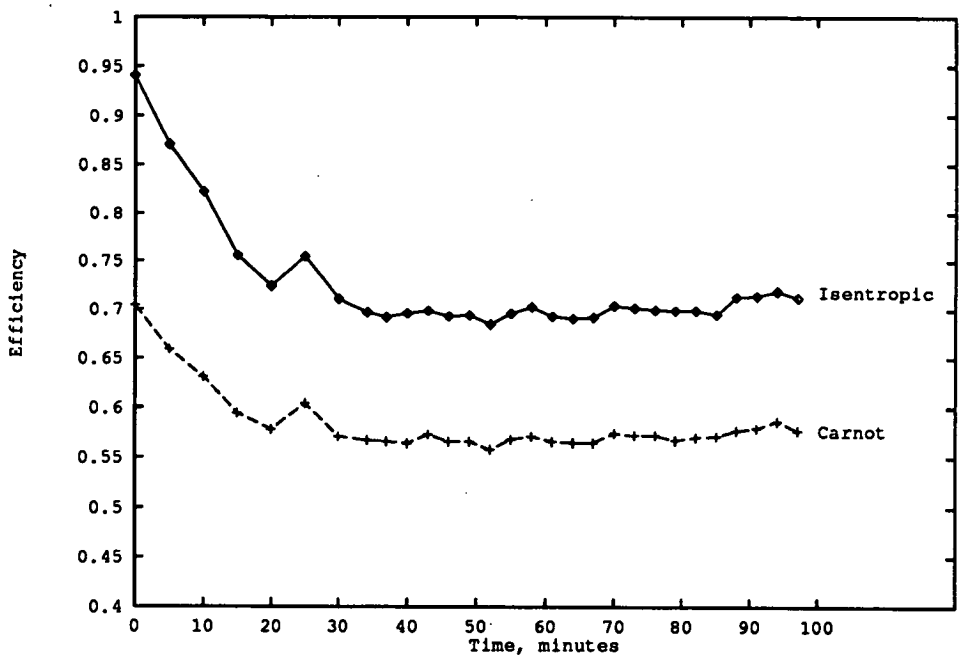

Figure 4.27: Variation of Carnot and Isentropic Efficiencies: December 7th Run 2

isentropic efficiency was again in the region 66–70%.

4.4 Experiments using a Binary Working Fluid

4.4.1 Introduction

The work described in Section 4.3 was carried out with a working fluid of pure R114; it was necessary to perform so much work in this way to gain familiarity with the plant. The work described in this Section was carried out in an attempt to determine whether the plant could actually perform a progressive separation of the working fluid; if a separation of the components were to be observed, this would vindicate the central

basis of the project.

The active holdup of R114 in the plant at the end of the initial series of experiments (June 1990) was between 5 and 6 litres of fluid. This was enough to run the plant with comfortable reserves for maintenance of liquid level in the storage vessels; there was however still significant capacity in the system. On 19th July, four litres of R113 were charged into the plant by induction through the compressor manifold while the compressor was running. This was done to enforce an initial mixing of the two components through as much of the plant as possible. It was estimated that the resulting "global" composition of the working fluid in the plant was 60 mol% R114.

The experimental work described in the following Sections was primarily concerned with determining the behaviour of the system and the variation of the active working fluid composition. The analysis presented will focus on a qualitative description of the behaviour of the plant, backed up by numerical analysis to demonstrate the composition shifts. The compositions quoted were obtained by use of computer programs, written by the author, which used the CSD equation of state to predict thermodynamic properties from measurable quantities. This equation of state had been used in the initial analysis of the performance of the plant (Section 4.3.4.4–Section 4.3.4.5) and was reckoned to be as accurate as proprietary data tables or specialised refrigerant property correlations.

In most of the work now described, the plant was run with both sides in operation; that is, with both condensers, both storage vessels, and both sides of the metering pump in operation. This is to be contrasted with the pure-fluid experimentation, where only one condenser and one storage vessel were used. The problems of control which arose from this mode of operation were considerable: in balancing the evaporator feed rate against the observed rate of rise of level, for example, two pump settings had to be juggled without causing major disturbance. The control of condenser pressures was also of importance; in previous work the condenser pressure had not been regulated. In these experiments, however, pressure control was important and involved empirical determination in real time of control parameters capable of implementing effective control action. The reason for this was that the condensing pressures affected the mean driving forces for heat transfer in the condensers. This was important because the throughputs of refrigerant which were achievable given the evaporator/compressor bottleneck could easily be condensed in the first unit alone. In order to enforce con-

densation in both condensers of the heat pump, the performance of the first unit (C–1) had therefore to be degraded, and one method which was attempted was to maintain a pressure difference between the two condenser units.

4.4.2 First Experiment

The first experiment carried out after the addition of R113 to the system was carried out principally in order to determine the characteristics of the binary working fluid in comparison to the pure working fluid. During this run there were two incidents of computer failure, caused by a defective cooling fan, and the zero position on one head of the metering pump drifted. The quantitative data which could be trusted were accordingly scanty. The experiment did nonetheless provide a valuable insight into the problems which lay ahead; therefore the analysis and discussion is qualitative. The progress of the experiment is described as an account of the response of the system to the manipulations of the control elements carried out as attempts at obtaining condensation on both sides of the heat pump.

4.4.2.1 Method and Preparation

Method The experiment was to be carried out with both condensers in line: the feed was to be taken from the heavy tank alone in the initial stage of operation. The intent was to observe the hot water temperature profile through the two condensers; a rise in temperature as the water passed through a condenser would indicate condensation. This was to be backed up by visual observation of condensate levels and relative rates of condensation on each side of the condenser bank. Evidence of a shift in composition would be provided by measurements of temperature and pressure in the storage tanks at regular intevals throughout the experiment: if there were some degree of component redistribution then the pressure in the heavy tank would fall with time, as the concentration of less volatile increased. The final measure of the degree of redistribution would be measured by a blowdown of the contents of each condensate pot to the storage: this would enable direct comparison of the composition in each

storage tank by reading of the pressures, and would also permit measurement of the amounts of condensate formed on each side.

Preparation The refrigerant charge was transferred (as far as possible) into the heavy storage tank before the experiment started. This was accomplished during the R113 charging: only the first condenser was used while the charging run was performed. The hot and cold water streams were assigned setpoints of 60 °C and 30 °C, in accordance with the earlier runs. The valves on the lines joining the two condensers were opened and the level controller for the heavy condensate receiver pot was connected to the condensate throttle valve. The light condensate level control was disabled: it was intended to observe the rate of accumulation in the sight glass of the receiver. The normal startup procedure was then attempted, using a compressor speed of 50% (*i.e.* 1500 rpm.) The feed pump rate was initially set to 40 litre/hr from the heavy tank, with no feed from the (empty) light tank.

4.4.2.2 Progress of Run

Operation The first, most noticeable difference between operation with a binary and a pure working fluid was the startup performance. The initial feed composition to the evaporator was in the region of 50% R114; thus the effective vapour pressure of the feed was much lower than that of the pure fluid. The lower vapour density, coupled with the geometry of the evaporator and the high pressure drop in the suction pipework, made it very difficult to circulate enough refrigerant to warm the plant up by condensation. It was found that the evaporator flooded within a few minutes of starting the feed pump: the compressor suction pressure dropped well below that of the evaporator, and liquid holdup was observed in the V/L separator attached to the evaporator. Whilst this was happening, it was observed that the condensation of the compressed vapour took place only in the first condenser, and that the condensate exit temperature corresponded closely to the boiling temperature of pure R114 under the indicated condenser pressure. This implied that the less volatile R113 was not reaching the condenser; it must therefore have been retained in the V/L separator, or absorbed into the compressor lubricating oil sump. The feed pump rate was therefore adjusted progressively downwards until a reasonably steady indicated evaporator liquid level

was displayed over a period of several minutes on the PC screen. The final feed rate which gave a steady level was 35 litre/hr, only 5 litre/hr less than the initial rate which caused the flood.

After the evaporator level was stabilised, there was still no indicated rise in water temperature through the light condenser: it was decided to try two strategies to improve this. The first was the control of the condenser pressures, described above; the second was to reduce the heat sink flowrate, thereby increasing the temperature rise experienced by the heat sink and thus narrowing the temperature approach in the first condenser. It was hoped that this would reduce the duty on the first condenser without reducing the quality of heat output.

It proved very difficult to obtain satisfactory control of pressure in the condensers: in an attempt to obtain controller settings which would enable steady pressure levels to be maintained, the control algorithm used for each loop was proportional only. In the event the two loops interacted: this was anticipated, of course, but the adjustment of the loops was difficult because the valve trim in CV1 was too large. This was known beforehand but as funds were not sanctioned for replacement valve trims nothing much could be done. All condensation appeared to take place in the first condenser until the control valve between the two condensers was opened beyond about 10%: then the compressor merely drew the bulk of vapour straight through the second condenser and the Badger valve, if this latter valve were open. The boilup rate in the evaporator and the total heat flux delivered to the heat sink stream would then fall, triggering an evaporator flood and consequent loss of steady state in the rest of the plant.

Condensate accumulation was observed only intermittently in the second receiver. This was nonetheless a better result than might appear: the formation of condensate was observed to occur after modifications to the control settings were made to encourage condensation. The reason for cessation of condensation seemed to be loss of control function rather than erroneous choice of control strategy by the author. For example, alteration of the condenser setpoint pressures to disable the first condenser did produce a stream of condensate from the second unit; this only died off when the control function was lost. The conclusion drawn was that pressure control would be difficult to set up but that given time it would be feasible.

The second strategy, that of altering the heat sink capacity rate, was also only partly successful. It did prove possible to force condensation in the second condenser by reduction of the water flow: it was difficult to maintain a stable régime of operation which maintained these conditions for long.

Pressure Variations Some quantitative data are appropriate and are presented here. These data were taken in two sets: this was enforced by a computer failure. The sampling period was 60 seconds; sampling started at the same time as the feed to the evaporator and the compressor drive were turned on. This run gave an indication of the startup characteristic of the pilot plant.

The variation of the cycle pressures with time is shown in Figure 4.28. This makes it clear that the two condensers operated at the same pressure throughout nearly all of the experiment: the apparent difference in pressure was caused by drifts in the electronics and instrument calibrations. The initial fluctuation in evaporator pressure is a symptom of the flooding behaviour described above: it may be seen that after about 2000 seconds of operation (half an hour) the plant had come close to steady state.

The variation of pressure in the storage tanks is shown in Figure 4.29, which also shows the evaporator pressure as a reference. This plot indicates that the light tank pressure remained below that of the heavy tank pressure until steady state was reached, when the light tank pressure rose rapidly to a steady value. The two storage tanks were at very similar temperatures and so the light tank contents must have been richer in R114 than those of the heavy tank. This was a primary aim of the experiment: to achieve condensate streams of differing composition. The lag between startup and appearance of lights in the storage was caused by the very slow condensation rate: condensate would not have been blown down by the level controller until about 0.5 litre of refrigerant liquid had collected in the lines attached to the second V/L separator.

Temperatures The temperature of refrigerant entering and leaving the evaporator is shown in Figure 4.30. The initial fluctuations in temperature and the close approaches of inlet and outlet temperature were associated with the flooding phenomenon: once

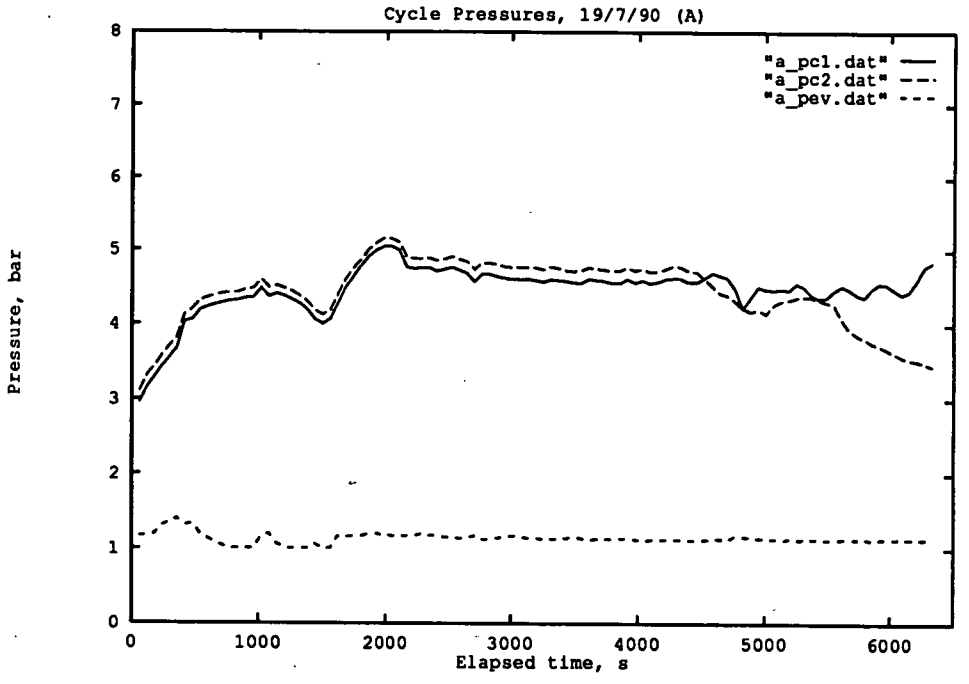

Figure 4.28: Variation of Cycle Pressures 19/7/90/A

a steady state had been achieved the temperature levels and degree of superheat performed by the unit were very stable.

The compressor suction and discharge temperatures are shown in Figure 4.31. The suction temperature was initially rather unstable: the observed temperature was lower than that of the gas leaving the evaporator for the initial part of the run. This cooling was probably provided by cold oil returning from the oil separator. The suction temperature stabilised more quickly than the discharge temperature: this effect had been observed in the experimentation with pure working fluid and was not surprising.

The variation of the temperature of the heat sink stream is shown in Figure 4.32, which is a plot of the water temperature at three points: the entrance to C–2; the exit from C–2, and the exit from C–1. This plot indicates clearly that for most of the run all condensation took place in the second condenser. The control of water temperature to the initial setpoint of 60 °C was good: after about 80 minutes of operation the water setpoint was reduced to 55 °C in an attempt to boost the condensation in C–2, and

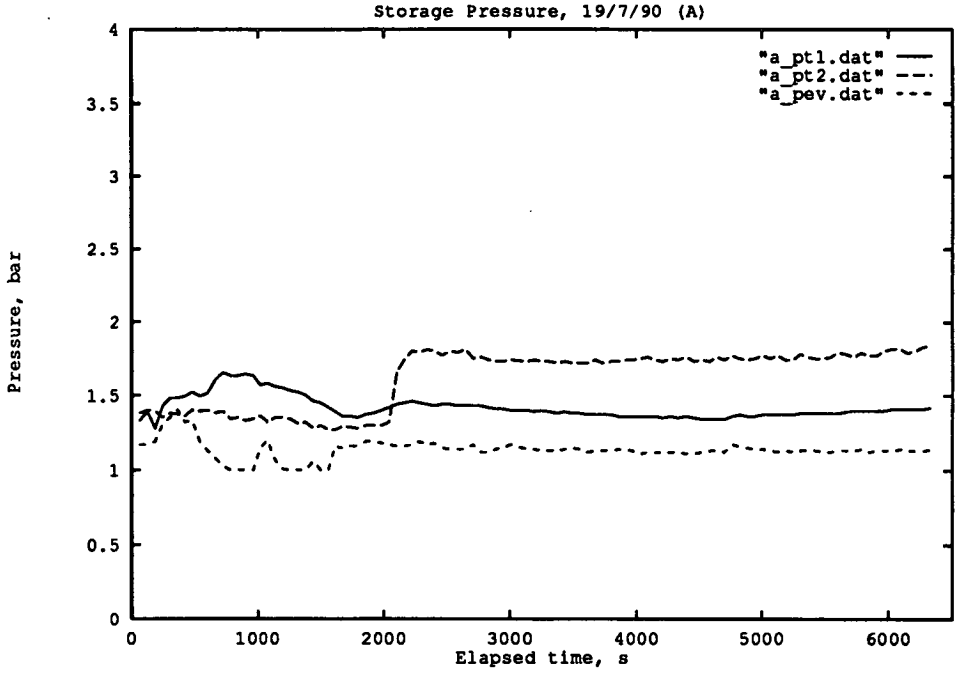

Figure 4.29: Variation of Storage Pressures, 19/7/90/A

this is evident on the temperature plot. At the same time as the reduction in water temperature the flowrate was reduced, with the aim of reducing the driving force in C–1. this did raise the water discharge temperature slightly but the effect was small.

The evaporator water temperature was well controlled to its setpoint of 30 °C: the mean heat flux delivered in the evaporator was so constant that it is not worth reproducing the evaporator water temperatures here. The heat flux delivered by the evaporator was rather disappointing: the final steady state attained was very close to the flood point and must thus represent an approximate limiting performance.

Heat Fluxes The instantaneous heat fluxes recorded by the computer were found to be affected by instrument noise to a surprisingly large extent: this was particularly true in the condenser. The fault lay not in the recorded temperatures—the plots of water temperature show a constant temperature increase—but in the recorded instantaneous flowrate of hot water. The average flow indicated by the rotameter setting was there-

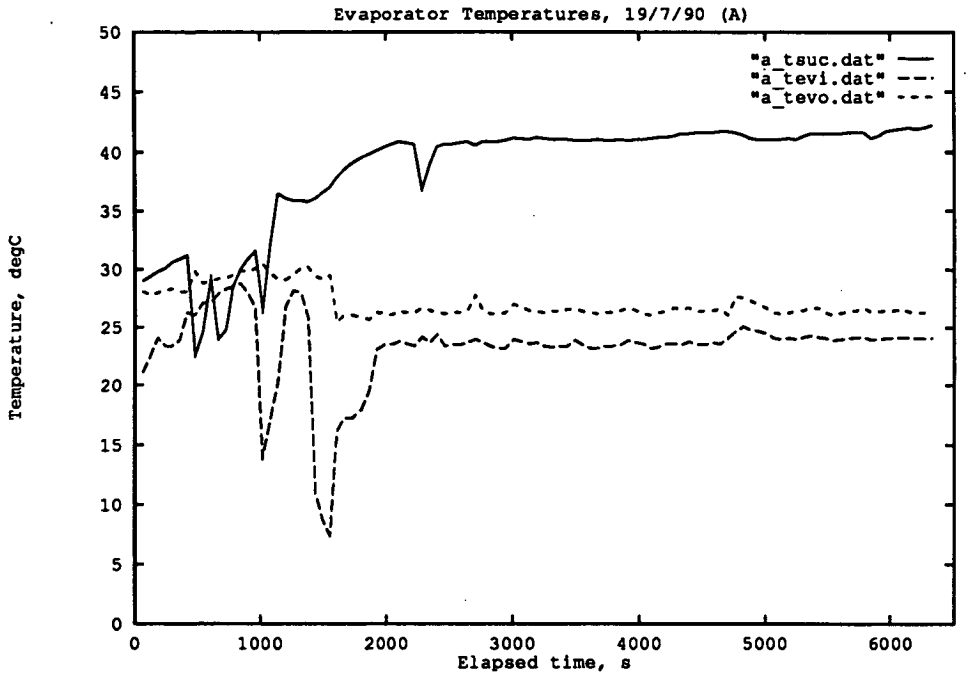

Figure 4.30: Evaporator Inlet and Outlet Temperatures, 19/7/90/A

fore used to estimate the steady-state condenser heat flux: this was about 2.5 kW. This agreed with the estimated flux of 2.4 kW, calculated from the thermodynamic properties of the refrigerant mixture and the metering pump setting. The evaporator steady-state heat flux was about 1.9 kW, compared to an estimated heat flux of 2.37 kW. The discrepancy in these two figures is analagous to that described in the analysis of the pure-fluid experiments.

Refrigerant Thermodynamics The Coefficient of Performance was estimated by treating the heat pump as a single-condenser system: this was entirely reasonable given the observed condensation patterns. In order to calculate the working fluid composition, these assumptions were made: the liquid in the evaporator was in equilibrium with the vapour leaving the unit; the condensate from C–1 was at its bubblepoint; the storage tanks were at equialibrium, and the unknown pressure drop between superheater and compressor suction could be treated as an adiabatic throttle. The CSD equation of state was used to generate bubblepoint curves from the measured temperatures and pressures at the points of assumed VLE: this gave an estimate of compositions in either

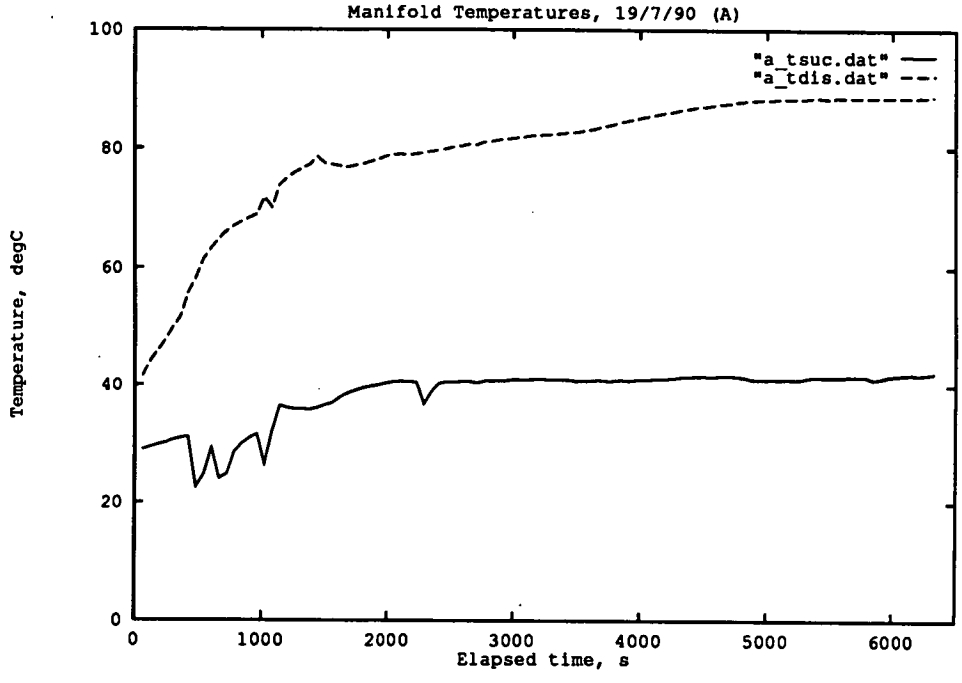

Figure 4.31: Compressor Manifold Temperatures, 19/7/90/A

phase. This analysis gave the following results, based on the mean temperature and

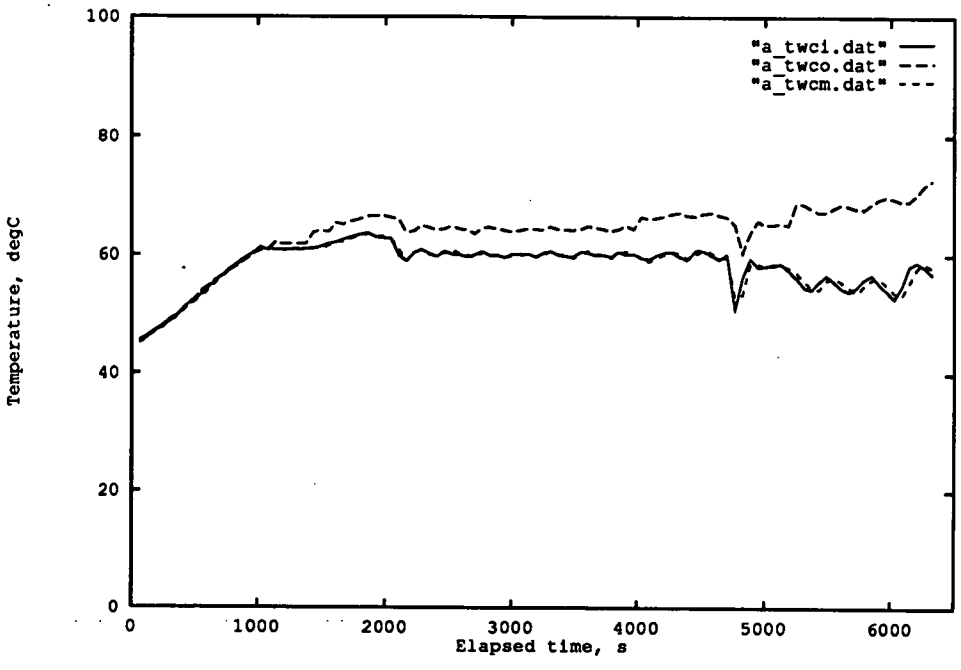

Figure 4.32: Condenser Water Temperatures, 19/7/90/A

pressures recorded over the most stable period of operation.

- Evaporator inlet : 23.5 °C at 1.14 bar, liquid 45 mol% R114, vapour 76 mol% R114
- Evaporator outlet: 26.5 °C
- Compressor suction: 40.5 °C at 0.85 bara (4″ Hg vacuum)
- Compressor discharge: 81.5 °C at 4.75 bara
- Condenser: 61.7 °C at 4.71 bar, liquid 73 mol% R114
- Heavy storage: 24.1 °C at 1.43 bara, liquid 61 mol% R114
- Light storage: 23.9 °C at 1.76 bara, liquid 84 mol% R114

These results show a pleasing consistency: the calculated vapour composition leaving the evaporator is within 3 mol% of the calculated condensate composition. If one allows

0.05 bar for pressure drop over the evaporator this error is reduced further. (The figure of 0.05 bar was not plucked from the air, but based on the average apparent level indicated by the differential pressure transducer connected over the evaporator.) The estimated circulating composition lies between those of the storage vessels, which is the intended state of affairs.

The COP was calculated by assigning compositions as appropriate from the above analysis: it was found to be 5.1 for this run. The Carnot COP of a cycle operating between 23.5 °C and 61.7 °C is 8, giving an apparent Carnot efficiency of 0.64 for these data. This is in agreement with the efficiencies found using pure R114. The equivalent Rankine cycle COP for pure R114, using the same temperatures and degree of suction superheat is 5.5: this may be caused partly by the properties of the mixture and partly by the very different operating pressures which prevailed in this experiment.

An important conclusion may be drawn from the compositions of liquid which were calculated above: the active circulating refrigerant was predominantly R114. In the evaporator there existed a permanent holdup of R113; it was suspected that this was also the case in the oil separator. This represented an undesirable state of affairs: had the solution circuit line been used then liquid from the evaporator could have been sprayed into the condenser to drop the pressure ratio of the cycle and thus boost thermodynamic efficiency. This was not tried for the simple reason that this experiment was the first ever performed with a mixed fluid and therefore was already full of imponderables. It should however be included in future work.

4.4.3 Second Experiment

The second experiment performed with the mixed working fluid was intended to demonstrate a progressive shift in composition of the circulating refrigerant in the plant. This was to be achieved by recording the temperatures and pressures in the storage tanks, and by monitoring the change in heat sink temperature over each condenser.

4.4.3.1 Method

The basic method was unchanged from the previous experiment: the compressor speed was set to 50%, the hot water tank temperature to 60 °C and the cold tank temperature to 30 °C. The plant was started up using the single-condenser configuration, with refrigerant being taken from the heavy tank only. The valves on the connecting pipework between the condensers were then opened and the system run with both condensers in operation. The intention was to measure the average rate of condensation in each condenser by periodic blowdown and measurement of level in the glass separator ranks. The composition of fluid in the tanks would be estimated from temperature and pressure measurement.

4.4.3.2 Results

This experiment gave inconclusive results. The apparent rate of condensation in the second condenser was very low; so low that there was no appreciable change in water temperature over the condenser. The problem lay in the low mass flowrates being circulated: the entire vapour stream was condensed in the first condenser and the control of condenser pressure was not sufficiently good to enable a split of the condensation process. At the end of the run nonetheless there was an observable quantity of condensate in the receiver attached to the second condenser. When this was blown down into the lights tank and allowed to equilibrate the estimated composition was better than 95% R114. The estimated composition of fluid in the heavy tank was 65%, and this had fallen from the initial estimated composition, indicating a transfer of R114 between the vessels. It was concluded that the composition split effect was probably taking place but that it was not possible to back this up from the observed variations in temperatures and condensation rates.

Evaporator flooding was again a problem in the startup of the pump: the unit eventually came to a steady state but careful adjustment of the feed rate was required to maintain this steady state. The *average* feed rate remained nearly constant at 32 litre/hr, giving a heat output of just over 2 kW. It was however found necessary to shift the pump rate up and down around this mean point until the rest of the cycle had

reached steady operating conditions. This was not seen as a major worry: the point of performing these experiments was in part to identify those process components which would affect the plant performance in dynamic operation.

Problems were also experienced with the metering pump during this experiment: the head attached to the lights tank ceased to pump. This was found to result from fouling of the valve seats by corrosion products and general crud: the pump was stripped down and cleaned after the experiments were completed. The discovery of corrosion products prompted replacement of the water filter element in the evaporator feed line. The presence of water was (optimistically) attributed to inhalation of moist air by the plant when opened or under partial vacuum, rather than to any leakage in the heat exchanger units. As these were all brazed items it was not practical to carry out a thorough inspection of the heat exchangers. A possible method of testing these units for leaks might have been to set all water flows to closed-circuit operation, then introduce different colours of dye into each water stream and examine the refrigerant storage vessels for any signs of an aqueous phase. This was left as a cunning plan for future users of the apparatus.

4.4.4 Single-Condenser Experiments

Two experiments were performed on successive days of operation, in which the plant was run in the single-condenser mode. This work was performed to assess the behaviour of the plant in this mode with a mixed working fluid for comparison against the results obtained using pure R114.

4.4.4.1 First Experiment: July 20th 1990

Two compressor speeds were investigated in this experiment: 50% and 75% of full speed. The evaporator feed rate was set by trial and error to give an apparent evaporator level close to the observed flood point: this was of necessity a process of trial and

error. The method used in the experiment was essentially that used for the pure fluid experiments, with the learning gained from previous two-fluid operation employed to overcome the flooding problems. The compressor was run at 50% speed for the first 35 minutes of the run, then switched up to the higher speed. The metering pump rate was initially set to 50 litre/hr on startup, then reduced to 32 litre/hr until the compressor speed was altered, when it was adjusted to 47 litre/hr. This adjustment was made in order to maintain the evaporator pressure and hence compressor suction conditions at similar values for both speed settings. The cold water stream temperature was set at 35 °C, the hot water stream at 65 °C. These higher temperatures were used to keep the evaporator pressure above atmospheric, because the evaporator pressure transducer gave only positive gauge pressure readings.

Variation of Pressures and Temperatures The variation of temperature in the evaporator is shown in Figure 4.33; this shows the refrigerant inlet and outlet temperatures and the water inlet and outlet temperatures. The temperatures of the refrigerant entering and leaving the compressor, the temperature of the condensate from C–1 and the water temperatures in C–1 are shown in Figure 4.34. The variation of pressure in the evaporator and condenser is shown in Figure 4.35.

The evaporator and condenser pressures stayed nearly constant over the experiment, even after the change in compressor speed. The degree of superheat during the compression process was markedly increased by the increase in speed: this may have been partly caused by an increase in the suction side pressure drop and partly by increased compression inefficiency. The indicated suction pressure at the manifold was 5 inches Hg vacuum (0.85 bara) at the first speed and 7 inches Hg (0.78 bara) at the second. The hot water exit temperature from C–1 stayed at approximately 75 °C: this constancy meant that the suction superheater could perform under constant conditions, and this explains the constancy of suction inlet temperature. The overall external lift was therefore 40 °, comparable to the experiments performed with pure R114.

The evaporator temperature plot shows a dramatic dip in refrigerant inlet temperature, the minimum temperature occurring at about the same time as the increase in compressor speed. This would seem to imply a change in circulating refrigerant composition, as the evaporator pressure remained constant. It is the author's opinion however

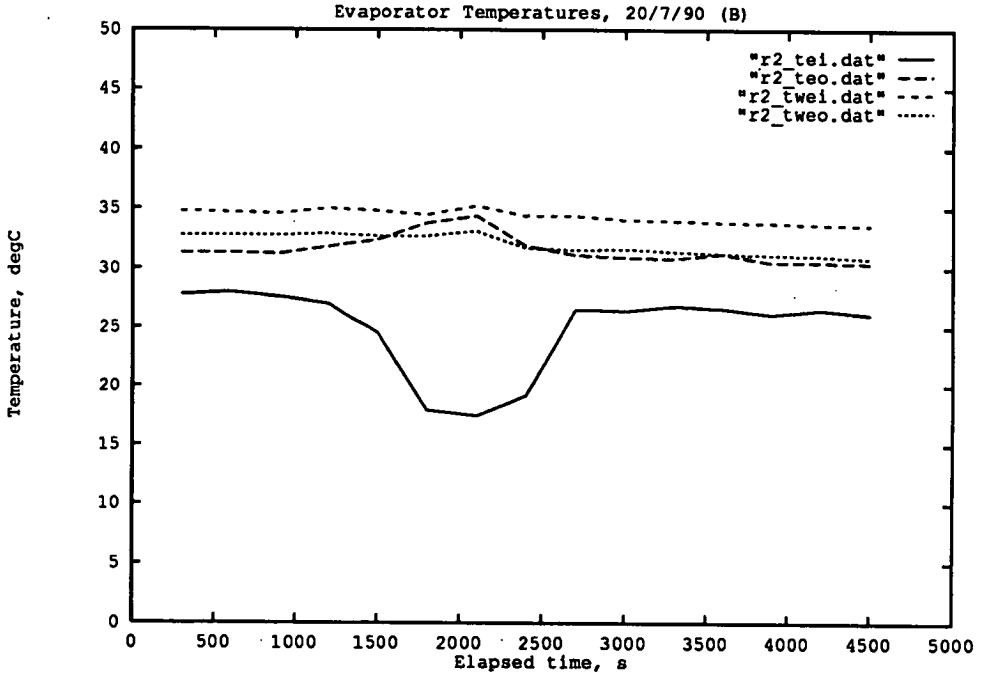

Figure 4.33: Variation of Evaporator Temperatures, 20/7/90 (pm)

that this was not the case: the conditions in the rest of the plant indicated no shift in holdups or compositions in the other holdup volumes. The explanation lies in the evaporator holdup: the evaporator pressure was measured at the top of the unit, in the vapour outlet. The refrigerant inlet was at the bottom of the unit and so would in fact be at a greater pressure then the outlet: hydrostatic head and pressure drop from the geometry would ensure this. Although not plotted in the thesis the recorded apparent levels in the evaporator were examined by the author. These figures are directly proportional to the pressure drop over the unit (they were measured with a differential pressure transducer). The apparent level shows a drop occurring over the same timescale as the change in inlet temperature: since the pressure at the top of the unit remained constant this implies a drop in the inlet pressure. This in turn implies a drop in refrigerant inlet temperature: the feed liquid was throttled into the evaporator because the storage tank was at a higher pressure than the evaporator. Any decrease in pressure would therefore increase the adiabatic temperature drop of this process; furthermore the temperature of a binary system at constant composition is a function of pressure.

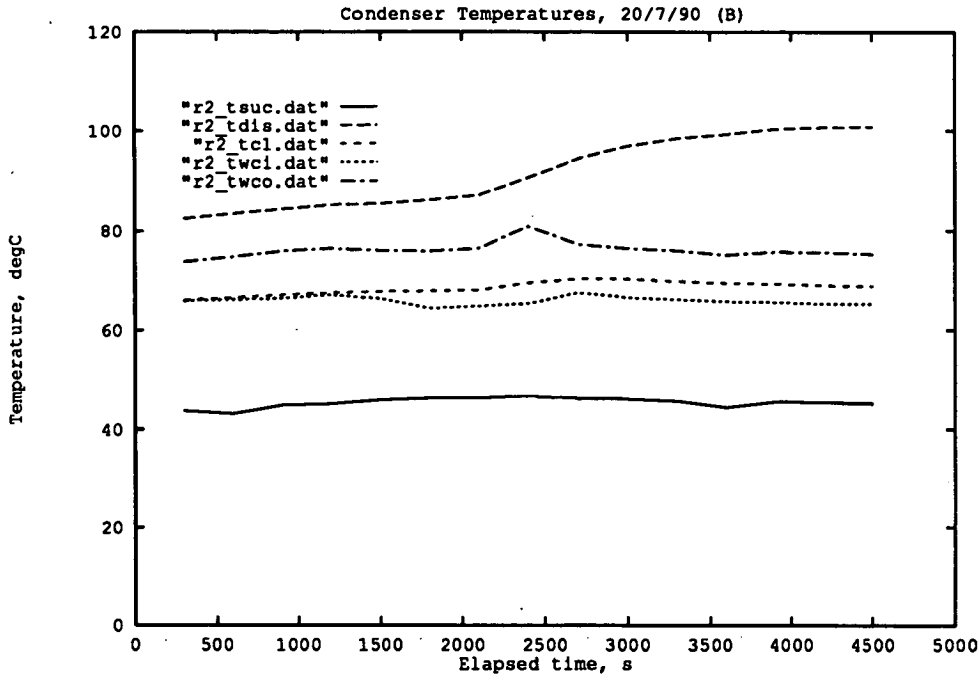

Figure 4.34: Variation of Compressor & Condenser Temperatures, 20/7/90 (pm)

Compositions The data were analysed using the CSD and CCOR equations of state to calculate the liquid compositions in the heavy tank and V/L separator (T–1) attached to the condenser. The vapour composition leaving the evaporator was also estimated but there was less certainty over the accuracy of this value. It was assumed that little superheat was performed by the evaporator in normal operation (it was run close to the flood point) but in fact there was a period of low level when superheat was performed: this is shown by the temperature plots above. The vapour compositions calculated using these data would be in error since the method of calculation assumed the refrigerant exit temperature in the evaporator was the dew temperature for the fluid mixture. The results are given below in Table 4.21, which lists the calculated vapour and liquid compositions in the evaporator; the liquid composition in the storage tank T–3 (*i.e.* evaporator feed), and the composition of the liquid in the condensate receiver T–1. All compositions are given as mol fractions of R114.

It may be seen that the agreement between the two equations of state is very good: they predict essentially identical liquid compositions, and vapour composition prediction

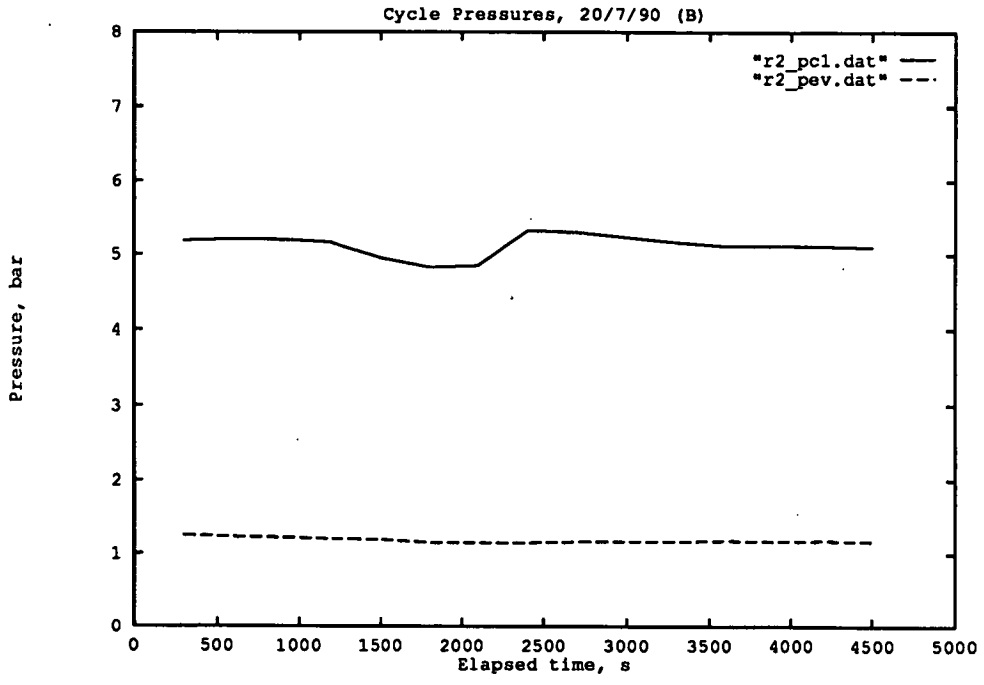

Figure 4.35: Variation of Cycle Pressures, 20/7/90 (pm)

differs by less than 5 mol%. The deviation in predicted evaporator composition and condensate composition was caused by superheat. The CCOR equation actually gives results which are in better internal agreement: the composition of evaporator product vapour is close to that of condensate in T–1. The results vindicate the investigation of both equations and indicate that a control program equipped with either equation for on-line property prediction would be of use.

Thermodynamic Performance The magnitude of heat flux in the condenser was about 2.5 kW at the first compressor speed and 3.5 kW at the second speed. These fluxes were again lower than was desired but they were not of overriding concern. The thermodynamic performance of the heat pump was determined by calculation of the state functions of the working fluid once composition in the active loop had been determined (see above). There was some uncertainty over the inaccuracy in the compressor manifold gauge readings: the two manifold pressure readings recorded above were assumed to be representative of the pressures experienced by the compressor throughout the experiment, and were used in the input to the thermodynamic property

	CSD Equation				CCOR Equation			
Time	Evaporator		T-3	T-1	Evaporator		T-3	T-1
hr	Liquid	Vapour	Liquid	Liquid	Liquid	Vapour	Liquid	Liquid
Data taken with compressor at 50% speed								
15:47	0.28	0.64	0.65	0.64	0.27	0.57	0.66	0.66
15:52	0.33	0.68	0.59	0.65	0.32	0.63	0.59	0.66
15:57	0.32	0.69	0.58	0.65	0.31	0.63	0.58	0.66
16:02	0.32	0.68	0.57	0.63	0.31	0.62	0.58	0.64
16:07	0.30	0.66	0.56	0.61	0.28	0.59	0.57	0.62
16:12	0.28	0.64	0.54	0.59	0.27	0.57	0.55	0.60
16:17	0.24	0.59	0.53	0.56	0.22	0.51	0.53	0.57
16:22	0.23	0.56	0.52	0.58	0.21	0.49	0.52	0.59
Data taken with compressor at 75% speed								
16:27	0.27	0.63	0.50	0.59	0.26	0.56	0.49	0.60
16:32	0.29	0.66	0.53	0.58	0.28	0.58	0.53	0.59
16:37	0.30	0.67	0.52	0.58	0.29	0.60	0.52	0.58
16:42	0.30	0.66	0.52	0.58	0.28	0.59	0.52	0.60
16:47	0.30	0.66	0.52	0.60	0.29	0.60	0.52	0.61
16:52	0.31	0.67	0.52	0.58	0.30	0.61	0.52	0.59
16:57	0.31	0.67	0.53	0.59	0.30	0.61	0.53	0.60
17:02	0.31	0.67	0.53	0.59	0.30	0.61	0.53	0.60

Table 4.21: Calculated Working Fluid Compositions, 20/7/90 (pm)

prediction program.

The results for the first compressor speed were very consistent: the COP was calculated to be 5.7 $\pm$ 0.2 for this speed. In the absence of better data on the composition the Lorentz COP was not determined, as this would be quite sensitive to errors in temperatuer and composition. The equivalent Carnot COP, calculated between the evaporator inlet temperature and the condensate temperature (bubble-point of evaporator to bubble-point of condenser) was on average 8.7 for the duty, giving a Carnot efficiency of about 65%. This was consistent with the previous work on pure fluids but should be treated with caution as an absolute measure of efficiency.

The results recorded at the second compressor speed are more interesting: they indicate that the compression efficiency changed more sluggishly than the rest of the cycle parameters. The calculated COP fell steadily after the speed change for 25 minutes before settling down to a (constant) value of 4.0 for the remainder of the experiment. This slow response was caused by the thermal inertia of the oil separator and its inventory of fluids: the increase in speed brought about a decrease in compression

efficiency but this was initially offset by the contents of the separator acting as a quench to the compression process. The discharge temperatures attained in the final part of the run were well above the compressor design conditions, which may help to explain the dramatic effect on performance of the speed change. Another important consequence of the increase in compressor speed was the drop in manifold pressure, which increase the compression ratio for the unit and would therefore affect the efficiency of compression.

4.4.4.2 Second Experiment: July 23rd 1990

This experiment was intended as a duplicate of the previous experiment, performed in order to confirm the observations made in that work. The setpoints were as described above but the plant was run for over six hours, at 50% compressor speed for most of the time. The speed was increased to 75% about 40 minutes before the end of data logging, in order to prove the increase in adiabatic temperature rise which this caused before. The longer run time resulted from repeated flooding of the evaporator, which required corrective action to retrieve the desired steady state. The temperatures, pressures and calculated compositions bore out the observations on COP and performance which were made in the previous work, and the same depth of analysis is not repeated since it sheds little new light on the plant performance. The interesting data from this work concern the behaviour of the evaporator.

Evaporator Performance The performance of the evaporator was erratic: it exhibited two steady states under identical liquid feed and vapour off-take rates, a cause of considerable vexation to the operators. The plant was brought up to temperature using a low metering pump setting of 25 litre/hr: this resulted in a stable steady state in the evaporator with a low measured level and a large increase in refrigerant temperature between inlet and outlet. The pressure in the evaporator was also low: almost atmospheric. These observations indicated that the evaporator was running empty, and so attempts were made to boost the performance by increasing the feed rate. An increase in flow of 5 litre/hr initiated the first flood. The level in the evaporator then climbed rapidly until the vapour product could support a level of several centimetres of liquid above the exit pipe datum (this was visible in the V/L separator) and there was no difference between the refrigerant inlet and exit temperatures. This was the

second stable state, and persisted until broken by stopping the feed to the evaporator altogether.

This behaviour was repeated throughout the experiment: it was found that a kind of hysteresis was involved. The feed rate which would trigger a flood was not the same as the rate which would cause the operating state to flip back from flooded to dry operation. It was not possible to identify unambiguously the cause of this behaviour, as nothing was known about the internal construction of the evaporator vapour space beyond an indication that the unit had over 50 times the bare-tube area for heat transfer. It is the author's speculation that the hysteresis may be partly ascribed to wetting effects and partly to the vertical orientation. In order to force fluid up the unit and out it would be necessary to exert a net force larger than the fluid's weight on it: the magnitude of this force would depend on the surface friction and surface tension. On the other hand a reduction in applied force sufficient to arrest the flood would only need to drop the applied force back to match the weight of the fluid. The lifting force on the liquid contents of the evaporator would be related to the boilup rate, which in turn would be a function of the feed rate and total pressure. This argument would therefore seem to explain the observed behaviour, although more detailed measurements would need to be done to quantify the effect.

The temperatures of water and refrigerant passing through the evaporator are shown in Figure 4.36: these show clearly the two steady states of the unit: the temperature difference between the feed and outlet is a good indicator of this. This could be used directly in feed rate control if the feed were a pure fluid (*i.e.* control on superheat) but some intermediate composition prediction would be necessary to apply this technique to a mixed-fluid system.

Behaviour of Compressor and Condenser The evaporator exhibited large fluctuations in its operating conditions: these did not carry through to affect temperature and pressure levels in the rest of the plant. The suction gas superheater levelled out the changes in refrigerant vapour temperature, enabling the compressor to run with a steady inlet temperature. The large pressure drop on the suction side also damped out the fluctuations in evaporator pressure. The condenser pressure remained reasonably constant, although some small deviations were observed. These were probably the only

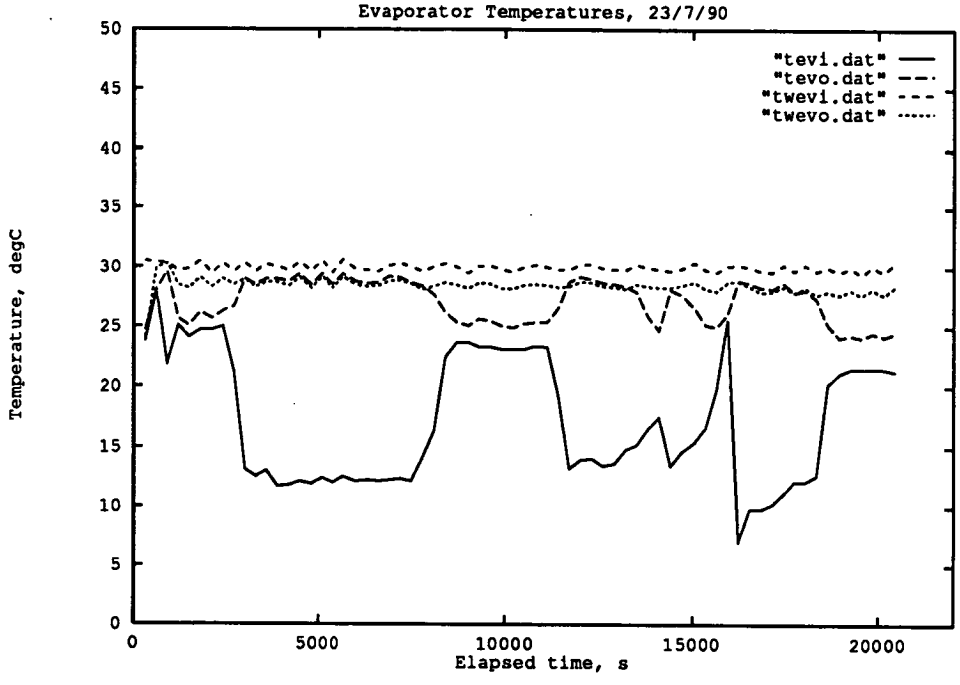

Figure 4.36: Variation of Evaporator Temperatures, July 23rd 1990

"knock-on" effect, caused by small changes in the refrigerant mass flow attendant on a change in metering pump rate. The temperature of water entering the condenser was controlled well to 60 °C for nearly all of the run, which made maintenance of steady refrigerant pressures and temperatures simple.

The variation of the compressor and condenser temperatures with time is shown in Figure 4.37; the variations in condenser and evaporator pressure are shown in Figure 4.38. The evaporator pressure dropped below atmospheric on several occasions; this is evident on close scrutiny of the pressure curve.

Thermodynamic Performance The data were not analysed in detail: comparison of the pressure and temperature levels with those attained in the previous experiment reveals that this experiment's results were very similar. A COP was determined for a few points in the middle of one of the stable, flooded states of the evaporator. This was 5.4 ± 0.2, in agreement with the previous work. The same increase in adiabatic tem-

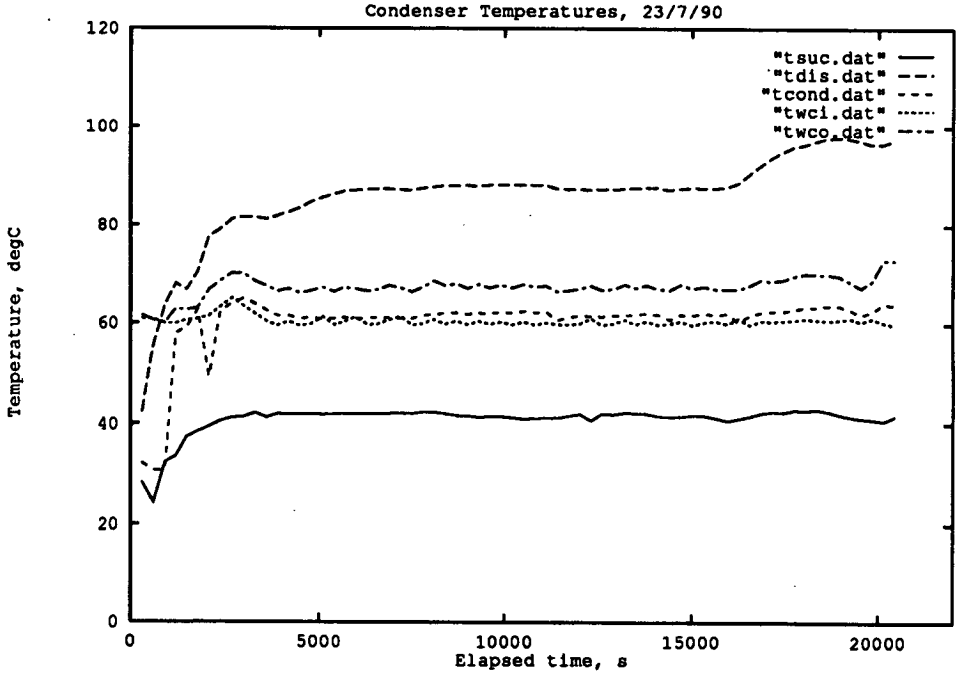

Figure 4.37: Compressor and Condenser Temperatures, July 23rd 1990

perature rise was observed, indicating that the effect of speed on compression efficiency was reproducible.

4.4.5 Effect of Condenser Water Flow

The last experiment performed by the author was intended to demonstrate the sensitivity of the degree of condensation in the first condenser to the water flowrate through the condenser bank. This was done as a more controllable method of effecting the condensation split than pressure control: time was no longer available to modify control loop settings. It was known that condensation did take place in the first condenser: the problem was that refrigerant flows in the plant had been too low for the desired water flowrates to affect the condensation process. This last experiment was therefore carried out with extremely low water flows, and this affected the quality of data obtained.

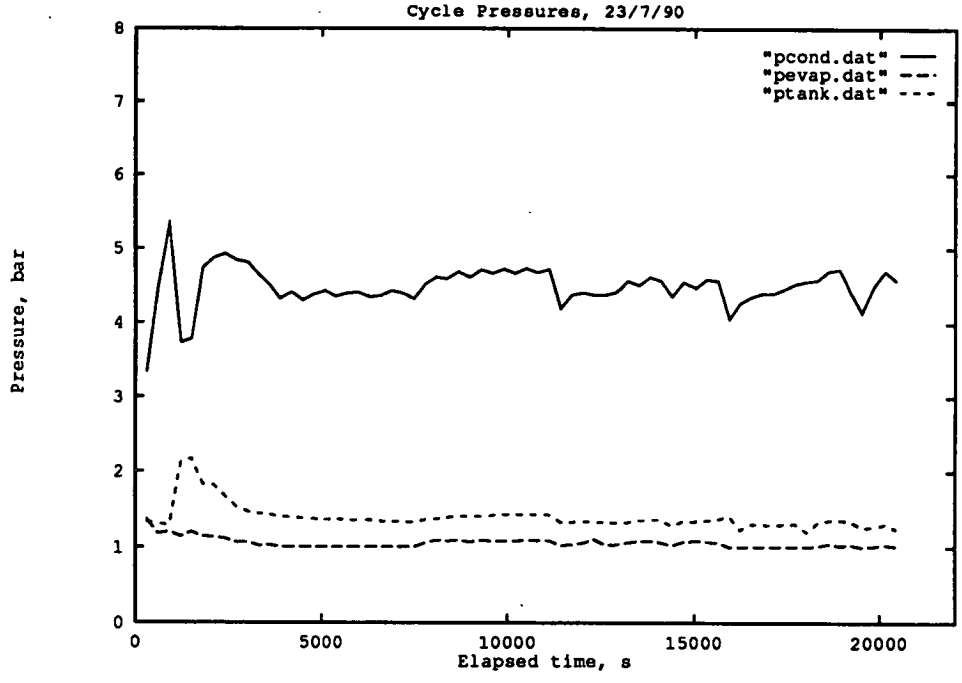

Figure 4.38: Condenser and Evaporator Pressures, July 23rd 1990

4.4.5.1 Procedure and Progress of Run

The plant was run in two-condenser mode, with the compressor at 50% speed, the cold water temperature at 40 °C and the hot water temperature at 70 °C. The water temperatures were raised to increase the evaporator pressure and hence increase the compressor suction gas density. The metering pump was still not functioning properly: the head attached to the light storage tank was not pumping a controlled flow but rather delivering irregular slugs of fluid. This was not an insurmountable problem: the rate of condensation was so slow in the second unit that accumulation in the tank was slow and could be vented back to the compressor suction.

The rig was brought to an emergency stop about halfway through the experiment in response to a hose failure on the heat sink flowmeter. The loss of the heat sink stream meant that the compressor had to be tripped out, and so the whole equilibrium of the pressurised part of the plant was disturbed. This will become obvious from the

plots of temperatures and pressures in the plant. An interesting observation was made about this time: there was no discernable condensation in the second condenser until *after* the restart. It was not immediately obvious why this should be so: one possible explanation might however be the following:

When the compressor was tripped, the condensers were vented back to the suction line: rather than an immediate, crashing stop, the unit was put on total recycle for a short time while the speed controller wound down the compressor. This had the effect of flushing the second condenser back to the suction. The geometry of the plant meant that this vent gas had to pass through the glass V/L separator, which was of course fitted with a pressure relief valve. The author observed condensation on the glass walls of this vessel during this flushing process: this was an indication of an elevated pressure in the vessel, as no such condensation was observed in normal operation. The indicated evaporator pressure peaked briefly above the set relief pressure of 25 psig; thus it is possible that a vent to atmosphere occurred in this process. If inerts had accumulated in the condenser bank then this would have purged them from the system; although the rig was routinely vented (from the top of C–2) after any maintenance the existence of subatmospheric pressures may have led to the slow induction of air. An inert blanket over the second condenser heat transfer surface would have acted as a severe disincentive to condensation, especially given the low refrigerant flows and oversized condenser areas.

After the restart, the water flow was initially set to about 5 litre/minute. Once the circulation of refrigerant had been re-established this was reduced to 1.6 litre/minute and the plant was allowed to find a meta-stable state. Rivulets of condensation had appeared in the sight glass attached to the second condenser's condensate receiver before the flow reduction: the rate of condensation was greatly increased by the change in water flow, prompting the decision to vary the water flow systematically to observe any effect on the condensation process. Four other water flows were chosen, corresponding to successive divisions on the water rotameter. The flow was adjusted to a new value then the plant was allowed to run for about 10–15 minutes, by which time the plant was at a near-steady state once more.

4.4.5.2 Results

The results obtained were of interest merely as indicators of the splitting of the condensation and separation of the working fluid. Over 100 data sets were sampled in the course of this run: these were taken at varying time intervals to record the dynamic response of the plant to deliberate disturbances of some of the process variables (*e.g.* the hot water flowrate). In view of the observed dichotomy in plant behaviour before and after the emergency shutdown only the performance after the break will be discussed; although the graphs include the data for the entire run to demonstrate the general behaviour before the trip occurred.

The variation of water temperature through the condenser bank is shown in Figure 4.39, in which the legend indicates: `twci`: water into C–2; `twcm`: water out of C–2, and `twco`: water out of C–1. This diagram shows that after the restart, in the period when water flow was slowly increased from a minimum value of 1.6 litre/min back to the original flow of 5 litre/min, the *total* temperature rise of the water passing through the condensers was nearly constant. The duty was split between the condensers: the size of the split in duty was related inversely to the water flowrate. This may be easily seen by comparison of the vertical distances between the three temperature curves on the plot. The accompanying plot in Figure 4.40 shows the variation of refrigerant condensate temperatures, with the water inlet and exit temperatures shown as a comparison. This bears out the observed condensation split: the temperature of the condensate in C–2 was above that of the inlet water for a time.

The water flowrate could have affected the proportion of condensation in the second condenser as a result of one of two possible phenomena: either the first condenser's capacity was limited by a thermal pinch, or a change in flow regime affected the overall heat-transfer coefficients in the exchangers. The water flow was certainly near-laminar in the main pipe run (Reynolds number of 2400) but was probably still turbulent in the heat exchangers.

The first of these is then the more likely explanation: the water exit temperature was in the range 85 °C–90 °C for much of the time, and was actually 7–10 ° higher than that of the condensate from C–1. The compressor discharge temperature is shown in

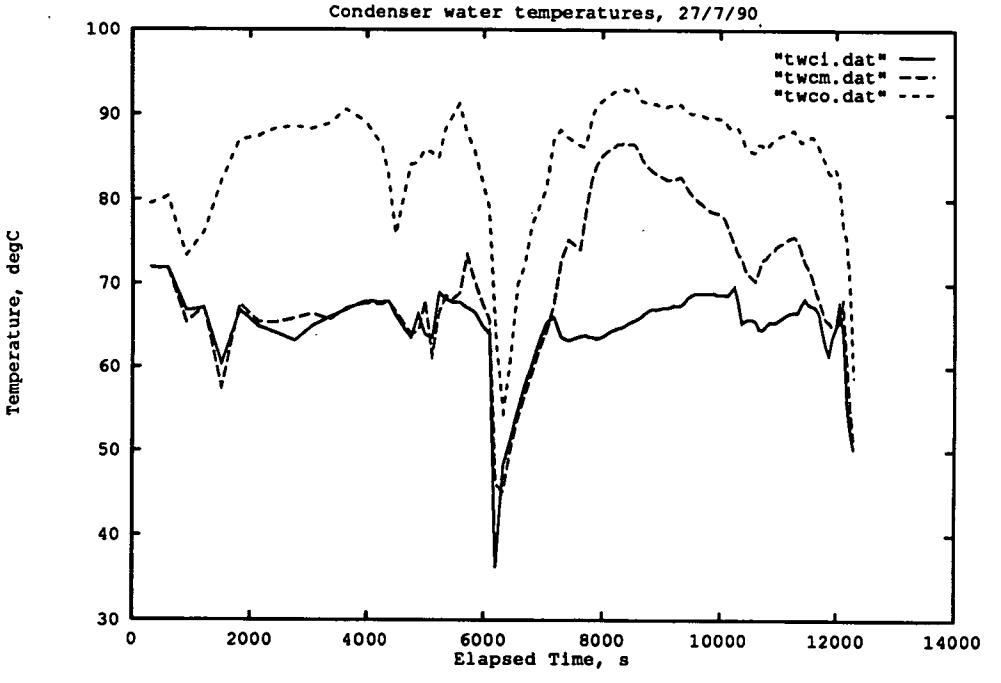

Figure 4.39: Variation of Condenser Water Temperatures, 27/7/90

Figure 4.41: it was reasonably consistent at just under 110 °C after attainment of a near-steady state. Previous work with the plant had led to the observation that the degree of superheat of compressed vapour would be of the same order as the degree of superheat of the suction vapour. The measured superheat (assuming low superheat in the evaporator) was in the range 15–20°, implying a dew temperature for the working fluid of about 90 °C. This was again in line with the earlier work, where it had been observed that the temperature of pure condensing R114 was invariably close to that of the water leaving the condenser bank.

The refrigerant storage tank pressures are shown in Figure 4.42 together with the evaporator pressure. This plot shows that after the restart, when R114-rich fluid was collecting in the condensate receiver attached to C–2, the pressure in the light storage tank began to rise until it was the highest in the low-pressure side of the plant. This was caused by passing of condensate into the tank: the tank itself was isolated from the evaporator and compressor suction because of the metering pump failure. The pressure in the heavy storage tank and in the evaporator dropped as this was happening,

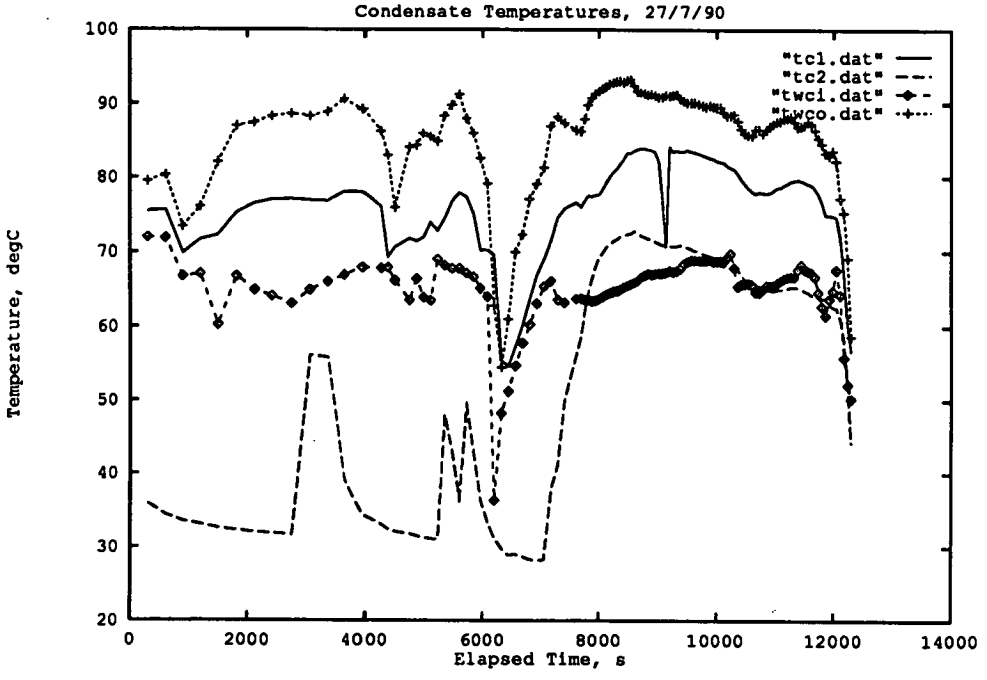

Figure 4.40: Variation of Condenser Refrigerant Temperatures, 27/7/90

indicating that the R114 concentration on that side of the storage was dropping. A progressive separation of the working fluid was therefore enforced, even under these low load conditions.

The variation in evaporator heat flux is plotted in Figure 4.43: it shows that in the period after the restart when the composition of working fluid was undergoing a continuous change, caused by the loss of R114 as condensate in C–2, the heat input fell by nearly 0.5 kW out of a flux of 3.5 kW, a change of 14%. This may be ascribed to the change in vapour pressure in the evaporator, and the result vindicates the principle of capacity control by composition regulation. The initial higher heat flux of nearly 4 kW was caused by the author's empirical rapid restart technique: any accumulations of R114-rich fluid were vented back to the evaporator from the tanks on restart to boost the throughput of the compressor. At the end of the experiment, the second condenser was blown down to storage, and this is the explanation for the second peak in evaporator heat flux: some of the R114 would have flashed back into vapour and gone round the circuit again before eventual condensation.

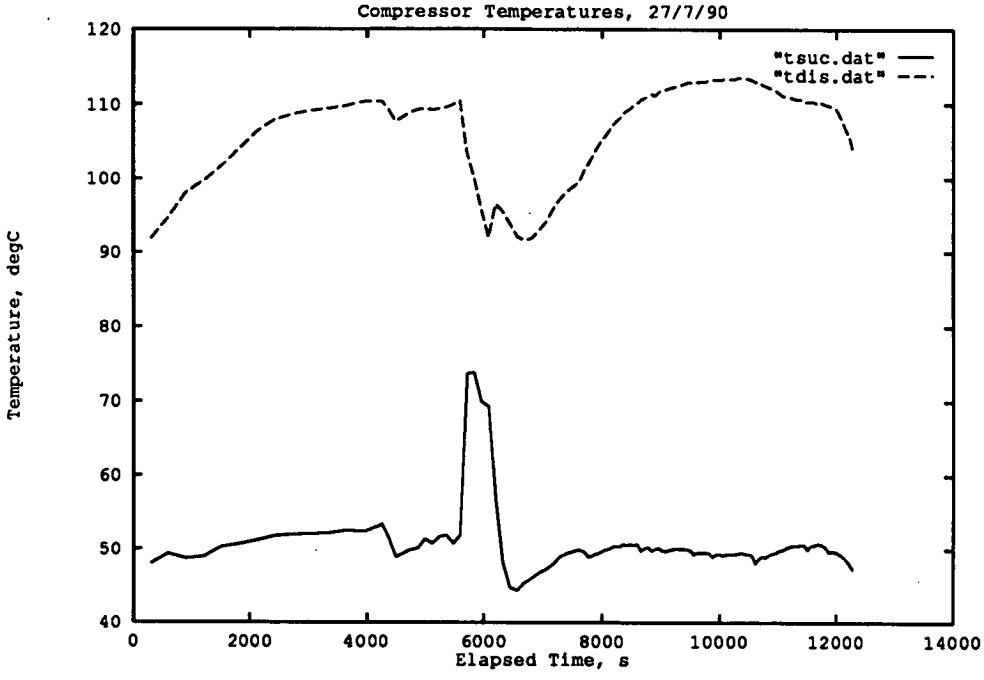

Figure 4.41: Compressor Suction & Discharge Temperatures, 27/7/90

4.4.5.3 Conclusions

This experiment, marred though it was by equipment failures, was of key importance to the aim of the project. It was possible to achieve a progressive separation of the active working fluid in the circuit by adjustment of the water flow to "pinch" the first condenser. This rather drastic control measure was required because of the low (compared to design) loads: the total heat flux was about 3 kW compared to a design rating of 10 kW. This turndown ratio was nonetheless in the desired range of capacity variation, and so it was essential to demonstrate that a condensation split could be achieved. There would be less of a problem in achieving this split at higher refrigerant flowrates: use of pressure control to affect the temperature profiles on the heat exchangers would then also assist the condensation split.

The progressive shift in the circulating refrigerant's composition resulted in a shift in the total heat output delivered by the plant. This demonstrated that the capacity of

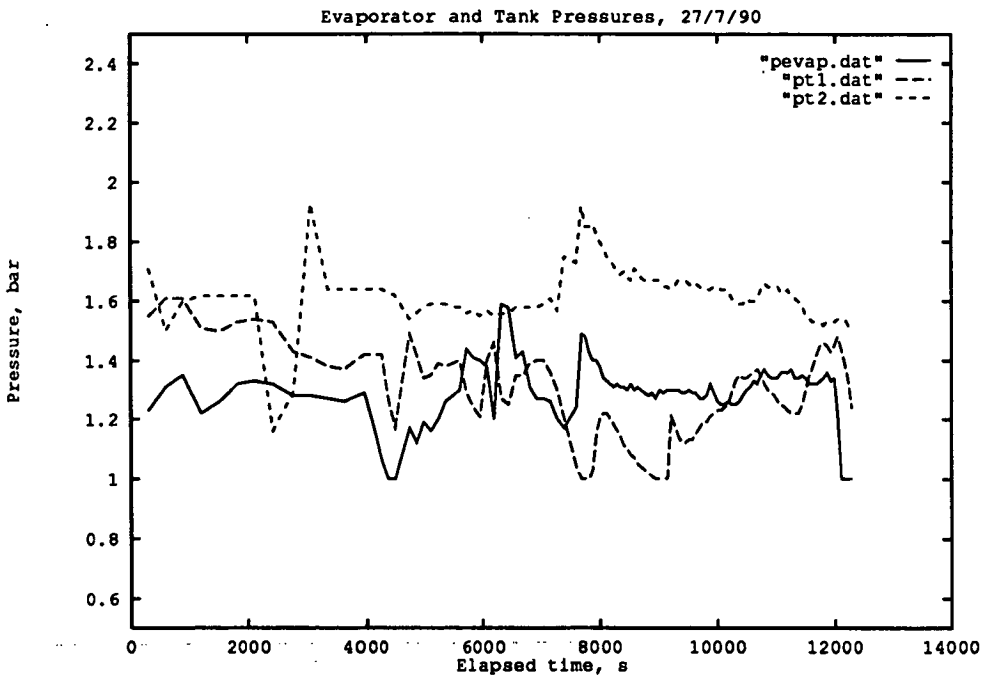

Figure 4.42: Storage and Evaporator Pressures, 27/7/90

the plant would shift at constant compressor speed. It may further be concluded that this represented a self-regulation: admittedly the composition shift was initiated by a deliberate reduction of the hot water flow, but exactly similar results would have been achieved had this alteration in flow been caused by a reduction in load or power input. The variation in water discharge temperature was small: the plant maintained high condensing temperatures throughout the composition shift, suggesting that were the experiment to be repeated with feedback control of water flow to maintain constant temperature, it would have been possible to maintain the product temperature at about 90 °C in an analogue of this experiment.

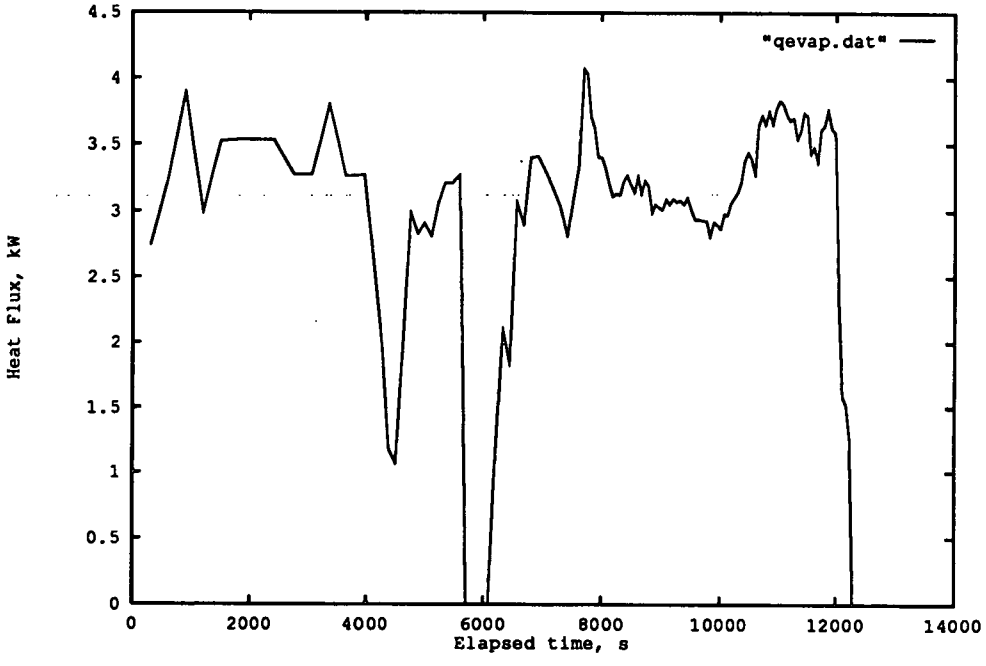

Figure 4.43: Measured Evaporator Heat Flux

Chapter 5

Computer Modelling

5.1 Sequential Model of the Heat Pump Evaporator

5.1.1 Description of the Unit

The evaporator for the heat pump pilot plant was supplied by Messrs Cal-Gavin Ltd. of Birmingham. This prototype design uses a water stream as heat source, evaporating refrigerant in vertical shells supplied by a common feed. The evaporator design has been sketched in Figure 3.3 in Chapter 3.

Liquid refrigerant is fed to the base of the shells *via* a manifold; thus the feed for each shell is at the same temperature. Furthermore, the level in each section of the unit must be the same, neglecting changes in apparent density of the fluid. The vapour produced is

taken off through a (larger bore) exit manifold at the top of the unit. The heat source, that is, the water stream, is piped into the top of shell 'A', thence to the bottom of shell 'B' and out through shell 'C'. This arrangement gives two counter-current and one co-current contacting arrangement: the general equation $\dot{Q} = \mathcal{F}UA\Delta T_{LM}$ may be used for each shell without need of the correction function $\mathcal{F}$. Unless the unit is run flooded, there will normally be some degree of superheat to the vapour product, within the limitations of the heat source capacity rate and temperature. The overall heat transfer, then, will be composed of evaporation followed by superheat, with differing resistances for each process. The analysis of experimental data on the unit must therefore incorporate methods of determining these resistances from the available measured quantities. The difficulty of this task for any unit depends on the nature of the area used for heat transfer, and it will be shown that this design of exchanger presents some difficulties of both modelling and data analysis.

The heat transfer surface used is a combination of extended surface (*i.e.* fins, and enhanced (*i.e. roughened*) surface. Without knowledge of the detailed composition of this surface it is not possible to obtain a good figure for the area available for heat transfer; this means that only experimental determination of heat transfer products (UA) rather than heat transfer coefficients (U) is possible. The tube side heat transfer resistance is lowered by the introduction of "Heatex" turbulence promoters: this should mean that the refrigerant-side resistance is the controlling factor in this unit. It should be appreciated that it will not be possible to construct a detailed mathematical model of this unit unless the internal geometry is precisely known: for the work described in this thesis this was *not* the case. The mathematical model presented here is extremely basic, yet it should give reasonable predictions which will match the experimental data to somewhere approaching the accuracy of the measured variables.

5.1.2 Description of Model

5.1.2.1 Assumptions Made

The derivation presented here is subject to the following assumptions:

- The evaporator feed is pure, saturated liquid at its bubble point.

- Heat leakage, either to or from the environment, is negligible.
- The evaporative heat transfer takes place only on those surfaces which are submerged in liquid; thus each shell of the evaporator has the same proportion of total area available for superheat.
- The variations in temperature and heat flux through the unit are so low that the heat transfer coefficients for evaporation and superheat will not change from shell to shell. The behaviour of the whole unit is then characterised by an overall coefficient for evaporation , U_e, and an overall coefficient for superheat, U_h.
- The observed refrigerant exit vapour flowrate and temperature is the result of the adiabatic mixing of the vapour streams from each shell.

5.1.2.2 Problem statement

The experiments carried out using pure refrigerant as the working fluid were the first part of the overall programme. At the time of working there were insufficient channels available on the thermocouple amplifier board: it was not possible to measure the water temperature at the inlet and outlet of each shell. This was later rectified but the lack of the two intermediate water temperatures meant that a direct calculation of the heat transfer coefficients for evaporation and superheat was not possible. The model described here was developed to accept a specified pair of heat transfer coefficients and calculate the expected performance of the unit, given inlet temperatures and water flowrate. The intention was to compare the predicted exit temperatures and total refrigerant throughput with that obtained by measurement. The problem specification was therefore taken as:

> Given an evaporator of the geometry described in Section 5.1.1, subject to the assumptions detailed above, find the outlet water temperature, outlet refrigerant vapour temperature and total refrigerant flow which correspond to the following specified process variables.
>
> - Water flowrate.
> - Water inlet temperature.
> - Refrigerant boiling temperature.
> - Heat transfer product $(UA)_e$ for evaporation.
> - heat transfer product $(UA)_h$ for superheat.

5.1.2.3 Notation

For the analysis the evaporator is split into three shells, corresponding to the actual shells found in the unit. Each shell is further split into an evaporator, where only latent heat is gained by the refrigerant, and a superheater, where dry, saturated vapour is superheated to an (initially) unknown exit temperature. The notation used in the analysis is straightforward: water temperatures are denoted by upper-case 'T', while temperatures on the refrigerant side are represented by lower-case 't'. The subscripts used are as shown in Figure 5.1, which shows the example of a counter-current shell. The same notation is used for a co-current shell. In addition to the unknown water exit temperature, there is an unknown midpoint temperature, T_M, which is the temperature of the water at the boundary between the superheating and evaporative sections of the exchanger. The heat flux in the evaporative section is denoted as $\dot{Q}_e$, that in the superheat section $\dot{Q}_h$.

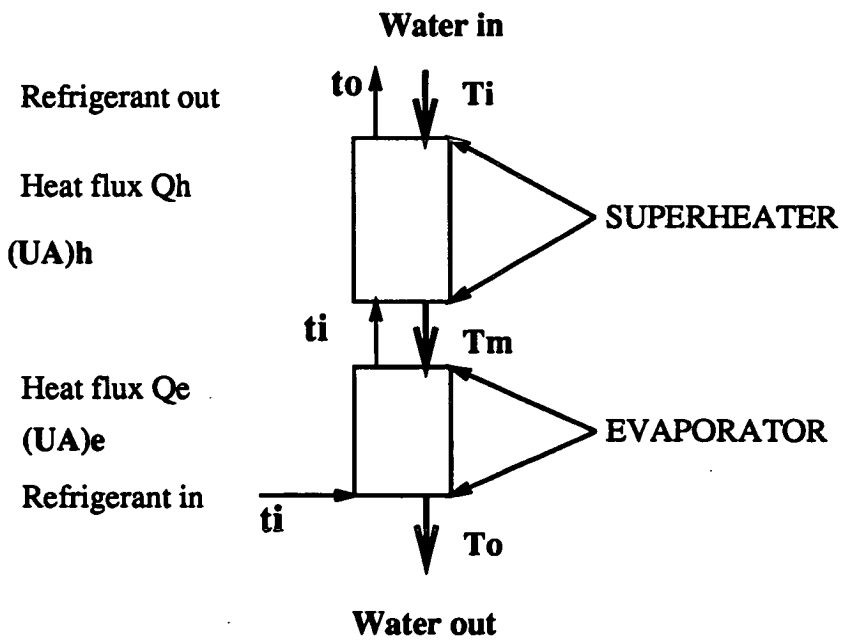

Figure 5.1: Notation for Evaporator Analysis

5.1.2.4 Counter-Current Shell

Evaporative Section The equations for this section are:

$$\dot{Q}_e = \dot{m}_R \lambda \tag{5.1}$$

$$\dot{Q}_e = \dot{m}_W Cp_W (T_M - T_o) \tag{5.2}$$

$$\dot{Q}_e = (UA)_e (LMTD)_e \tag{5.3}$$

$$(LMTD)_e = \frac{T_M - T_o}{\ln\left[\frac{T_M - t_i}{T_o - t_i}\right]} \tag{5.4}$$

where the symbols λ, Cp represent latent and specific heats. Refrigerant properties are denoted by subscript 'R', water by subscript 'W'.

The primary variables in the above equation set are: $\dot{m}_R, \dot{m}_W, t_i, T_M, T_o, (UA)_e$ and $\dot{Q}_e$, *i.e.* 7 variables. (All other variables used above have definitions in terms of these variables.) There are 3 independent equations (Equation 5.1, Equation 5.2 and Equation 5.3) and so the system has 4 degrees of freedom. Of the variables itemized, only $\dot{m}_W$ and t_i were measured in the experimental work: this leaves 2 degrees of freedom. A reasonable choice of the remaining two set variables is the pair $(UA)_e, T_M$, yielding a solution as follows:

Introducing the auxiliary quantities $\Delta_W = (T_M - T_o)$, $I = (T_M - t_i)$ and $W = \dot{m}_W Cp_W$, Equation 5.3 may be written as:

$$W\Delta_W = (UA)_e \frac{\Delta_W}{\ln\left[\frac{I}{I-\Delta_W}\right]} \tag{5.5}$$

$$\Rightarrow \quad \ln\left[\frac{I}{I-\Delta_W}\right] = \frac{(UA)_e}{W} \tag{5.6}$$

$$\Rightarrow \quad \frac{I}{I-\Delta_W} = \exp\left(\frac{(UA)_e}{W}\right) \tag{5.7}$$

$$= \quad G_e$$

The water temperature drop and refrigerant mass flow may then be found using Equation 5.1 and Equation 5.2, giving:

$$\Delta_W = \frac{I(G_e - 1)}{G_e} \tag{5.8}$$

$$\dot{m}_R = \left(\frac{W\Delta_W}{\lambda}\right) \tag{5.9}$$

Superheat Section Define auxiliary variables $\Delta_R = t_o - t_i, \Delta_W = T_i - T_M, R = \dot{m}_R Cp_R, W = \dot{m}_W Cp_W, A = T_i - t_i$. The governing equations then become:

$$\dot{Q}_h = \dot{m}_R Cp_R (t_o - t_i) = R\Delta_R \tag{5.10}$$

$$\dot{Q}_h = \dot{m}_W Cp_W (T_i - T_M) = W\Delta_W \tag{5.11}$$

$$\dot{Q}_h = (UA)_h (LMTD)_h \tag{5.12}$$

$$(LMTD)_h = \frac{(T_i - t_o) - (T_M - t_i)}{\ln\left[\frac{T_i - t_o}{T_M - t_i}\right]} \tag{5.13}$$

$$= \frac{\Delta_W - \Delta_R}{\ln\left[\frac{A - \Delta_R}{A - \Delta_W}\right]}$$

By analogy with the evaporative section, the independent variables are: $\dot{m}_R, \dot{m}_W, t_i, t_o, T_i, T_M, (UA)_h$ and $\dot{Q}_h$, giving 8 in total. The number of independent equations is still 3 (Equation 5.10, Equation 5.11 and Equation 5.12), so there is an additional degree of freedom in this system. The measurable quantities are $\dot{m}_W, T_i$ and t_i, yielding a final problem with 2 degrees of freedom if these measurables are used. If the pair $(UA)_h, \dot{m}_R$ is specified, a direct solution is obtained as follows:

Putting $(W/R) = K$ gives $\Delta_R = K\Delta_W$ and hence

$$W\Delta_W = (UA)_h \frac{\Delta_W (1 - K)}{\ln\left[\frac{A - K\Delta_W}{A - \Delta_W}\right]} \tag{5.14}$$

$$\Rightarrow \quad ln\left[\frac{A - K\Delta_W}{A - \Delta_W}\right] = \left(\frac{(UA)_h}{W}\right) = \ln G_h \tag{5.15}$$

$$\Rightarrow \quad \frac{A - K\Delta_W}{A - \Delta_W} = G_h \tag{5.16}$$

$$\Rightarrow \quad \Delta_W = \frac{A(G_h - 1)}{G_h - K} \tag{5.17}$$

The solution is completed by Equation 5.17, since the refrigerant exit temperature may be determined from the water temperature change.

Solution of Both Sections The solutions given above for each section of the shell required specification of two unknowns: for the evaporative section $(UA)_e, T_M$ and for

the superheating section $(UA)_h, \dot{m}_R$. If it is assumed that the heat transfer products are specified in advance, then a means of determining the refrigerant mass flow and water intermediate temperature is required, as neither of these quantities is observable. An effective way of doing this is to iterate on either of the two variables; by specifying one the complete solution to its section is obtained, which in turn provides the information necessary to calculate a solution to the other section. The water intermediate temperature was chosen as the iteration variable: it is bounded by the inlet temperatures of water and refrigerant, both of which are known. This is preferable, since the LMTD will not be defined should a physically impossible value of T_M be generated. Further, it is possible to make a good first guess from the relative magnitudes of the heat transfer products.

Algorithm 5.1 Single Counterflow Shell Solution

Step 1: *Specify* $(UA)_e, (UA)_h, \dot{m}_W, T_i, t_i$

Step 2: *Make an initial guess of* T_M. *A good guess is:*
$T_M = T_i + (T_i - t_i) \times (UA)_h/(UA)_e$

Step 3: *Solve the evaporative section to find a refrigerant mass flow* $\dot{m}_R$.

Step 4: *Using the value of* $\dot{m}_R$ *from the previous step, calculate the superheat section and obtain a new value of* T_M *from Equation 5.17*

Step 5: *Test the two values of* T_M*: if they agree to the experimental accuracy then break the iteration*

Step 6: *Update the value of* T_M *by a safe method* e.g. *the bounded secant algorithm, or bisection, then return to step 3*

5.1.2.5 Co-Current Shell

The case of a shell with co-current flow is slightly different, as the evaporator is the first section to contact the water stream. As a result the final equations for each shell are not exactly the same as those presented in the previous section. The notation used in this Section is identical, however, and will not be repeated here. The relevant equations are as follows:

Evaporative Section

$$G_e = \exp\left(\frac{(UA)_e}{W}\right) \tag{5.18}$$

$$\Delta_W = \frac{I(G_e - 1)}{G_e} \tag{5.19}$$

Superheat Section

$$A = T_M - T_i \tag{5.20}$$

$$K = \dot{m}_W Cp_W / \dot{m}_R Cp_R \tag{5.21}$$

$$G_h = exp\left(\frac{(1+K)(UA)_h}{W}\right) \tag{5.22}$$

$$\Delta_W = \frac{A(G_h - 1)}{G_h(K+1)} \tag{5.23}$$

The algorithm used for the co-current solution is identical to that described by Algorithm 5.1, save for the initial guess of T_M. The initial guess for the co-current case is $T_M = T_i + (T_i - t_i) \times (1 - (UA)_h/(UA)_e)$, which gives a sensible starting value within the bounds of feasible T_M.

5.1.2.6 Solution of Evaporator

The evaporator consists of two counter-current shells and one co-current shell. From the Problem Statement (Section 5.1.2.2), the known variables may be taken as the refrigerant inlet temperature, water inlet temperature and water flowrate. Then the algorithm for solution of the complete evaporator problem is as follows:

Algorithm 5.2 Evaporator Calculation

Step 1: *Specify the following variables:*
$\dot{m}_W, T_i, t_i, (UA)_e, (UA)_h$

Step 2: *Determine the refrigerant latent and specific heats from* t_i.

Step 3: *Solve Shell 'A' using Algorithm 5.1: store the values of refrigerant flowrate, refrigerant exit temperature and water exit temperature.*

Step 4: *Using the information generated from the previous step, solve Shell 'B' and store the exit conditions and refrigerant flow.*

Step 5: *Solve Shell 'C' and store the exit conditions.*

Step 6: *Sum the capacities of each shell to get the total capacity.*

Step 7: *Perform an adiabatic mixing of the refrigerant vapour streams to obtain an overall exit temperature for the vapour.*

Step 8: *Report all temperatures, capacity and heat loads.*

5.1.3 Application

The evaporator model described above was implemented in the 'C' language on the departmental Sun network. The source code could be compiled without modification on a PC system, although the calculations described here were carried out on the workstations for convenience. In addition to the implementation of the evaporator, the program was fitted with correlation functions for the properties of pure refrigerants: these are more fully described in Chapter 6. The source code for the final version of the program is contained in Appendix C: in essence it follows the procedure described by Algorithm 5.2 with minor enhancements. Provision is made to perform calculations over ranges of heat transfer product, with output in a form suitable for generation of contour or surface plots using the UNIMAP package. This enables quick visualisation of the effect of each specified parameter on the main calculated parameters.

5.1.4 Results

The model requires specification of five parameters, namely $\dot{m}_W, T_i, t_i, (UA)_e, (UA)_h$. Removing the two heat transfer products from the required inputs (they will each be stepped through a set range by the program) leaves three specified variables. A set of these inputs was established from the design basis of the evaporator, namely:

- Water flowrate of 15 litre/min *i.e.* 0.25 kg/s
- Refrigerant boiling temperature of 20 °C
- Water inlet temperature of 35 °C

In order to explore the effect of variation in these variables on the performance of the evaporator it was necessary to generate data for three parameters: total capacity; refrigerant exit temperature, and water exit temperature. It was necessary to choose a method of data representation which would clearly illustrate the influence of the five specified parameters on the overall performance of an evaporator of this configuration.

The UNIMAP package may be used to produce representations of three-dimensional surfaces, given sets of co-ordinate triplets. It was decided to represent the predictions of the model as sets of three such surfaces: in each plot the base co-ordinates would be the evaporative heat-transfer product, and the ratio of superheating heat-transfer product to evaporative heat transfer product. The three ordinates chosen were: refrigerant flowrate (the evaporator capacity); refrigerant vapour exit temperature, and water exit temperature. It would be possible to plot a fourth graph, of total heat load: this is however a linear function of water exit temperature and so the shape of the surface will resemble that of the water temperature plot.

A representative set of graphs have been included by way of illustration. These were generated using a water flow of 0.225 kg/s, inlet temperature 30 °C, evaporating pure R114 at 15 °C. These values were typical of those observed in operation of the plant.

The capacity is shown in Figure 5.2: this shows capacity reaching some asymptotic value of about 0.35 kg/s for these inlet conditions.

The variation of refrigerant exit temperature is shown in Figure 5.3: this also exhibits asymptotic behaviour, but the asymptote condition is of course achieved at the expense of capacity.

The variation of water exit temperature (heat flux) is shown in Figure 5.4: this indicates that beyond an evaporative UA of about 2.8 kW/K the evaporator is pinched, and any increase in area would have negligible effect. It also indicates quite clearly that superheat will never control the heat duty to any extent.

5.2 Rigorous (Simultaneous) Evaporator Models

5.2.1 Motivation for Development

The model described in this Section followed on from the the sequential model described in Section 5.1. The basis of the model remained similar to that of the sequential: the evaporator was considered as a set of three evaporator/superheater pairs. The major differences lay in the choice of constraints and in the solution of the governing equations. This model was based on the simultaneous solution of the entire equation set. This method was chosen to enable calculation of heat transfer coefficients from experimental datasets. By contrast the sequential model required prior specification of heat transfer coefficients and was therefore restricted to prediction of the performance of an evaporator of the Cal-Gavin configuration. The experimental datasets contained measured values of certain data, predicted by the sequential model, which could be used as constraints in place of the heat transfer coefficients. These are described in the following text.

The feed vapour fraction was also introduced as a constraint in the rigorous model, to be specified before the start of the calculation. This was necessary for analysis of most of the experimental data, since the refrigerant storage tank was usually at a higher pressure than the evaporator: the liquid drawn from the tank by the feed pump would therefore undergo a throttle over the pump loading valve, producing a two-phase feed. In principle this vapour fraction could be calculated from the observed temperatures and pressures in the storage tank and evaporator; in practice it was necessary to calculate the fraction as that value which compensated for any additional heat leakage into the system. As described in Chapter 4, there was a consistent deviation between the evaporator heat flux indicated by measurements of water temperature and the calculated flux obtained from the change of state of the refrigerant between the tank and the evaporator outlet. The reasons for this have been discussed in Chapter 4; in any event the effect was known and had to be allowed for in the design of the model.

5.2.2 Development of Model

The development outlined here is very similar to that used for the sequential model; the main differences lie in the choice of process constraints and unknowns.

5.2.2.1 Assumptions Made

The derivation presented here is subject to the following assumptions:

- The evaporator feed is pure, saturated refrigerant, either saturated liquid or a two-phase mixture in equilibrium.
- Heat leakage from the environment into the system may occur but will be accounted for by use of a modified feed vapour fraction.
- The evaporative heat transfer takes place only on those surfaces which are submerged in liquid; thus each shell of the evaporator has the same proportion of total area available for superheat.
- The variations in temperature and heat flux through the unit are so low that the heat transfer coefficients for evaporation and superheat will not change from shell to shell. The behaviour of the whole unit is then characterised by an overall coefficient for evaporation , U_e, and an overall coefficient for superheat, U_h.
- The observed refrigerant exit vapour flowrate and temperature is the result of the adiabatic mixing of the vapour streams from each shell.
- The variations in temperature driving force in any section of the evaporator are such that the logarithmic mean temperature differences occurring in the statement of the heat transfer equations may be replaced by the arithmetic mean temperature difference over that section.
- Specific heats of both refrigerant and water have constant values; the latent heat of vapourisation of refrigerant is also constant for a given set of inlet conditions.

These assumptions are very similar to those made in Section 5.1, save for the use of vapour fractions and the approximation of log-mean temperature differences by arithmetic mean temperature differences. This latter step was a useful simplification of the problem as it reduced the amount of calculation necessary in the iterative solution, and reduced the non-linearity of the equation set by elimination of the need to include logarithmic functions in the heat transfer equations.

5.2.2.2 Derivation of Equations

Each shell is regarded as a pair of heat exchangers, an evaporator and a superheater in series. For each of these sub-units two equations may be written: one expressing the

heat balance and one expressing the rate of heat transfer in that section as a function of driving force and heat transfer product. This gives $3 \times 2 \times 2 = 12$ equations; in addition there is an overall mass balance on the refrigerant streams, a heat balance on the refrigerant outlet manifold, and the overall heat balance relating the heat gained by refrigerant to heat lost by water, giving fifteen equations in all.

The model has the following variables: five refrigerant temperatures; seven water temperatures; five mass flowrates; two heat transfer products; one vapour fraction; two specific heats, and one latent heat. The thermodynamic properties are fixed, leaving twenty unknowns. The system therefore has five degrees of freedom. A minimal set of specified constraints could then be: total mass flow of refrigerant; water flowrate; inlet temperatures of both water and refrigerant, and feed vapour fraction. This was the initial set of constraints chosen: it agrees with common sense, since all the properties are associated with inlet streams to the unit.

In fact, the final version of the program, the only one discussed here, solved a reduced version of the problem, in which the refrigerant and water temperatures were specified. This was done in an attempt to analyse experimental datasets, which contained these quantities in addition to the initial specified quantities. Rather than specify the feed vapour fraction directly, the overall heat balance was used to compute the feed vapour fraction which would satisfy the heat balance. The computer program written to implement this model first requested input of the fixed temperatures and flows, then computed the feed vapour fraction, presented this knowledge, and asked for confirmation before proceeding to the solution. This was necessary as instrument error in some of the datasets would have led to impossible conditions, had the data been entered "blind".

The original structure of the problem was left intact in the program code for simplicity and speed of coding. The original listing (see Appendix C) appears to set up and solve a fourteen equation problem, but two of these equations are redundant. The rewriting of the code into a more economical form was left for the author's successor.

Notation The notation used in the following derivation may be summarised as follows:

- The refrigerant temperatures are represented by lower-case t; the water temperatures by upper-case T.

- The inlet refrigerant and water temperatures are given the subscript 0; thereafter the subscripting is sequential for the water side. The exit water temperature for shell "A" is denoted by T_1, that of shell "B" by T_2, and the final exit temperature by T_3.
- The temperature of water at the point in each shell where the boundary between evaporation and superheat is assumed to lie is denoted by the additional subscript letter M. The refrigerant vapour exiting each shell will have a different temperature: the vapour produced by shell "A" has temperature t_1 *etc.*
- The flowrate of refrigerant is generally denoted by $\dot{m}_R$. Each shell will have a slightly different flow, denoted by an additional subscript corresponding to the shell label. (*e.g.* $\dot{m}_{R,A}$)
- The water flowrate is replaced by the heat capacity rate W, defined as the product of mass flowrate and specific heat capacity.
- The heat transfer products (defined by $\frac{\text{Heat Flux}}{\text{Driving Force}}$) are denoted by (UA), with subscript e denoting evaporation and h denoting superheat.
- The feed vapour fraction is denoted by α; the latent heat of vapourisation is λ, and specific heats are denoted by the symbol C_p.

Constraints The constrained quantities are listed here in the notation used in the listing of the model's constituent equations.

- Water mass flowrate: $\dot{m}_W$
- Refrigerant total mass flow: $\dot{m}_R$
- Water inlet temperature: T_0
- Refrigerant inlet (boiling) temperature: t_0
- Water exit temperature: T_3
- Refrigerant exit temperature: t_4
- Feed vapour fraction (calculated): α

Shell A The equations governing the first shell of the evaporator, which is in counter-current flow, are:

$$\dot{m}_A(1-\alpha)\lambda - W\,(T_{M,A} - T_1) = 0 \tag{5.24}$$

$$W\,(T_{M,A} - T_1) - \frac{(UA)_e}{2}\,[T_{M,A} + T_1 - 2t_0] = 0 \tag{5.25}$$

$$C_{p,R}\dot{m}_A\,(t_1 - t_0) - W\,(T_0 - T_{M,A}) = 0 \tag{5.26}$$

$$W\,(T_0 - T_{M,A}) - \frac{(UA)_h}{2}\,[T_0 + T_{M,A} - t_1 - t_0] = 0 \tag{5.27}$$

Shell B The equations for the second shell, in co-current flow, are:

$$\dot{m}_B(1-\alpha)\lambda - W\,(T_1 - T_{M,B}) = 0 \tag{5.28}$$

$$W\,(T_1 - T_{M,B}) - \frac{(UA)_e}{2}\,[T_{M,B} + T_1 - 2t_0] = 0 \tag{5.29}$$

$$C_{p,R}\dot{m}_B\,(t_2 - t_0) - W\,(T_{M,B} - T_2) = 0 \tag{5.30}$$

$$W\,(T_{M,B} - T_2) - \frac{(UA)_h}{2}\,[T_{M,B} + T_2 - t_2 - t_0] = 0 \tag{5.31}$$

Shell C The equations for the last shell are identical in form to those for the first shell:

$$\dot{m}_C(1-\alpha)\lambda - W\,(T_{M,C} - T_3) = 0 \tag{5.32}$$

$$W\,(T_{M,C} - T_3) - \frac{(UA)_e}{2}\,[T_{M,C} + T_3 - 2t_0] = 0 \tag{5.33}$$

$$C_{p,R}\dot{m}_C\,(t_3 - t_0) - W\,(T_2 - T_{M,C}) = 0 \tag{5.34}$$

$$W\,(T_2 - T_{M,C}) - \frac{(UA)_h}{2}\,[T_2 + T_{M,C} - t_3 - t_0] = 0 \tag{5.35}$$

Other Equations These equations are statements of the mass and heat balances on the mixing of the refrigerant vapour streams into the specified stream leaving the unit.

$$\dot{m}_R - (\dot{m}_A + \dot{m}_B + \dot{m}_C) = 0 \tag{5.36}$$

$$\dot{m}_R t_4 - (\dot{m}_A t_1 + \dot{m}_B t_2 + \dot{m}_C t_3) = 0 \tag{5.37}$$

The overall heat balance for the unit, which was used in the final implementation of the model but was *not* used in the set of equations to be solved, was:

$$\dot{m}_R\left[(1-\alpha)\lambda + C_{p,R}\left(t_4 - t_0\right)\right] = W\left(T_0 - T_3\right) \tag{5.38}$$

This equation is a one-dimensional linear equation in the feed vapour fraction (as a result of the choice of constraint); the vapour fraction could thus be eliminated from the problem in advance of solution.

5.2.2.3 Computer Implementation

The model was implemented in the C language, using a subset of the ANSI draft standard for the language which would be acceptable both to PC and workstation C compilers. The steps followed by the program are summarised by the following Algorithm 5.3:

Algorithm 5.3 Implementation of Rigorous Evaporator Model

Step 1: *Set up thermodynamic property routines for refrigerant to be used*

Step 2: *Read specification set from user via keyboard*

Step 3: *Calculate necessary vapour fraction; report on the consistency of constraints by performing heat balance.*

Step 4: *If constraints are accepted by user, proceed, else return to step 2*

Step 5: *Set up initial conditions for the unknown variables by educated guesswork, backed up by physical constraints.*

Step 6: *Attempt to solve the non-linear equation set by Newton-Raphson iteration using an analytic Jacobian.*

Step 7: *Analyse the solution vector returned by the iteration for success; report results and print warnings if results are inplausible or unconverged.*

The nature of the equation set permitted easy derivation of all the residual functions with respect to the unknown variables, justifying the use of an analytic Newton-Raphson solution technique rather than a quasi-Newton method using periodic updates

to an approximate Jacobian matrix. The Newton-Raphson method requires solution of a set of simultaneous linear equations, and this was performed using the Crout algorithm for LU decomposition of a non-singular matrix (the N-R solver routine had a built-in check against singularity of the Jacobian which would break the iteration if necessary). It would have been possible to implement a more rapid solution algorithm for this step of the iteration, as the equation set was rather sparse; this was not done. The Crout algorithm had already been coded, debugged and tested by the author, and found to sufficiently rapid for his requirements. This would be another area of the code which could be made more elegant in future revisions. The version of the algorithm used was the one given in the all-purpose numerical text by Press *et al.* [89].

The thermodynamic properties of refrigerant were calculated using the specialised property correlations developed by Downing [24]. The subroutines used in this program were lifted wholesale from other work carried out by the author, described in Chapter 6.

The coding of the model was straightforward; the amount of arithmetic to be performed at each function evaluation was reduced by appropriate definition of auxiliary quantities (*e.g.* the latent heat λ was replaced by the *effective* latent heat $(1-\alpha)\lambda$ in the evaporative heat balance equations. The original source code contains comment statements explaining these steps. This source code was given the name **RIGEVAP** (for RIGorous EVAPorator): it was completely self-contained to ease portability of updated source files between the different machines on which it was compiled.

5.2.3 Results

The rigorous model, in the **RIGEVAP** incarnation, was used in the analysis of experimental datasets, garnered from the experimental work performed on the pilot plant. The output from the program has been quoted in Chapter 4, Section 4.3. The reader is referred to that Section for examples of the type of results produced by the model. In general, there seemed to be few problems with the convergence of the equation set to a realistic solution; the only problems would come if a dataset were entered which violated the heat balance in such a way as to cause nonsensical starting guesses for some of the variables to be computed. The program could be used as the basis for a more sophisticated model incorporating better description of pressure drop and heat transfer effects: it was however entirely satisfactory for the author's purposes.

5.3 Heat and Mass Balance of the Two-Fluid Heat Pump

5.3.1 Introduction

The solution of the heat and mass balances for the simplified process flowsheet described in Chapter 3 could be achieved without iteration on stream compositions; the hand-calculation operation sequence has already been described in Chapter 3. A computer program , **SIMTRY2**, was written in imp80 to automate this calculation procedure. The order of operations was essentially similar to that followed in the hand calculation, except that the CSD equation of state was used to predict the thermodynamic properties of the working fluid mixture at all points in the cycle. There were two main reasons for devotion of time to this after the plant design had been formalised: different pairs of fluids could be tested for a set of fixed process conditions with little effort; and the use of this equation of state would allow inclusion of better VLE predictions in the high-pressure sections of the plant.

The source code for this program has not been included in the thesis because of its length. A brief description is given here of the method used to construct the program. The main plant items in the flowsheet (*e.g.* partial condensers) were modelled by subroutines which calculated all output streams from given input streams. These unit subroutines were then joined together by a calling routine which managed the transfer of stream data between units. This structure is standard practice in most flowsheeting programs, such as ICI's FLOWPACK, and should need no further clarification here.

Although the calculation method did not require iteration to guess a stream composition, many subsidiary iterations had to be performed in the calculation of individual units. The solution of VLE (dew or bubble points) was performed rigorously at every asking; all stream mixings were performed as adiabatic mixings, and throttling calculations were performed using Ponton's method for the generalised non-adiabatic flash problem. These refinements to the hand calculation technique yielded a program whose execution time on the Edinburgh mainframe was considerable. A less hastily-coded program would have used forms of correlation functions to fit phase equilibrium data generated by the equation of state; this technique would remove much of the costly iteration with little or no effect on the final accuracy of solution.

A selection of output data is included: these data were generated by running the program with essentially similar fixed process parameters to those used in the manual design calculation. The working fluids used in the runs were: R114/R113 (used in the

actual pilot plant) and R12/R114 (should give a higher capacity).

5.3.2 Inputs and Outputs

The inputs to the program were:

- Working fluid components
- Composition range of working fluid passing through the compressor
- Dew temperature in each of the partial condensers
- Dew temperature in the evaporator
- Isentropic compression efficiency
- Ratio of product vapour to feed in each partial condenser

The output from the program consisted of a report of all real streams' temperature, pressure, composition, enthalpy, entropy and availability, followed by a list of the main energy fluxes for the cycle. If the program were run with a stepping range of specified working fluid compositions, then the output included a summary file which listed the COP, volumetric heating capacity, volumetric work requirement and exergetic efficiency of the cycle at each set condition. (These quantities are defined in Chapter 3.)

5.3.3 Results

5.3.3.1 Base-Case Inputs

A set of inputs corresponding to those used in the plant design was specified as the base case or reference. These were:

- **Composition range:** 0–1 mol fraction MVC.
- **Dew temperature in C–1:** 85 °C

- **Dew temperature in C–2:** 75 °C
- **Dew temperature in evaporator:** 20 °C
- **Isentropic compression efficiency:** 0.700
- **Vapour split in C–1:** 0.5
- **Vapour split in C–2:** 0.025

Two working fluid mixtures were examined: R114/R113, the chosen working pair for the plant, and R12/R114. It was anticipated that the former pair would exhibit a wider range in volumetric capacity and work requirement than the latter, as the difference in volatility between the components was greater for the former mixture. The latter pair should however exhibit a larger maximum capacity, since the more volatile (R12) of the second mixture was considerably more volatile than R114, the more volatile of the first mixture. The effect of composition on COP was unclear. It was hoped that the thermodynamic properties predicted by the equation of state would be sufficiently realistic to reveal the maxima in COP which had been found by other workers using nonazeotropic mixtures as working fluids (see Chapter 2). Any such variation could not be predicted *a priori*; the author's heat pump cycle was markedly different in specification and unit order from those examined by previous workers, which would have an effect on the cycle performance.

Coefficients of Performance The variation in COP with mol fraction of more volatile is shown in Figure 5.5 for both fluid mixtures. The plot for the R114/R113 mixture reveals a maximum in COP at about 0.15 mol fraction and a minimum at about 0.85 mol fraction. By contrast the plot for the R12/R114 mixture reveals no maximum but a minimum at 0.85 mol fraction.

Volumetric Capacities The volumetric capacity curves for each mixture are shown in Figure 5.6. Both pairs of fluids exhibit smoothly increasing capacity as a function of composition. It is evident that the R12/R114 mixture gives greater overall capacity than the R114/R113 mixture; the relative *change* in capacity however is greater for R114/R113 than for R12. In the case of R114/R113, the ratio of the capacity of pure R114 to that of pure R113 is 3.7; the equivalent figure for R12/R114 is 2.6, indicating a superior performance for R113/R114 in terms of capacity modulation potential.

Volumetric Work Requirement The volumetric work requirement (ratio of compression work to specific suction volume) is shown for both fluids in Figure 5.7. The patterns of curve correspond closely to those for the volumetric heating capacity.

5.4 Conclusions

The programs developed by the author and described in this chapter could be used to perform exhaustive explorations of evaporator performance heat pump cycle performance. A relatively smalll number of results have been presented here: these were chosen to illustrate the general features of the equipment which were revealed by the programs. The further usage and development of this modelling work was left for future users of the programs; the requirements of the experimental programme forbade more work on modelling.

Figure 5.2: Capacity of Cal-Gavin Evaporator

Refrigerant Exit Temperature

Figure 5.3: Cal-Gavin Evaporator Refrigerant Exit Temperature

Figure 5.4: Cal-Gavin Evaporator Water Exit Temperature

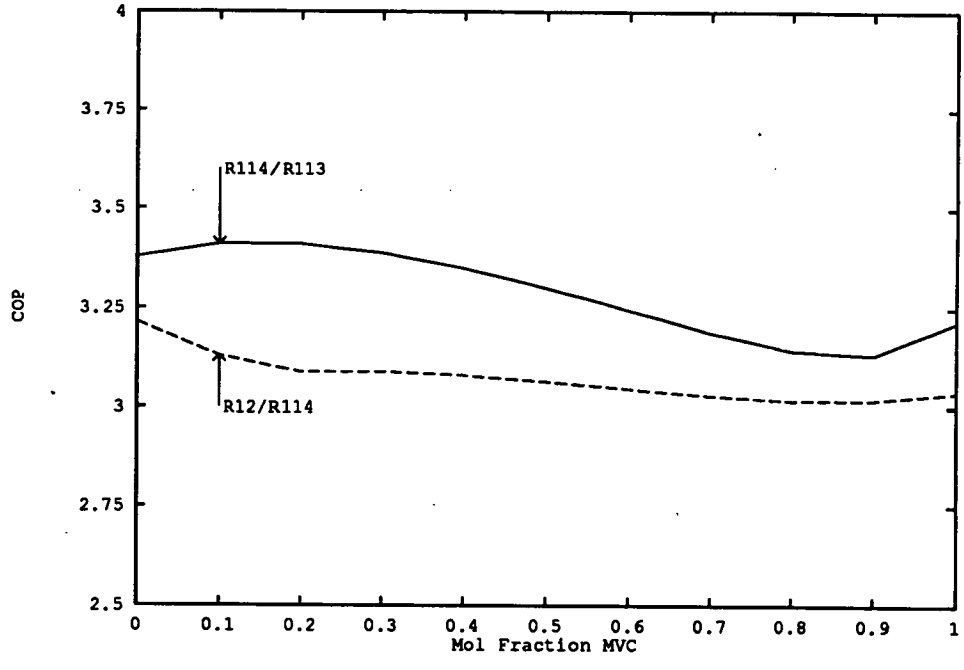

Figure 5.5: Base Case: Variation of COP with Composition

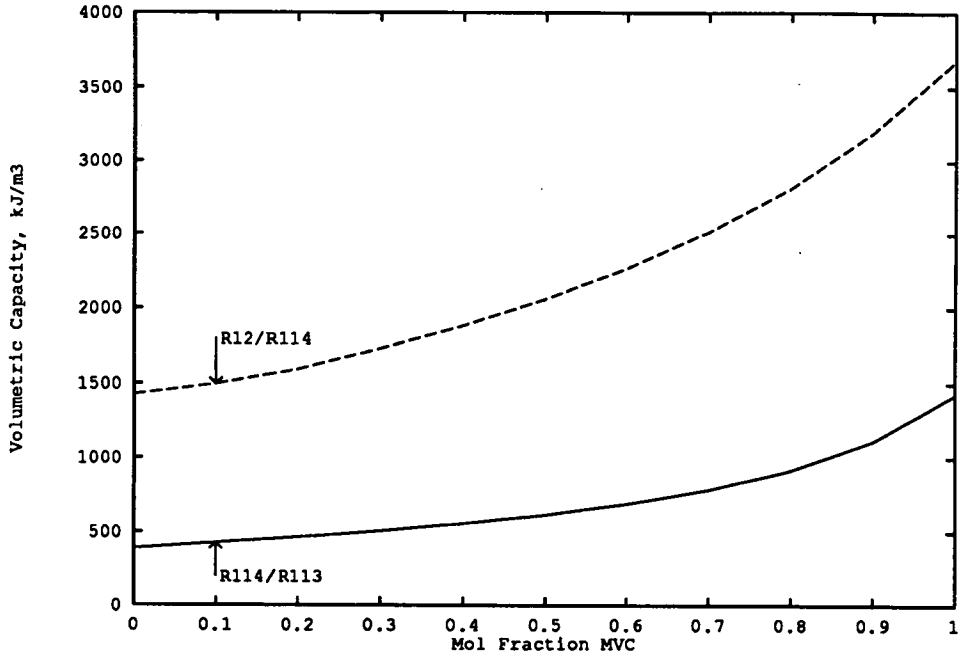

Figure 5.6: Base Case: Variation of Volumetric Capacity

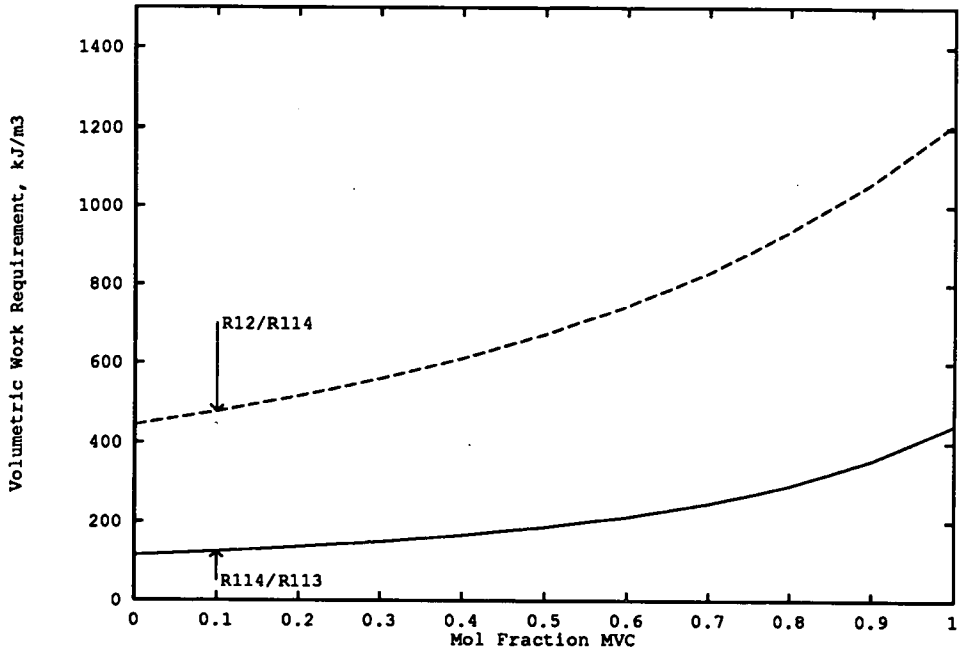

Figure 5.7: Base Case: Variation of Work Requirement

Chapter 6

Thermodynamics of CFC Mixtures

6.1 Introduction

The calculation of the thermodynamic properties of the working fluid is essential in the analysis of any heat pump cycle. There exists a variety of methods of property calculation and representation; the best of these must always be those which represent direct correlations of data obtained from experimental work. In the case of pure fluids the construction of such relations is surprisingly straightforward; many important thermodynamic properties may be correlated to a high degree of accuracy with simple algebraic functions of temperature, pressure and/or density. These relations generally hold for nearly all parts of the liquid-vapour phase diagram, except in the vicinity of the critical point, where it is known that no analytic function may truly represent the behaviour of the fluid. Should the reader be unconvinced, recall that

the constant-pressure heat capacity C_p of a fluid is infinite at the critical point. This quantity represents the rate of change of enthalpy, therefore this implies a discontinuity in the enthalpy function.

It is often the case, however, that inadequate or incomplete data exist for the fluid of interest. In this case recourse must be made to predictive or interpolative techniques to fill in the unknown portions of the fluid's behaviour. Much work has been done in this field, notably using the *Principle of Corresponding States*, which in essence demands that all substances behave in much the same way at the same unique reduced state. A reduced state is defined by expression of the appropriate number of defining state functions as dimensionless ratios of their values at the given state to their values at the critical point. One might therefore expect any generalised correlations to make use of one or more of the critical properties as a required input. In practice the critical temperature and critical pressure are used; the critical volume is most difficult to measure to high accuracy and so is not often used for property correlation.

It has been found that really general property correlations require additional data in addition to the critical point; a very common property which is used is the Pitzer acentric factor, conventionally denoted by ω. This is defined by the relation:

$$\omega = -\log_{10} P_R^* - 1.000 \tag{6.1}$$

where P_R^* is the reduced vapour pressure at a reduced temperature $T_R = 0.7$. The acentric factor is related to the *sphericity* of a molecule and is zero for noble gases such as argon, whose molecules are essentially spherical. The greater the deviation from the spherical shape, the greater the acentric factor.

The acentric factor is commonly taken with the critical temperature and pressure to form a set of required specifications on which other properties are correlated, and this has been found to be adequate for many purposes. Specific instances of such correlations are discussed later in the chapter.

In the case of mixture property calculation, the effort required to obtain a comprehensive map of the mixture's behaviour may be prohibitive, as a result of the additional degrees of freedom which the independent mol fractions represent. Therefore much effort

has been put into the accurate prediction of properties of a mixture from the known properties of its components (which may be very well known and correlated). This task is made difficult by the effects of interaction between unlike molecules; the mere proximity of unlike molecules may also affect the interactions between like molecules. Nonetheless there exist techniques of mixture property prediction which overcome these problems to a greater or lesser extent; these will be touched upon below.

The subject of this chapter is the derivation of the thermodynamic properties of CFC refrigerant fluids and their mixtures. The work described here was carried out in order to obtain thermodynamic properties of some fluids proposed as the next generation of "ozone-friendly" CFC replacement refrigerants. At the commencement of this work, little or no data were available beyond the critical properties and acentric factor for these fluids (sometimes not even these few data were to hand!), yet it was desired to obtain sufficient information to perform evaluation of heat pump cycle performance using these fluids. This need for data led to an investigation by the author of the available techniques, including those which had been used for prediction of CFC properties in the past. A review of the literature pertinent to this subject is contained in Chapter 2: this has been separated from this chapter to allow a clear view of the forest of results, unencumbered by the spreading oaks of detail.

The core of the work decribed here was the use of a generalised cubic equation of state, the *Cubic Chain-Of-Rotators* (CCOR) equation, to obtain the thermodynamic properties of CFC fluids and their binary mixtures. The reasons for the choice of this equation will be made clear in the subsequent text; it is one of several equations to use the critical temperature, pressure and acentric factor as the required inputs. It was first presented in 1982 by Lin *et al.* [55]

The properties of pure fluids predicted by this equation are compared with the predictions of more accurate but more complex equations, and the deviations in properties exhibited by several fluids are compared in terms of reduced properties. It will be shown that the errors in predicted volumetric properties follow similar patterns when taken in dimensionless form for this family of fluids. The effect of optimisation of the equation's fluid-specific parameters on these errors is also demonstrated.

The extension of the CCOR equation to the prediction of mixture properties is analysed by comparison with experimental measurements of vapour-liquid equilibrium (VLE) states for several binary mixtures of CFC fluids; some are azeotropic, others non-azeotropic in nature.

A parallel thread of work was the implementation of other methods of thermodynamic property prediction, both as a means of generating reference data and as a source of information to be used in the experimental portion of the work. Another, more complex, equation of state was used to generate data on properties of mixtures; this was the *Carnahan-Starling-DeSantis* (CSD) equation, which has been used with great success by other workers [72] to calculate data on CFC mixtures. In addition, a set of correlation functions developed by Downing were coded to provide high-accuracy data on certain pure CFC fluids (notably R114, which was used in the experimental programme). These equations are described below; they provided another useful method for generation of data for quantitative data analysis.

6.2 Current Prediction Techniques

6.2.1 Pure Fluids

Good property correlations already exist for those pure fluids which have traditionally been used in heat pumping applications. This is only natural, as the CFC refrigerants have been used since the 1920's and represent a key component of a major global technology. The properties of interest to the designer—density and enthalpy of saturated liquid; latent heat and vapour pressure as temperature functions, and vapour phase properties—have been supplied by manufacturers in tabular form for many years. (See, for example, the literature supplied by Imperial Chemical Industries plc [38].) The tables of these properties commonly to be found in the literature have normally been generated using equations fitted to experimental datasets. The benefit of fitting such relations is that it smooths out datasets and averages away experimental scatter on datasets. Downing [24] presented typical relations in equation form in 1974: his paper is widely cited in the literature, indicating the wide use of his correlations. These take the following form:

1. A 6-term polynomial correlation of liquid density with (reduced) temperature.
2. An extended, 6-term Antoine-type correlation of vapour pressure with temperature.

3. A 15-term version of the Martin-Hou equation of state to describe the vapour phase volumetric behaviour and hence its energetic properties.

4. A 5-term perfect gas heat capacity correlation.

5. Derived formulae for the enthalpy, entropy and real gas heat capacity of the vapour, using the constants for the equation of state and perfect-gas heat capacity correlations.

6. A derived formula, using Clapeyron's Law in conjunction with the vapour pressure correlation, which yields the latent heat of vapourisation from the temperature and phase volumes.

Manufacturers of refrigerants now often supply this information both as tables and as correlations similar to those used by Downing. This will also be the case in the future for CFC replacement refrigerants.

6.2.2 Mixtures

The calculation of properties of CFC refrigerant mixtures is more complex than the equivalent pure-fluid task, as a result of the extra degree(s) of freedom possessed by a binary (or more complex) mixture. The simplest approach taken has been to assume that mixtures may be treated as ideal mixtures, for which Raoult's Law describes the vapour-liquid equilibrium. In this case the properties of the liquid phase may be obtained as molar averages of the equivalent pure component properties under the same temperature and pressure; the vapour phase properties may be obtained by use of the accepted (Martin-Hou) equation, using simple mixing rules to obtain constants for the mixture. This approach may give reasonable results for some mixtures but it may fail for azeotropic mixtures. It may also give predictions which are not thermodynamically consistent, when for example liquid phase properties are desired at a temperature above the critical temperature of one component.

A method of property calculation which is internally consistent and may be applied to both liquid and vapour phases is required. One such method is to use an equation of state which is applicable to both phases, in contrast to the Martin-Hou equation, which only describes vapour behaviour. There exist many equations which have been used

as predictors or correlators of thermodynamic data by both academic and industrial workers. These range from the highly accurate, multi-parameter equations of *e.g.* Bender, through well-known equations based on the Benedict-Webb-Rubin (BWR) equation, to the cubic equations, which are the simplest class of equations capable of these duties. Nearly all equations of state which are practically useful take the form:

$$Z = \left(\frac{Pv}{RT}\right) = 1 + \Delta Z(v, T, \underline{x}) \tag{6.2}$$

where $\underline{x}$ represents the composition vector of the fluid. The nature of process problems means that temperature and pressure are the normal independent variables, implying a need to invert the equation of state to find the molar volume before proceeding further in property calculation. This is one of the reasons for the popularity of cubic equations, for which there exists an algebraic solution technique. In order to represent both phases, of course, a cubic represents the simplest function having three real roots which may be fitted to the general isotherm curve of a fluid in a pressure-volume plot.

The other commonly-used technique is to use activity coefficient models to describe the liquid phase behaviour; the vapour phase properties may then be found by any desired method for which sufficient data are available. The activity coefficients may be derived directly from experimental data, or predicted using methods such as UNIQUAC, the well-known group-contribution route to activity coefficients. This method can be highly accurate but it does not guarantee consistency between the properties of the phases.

The work done on predicting properties of refrigerant mixtures in recent years is more fully documented in Chapter 2; all of the methods outlined in the preceding paragraphs have been used, with varying success. Inspection of the recent literature reveals that most recent efforts have used the equation of state approach, and this is the method which will be discussed at length in this Chapter.

6.2.3 Drawbacks of Equations of State

Before proceeding to describe the work performed by the author using equations of state, it is apposite to inform the reader of the drawbacks associated with this method. These limitations helped to guide the author in taking some decisions regarding choice of equation, implementation, *etc.*, so should be borne in mind in reading future paragraphs.

6.2.3.1 The Accuracy-Convenience Tradeoff

The multi-term equations are useful if sufficient good thermodynamic data are available to permit determination of the parameters by regression analysis. If these data are *not* however available, then the use of these equations is precluded. Another drawback of such equations may be the complexity of ensuing calculations: this can lead to a significant requirement of computing power. While this may seem to be irrelevant given the pace of workstation and microcomputer development, in practice it is still important; for example most of the time required by process simulators is used in calculation of physical properties. In this regard the use of the large equations, such as Bender's equation, will be extremely expensive and may not be justified if the final results are being fed into another, "top-level", calculation. There must therefore be some element of tradeoff in the selection of an equation of state to perform a given task; the benefits of high-accuracy data must be assigned some notional cost for comparison against the costs of obtaining these data and implementing the complex equation of state. Typical uses of such large equations are in detailed design of large-scale processes operating on well-known fluids. Examples are: simple hydrocarbon mixtures, or cryogenic fluid systems. In such cases the scale of operation may be so great that a small increase in the accuracy of available design data may pay dividends in capital and/or operating costs of the final equipment. By contrast, for initial design of a process the nitty-gritty is not so important as the ability to explore many alternative options in a short space of time, so a faster technique may be more desirable than an accurate one.

6.2.3.2 Extension to Mixtures

The properties of a pure fluid are relatively straightforward to predict, as there is only one type of intermolecular interaction in each phase which may affect the behaviour of the substance. For most purposes the behaviour of interacting molecules may be assumed to be dependent mainly on the temperature of the system (and hence their average kinetic energy). Except in the region of the critical point, experience has shown that the effect of temperature may be quantified by smooth, analytic functions—temperature dependent parameters incorporated into equations of state. The situation is not quite so simple for mixtures: the parameters of the equation of state are no longer functions of temperature only, but also of composition. This functional behaviour must be crystallised into a set of recipes for the production of parameters for any given specified temperature and composition. Such recipes are termed *mixing rules.*

The problem in derivation of mixing rules is simple: they must predict the effect of composition on interactions between like and unlike molecules from only information on interaction between like molecules. In fact, the situation is worse yet, since even interactions between like molecules may be affected by the proximity of other, unlike molecules! The perfect mixing rule has not yet been derived, although many people have tussled with the problem for years. The author used only one mixing rule, the van der Waals rule, which is:

$$M_m = \sum_{i=1}^{N} \sum_{j=1}^{N} x_i x_j M_{ij} \tag{6.3}$$

where M_m represents a mixture parameter; M_{ii} is the equivalent parameter for component i, and M_{ij} $(i \neq j)$ is the so-called *cross constant.* The cross constant represents the effect of interaction between species i and species j, and is found from the parameters M_{ii} and M_{jj} by combining them in an arbitrary numerical recipe which may also include *another* parameter, the *interaction constant.*

There have been attempts to predict these interaction constants on an *ad hoc* basis, using characteristic properties of each molecular species (see *e.g.* Pesuit [83]) but the only sure way to obtain a meaningful interaction constant for a given mixture is by regression on a set of experimental equilibrium data to find an optimal interaction constant. This is a *post hoc* analysis and is limited in its utility for the following

reasons:

- The objective function to be minimised must be carefully selected and documented: normally it is the Gibbs energy of the system, or a sum of residual differences in fugacity between components in different phases. However it is possible to conceive of other criteria which could be used in constructing the objective function, and these might affect the final result.
- The value of interaction constant yielded by the optimization may be dependent on the mixing rules used. This may restrict applicability of interaction constants cited in the literature.
- The interaction constant may be invariant, or it may be a function of temperature. If the latter is true, then there are obvious problems of extrapolation beyond the range of temperatures for which experimental data are available.

6.2.3.3 Computational Overhead

The final major problem discussed here is that of the computational overhead involved in use of an equation of state to calculate thermodynamic properties. This has been touched upon in previous paragraphs and is expanded here to avoid obfuscation in later discussion of the author's implementation of various equations.

A typical example of increasing overhead is supplied by the calculation of an equilibrium vapour pressure for a binary mixture. For a pure fluid, vapour pressure may be well correlated by an analytic function of temperature, using only a few fluid-specific parameters. One of the more complex relations in common use may be represented by:

$$\ln P_i^* = A + \frac{B}{T+C} + DT + E \ln T \tag{6.4}$$

where P^* is the vapour pressure and T is the absolute temperature. The use of this equation requires four additions, three multiplications and two logarithmic operations (taking logs requires much the same time as raising to powers). If Raoult's Law is then used to find an approximate bubblepoint, the result is:

$$P_{bub} = \sum_{i=1} N x_i P_i^* = P_2^* + x_1 (P_1^* - P_2^*) \tag{6.5}$$

so the total overhead is: eight additions, six multiplications and four logarithm operations to find the vapour pressures, then two additions and a multiplication to find the bubble pressure.

If an equation of state is used to find the pure component vapour pressures, the overhead increases significantly. An initial guess at pressure must be made, then an iteration must be performed to solve the equation:

$$\mu_{vap} - \mu_{liq} = 0 \tag{6.6}$$

where μ is the chemical potential of the species in either liquid or vapour phase. One of the best ways of performing this iteration is to use the Newton-Raphson scheme with analytic derivative to solve the equivalent equation:

$$\log \phi_{vap} - \log \phi_{liq} = 0 \tag{6.7}$$

in which ϕ represents the fugacity coefficient of the substance. It may be shown that the Newton-Raphson algorithm gives the following formula for update of an approximation to the vapour pressure satisfying the fugacity equality Equation 6.7. The quantity $\ln \phi$ is defined by Equation 6.24 in terms of the compression factor Z. Substitution of Equation 6.24 into Equation 6.72 yields:

$$f(P) = \ln (\phi_v / \phi_l) = \int_0^P \left(\frac{Z_v - Z_l}{P} \right) dP \tag{6.8}$$

from which the derivative of the iteration function $f(P)$ with respect to pressure is simply given by:

$$f'(P) = \left(\frac{Z_v - Z_l}{P}\right) \tag{6.9}$$

The Newton-Raphson algorithm using analytic derivative to solve $f(x) = 0$ is:

$$x_{new} = x_{old} - \frac{f(x_{old})}{f'(x_{old})} \tag{6.10}$$

and substituting the expressions above for $f(P)$ and $f'(P)$ gives the update on the initial guess of pressure in recursive form as:

$$P^*_{new} = P^*_{old} \times \left[\frac{(Z_{vap} - Z_{liq}) - \ln(\phi_{vap}/\phi_{liq})}{(Z_{vap} - Z_{liq})}\right] \tag{6.11}$$

This update requires only two additions, three multiplications and one logarithm; hidden in the equation, however, are the calculation of equation of state parameters and the inverson of the equation to find vapour and liquid volumes from set temperature and pressure. As most calculations converge to an acceptable accuracy in not less than two iterations (including the initial guess), it is plain that the update alone is almost as costly as the most complex of straightforward vapour pressure correlations. The use of an equation of state to find vapour pressures for use in Raoult's Law does not therefore normally make good sense if there is an alternative correlation available.

A more accurate method of obtaining the bubble pressure is to solve the simultaneous equation set relating the component fugacities in both liquid and vapour phases:

$$\phi^1_{vap} y - \phi^1_{liq} x = 0 \tag{6.12}$$

$$\phi^2_{vap}(1-y) - \phi^2_{liq}(1-x) = 0 \tag{6.13}$$

This problem is in fact normally specified as: given temperature and mol fraction in one phase, find the pressure; the mol fraction in the other phase, and the liquid and

vapour phase volumes. There are therfore four unknowns, implying solution of a set of four non-linear equations. If this is attempted then the computational overhead becomes many times that of the simpler problem represented by Equation 6.7. Use of the Newton-Raphson algorithm requires the costly derivation of the Jacobian matrix of partial derivatives, followed by inversion of a set of four simultaneous linear equations, to perform the update step. Before this may be done, the equations of state parameters for each phase must be found; the equation of state must be inverted for each phase, and fugacity coefficients for each component in each phase must be calculated. This last step in particular is far more costly than the equivalent step in the pure-fluid calculation, as a result of the nature of the defining equations for mixture fugacity coefficients. In fact, many published algorithms for solution of the multicomponent VLE problem use so-called *quasi-Newton* methods, which employ local approximations to the Jacobian matrix, updated only when necessary to improve accuracy. Although these save significant amounts of computation, especially if an LU decomposition technique is used to decompose the Jacobian, the final overhead is still (relatively) large.

6.2.4 The Silver Lining

The analysis of the drawbacks to use of equations of state may have led the reader to conclude that this method of property prediction is not worth the effort. There are very good reasons for persevering, though; one of the most important is the absolute consistency of the predictions between phases. There will be errors in the final results but these might not be significant for most applications. Furthermore the technique is extendible to mixtures of many components with the only consequence that computational overhead increases. The problem of computational overhead should also be regarded in the context of the rapid pace of development of computing hardware; today's desktop presonal computers are certainly capable of execution of thermodynamics programs using equations of state in reasonable timescales. The awesome power of engineering workstations is furthermore available at ever-falling prices, although the substitution of brute power for elegant programming and cunning solution algorithms is not necessarily a wise action. A final comment on the reduction of overhead: because the results generated by equations of state are generally smooth functions, they may be fitted to the conventional correlations, such as Equation 6.4 for vapour pressure. Thus the complex iterative calculations associated with phase equilibrium problems may be replaced by polynomials or similar functions; these may be used in conjunction with other results, such as enthalpy or entropy prediction, which may be calculated directly

from the equation of state. This would preserve consistency but accelerate computation and is thus suited to incorporation in *e.g.* flowsheeting programs.

6.3 Fundamentals

A brief summary is given here of the exact thermodynamic results which may be used to obtain any desired thermodynamic property from a closed-form, pressure-explicit equation of state. The reader is referred to a standard thermoydynamics text for more detailed exposition of these results. (See, for example, Bett, Rowlinson and Savile [9].) In the following discussion, the fluid will be treated as having constant composition until the derivation of those results dealing explicitly with properties of mixture components. The same expressions for *e.g.* enthalpy departure function are valid both for pure fluids and for mixtures of constant composition. It should be borne in mind that, unless stated otherwise, the properties referred to are regarded as *intensive* properties: for example, *specific* volume, *specific* enthalpy. These properties are obtained on a molar basis by convention (*e.g.* enthalpy has units of kJ/kmol).

Equation of State: Useful Mathematical Properties Recall from Equation 6.2 that the equation of state is explicit in pressure as a function of temperature, specific volume (or equivalently, density) and composition. All of the equations used in this work are analytic functions which are smooth and continuously differentiable. The partial derivatives of pressure with respect to temperature, volume and each independent mol fraction are therefore meaningful quantities. This is of key importance. Of course, this means that the equations can only be approximations to the real fluid behaviour, as there are discontinuities in isotherms at phase-change points, for example. In practice a pure-fluid isotherm which passes through the two-phase region is approximated by a curve with an even number of turning points between the liquid and vapour roots.

Definitions of Perfection To avoid confusion, the definitions of perfect gases and ideal mixtures are laid out here in advance. Molar quantities are written in lower-case, total quantities in upper-case.

A *perfect gas* of invariant composition is taken to be a fluid satisfying the equation of state:

$$P = \frac{nRT}{V} = \frac{RT}{v} \tag{6.14}$$

where V represents the total volume occupied by n mol of gas and v is the specific molar volume.

The molar Gibbs energy of a perfect gas is given by the relation:

$$g^\circ = \Psi(T) + RT\ln(P/P^\theta) \tag{6.15}$$

The measure of free energy normally used by engineers is the fugacity f, defined by the relation:

$$g = \Psi(T) + RT\ln(f/f^\theta) \tag{6.16}$$

The fugacity has the units of pressure and approaches the value of pressure in the limit of zero density, *i.e.* perfect gas behaviour. In the defining relations Equation 6.15 and Equation 6.16 the quantities superscripted with θ represent standard-state quantities, normally taken as unity. A useful quantity is the *fugacity coefficient* ϕ, defined as the ratio of fugacity to pressure. This goes to unity in the limit of zero pressure.

The *chemical potential* of a component i in a mixture is defined by the relation:

$$\mu_i = \left(\frac{\partial G}{\partial n_i}\right)_{T,P,n_j} \tag{6.17}$$

where G denotes the total Gibbs energy and n_i is the number of moles of component i present. The total Gibbs energy of a mixture is then given by:

$$G_{mix} = \sum_i n_i \mu_i \tag{6.18}$$

The chemical potential of component i in a perfect gas mixture is given by:

$$\mu_i = \Psi_i(T) + RT \ln (P y_i) \tag{6.19}$$

where y_i denotes the mol fraction of component i, and Ψ_i is a function of temperature only (cf. Equation 6.15).

An *ideal mixture* is defined to be one whose conponents have chemical potentials satisfying the relation:

$$\mu_i = \mu_i^\circ + RT \ln y_i \tag{6.20}$$

where μ_i° denots the chemical potential of pure i under the same conditions as the mixture. NB: it is possible to have an ideal mixture of imperfect gases!

Finally, a reminder that system has a unique thermodynamic state characterised by the number of degrees of freedom available to the system. The degrees of freedom are given by Gibbs' Phase Rule:

$$(DOF) = \text{Components} - \text{Phases} + 2 \tag{6.21}$$

The state of the system is fixed by specifying the values of as many state functions as there are degrees of freedom. A state function is independent of the quantity of material *i.e.* intensive, and has the property that the change in that function's value between two fixed states is independent of the pathway between the two states.

Use of Departure Functions The most convenient approach to calculation of thermodynamic properties from an equation of state uses the concept of the departure function (or deviation function). A departure function measures the difference between the value of some thermodynamic state function of a real fluid and the value of that function of a perfect gas under the same conditions. The departure functions behave in exactly the same way as any normal state function; the same functional relationships hold between departure functions as do between the functions themselves. The especial utility of these functions is that they permit relation of quantities such as enthalpy and entropy to arbitrary reference states without need for specification of absolute zeros.

The notation used here for a departure function is Δ, for example Δh as the enthalpy departure function. Another frequently used notation is $(h - h^\circ)$. Some texts present departure functions as the difference between the perfect-gas quantity and the real quantity, that is, as the negative of the functions used in this work.

Compression Factor The compression factor deviation takes the simple form $\Delta Z = Z - 1$. It is a useful quantity in the derivation of the other departure functions; it follows directly from the equation of state when written in the form of Equation 6.2.

Gibbs Energy Departure: Fugacity Coefficient Examination of Equations 6.15 and Equation 6.16 yields the fugacity coefficient, equivalent to the dimensionless molar Gibbs energy departure:

$$\Delta g = g - g^\circ = RT \ln(f/P) = RT \ln \phi \tag{6.22}$$

This may be derived from the compression factor deviation by use of the Maxwell relation:

$$\left(\frac{\partial g}{\partial P}\right)_T = v \tag{6.23}$$

By manipulation of Equations 6.15, 6.16 and using Equation 6.23, it may be shown

that the fugacity coefficient is related to the compression factor departure by:

$$\begin{aligned} \ln\phi &= \int_0^P \left(\frac{Z-1}{P}\right) dP \\ &= \int_1^Z \left(\frac{Z-1}{Z}\right) dZ - \int_\infty^V \left(\frac{Z-1}{V}\right) dV \\ &= (Z-1) - \ln Z - \int_\infty^V \left(\frac{Z-1}{V}\right) dV \end{aligned} \tag{6.24}$$

Internal Energy Departure The variation of internal energy with volume is given by the relation:

$$\left(\frac{\partial U}{\partial V}\right)_T = T\left(\frac{\partial P}{\partial T}\right)_V - P \tag{6.25}$$

As the internal energy of a perfect gas is a function of temperature only, the internal energy departure function follows directly:

$$\begin{aligned} \Delta U &= \int_\infty^V \left[T\left(\frac{\partial P}{\partial T}\right)_V - P\right] dV \\ &= RT^2 \int_\infty^V \left(\frac{\partial (Z-1)}{\partial T}\right)_V dV \end{aligned} \tag{6.26}$$

Enthalpy Departure The enthalpy departure function is simply obtained from Equation 6.26 by:

$$\Delta H = \Delta U + RT(Z-1) \tag{6.27}$$

Entropy Departure The entropy departure function is given by the relation:

$$\Delta S = R\int_{\infty}^{V}\left[\frac{(Z-1)}{V} + \frac{T}{V}\left(\frac{\partial(Z-1)}{\partial T}\right)_V\right] dV \tag{6.28}$$

Mixture Fugacity Coefficient The mixture fugacity coefficient ϕ_i of component i is related to the chemical potential of the component, in the same way that the fugacity coefficient of a pure fluid is related to the molar Gibbs energy. The fugacity coefficient may be expressed as:

$$\begin{aligned}\phi_i &= \ln\left(\frac{f_i}{Py_i}\right) \\ &= -\frac{1}{RT}\int_{\infty}^{V}\left[\left(\frac{\partial P}{\partial n_i}\right)_{T,V,n_j} - \frac{RT}{V}\right] dV - \ln Z\end{aligned} \tag{6.29}$$

Enthalpy Formulae The enthalpy of a pure fluid at an arbitrary state $h(T, P(v))$ is related to the enthalpy at a reference state $h^*(T^*, P^*(v^*))$ by use of the enthalpy departure function $\Delta h(P,T)$ and the perfect gas heat capacity C_p°. The relevant formula is:

$$h(P(v),T) = h^* + \Delta h(P(v),T) + \int_{T^*}^{T} C_p^\circ\, dT - \Delta h(P^*(v^*),T^*) \tag{6.30}$$

where the implicit dependence of pressure on specific volume is indicated by denoting pressure as $P(v)$.

The extension of Equation 6.30 to mixtures is straightforward. The mixture enthalpy is denoted by h_m; the enthalpy of a pure component i is denoted by h_i. The enthalpy of a mixture of N components with specific volume v_m at temperature T and pressure P is then given by:

$$h_m(v_m,T,\underline{y}) = \sum_{i=1}^{N} y_i h_i^* + \Delta h_m(P(v_m),T) + \sum_{i=1}^{N} y_i\left[\int_{T_i^*}^{T} C_{p_i}^\circ\, dT - \Delta h_i(P_i^*(v_i^*),T_i^*)\right] \tag{6.31}$$

In Equation 6.31, the component reference enthalpies may be taken at different reference temperatures and pressures. The reference states for each component may then be chosen at will, and the enthalpies at the reference states assigned arbitrary values. The enthalpy of mixing (Δh_{mixing}) of a mixture may be computed by manipulation of Equations 6.30 and 6.31:

$$\Delta h_{mixing} = \Delta h_m(v_m, T) - \sum_{i=1}^{N} y_i \Delta h_i(v_m, T) \tag{6.32}$$

There are two common conventions used in work with refrigerants: the first assumes the enthalpy of a pure saturated liquid at -40 °C is zero; the second assigns an enthalpy of 100 kJ/kg to saturated liquid refrigerant at 0 °C. Throughout the author's work the former convention was used.

Entropy Formulae The entropy of a pure fluid with specific volume v and at temperature T, relative to a reference state (v^*, T^*) is given by Equation 6.33:

$$s(v,T) = s^*(v^*,T^*) + \Delta s(v,T) + \int_{T^*}^{T} \left[\frac{C_v^\circ}{T}\right] dT + R\ln\left(\frac{v}{v^*}\right) - \Delta s(v^*,T^*) \tag{6.33}$$

The extension of Equation 6.33 to mixtures is rather more complex than the corresponding enthalpy formula, Equation 6.31, as the entropy of mixing of an ideal mixture must be included in the formula:

$$\begin{aligned} s_m(v_m, T_m, \underline{y}) &= \sum_{i=1}^{N} y_i \left[\int_{T_i^*}^{T} \left[\frac{C_{v_i}^\circ}{T}\right] dT - \Delta s_i(v_i^*, T_i^*)\right] \\ &+ R\sum_{i=1}^{N} y_i \ln\left(\frac{v_m}{v_i^*}\right) - R\sum_{i=1}^{N} y_i \ln y_i + \sum_{i=1}^{N} y_i s_i^* \end{aligned} \tag{6.34}$$

The entropy of mixing may be found from Equations 6.33 and 6.34 in exactly the same way as the enthalpy of mixing.

The convention for reference used by the author was that the entropy of a pure saturated liquid was zero at -40 °C; the other common convention assigns an entropy of 1 kJ/kg K to pure, saturated liquid at 0 °C.

6.4 Property Prediction Using the CCOR Equation

6.4.1 Why The CCOR Equation?

The aim of the work was to obtain thermodynamic data for CFC fluids from the minimum of data, using an equation of state. Many equations of state have been used in the chemical industries for property prediction; however most require prior knowledge of at least some phase equilibrium data, in order to fit fluid-specific parameters. A survey was carried out to identify several equations which could use only well-known constant properties of fluids— the critical properties and acentric factor— to produce thermoydynamic data for both liquid and vapour phases. The simplest equations capable of such a task would be cubic in form, but other, more complex, equations were also considered.

Out of the many candidates the following were identified: all require knowledge of the critical temperature, critical pressure and acentric factor.

1. **Lee-Kesler (LK):** This is a generalisation of the complex, empirical Benedict-Webb-Rubin equation of state.
2. **Carnahan-Starling-DeSantis (CSD):** This equation, a fifth-order polynomial in volume, has been used with succes to calculate properties of CFC mixtures.
3. **Soave-Redlich-Kwong (SRK):** This is one of the best-known cubic equations of state, used frequently for hydrocarbon mixtures.
4. **Peng-Robinson (PR):** Another cubic equation, developed for VLE calculations.

5. **Cubic Chain-Of-Rotators (CCOR):** A cubic approximation to a more complex, theoretically derived equation, the *Chain-Of-Rotators* equation.

The Lee-Kesler equation was initially considered, on the grounds of the high accuracy claimed by the published literature. It was finally rejected because of its complex nature; a problem with this equation is the existence of multiple spurious volume roots which can foul up the solution in subtle ways. The CSD equation was implemented in order to provide reference data for mixtures of the well-known CFC fluids; it could not be used for prediction of data for new fluids, as it requires determination of six fluid-specific constants for use. It is described in more detail in Section 6.5.1.

The other candidates were all cubic equations; all seemed to give good prediction of vapour pressure and mixture VLE. The cubic form was more attractive from the computational viewpoint than any more complex equation, as it could be inverted using a direct algebraic formula. The final decision was made in favour of the CCOR equation because the literature indicated significantly better prediction of liquid phase properties than either the PR or SRK equations. There seemed little advantage in slavishly copying work by other workers on use of the PR and SRK equations if the CCOR equation gave equally good results: much of the tedious programming load would be present irrespective of the final equation chōsen.

6.4.2 Prediction of Minimum Data Requirements

The CCOR equation, as described in the papers by Lin [55], Guo [29, 30] and Leet [54], requires a knowledge of the critical temperature, critical pressure and acentric factor. In order to obtain a complete set of thermodynamic data, it would also be necessary to obtain a function describing the variation of the perfect-gas heat capacity with temperature. This quantity is normally represented by a quadratic or cubic polynomial in temperature: for many fluids the polynomial coefficients have been tabulated in *e.g.* Sinnott [106]. At the time this work was started, not all the above data were available for some of the compounds of interest; the only information on some fluids was the normal boiling point and structural formula. Some way had therfore to be found of estimating the missing data from this bare minimum of knowledge.

The following paragraphs describe the methods used to obtain necessary data for novel CFC replacements; the results of the methods were analysed by using them to obtain the properties of well-known CFC fluids. Most of the methods are *group contribution* schemes: the structure of the molecule is split into smaller building blocks, which are assumed to make discrete contributions to the final result. The contributions from each group present in the molecule are obtained from a table of universal contributions and summed to yield the final result.

6.4.2.1 Critical Properties and Acentric Factor

The methods used in the original work were taken from Section 3 of Perry [82]. After this work was performed, Shigaki *et al.* [105] published their work on CFC critical property prediction; this is noted but the formulae given by Shigaki were not used.

Critical Temperature The critical temperature was estimated using Lydersen's correlation between the boiling point and critical point:

$$T_c = \frac{T_b}{0.567 + \sum \Delta_T - (\sum \Delta_T)^2} \tag{6.35}$$

where the sum of group contributions is denoted by $\sum \Delta_T$. In this correlation the critical temperature must be in the same units of absolute temperature, that is, in either Kelvin or degrees Rankine.

Critical Pressure The rule used for critical pressure was again due to Lydersen, and may be expressed as:

$$P_c = \frac{MW}{(0.34 + \sum \Delta_P)^2} \tag{6.36}$$

where MW is the molecular weight and the critical pressure P_c is calculated in atmospheres.

Critical Volume The critical volume was estimated in two ways: a rule suggested by Lydersen, and a more complex rule due to Vetere. The errors associated with the latter method are listed under the heading v_c^* in Table 6.1.

Lydersen's expression for critical volume is:

$$V_c = 40 + \sum \Delta_V \tag{6.37}$$

with the volume V_c in cm^3/mol. Vetere's rule is:

$$V_c = 33.04 + \left(\sum_i M_i \times \Delta V_i \right)^{1.029} \tag{6.38}$$

where again the volume is in cm^3/mol and the quantity M_i is the molecular weight of contributing group i.

Acentric Factor The best correlation available for acentric factor was that due to Lee and Kesler, as quoted in Perry. This relates the acentric factor ω to the critical pressure and the reduced boiling temperature:

$$\omega = \frac{-\ln P_c - 5.92714 + 6.09648\theta^{-1} + 1.28862 \ln \theta - 0.169347\theta^6}{15.2518 - 15.6875\theta^{-1} - 13.4721 \ln \theta + 0.43577\theta^6} \tag{6.39}$$

where the critical pressure is in atmospheres and θ is the ratio of the normal boiling temperature to the critical temperature.

The methods described above were tested on the following fluids: R11, R12, R113, R114, R22 and RC318. The results of the predictions are summarised in Table 6.1. In this Table, the errors are shown as fractional (relative) errors.

Fluid	δP_c	δT_c	δv_c	$\delta \omega$	δv_c^*
R11	+5.76	-0.40	-0.19	+6.19	+1.34
R12	+11.0	-0.76	-0.03	+18.4	-0.62
R22	+1.38	+6.67	+1.98	-28.0	+2.06
R113	-2.82	-0.62	-0.43	+2.38	+2.69
R114	-0.5	+0.7	-0.3	-1.0	+1.9
RC318	-3.67	-4.64	+2.70	-35.0	+1.86

Table 6.1: Errors in Estimating Properties of CFC Fluids

The best-correlated properties were the critical temperature and the critical volume as found from the Vetere formula, Equation 6.38. The acentric factor was worst correlated; this may be because the Lee-Kesler formula was developed for use with hydrocarbons. The critical pressure was well correlated for the large molecules tested; the conclusion drawn was that for the projected CFC replacements, which all have two or three carbon atoms in each molecule, this property would be adequately correlated. Nonetheless this test shows that even accepted correlations may give errors of several percent and should as a consequence only be used if experimental measurements are not available.

Perfect-Gas Heat Capacities The variation of the perfect gas heat capacity with temperature must be known in order to obtain a complete set of thermodynamic data; the accepted correlations of heat capacity are nearly all simple quadratic or cubic polynomials in temperature. The polynomial constants may be obtained from the group contribution tables quoted in Perry, Section 3 [82].

Shigaki's Formulae The paper cited above by Shigaki and co described several new correlations of T_b, T_c, P_c, ω which have been developed specifically for CFC fluids. The formulae given were tested extensively by the authors on a wide selection of chloro– and fluoro–hydrocarbons; the rms deviations on the critical temperature, critical pressure and acentric factor were 1%, 3% and 3% respectively. This represents a significant improvement over the equations decribed above, and would be incorporated in any new implementation of this section of work.

6.4.3 Computational Details

6.4.3.1 Introduction

In this Section the computation of thermodynamic properties from an equation of state is discussed in some detail. The equations defining the important thermodynamic state functions listed in Section 6.3 are given for the CCOR equation. The rate-determining processes associated with use of an equation of state are identified; indications are given of the relative amounts of CPU time required for such tasks. Details are given of the algorithms employed in key calculations; these include steps necessary in dealing with the nitty-gritty of equation solving to ensure convergence of iterations.

6.4.3.2 CCOR Equation Recipes

Equation Of State The CCOR equation is normally written in the direct pressure-explicit form:

$$P = \frac{RT}{v - 0.42b} + \frac{RTb(0.77 + 0.055c^R)}{v(v - 0.42b)} - \frac{a}{v(v + c)} - \frac{bd}{v(v - 0.42b)(v + c)} \tag{6.40}$$

The equation has five fluid-specific parameters: a, b, c, d, c^R. These have been correlated with the critical temperature, critical pressure and acentric factor by Lin [55]. The parameters a and c are functions of temperature. The equation of state is constrained to fit the critical point; van der Waals' relations, which describe the isotherm curve's behaviour at the critical point were used by Lin *et al.* in the derivation of the following expressions for the parameters. (Reminder: van der Waals' relations are given by Equations 6.41–6.43.)

$$v = v_c \tag{6.41}$$

$$\left(\frac{\partial P}{\partial v}\right)_T = 0 \tag{6.42}$$

$$\left(\frac{\partial^2 P}{\partial v^2}\right)_T = 0 \tag{6.43}$$

By constraining the equation to fit the critical point exactly, some distortion of the shape of the phase envelope is inevitable, as the critical point cannot be part of an analytic description of a real fluid's behaviour. The CSD equation of state, described in Section 6.5.1, is not constrained to fit the critical point of the fluid it describes, although the equation does exhibit turning points which satisfy van der Waals' relations. As a consequence it yields good accuracy provided the critical region is not closely approached. For most practical heat pumping or refrigeration applications the critical region is of little interest, so this is no handicap.

EoS Parameters The parameters of the CCOR equation are defined by the following relations:

$$a = \alpha(T_r)\Omega_a R^2 T_c^2 / P_c \tag{6.44}$$

$$b = \Omega_b RT_c / P_c \tag{6.45}$$

$$c = \gamma(T_r)\Omega_c RT_c / P_c \tag{6.46}$$

$$d = \Omega_d R^2 T_c^2 / P_c \tag{6.47}$$

$$c^R = 24.863\omega - 33.368\omega^2 + 57.266\omega^3 \ (\omega \geq 0) \tag{6.48}$$

$$= 0 \ (\omega < 0)$$

The Ω factors in Equations 6.44–6.47 have been correlated by Lin with the acentric factor and critical compressibility z_c. The author used the Pitzer correlation $z_c = 0.291 - 0.08\omega$ to obtain the critical compressibility from the acentric factor, as this was the method used by Lin *et al.* in their work. The effect of using this correlation is small: for example, the true critical compressibility of R114 is 0.275; the value given by Pitzer's correlation is 0.271, an error of 1.5%. This is typical of the errors found using this correlation for the smaller CFC molecules; the error in the critical volume is probably of this magnitude, implying no difference between the two methods.

The Ω correlations are given by Equations 6.49–6.52

$$\Omega_b = 0.4756 - 3.396 z_c + 8.236 z_c^2 \tag{6.49}$$

$$\Omega_c = 0.42\Omega_b + 1 - 3z_c \tag{6.50}$$

$$\Omega_a = \Omega_c (1 + 0.42\Omega_b) + \Omega_b \left(0.77 + 0.055 c^R\right) + 3z_c^2 \tag{6.51}$$

$$\Omega_d = \Omega_c \left(0.77 + 0.055 c^R\right) + 0.42\Omega_a - z_c^3 / \Omega_b \tag{6.52}$$

The temperature dependence of the parameters a and c is represented by the scaling functions $\alpha(T_r)$ and $\gamma(T_r)$; these functions take *reduced* temperature $T_r = T/T_c$ as their argument. The functions, as used by Lin, are:

$$\alpha(T_r) = \left(1 + A_1(T_r^{-(1/4)} - 1) - A_2(1 - T_r^2)\right)^2 \ (T_r \leq 1) \tag{6.53}$$

$$= \exp\left(A_3(T_r - 1) - A_4(\sqrt{T_r} - 1)\right) \ (T_r > 1)$$

$$\gamma(T_r) = \exp\left(C_1\left(1 - T_r^{C_2}\right)\right) \tag{6.54}$$

where:

$$A_1 = 2.66709 + 5.51328\omega - 2.65333\omega^2 \tag{6.55}$$

$$A_2 = 0.18471 + 0.38357\omega - 0.32706\omega^2 \tag{6.56}$$

$$A_3 = 0.38349 + 4.88358\omega + 14.2113\omega^2 \tag{6.57}$$

$$A_4 = 1.17543 + 14.3109\omega + 30.5032\omega^2 \tag{6.58}$$

$$C_1 = 7.04333 - 5.00422\omega + 1.88597\omega^2 \quad (6.59)$$

$$C_2 = 0.23177 + 0.16986\omega + 0.03179\omega^2 \quad (6.60)$$

Fugacity Coefficient The fugacity coefficient for a fluid of invariant composition is given by:

$$\begin{aligned} \ln\phi &= \left[\frac{d}{0.42RT(c+0.42b)} - \frac{1.19+0.055c^R}{0.42}\right]\ln\left(\frac{v-0.42b}{v}\right) \quad (6.61)\\ &+ \left[\frac{a(c+0.42b)-bd}{RTc(c+0.42b)}\right]\ln\left(\frac{v}{v+c}\right)\\ &+ Z - 1 - \ln Z \end{aligned}$$

Internal Energy Departure Function The internal energy departure function is given by:

$$\begin{aligned} \Delta u &= \frac{1}{c}\left[a - T\left[a' - \frac{ac'}{c}\right] - \frac{Tbdc'}{c(c+0.42b)}\left[\frac{1}{c} + \frac{1}{c+0.42b}\right]\right]\ln\left(\frac{v+c}{v}\right) \quad (6.62)\\ &+ \frac{d}{0.42(c+0.42b)}\left[\frac{Tc'}{c+0.42b} + 1\right]\ln\left(\frac{v-0.42b}{v}\right)\\ &+ \frac{Tc'}{c(v+c)}\left[a - \frac{bd}{c+0.42b}\right] \end{aligned}$$

where the quantities a' and c' denote the temperature derivatives of the parameters a and c. These temperature derivatives are given by Equations 6.63 and 6.64:

$$\begin{aligned} \frac{a'}{\Omega_a R^2 T_c/P_c} &= \sqrt{\alpha(T_r)}\left[4A_2T_r - \frac{A_1}{2}T_r^{-(5/4)}\right] \ (T_r \le 1) \quad (6.63)\\ &= \alpha\left[A_3 - \frac{A_4}{2\sqrt{T_r}}\right] \ (T_r > 1) \end{aligned}$$

$$\frac{c'}{\Omega_c R/P_c} = -C_1C_2T_r^{C_2-1}\gamma(T_r) \quad (6.64)$$

Cross Constants The equation of state parameters for the mixture are obtained using the van der Waals mixing rule, Equation 6.3. The cross constants M_{ij}, $(i \neq j)$,

are found from these recipes:

$$a_{ij} = (1-k_a)(a_{ii}a_{jj})^{1/2} \quad (6.65)$$

$$b_{ij} = (b_{ii}+b_{jj})/2 \quad (6.66)$$

$$c_{ij} = (1-k_c)(c_{ii}+c_{jj})/2 \quad (6.67)$$

$$d_{ij} = (d_{ii}d_{jj})^{1/2} \quad (6.68)$$

$$c^R_{ij} = \left(c^R_{ii}+c^R_{jj}\right)/2 \quad (6.69)$$

The quantities k_a, k_c are the interaction constants discussed in Section 6.2.3.2. These are normally set to zero in the absence of sufficient experimental data to permit determination of the constants by regression.

Mixture Fugacity Coefficient In this formula for ϕ_i, the notation Σ_M is shorthand for the quantity $2\sum_{k=1}^{N} y_k M_{ik}$, where the sum is performed over all components and the letter M stands for any one of the five parameters. This quantity arises from the derivation of the expressions for mixture constants with respect to mole fraction; as a consequence the computation of the component fugacity in a mixture is much more expensive than the equivalent pure-fluid fugacity coefficient.

$$\begin{aligned}
\ln\phi_i &= -\ln Z \\
&- \left[2.833 + 0.13095c^R_{ii} + \frac{1}{0.42bRT(c+0.42b)}\left[\frac{d(0.42\Sigma_b+\Sigma_c)}{c+0.42b} - \Sigma_d\right]\right] \\
&\times \ln\left(\frac{v-0.42b}{v}\right) \\
&+ \frac{1}{RTc}\left[\Sigma_a - \frac{a\Sigma_c}{c} + \frac{1}{c+0.42b}\left[bd\left[1+\Sigma_c\left[\frac{1}{c}+\frac{1}{c+0.42b}\right]+\frac{0.42\Sigma_b}{c+0.42b}\right] - b\Sigma_d - d\Sigma_b\right]\right] \\
&\times \ln\left(\frac{v}{v+c}\right) \\
&+ \frac{\Sigma_b}{v-0.42b}\left[1.19+0.055c^R - \frac{d}{RT(c+0.42b)}\right] + \frac{\Sigma_c}{RTc(v+c)}\left[\frac{bd}{c+0.42b} - a\right]
\end{aligned} \quad (6.70)$$

6.4.3.3 Basic Calculation Steps

The equation of state method was analysed to identify those operations which would be: common to all equations of state; frequent in occurrence, and necessary precursors to production of the desired data. It would be necessary to devise efficient strategies for these tasks in order to minimise the computational overhead involved in generation

of data. It was desired to achieve maximum speed in all calculations because of the possibility of inclusion of the property calculation subroutines as part of the control program for the pilot plant on which the author's experimental program was to be executed. While a delay of a few seconds in generation of a printed table of saturation properties would be entirely acceptable if the data were not required instantly, such a delay would prevent incorporation of data derived from experimental measurement into a real-time control strategy. It should also be emphasised that in coding of property prediction subroutines it always makes good sense to employ all possible time-saving tricks compatible with accuracy; in the real world every second of CPU time must be paid for. The operations identified as occurring most frequently were:

1. Calculation of the equation of state parameters
2. Calculation of the temperature and composition derivatives of these parameters.
3. Implementation of mixing rules to create mixture parameters from pure-component parameters.
4. Solution of the equation for volume, from specified temperature, pressure and composition.
5. Determination of the vapour pressure of a pure component.
6. Solution of the dew or bubble point problem.
7. Solution of a fixed-enthalpy or isothermal flash from a known feed.

The first five tasks may be regarded as the fundamental, "rate-determining" steps; they must be performed repeatedly in any more complex calculation, such as a vapour pressure calculation. A major reason for the profusion of cubic equations of state has been the supposition that the inversion of the equation of state for volume is the most time-consuming step of all in equation of state calculations. In fact, it has been shown [62, 114] that, for multicomponent mixtures, the calculation of equation parameters and parameter derivatives may require as much or more time than the inversion of the equation of state. This is partly caused by the great effort devoted to efficient solution algorithms for equations of state; however the main reason is the time consumed in implementing even the simplest of mixing rules, such as Equation 6.3. The time requirement for calculation of the parameters is still less than the time required to solution; even so the difference is small.

The first few steps were studied by the author in an attempt to assess the time required to perform each operation, using a cubic equation of state (the CCOR equation) and a non-cubic equation (the CSD equation, discussed in Section 6.5.1). The absolute time requirements for each task are of course dependent on the machine and programming language used to carry out the tests; it is the relative size of each task that indicates its importance. The times for each task are shown in Table 6.2, which shows the results of tests performed on an IBM–XT compatible running at 10 MHz, using GW–BASIC as the programming language. The times given for each task are in seconds.

Task	CCOR time sec	CSD time sec
Parameters (pure fluid)	0.054	0.054
Parameters (binary mixture)	0.180	0.100
Parameter derivatives	0.048	0.049
Vapour Solution	0.160	0.380
Liquid Solution	0.160	0.680

Table 6.2: Speed Tests for CCOR and CSD Equations

These tests showed quite clearly that the analytic solution of the CCOR equation was faster than the numerical solution of the CSD equation; furthermore the time required was always the same, irrespective of phase, as the solution was performed according to a fixed algebraic recipe. Furthermore, if a pure fluid's saturation properties were desired, then one call to the cubic solution routine would yield both liquid and vapour phase volumes. The solution times for the CSD equation were quoted as the mean solution time over a range of reduced temperatures, using the initial guesses for volume which were recommended in the source literature. In fact, the higher the reduced temperature, the longer the solution time.

The calculation of pure-fluid parameters and temperature derivatives took the same time for both equations because both equations have two temperature-dependent parameters; the computation of these parameters involves roughly similar steps. The CSD equation parameters were significantly less costly to evaluate for a binary mixture than the CCOR equation; this shows the effect of the mixing rule overhead, as the CCOR equation has five parameters to be mixed, whereas the CSD equation only has two parameters. Nonetheless, the total time involved in computing a volume root (parameter evaluation followed by inversion) was less for the cubic than for the non-cubic equation.

Good Housekeeping At this point brief mention is made of some of the techniques used by the author to reduce computational load in implementation of these equations

of state. Every effort was made to reduce the number of floating-point multiplications; where formulae called for integers to be multiplied into real numbers the multiplication was replaced by addition. (on a PC, floating-point multiplication incurs about seven times the overhead of floating-point addition.) Complex formulae were factored before coding, to reduce the number of arithmetic operations required in their evaluation. Intermediate storage in local variables was used to avoid repetition of calculation steps where possible; examination of Equation 6.70, for example, shows considerable scope for this. Where iteration schemes were to be used, the Newton-Raphson algorithm with analytic derivative was preferred if it was possible to obtain an expression for the derivative; this permitted the coding of a compact convergence algorithm. As the calculation of the equation of state parameters was known to be relatively costly, repetition of parameter calculations was avoided where possible. In the case of the CCOR equation in particular, the calculation of mixture parameters was split into composition and temperature dependent subroutine steps to avoid unnecessary repetition of either operation on a call to the parameter subroutines. The cumulative effect was to increase the number of required parameters passed between subroutines and to increase the use of storage; the reduction in floating-point overhead more than compensated for the memory-access overhead.

6.4.4 Algorithmics

In this Section are given the algorithms used to perform various complex calculations . In some cases this is a simple list of operations; in others a more complex, iterative algorithm is described. These algorithms were all used in the programs described in Section 6.4.5.1, which discusses the programs written by the author for property prediction.

6.4.4.1 Initialisation

In order to use the CCOR equation for a given fluid, certain data structures had to be initialised by the program. The necessary initialisation steps were: determination of the fluid(s) to be used; calculation of the equation of state parameters using the equations in Section 6.4.3.2; determination of the datum states for enthalpy and entropy, and specification of the bounding parameters for the relevant problem. These

steps are formalised in Algorithm 6.1, which details the steps involved. In order to avoid repetitive typing of the basic parameters required, input of this information was performed *via* text files, constructed to a standard input format. Hence some small amount of work with a text editor was required to write a data file for every new fluid.

Algorithm 6.1 CCOR Equation Initialisation Procedures

Step 1: *Read name of data file for relevant fluids from keyboard.*

Step 2: *Check existence of specified data files: if not available return to previous step.*

Step 3: *Determine whether to use default or optimised equation parameters; if optimised parameters, read them from keyboard or file, otherwise calculate the default parameters.*

Step 4: *Using the relations given in Section 6.3, calculate and store the values of temperature, pressure, volume, fugacity coefficient, enthalpy and entropy departure functions at the desired datum state: saturated liquid at -40°C. Perform this for each component to be used.*

Step 5: *Interrogate user for details of output format: screen or file, plain text or text inclusive of formatting commands, etc.*

Step 6: *Read calculation control parameters from keyboard; perform appropriate conversions of units and allocation of intermediate storage.*

Step 7: *Open and initialise any disc files required, checking for existence and confirming any overwrites before proceeding.*

6.4.4.2 Evaluation of Parameters

The evaluation of the equation of state parameters for a pure fluid was straightforward; the three invariant parameters were obtained during the initialisation steps (Algorithm 6.1), leaving only the calculation of parameters a and c. In the case of a mixture, all five parameters had to be concocted. Therefore this task was split into two stages: firstly, calculation and storage of the five parameters for each component at the desired temperature; secondly, use of the specified mol fraction vector to combine the pure-fluid parameters into a vector of mixture parameters.

6.4.4.3 Solution of the Equation of State

This was straightforward in the case of a pure fluid; in the case of a mixture there could be problems of root selection at temperatures near the critical point. These were not really addressed in detail, as the bulk of the work performed with the CCOR equation did not stray into such problematic regions. A more thorough approach would be required to render this algorithm reliable in the critical mixture region: this would require in addition a link to the calling routines to adjust specifications of temperature, pressure and mol fraction to ensure existence of appropriate roots of the right type.

Algorithm 6.2 Inversion of the CCOR Equation

Step 1: *Using the temperature, pressure and parameters* a, b, c, d, c^R *as input, rearrange the equation of state into standard cubic form, i.e.* $v^3 + K_1 v^2 + K_2 v + K_3 = 0$. *The coefficients* K_1, K_2, K_3 *are given by Equation 6.71.*

Step 2: *Solve the cubic equation using the algorithm quoted in Perry [82] Section 2. Check the number of real roots (returned by the equation-solving algorithm).*

Step 3: *If only one real root exists: check magnitude of root against critical volume and desired phase. Print warning if magnitude is incompatible with the desired phase. If a mixture is used, check against the calculated volume, found using Equation 6.79.*

Step 4: *If three real roots exist, smallest is liquid root, largest is vapour root. Make choice based on desired phase (may wish both).*

$$\begin{aligned} V^\circ &= RT/P \\ K_1 &= c - 0.42b - V^\circ \\ K_2 &= -\left[0.42bc + V^\circ(c + b(0.77 + 0.055c^R)) - a/P\right] \\ K_3 &= -b\left[V^\circ c(0.77 + 0.055c^R) + (0.42a - d)/P\right] \end{aligned} \tag{6.71}$$

6.4.4.4 Pure-Fluid Vapour Pressure

The calculation of vapour pressure from first principles requires determination of pressure and liquid and vapour phase volumes which ensure an equivalence of fugacities between the liquid and vapour phases. There are therefore three unkown quantities; as the solution of the equation from specified temperature and pressure yields both phase volumes, the problem may be coded as a one-dimensional iteration. This is merely a consequence of the phase rule: once temperature *and* pressure have been set, then the volumes are no longer independent. The iteration function used by the author in this solution was:

$$f(P) = \ln \phi_v(P^*(v_v), T) - \ln \phi_l(P^*(v_l), T) = 0 \tag{6.72}$$

in which the interdependence of pressure, liquid and vapour volumes is implied. This function permitted an elegant implementation of the Newton-Raphson algorithm, from Campbell [11], which is explained in Section 6.2.3.3. The vapour pressure was updated according to Equation 6.11— typically this would result in convergence after 3–4 iterations at worst.

The initial guess of vapour pressure, required to start off the iteration, was made by fitting a two-term Antoine equation to the vapour pressure curve between the normal boiling point and the critical point:

$$\ln P^* = A + B/T \tag{6.73}$$

in which the values of A and B could be obtained in terms of the critical point and the normal boiling point by algebraic manipulation. This method was found to be quite adequate. Campbell [11] gives a more complex method of choosing the initial guess based on finding the turning points of the isotherm curve by algebraic manipulation of a cubic equation of state. The same principle was used by Morrison and McLinden [70] for the CSD equation of state; their method involved bracketing the turning points by numerical methods. There seemed little point in substituting either method for the simple empirical guess provided by the author's own method. The procedure is formally encapsulated in Algorithm 6.3 and flowcharted in Figure 6.1.

Algorithm 6.3 Pure-Fluid Vapour Pressure Calculation

Step 1: *Specify temperature: check against critical temperature. If temperature is above critical temperature, break iteration.*

Step 2: *Specify stopping criteria for iteration (normally a residual of less than 10^{-6} on the iteration function Equation 6.72) and the maximum iteration count.*

Step 3: *Calculate parameters of equation of state.*

Step 4: *Using the two-term vapour pressure relation, Equation 6.73, make an initial guess of pressure.*

Step 5: *Solve the equation of state for both phase volumes; compute the value of the iteration function and the phase compression factors.*

Step 6: *Check the size of the iteration function and the magnitude of the update; break iteration if either is sufficiently small.*

Step 7: *Update pressure and return to step 5.*

Step 8: *If the procedure reaches here, warn of unconverged variables. Stop.*

6.4.4.5 Pure-Fluid Saturation Temperature

This computation corresponds to that described above for vapour pressure; there were however certain unavoidable differences in the solution method. As temperature was the unknown in this problem, the equation of state parameters had to be evaluated at each step. The iteration function used was still the difference between the logarithms of liquid and vapour fugacity coefficients. The starting guess of temperature was found from the 2-term Antoine relation, Equation 6.73; thereafter the secant method was employed to update the temperature guess.

Algorithm 6.4 Pure-Fluid Saturation Temperature Calculation

Step 1: *Specify pressure: if pressure is greater than critical pressure break iteration.*

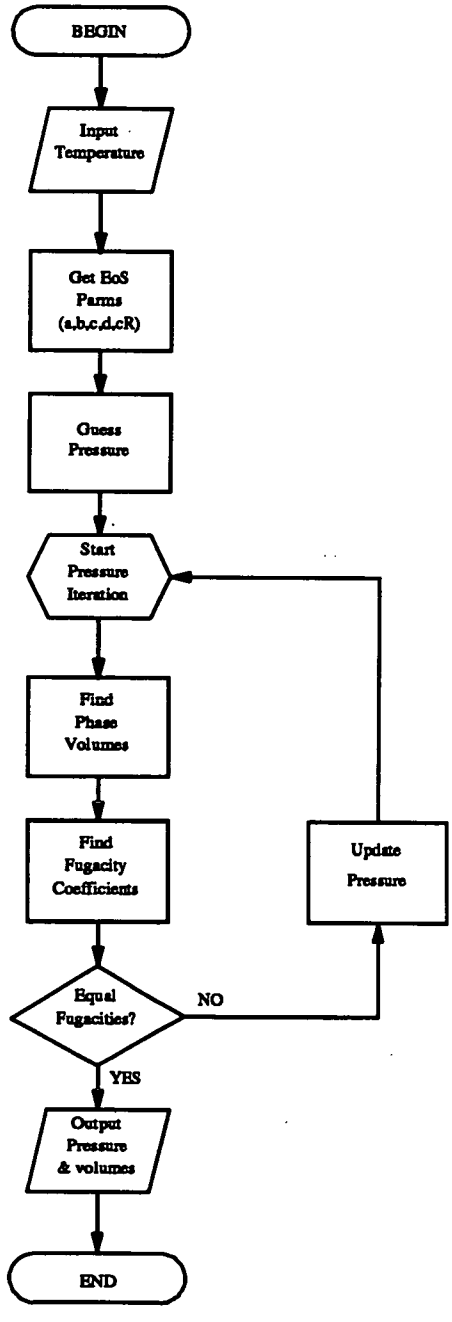

Figure 6.1: Pure Fluid Vapour Pressure Calculation Algorithm

Step 2: *Specify constraints on iteration, as for vapour pressure calculation.*

Step 3: *Make initial guess of saturation temperature based on Equation 6.73*

Step 4: *Calculate equation of state parameters.*

Step 5: *Solve equation of state for phase volumes; calculate function value.*

Step 6: *Test function value for convergence: if converged to tolerance, break.*

Step 7: *If this is first step, set the new guess of temperature by using a temperature step of 1 degree from the first guess, then store the first values of temperature and iteration function and go to step 4*

Step 8: *Update the temperature using the secant algorithm and the previous step's function and temperature values. If the updated temperature is sufficiently close to the previous value, break, otherwise return to step 4.*

Step 9: *If the iteration reaches here, warn of unconverged variables, then stop.*

6.4.4.6 Enthalpy and Entropy

The calculation of enthalpies and entropies was a non-iterative process, once the temperature, pressure, volume and composition were known. The calculation process involved: computation of the enthalpy departure function for the fluid at the specified conditions; evaluation of the perfect-gas function changes between the datum states and the desired state, and combination of these quantities with the datum state departure functions obtained during initialisation (Algorithm 6.1) to yield a final enthalpy or entropy.

6.4.4.7 Binary Dew/Bubble Pressure

The calculation of dew pressure of a multicomponent mixture is significantly more difficult than the pure-fluid problem. With multiple components, there may be difficulties with the shape of the two-phase region: the computational load is also very much greater than that of the pure-fluid solution. The only case treated here is that of the

general binary dew or bubble pressure evaluation. In this problem, the temperature and mol fraction more volatile in one phase are specified; the unknowns are pressure, mol fraction in the other phase, and the phase volumes. There are two degrees of freedom and two constraints which must be satisfied, namely Equation 6.12 and Equation 6.13.

The method chosen to solve the VLE problem was based on an algorithm developed by Morrison and McLinden [70] for use with the CSD equation of state. This was a nested iteration: an outer loop to converge the pressure; an inner loop to converge the unknown phase composition, with phase volumes being evaluated as required to enable calculation of the component fugacities in each phase. The alternative would have been to set up a simultaneous system to be solved using the multi-dimensional version of the Newton-Raphson algorithm, or a generalisation of the secant algorithm. The nested approach was preferred because it involved only one-dimensional iteration loops; the iteration variable in each loop could be kept within safe limits by the iteration schemes. Each loop was converged using the secant algorithm: the update step results were monitored and compared with limits on the variable, found from previous iteration steps. If a secant step would take the iteration outside acceptable limits, a false position step was employed instead. Thus each loop should eventually converge, providing that limits on the iteration variable had been found. The limits were found by monitoring the sign of the residual function used in each loop: a sign change between iterations would signify a bracketing of the root.

The iteration functions were obtained by manipulation of the component fugacity coefficients into auxiliary constants z_j, defined by:

$$z_j = x_{p,j} \times \left(\frac{\phi_{p,j}}{\phi_{i,j}} \right) \quad (j = 1,2) \tag{6.74}$$

where x denotes mol fraction, the suffix p denotes *parent* (known) phase and i denotes *incipient* (unknown) phase. These quantities are closely related to the familiar equilibrium constants $K_j = (y_j/x_j)$ $(j = 1,2)$. The iteration function for the incipient phase composition was simply:

$$f_x(x_i) = \frac{z_1}{z_1 + z_2} - x_i \ (P \text{ constant}) \tag{6.75}$$

where x_i is the mol fraction more volatile in the incipient phase.

The iteration function used for the pressure update was:

$$f_P(P) = 1.0 - (z_1 + z_2) \tag{6.76}$$

The proof that these iteration functions satisfy Equations 6.12 and 6.13 is left to the reader. It should be apparent from inspection of Equation 6.75 that this function is a residual of the incipient composition; this is used in the initial update of incipient phase composition.

The procedure is summarised for the fixed-temperature problem in Algorithm 6.5, which may be used to find either dew or bubble point conditions, given temperature and one phase composition. The path of the algorithm is mapped out in the flow chart of Figure 6.2; the source code for the final version of the algorithm is contained in Appendix listapp as a further reference. The following paragraphs describe in detail the update formulae, checks and safeguards which were built into the algorithm to ensure convergence.

Initial Estimates The initial estimate of pressure was calculated using Raoult's Law in its simplest form, yielding:

$$P^0_{bub} = x_p p^*_1 + (1 - x_p) p^*_2 \tag{6.77}$$

$$P^0_{dew} = \frac{p^*_2}{1 + x_p \left[\frac{p^*_2}{p^*_1} - 1\right]} \tag{6.78}$$

where Equation 6.77 gives the initial guess P^0_{bub} for a bubble pressure and Equation 6.78 the initial guess P^0_{dew} for a dew pressure.

The initial composition guess in the algorithm as derived by Morrison [70] was that the composition of the incipient phase should equal that of the parent phase. This avoided spurious calculation in the cases where either an azeotrope or a single-phase fluid was the subject of the calculation. The author found, however, that for VLE away from the critical region, a faster convergence (fewer pressure iterations) was given by use of Raoult's Law to generate an initial guess on the unknown composition.

Consistency Checks Although the CCOR equation (cubic) was inverted by an analytic procedure, two heuristic checks on the calculated volume of each phase were used whenever the equation was inverted. The need for such checking with cubic equations

has been discussed by Poling [85]. In essence this is only a problem with mixtures, where combinations of pressure, temperature and composition may cause the calculation of equation parameters which only yield one real root. This root may lie on the wrong side of the critical point; or it may lie below the minimum (excluded) volume of the equation of state. Especially near the critical region, for example at temperatures above the critical of one of the components, there may only be a very small range of feasible $(P, T, \underline{x})$ which yield sensible phase volumes. Thus a poor starting guess of any variable, or an overshoot by an iteration convergence method, may cause an excursion from the two-phase region. The two checks on calculated volume were used to ameliorate this problem

The first check tested the volume against the minimum possible volume for the CCOR equation, $v_{min} = 0.42b$. If the volume failed this test, it was reset: for liquid phases the reset volumes was $v_{new} = 0.8 \times v_{c,mix}$; the vapour phase volume was reset to the perfect gas volume $v_{pg} = RT/P$. No alteration was made to the iteration variables (pressure, unknown phase composition) at this stage. This check was really intended to pick up bad liquid-like volume roots, for which the volume dependence of fugacity would be small: so the use of a meaningful volume root would not cause a great change in the iteration function value.

The second test used a calculated critical volume to assess the stability of the incipient (unknown) phase. This was intended to detect an excursion from the two-phase region caused by an infeasible pressure guess: should this be the case then the current guess of pressure was perturbed to try to force formation of a second phase. This was a safe procedure: the pressure of any two-phase system would be bounded between the critical pressure of the more volatile and the vapour pressure of the less volatile, except in the case of a positive-boiling azeotrope approaching its critical point. In the latter case the composition iteration would be instantly satisfied by the initial guess of $x_i = x_p$, leaving the pressure iteration to find the azeotropic critical pressure. The mixture critical volume was calculated using Li's equation for mixture critical volume, Equation 6.79, in the form cited in Perry [82] Section 3.

$$v_{c,mix} = y v_{c,1} + (1-y) v_{c,2} - \frac{y(1-y)\left(v_{c,1} + v_{c,2}\right)^2}{v_{c,1} - v_{c,2}} \qquad (6.79)$$

where $v_{c,mix}$ represents the mixture critical volume and $v_{c,i}$ $(i = 1, 2)$ represent the component critical volumes. The current pressure guess was updated if the calculated incipient phase volume lay on the same side of the critical point as the parent phase volume. This technique proved extremely effective in extending the range of the algo-

rithm: before this was introduced to the solution, the algorithm was prone to failure at temperatures higher than the critical temperature of the more volatile. This could yet be improved: the approximation to true critical volume represented by Equation 6.79 prevents unambiguous detection of the critical point. The algorithm will unnecessarily perturb the pressure once the difference between the true (unknown) critical volume and the incipient phase volume is less than the distance between the approximate critical volume and the incipient volume. This was not however felt to be a major problem; there exist algorithms [26, 33, 68] for calculation of true mixture critical volumes using an equation of state, which could be used in advance to fit the critical volume locus as a function of mol fraction.

Iteration Update Methods Both pressure and composition were updated using a combination of the secant method and the rule of false position. These methods are expressed by Equation 6.80 and Equation 6.81 for the general case of an iteration variable x and an iteration function $f(x)$, where the function should disappear at the root. The formulae both express the updated value at the $j+1$th iteration in terms of previously-calculated iteration data. In Equation 6.81 the subscripts *pos* and *neg* refer to previously calculated $(x, f(x))$ points where the function took a positive or negative value.

$$x_{j+1} = x_j - f_j \times \frac{x_j - x_{j-1}}{f_j - f_{j-1}} \tag{6.80}$$

$$x_{j+1} = x_j - f_{pos} \times \frac{x_{pos} - x_{neg}}{f_{pos} - f_{neg}} \tag{6.81}$$

Both Equation 6.80 and Equation 6.81 require some prior knowledge of the behaviour of the iteration function; in the case of the secant method two previous (arbitrary) points are required, while the false position method requires points bracketing the root to be found. In addition to the initial guess of either iteration variable, some means of generating a second guess was required to initialise the secant method. The second guess at pressure was set to 100.1% of the starting guess: this was wholly empirical but gave satisfactory results. The second guess at any composition iteration was found by summing the first guess and the value of the composition iteration function; the quantity $z_1/(z_1 + z_2)$ in Equation 6.75 will be equal to the incipient phase composition at the root.

The use of false position was enabled by a check of the function sign after every function evaluation, with the (x, f_x) pair being placed in storage for future use if required. The criterion for preference of a false position update was that the update on x generated by

Equation 6.80 should not lie outside the limits $[x_{pos}, x_{neg}]$, if these had been established.

Pressure Correction The occasional need for correction of the pressure guess during a composition iteration step has been explained above. For a dewpoint calculation (incipient phase liquid) the absence of a stable incipient phase implies a need to *increase* the pressure; for a bubblepoint calculation the pressure should be reduced. The initial method of correction was to employ a half-interval step between the current pressure and the relevant physical constraint on feasible pressure. This was rejected after practical trials revealed it to be too clumsy: frequently the corrected pressure would cause the parent phase volume to become inconsistent with the type of phase required, and the whole iteration would lurch drunkenly around the P–x plane before crashing to a halt at a spurious root. A second correction was tried: a small fraction of the distance (2.5%) between the current pressure and the relevant pressure limit was added to the pressure to form the update. This was successful; although the speed of the algorithm was impaired by use of a small pressure step the success rate of the routine was much improved.

Algorithm 6.5 Calculation of Binary Dewpoint (Temperature Fixed)

Step 1: *Specify temperature and composition of known (parent) phase. If interaction constants are to be used, specify these here.*

Step 2: *Find the pure component vapour pressures and estimate the dew pressure from Equation 6.78. If the system temperature is above the critical temperature of one of the components, use the critical pressure for that fluid.*

Step 3: *Calculate the critical volume for the parent phase composition from Equation 6.79.*

Step 4: *Calculate the equation of state parameters for each pure component at the system temperature: combine these to make the mixture parameters for the parent phase.*

Step 5: *For the given pressure, solve the equation of state for the parent phase volume.*

Step 6: *Check the phase volume: if the volume is below the minimum feasible volume for the equation of state, reset the phase volume to a feasible value.*

Step 7: *Calculate the fugacity coefficient of each component in the parent phase.*

Step 8: *Set an initial guess of incipient composition: for the first time round the pressure (outer) iteration loop, use Raoult's Law, thereafter use the converged value from the previous composition iteration. If the previous composition iteration did not converge, set the composition to the parent phase composition.*

Step 9: *Calculate the equation of state parameters for the incipient phase and solve for volume. Check the phase volume as before: if it is unsatisfactory, adjust to a feasible value.*

Step 10: *Calculate the critical volume for a mixture with the current incipient composition.*

Step 11: *Test the incipient volume against the critical volume: if the incipient volume lies on the wrong side of the critical volume, do the following:*

1. *Reset the pressure guess, by adding a small fraction of the interval between the current pressure and the relevant pressure constraint. If the incipient phase is liquid, the pressure constraint is the critical pressure of the more volatile, otherwise the constraint is the vapour pressure of the less volatile.*
2. *Calculate the parent phase volume and fugacity coefficients at the new pressure.*
3. *Reset the composition iteration convergence flags and goto step 9.*

Step 12: *Calculate the incipient phase fugacity coefficients and evaluate the auxiliary variables z_1, z_2. Calculate the value of the iteration function f_x from Equation 6.75.*

Step 13: *Store the current values of x_i and $f_x(x_i)$ in slots according to the sign of f_x: the objective is to maintain stored values of $(x_i, f_x(x_i))$ on either side of the composition root.*

Step 14: *Test the composition loop for convergence, by comparing the magnitude of f_x against a preset tolerance. If converged, flag this and go to step 18.*

Step 15: *If this is the first composition iteration: store the current x_i and f_x; increment the value of x_i (by addition of f_x), then go to step 9.*

Step 16: *Use the previously-stored values of x_i, f_x to perform an iterative correction to x_i by the secant method. Check the updated value of composition: if less than zero, or greater than unity, set to zero or one accordingly.*

Then, if the root has been bracketed (both a positive and a negative value of f_x found), do:

1. *Find the maximum and minimum constraints on x_i by inspection of the values of x_i from previous steps which bracket the root.*
2. *If the updated value of x_i lies outside the interval indicated by the bracketing compositions, perform a second update by the rule of false position, using the boundary values of x_i and f_x to give a safe new value of x_i.*

Step 17: *Store current values of x_i and f_x, then return to step 9.*

Step 18: *Calculate the pressure iteration function f_P.*

Step 19: *Store the (P, f_P) pair according to the sign of f_P, as done for composition in step 13.*

Step 20: *Check the pressure loop for convergence: if converged, break and go to step 23.*

Step 21: *If this is the first time round the pressure loop, perturb the pressure by a small fraction (0.1%) and go to step 5. Otherwise update the pressure by the same combination of secant and false position steps as used for the composition iteration above.*

Step 22: *Return to step 5*

Step 23: *Test the convergence flags for the pressure and incipient composition iterations: use these to decide the return code for the iteration. If either of the iterations was unconverged, print appropriate warnings to the standard error file. Return the final values of the pressure, incipient phase composition, liquid and vapour volumes to the calling routine.*

6.4.4.8 Isentrope Calculation

The calculation of an isentrope is required in the analysis of a real compression heat pump cycle, in order to estimate the compression efficiency from given suction and discharge conditions. The object of the calculation is to calculate the isentropic efficiency η and the specific enthalpy change associated with the transition between the states at the compressor suction and discharge. Specified quantities are normally: composition; suction side temperature and pressure, and discharge temperature and pressure.

The basic procedure finds a state point at the discharge pressure which implies no gain or loss in entropy during the compression process. The enthalpy of the fluid at this state (which represents reversible, adiabatic compression) is then combined with the actual enthalpy at the discharge to find η, using Equation 4.5. There is a subtlety: the shape of some fluids' phase envelopes may mean that the fluid is in the two-phase region at either the real discharge or the reversible adiabatic discharge state. This must therefore be checked for during the calculation.

The adiabatic reversible discharge temperature may be calculated from the actual discharge temperature if the difference in entropy between the fluid at the reversible discharge temperature and the real discharge temperature is known. As the process of reversible compression by definition implies no change in entropy between suction and discharge, the entropy difference is known, yielding the following relations:

$$S_{dis} - S_{rev} = S_{dis} - S_{suct} \tag{6.82}$$

$$= \int_{T_{rev}}^{T_{dis}} \left[\frac{C_p}{T}\right] dT_{P=P_{dis}} \tag{6.83}$$

where the subscript *rev* refers to reversible exit state, *suct* refers to suction conditions, and *dis* to actual discharge conditions. This relation may be rearranged to yield an explicit equation for T_{rev}:

$$T_{rev} = T_{dis} \times \exp\left(\frac{S_{suct} - S_{dis}}{C_p}\right) \tag{6.84}$$

Algorithm 6.6 Calculation of Isentropic Efficency of Compression

Step 1: *For specified discharge pressure, calculate the saturation (dew) temperature of the fluid and compare against the given discharge temperature.*

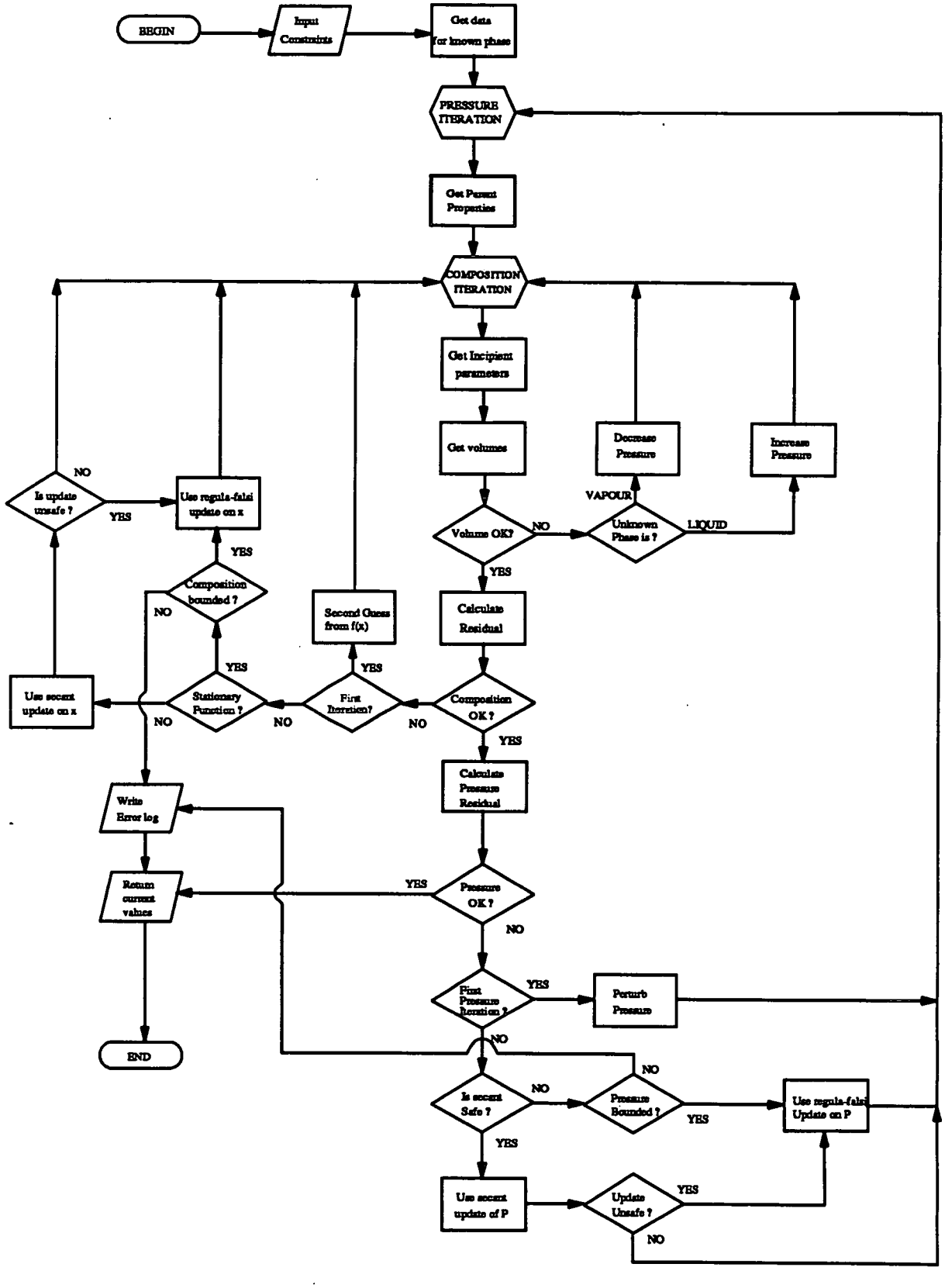

Figure 6.2: Flow Chart for Fixed-Temperature Binary Dewpoint Calculation

if the discharge temperature is not higher than the saturation temperature, print warning and break.

Step 2: *Invert the equation of state to find the molar volume of the fluid at suction and discharge. Use these molar volumes to calculate the enthalpy and entropy at both points.*

Step 3: *Calculate the constant-pressure specific heat of the fluid at the discharge temperature. Use this in Equation 6.84 to find the temperature T_{ad} which corresponds to a reversible adiabatic compression over the same pressure ratio.*

Step 4: *If the value of T_{ad} indicated by Equation 6.84 is less than the saturation temperature of the fluid at that temperature, then the vapour fraction of a two-phase mixture having the same entropy as the suction gas must be found: this may be calculated directly for the pure fluid, but for a real gas mixture the calculation will be iterative.*

Step 5: *After determination of the reversible discharge state, calculate the enthalpy of the fluid at this state. Substitue the enthalpy in Equation 4.5 to yield the isentropic efficiency of the process.*

6.4.5 Pure Fluid Results

6.4.5.1 Implementation Of The CCOR Equation

The initial work with the CCOR equation was programmed in the language imp80; the programs were compiled and run on the Edinburgh University EMAS-A mainframe, whose operating system was also written in imp80. The author's first programs all dealt with properties of pure fluids; since then nearly all the functions of the early programs have been superseded by programs written in the C language, for compilation on *either* a PC-compatible microcomputer *or* a Sun engineering workstation. The shift in programming language was dictated by the desire to run substantially similar programs on all the hardware available to the author in the Department of Chemical Engineering; the pilot plant described in Chapter 3 had a control system program written in C, while the bulk of the department's computing power lay in its network of workstations.

The implementation of the equation of state in a useful form required the preparation of a set of subroutines, to be linked into complete programs as required. These were divided into three classes: non-iterative functions; iterative calculations, and input-output routines. The final versions of the input-output routines were compatible with the subroutines written to implement the CSD equation, described in Section 6.5.1. The complete source code for all the subroutines necessary in order to calculate any desired property of a pure fluid or binary mixture occupied less than 80 kB of disc space, showing that the core routines for an equation-of-state-based property package need occupy relatively little space. The input and output for all the programs written was deliberately spartan; this made transfer of code between compilers straightforward. Had the code been "for public consumption" then the code for the input-output interface would have been far larger than the number-crunching code; happily it was not necessary to develop such an interface in order to obtain thermodynamic data for purposes of research and comparison with other data sources.

6.4.5.2 Data Generation Details

The CCOR equation was used to predict sets of saturation data for eight well-known CFC fluids: R11, R12, R13, R22, R23, R113, R114 and RC318. The equation was used in its general form, that is, with the critical temperature, critical pressure and acentric factor being used to calculate all the necessary parameters for the equation. The acentric factors were calculated from the definition given by Equation 6.1, using the high-accuracy Antoine equations for each fluid available in the literature [24]. Critical temperatures and pressures were taken from the standard sources [106, 82, 24].

These datasets were then compared against tables of data from the literature [82, 24]. Each dataset spanned roughly the same reduced temperature range of 0.5–1: this enabled direct comparison to be drawn with the patterns of error in property predictions for each fluid. The properties compared against the literature data were: vapour pressure; liquid volume, vapour volume and latent heat of vapourisation. In order to interpolate between data points, some of the literature datasets were supplemented using the high-accuracy correlations of Downing [24] (see Section 6.5.2). These correlations were checked against the available data and found to be in excellent agreement; their use would not affect the shapes of the error curves which were obtained.

The following sections present the results of the comparison in graphical form; tabulated summaries of the results are included after the graphs. In each of the error curve graphs,

all of the fluids' error curves are shown on the same plot: the curves are tagged with the refrigerant acronym for the appropriate fluid *e.g.* R11. The full name of each fluid is given in the tabular summary Table 6.3. Where predicted data and reference data are shown on the same plot the predicted data are shown as smooth lines, the reference data as points.

The CCOR equation was also used to predict the properties of several of the proposed CFC replacement fluids: R134a, R123, R124, R125, R32. The predictions are shown in the appropriate section and, where possible, they are compared with recently-published data from the manufacturers' publications [40, 39]. The critical properties and acentric factor of these fluids were originally calculated from the correlations presented in Section 6.4.2.1; these predictions have been published by the author [58]. The data presented in this section were however calculated using values of critical temperature, pressure and acentric factor supplied from the literature, as these became available.

6.4.5.3 Vapour Pressure

The prediction of vapour pressure for all of the test fluids is shown in Figure 6.3, which shows the vapour pressure in bar as a function of temperature in Kelvin, up to the critical point of each fluid. This figure shows the predicted vapour pressures to be in good agreement with the actual pressures over the whole range shown.

The vapour pressure curves of the new fluids are shown in Figure 6.4, which has the same format as Figure 6.3. In this figure the vapour pressure curves for R12 and RC318 have been include for reference; it is immediately obvious that the system R12/R134a should exhibit azeotropy, because the vapour pressure curves of these fluids intersect. (Such an intersection is called a *Bancroft Point.*) The fluid RC318 is shown because it was one of the favoured fluids for use in the pilot plant; with a volatility close to R114 and R124 it may be a useful high-temperature working fluid.

The relative error in the prediction of vapour pressure for each fluid was calculated and plotted; the plots are shown in Figure 6.5, which is a plot of relative error against reduced temperature. The error curves for all of the fluids investigated follow the same pattern; the largest deviation is shown to be roughly 3%, at a reduced temperature between 0.6 and 0.7. This graph indicates that the CCOR equation can be used to give good predictions of vapour pressure over a wide temperature range.

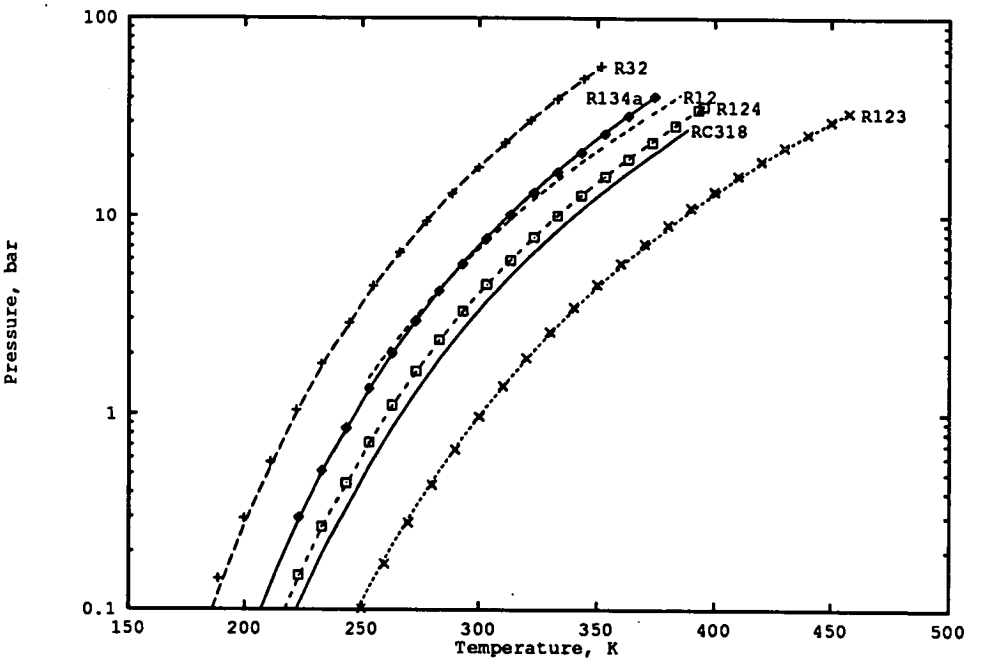

Figure 6.3: Vapour Pressure Curves of Reference Fluids

6.4.5.4 Phase Volumes

Typical Phase Envelopes The saturated liquid and vapour volumes predicted by the CCOR equation for each reference fluid are not shown here for reasons of space. Instead two illustrative fluids are chosen by way of example. The phase envelope of R12 is normally termed "straight", while that of R114 is "skewed"; these terms refer to the shape of the vapour volume boundary. A fluid such as R12 has the property that the adiabatic, reversible compression of saturated vapour causes an increase in vapour superheat, that is, an isentropic path leads *away* from the phase boundary. In the case of a fluid resembling R114, the compression of saturated vapour may cause the fluid to cross the two-phase boundary, resulting in the formation of liquid during the compression process. Such fluids are characterised by high gas heat capacities; when plotted on temperature-entropy or pressure-enthalpy charts, the two-phase region appears kinked. (See [64] for a discussion of the characteristics of phase envelopes.)

The pressure-volume envelope of R12 is shown in Figure 6.6, that of R114 in Figure 6.7. In both of these diagrams two sets of data are plotted: the points represent

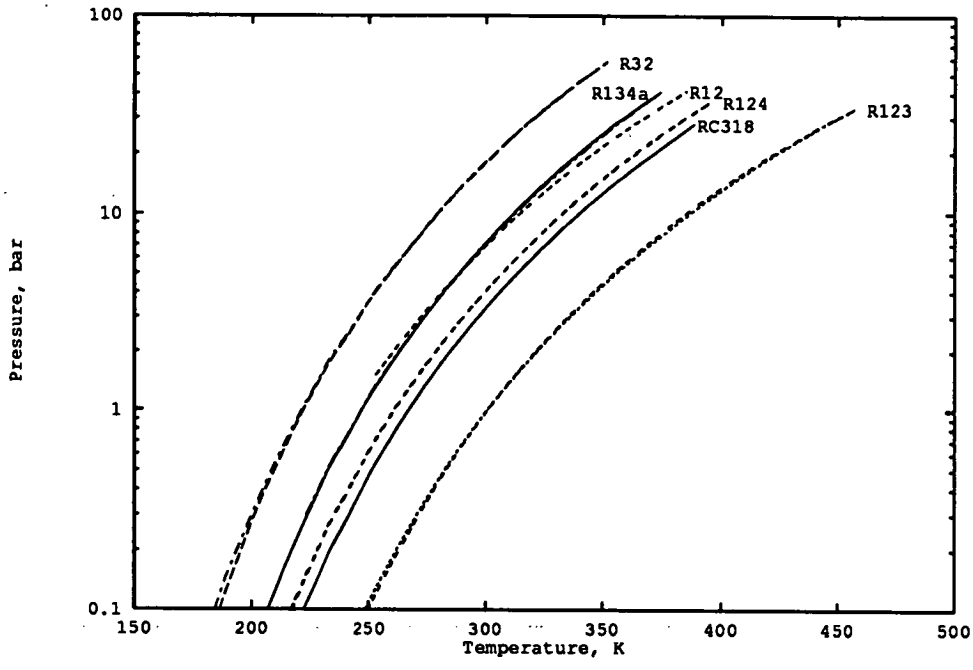

Figure 6.4: Vapour Pressure Curves of New Refrigerant Fluids

tabulated reference data, the lines the predictions of the CCOR equation. The fit appears excellent, but it should be noted that the plots use logarithmic co-ordinates, whose effect is to reduce the apparent deviation between the two sets of data at high reduced temperatures.

Liquid Volume Errors The fit of the CCOR equation's predictions to saturated liquid volume is shown in Figure 6.8: as for vapour pressure, there exists a strong similarity in the shape of the error curves for each fluid tested. The fit of liquid volume appears to be best for the smaller molecules such as R11 and R12. The worst-predicted fluid was RC318; this exhibited an average absolute deviation (AAD) of 7% in prediction of liquid volume. This prompted the author to seek for a reason why this should be so; the conclusion drawn was a possible shortcoming of the correlations presented in the literature for the CCOR equation parameters.

The source literature [55, 29, 30, 45, 54] recommends calculation of a critical compressibility z_c from the Pitzer relation $z_c = 0.291 - 0.08\omega$, where ω, the acentric factor, is one of the three required fluid properties. This critical compressiblity is then used to calcu-

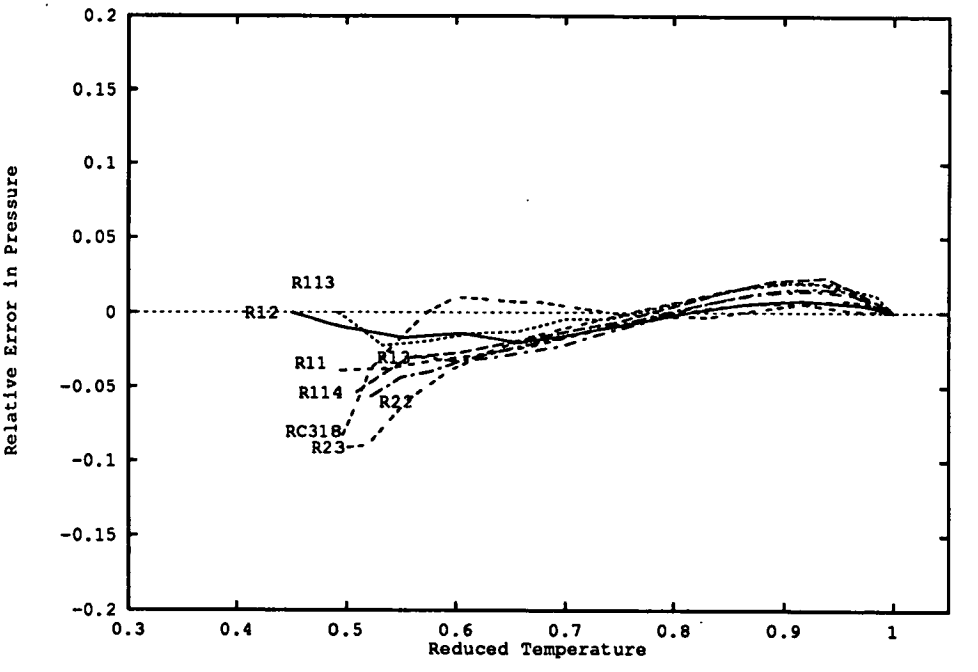

Figure 6.5: Error in CCOR Pressure Prediction for CFC Fluids

late intermediate parameters, using for example Equation 6.49. In the case of RC318, the critical compressibility is $z_c = 0.2780$, using the data quoted in [82]. The acentric factor, calculated from the definition Equation 6.1 is $\omega = 0.357$. If this is then used to compute a critical density from the Pitzer correlation the resultant value $z'_c = 0.2630$ — a difference of 5.4%. The importance of this error is that the critical compressibility terms in the defining relations Equation 6.49–6.52 are mostly non-linear; so the error is propagated throughout all the equation parameters.

It would not be sensible to attempt a reversal of this effect by inversion of the Pitzer correlation to find a pseudo acentric factor; because of the loss of accuracy which the form of the equation would cause ($d\omega/dz_c$ is large). Should this be attempted the result is an increase in the accuracy of liquid volume prediction and a large increase in the inaccuracy of predicted vapour pressure and vapour volume. The conclusion is that some kind of parameter optimisation to find the intermediate parameters A_1–A_4, C_1–C_2 would be the best method of attack to reduce this error, unless recourse were made to the volume translation technique of Péneloux [79] discussed in Chapter 2.

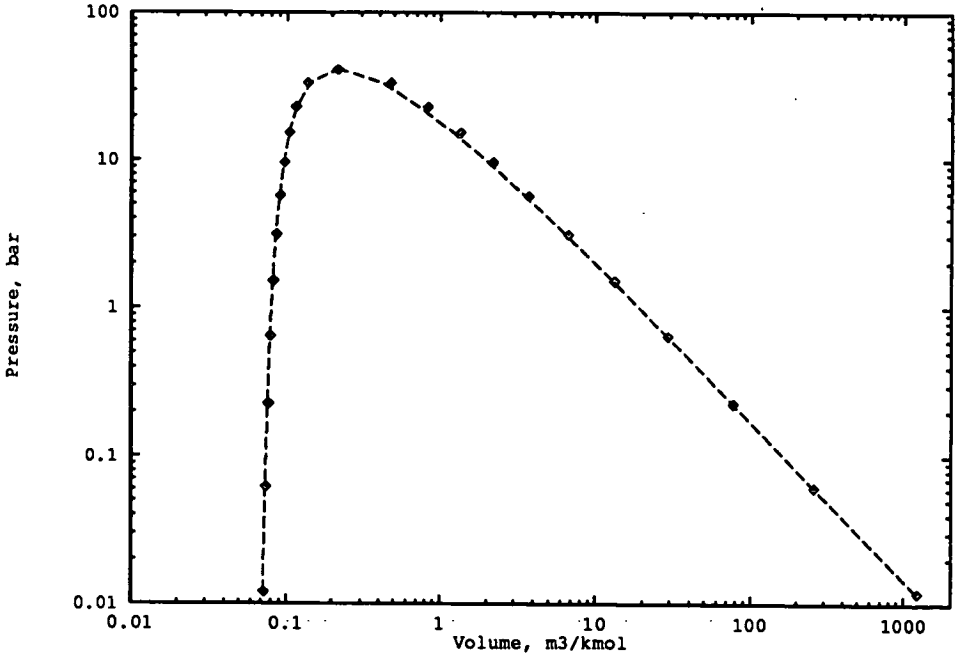

Figure 6.6: Pressure-Volume Envelope of R12

Vapour Volume Errors The predictions of vapour volume errors for each of the test fluids again followed similar paths in the error-reduced temperature plot. This is shown as Figure 6.9.

It may be seen by comparison with Figure 6.8 that the predicted saturated vapour volume was subject to much larger errors at high reduced temperatures. The intersection of the vapour error curve occurs at a reduced temperature of roughly 0.65; this corresponds with the reduced normal boiling point of most CFC fluids. The vapour volume is over-predicted at lower reduced temperatures and drastically under-predicted at high reduced temperatures. This should be borne in mind when examining the average absolute deviation in vapour volume: in contrast to the liquid volume, where the AAD gives a good estimate of the error in volume over a large temperature range, the AAD on vapour volume is much less useful.

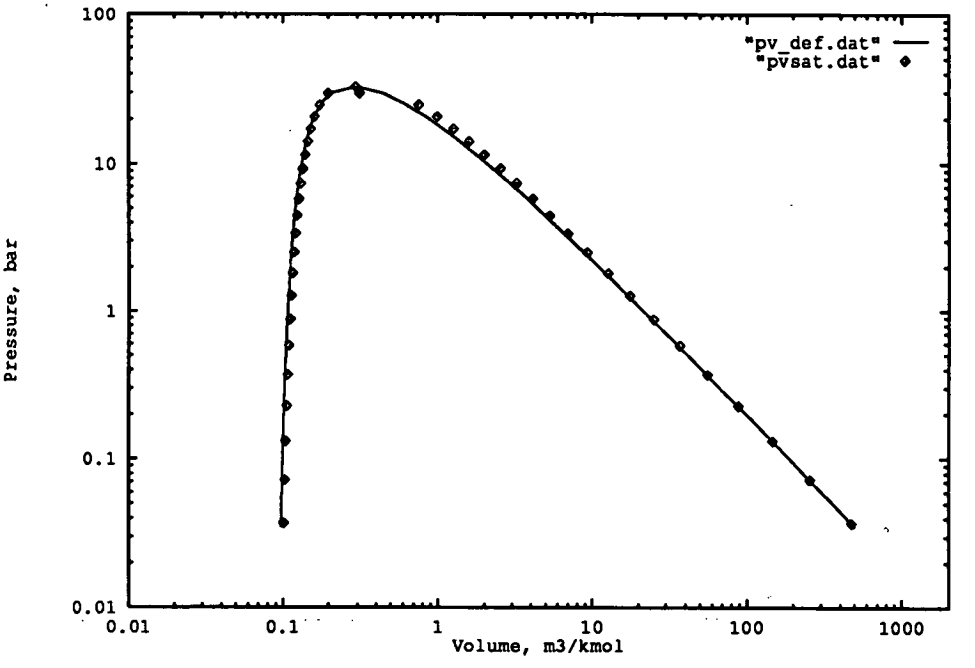

Figure 6.7: Pressure-Volume Envelope of R114

6.4.5.5 Latent Heat of Vapourisation

The latent heat was the property subject to the largest errors at high reduced temperature. This was to be expected; recall that the latent heat is given by Clapeyron's (exact) relation, Equation 6.85, which links the latent heat, volume change between phases, and rate of change of vapour pressure with respect to temperature.

$$\Delta H_{lat} = (H_V - H_L) = T\left(\frac{\partial P}{\partial T}\right)_\sigma (V_V - V_L) \tag{6.85}$$

An error in prediction of either phase volume therefore has a direct effect on the latent heat prediction, as does the shape of the vapour pressure curve. Inspection of the error curves in the previous Figures reveals that the major source of error in latent heat predictions from the CCOR equation will be the vapour volume error. One would therefore expect a correspondence in the shape of the vapour volume and latent heat error curves, and this is so. Figure 6.10 shows the latent heat error variation with reduced temperature.

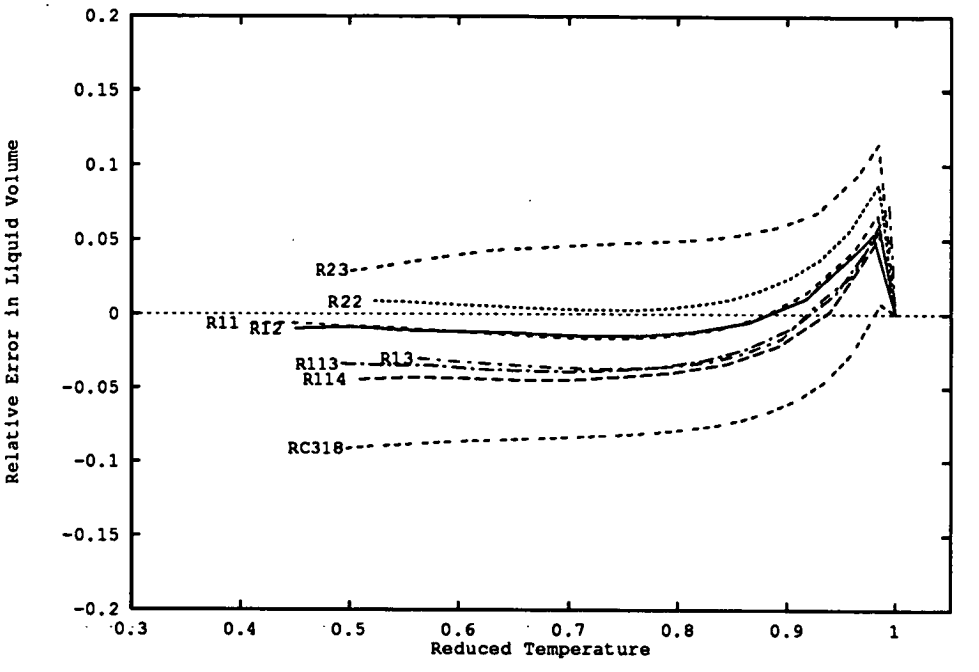

Figure 6.8: Error in Predicted Liquid Volume

The error in latent heat is much greater than that on the vapour volume at low temperatures—up to twice the size—because of the nature of the thermodynamic relations between the volumetric and energetic properties of a fluid. These are ill-conditioned equations; this explains the extremely high accuracy required of experimental data in the preparation of enthalpy tables from measurements of temperature, pressure and volume changes. Nonetheless, the latent heat is well predicted up to a reduced temperature of about 0.8. This means that the use of the CCOR equation as a source of quantitative enthalpy data for heat pump analysis need not be ruled out.

6.4.5.6 Summary of Pure Fluid Prediction Results

The average absolute deviations (AAD) in predicted properties for each fluid tested are shown in Table 6.3. This shows: the number of points used; the reduced temperature range covered, and the AAD on each property as a percentage, The reference data were taken either from the sources listed in Downing [24], or directly from the thermodynamic property tables in [82].

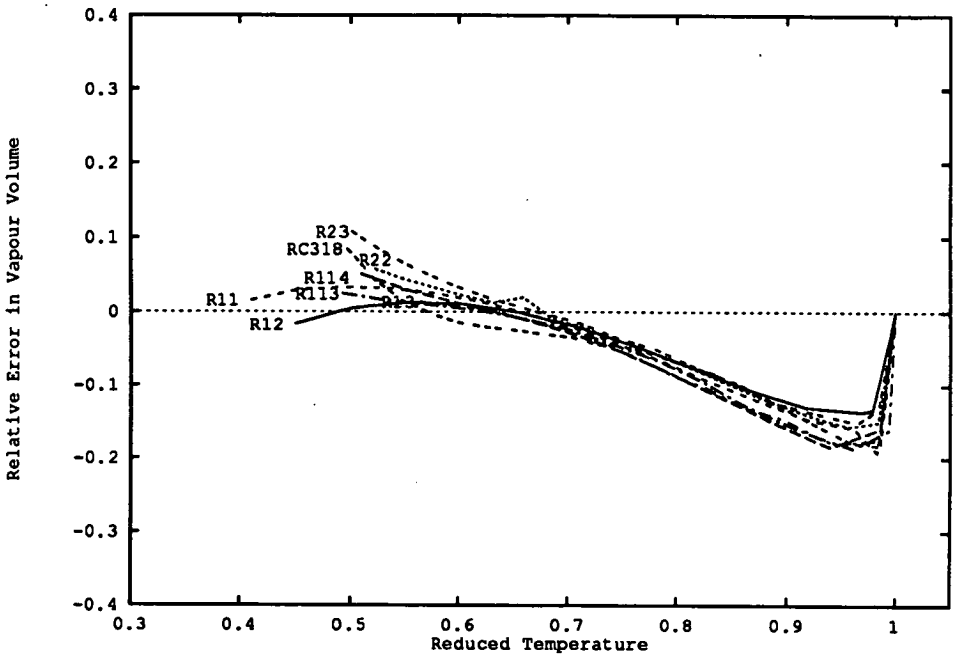

Figure 6.9: Error in Predicted Vapour Volume

The mean error in prediction of vapour pressure, taken in conjunction with the shape of the general pressure error curve Figure 6.5, demonstrates that the CCOR equation gives satisfactory quantitative prediction of vapour pressure over the range of reduced temperature studied. The liquid volume is well correlated for the smaller fluids although the spread of errors over all the test fluids is larger than for the vapour pressure. The error in liquid volume prediction for each fluid appears to be relatively invariant with temperature, suggesting that a modification to one of the invariant parameters of the equation of state might improve the prediction of this volume.

The average absolute deviation in vapour volume was considerably lower than the maximum volume errors exhibited by the equation; the skewed shape of the error curve for this property caused this. The range of temperature for R13 was deliberately restricted to $T_r > 0.56$ in order to better assess the average deviations on latent heat and vapour volume in the region where these properties were worst correlated by the CCOR equation. It can be seen that the vapour volume is not really correlated with satisfactory accuracy above a reduced temperature of 0.85. The error in latent heat is directly affected by, and similar to, the error in vapour volume prediction, for the reasons discussed above.

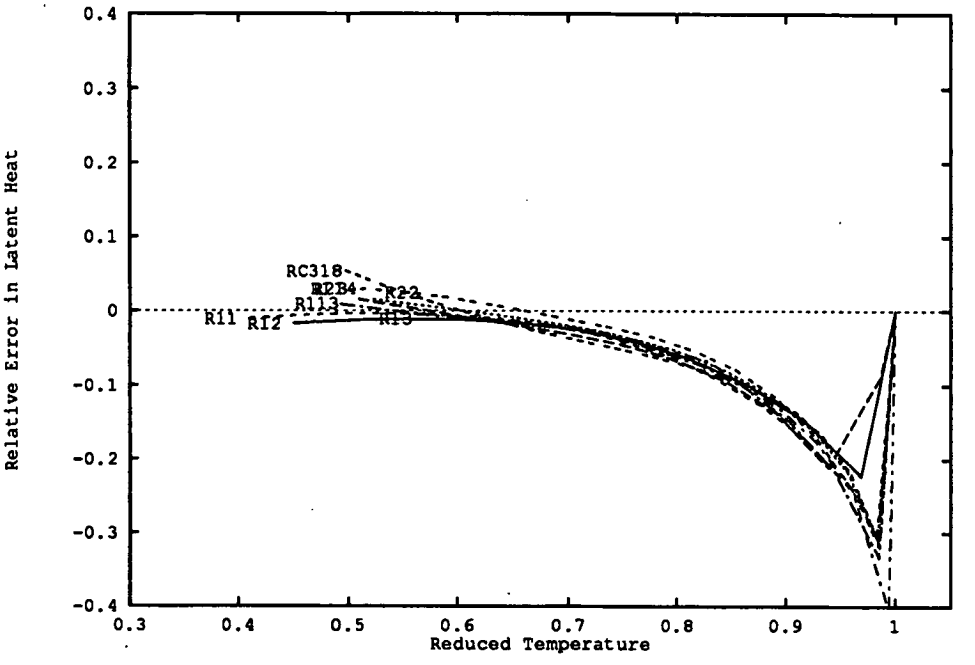

Figure 6.10: Error in Predicted Latent Heat of Vapourisation

It should be borne in mind that the reference data themselves may be partly responsible for the large apparent errors in vapour volume prediction; the data tables quoted in some of the sources may contain calculated rather than directly measured data. No indication is given of the accuracy or nature of many of the data quoted in Perry, for example. Near the critical point it is notoriously difficult to obtain accurate data because the fluid properties exhibit rapid rates of change as the critical point is approached. This in itself does not constitute an explanation of the clear deviation in vapour volume, which starts at a reduced temperature of about 0.8 and is evidently an inherent characteristic of the equation.

In the critical region the CCOR equation differs from the more complex CSD equation, which cannot be used much above a reduced temperature of 0.95: all fluids obeying the CSD equation of state must have a critical compressibility of 0.3516. The CSD equation *overpredicts* latent heat at high reduced temperatures, because its critical point is higher than that of a real fluid. The vapour phase volume predicted by the CSD equation therefore decreases more slowly in the true near-critical region than it must to meet the true critical point. This is demonstrated by Table 6.4, which shows the vapour pressure and latent heat of R12 over the temperature range 90 °C–110 °C, *i.e.*

Fluid	Range of T_r	N_{pts}	AAD-(P)	AAD V_L	AAD-V_V	AAD-(ΔH)
R11(CCl_3F)	0.41–1.0	16	1.5	1.6	6.1	7.0
R12(CCl_2F_2)	0.45–1.0	15	0.8	1.6	5.4	5.6
R13($CClF_3$)	0.56–1.0	15	1.5	3.1	7.7	8.7
R22($CHClF_2$)	0.52–1.0	18	1.8	1.5	6.6	6.8
R23(CHF_3)	0.50–1.0	16	2.6	5.0	7.1	7.3
R113(CCl_2FCClF_2)	0.49–1.0	15	1.1	3.1	6.6	7.3
R114($CClF_2CClF_2$)	0.50–1.0	14	1.8	3.5	7.3	6.0
RC318(C_4F_8)	0.50–1.0	20	1.0	6.9	7.0	7.6
MEAN	—	—	1.5	3.3	6.7	7.0

Table 6.3: Summary of Errors in Prediction of CFC Thermodynamic Properties

a reduced temperature range of 0.94–0.99. In this table the predictions of the CCOR and CSD equations are compared against the same set of reference data used in the earlier comparison work. The agreement of vapour pressure prediction by the CCOR equation with the reference data is excellent, whereas the CSD equation underpredicts the vapour pressure in this region of reduced temperature. Whereas the CCOR equation underpredicts the latent heat at 100 °C by 22%, the CSD equation overpredicts by 12%. At 105 °C the errors in latent heat from both equations' predictions have the same magnitude (25%) but opposite signs, and at 110 °C—two degrees away from the critical point—the CSD equation has become far less accurate than the CCOR equation.

	CCOR		CSD		Reference	
T	P	λ	P	λ	P	λ
°C	bar	kJ/kg	bar	kJ/kg	bar	kJ/kg
90	28.1	65.7	27.3	82.3	27.9	80.0
95	30.8	57.5	28.9	76.0	30.6	71.7
100	33.6	48.1	32.6	69.0	33.4	61.8
105	36.3	36.6	35.5	61.2	36.5	49.1
110	39.8	19.4	38.5	52.2	39.8	28.6

Table 6.4: Comparison of CCOR and CSD Equations for R12 near the Critical Point

The most likely cause of the deviations in vapour volume and latent heat is the constraint of the critical point on the equation of state; this has been shown [71] to cause distortion of the phase envelope below the critical point, as a direct consequence of the non-analytic behaviour of all fluids in the near-critical region. The accurate description of the vapour pressure and critical point by the CCOR equation has therefore been won at the cost of poor vapour phase performance in the sub-critical region. This may be an inevitable tradeoff; after all, it is quite remarkable that a fluid's volumetric behaviour can be described with *any* degree of quantitative accuracy by a simple family of cubic polynomial functions!

6.4.5.7 Parameter Optimisation

Optimisation Strategy The error curves obtained from the comparison of the generalised CCOR equation's property prediction showed that there was scope for improvement of the accuracy of the equation's phase volume prediction. The strong similarity between the variations of errors with reduced temperature across the range of test fluids suggested a possible method of improvement: an optimisation of the temperature-dependent parameters of the equation of state. This would be carried out by determination of the optimum values of the $\alpha(T_r), \gamma(T_r)$ functions over a range of reduced temperatures. An alternative strategy would be to attempt to discover a temperature variation function for some or all of the normally invariant equation parameters b, d, c^R which would yield improved property prediction. Of these parameters, only b would be an obvious candidate, as it represents the closest approach distance of molecules, which is a decreasing function of temperature (see Morrison [70]).

The author chose to restrict the optimisation to the functions α and γ, by analogy with the work of Leet [54] in fitting the CCOR equation to polar fluids. This provided an indication that the optimisation procedure had been tried before, with apparent success. The pursuit of other objective functions or type of functional fit to parameters would have occupied too much time; a *really* detailed exploration of the subject would justify a doctoral project in its own right.

The optimisation process was based on the need to improve the fit of predicted properties over a set of saturation temperatures; the objective function $F(\alpha, \gamma)$ for the minimisation was defined by Equation 6.86 as a straightforward sum of least squares at each temperature used.

$$F(\alpha, \gamma) = \omega_P \varepsilon_P^2 + \omega_{V_g} \varepsilon_{V_g}^2 + \omega_{V_f} \varepsilon_{V_f}^2 \tag{6.86}$$

where ω denotes a weighting factor and ε denotes a relative error in a property, that is:

$$\varepsilon_M = \frac{\text{Reference Value - Predicted Value}}{\text{Reference Value}} \tag{6.87}$$

where M denotes one of pressure P, liquid volume V_L or vapour volume V_V.

Implementation The optimisation was performed by a program written in imp80 by the author; this used a "black-box" optimisation subroutine culled from the Chemical Engineering software library to find the (α, γ) pair which minimised the objective

function at a given temperature. The subroutine used Powell's algorithm, described in Press *et al.* [89] to perform the minimisation. The objective function was evaluated by a subroutine written by the author, which solved the vapour-liquid equilibrium problem for the specified set of temperature and equation parameters. This ensured that the fundamental condition for phase equilibrium was satisfied by each guess at the optimum parameter set.

The optimisation program accepted a set of PVT data for a given fluid as input, then called the minimisation subroutine repeatedly to find a set of optimum parameter pairs. These were then fitted to functions having the same form as the defining relations Equation 6.53 and Equation 6.54, in order to find the parameters A_1, A_2, C_1, C_2. These secondary optimisations were also performed using the Powell algorithm routine, this time to minimise the functions F_α and F_γ of Equation 6.88 and Equation 6.89.

$$F_\alpha(A_1, A_2) = \sum_{i=1}^{N} \left[\frac{\alpha_{opt,i} - \alpha_{calc,i}}{\alpha_{opt,i}} \right]^2 \tag{6.88}$$

$$F_\gamma(C_1, C_2) = \sum_{i=1}^{N} \left[\frac{\gamma_{opt,i} - \gamma_{calc,i}}{\gamma_{opt,i}} \right]^2 \tag{6.89}$$

This procedure was tested on some common CFC fluids with equal weight on all three properties—pressure, liquid volume and vapour volume—to assess its effectiveness in reducing the major errors. By way of comparison the program was also run with a zero vapour volume weight, to assess the gain in accuracy of vapour pressure and liquid volume prediction. The parameters found by the optimisation program are summarised in Table 6.5; the statistical performance of each optimisation is summarised in Table 6.6. In both of these tables the weighting factors are indicated by "ALL" for equal weight on all three properties, or "NOVAP" for the optimisation omitting vapour volume from the objective function.

Table 6.6 shows the relative error ε on each of the pressure, liquid and vapour volume predictions, averaged over the whole dataset for each fluid. The standard deviations of these errors are included for comparison. The prediction of pressure and liquid volume error was improved by the optimization when volume was omitted: the inclusion of the volume error made the pressure prediction worse: the increase in liquid volume prediction error was too small to be significant. Although the mean vapour volume error appears small, this is deceptive; the error curves exhibited by the results obtained using

Fluid	Weighting	N_{pts}	T_r Range	A_1	A_2	C_1	C_2
R11	ALL	24	0.55–0.96	3.09978	0.146132	4.11784	0.414642
	NOVAP	24	0.55–0.96	3.37653	0.205559	4.92562	0.340507
R12	ALL	26	0.52–1.0	3.265092	0.181905	4.96341	0.337086
	NOVAP	26	0.52–1.0	3.51031	0.238701	6.20857	0.264297
R22	ALL	22	0.60–0.89	3.366133	0.153636	4.54314	0.372787
	NOVAP	22	0.60–0.89	3.75479	0.232326	5.62640	0.295968
R113	ALL	17	0.55–0.86	3.67085	0.202143	4.84906	0.354964
	NOVAP	17	0.55–0.86	3.94129	0.260625	5.49038	0.309904
R114	ALL	24	0.66–0.94	3.02348	0.086189	3.65556	0.482918
	NOVAP	24	0.62–0.94	3.74347	0.223053	5.90605	0.288647
RC318	ALL	31	0.65–0.96 3.68247	0.188259	4.93781	0.347980	
	NOVAP	31	0.65–0.96	4.32019	0.307902	7.984119	0.209824

Table 6.5: Summary of Parameter Optimisation Results

Fluid	Weighting	ε_P %	σ_P bar	ε_{V_f} %	σ_{V_f} m^3/kmol	ε_{V_g} %	σ_{V_g} m^3/kmol
R11	ALL	2.7	0.71	0.5	0.001	2.1	0.162
	NOVAP	0.0	0.00	0.0	0.000	5.6	0.344
R12	ALL	3.0	0.79	0.7	0.001	2.3	0.106
	NOVAP	0.0	0.00	0.0	0.000	6.4	0.227
R22	ALL	2.8	0.47	0.4	0.001	2.3	0.102
	NOVAP	0.0	0.00	0.0	0.000	5.6	0.223
R113	ALL	2.5	0.24	0.3	0.001	2.1	0.366
	NOVAP	0.0	0.00	0.0	0.000	5.0	0.763
R114	ALL	4.2	0.60	0.8	0.001	3.3	0.173
	NOVAP	0.0	0.00	0.0	0.00	8.6	0.389
RC318	ALL	3.2	0.47	0.6	0.001	2.5	0.150
	NOVAP	0.0	0.00	0.0	0.00	6.7	0.332

Table 6.6: Summary of Parameter Optimisation Statistics

the optimised parameter set will be discussed below. In this discussion, two example fluids (R12 and R114) will be discussed in detail; the general conclusions will be drawn in Section 6.4.5.8. These two example fluids were chosen because of the shapes of their phase envelopes: this has been previously discussed on page 327.

Example 1: R12 Optimisation The fits of the optimised parameter sets, found for R12 with equal weight on all parameters, to the fitting functions Equation 6.53 and Equation 6.54 are shown in Figure 6.11 and Figure 6.12. These figures, plots of the values of the α and γ functions against reduced temperature, show that the two-tier optimisation process succeeded in fitting a good approximation to the optimum data sets. The plots also show the variation of α and γ which would be obtained by

using the *default* correlations for the parameters A_1, A_2, C_1, C_2 given in the source literature. It is clear that the optimisation procedure had only a small effect on the equation of state; the two function plots are close to co-incident for much of the reduced temperature range.

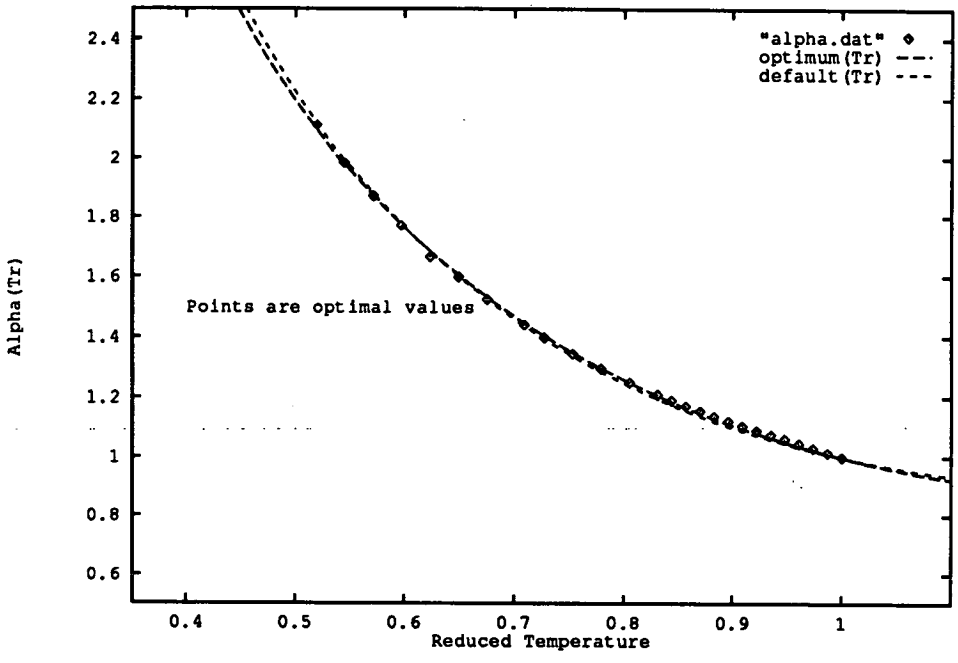

Figure 6.11: Variation of the α Function of R12 with Reduced Temperature

The error curves for the properties of R12, calculated from the optimised parameter set listed in Table 6.5, are shown in Figures 6.13–6.16, which take the same format as those described in Section 6.4.5.6. These show that the optimisation process succeeded in improving only the liquid volume prediction with any degree of consistency: the vapour volume prediction was slightly improved in the near-critical region but *worsened* below the normal boiling point. The vapour pressure error was also increased over most of the range covered, especially at the lower end of the reduced temperature scale. The latent heat prediction was also worsened by the optimisation over the *useful* reduced temperature range (pressure below 25 bar implies reduced temperature less than 0.9 for R12). The benefits of the optimisation results in this case were not worth the unwanted side-effects. An illustration of this is provided by Figure 6.17, which shows the phase envelope of R12, plotted on the pressure-enthalpy chart. This chart shows: the reference data (as points); the phase boundary, predicted from the default parameters (key **ph_def.dat**), and the envelope obtained from the optimised parameters (key **ph_opt.dat**). The effect of the optimisation was to shrink the envelope

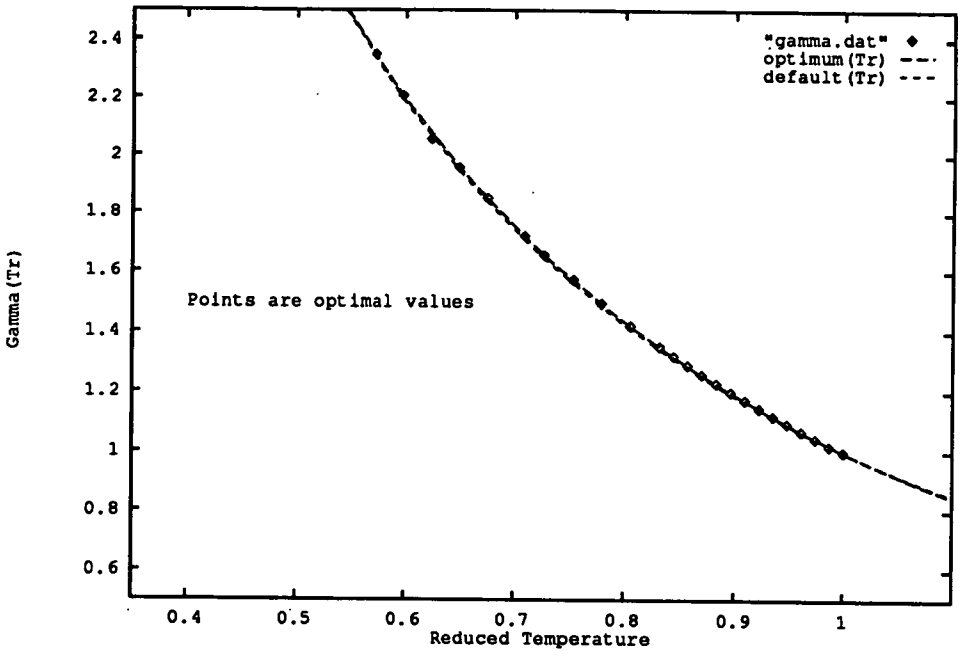

Figure 6.12: Variation of the γ Function of R12 with Reduced Temperature

and alter its shape further away from the reference data. These data were plotted on the basis of equal enthalpies of saturated liquid at 0 °C: the shift in critical point is evident, although not major for this fluid.

The data resulting from the optimisation performed using no vapour volume error have not been plotted for reasons of space: the plots merely reveal that the optimum parameters in such a scenario are very close to those given by the default correlations. The use of the parameters obtained from this case study produced error curves which were practically identical to those obtained from the default parameters; the phase envelope on the pressure-enthalpy chart was also indistinguishable from that given by the default parameters.

Example 2: R114 Optimisation The fit of parameters for R114 was carried out over a smaller reduced temperature range than for R12, and this had a noticeable effect on the shapes of the optimum parameter functions. The α and γ curves for R114 are plotted in Figure 6.18 and Figure 6.19, which follow the format of Figure 6.11 and Figure 6.12. The optimised-parameter curve of R114 clearly deviates from the default

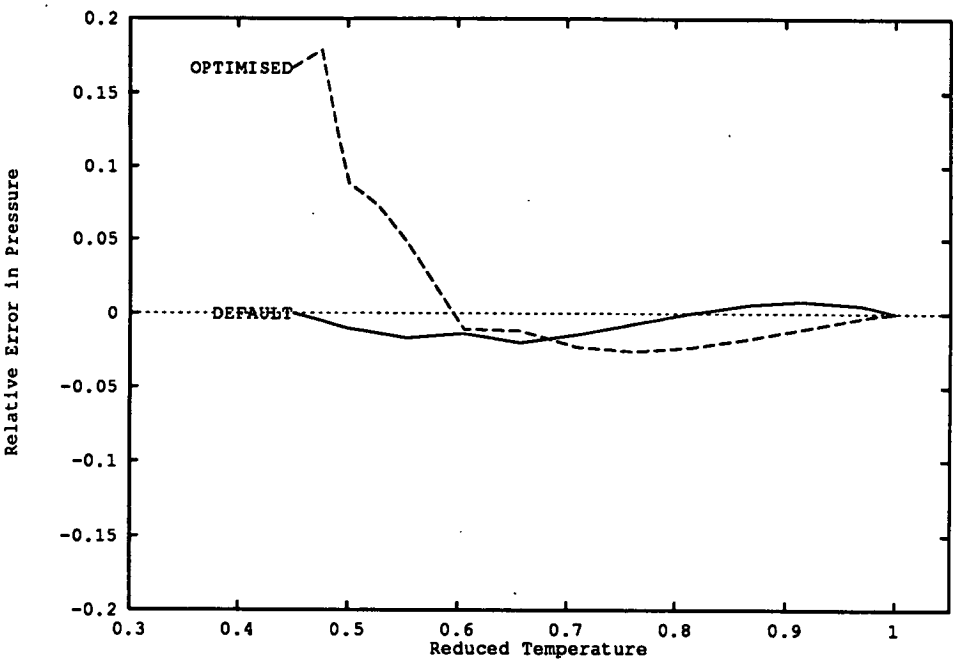

Figure 6.13: Error on Predicted R12 Vapour Pressure from Optimised CCOR Parameters

parameter curve away from the optimised region.

The effects of this deviation from the default curves (which give reasonable predictions at low reduced temperatures) are obvious from inspection of Figures 6.20–6.23, the error curve plots from the optimised parameter sets. The vapour pressures predicted by the equation at low reduced temperatures were far higher than the actual pressures: this explains the under-prediction of vapour volume in the same region. The only property to be consistently improved, as before, was the liquid volume: the latent heat prediction was especially bad for this case. Finally, the shape of the phase envelope was distorted by use of these parameters. In Figure 6.24 the three sets of data plotted—reference, default and optimum results—were assigned the same critical enthalpy. The default parameters gave an acceptable match to the reference envelope over most of the range; the optimised parameter set distorted the envelope and changed the slope of the liquid branch ($\partial P/\partial h_f$). It is clear that, for this combination of fluid, input data set and objective function, the "optimisation" was counter-productive. The second optimisation (with no vapour volume error in the objective function) gave the same general result as for R12: no improvement of the vapour phase, some small improvement

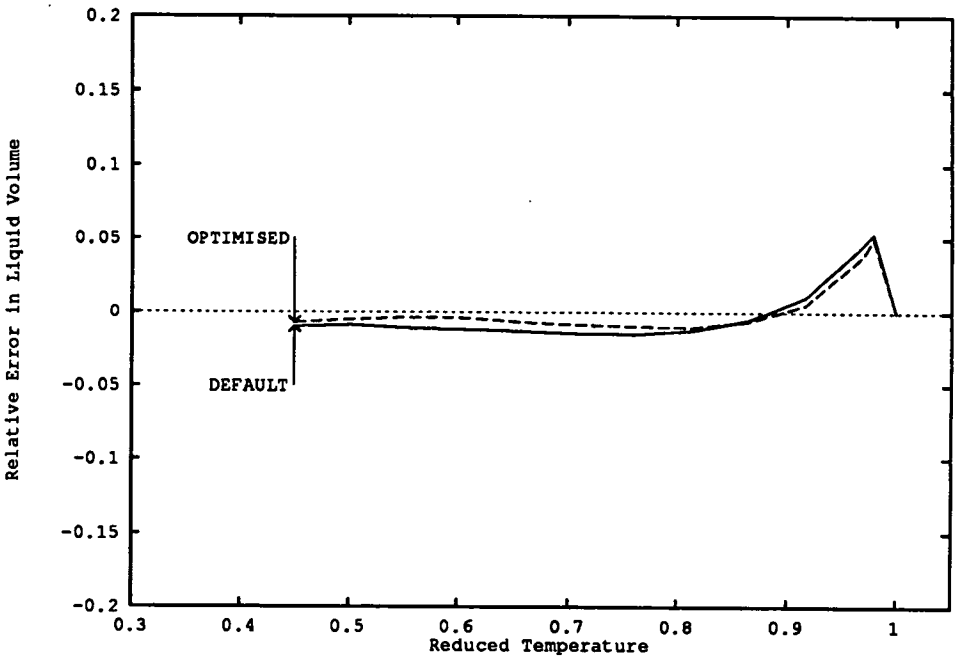

Figure 6.14: Error on Predicted R12 Liquid Volume from Optimised CCOR Parameters

in vapour pressure and liquid volume but no change in the enthalpy prediction.

Alternative Optimization Method The results discussed above were all generated using the original optimisation program, which used Powell's method to minimise the objective function. A second strategy was also tried, written using the author's own C language subroutines. This method relied on the fact that an extremum of the objective function would coincide with the condition of Equation 6.90: all first derivatives of the function with respect to the parameter set would vanish at an extremum.

$$\nabla F(\underline{x}^{\circ}) \equiv \underline{0} \tag{6.90}$$

where F represents the objective function and x° the vector of parameters which yield an extremum. The basis of the method, then, was to set up and solve (by numerical methods) the equations:

$$f_1(\alpha,\gamma) = \left(\frac{\partial F}{\partial \alpha}\right)_{\gamma} = 0 \tag{6.91}$$

$$f_2(\alpha,\gamma) = \left(\frac{\partial F}{\partial \gamma}\right)_{\alpha} = 0 \tag{6.92}$$

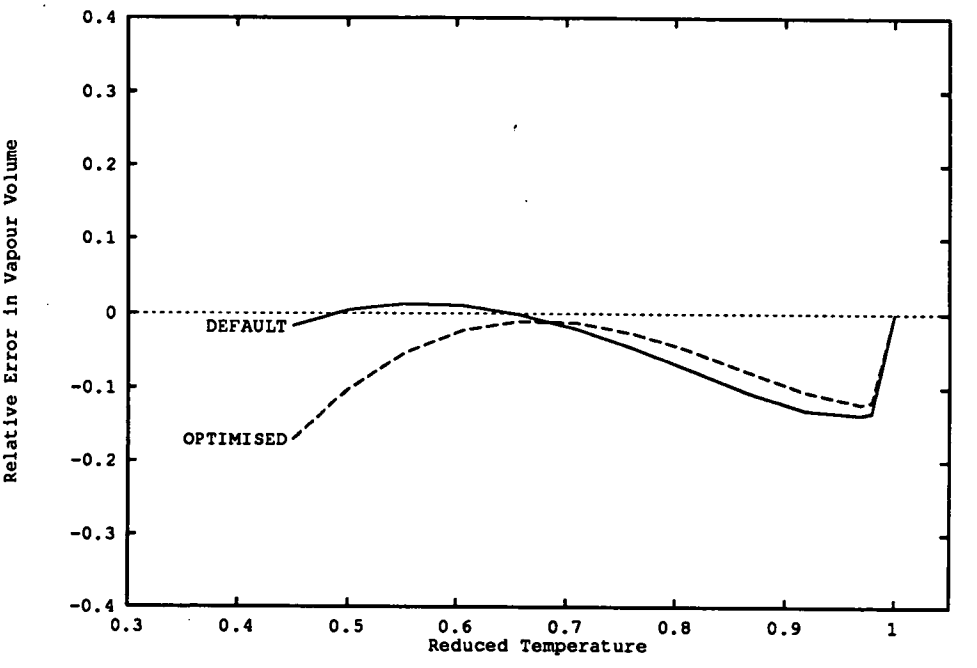

Figure 6.15: Error on Predicted R12 Vapour Volume from Optimised CCOR Parameters

The implementation of this method used the Newton-Raphson algorithm with numerical derivative evaluation to solve this equation system: little subtlety was employed in the coding, beyond checking at each iteration for a stationary function value. The results yielded by this method agreed with the original work: it proved impossible to obtain a real improvement in the vapour volume prediction if the liquid volume error were also included in the objective function. (By contrast, the presence of the vapour volume error did not seem to affect the liquid volume prediction to any great extent.)

The utility of this second approach was that it permitted a study of the nature of the objective function: the previous program did not give an easy indication of the existence of a true minimum. The main drawbacks of this method of minimisation are often cited [89] as its lack of discretion and its slowness. The first derivatives may vanish at a local rather than global minimum, at a maximum or saddle point; the iteration may converge with painful slowness if the minimum is flat. In this study, these drawbacks were useful: by study of the progress of an iteration it was possible to deduce much about the shape of the objective function and the effect of each of the three errors on the chances of finding a true minimum.

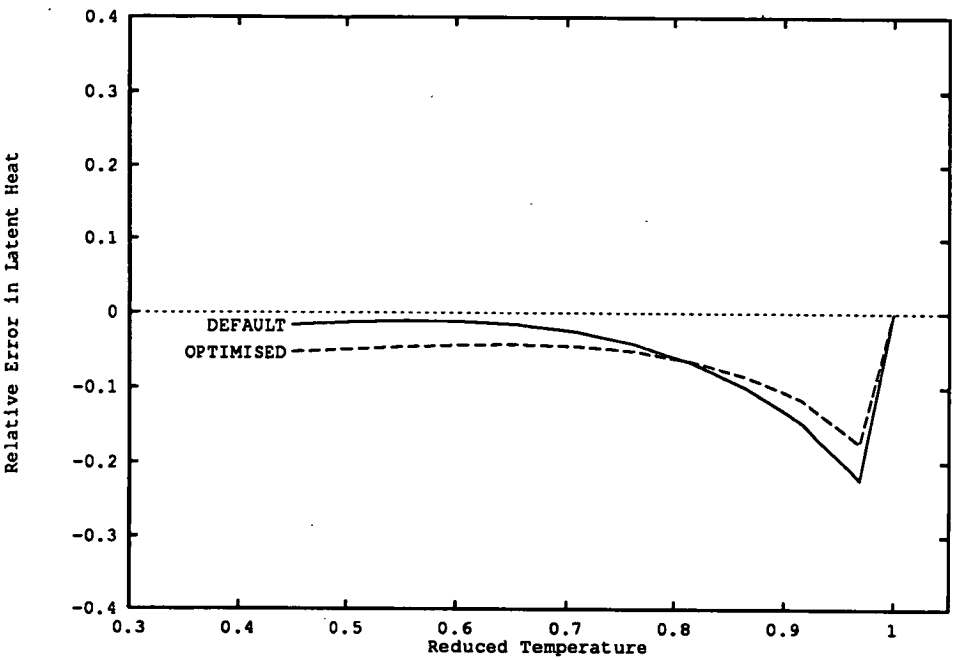

Figure 6.16: Error on Predicted R12 Latent Heat from Optimised CCOR Parameters

The iteration would always find a minimum if pressure and liquid volume error alone were used in the objective function. The addition of the vapour volume error however seemed to alter the character of the objective function, especially at high reduced temperatures. In these latter cases, one or both of the gradient functions would not converge to a root: the objective function appeared to be almost but not quite flat. If sufficient proportion of the vapour volume error were fed into the objective function— typically if equal weighting were used— then the iteration would stray away from the feasible region into a space where there existed only one real volume root of the equation of state, causing failure of the calculation. The typical behaviour of the iteration is described in Table 6.7 for archetypal objective functions to illustrate more clearly this point. In Table 6.7, the errors are categorised into three classes: "BETTER", signifying a deterioration from the performance of the default; "SAME", signifying little or no deviation from the error curves resulting from the use of the default parameters, and "WORSE", indicating an improvement in prediction as a result of the optimisation.

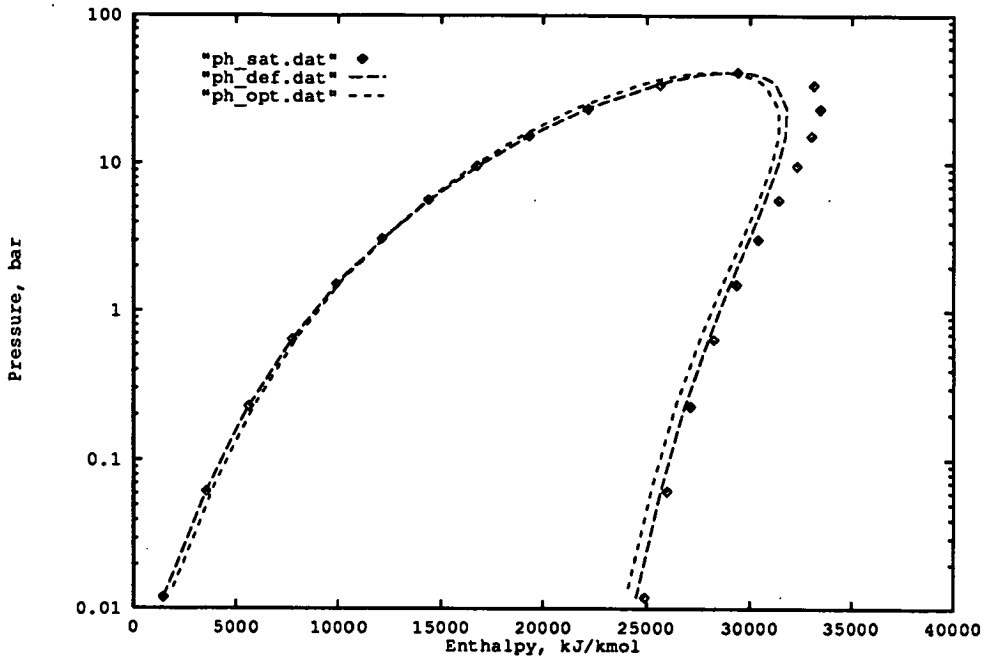

Figure 6.17: Phase Envelope of R12 in Pressure-Enthalpy Co-ordinates

6.4.5.8 Discussion of Optimisation Results

The optimisation procedure described in Section 6.4.5.7 did not seem to yield any real improvement in property prediction for the fluids studied: although only two fluids' properties were explained in detail here, the rest of the fluids investigated gave very similar results. There may be several reasons for this: some of these might have been eliminated given sufficient time, but this was not possible in the context of the

Weighted	Effect on Errors		
	P	v_f	v_g
P only	BETTER	SAME	SAME
v_f only	WORSE	BETTER	WORSE
v_g only	SAME	SAME	WORSE
P, v_f	BETTER	BETTER	SAME
$P v_g$	BETTER	SAME	WORSE
v_f, v_g	WORSE	BETTER	WORSE
P, v_f, v_g	BETTER	BETTER	SAME

Table 6.7: Effect of Objective Function Weights on Optimisation Results

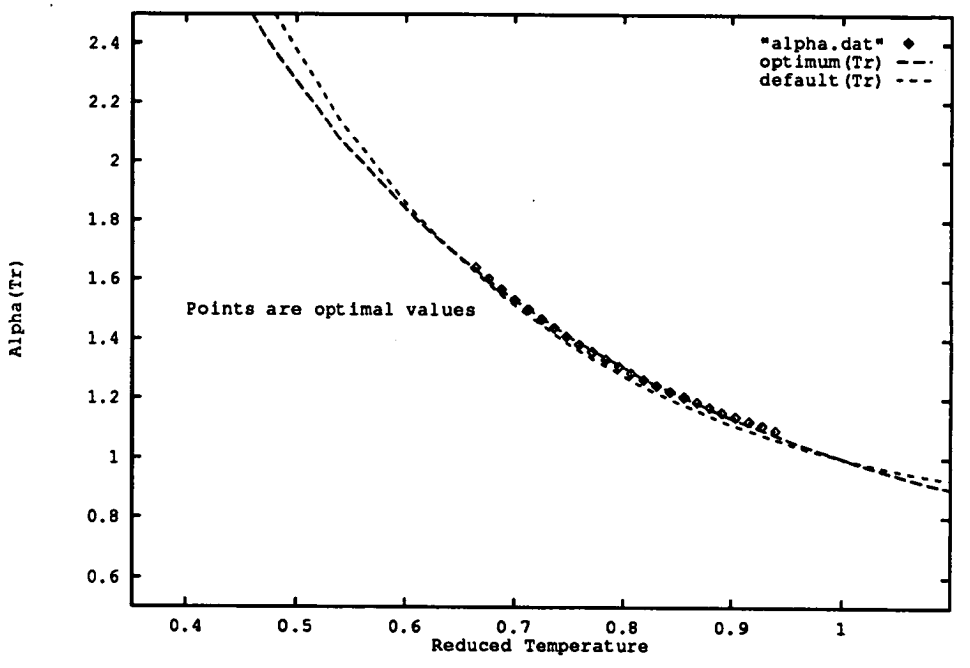

Figure 6.18: Variation of the α Function of R114 with Reduced Temperature

project. The main conclusions to be drawn, both from the original results and the work summarised in Table 6.7, are as follows:

- The equation parameters α and γ may be optimised to give improved prediction of one or both of the vapour pressure and saturated liquid volume.
- The vapour volume prediction at high reduced temperatures could not be improved by the optimisation scheme used.
- In order to obtain parameters which gave vapour volumes no worse than those given by the default parameters, the optimisation had to include both pressure and liquid volume. All other combinations made matters worse.

Faced with the intransigent behaviour of the equation with regard to vapour phase prediction, the conclusion is that the form of the equation must be the stumbling block. A cursory attempt was made, using an extension of the vanishing-gradient principle described in Section 6.4.5.7, to fit a third equation parameter to a temperature function. The parameter used was b, the closest approach parameter. Although it proved possible

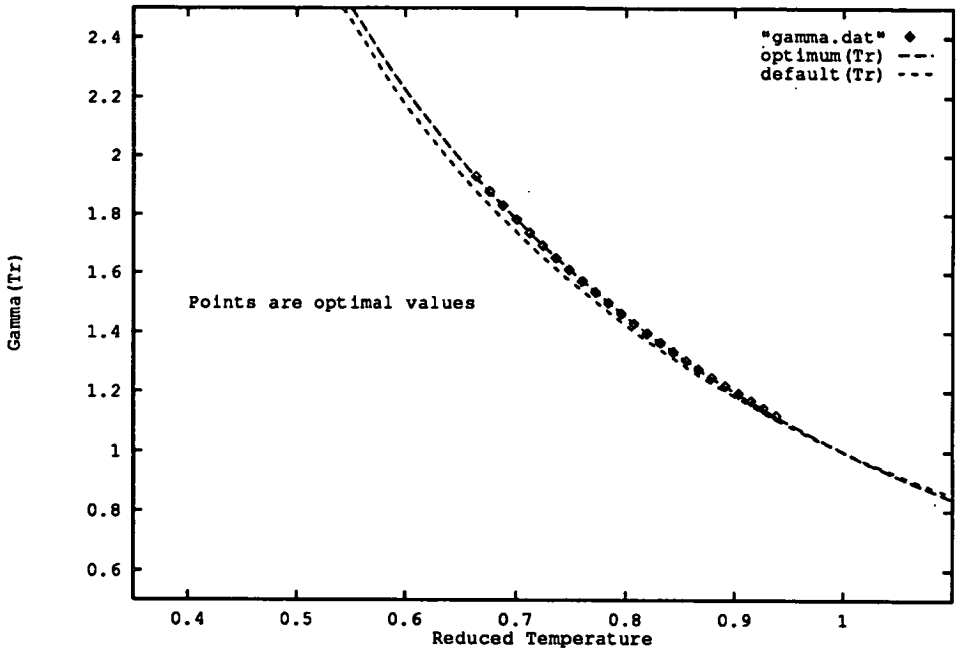

Figure 6.19: Variation of the γ Function of R114 with Reduced Temperature

to obtain a minimum if vapour volume were omitted from the objective function, the optimisation was not successful at improving the vapour volume prediction in general. The only exception was that, were pressure and liquid volume both omitted from the objective function, then this would yield a better vapour volume fit than the default case. This result was useless: the predicted vapour pressures were very poor in that case. No further attempts were made to explore the possibilities of the remaining equation parameter d, as it was suspected this would be futile.

To summarize: the equation of state has its strengths in liquid phase property prediction, where it gives good prediction of liquid volume and vapour pressure to within a few percent over a wide range of reduced temperature. This was not surprising: the original developers of the equation, Kim [45] based the equation on a theory of molecular behaviour at high densities with the specific aim of improving the liquid phase predictions. The vapour phase volume prediction seems to be immune to cajolery; this probably indicates that the only method of improvement would be the addition of extra volume terms on the right-hand side of the equation of state. This would of course lead to the development of an entirely new equation (non-cubic), and was not in the scope of the project work.

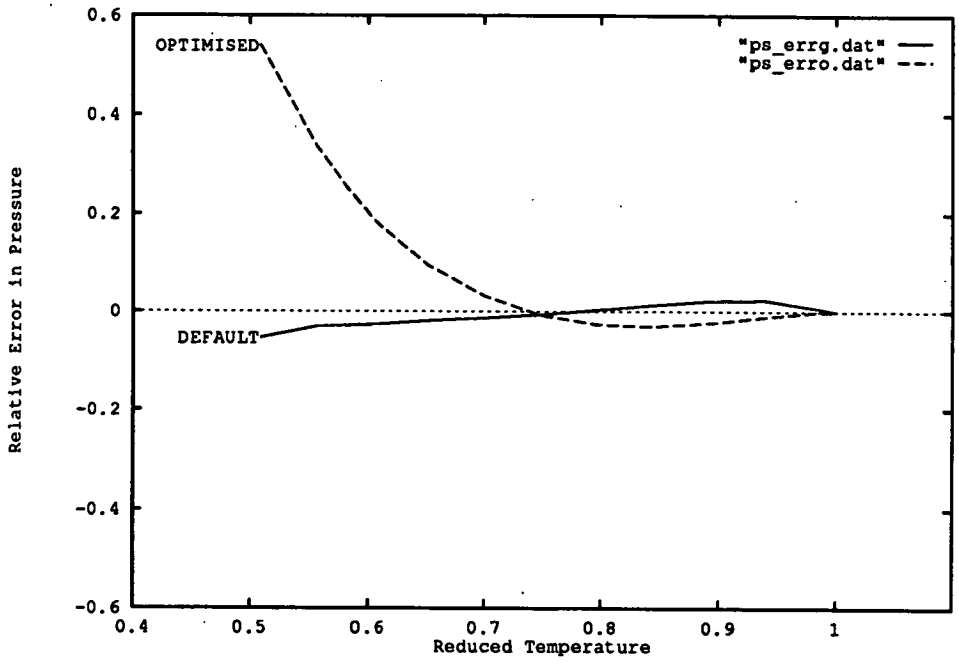

Figure 6.20: Error on Predicted R114 Vapour Pressure from Optimised CCOR Parameters

6.4.6 Mixture Results

6.4.6.1 Introduction

In this Section are presented the results of the authors' exploration of the prediction of properties of binary refrigerant mixtures. This was intended to assess the ability of the CCOR equation to predict vapour-liquid equilibrium data of refrigerant mixtures without recourse to parameter fitting. This would then give an indication of the likely accuracy of predictions made about systems for which no experimental data were available.

Sources of Reference Data There exist in the literature relatively few articles reporting experimental measurements on binary refrigerant mixture systems; although the number of publications has increased rapidly in the recent past. There were

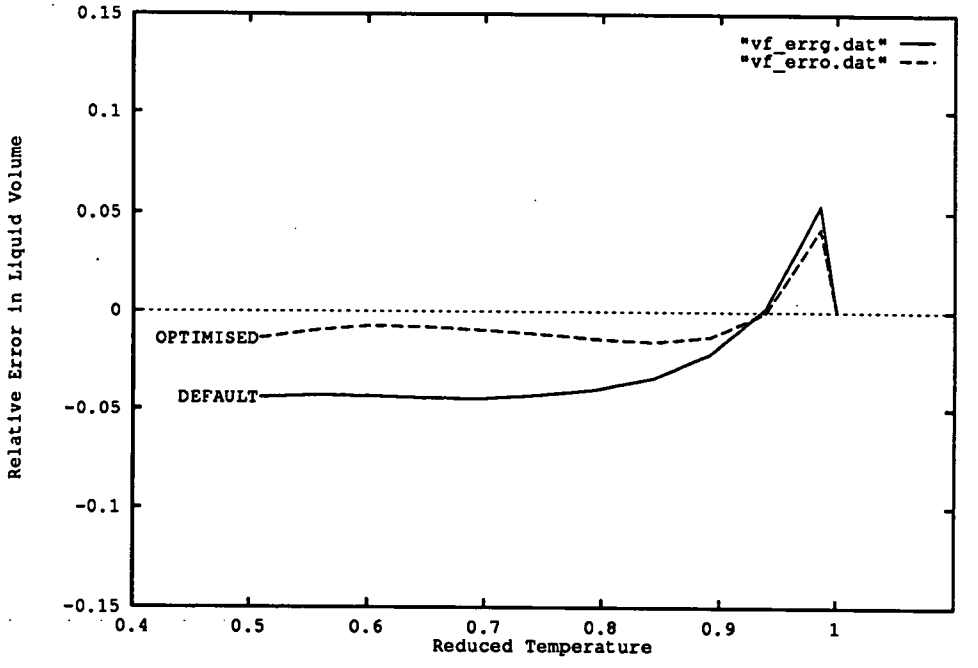

Figure 6.21: Error on Predicted R114 Liquid Volume from Optimised CCOR Parameters

nonetheless too many to include in this Thesis: accordingly a representative subset of fluid pairs was analysed, and the results are presented in the following text. In order to demonstrate the ability of the CCOR equation to cope with a variety of fluids, the mixtures chosen included near-ideal pairs, supercritical mixtures and azeotropes. To the best of the author's knowledge, most of the recent publications of data on refrigerant mixture VLE have been included in this study. Further information on the sources of experimental data is given in the following text and in Chapter 2. The data sources quoted contain information on more fluid pairs and could be consulted for reference were such data of interest to the reader.

Calculation Method The calculations were performed using the author's property subroutines written in C; these represented the most advanced version of the source code. The key to the calculations was the binary VLE algorithm developed by the author and described as Algorithm 6.5 in Section 6.4.4. This enabled exploration of the predictive ability of the equation in regions where the more volatile component was above its critical temperature. The program written to implement the equilibrium solution allowed the specification of arbitrary values for the two interaction constants

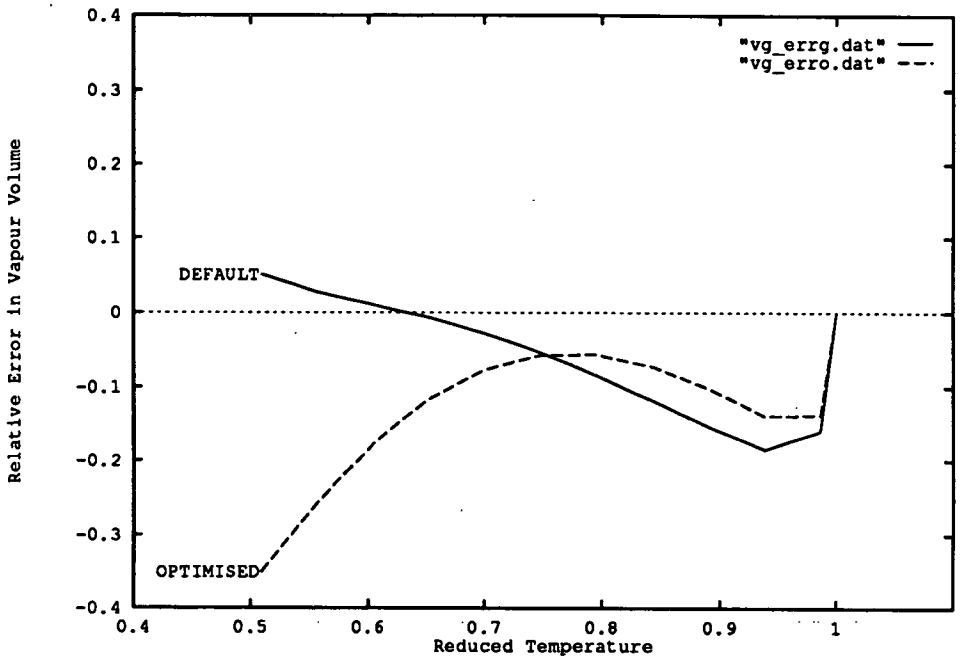

Figure 6.22: Error on Predicted R114 Vapour Volume from Optimised CCOR Parameters

k_a, k_c associated with the CCOR equation. This facility was used to examine the effect of each of these adjustable parameters on the predictions of pressure, volume and equilibrium composition. No attempt was made to determine an optimum pair of interaction constants for each fluid; time was too scarce to permit this. It will however be demonstrated in the text that there should exist an optimum (k_a, k_c) pair for each set of equilibrium data; a specimen optimisation was performed for the R22/R11 system as a demonstration.

Presentation of Results The bulk of the results presented here are in graphical form: this was a compact way of presenting large groups of data, which offered a quick comparison between the results of the author's work and that of other workers. The fit of an equation's predictions over a range of independent variables is much easier to assess in this way than by comparison of mean errors; this was demonstrated in Section 6.4.5.

The graphs presented follow straightforward notational conventions: experimental mea-

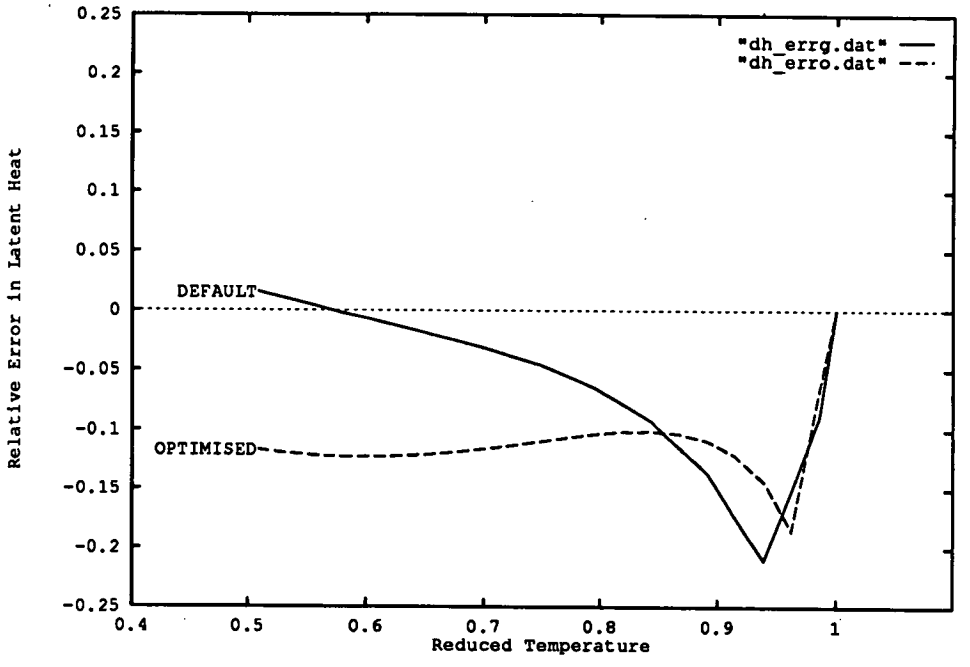

Figure 6.23: Error on Predicted R114 Latent Heat from Optimised CCOR Parameters

surements are plotted as points, predictions of an equation of state are plotted as lines. Many of the graphs show several datasets to enable comparison of predictions: where possible these have been distinguished by unique text labels in the body of the figure.

The data sources used for this study differed in the presentation of measurements: some workers measured compositions in both phases; others only measured liquid phase properties. All of the data sources contain measurements of temperature and pressure but only some contain measurements of specific volumes. The average absolute deviation (AAD) between predicted and measured datasets is given where appropriate as an indication of the accuracy of fit of the equation of state.

6.4.6.2 The R12/R114 System

This system has been studied by Kubota and by Ström [51, 113]; Kubota's paper reports isothermal data, while Ström's work dealt with the isobaric equilibrium. In each case measurements were made of the liquid and vapour phase compositions for a

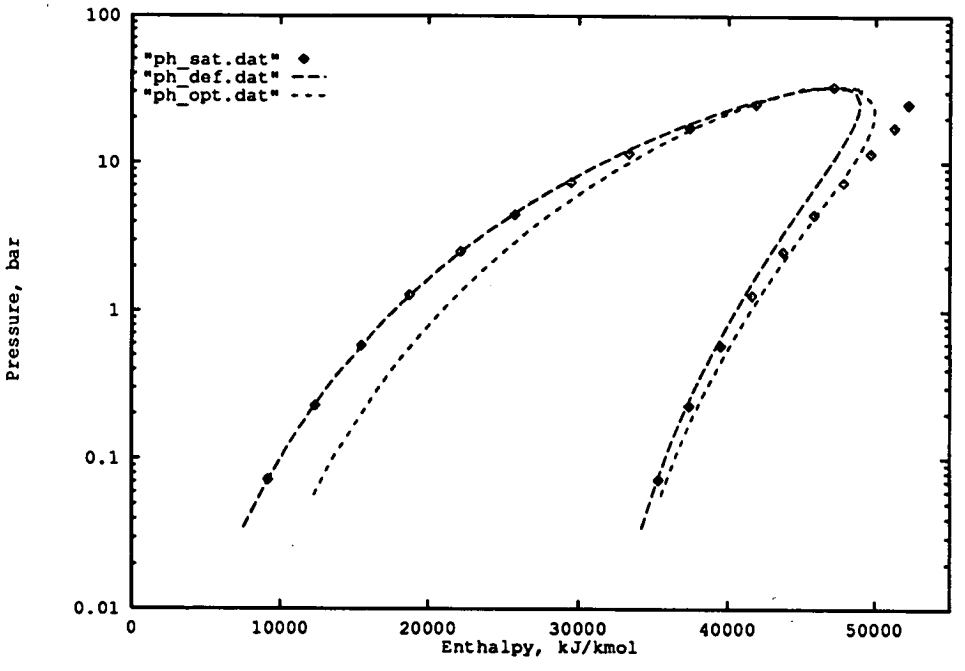

Figure 6.24: Phase Envelope of R114 in Pressure-Enthalpy Co-ordinates

given temperature and pressure.

Comparison with Kubota's Data The CCOR equation was used with both interaction constants set to zero to generate sets of data from the same fixed conditions used by Kubota: a range of liquid mole fractions at temperatures of 10 °C and 40 °C. The results are plotted as boiling-point diagrams in Figure 6.25. This indicates a good fit to the phase envelope by the CCOR equation predictions at both temperatures.

Comparison with Ström's Data The source gives tabulated measurements of temperature, liquid mol fraction and vapour mol fraction over the whole composition range at several pressures. The predicted data were generated in two ways: firstly by performing a bubble point calculation using the measured liquid mol fraction and pressure as inputs, secondly by performing an isothermal phase split calculation from the measured temperature and pressure. This allowed assessment of the sensitivity of the results from each calculation method.

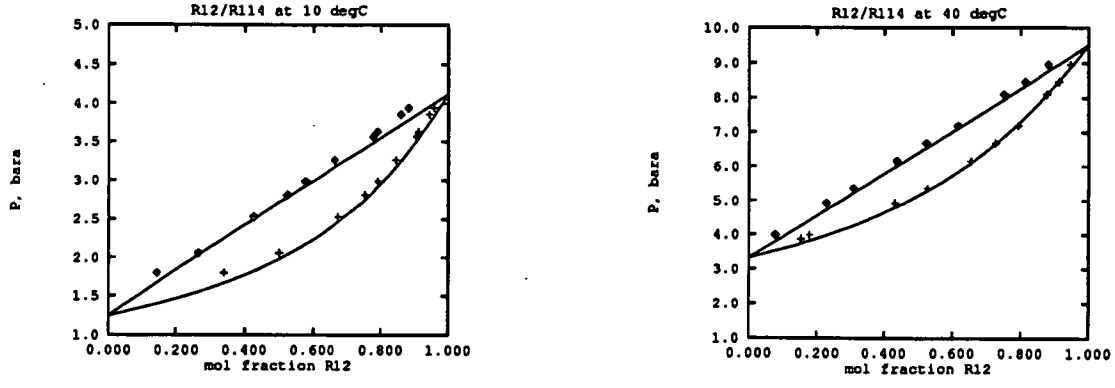

Figure 6.25: The R12/R114 system at 10 °C and 40 °C

The boiling-point diagrams for R12/R114 under 3.5 and 8.85 bar are shown in Figure 6.26. This indicates a good correspondence between the predictions of the CCOR equation and the measured data. Ström's paper comments that this system is nearly ideal; this explains the quality of the prediction.

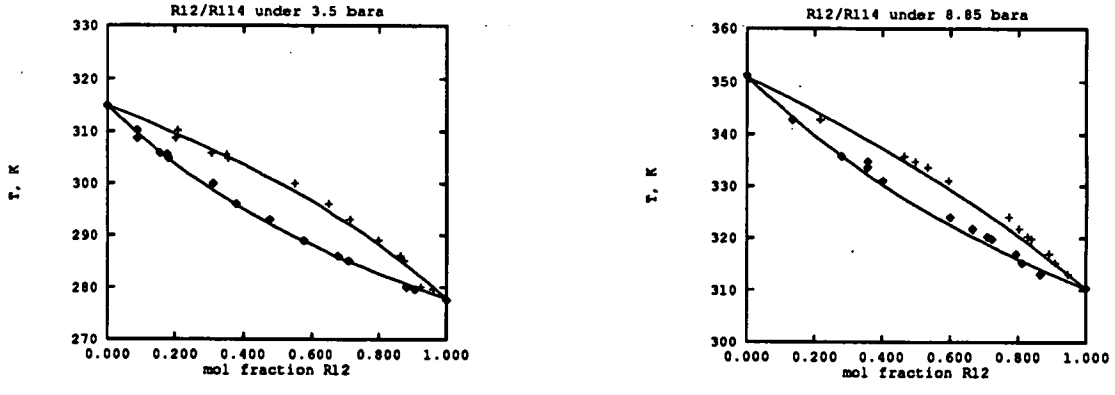

Figure 6.26: The R12/R114 system under 3.5 and 8.85 bara

The source of these data quoted an estimated uncertainty of 1–2 mol% on composition: the AAD on calculated vapour composition from the bubblepoint calculation was 1.1%, averaged over three system pressures: 3.5, 8.85 and 14.5 bar. The AAD in predicted bubble temperature in this case was 0.4 K at 3.5 bar, 0.9 K at 8.85 bar and 1.0 K at 14.5 bar. The AAD on liquid composition prediction from specified (T,P) was 2.1%, the AAD on vapour composition 2.7% from the same method.

Behaviour of R12/R114 at High Temperatures It was concluded that the CCOR equation could represent the behaviour of the R12/R114 system with reasonable accuracy; this led the author to use this system as a test of the dewpoint algorithm, Algorithm 6.5, in the region above the critical temperature of the more volatile. The results are shown in Figure 6.27, which is a plot of the phase envelope at several differ-

ent temperatures in pressure-composition co-ordinates. The algorithm converged to a non-trivial solution except in the immediate vicinity of the critical point, where the feasible (P, x) region was very small. This only happened when the composition difference between the phases was very small: for example, the program converged the dewpoint at $T = 130°C$, $y = 0.4210$ to a successful solution of $P = 35.151$ bar, $x = 0.4201$. At this point the difference in volume between the phases was less than 0.004 m^3/kmol. The algorithm failed for the analagous bubblepoint solution: this was caused by the slight error in the approximate (calculated) critical volume, used as the criterion for phase stability. The adaptation of the existing algorithm to deal with solution up to the critical point was not attempted; such a modification would need to make more subtle adjustments to the iteration variables in order to prevent the iteration from straying from the straight and narrow path of convergence.

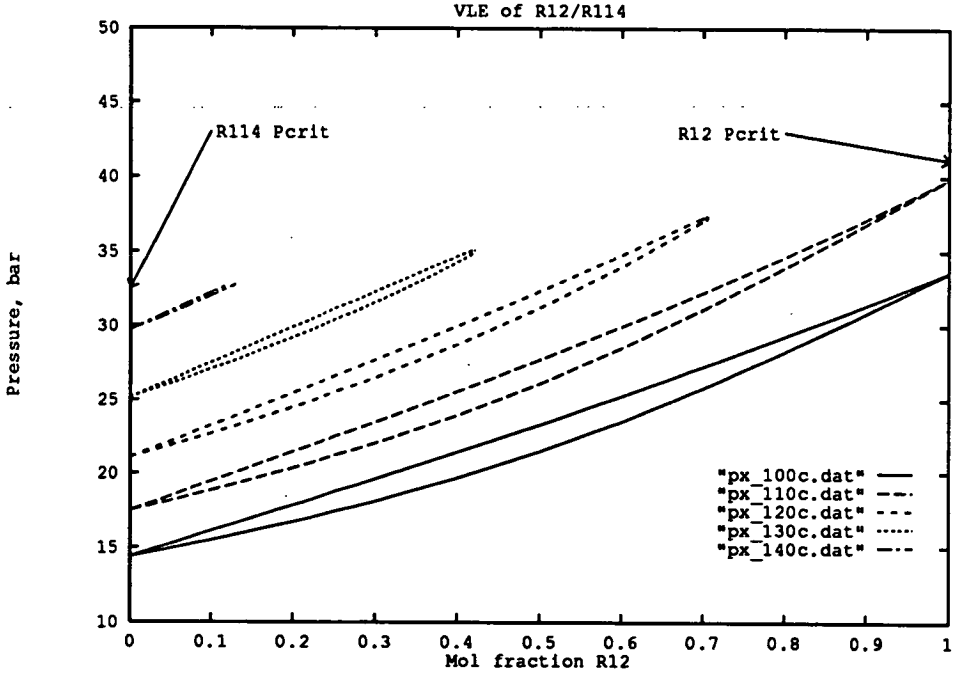

Figure 6.27: Phase Envelope of R12/R114 between 100 °C and 140 °C

6.4.6.3 The R22/R114 System

This system was studied by Ström, Kubota, Valtz, Hasegawa and Kagawa [113, 51, 119, 32, 43]. Ström's data were taken under isobaric conditions; the data of Kubota and Valtz were measured under isothermal conditions. Hasegawa's publication included an

extensive tabulation of single-phase pressure, density and temperature measurements for a set of five fixed compositions: however the only data of interest were his set of dew and bubble point measurements. Kagawa's paper [43] does not contain experimental data *per se*, rather a pictorial representation of the R22/R114 phase envelope in (T, ρ, x) co-ordinates, together with approximate polynomial fits to the data. For this reason no attempt was made at comparison with data from Kagawa's paper.

Comparison with Kubota's Data The comparison with Kubota's data is shown in Figure 6.28, the boiling point diagrams at 40 °C and 65 °C. The fit is excellent at both temperatures.

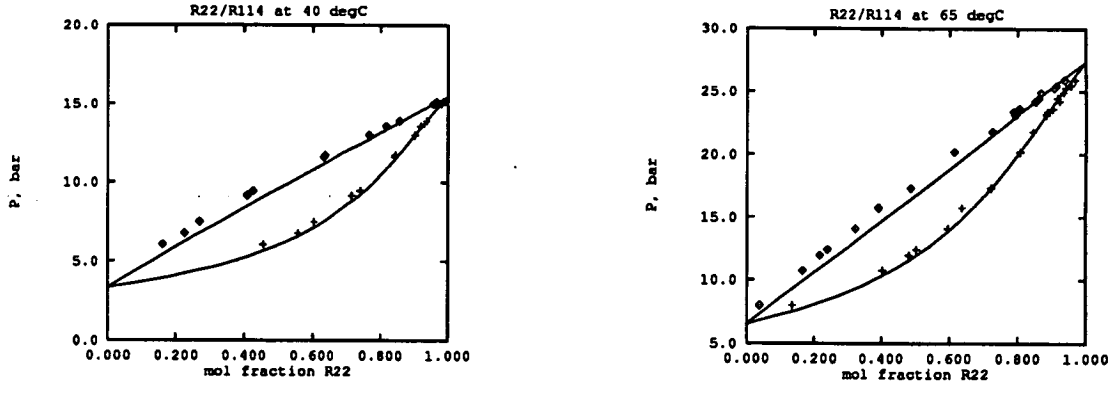

Figure 6.28: The R22/R114 system at 40 °C and 65 °C

Comparison with Ström's Data The uncertainty on composition for this system was quoted as in the range 1–2%, but the reference warns of inconsistency in the data at low mol fractions of R22. This inconsistency was ascribed to impurities in the supply of R114 used for the experiments. The statistical analysis of the predictions of the CCOR equation for this system also indicated the largest errors in composition were at low mol fractions of R22: this is visible in Figure 6.29. The AAD on liquid composition obtained using these data was 3.5%, while the AAD on vapour mol fraction was 3.9%. These deviations are larger than those found for the R12/R114 system but they should be viewed in the context of the comparisons with other workers' datasets for the R22/R114 system.

Comparison with the Data of Valtz The data of Valtz were taken at four temperatures: 25, 50, 75 and 100 °C. The quoted measurements are of bubble pressure and saturated liquid specific volume, over a series of liquid mol fractions. When used with both interaction constants set to zero, the CCOR equation gave an average deviation

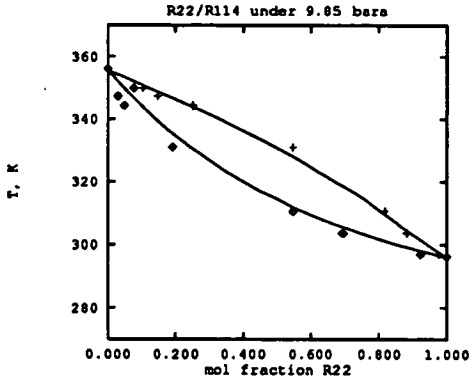

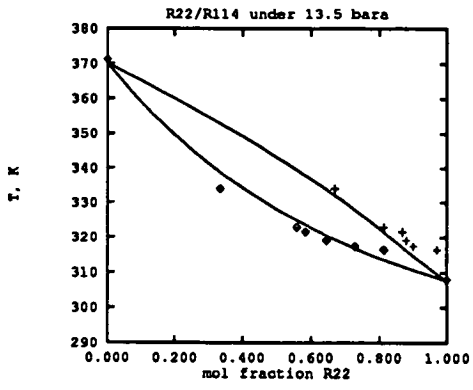

Figure 6.29: The R22/R114 system under 9.85 and 13.5 bara

on bubble pressure of 0.18 bar, with a standard deviation of 0.12 bar. It is concluded that the bubble pressure is well represented by the CCOR equation.

When both interaction constants were set to zero, the equation did not correctly predict the variation of molar volume with composition, although the deviation in liquid volume for the first three temperatures was 5.6 ml/mol—an error of about 5%. At the last temperature the prediction of liquid volume was greatly in error: this behaviour was also found by Valtz, using the Peng-Robinson equation of state: the deviations in liquid volume prediction from the CCOR equation do however appear to be less than those given by the Peng-Robinson equation in Valtz' work. The sharp increase in liquid volume with increasing R22 mol fraction arises because at 100 °C the mixture is above the critical point of R22. This behaviour was also noted in the R22/R11 system, described in Section 6.4.6.6 below.

Hasegawa's Data The vapour-liquid equilibrium data included in Hasegawa's paper [32] were given for four fixed compositions, and comprised several measurements of the dew and bubble temperature and pressure for each composition. These were used by Hasegawa to infer the critical locus of the R22/R114 system. Most of these measurements were made in the near-critical region; it was not possible to obtain non-trivial solutions using the dewpoint algorithm in this case. The problem lay in the detection of a feasible region: the iteration was monitored, revealing that the problem lay in determining an initial guess at incipient composition which would allow the formation of two phases.

6.4.6.4 The R22/R12 System

The mixture of R22 and R12 is known to exhibit azeotropy: this system in its azeotropic state is referred to as R501. This has been studied by several workers, notably: McLinden and Morrison [71, 72], Kagawa [43], and Ström [113]. The data contained in Ström's paper were used for the comparison work.

Ström measured equilibrium temperature and phase compositions for two system pressures, 9.85 and 13.95 bar. He found that the system exhibited a definite azeotrope at the lower pressure but not at the higher pressure, although the phase envelope at the higher pressure was very narrow at high R22 mol fraction. The predictions of the CCOR equation with both interaction constants set to zero are shown in Figure 6.30, which shows the boiling-point diagram for the system at 13.95 bar (the more imperfect VLE case). The equation fails to detect the true behaviour of the phase envelope in this case: this behaviour is also displayed by other equations of state, such as the CSD equation, if no interaction constants are used for this system.

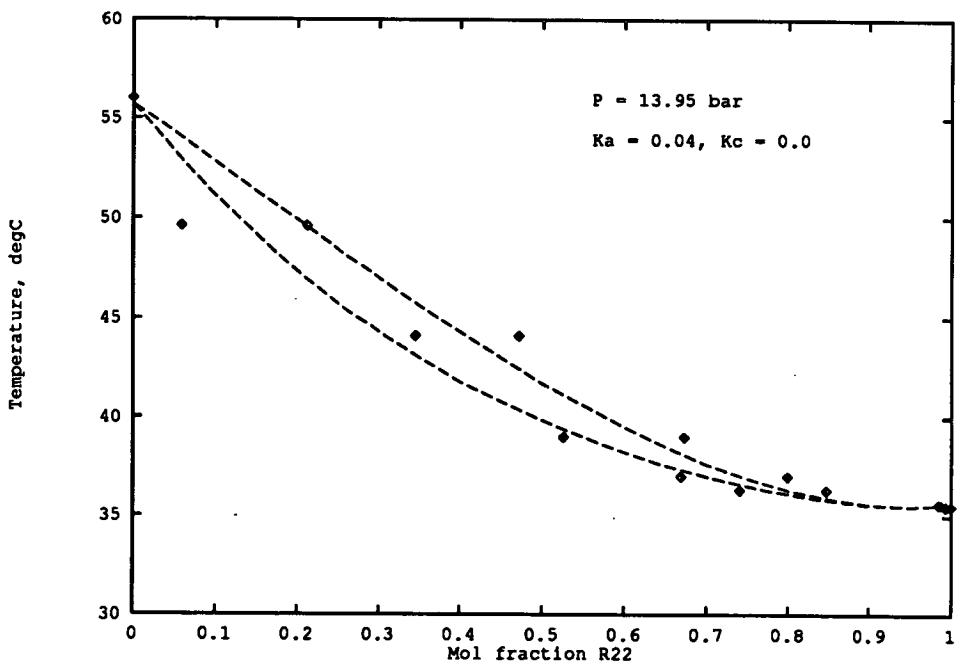

Figure 6.30: Boiling-Point Diagram of R22/R12 under 13.95 bar

The phase envelope's shape was however correctly predicted by Ström, using the SRK

and CSD equations with a non-zero interaction constant: this suggested that adjustment of one or other of the two CCOR interaction constants might improve the predictions of the equation. After experimentation it was found that a non-zero value of k_a would deform the phase envelope in the required direction: see Section 6.4.6.6 for a further demonstration of the effect of the interaction constants on the equation's predictions. This is shown in Figure 6.31, which shows the predictions of the equation with $k_a = 0.04$. (This value was chosen by comparison with Ström's optimised interaction constant of 0.045 for the SRK equation.) As this value was not optimised for the CCOR equation—indeed, it will be shown in Section 6.4.6.7 that an optimum data prediction would probably require a non-zero value for both k_a and k_c—no mean deviations were calculated for this system. The fit indicated by Figure 6.31 suggests, however, that the predictions could be made as accurate as the quoted uncertainty on the experimental data (1–2 mol%).

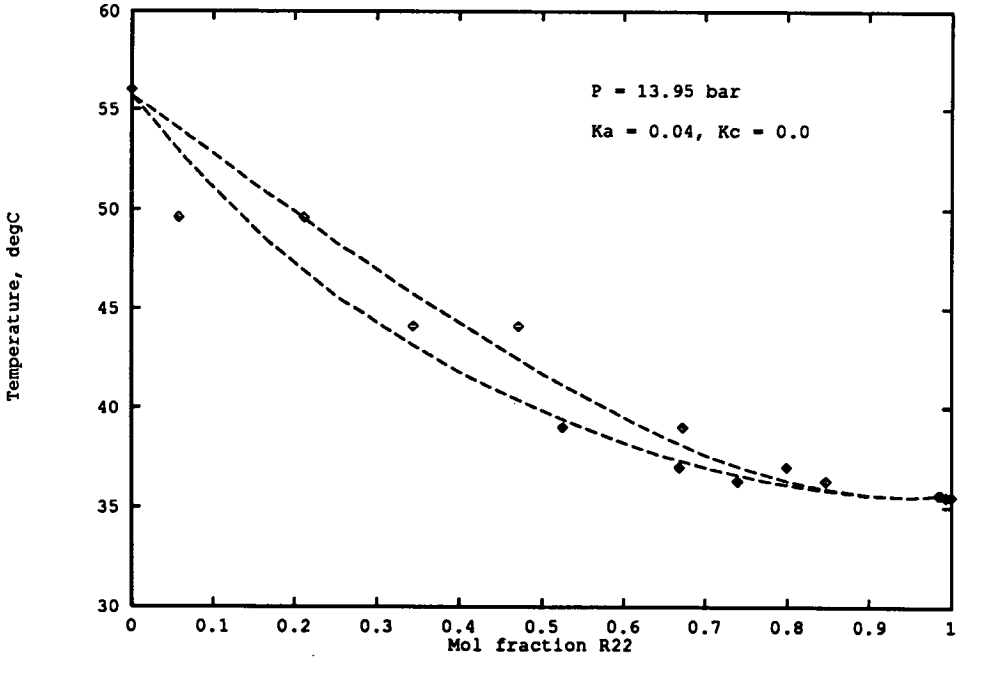

Figure 6.31: R22/R12 Under 13.95 bar: Effect of k_a

6.4.6.5 The System Methylene Chloride (R30)/R113

The mixture of methylene chloride, CH_2Cl_2, with R113 is known to exhibit azeotropy; the azeotrope formed under atmospheric pressure is listed in Horsley [35], with an

azeotropic composition of 48% R30 by mass ($x_{R30} = 0.6708$), boiling at 37.5 °C (Boiling points of the components are: R30, T_b = 40.3° C, R113, T_b = 47.5° C). Without using interaction constants, the CCOR equation correctly predicts the existence of an azeotrope under atmospheric pressure: the azeotropic temperature is predicted as 38.9 °C at a composition of $x_{R30} \approx 0.75$. If k_a is set to 0.025 and k_c to zero, the CCOR equation predicts the boiling point of the azeotrope as 37 °C, with a composition of $x_{R30} \approx 0.69$: thus the use of interaction constants could result in very good quantitative prediction of the azeotrope's behaviour. The predictions are shown in Figure 6.32.

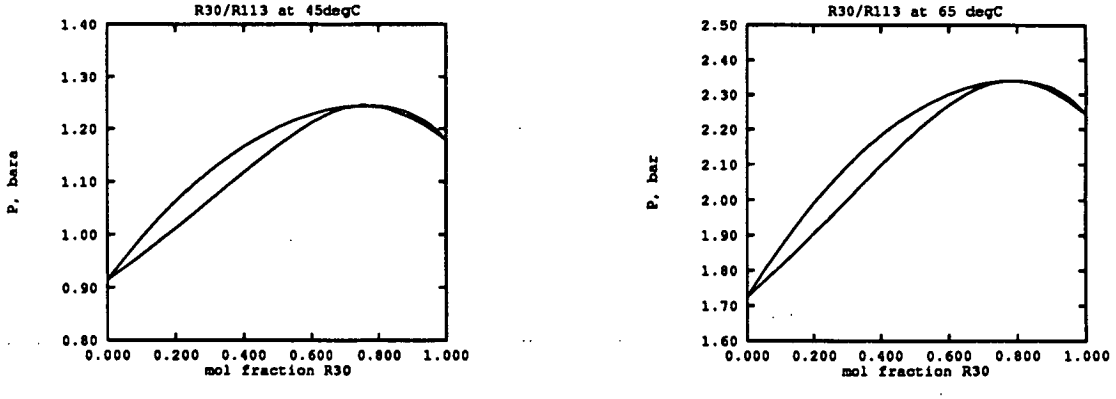

Figure 6.32: R30/R113 at 45 °C and 65 °C

6.4.6.6 The System R22/R11

This system was studied by Meskel-LeSavre and co-workers [66], who obtained measurements of bubble pressure and saturated liquid volume for a range of mol fractions at four temperatures: 25, 50, 75 and 100 °C (this last temperature is above the critical temperature of R22). Meskel-LeSavre also used the Peng-Robinson equation, with an optimised interaction parameter, to fit his data: the value of this interaction constant was $k_{P\_R} = 0.047$. The reported mean error on pressure using the Peng-Robinson equation with $k_{P\_R} = 0.0$ was ten times the experimental precision *i.e.* 1.0 bar. The reported mean error on pressure using the optimised interaction constant was of the order of 0.1 bar "most of the time". The figure quoted for liquid volume prediction error was 5%, but the plots of predicted volume (with optimised k_{P_R}) showed deviations much greater than this at high temperatures.

Bubble Pressures The bubble pressures predicted by the CCOR equation with $k_a = k_c = 0.0$ are shown in Figure 6.33. This shows the progressive departure from ideality of the system: at the lowest temperature the experimental data lie on what is a virtual

straight line, hence obey Raoult's Law, but as the temperature increases the locus of bubble pressures develops a distinct curve. The plot also shows the predictions of the CSD equation of state, with its single interaction parameter k_a set to zero. It is evident that the predictions of the cubic equation are *no worse* than the predictions of the more complex equation for this system. Both equations underpredict the bubble pressure: the greatest deviations lying near the middle of the composition range, corresponding to the widest section of the phase envelope.

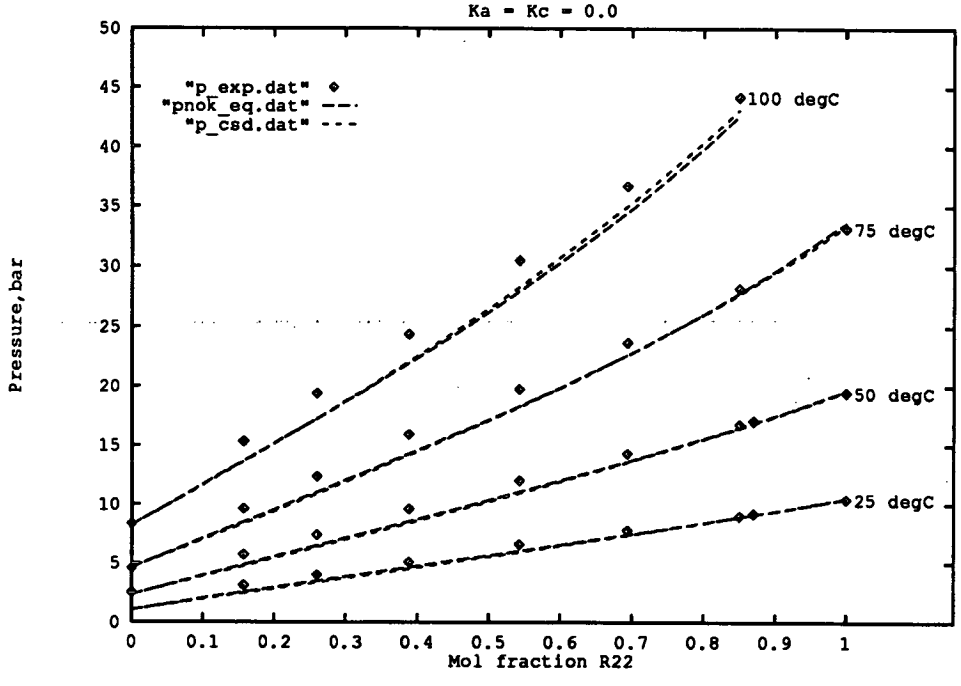

Figure 6.33: R22/R11 Bubble Pressures

Liquid Volumes The predicted liquid volumes are shown in Figure 6.34, with the predictions of the CSD equation as a reference. It is clear that in this case the CCOR equation is inferior to the CSD equation; the former fails correctly to predict the minimum in molar volume at the higher temperatures. At the highest temperature the equation also predicts a much more rapid increase in volume than the measured data indicate; the effect of the R22 critical point is evident here. This variation in liquid volume was also detected for the R22/R114 system, Section 6.4.6.3. The plots of predicted liquid volume contained in Meskel-LeSavre's paper show a similar behaviour; they also show that the errors in liquid volume are smaller for the CCOR equation, which predicts the pure-component liquid volumes with a greater accuracy than does the Peng-Robinson equation.

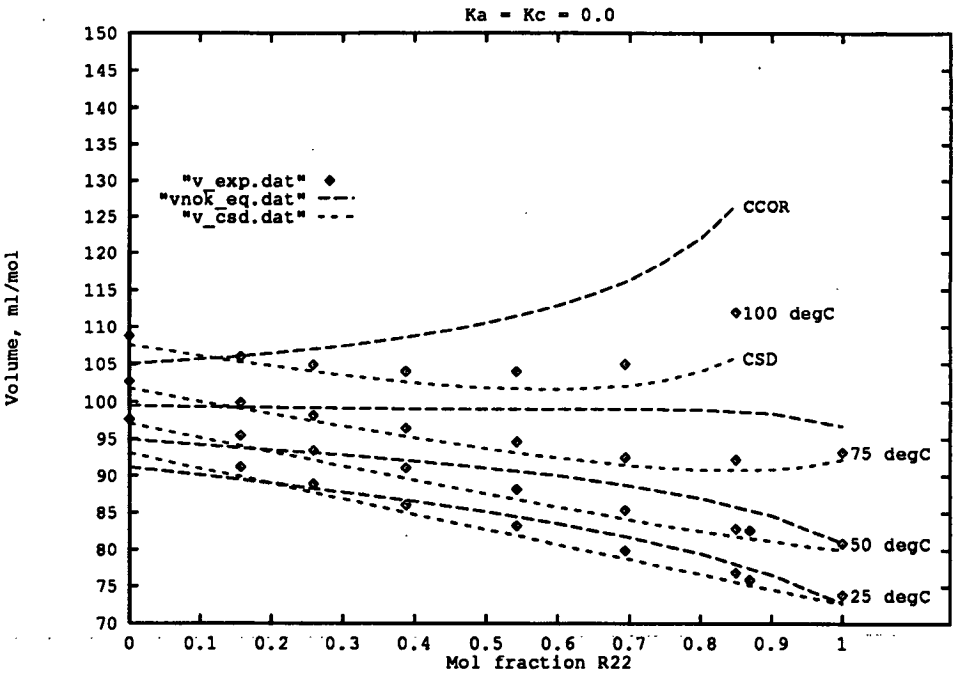

Figure 6.34: R22/R11 Liquid Volumes

Statistics The average absolute deviation (AAD) and standard deviation σ_{N-1} were calculated for each set of predicted pressure and liquid volume; the results are summarised in Table 6.8.

Temperature	Pressure		Liquid Volume	
°C	AAD, bar	σ, bar	AAD, cm^3/mol	σ, cm^3/mol
25.0	0.31	0.24	1.3	0.6
50.0	0.58	0.38	2.0	1.2
75.0	0.96	0.58	3.5	2.3
100.0	1.8	0.84	6.2	5.2

Table 6.8: Deviations in Predicted Bubble-Point Properties of the R22/R11 System

6.4.6.7 Effect of Interaction Constants

The effect of the two interaction constants k_a and k_c was investigated by use of the data for the R22/R11 system as a reference. It had previously been found (see Section 6.4.6.4 that the prediction of dew and bubble pressure for an azeotropic system was improved by use of a non-zero value of k_a. The chosen reference system was nonazeotropic but

offered useful data over a wide range of temperatures.

The method of investigation was simple: the interaction constants were assigned small non-zero values and the bubble-point properties of the mixture were calculated at each temperature used in the reference data [66]. The resulting predictions of pressure and liquid volume were then plotted against mol fraction; on the same plots were shown the experimental data. These figures followed the same format as Figure 6.33 and Figure 6.34. The aim of the exercise was to determine whether the effects of each interaction constant on pressure and volume prediction would lead to the existence of an optimum pair which minimised the error on both pressure and volume. It was suspected that this would be the case: Meskel-LeSavre had been able to optimise a single interaction constant (for the Peng-Robinson equation) which improved pressure prediction but not volume prediction. The use of a second interaction constant in the CCOR equation might therefore give some scope to improving the prediction of volume, in particular in coercing the correct qualitative description of the variation of liquid volume with mol fraction at high temperatures.

Effect of k_a The interaction constant k_a was set to 0.05 (by analogy with the optimum value of k_{P_R} found by Meskel-LeSavre) and the bubble-point properties of R22/R11 were calculated at 25, 50, 75 and 100 °C. The effect of this perturbation on pressure prediction is shown in Figure 6.35, which indicates an elevation of the predicted pressure as a result of the increase in k_a. The corresponding effect on prediction of liquid volume is shown in Figure 6.36, which shows a corresponding increase in the predicted liquid volume. The overall effect is to improve the accuracy of the pressure prediction at the expense of the prediction of the variation of liquid volume with composition.

Effect of k_c The interaction constant k_c was also set to 0.05 and the bubble-point properties recalculated: the results are shown in Figure 6.37 and Figure 6.38. The effect of k_c is opposed to that of k_a: a non-zero value of the k_c parameter depresses predicted bubble pressure and reduces predicted liquid volume. It is shown by Figure 6.38 that a non-zero value of k_c will improve the *qualitative* prediction of liquid volume: the characteristic minimum in the variation of molar volume with composition is displayed by this set of predicted data.

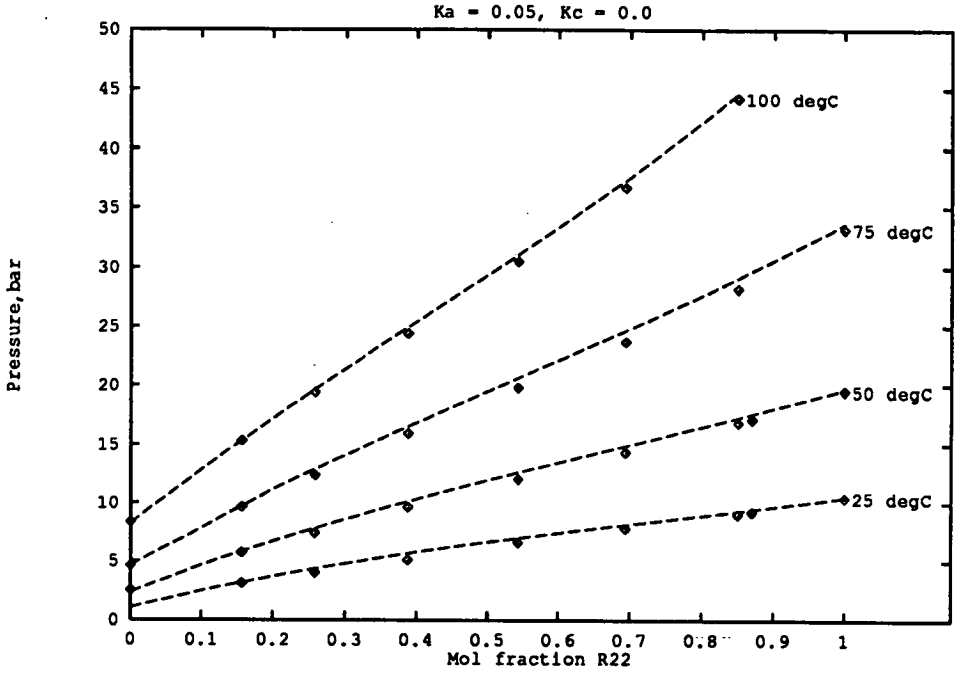

Figure 6.35: R22/R11 Bubble Pressure: Effect of k_a

Effect of *both* Interaction Constants The opposing effects of the two interaction constants demonstrated above suggested that a combination of non-zero values for both parameters should lead to an optimum set of predicted data. A further set of data were generated, using both interaction constants set to 0.05: the results are shown in Figure 6.39 and Figure 6.40. The prediction of both pressure and liquid volume is improved, even at the highest temperature, where the more volatile is at a super-critical temperature. (The highest liquid mol fraction quoted by Meskel-LeSavre was $x_{R22} = 0.8505$; the critical composition corresponding to a critical temperature of 100 °C was predicted by the CCOR equation to lie close to $x_{R22} = 0.89$.) The goodness of the improved fit suggests that, for k_a at least, a good approximation to the optimum value may be given by optimised interaction constants for other cubic equations of state used on the same system.

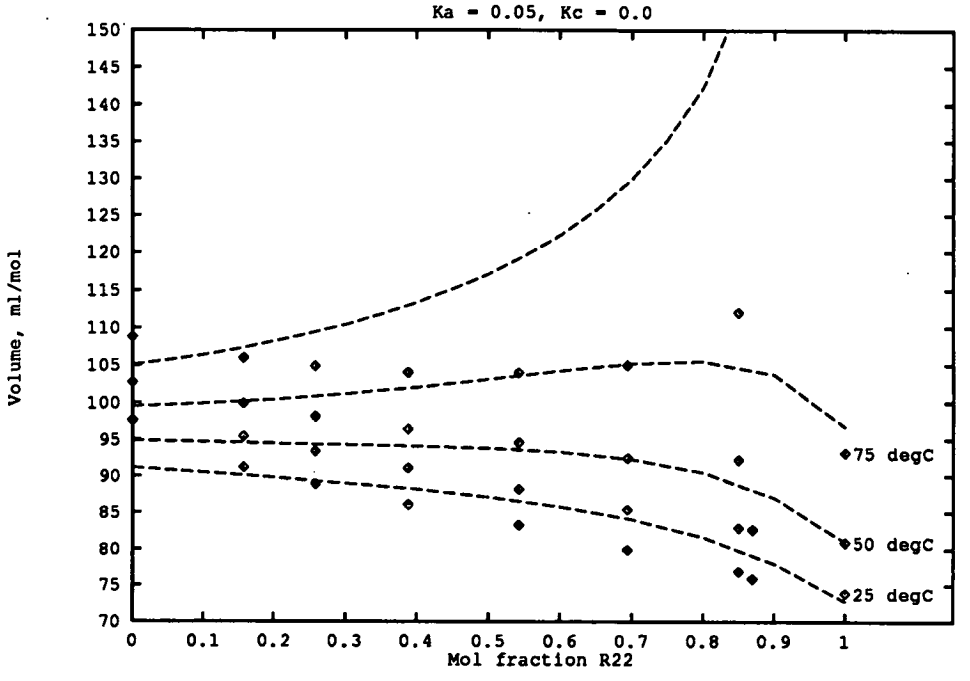

Figure 6.36: R22/R11 Liquid Volume: Effect of k_a

6.4.6.8 Determination of Optimum Interaction Constants

A strategy for determination of an optimum pair of interaction constants was developed: the minimisation of an objective function (O.F.) composed of squares of errors in predicted quantities. This scalar function was a highly non-linear function of the (two-dimensional) interaction constant vector, expressed by Equation 6.93 in terms of errors on pressure P, liquid phase volume v_f and vapour phase composition y, where N experimental data measurements were used.

$$F_{min}(k_a, k_c) = \sum_{i=1}^{N} \left[\omega_p \varepsilon_p^2 + \omega_f \varepsilon_{v_f}^2 + \omega_y \varepsilon_y^2\right] \tag{6.93}$$

The minimisation of the objective function was achieved by use of Powell's method, in the form given in Press [89]. This method required two auxiliary subroutines: one to bracket the minimum of the O.F. in a given direction, and one to minimise the function along a given direction. The line minimisation was a one-dimensional problem, although operating on a vector: it was performed by Brent's algorithm, with the Golden Section method as a standby in case Brent's method attempted to step outside the bracketing

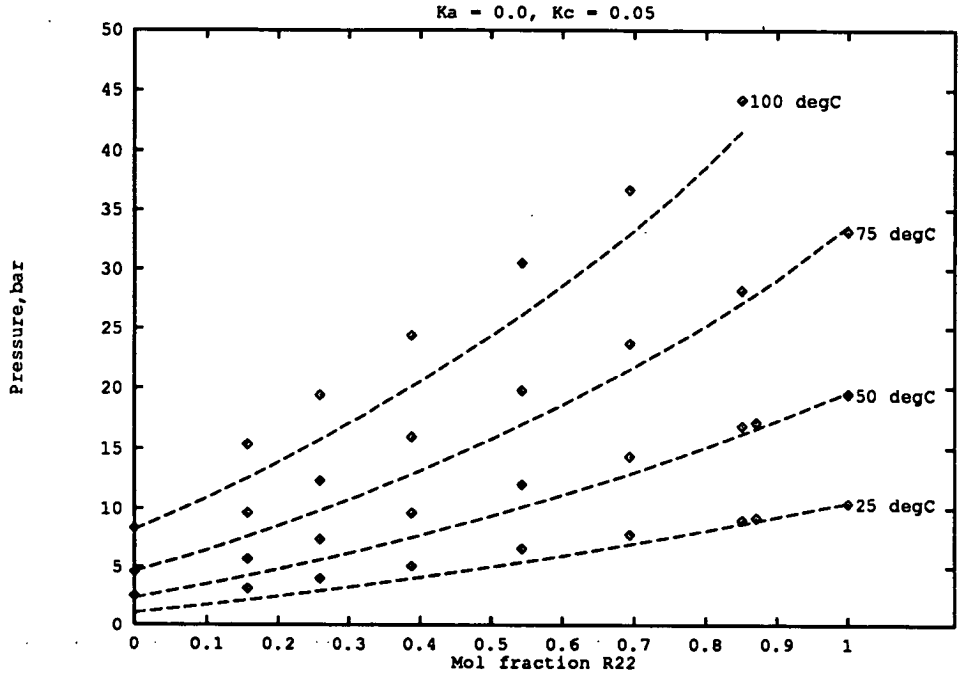

Figure 6.37: R22/R11 Bubble Pressure: Effect of k_c

bounds. These numerical techniques are described in full in Press' book: the author's code was a close translation of the original FORTRAN77 source given in that book and is not recorded here.

Implementation The objective function was evaluated by repeated calls to the author's dew/ bubble point subroutine `CCORdewbubpt()` for each point in the reference data set: the fixed parameters were temperature and liquid composition. This method was in some respects inefficient, since on each call to the bubblepoint subroutine the pure-component equation-of-state parameters were evaluated. Most of the experimental datasets were recorded at constant temperature, so this overhead could have been reduced. Moreover, the tolerance on the bubblepoint iteration variables was fixed (1×10^{-9} on fugacity difference) but in the initial stages of the optimisation a looser tolerance would have been acceptable. As time was by now extremely scarce, no attempt was made to increase the code speed: the time spent in so doing would negate the extra time spent in computation.

The final version of the code required ≈ 12 minutes to execute on a PC–XT with maths

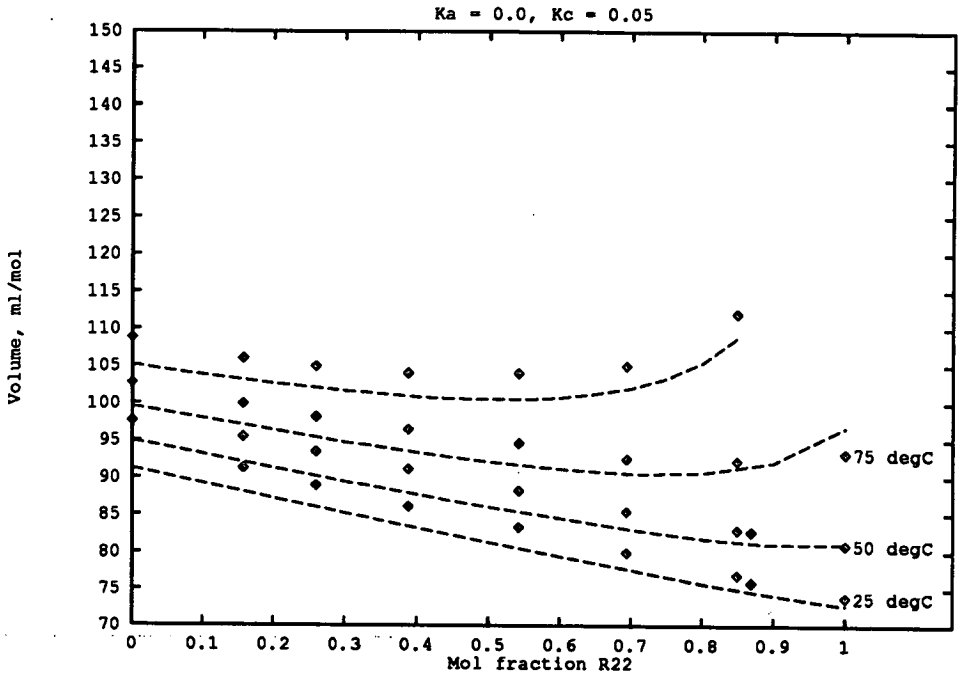

Figure 6.38: R22/R11 Liquid Volume: Effect of k_c

co-processor, using a set of seven experimental data points. This is to be compared with an execution time of a fraction of a second for a single bubblepont calculation on the same machine. In all the optimisations performed, the objective function was composed of pressure and liquid volume errors only, with equal weight given to each quantity. The criterion for attainment of the minimum was that the fractional change in the objective function between the present and the last point tried should be less than 0.0001. The starting position was taken as the origin for the first iteration: if several datasets on the same fluid were to be optimised, then the starting values for the interaction constants at the second and later temperatures were the optimum values found from the previous optimisation. This was found to speed up the convergence of the iteration method: the time taken to converge to the optimum for the same set of seven points was reduced from 12 to 8.5 minutes by this strategy.

Results The optimisation procedure was tested on the R22/R11 system, using the data of Meskel-LeSavre and his co-workers [66]. These data had previously been used to explore the effect of k_a and k_c on the predictions of the bubblepoint properties. The optimum interaction constants were found to vary with temperature: the results of the

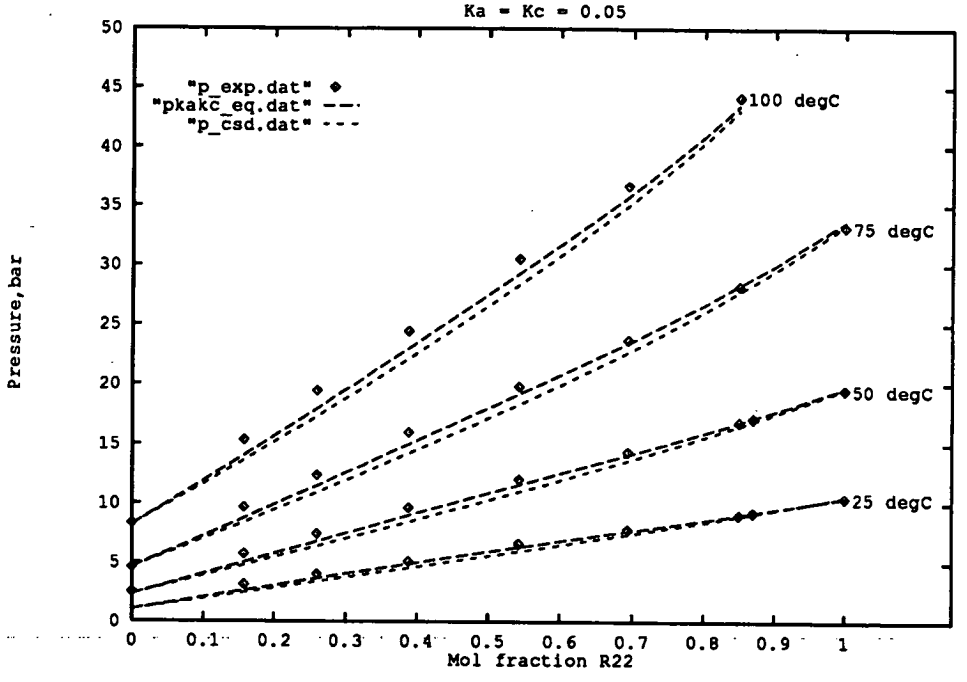

Figure 6.39: R22/R11 Bubble Pressure: Effect of k_a and k_c

optimisations are shown in Table 6.9.

T °C	k_a —	k_c —	N —	δ_p bar	σ_p bar	δ_{v_f} m^3/kmol	σ_{v_f} m^3/kmol
25.0	0.0478	0.0214	6	0.14	0.08	1.4	0.7
50.0	0.0756	0.0546	7	0.26	0.13	1.7	0.8
75.0	0.0889	0.0755	6	0.41	0.28	2.1	1.1
100.0	0.1038	0.0978	6	0.51	0.27	3.0	2.0

Table 6.9: Results of Interaction Constant Optimisation for R22/R11

A direct comparison was made between the predictions of the CCOR equation and Meskel-LeSavre's work with the Peng-Robinson equation. The CCOR equation's predictions of bubble pressure were as good as those of the PR equation; the CCOR equation was markedly superior in prediction of the saturated liquid volume. This had been anticipated: the Peng-Robinson equation used only one adjustable parameter. The results of the optimisation are illustrated in Figure 6.41 and Figure 6.42, which show the predictions of the unoptimised CCOR equation for comparison. The improvement in prediction, especially at the higher temperatures, is obvious. The qualitative prediction of the shape of volume curve is improved: at high temperatures the minimum in volume is predicted. The increase in absolute deviation of pressure at higher

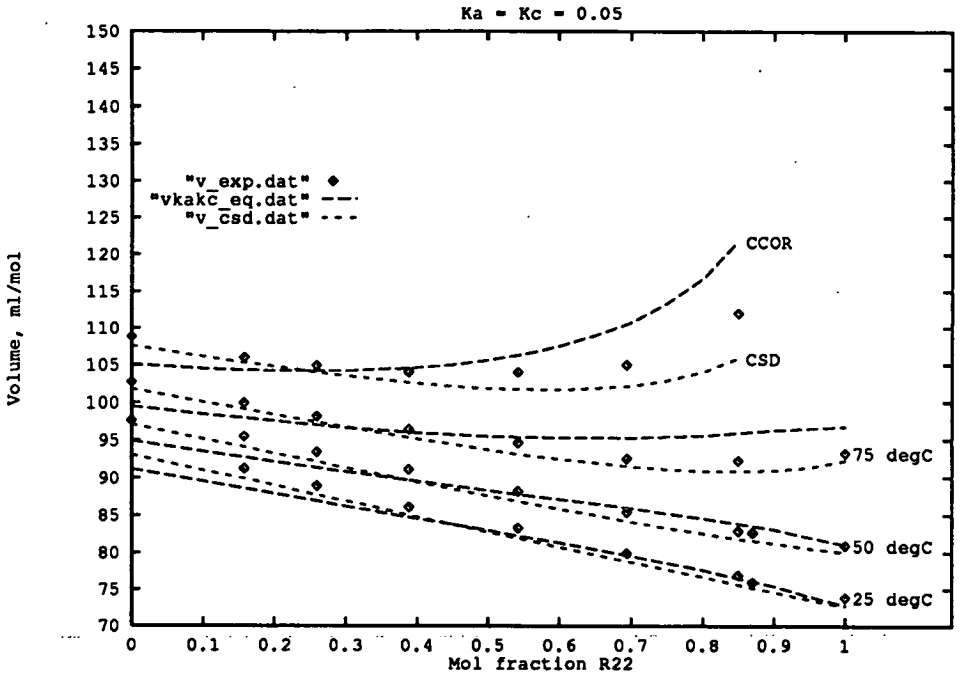

Figure 6.40: R22/R11 Liquid Volume: Effect of k_a and k_c

temperatures could be expected as a consequence of the use of relative errors in the objective function.

6.4.7 Conclusions

The following conclusions have been drawn by the author on completion of his investigation of the CCOR equation of state as a source of thermodynamic data for refrigerant fluids:

- The CCOR equation could be applied with some success to CFC fluids using the bare minimum of measured data on those fluids' physical properties. The availability of accurate group-contribution methods for the prediction of critical properties enabled application of the CCOR equation to fluids on which almost no data were openly available.

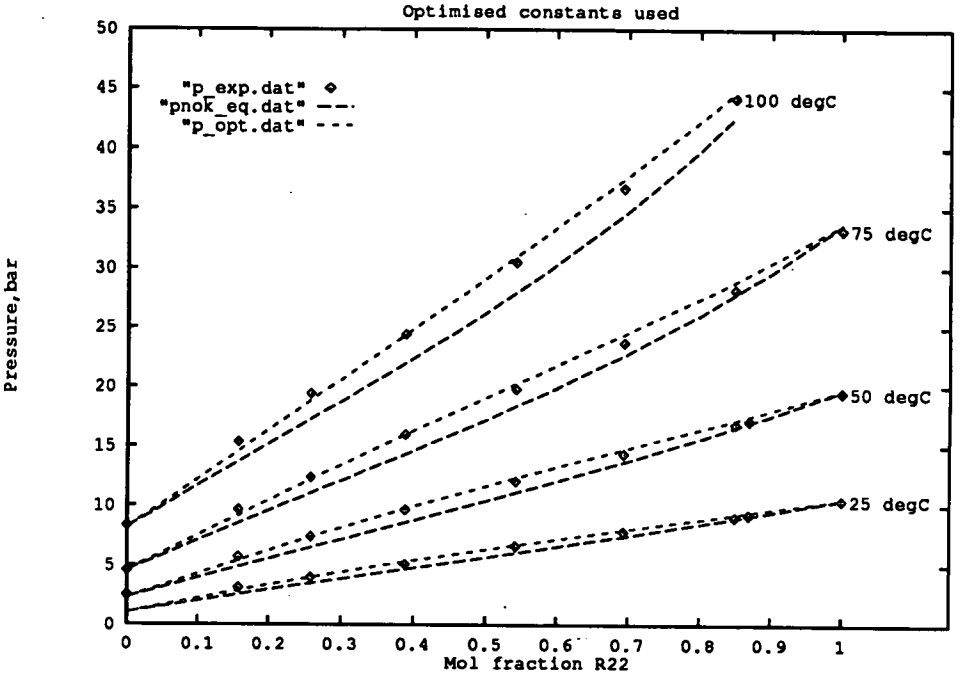

Figure 6.41: R22/R11 Bubble Pressure: Optimised Interaction Constants

- The CCOR equation predicted the vapour pressures of all CFC fluids tested to an average accuracy of 1%, which is as good as any other generalised cubic equation.
- The prediction of saturated liquid volume by the CCOR equation was superior to those of the other well-known cubic equations which have been applied to refrigerant fluids.
- The CCOR equation underpredicted saturated vapour volume at high reduced temperatures, causing an associated error in the prediction of latent heat of vapourisation.
- The equation predicted the VLE of some binary refrigerant mixtures well without the use of empirical interaction constants. In all test cases the equation's predictions were no worse than those of other equations of state if no interaction constants were used.
- The CCOR equation could be used with success to predict the VLE of a mixture at temperatures higher than the critical temperature of the more volatile.
- The successful convergence of phase-equilibrium iterations in this region required the derivation of a solution algorithm capable of keeping the iteration variables

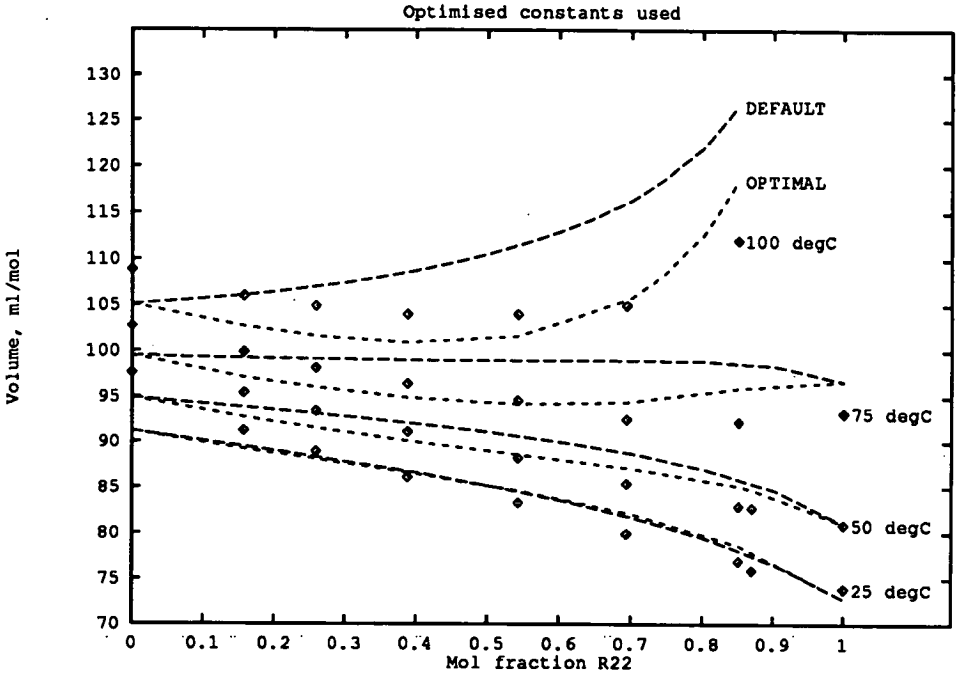

Figure 6.42: R22/R11 Saturated Liquid Volume: Optimised Interaction Constants

inside feasible limits. The author's modified solution algorithm functioned successfully except in the immediate vicinity of the mixture critical point but could be further improved.

- The qualitative and quantitative predictions of mixture properties by the CCOR equation could be improved by use of two interaction constants, k_a and k_c to modify the mixture parameters a and c. It was shown that an optimum pair of interaction constants should exist for any mixture: a set of optimised interaction constants was obtained for the R22/R11 system.

The CCOR equation seems to offer improved prediction of liquid phase properties of refrigerant fluids as compared to other generalised cubic equations of state. The equation is not as powerful as the CSD equation of state but has the advantage of minimal prior parameter-fitting requirement. It therefore has attraction as a source of data on mixtures of proposed CFC replacements fluid mixtures.

6.5 Other Property Prediction Methods

In this section the other methods of thermodynamic property prediction referred to by the author are briefly discussed: the reader is referred to the literature or Chapter 2 for more detailed information.

6.5.1 Implementation of CSD Equation

The Carnahan-Starling-DeSantis (CSD) equation of state was originally developed for use with hydrocarbon mixtures but has been used with success by several workers to predict the properties of refrigerants and their mixtures [71, 70, 72]. The equation is based on a theoretical model fluid—the so-called *hard-sphere* fluid—and in this respect is similar to the Chain-Of-Rotators (COR) equation to which the CCOR equation is an approximation. (This means *inter alia* that the prediction of high-density fluid properties should be good.) It is conventionally written in terms of compression factor due to repulsive and attractive terms, the former being due to the hard-sphere behaviour, the latter to long-distance interactions between molecules. The normal form of the CSD equation is given by Equation 6.94, in which the quantities a and b are the two temperature-dependent parameters of the equation and the other symbols take their usual meaning.

$$\begin{aligned} Z &= Z_{h-s} + Z_{attr} \\ &= \frac{1 + y + y^2 - y^3}{(1-y)^3} - \frac{a}{RT(v+b)} \quad y = b/(4v) \end{aligned} \tag{6.94}$$

The equation-of-state parameters a and b are both defined by three-constant functions of temperature, making a total of six constants which must be calculated for any fluid to which the equation is to be applied. The regression load is not heavy: the functional forms of the relations defining a and b are both quadratics. Sufficient data on the saturation properties of the pure fluid are nonetheless required over the temperature range of interest, making the equation limited in use as a predictor from first principles. Morrison and McLinden [72] give algorithms and FORTRAN77 source for most applications of the CSD equation, including a parameter fitting routine.

The CSD equation is a fifth-order polynomial in volume and so must be solved by numerical methods, in contrast to the cubic equations of state. Its simple form permits use of a fast method of solution using derivative information: the author used Newton-Raphson iteration in his implementation. The range of application for pure fluids is up to reduced temperatures of ≈0.95, which is no restriction in practical terms for heat pump work. The equation has a critical point but it predicts the critical compressibility of all fluids to be 0.316, which is too large for CFC fluids. The advantages of using an equation which does not fit the critical point (as opposed to those such as the CCOR equation, which are constrained to it) have been detailed by Morrison [71].

No results of application of the CSD equation have been included: the information is available in the literature. It has been shown that in the valid reduced temperature range the CSD equation will correlate the vapour pressure, liquid and vapour phase volumes to at least the accuracy of available measured data for pure fluids. The equation may also represent the volumetric and energetic properties of binary mixtures to a high accuracy, even using only the simple van der Waals' mixing rules. The equation gives a good description for example of the variation of heat of mixing with composition, which is a stiff test of an equation of state's ability to predict the second-order thermodynamic properties. The author used the CSD equation to generate data for comparison with the CCOR equation; it was also used to generate data on the R113/R114 mixture for analysis of results from the operation of the pilot plant.

6.5.2 Pure Fluid Correlations; the Martin-Hou Equation

The Martin-Hou equation [24] is now the accepted equation for correlation of the properties of pure refrigerant vapours. It is not applicable to the liquid phase but covers a wide range of vapour densities, up to and beyond the critical point. It is normally written as an expression for pressure:

$$P = \frac{RT}{v-b} + \sum_{k=2}^{5} \frac{F_k}{(v-b)^k} + \frac{F_6}{e^{\alpha v}(1 + C'e^{\alpha v})} \tag{6.95}$$

where the parameters F_k are functions of temperature, defined by:

$$F_k = A_k + B_k T + C_k \exp(-KT/T_c) \tag{6.96}$$

The full, six-term equation therefore requires the molecular weight, critical temperature

and nineteen fluid-specific parameters to be determined from measured data. The sixth term need not however be used in the calculation of vapour properties under the normal range of temperatures and pressures encountered in refrigeration or heat pump cycles, reducing the number of required constants to fourteen.

The form of the Martin-Hou equation makes derivation of the departure functions straightforward; it also permits inversion of the equation by the Newton-Raphson method using analytic derivatives. This gives a rapid solution of the equation for volume at given temperature, except near the critical point where the quantity $(\partial P/\partial V)_T$ approaches infinity. The large number of parameters are a drawback in the application of the equation to gas mixtures: in this case the largest single CPU requirement may be for combination of pure-fluid parameters to form mixture parameters.

Chapter 7

Conclusions

This chapter summarises the conclusions drawn by the author from the results of the work described in this thesis. The conclusions are divided into two sections: those dealing with the experimental programme, and those relating to the work on thermodynamic property prediction for refrigerant mixtures. The author's suggestions for future work as a continuation of this project are then presented.

7.1 Experimental Programme

The experimental program was a qualified success. The pilot plant design was advanced from a bare concept to a working heat pump, which was commissioned and operated, albeit over a period of time which was too short to achieve all of the experimental objectives. The lessons to be learned from the experimental work carried out by the author are summarised below.

7.1.1 Design and Hardware

The original pilot plant design was fundamentally correct: the twin condenser system would enforce a composition shift over a range of input working fluid compositions. There were however numerous modifications made to the plant throughout the work programme: these were made to compensate for shortcomings of the original hardware selected as the plant components. The evaporator in particular was poorly suited to the task of total evaporation over the range of vapour densities and feedrates used. The problems caused by the evaporator led to significant delays in advancement of the programme; in turn this increased the pressure to progress to the next stages of the investigation before the initial topics had been made the subject of repeated experiment. This should be remembered when contemplating the exhaustive analysis of data from the small number of experiments performed using pure R114 as the working fluid; more experimentation would have led to better correlations of the behaviour of the heat pump and components with the independent process variables.

The compressor performed well in the plant work, given that it was designed for lower operating temperatures and a single working fluid. The variable speed drive unit was reliable and efficient, although its transfer function was non-linear, which made prediction of throughput at high speeds rather imprecise. The associated oil separation unit also performed well once the compression path had been moved away from the saturation region. This enabled the prediction of vapour-liquid equilibrium in the separation pots and storage tanks very much more simple.

The welded plate heat exchangers performed too well: the first condenser, sized for 4 kW, could easily transfer 6 kW of heat with a driving force of less than 10° between condensing fluid and heat sink. this caused problems when the time came to attempt splitting of the condensation process but indicates that plate heat exchangers can be used in a pressurised refrigeration/heat pump plant.

The double-pipe subcoolers and the suction vapour superheater also performed extremely well, each transferring at least a kilowatt of heat under operational conditions. These ancillary units made operation of the plant quite straightforward: in a hypothetical second design their duties would be supplied by internal refrigerant streams where possible. Further work with the existing plant was planned, in which the heat duties measured in these units would have been used to calculate efficiencies of cycles with internal heat exchange.

The instrumentation and control system could be classified as a triumph of ingenuity or as a frustrating near-miss, depending on one's outlook. There were still unresolved problems of interference, signal fluctuation and control at the end of the work, but against this it must be said that the equipment was put in place at very little net cost. That it functioned at all was no mean feat, and a tribute to the support provided by Matthew Rea (workshop services manager). In fact the quality of data obtained was good enough for quantitative analysis of most parts of the plant. In developing the instrumentation system for the plant the experience of interfacing PC technology to complex real-time plant within Edinburgh University was substantially advanced over a short time-scale. Most, if not all of the shortcomings described in the previous text would certainly be overcome in a rebuild or second plant design.

The control and analysis software written by the author was adequate for easy operation of the plant but could have been further improved for a further series of work. The text has described how a set of computer programs were used in operation and analysis: the original intent was to produce an integrated program which would perform the several tasks of control, recording and analysis in real time: this was frustrated by time and hardware limitations. A substantial increase in PC power would be required to achieve the original objectives. This does not invalidate the original vision, rather it suggests a way forward.

7.1.2 Experimental Results

The results were disappointing mainly in their quantity: those experiments where steady-state operation was achieved gave good data which in turn enabled meaningful identification of the thermodynamic efficiency of the plant and identification of those components whose contribution to inefficiency was greatest.

Tne work with pure fluids established that the compressor efficency was a function both of gas density and of pressure ratio. The use of pure fluid enabled analysis of the overall cycle performance with a high degree of confidence in the results: the plant's performance compared favourably with other compression heat pump cycles operating with similar lifts and temperature levels.

The performance of the prototype evaporator was roughly characterised, although insufficient experimental measurements were available to determine numerical values of heat transfer coefficients. The inferred heat transfer products (UA) were nearly constant for all the evaporator feed rates used, and were found to vary almost linearly with the pressure drop over the evaporator. This indicated that the boilup rate for the evaporator was fixed by the level of liquid in the shells; there was a maximum boilup rate beyond which the vapour velocity would be sufficient to blow the charge of liquid out of the top of the evaporator.

The experimentation with a mixed working fluid gave some quantitative data which indicated that the thermodynamic efficiency of the heat pump was the same for the mixed fluid as for pure R114: only a few compositions of working fluid were however used. The principle of composition estimation from simultaneous temperature and pressure readings was verified: calculation of the active refrigerant composition by use of three different sets of temperature and pressure readings from different parts of the plant gave values which agreed within 5% on molar composition.

The principle of capacity self-regulation in response to change in process heat load was verified by experiment: the active composition shifted in response to a controlled perturbation in the heat sink flowrate. This indicated that the basic concept underpinning the research was in practice viable. If the capacity of the plant shifted in response to a change in heat load it would do the same in response to a change in work input.

A progressive separation of working fluid into the storage receivers was observed in the course of experimental work. The relative rate of condensation and hence the rate of composition shift was found to be a function of the heat sink flowrate, which in effect pinched the performance of the first condenser. It was difficult to initiate this shift in composition but this may be attributed to the learning process and to minor hardware problems. The shift in composition at the end of each run was typically of the order of 30–40 mol%: the condensate produced in the second condenser was nearly pure R114 while the equilibrium composition of fluid in the heavy side of the plant seemed to be in the range 50–60 mol% of R114. This split was of course influenced by the relative amounts of the two refrigerants in the inventory.

7.2 Thermodynamic Property Prediction

A review of the methods available for the correlation of the thermodynamic properties of halogenated alkane fluids was carried out: on the basis of this review the Cubic Chain-Of-Rotators (CCOR) equation of state was investigated for the purpose of obtaining data on some suggested refrigerant replacement fluids, whose properties were not yet tabulated in the open literature. The equation was tested by comparison with the predictions of recognised pure refrigerant property correlation techniques; by comparison with experimental measurements on pure fluids and binary systems, and by comparison against other equations of state. The equation was chosen because of its general nature: it required knowledge only of the critical properties and acentric factor of a fluid, in conjunction with perfect gas heat capacity data. These could all be obtained from the literature or predicted using standard methods for the fluids of interest in this work.

The CCOR equation was found to be superior to other cubic equations in its prediction of liquid phase properties: both for pure fluids and for mixtures it predicted liquid phase volumes which were of quantitative accuracy. It exhibited a characteristic underprediction of saturated vapour volumes at reduced temperatures greater than 0.85, which affected the latent heat prediction.

It was found that the CCOR equation exhibited similar errors in the saturation properties of fluids at the same reduced temperature: these characteristic error curves were obtained by the author for a set of refrigerant fluids on which there existed comprehensive tabulations of data. It was also found that, by fitting four parameters to saturation volumetric properties, the prediction of vapour pressure and saturated liquid volume could be improved. The prediction of saturated vapour volume was not howevere improved by any of the optimisation techniques tried, and it was concluded that the form of the equation was to blame for this.

The equation was able to represent well the vapour-liquid equilibrium of binary refrigerant mixtures if two non-zero interaction constants were fitted to experiental data. If no interaction constants were fitted to the data, the accuracy of prediction was dependent on the fluid mixture. The equation was able to predict azeotropic behaviour, although the existence of an azeotrope would generally not be predicted unless the interaction constant acting on the attractive force parameter was given a non-zero value.

The CCOR equation used with zero interaction constants predicted bubble and dew pressures with an accuracy which was no worse than that of other equations of state. Its predictions of saturated liquid volumes were better than those of the Redlich-Kwong-Soave and Peng-Robinson equations but were inferior to those of the Carnahan-Starling-DeSantis equation of state commonly used to predict properties of refrigerant mixtures. If optimised interaction constants were used the prediction of both pressure and volume could be significantly improved. This was demonstrated by the author for the specimen system of R22/R11.

7.3 Recommendations For Future Work

The basis for future research must lie in further investigation of the dynamic behaviour of a split-condenser heat pump cycle similar to the author's prototype. To this end it would be advisable to develop dynamic simulations of the key components in the cycle as an aid to experimental planning. The plant built by the author consisted of components with widely differing time constants, and so a dynamic simulation of the whole plant would have all the problems associated with stiff systems of differential equations. This should not be a barrier to progression of such work but it should be recognised that this could form the basis of a doctoral project on its own.

Work with the existing plant could be carried out along the original research plan: in order to achieve the design throughputs of refrigerant the evaporator would need to be replaced with a unit capable of maintaining a higher suction pressure at high compressor speeds. This would enable operation in a R114-rich régime rather than in the R113-rich zones used by the author. Another advisable modification would be the refit of control valve trims more closely suited to the duties required of them; this would make implementation of automatic condenser pressure control more simple. The use of condenser pressure control as a means of affecting the composition shift was not properly investigated but is certainly worthy of research.

A more rigorous characterisation of the speed of composition shift and the factors which affect the response to a change in load would be an essential part of further work. As well as changing the heat sink flow to simulate a shift in load, the compressor work input should be varied: this could be done using the electronic speed control from the

control computer. If a more sophisticated computer control system were used, or a second computer were dedicated to compressor drive, then the compressor speed could be varied in any desired manner. Thus a typical wave energy spectrum could be used to mimic the work available from a wave energy absorber as part of a compressor drive.

The plant was built with subcoolers, flash vapour return lines and a liquid injection line connecting evaporator to condenser. These items were all included in order to gain quantitative data on their effect on the thermodynamic efficiency of the heat pump cycle and their effect on composition shift. Only the subcoolers were used in the author's work, and these only as a means of stabilising the tank pressures. The analysis of these units could form another part of the work.

In the longer term a second plant should be built, using operating experience gained from the author's plant. The glassware components in the plant are "weak links" and would need to be replaced if any more volatile fluids were to be studied. The best way forward would probably be to cannibalise the original plant once sufficient data to enable better cycle design and equipment specification had been obtained. More sophisticated instrumentation would also be required; replacement of gauge pressure transducers with absolute pressure transmitters, for example. Facility for occasional sampling of refrigerant composition for chromatographic analysis should be included, and direct mass flow measurement of the refrigerant flow round the plant would be of great use in obtaining more certain estimates of performance. Measurement of evaporator product rate and condensate rates would have been of great use in determining the performance of the heat exchangers and compressor.

The development of control hardware to regulate the plant control loops would form an interesting task. The condensation split could be measured quantitatively if the heat fluxes in each condenser were measured, by *e.g.* measurement of water temperature rise in each unit. The relative split could then be used as a control function. Further, if a numerical map of the two-phase space of the working fluid were stored in hardware then measurements of temperature and pressure could be used to infer compositions, from which adjustments to control element positions could be made in order to tune the active composition to meet process requirements. A similar strategy could be used to develop the control equipment necessary to regulate feed to the evaporator from each tank: since a real plant would not use a metering pump for this task a simpler method of ensuring selective feeding of fluids would be necessary.

The thermodynamic property prediction software developed by the author could be

taken and developed as the basis for a heat pump cycle design program. This is hardly original work; it is more of a necessary chore than a startling innovation. The author's original intention was to use the CCOR equation for real-time analysis of the pilot plant performance, and the best means of achieving this could be a useful section of work in a future programme. This would enable the concept of controlling using composition maps to be tested on a working plant. The algorithms developed by the author could be refined further; methods of speeding up the calculation procedures by selective curve-fitting of equation predictions should be investigated.

Bibliography

[1] Lena Åhlby. *Compression/Absorption Cycles for Large Heat Pumps: System Simulations.* PhD thesis, Chalmers Technical University, Department of Heat and Power Technology, CTU Göteborg, Sweden, 1987.

[2] G. Alefeld. Kompressions- und Expansionsmaschinen in Verbindung mit Absorberkreisläufen. *Brennstoff-Wärme-Kraft*, 34(3):142–152, 1982.

[3] E. Altenkirch. Die Kompressionskältemaschine mit Lösungskreislauf. *Kältetechnik*, 2(10):251–259, 1950.

[4] E. Altenkirch. Der Einfluß endlicher Temperaturdifferenzen auf die Betriebskosten von Kompressionskälteanlagen mit und ohne Lösungskreislauf. *Kältetechnik*, 3(8):201–205, 1951.

[5] L. Asselineau, G. Bogdanić, and J. Vidal. Calculation of thermodynamic properties and vapor-liquid equilibria of refrigerants. *Chemical Engineering Science*, 33(9):1269–1276, 1978.

[6] M. Benedict, G. B. Webb, and L. C. Rubin. *Journal of Chemical Physics*, 8:334ff, 1940.

[7] S. Beret and J. M. Prausnitz. Perturbed Hard-Chain theory: an equation of state for fluids containing small or large molecules. *AIChE Journal*, 21(6):1123–1132, 1975.

[8] Thore Berntsson and Hans Schnitzer. Some technical aspects on nonazeotropic mixtures as working fluids. In *Second International Symposium on the Large-scale Application of Heat Pumps, York 1984*, Cranfield, United Kingdom. British Hydromechanics Research Association, British Hydromechanics Research Association.

[9] K. E. Bett, J. S. Rowlinson, and G. Saville. *Thermodynamics for Chemical Engineers.* The Athlone Press, London, first edition, 1982.

[10] E. Brousse, B. Claudel, and C. Jallut. Le diagramme enthalpie-pression-composition. Application en distillation aux pompes à chaleur. *Entropie*, 112:29–34, 1983.

[11] Scott W. Campbell. A good initial estimate for pure-component vapor pressures in equation of state calculations. *Industrial and Engineering Chemistry Research*, 27(7):1333–1335, 1988.

[12] N. F. Carnahan and K. E. Starling. *Journal of Chemical Physics*, 51:635ff, 1969.

[13] C. H. Chien, R. A. Greenkorn, and K. C. Chao. Chain-Of-Rotators equation of state. *AIChE Journal*, 29(4):560–571, 1983.

[14] H. Connon and D. Drew. Ermittlung und Anwendung der Thermodynamischen Eigenschaften eines nicht-azeotropen Kältemittelgemisches. *Ki Klima Kälte Heizung*, 11(4):155–159, 1983.

[15] Brian H. Cooke. *The Design and Performance of an integrated Heat Pump-Latent Heat Store Water Heating System.* PhD thesis, University of Edinburgh, Department of Chemical Engineering, Edinburgh, United Kingdom, 1987.

[16] William D. Cooper. Refrigerant compositions. European Patent Application 0021416, 1981.

[17] A. J. Crerar. *Wave Powered Desalination.* PhD thesis, University of Edinburgh, Department of Chemical Engineering, Edinburgh University, 1989.

[18] A. J. Crerar, R. E. Low, and C. L. Pritchard. Wave Powered Desalination. In *Proceedings of the 3rd World Congress on Desalination and Water Re-use, Volume 4*, Netherlands, 1987. International Desalination Association, Elsevier.

[19] A. J. Crerar, C. L. Pritchard, and S. H. Salter. Wave Power for Desalination by direct Vapour Compression. In *Proceedings of the 5th International Conference on Energy Options*, London, United Kingdom, 1987. Institution of Electrical Engineers, Institution of Electrical Engineers.

[20] R. DeSantis, F. Gironi, and L. Marrelli. Vapor-liquid equilibrium from a hard-sphere equation of state. *Industrial and Engineering Chemistry: Fundamentals*, 15(3):183–189, 1976.

[21] P. Domanski. Modelling of a heat pump charged with a non-azeotropic refrigerant mixture (final report). Technical Note NBS/TN-1218, National Bureau of Standards, Gaithersburg, Maryland, United States, 1986.

[22] P. A. Domanski and D. A. Didion. Equation of state-based thermodynamic charts for nonazeotropic refrigerant mixtures. *ASHRAE Transactions*, 91(1):250–259, 1985.

[23] M. D. Donohue and J. M. Prausnitz. Perturbed Hard-Chain Theory for fluid mixtures: Thermodynamic properties for mixtures in natural gas and petroleum technology. *AIChE Journal*, 24(5):849–860, 1978.

[24] R. C. Downing. Refrigerant equations. *ASHRAE Transactions*, 80(2):158–169, 1974.

[25] B. J. Eiseman. The azeotrope monochlorodifluoromethane and dichlorodifluoromethane. *Journal of the American Chemical Society*, 79:6087ff, 1975.

[26] J. R. Elliott and T. E. Daubert. Evaluation of an equation of state method for calculating the Critical properties of mixtures. *Industrial and Engineering Chemistry Research*, 26(8):1686–1691, 1987.

[27] J. Gmehling, D. D. Liu, and J. M. Prausnitz. High-pressure vapour-liquid equilibria for mixtures containing one or more pure components. *Chemical Engineering Science*, 34:951–958, 1979.

[28] Truls Gundersen. Numerical aspects of the implementation of cubic equations of state in flash calculation routines. *Computers and Chemical Engineering*, 6(3):245–255, 1982.

[29] T-M. Guo, H. Kim, H-M. Lin, and K-C. Chao. Cubic Chain-Of-Rotators equation of state 2: Polar substances. *Industrial and Engineering Chemistry: Process Design and Development*, 24(3):764–767, 1985.

[30] T-M. Guo, H. Kim, H-M. Lin, and K-C. Chao. Cubic Chain-Of-Rotators equation of state 3: Mixtures of polar substances. *Industrial and Engineering Chemistry: Process Design and Development*, 24(3):768–773, 1985.

[31] K. Hansen. Computer simulations of real heat pump processes with non-azeotropic R22/R114 mixtures. In *VDI-Berichte 539: Proceedings of the International VDI Seminar Zürich 10–12 September 1984*, Düsseldorf, Germany, 1984. Verein der Deutschen Ingenieur (VDI), VDI-Verlag.

[32] N. Hasegawa, M. Uematsu, and K. Watanabe. Measurements of PVTx properties for the R22+R114 system. *Journal of Chemical and Engineering Data*, 30(1):32–36, 1985.

[33] R. A. Heidemann and A. M. Khalil. *AIChE Journal*, 26:726ff, 1980.

[34] Y. Higashi, Y. Kabata, M. Uematsu, and K. Watanabe. Measurements of the Vapor-Liquid Coexistence Curve for the R13B1+R114 System in the Critical Region. *Journal of Chemical and Engineering Data*, 33(1):23–26, 1988.

[35] L. H. Horsley, editor. *Azeotropic Data–III.* American Chemical Society, 1978.

[36] S. Hosotoni, Y. Maezawa, M. Uematsu, and K. Watanabe. Measurements of PVTx properties for the R13B1+R114 system. *Journal of Chemical and Engineering Data*, 33(1):20–23, 1988.

[37] G. D. Ikonomou and M. D. Donohue. Thermodynamics of hydrogen-bonded molecules: the Associated Perturbed Anisotropic Chain Theory. *AIChE Journal*, 32(10):1716–1725, 1986.

[38] Imperial Chemical Industries plc. *Thermodynamic properties of Arcton 114 (SI Units).*

[39] Imperial Chemical Industries plc. *Thermodynamic properties of Klea 123 (SI Units).*

[40] Imperial Chemical Industries plc. *Thermodynamic properties of Klea 134a (SI Units).*

[41] R. M. Jakobs. Die Anwendung von nichtazeotropen Zweistoff-Kältemittel in Wärmepumpen . *Temperatur Technik*, 17(6):128–135, 1979.

[42] Joseph Joffe. The Martin equation applied to high-pressure systems with polar components. *Industrial and Engineering Chemistry Research*, 26(4):759–762, 1987.

[43] N. Kagawa, N. Hasegawa, and Y. Takaishi. Thermodynamic state surface of binary mixture R12+R22 and R22+R114 systems. In *American Society of Mechanical Engineers Winter Meeting 1983*, New York, 1983. American Society of Mechanical Engineers.

[44] D. Q. Kern. *Process Heat Transfer.* McGraw Hill, New York, international student edition, 1965.

[45] H. Kim, H-M. Lin, and K-C. Chao. Cubic Chain-Of-Rotators equation of state. *Industrial and Engineering Chemistry: Fundamentals*, 25(1):75–84, 1986.

[46] M. Kriebel. Liquid-vapor phase equilibria of the binary system difluoromonochloromethane (R22)—difluorodichloromethane (R12). *Kältetechnik*, 19:8–14, 1967.

[47] H. Kruse. The advantages of non-azeotropic mixtures for heat pump application. *International Journal of Refrigeration*, 4(3):119–135, 1981.

[48] H. Kruse. Improving industrial heat pumps by applying refrigerant mixtures. *Journal of Heat Recovery Systems*, 4(5):359–363, 1984.

[49] H. Kruse. Improving industrial heat pumps by applying refrigerant mixtures. In *Congress on Energy Economics and Management in Industry, Albufeira, Portugal (1984)*, 1984.

[50] H. Kruse and R. Jakobs. Die Bedeutung der nichtazeotropen Zweistoff-Kältemittel beim Einsatz in Wärmepumpen und Kälteanlagen. *Ki-Klima-Kälte-Ingenieur*, 7–8(6):253–260, 1977.

[51] H. Kubota, T. Ikawa, Y. Tanaka, T. Makita, and K. Miyoshi. Vapor-Liquid Equilibria of non-azeotropic halogenated hydrocarbon mixtures under high pressure. *Journal of Chemical Engineering of Japan*, 23(2):155–159, 1990.

[52] P. F. Launay. Improving the efficiency of refrigerators and heat pumps by using a non-azeotropic mixture of refrigerants. Technical Note ORNL/SUB-SI/7762/1, Oak Ridge National Laboratory, Oak Ridge, Tennessee, United States, 1981.

[53] B. I. Lee and M. G. Kesler. A generalized thermodynamic correlation Based on Three-Parameter corresponding states. *AIChE Journal*, 21(3):510–527, 1975.

[54] William A. Leet, Ho-Mu Lin, and Kwang-Chu Chao. Cubic Chain-Of-Rotators equation of state II for strongly polar substances and their mixtures. *Industrial and Engineering Chemistry: Fundamentals*, 25(4):695–701, 1986.

[55] H-M. Lin, T. M. Guo, and K-C. Chao. Cubic Chain-Of-Rotators equation of state and VLE calculations. *Fluid Phase Equilibria*, 13:143–152, 1983.

[56] A. Lorenz. Zur Anwendung binärer Kältemittelgemische in Kompressionskälteanlagen. *Luft- und Kältetechnik*, 6:296–301, 1973.

[57] A. Lorenz. Untersuchungen zum Einsatz des nichtazeotropen Zweistoffkältemittels R12/R11 in Kompressionskältemaschinen. *Luft- und Kältetechnik*, 11(1):33–37, 1975.

[58] R. E. Low. Techniques for thermodynamic property prediction with reference to microcomputer applications. In *Second International Workshop on Advanced Heat Pumps*, Inffeldgasse 19, Graz, Austria, 1988. Technical University of Graz, Technical University of Graz.

[59] R. E. Low and C. L. Pritchard. Prediction of thermodynamic properties of cfc mixtures using the ccor equation of state. In *4th International Conference on Application and Efficiency of Heat Pump Systems in Environmentally Sensitive Times*, Cranfield, United Kingdom, 1990. British Hydromechanics Research Group, BHR Group.

[60] R. E. Low and C. L. Pritchard. Thermodynamic properties of refrigerant mixtures from the CCOR equation of state. In *ThirdInternational Workshop on Advanced Heat Pumps*, Inffeldgasse 19, Graz, Austria, 1990. Technical University of Graz, Technical University of Graz.

[61] J. J. Martin. *Industrial and Engineering Chemistry: Fundamentals*, 18:81ff, 1979.

[62] P. M. Mathias, J. F. Boston, and S. Watanasiri. Effective utilisation of equations of state for thermodynamic properties in process simulation. *AIChE Journal*, 30:182–186, 1984.

[63] R. C. McHarness and D. D. Chapman. Refrigerating capacity and performance data for various refrigerants, azeotropes and mixtures. *ASHRAE Transactions*, 67:441–464, 1961.

[64] Mark O. McLinden and David A. Didion. Quest for alternatives. *ASHRAE Journal*, pages 32–42, December 1987.

[65] J. T. McMullan and R. Morgan. *Heat Pumps*. Adam Hilger, Bristol, United Kingdom, 1981.

[66] M. Meskel-LeSavre, D. Richon, and H. Renon. Bubble pressures and saturated liquid molar volumes of trichlorofluoromethane–chlorodifluoromethane mixtures.

representation of refrigerant-Mixture vapor-liquid equilibrium data by a modified form of the Peng-Robinson equation of state. *Fluid Phase Equilibria*, 8:37–53, 1982.

[67] Michèle Meskel-LeSavre, Dominique Richon, and Henri Renon. Bubble pressures and liquid molar volumes of the system chlorotrifluoromethane–1,1,2-trichlorotrifluoromethane. *Journal of Chemical and Engineering Data*, 27(2):160–165, 1982.

[68] Michael L. Michelsen. Calculation of phase envelopes and critical points for multicomponent mixtures. *Fluid Phase Equilibria*, 4:1–10, 1980.

[69] T. Midgley. From the periodic table to production. *Industrial and Engineering Chemistry: Process Design and Development*, 29:241–244, 1937.

[70] G. Morrison. The importance of including the liquid phase in equations of state for nonazeotropic refrigerant mixtures. *ASHRAE Transactions*, 91(1):260–273, 1985.

[71] G. Morrison. Two refrigerant mixtures and the Hard-Sphere fluid. *ASHRAE Transactions*, 91:929–943, 1985.

[72] G. Morrison and M. O. McLinden. Application of a hard-sphere equation of state to refrigerants and their mixtures: Final report. Technical Note 1226, National Bureau of Standards, 1986.

[73] F. Moser and H. Schnitzer. Mixtures of two or more refrigerants as working fluids for compression heat pumps. In *VDI-Berichte 539: Proceedings of the International VDI Seminar Zürich 10–12 September 1984*, Düsseldorf, Germany, 1984. Verein der Deutschen Ingenieur (VDI), VDI-Verlag.

[74] V. Mučić and B. Scheuermann. Zweistoff–Kompressions–Wärmepumpe mit Lösungskreislauf. *Fernwärme International*, 13(2):79–81, 1984.

[75] V. Mučić and B. Scheuermann. Zweistoff–Kompressions–Wärmepumpe mit Lösungskreislauf. Technical Report BFT–FB–T–84–197, Bundesministerium für Forschung und Technologie, Karlsruhe, Germany, 1984.

[76] M. Narodoslawsky et al. Ethyl chloride: a viable alternative for medium and high-temperature compression heat pump cycles. In *4th International Conference on Application and Efficiency of Heat Pump Systems in Environmentally Sensitive Times*, Oxford, United Kingdom, 1990. BHR Group, Scientific & Technical Information Limited.

[77] N. Narodoslawsky and F. Moser. New compression media as replacements for CFCs. *International Journal of Refrigeration*, 13(2):264ff, 1988.

[78] H. Ofner, H. Schnitzer, and F. Moser. The economy of nonazeotropic refrigerant mixtures in compression heat pumps. *Journal of Heat Recovery Systems*, 6(4):313–321, 1986.

[79] A. Peneloux, E. Rauzy, and R. Frese. *Fluid Phase Equilibria*, 8:7ff, 1982.

[80] D-Y. Peng and D. B. Robinson. *Industrial and Engineering Chemistry: Fundamentals*, 15:233ff, 1976.

[81] W. A. Pennington and W. H. Reed. Azeotrope of 1,1-difluoroethane and dichlorodifluoromethane as a refrigerant. *Chemical Engineering Progress*, 46:464–466, 1950.

[82] R. H. Perry and Don Green, editors. *Perry's Chemical Engineer's Handbook.* McGraw Hill, New York, sixth edition, 1986.

[83] David R. Pesuit. Binary interaction constants for mixtures with a wide range in component properties. *Industrial and Engineering Chemistry: Fundamentals*, 17(4):235–242, 1978.

[84] U. Plöcker, H. Knapp, and J. M. Prausnitz. *Industrial and Engineering Chemistry: Process Design and Development*, 17:324ff, 1978.

[85] Bruce E. Poling, Edward A. Grens II, and John M. Prausnitz. Thermodynamic properties from a cubic equation of state: Avoiding trivial roots and spurious derivatives. *Industrial and Engineering Chemistry: Process Design and Development*, 20(1):127–130, 1981.

[86] A. Polt. Representation of thermodynamic properties of fluids for Organic Rankine Cycles by the Bender equation of state. In *VDI-Berichte 539: Proceedings of the International VDI Seminar Zürich 10–12 September 1984*, Düsseldorf, Germany, 1984. Verein der Deutschen Ingenieur (VDI), VDI-Verlag.

[87] J. W. Ponton. Rapid approximate vapour-liquid equilibrium calculations. *Computers and Chemical Engineering*, 11(5):537–541, 1987.

[88] S. Pourreza-Djourshari and R. Radermacher. Calculation of the performance of vapour compression heat pumps with solution circuits using the mixture R22–DEGDME. *International Journal of Refrigeration*, 9(7):245–250, 1986.

[89] Press, Flannery, Teupolsky, and Vetterling. *Numerical Recipes: The Art of Scientific Computing.* Cambridge University Press, Boston, Massachusetts, 1986.

[90] C. L. Pritchard and R. E. Low. A self-regulating heat pump for systems with variable power input. In *Second International Workshop on Advanced Heat Pumps*, Inffeldgasse 19, Graz, Austria, 1988. Technical University of Graz, Technical University of Graz.

[91] C. L. Pritchard and R. E. Low. A self-regulating heat pump for renewable energy applications. In *4th International Conference on Application and Efficiency of Heat Pump Systems in Environmentally Sensitive Times*, Cranfield, United Kingdom, 1990. British Hydromechanics Research Group, BHR Group.

[92] C. L. Pritchard and R. E. Low. A self-regulating heat pump for systems with variable power input. In *ThirdInternational Workshop on Advanced Heat Pumps*, Inffeldgasse 19, Graz, Austria, 1990. Technical University of Graz, Technical University of Graz.

[93] C. L. Pritchard and R. E. Low. A self-Regulating heat pump to utilize wind and wave energy resources. *Energy Sources*, 12:15–24, 1990.

[94] R. Radermacher. Advanced versions of heat pumps with zeotropic refrigerant mixtures. *ASHRAE Transactions*, 92:52–59, 1986.

[95] C. L. Ramet and A. Rojey. Application of mixed refrigerants to compression heat pumps. In *VDI-Berichte 539: Proceedings of the International VDI Seminar Zürich 10–12 September 1984*, Düsseldorf, Germany, 1984. Verein der Deutschen Ingenieur (VDI), VDI-Verlag.

[96] O. Redlich and J. N. S. Kwong. *Chemical Review*, 44:233ff, 1949.

[97] A. Rojey et al. Pompe a chaleur fonctionnant avec un mélange de fluides. Technical Report EUR 6848FR, European Communities' Energy Commission, Luxembourg, 1980.

[98] A. Rojey et al. Pompe de chaleur fonctionnant avec un mélange de fluides. *Revue de l'Institut Français du Pétrole*, 36(2):183–190, 1981.

[99] S. H. Salter. Progress on Edinburgh Ducks. In *IUTAM Symposium on the Hydrodynamics of Ocean Wave Energy Utilization*. I.U.T.A.M., 1985.

[100] S. H. Salter. Wave powered Desalination. In *Proceedings of the 4th Conference on Energy for Rural and Isolated Communities*, London, United Kingdom, 1985. Institution of Electrical Engineers.

[101] J. A. Sandarusi, A. J. Kidnay, and V. F. Yesavage. Compilation of parameters for a polar fluid Soave-Redlich-Kwong equation of state. *Industrial and Engineering Chemistry: Process Design and Development*, 25(4):957–963, 1986.

[102] H. Schnitzer and T. Berntsson. Binäre Kältemittelgemische für Kompressionswärmepumpen. *Brennstoff-Wärme-Kraft.*

[103] Hans Schnitzer and Thore Berntsson. Improving the COP of compressing heat pumps through the use of nonazeotropic mixtures. In *Second International Symposium on the Large-scale Application of Heat Pumps, York 1984*, Cranfield, United Kingdom. British Hydromechanics Research Association, British Hydromechanics Research Association.

[104] H. Schwind. Über die Verwendung binärer Kältemittelgemische und deren Darstellung im Enthalpie, Druck-Diagramm. *Kältetechnik*, 14(4):98–105, 1962.

[105] Y. Shigaki et al. Estimation of the basic properties (T_b, T_c, P_c and ω) of fluorocarbon refrigerants (freons). *International Chemical Engineering*, 28(3):447–454, 1988.

[106] R. K. Sinnott. *Chemical Engineering Volume 6: Design*. Pergamon, Oxford, first edition, 1983.

[107] G. Soave. *Chemical Engineering Science*, 27:1197ff, 1972.

[108] Fred P. Stein and Patricio C. Proust. Vapor-Liquid Equilibria of the Trifluoromethane–Trifluorochloromethane System. *Journal of Chemical and Engineering Data*, 16(4):389–393, 1971.

[109] W. F. Stoecker and C. I. McCarthy. Simulation and performance of a system using an R-12/R114 refrigerant mixture. Technical Report ORNL/SUB-SI/7762/301, Oak Ridge National Laboratory, Oak Ridge, Tennessee, United States, 1984.

[110] W. F. Stoecker and D. J. Walukas. Conserving energy in refrigerators through the use of refrigerant mixtures. *ASHRAE Transactions*, 87(1):279–291, 1981.

[111] M. Stokar. Compression heat pump with solution circuit part 2: Sensitivity analysis of construction and control parameters. *International Journal of Refrigeration*, 10:134–142, May 1987.

[112] M. Stokar and C. H. Trepp. Compression heat pump with solution circuit part 1: Design and experimental results. *International Journal of Refrigeration*, 10:87–96, March 1987.

[113] K. Ström, U. Gren, and K. Ljungkvist. Representation of vapor-liquid equilibrium data for binary refrigerant mixtures. *Journal of Chemical and Engineering Data*, 34(2):252–257, 1989.

[114] R. J. Topliss, D. Dimitrelis, and J. M. Prausnitz. Computational aspects of a non-cubic equation of state for phase-equilibrium calculations. effect of density-dependent mixing rules. *Computers and Chemical Engineering*, 12(5):483–489, 1988.

[115] Constantine Tsonopoulos. An empirical correlation of second virial coefficients. *AIChE Journal*, 20(2):263–272, 1974.

[116] M. Uematsu, K. Watanabe, and N. Kagawa. Role of the thermophysical properties study of the binary refrigerant mixtures for ORC technology. In *VDI-Berichte 539: Proceedings of the International VDI Seminar Zürich 10–12 September 1984*, Düsseldorf, Germany, 1984. Verein der Deutschen Ingenieur (VDI), VDI-Verlag.

[117] B. Vakil. Thermodynamics of heat exchange in refrigeration cycles with non-azeotropic mixtures. In *XVIth International Congress of Refrigeration (Paris 1983) Proceedings Volume II*, pages 305–310. International Institute of Refrigeration, 1983.

[118] H. B. Vakil. Vapor compression cycle device with multi-component working fluid and method of modulating its capacity. U. S. Patent 4179898, 1979.

[119] A. Valtz, S. Laugier, and D. Richon. Bubble pressures and saturated liquid molar volumes of dichloromonofluoromethane–fluorochloroethane binary mixtures: Experimental data and modelling. *International Journal of Refrigeration*, 9:282–289, September 1986.

[120] A. Valtz, S. Laugier, and D. Richon. Bubble pressures and saturated liquid molar volumes of trifluorotrichloroethane–fluorochlorohydrocarbon mixtures: Experimental data and modelization. *Journal of Chemical and Engineering Data*, 32(4):397–400, 1987.

[121] L. Vamling, M. Hogberg, and T. Berntsson. CFC alternatives for high-temperature heat pump applications. In *4th International Conference on Application and Efficiency of Heat Pump Systems in Environmentally Sensitive Times*, Oxford, United Kingdom, 1990. BHR Group, Scientific & Technical Information Limited.

[122] P. Vimalchand, I. Celmins, and M. D. Donohue. VLE calculations for mixtures containing multipolar compounds using the Perturbed Anisotropic Chain Theory. *AIChE Journal*, 32(10):1735–1737, 1986.

[123] K. Watanabe and M. Uematsu. Thermodynamic properties of Perfluorocarbons for industrial waste heat recovery systems. In *VDI-Berichte 539: Proceedings of the International VDI Seminar Zürich 10–12 September 1984*, Düsseldorf, Germany, 1984. Verein der Deutschen Ingenieur (VDI), VDI-Verlag.

[124] B. Whittaker. Recent developments in wave energy systems. In *Proceedings of the 5th International Conference on Energy Options*, London, United Kingdom, 1987. Institution of Electrical Engineers, Institution of Electrical Engineers.

[125] Zhong Xu and Stanley I. Sandler. Temperature-dependent parameters and the Peng-Robinson equation of state. *Industrial and Engineering Chemistry Research*, 26(3):606–616, 1987.

[126] F. Ziegler and G. Hämmer. Experimental results of a double-lift compression-absorption heat pump. In *4th International Conference on Application and Efficiency of Heat Pump Systems in Environmentally Sensitive Times*, Cranfield, United Kingdom, 1990. British Hydromechanics Research Group, BHR Group.

Appendix A

Nomenclature

The following symbols have been commonly used without explanation in the body of the text and as such are here defined for reference.

a, b, c, d, c^R	parameters of CCOR equation	
Cp,Cv	heat capacity	kJ/kmol K
d	diameter	m
f	fugacity	kPa
h,H	enthalpy	kJ/kmol
h	heat transfer coefficient	kW/m^2 K
k	thermal conductivity	W/m K
K	polytropic index	
L	length	m
m	mass	kg
n	number of mol	mol
N	number of components	
N	polytropic index	
P	pressure	kPa
q,Q	heat or heat flux,	kJ (kW)
R	Gas Constant	kJ/kmol K
s,S	entropy	kJ/kmol K
t,T	temperature	K
U	internal energy	kJ/kmol
U	overall heat transfer coefficient	kW/m^2 K
v,V	volume	m^3/kmol
x	mol fraction in liquid phase	
y	mol fraction in vapour phase	
z	mol fraction (phase immaterial)*or* compression factor	
Z	compression factor (Pv/RT)	

Sub- and Superscripts

$\dot{q}$	flux *e.g.* heat flux
°	perfect gas state
′	temperature derivative
a	actual or achieved quantity
c	critical state
C	Carnot cycle parameter
cmp,comp	compressor
co,cond	condenser
dis,disch	compressor discharge
ev,evap	evaporator
exp	experimental quantity
i,j,k	component indices
i	inside (of tubes or pipes)
l	liquid phase
L	Lorenz cycle parameter
o	outside (of tubes or pipes)
p	constant pressure
r	reduced property
R	Rankine cycle parameter
sc	sub-cooled, subcooler
si	sink
so	source
suc,suct	compressor suction
v	constant volume *or* vapour phase

Greek letters

α	temperature function of CCOR equation
γ	temperature function of CCOR equation
γ	ratio of specific heats
ε	Carnot efficiency
η	isentropic compression efficiency
ϕ	fugacity coefficient
Π	Pressure ratio
ρ	density
Ω_M	parameter of CCOR equation (M one of $a, b, c, d,$)
ω	acentric factor

Dimensionless Groups

COP	Coefficient of Performance
Nu	Nusselt Number
Pr	Prandtl Number
Re	Reynolds Number

Appendix B

Operation of Heat Pump Plant

B.1 General Remarks

The notes in this Appendix describe procedures for the safe startup and operation of the heat pump pilot plant. It is useful to outline the general principles which guided the derivation of these procedures: this should help to clarify the reasons for each stage described below. The paramount requirement is that the plant be operated in a way which minimises any risk, either to material or to laboratory personnel.

The plant uses working fluids which are not themselves a grave toxicological hazard: nonetheless it is important to avoid any leakage of the fluids, since high airborne concentrations of refrigerant vapour may cause hallucinations or sickness. The cost of refrigerant fluids is another good reason for ensuring that the plant pipework be as gas-tight as possible.

The apparatus uses both 240V, 50 Hz single-phase and 440V, 50 Hz three-phase elec-

tricity supplies: these present an obvious potential for hazard. Care should therefore be taken in the vicinity of the plant to aviod water spills near wiring. Furthermore, the cabling of the electricity supply and of the plant's instruments should be carefully connected and installed to avoid accidental shocks. Most of the instrumentation cabling carries low-voltage, low-current signals to the computer interface rack; this wiring is conducted through trunking on the floor for the above reasons.

The major remaining potential hazard is the fabric of the plant itself, which contains a refrigerant whose vapour pressure is normally positive gauge even at room temperature. Failure of any component may result in at least loss of part of the charge; in addition some projectile shrapnel may be thrown into the laboratory. Therefore the utmost care is required to keep all parts of the plant below their design pressures at all times.

B.2 Initial Checklist

This list should be used before any attempt is made to start the hest pump.

B.2.1 Compressor

1. Switch the 3-phase power supply off at the junction box.
2. Open the hand valves and check valves on both oil return lines. Check valves are open when the handle is parallel to the pipe axis; a hand valve is opened by counter-clockwise turning.
3. Open the check valve on the vapour line before the suction filter.
4. Ensure that the isolation valves on the refrigerant charging manifold are shut; check the cap on the manifold external connection is tight.
5. If the compressor manifold has the service valves mounted, ensure that these are open (at least $\frac{1}{2}$" of valve stem visible). If they are not open, use the loose handwheel attached to the frame to turn them.
6. Ensure that the switches on the compressor control box are set to STOP, PC control, as indicated. Check that the control line from the PC and the trip signal lines are connected: turn the power switch to OFF.

B.2.2 Metering Pump

1. Open the valves on the pump head inlets to allow refrigerant to be drawn from either or both tanks.
2. Open the check valve in the evaporator liquid feed line. Also check that the hand valve between head 2 of the pump and the junction with the discharge of head 1 is open.
3. Ensure that the valve in the solution circuit (between pump and condenser C1) is closed.
4. Plug in the power cable and check that the control wires from the PC are plugged into the correct heads of the pump. The cable for head 1 has one black band near the plug; that for head 2 has twin black bands.

B.2.3 Solenoid Valves

1. Throw all the control switches on the relay box to the right (AUTO) position.
2. Check the control cable is plugged in.
3. Disconnect the power cable from the mains.

B.2.4 Cold Water Circuit

1. Check that there is water in the tank. If not, open the ballcock feed valve and allow tank to fill. Make sure that the drain line valve is closed.
2. Check that the heater element power lines are plugged in to the relay box. Plug the relay box cables into the mains supply and check that the control line from the PC is plugged into the box. Throw all switches to AUTO (PC control).
3. Open the pump suction valve.
4. Open the hand valve at the base of the cold water rotameter.
5. Close the valve on the bypass line (line which runs to the Alfa-Laval plate heat exchanger).

6. Open the check valves on the pressure transmitter over the orifice plate. Open the bypass valve on this unit.

7. Switch on the pump and allow to run until the system is full of water and the rotameter float is showing a steady flow.

8. Wait until no more air bubbles may be seen flowing from the pressure transmitter through the PVC connector tubes, then shut the bypass valve on the transmitter.

The pump may be left running, or switched off. If switched off, then the pressure transmitter should be flushed through again on the next startup to remove any air bubbles.

B.2.5 Hot Water Circuit

1. Check that there is water in the tank. If not, fill from the mains line.

2. Set a low flow (0.5 l/min) using the hand valve on the cold water feed line, reading the flow of the small rotameter on this line. If no flow through this line, check the position of the valves on the line between the water mains pipe and the rotameter.

3. Open the pump suction valve.

4. Open the hand valve at the base of the hot water rotameter. Check that the flow control valve on this line is open. If it is not, and the air supply is switched off, then technical help is required, as it should fail open. In this case the valve stem motion needs to be checked.

5. Open the check and bypass valves on the pressure transmitter assembly.

6. Check that the heater power cable is plugged in at both ends.

7. Switch on the pump and allow to run until the rotameter indicates a steady flow, then shut the pressure transmitter bypass line.

As for the cold water circuit, the transmitter needs to be bled of air every time the pump is started up.

B.2.6 Mains Water

The mains water flows through each subcooler are not critical to startup but it is a good precaution to switch these on at the same time as the cold water makeup supply to the heat source tank is checked. The flows of water to the subcoolers are controlled by the hand valves mounted on a panel on the main board, above the top of the glass storage tanks. Likewise, switch on the flow of water through the glass tank cooling coils.

B.2.7 Compressed Air

Leave this off until the compressor is started: however it may be set to a supply pressure at the manifold of 15–30 psig beforehand, then shut off using the green hand valve.

B.2.8 Final Checks

- Is there a satisfactory flow of water through each circuit?
- Are the compressor and pump valves set to avoid dead-ending either unit?
- Can the compressor and pump draw feed from the evaporator and storage respectively?
- Are the heaters and solenoid valve relay boxes ready to be switched on?

B.3 Startup Procedure

Now it is possible to begin startup, switching on the plant one stage at a time.

1. Check the connections of all power cables to thermocouple boxes, instrument rack and PC. Check also that the instrument signal cables are all plugged in properly.

2. Disconnect the control outputs from the level controller card, as these will not function properly until the plant has run for sufficient time to allow accumulation of a reference head of condensate in the level measurement loop. (Until then, do level control on the separation pots by hand, plugging and unplugging the control cables to the control card.)

3. Switch on the power to the PC and rack system. Power up the PC and let it go through the bootup procedure.

4. Go to the hard disk directory holding the control software. Check that the executable files RP_NEW.EXE, TEMPRD5.EXE and PLOTCH.EXE are present.

5. Start the monitoring program (RP_NEW.EXE).

6. Switch the temperature scan ON, using a scan period of about 10 seconds. If no message appears in the ALARM window, the scan is OK. Otherwise, check the cables connections to the CIL boxes and repeat.

7. Check the indicated tank pressures with the gauge pressure readings. If a pure fluid is being used, check the pressure and indicated temperature against vapour pressure tables. If the pressure is significantly higher than the vapour pressure, there is air in the system. In this case, crack one of the joints on the tank top and allow gas to vent from the tank for a few seconds, then retighten. Wait for a few minutes, then check the integrity of the joint with the refrigerant leak detector torch.

8. Check the flowrates indicated by the program against the rotameter calibration charts. If there is a significant deviation, try flushing through the bypass line of the pressure transmitter.

9. Plug in the power supplies to the heater element and solenoid valve relay boxes.

10. From the PC, switch on the heater elements and check the tanks for signs of operation (bubbles rising, hissing sounds, convection patterns.) Switch the heaters off again.

11. Using the PC, switch the solenoid valves and check that they function. Leave both valves SHUT.

12. Set target temperatures for the hot and cold water streams from the console, selecting the Auto control option from the screen display. Typical starting setpoints might be 60 °C for the hot water and 30 °C for the cold water. These will take about 20 minutes to reach the setpoints from cold, as the whole pipework and associated units need to be warmed up too.

13. At the same time as starting the water heaters, switch on the the tape heater wrapped around the compressor oil separator.

14. When the water temperatures have come close to setpoints, use the PC to set the metering pump to about 25% on each head. If using a pure working fluid, the initial takeoff should be from the tank with most liquid; if using a mixture, start up using the tank with the higher vapour pressure, as this will give a higher heat output.

15. Connect the power to the compressor and metering pump. Switch the pump motor on and observe the indicated evaporator level. When this reaches about 30 cm, or if the evaporator pressure exceeds 20 psig, start the compressor at a setting of about 20%. Leave the compressor running at this speed for several minutes. If the evaporator level continues to rise, switch the pump off. The purpose of running the compressor in this way, developing no great pressure lift and returning gas to the suction, is to pump excess oil from the casing back into the oil separator. If this is not done, the compressor may stall with unpleasant thumping noises as a vane impacts against a slug of oil.

16. Open the compressed air supply valve and check that all the control valve pressure indicators are showing about 3 psig. Shut the control valve and bypass valve on the lines between the two condensers. The control valve on the hot water line should be left full open, all others should be shut.

17. Once the compressor has run for several minutes, shut the secondary oil return line check valve (The secondary line runs from the top of the oil separator to the compressor suction.) Set the other valves in the suction line to bypass the filter element. The compressor should now draw vapour from the evaporator, causing the pressure there to drop and heat to be transferred in the unit. If there are no unusual noises from the compressor, it is probably safe to increase its speed.

The above steps constitute the basic startup procedure. The task now is to warm up the fabric of the plant and achieve stable steady states in the evaporator and condenser. The plant is run initially using only the first condenser, as this makes it easier to recover refrigerant and maintain a cyclic operation. There will be a tendency for refrigerant to collect in the oil separator until the compressor and its charge of oil have warmed up, so there will be a delay of some minutes before condensate is observed to accumulate in the receiver attached to the first condenser. The heater tape on the separator is meant to reduce this problem. Another useful procedure is to crack open the secondary return line for 30s every few minutes until there is at least 15 °C of superheat observed on the compressor suction gas; this will return any liquid formed in the compression process to the suction.

It is important to keep watch on the quantities of refrigerant distributed throughout the plant. The evaporator should be run so that there is a small degree of superhet observed, but should not be run flooded if this can be avoided. This requries constant adjustment of the metering pump settings. The level of condensate in the receiver should also be watched: once this has started to accumulate in appreciable quantity,

try connecting the hardware controller card to the throttle valve on the receiver liquid outlet. If this does not control the level but rather results in a continuous blowdown, there is still insufficient liquid in the reference leg of the transducer. This will be cured with a few more minutes of operation. In the interim, open and shut the control valve by hand (connect the control line to the card to open the valve, disconnect to close) to let refrigerant back into the storage tank.

For obvious reasons of safety, watch the pressures recorded in the evaporator and storage tanks. The maximum safe working pressures are 25 psig for the evaporator, 35 psig for the storage. Each of these units is protected by a relief valve but this should not be relied on to compensate for overpressure. The storage tank pressure may be lowered by opening the solenoid valve on the tank vapour outlet; this connects the tank to the compressor suction. The evaporator pressure may be reduced by: increasing the compressor speed; stopping the flow of water through the evaporator, or reducing the refrigerant feed rate.

The initial target of operation should be attainment of a steady state of operation, in which the pressure levels and temperatures in the refrigerant pipework are stable with time. Once cyclic operation has been attained, and refrigerant is returning to the storage tank from the condenser, it is reasonable to increase the compressor speed and feed pump rate. This will alter the pressure levels in the evaporator and condenser if nothing else is changed but the system should settle down fairly quickly to a change in speed. The slow part of the procedure is the establishment of cyclic operation, which usually requires that the whole system be completely warmed up.

B.4 Normal Operation

Once an initial steady state has been reached, it is possible to bring the hardware level controller on line and to introduce the second condenser unit. The control problem now becomes more complex, as the split of the condensation process between the two condensers is a function of the hot water (heat sink) capacity rate and the compressor throughput. Use the flow control valve between the first and second condenser and the valve between the second condenser and compressor suction to control the pressure in each condenser: maintaining a higher pressure in the first condenser than the second should cause flow of vapour to the second unit. A reduction of water flowrate will also increase the proportion of condensation taking place in the second condenser, by reducing the driving force in the first unit. The degree of condensation is easily seen by looking at the measured water temperatures at the inlet and outlet of each condenser.

Once condensation is achieved in both units, the second head of the metering pump may be brought into play. The settings of the pumpheads must be adjusted so that the level in each storage tank stays approximately constant; in other words, so that the rate of condensation in each condenser is balanced by the feed rate from the associated storage. This control problem has not been automated by the author, so this requires careful adjustment of all the process variables by the operator.

B.5 Shutdown Procedure

A normal, controlled shutdown should be performed with the following aims:

- Safety: avoidance of hazard caused by sudden alteration of the system.
- Steady reduction of the pressure levels in the refrigerant system.
- Collection of refrigerant in the low-pressure storage at the end of the run.

The procedure used by the author to shut down the plant is as follows:

1. Switch all the tank heaters off and disable tank temperature control.
2. Open the cold water bypass line through the plate heat exchanger, which will cause heat to be dumped from the hot water circuit to the cold water circuit.
3. Switch the metering pump off.
4. Reduce the compressor speed to about 35% of maximum.
5. Partially open the drain line valve on the cold water tank, to force makeup of cold water from the mains *via* the ballcock. This dumps heat into the drain.
6. Continue to run the compressor for several minutes, observing the pressure in the condensers fall as the heat sink temperature falls. Watch the glass tank pressures and liquid levels: if either becomes too high, a careful use of the isolation valves attached to the storage tanks should enable transfer of refrigerant to the other vessel. The purpose of running the compressor, rather than shutting it off immediately, is to extract as much refrigerant as possible from the evaporator and oil separator. To this end, shut the check valve on the evaporator feed; also shut the valves on the metering pump feed lines.

Once the heat fluxes in the evaporator and condensers have reduced to zero, or very small values, there is no more refrigerant in the active pipework and the compressor may be switched off. Shut off the compressor and compressed air supply. Switch off the water pumps. Shut the drain valve on the cold water tank and switch off all mains water flows through the rig. The plant is now shut down. The control program may be halted and the instrument system switched off. Also switch off the mains supplies to the pump motors, relay boxes and compressor control box.

Emergency Stop The control program has an emergency stop procedure which merely switches all control outputs to zero and displays an appropriate message. To achieve a manual emergency stop (which may be necessary should the computer fail):

1. Cut power to the compressor, metering pump and cold water pump.
2. Switch off the compressed air supply: this should cause all control valves to fail to their safe positions.
3. Boost water flow through the condensers to maximum, simultaneously switching off the power to the tank heater elements. If all else fails pull out the power cables.
4. Increase mains water flow through the subcoolers and tank cooling coils to maximum.

Initiating an emergency stop will disrupt the equilibrium of the plant and so may terminate an experiment. The main reason for using such a drastic option is to deal with an equipment failure, for example a pipe fracture, where all refrigerant flow must be halted as soon as possible. Normally it should be possible to deal with problems such as overpressure by less radical measures.

Appendix C

Program Listings

This Appendix holds the source code listings for all, or parts of, the programs written by the author as part of the research work which have been referenced in the body of the thesis. In order to keep the size of this Appendix below the size of the rest of the work, only key routines are reproduced here.

C.1 Programs Used with Pilot Plant

C.1.1 Main Control Program

The main() function from the source code of the heat pump pilot plant is given here as an accompaniment to the explanation of that program's function included in Chapter 3. The code for this includes references to many subroutines not included in this Appendix:

the names of these are mostly self-explanatory.

```
/* Global variables, to be used in other routines etc. */
/* These are all controlling variables and must be visible to the */
/* routines for alarms, control of outputs and so on. */

char *options[7]; /*Menu titles list. */
control_info *convar[4]; /*Info on the controlled signals*/
logical pumpmode=OFF; /*Flag for pump motor control  */
logical valvemode=OFF; /* "     "  solenoid valves */
logical heatmode=OFF; /* "     " tank heaters */
logical hwheater=OFF,cwheater1=OFF,cwheater2=OFF;
logical Tflag=OFF,quit=FALSE;
logical bflag=OFF,fflag=OFF;
file_info *bfil,*ffil;
byte pumpmotor=0; /*Controls the pump motor; */
double iscan=5.,Tscan=5.; /*Scanning frequencies in sec. */
double hw_set=60.0,cw_set=30.0; /*water temperature setpoints */
double hw_dead=0.5,cw_dead=0.5; /*dead bands for water control */
double write_every=60.0; /*File update interval in sec. */
int Tbits[2][16]; /*Array of CIL box ints */
double T[2][16]; /*Array of temperatures */
double invals[16]; /*Array of analogue inputs */
int inbits[16]; /* ""         ""      "" */
int CWhole=0; /*Orifice plate size indices for*/
int HWhole=1; /* flow meters (0=8mm,1=5mm,..)*/
double pump1,pump2; /*Positions of metripump heads */
double p1rate,p2rate; /*Pump rates in litre/min */
double Tload=25.0,dTc,dTev; /*Temperature signals */
double Pc1=0.0,Pc2=0.0,Pt1,Pt2,Pev; /*Pressure values */
double level; /*Evaporator level in cm. */
double CWrate,HWrate; /*Water flowrates in litre/min */
double Qevap,Qc1,Qc2,Qphe,Qct; /*Heat exchanger heat fluxes */
double Wcomp,cmp_spd=0.0,cmp_cur;/*Compressor parameters */
double COPa,COP1; /*Coefficients of Performance */


/********************** End of includes and defines **********************/

main()
{
/* This is the main() function for the heat pump monitor program.
*/
time_t now,ithen,Tthen,fthen; /*Time variables for clocking */
clock_t cstart,cnow; /*scan rates, control, etc. */
```

```
int hitkey;
double cstep,tcbuf;

popup_info *menu[NMENUS]; /*Info for each popup window */
MENUFUNC fnlist[NMENUS]; /*Array of menu functions. */

/********************** End of variable definitions for main() **********/

/* Call set-up routines to reset screen, initialise I/O cards, etc */

get_orifice_settings(&HWhole,&CWhole);
initialise();
setup_menus(options,menu,NULL,fnlist);
refresh_screen();
popup_menu(options,NMENUS,menu,fnlist,NULL);

/****** Now start looping round the main control instructions */
time(&Tthen);
fthen=ithen=Tthen;
cstart=clock();
while(quit==FALSE) /* START LOOP */
{
now=show_time();/*retrieve time and display it */
cnow=clock(); /*use clock() for control timestep */
cstep=(double)(cnow-cstart)/CLK_TCK;

/* Scan controlled pressure inputs */
Pc1=PDCR_35barg(13);
Pc2=PDCR_35barg(7);

/* Read independent thermocouple */
Tload=(double)sample_ADchan(THERMOCOUPLE)/TGAIN;

/* Read evaporator level indication signal */
level=evap_level(5,T[1][8]);
/* Take control action on the software control loops */
do_control(cstep,Tload,Pc1,Pc2,cmp_spd);
cstart=cnow;

/* Scan temperatures when required */
if(Tflag==ON&&difftime(now,Tthen)>=Tscan)
{
scan_temps(Tbits,T);
use_window(OUTPUT);
swap_colours();
print_temps(T);
```

```
swap_colours();
Tthen=now;

/* Update control action on heater switches */
if(heatmode==ON)
{
if(T[0][12]<(hw_set-hw_dead))
hwheater=ON;
else if(T[0][12]>(hw_set+hw_dead))
hwheater=OFF;
if(T[1][12]<(cw_set-cw_dead))
cwheater1=ON;
else if(T[1][12]>(cw_set+cw_dead))
cwheater1=OFF;
switch_heaters();
}
}

/* Scan analogue inputs if time is right... */
if(difftime(now,ithen)>=iscan)
{
scan_inputs();
display_inputs();
if(pumpmode==ON) /* Control pump */
{
if(level>48.0)
switch_pump(OFF);
else if(level<20.0)
switch_pump(ON);
}
ithen=now;
}

/* Check for a keypress using kbhit() */
use_window(SCREEN);
if(kbhit())
{
if((hitkey=getch())==0)
{ /* Shut down plant AT ONCE */

if((hitkey=getch())==FKEY_1)
EmergencyStop();
}
/* Activate menu on press of <Return> key */
else if(hitkey==CARR_RET)
popup_menu(options,NMENUS,menu,fnlist,NULL);
```

```
}

/* Update data log files if the time is right... */
if(difftime(now,fthen)>=write_every&&write_every>0.0&&fflag==ON)
{

use_window(ALARM);
clrscr();
beep();
cprintf("Updating record file %s\r\n",ffil->name);
update_files(&now);
clrscr();
fthen=now;
}
} /*END OF MAIN PROGRAM LOOP */

terminate(); /*Tidy up files, etc. and quit */
} /* END OF ROUTINE */
```

C.2 Evaporator Modelling Routines

C.2.1 Sequential Evaporator Model

These subroutines were the core of the sequential evaporator model, which took specified inlet conditions and heat transfer coefficients and calculated the evaporator capacity and output temperatures. There are three subroutines:

- `counter_shell()`: Routine to solve a single evaporator/superheater shell, assuming countercurrent water/refrigerant flow.
- `coflow_shell()`: Analagous to `counter_shell()`, this solves for the case of a co-current flow shell.
- `solve_evaporator()`: Routine to solve the complete three-shell evaporator in the original configuration supplied by Cal-Gavin Ltd.

```
int counter_shell(Mw,Twi,Tri,UAe,UAh,Cpg,lam,Two,Tro,Mr)
double Mw,Twi,Tri,UAe,UAh,Cpg,lam,*Two,*Tro,*Mr;
{
/* Routine to solve one shell of the evaporator. The assumption is that
the refrigerant is pure, saturated liquid at its bubblepoint
when entering the unit. Flow is counter-current.
The required inputs are:
Mw....mass flow of water in kg/s
Twi...inlet water temperature in degC
Tri... "      "       "        "   "
UAe...assumed heat transfer product for evaporation, kW/K
UAh...  "      "      "         "    "   gas superheat, kW/K
Two...address of variable to hold outlet water temperature
Tro...  "      "    "      "   "    "    gas       "
Mr....  "      "    "      "   "    "    gas flowrate, kg/s
*/

double Told,Tnew,G,K,W,R,I,A1,A2,fold,fnew;
double dTe,dTh;
int i,flag;

/* Now calculate useful numbers, like the water stream capacity rate */
W=Mw*4.184; /*CW heat capacity rate in kW/K */
lam=W/lam; /* Useful for the calculation of mass flow */

/* Initialise the guess on intermediate temperature */
Tnew=Twi-(Twi-Tri)*UAh/UAe;

/* Auxiliary parameters... */
I=Twi-Tri;
A1=exp(UAe/W);
A1=1.0-1.0/A1;
A2=UAh/W;
flag=0;
for(i=1;i<25;i++)
{
/* Solve the evaporator for the latest dT */
dTe=(Tnew-Tri)*A1;
*Mr=lam*dTe;
/* Now solve the superheater: */
R=(*Mr)*Cpg;
K=W/R;
G=exp((1.0-K)*A2);
dTh=I*(G-1.0)/(G-K);
fnew=Twi-dTh-Tnew;
```

```
if(i==1)
{
fold=fnew;
Told=Tnew;
Tnew=Twi-dTh;
continue;
}
if(fabs(fnew)<0.05) /* Test for convergence */
{
flag=1;
break;
}
Tnew=Tnew-fnew*(Tnew-Told)/(fnew-fold);
fold=fnew,Told=Tnew;
} /* End of iteration loop */

/* Calculate exit temperatures */
*Two=Twi-(dTh+dTe);
*Tro=Tri+K*dTh;
return(flag);
}
/******************** End of counter_shell() ************************/

int coflow_shell(Mw,Twi,Tri,UAe,UAh,Cpg,lam,Two,Tro,Mr)
double Mw,Twi,Tri,UAe,UAh,Cpg,lam,*Two,*Tro,*Mr;
{
/* Routine to solve one shell of the evaporator. The assumption is that
the refrigerant is pure, saturated liquid at its bubblepoint
when entering the unit. Flow is co-current.
The required inputs are:
Mw....mass flow of water in kg/s
Twi...inlet water temperature in degC
Tri... "      "       "        "   "
UAe...assumed heat transfer product for evaporation, kW/K
UAh...  "      "      "         "    "   gas superheat, kW/K
Two...address of variable to hold outlet water temperature
Tro...  "      "    "      "   "    "    gas       "
Mr....  "      "    "      "   "    "    gas flowrate, kg/s
*/

double Told,Tnew,G,K,W,R,Ie,Ih,A1,A2,fold,fnew;
double dTe,dTh;
int i,flag;

/* Now calculate useful numbers, like the water stream capacity rate */
W=Mw*4.184; /*CW heat capacity rate in kW/K */
```

```
lam=W/lam; /* Useful for the calculation of mass flow */

/* Initialise guess at intermediate temperature */
Tnew=Twi-(Twi-Tri)*(1.0-UAh/UAe);

/* Auxiliary parameters... */
Ie=Twi-Tri;
A1=exp(UAe/W);
A1=1.0-1.0/A1;
A2=UAh/W;
flag=0;

for(i=1;i<25;i++) /* Start iteration loop */
{
/* Solve the evaporation section for the latest dT */
dTe=Ie*A1;
*Mr=lam*dTe;
/* Now solve the superheater: */
R=(*Mr)*Cpg;
Ih=Tnew-Tri;
K=W/R;
G=exp((1.0+K)*A2);
dTh=Ih*(G-1.0)/(G*(K+1.0));
fnew=Twi-dTh-Tnew;
if(i==1)
{
fold=fnew;
Told=Tnew;
Tnew=Twi-dTh;
continue;
}
if(fabs(fnew)<0.05) /* Test for convergence */
{
flag=1;
break;
}
Tnew=Tnew-fnew*(Tnew-Told)/(fnew-fold);
fold=fnew,Told=Tnew;
} /* End of iteration loop */

/* Calculate water and refrigerant exit temperatures */
*Two=Twi-(dTh+dTe);
*Tro=Tri+K*dTh;
return(flag);
}
/******************** End of coflow_shell() ************************/
```

```
double solve_evaporator(Mw,Mr,Tw,Tr,UAe,UAh,lam,Cpg)
double Mw,Mr[],Tw[],Tr[],UAe,UAh,lam,Cpg;
{
/*  Calling routine to solve the evaporator in the normal configuration,
given inlet conditions and heat transfer products.
Parameters:
Mw Water flowrate, kg/s
Mr refrigerant flowrates in each shell, kg/s
Mr0...total flowrate
Mr1...flow in shell 1 (counter-current)
Mr2...flow in shell 2 (co-current)
Mr3...flow in shell 3 (counter-current)
Tw Water temperatures, Kelvin
Tw0...inlet temperature
Tw1...exit from shell 1
Tw2...exit from shell 2
Tw3...exit from shell 3
Tr Refrigerant temperatures, Kelvin
Tr0...boiling temperature
Tr1...exit from shell 1
Tr2...exit from shell 2
Tr3...exit from shell 3
Tr4...combined exit temperature
UAe Evaporative heat transfer product, kW/K
UAh Superheating heat transfer product, kW/K
lam latent heat of refrigerant, kJ/kg
Cp Specific heat of refrigerant vapour, kJ/kgK

*/
double duty;

/* Check the value of UAe: if it's zero then the evaporator does no
work, so set data accordingly and return...
*/
if(UAe==0.0)
{
Tw[1]=Tw[2]=Tw[3]=Tw[0];
Tr[1]=Tr[2]=Tr[3]=Tr[4]=Tr[0];
Mr[0]=Mr[1]=Mr[2]=Mr[3]=0.0;
duty=0.0;
}
else
{
counter_shell(Mw,Tw[0],Tr[0],UAe,UAh,Cpg,lam,&Tw[1],&Tr[1],&Mr[1]);
coflow_shell(Mw,Tw[1],Tr[0],UAe,UAh,Cpg,lam,&Tw[2],&Tr[2],&Mr[2]);
```

```
counter_shell(Mw,Tw[2],Tr[0],UAe,UAh,Cpg,lam,&Tw[3],&Tr[3],&Mr[3]);
Mr[0]=Mr[1]+Mr[2]+Mr[3];
Tr[4]=(Mr[1]*Tr[1]+Mr[2]*Tr[2]+Mr[3]*Tr[3])/Mr[0];
duty=4.184*Mw*(Tw[0]-Tw[3]);
}
return(duty);
} /* END OF ROUTINE */
```

C.2.2 Rigorous (Simultaneous) Evaporator Model

The only routine reproduced here is the routine which evaluated the values of the equation residuals; it was called by a multi-dimensional Newton-Raphson iteration algorithm routine. This was also written by the author but there was nothing exceptional about the code which justified its inclusion here.

```
void evapfns(x,fx,dfdx)
double x[],fx[],*dfdx[];
{
/*  Parameters:
x vector of current variable values
fx vector to hold residuals of the model equations
dfdx matrix to hold the Jacobian of the model equation set.
*/
/* Function to evaluate the residuals and their partial derivatives for
the rigorous evaporator model. Explanation of the variables follows.
The problem has 14 unknowns, numbered 0-13. The actual dimension of
the vector 'x' is 21: the physical properties and fixed parameters
are passed into this routine in slots 14-20. Temperatures are in
Kelvin throughout. NB that the log-mean temperature differences
which should appear in thse equations have been replaced by arithmetic
means to simplify the form of the equations.

Description of variables:

Index Description
-------------------------------------------------------------------------
0 Feed of refrigerant to shell 'A'
1   "   "     "        "   "   'B'
```

```
2   "   "     "        "   "   'C'
3 Refrigerant exit temperature from shell 'A'
4 Refrigerant exit temperature from shell 'B'
5 Refrigerant exit temperature from shell 'C'
6 Combined refrigerant exit temperature
7 Intermediate water temperature for shell 'A'
8 Shell 'A' water exit temperature
9 Intermediate water temperature for shell 'B'
10 Shell 'B' water exit temperature
11 Intermediate water temperature for shell 'C'
12 Evaporative heat transfer product, (UA)e in kW/K
13 Superheating heat transfer product, (UA)h in kW/K

Description of fixed parameters:

Index Description
-------------------------------------------------------------------------
14 Refrigerant boiling point tb
15 Water inlet temperature Twi
16 Water exit temperature Two
17 Refrigerant total mass flow, mr in kg/s
18 Water capacity rate (mw.Cpw) in kW/K
19 Refrigerant latent heat at tb in kJ/kg
20 Refrigerant (saturated) vapour specific heat at tb in kJ/kgK
21 Feed vapour fraction (in range 0-1)

Description of equations:

Index Description
-------------------------------------------------------------------------
0 Heat balance on evaporative part of shell 'A'
1 Heat transfer relation for evaporative part of shell 'A'
2 Heat balance on superheat section of shell 'A'
3 Heat transfer relation for superheat section of shell 'A'
4 Heat balance on evaporative part of shell 'B'
5 Heat transfer relation for evaporative part of shell 'B'
6 Heat balance on superheat section of shell 'B'
7 Heat transfer relation for superheat section of shell 'B'
8 Heat balance on evaporative part of shell 'C'
9 Heat transfer relation for evaporative part of shell 'C'
10 Heat balance on superheat section of shell 'C'
11 Heat transfer relation for superheat section of shell 'C'
12 Refrigerant mass balance on feed manifold
13 Refrigerant heat balance on outlet manifold

*/
```

```
int i,j;
double Ue2,Uh2,tb,tb2,W,lam,Cr,Twi,Two;

/* Assign useful constants here to reduce working */
tb=x[14];
tb2=tb+tb;
Twi=x[15];
Two=x[16];
W=x[18];
lam=x[19];
Cr=x[20];
Ue2=x[12]/2.0;
Uh2=x[13]/2.0;

/* Assign equation residuals here... */
/* Shell A equations... */
fx[0]=x[0]*lam-W*(x[7]-x[8]);
fx[1]=W*(x[7]-x[8])-Ue2*(x[7]+x[8]-tb2);
fx[2]=Cr*x[0]*(x[3]-tb)-W*(Twi-x[7]);
fx[3]=W*(Twi-x[7])-Uh2*(Twi+x[7]-x[3]-tb);
/* Shell B equations... */
fx[4]=x[1]*lam-W*(x[8]-x[9]);
fx[5]=W*(x[8]-x[9])-Ue2*(x[8]+x[9]-tb2);
fx[6]=x[1]*Cr*(x[4]-tb)-W*(x[9]-x[10]);
fx[7]=W*(x[9]-x[10])-Uh2*(x[9]+x[10]-x[4]-tb);
/* Shell C equations... */
fx[8]=x[2]*lam-W*(x[11]-Two);
fx[9]=W*(x[11]-Two)-Ue2*(x[11]+Two-tb2);
fx[10]=x[2]*Cr*(x[5]-tb)-W*(x[10]-x[11]);
fx[11]=W*(x[10]-x[11])-Uh2*(x[10]+x[11]-x[5]-tb);
/* Other equations... */
fx[12]=x[17]-(x[0]+x[1]+x[2]);
fx[13]=x[17]*x[6]-(x[0]*x[3]+x[1]*x[4]+x[2]*x[5]);

/* Now assign the derivative (Jacobian) matrix (many zeroes!) */

for(i=0;i<14;i++)
for(j=0;j<14;j++)
dfdx[i][j]=0.0;

dfdx[0][0]=dfdx[4][1]=dfdx[8][2]=lam;
dfdx[0][7]=dfdx[4][8]=dfdx[8][11]=dfdx[6][9]=dfdx[10][10]=-W;
dfdx[0][8]=dfdx[2][7]=dfdx[4][9]=dfdx[6][10]=dfdx[10][11]=W;
dfdx[1][7]=dfdx[5][8]=dfdx[9][11]=W-Ue2;
dfdx[1][8]=dfdx[5][9]=-W-Ue2;
```

```
dfdx[3][7]=dfdx[7][10]=dfdx[11][11]=-W-Uh2;
dfdx[7][9]=dfdx[11][10]=W-Uh2;
dfdx[3][3]=dfdx[7][4]=dfdx[11][5]=Uh2;
dfdx[12][0]=dfdx[12][1]=dfdx[12][2]=-1.0;
dfdx[1][12]=-(x[7]+x[8]-tb2)/2.0;
dfdx[2][0]=Cr*(x[3]-tb);
dfdx[2][3]=x[0]*Cr;
dfdx[3][13]=-(Twi+x[7]-x[3]-tb)/2.0;
dfdx[5][12]=-(x[8]+x[9]-tb2)/2.0;
dfdx[6][1]=Cr*(x[4]-tb);
dfdx[6][4]=Cr*x[1];
dfdx[7][13]=-(x[9]+x[10]-x[4]-tb)/2.0;
dfdx[9][12]=-(x[11]+Two-tb2)/2.0;
dfdx[10][2]=Cr*(x[5]-tb);
dfdx[10][5]=Cr*x[2];
dfdx[11][13]=-(x[10]+x[11]-x[5]-tb)/2.0;
dfdx[13][0]=-x[3];
dfdx[13][1]=-x[4];
dfdx[13][2]=-x[5];
dfdx[13][3]=-x[0];
dfdx[13][4]=-x[1];
dfdx[13][5]=-x[2];
dfdx[13][6]=x[17];

}
/***************** End of evapfns() ***********************************/
```

C.3 CCOR Equation of State Routines

C.3.1 Pure Fluid Vapour Pressure Routine

This routine is the final implementation of Algorithm 6.3. It calculates the vapour pressure of a fluid at a specified temperature by Newton-Raphson iteration

```
int CCORsatPVT(T,a,b,c,d,cr,Ps,vf,vg)
```

```
double T,a,b,c,d,cr;
double *Ps,*vf,*vg;
{
/* This routine finds saturated vapour pressure from first principles,
by iterating on pressure to obtain equality of fugacity coefficient
between phases. The return value is the number of iterations used
if the routine converges, 0 for non-convergence after 25 iterations,
or negative non-zero to indicate a problem.
Parameters:
T temperature in Kelvin
a,b,c,d,cr equation of state parameters at temperature T
Ps on entry, contains first pressure guess. On
return, contains final answer.
vf,vg addresses to hold liquid and vapour volumes at
the final pressure

The iteration is converged using Newton-Raphson with an analytic
derivative: the nature of the problem means that the update is a
simple multiple of the previous guess (the multiplying factor is the
local variable 'correct').
*/
double fg,fl,fdiff,correct,vloc[2],vo,RT;
int i,maxit,flag,nroots;

RT=Rg*T;
maxit=25,flag=0;

/* Start iteration loop */
for(i=0;(i<maxit)&&(!flag);i++)
{
/* Solve the equation of state for volume */
nroots=CCORvol(*Ps,T,a,b,c,d,cr,vloc);
if(nroots==1) /*There is a problem-probably T>Tc */
{
flag=-1;
fprintf(stderr,"CCORsatPVT():Only one real volume root: values follow:\n");
fprintf(stderr,"T:%4.3f P:%5.4e v:%5.4e\n",T,*Ps,vloc[0]);
break;
}
/* Find the fugacity of each phase */
fl=CCORlnphi(vloc[0],T,*Ps,a,b,c,d,cr);
fg=CCORlnphi(vloc[1],T,*Ps,a,b,c,d,cr);
*vf=vloc[0],*vg=vloc[1];
/* Calculate the iteration function */
fdiff=fg-fl;
```

```
/* Calculate the required pressure update factor */
correct=1.0-RT*fdiff/((*Ps)*(*vg-*vf));
if(fabs(fdiff)<=1.0E-7)
{
flag=i+1;
break;
}
/* Correct the pressure guess */
(*Ps)*=correct;
} /* END OF ITERATION LOOP */
if(!flag)
fputs("CCORsatPVT():Unconverged vapour pressure.\n",stderr);
return(flag);
} /*END OF ROUTINE */
```

C.3.2 Binary Mixture Dewpoint Calculation

This is the source code for the algorithm developed by the author to solve the fixed-temperature, binary dewpoint problem, described in Chapter 6. The algorithm has been formalised as Algorithm 6.5; it is also represented by Figure 6.2.

C.3.2.1 Referenced Subroutines

The following subroutines are referenced in the body of the algorithm; their functions are summarised here but the source code for the routines is omitted.

- `Pstar()`: Antoine-type correlation of pure component vapour pressure.
- `getCCORconsts()`: Calculates the pure component CCOR equation parameters at a given temperature and stores them to an array.
- `mixCCORconsts()`: Uses the equation of state parameters calculated by `getCCORconsts()` to generate parameters for a mixture of specified composition.
- `CCORvol()`: Solves the equation of state for a given temperature, pressure and composition; returns all real volume roots to the equation for processing by the calling routine.

- `getmixsums()`: Calculates auxiliary quantities (the composition derivatives of the equation of state parameters) for use in the calculation of component fugacity coefficients.
- `CCORlnphimix()`: Calculates all component fugacity coefficients from given P, v, T, x
- `CRITICAL_...()`: Macros to access the critical properties of the pure components (which were stored in global data arrays).
- `logical ...` a special enumerated variable defined by the author: takes the values TRUE or FALSE, by analogy with the FORTRAN `LOGICAL` variable type.

C.3.2.2 Main Source Code

The following source code was reproduced from a debugged and proven source code file. The comment statements included in this code explain the parameters and return codes used by the subroutine.

```
int CCORdewbubpt(T,xp,fa12,fc12,type,Pout,xi,vi,vp)
double T,xp,fa12,fc12;
int type;
double *Pout,*xi,*vi,*vp;
{
/* This solves for a dew or bubble point of a binary mixture at given
temperature and parent phase composition, using a nested iteration
process. The outer loop converges the pressure, while an inner loop
converges composition of the incipient phase. The solution for each
loop is achieved using a modified secant method, which obtains values
bracketing the root and updates these every step. Should an update
obtained by the secant step move away from the root, then a
false-position step is employed instead, to guarantee convergence.
The return values are:
0...the routine converged pressure and composition with success.
1... "   "   "   "     " neither pressure, nor composition.
2... "   "   "   "     " pressure but not composition.
3... "   "   "   "     " composition but not pressure.

The parameters passed in are:
T....temperature of system
xp...composition of known 'parent' phase
fa12..interaction constant for the 'a' parameter of the equation.
fc12..interaction constant for the 'c' parameter of the equation.
```

```
type..either 0 or 1, this denotes whether to solve for dew or bubble
point.
Pout...address for storage of the final pressure.
xi..... "   "   "   "   "  "   "  incipient phase composition.
vi..... "   "   "   "   "  "   "  incipient volume.
vp..... "   "   "   "   "  "   "  parent volume.

The notation of local variables is as follows:
A suffix of 'p' denotes parent (i.e. specified) phase.
A suffix of 'i'  "  "  incipient (i.e. unknown) phase.
A prefix of 'fp' "  "  value of the pressure iteration function.
A prefix of 'fx' "  "    "   "   "  composition "    "    "  "
mu...fugacity coefficient.
P....pressure variable.
v....volume
x....composition
*/
double P[2],vil[2],vpl[2],fx[2],fp[2],mup[2],mui[2];
double x[2],ap,bp,cp,dp,crp,ai,bi,ci,di,cri,psums[5],isums[5],**M;
double ppos,pneg,xpos,xneg,fppos,fpneg,fxpos,fxneg;
double pmax,pmin,xmax,xmin,fxnew,fpnew,tol,z1,z2,ps1,ps2,Vcmp,Vcmi,RT;
double vc1,vc2,vcfact;
int ip,ix,i,j,k,parm,itmax,nroots,retval=1,pflag;
logical pconverged,xconverged,pposflag,pnegflag,xposflag,xnegflag;
logical firstxloop,firstPloop;
double Pstar();
char *errs[4];

M=(double **)calloc(3,sizeof(double *));
for(i=0;i<3;i++)
M[i]=(double *)calloc(5,sizeof(double));

errs[0]="CCORdewbubpt() converged";
errs[1]="pressure and composition";
errs[2]="composition";
errs[3]="pressure";

/*Assign mol fraction vector to initial guess of xp=xi and find parent */
/*phase parameters. */
tol=1.0E-8;
getCCORconsts(T,fa12,fc12,M);
mixCCORconsts(xp,&ap,&bp,&cp,&dp,&crp,M);
RT=Rg*T;
/*Initialise pressure loop control variables, make initial guess of P. */
if(T<=CRITICAL_TEMP(MVC))
ps1=1.E5*Pstar(T,MVC);
```

```
else ps1=CRITICAL_PRESS(MVC);
ps2=1.E5*Pstar(T,LVC);
if(type==DEWPT) /*Dewpoint */
{
*Pout=ps2/(1+xp*(ps2/ps1-1.0));
*xi=1.0-*Pout*(1.0-xp)/ps2;
}
else
{
*Pout=xp*ps1+(1.0-xp)*ps2;
*xi=1.0-ps2*(1.0-xp)/(*Pout);
}

/* Calculate the approximate mixture critical volume for the parent
phase using Li's equation (Perry VI p3-267) */
vc1=CRITICAL_VOL(MVC);
vc2=CRITICAL_VOL(LVC);
vcfact=(vc1-vc2)*(vc1-vc2)/(vc1+vc2);
Vcmp = xp*vc1 + (1.0-xp)*vc2 - xp*(1.0-xp)*vcfact;

pconverged=pposflag=pnegflag=FALSE;
firstPloop=TRUE;
itmax=50;

/* Start pressure iteration loop HERE */
for(ip=1;ip<=itmax;ip++)
{

/*Find parent phase volume */
nroots=CCORvol(*Pout,T,ap,bp,cp,dp,crp,vpl);
if(nroots==3)
*vp=(type==0)?vpl[1]:vpl[0];
else *vp=vpl[0];
if((*vp<0.42*bp)) /* Test for safe volume */
*vp=(type==0)?RT/(*Pout):0.8*Vcmp;

/* Test parent phase volume against critical volume */
if( (*vp>Vcmp&&type==BUBBLEPT)||(*vp<Vcmp&&type==DEWPT) )
{
if(type==BUBBLEPT)
*Pout+=0.25*(ps1-*Pout);
else
*Pout+=0.025*(*Pout-ps2);
continue;
}
```

```
/*Find parent phase component fugacities */
for(i=0;i<2;i++)
{
getmixsums(i,xp,psums,M);
mup[i]=CCORlnphimix(*vp,T,*Pout,ap,bp,cp,dp,crp,psums);
}
xconverged=xposflag=xnegflag=FALSE;
firstxloop=TRUE;

/*******Start composition iteration loop HERE */
for(ix=1;ix<=itmax;ix++)
{
/*Find parameters for current value of xi */
mixCCORconsts(*xi,&ai,&bi,&ci,&di,&cri,M);

/*Solve EoS for incipient phase volume */
nroots=CCORvol(*Pout,T,ai,bi,ci,di,cri,vil);
if(nroots==3)
*vi=(type==DEWPT)?vil[0]:vil[1];
else *vi=vil[0];

/* Calculate incipient phase critical volume */
Vcmi=(*xi)*vc1+(1.0-(*xi))*vc2 -(*xi)*(1.0-*xi)*vcfact;

if((*vi<0.42*bi)) /* Test volume */
*vi=(type==1)?(RT/(*Pout)):(0.8*Vcmi);

/*Test for existence of liquid phase */
if( ( (*vi)<Vcmi&&type==BUBBLEPT)||((*vi)>Vcmi&&type==DEWPT))
{ /*No stable incipient phase...restart the */
/*iteration from a different pressure. */
if(type==DEWPT)
{
*Pout+=0.25*(ps1-*Pout);
}
else
{
*Pout-=0.025*(*Pout-ps2);
*xi=1.0-ps2*(1.0-xp)/(*Pout);
}

/*Find parent phase volume */
nroots=CCORvol(*Pout,T,ap,bp,cp,dp,crp,vpl);
if(nroots==3)
*vp=(type==DEWPT)?vpl[1]:vpl[0];
else *vp=vpl[0];
```

```
if((*vp<0.42*bp))
*vp=(type==0)?(RT/(*Pout)):(0.8*Vcmp);
/*Find parent phase component fugacities */
for(i=0;i<2;i++)
{
getmixsums(i,xp,psums,M);
mup[i]=CCORlnphimix(*vp,T,*Pout,ap,bp,cp,dp,crp,psums);
}
xconverged=xposflag=xnegflag=FALSE;
firstxloop=TRUE;
continue;
}
/*Find the incipient phase component fugacities */
for(i=0;i<2;i++)
{
getmixsums(i,*xi,isums,M);
mui[i]=CCORlnphimix(*vi,T,*Pout,ai,bi,ci,di,cri,isums);
}
/*Calculate auxiliaries z1,z2 and value of composition */
/*iteration function fx.  */
z1=xp*exp(mup[0]-mui[0]);
z2=(1.0-xp)*exp(mup[1]-mui[1]);
fxnew=z1/(z1+z2)-*xi;
                /*Update the root bounds */
if(fxnew<0)
{
xnegflag=TRUE;
fxneg=fxnew,xneg=*xi;
}
else
{
xposflag=TRUE;
fxpos=fxnew,xpos=*xi;
}
/*Test for convergence of the composition */
if(fabs(fxnew)<=tol)
{
xconverged=TRUE;
break;
}

if(firstxloop==TRUE)
{
x[0]=*xi,fx[0]=fxnew;
*xi+=fxnew;
firstxloop=FALSE;
```

```
continue;
}
x[1]=*xi,fx[1]=fxnew;

/* Check safety of secant step  */
if(fabs(fx[1]-fx[0])<1.e-20)
{
/* Try a false-position step */
if(xposflag==TRUE&&xnegflag==TRUE)
{
if(xneg<xpos)
xmax=xpos,xmin=xneg;
else
xmax=xneg,xmin=xpos;
*xi=xpos-fxpos*(xpos-xneg)/(fxpos-fxneg);
fx[0]=fx[1],x[0]=x[1];
continue;
}
else
{
fprintf(stderr,"CCORdewbubpt(): no change in fx\n");
break;
}
} /* End of code for unsafe secant */

/* The secant step is safe to take */
*xi-=fx[1]*(x[1]-x[0])/(fx[1]-fx[0]);
if(*xi>1.0) *xi=1.0;
if(*xi<0.0) *xi=0.0;
if(xposflag==TRUE&&xnegflag==TRUE)
{
if(xneg<xpos)
xmax=xpos,xmin=xneg;
else
xmax=xneg,xmin=xpos;
if(*xi<xmin||*xi>xmax)
*xi=xpos-fxpos*(xpos-xneg)/(fxpos-fxneg);
}
fx[0]=fx[1],x[0]=x[1];
} /*******END OF COMPOSITION ITERATION LOOP */
fpnew=1.0-(z1+z2);
if(fpnew<0)
{
pnegflag=TRUE;
pneg=*Pout,fpneg=fpnew;
}
```

```
else
{
pposflag=TRUE;
ppos=*Pout,fppos=fpnew;
}
/*Test pressure iteration function for convergence */
if(fabs(fpnew)<=100.0*tol)
{
pconverged=TRUE;
break;
}
if(firstPloop==TRUE)
{
P[0]=*Pout,fp[0]=fpnew;
*Pout*=1.001;
firstPloop=FALSE;
continue;
}
P[1]=*Pout,fp[1]=fpnew;

/* Check safety of secant update */
if(( fabs(fp[1]-fp[0])<=1.e-20) || P[0]==P[1])
{
/* try a false-position update */
                        if(pposflag==TRUE&&pnegflag==TRUE)
{
pmin=(ppos<pneg)?ppos:pneg;
pmax=(ppos<pneg)?pneg:ppos;
*Pout=ppos-fppos*(ppos-pneg)/(fppos-fpneg);
fp[0]=fp[1],P[0]=P[1];
continue;
}
else
{
fprintf(stderr,"CCORdewbubpt(): no change in fp\n");
break;
}
} /* End of case for unsafe secant */

*Pout-=fp[1]*(P[1]-P[0])/(fp[1]-fp[0]);
if(pposflag==TRUE&&pnegflag==TRUE)
{
pmin=(ppos<pneg)?ppos:pneg;
pmax=(ppos<pneg)?pneg:ppos;
if(*Pout<pmin||*Pout>pmax)
*Pout=ppos-fppos*(ppos-pneg)/(fppos-fpneg);
```

```
}
fp[0]=fp[1],P[0]=P[1];
} /******END OF PRESSURE ITERATION LOOP ********/

/* Now decide the return code... */
if(xconverged==TRUE&&pconverged==TRUE)
retval=0;
else
retval=(xconverged==FALSE&&pconverged==FALSE)?1:((xconverged==FALSE)?2:3);
free(M[0]);
free(M[1]);
free(M[2]);
free(M);
if(retval!=0) /*i.e. if unconverged */
{
fprintf(stderr,"CCORdewbubpt(): unconverged variables.\n");
fprintf(stderr,"Failed on: %s\n",errs[retval]);
}
return(retval);
}
/****************** End of CCORdewbubpt() *******************************/
```

Appendix D

Instrumentation Details

This appendix contains additional information on the instrumentation system which was used on the pilot plant.

D.1 Temperature Measurement

The temperatures throughout the plant were measured using K-type thermocouples, made in the department workshop. These were mounted in stainless steel pockets screwing into standard nipple glands. Each thermocouple was numbered: this number was written on the pcket mounting, attached to the connection wire and reproduced on the end connector plug of each line. The thermocouples were linked to the control PC using amplifier boxes manufactured by CIL Microsystems Ltd. Two PCI 1002 boxes were used: each box could accommodate 2 analogue voltage (0–1V) and 12 thermocouple signals. Internal cold junction compensation was built into the boxes, and the signals were returned to the PC as 12-bit digital numbers *via* an IEEE-488 interface. The form of this interface was non-standard,. and in order to enable the

IBM IEEE adapter to communicate with the boxes line 5 of the interface was disabled by disconnection of the wire inside the connecting multicore cable. This was clearly marked on the connector used. The identification of the thermocouples with box and channel slots is made in the following table:

Number	Name	Box	Channel
1	Compressor Suction	1	4
2	Compressor Discharge	1	5
3	Heavy Condensate	1	6
4	SC1 refrigerant out	1	7
5	Heavy storage tank	1	8
6	Light Condensate	2	4
7	SC2 refrigerant out	2	5
8	Light storage tank	2	6
9	C–1 vapour outlet	1	9
10	C–2 vapour outlet	2	7
11	Evaporator feed	2	8
12	Evaporator outlet	2	9
13	Water mains	1	15
14	Hot water tank	1	10
15	C–2 water inlet	1	11
16	C–2 water outlet	1	12
17	C–1 water outlet	1	13
18	PHE hot water outlet	1	14
19	DELETED		
20	Evaporator water in	2	13
21	Evaporator water out	2	14
22	PHE cold water outlet	2	15
23	DELETED		
24	DELETED		
25	DELETED		
27	Evaporator water from shell 1	2	10
28	Evaporator water from shell 2	2	11
29	Evaporator water from shell 3	2	12

Table D.1: Thermocouples Mounted on Pilot Plant

D.2 Pressure Measurement

Five pressure transducers were linked to the instrumentation system; details of these are given below. The interface circuitry for these units was designed and built by Matthew Rea. The I/O channel entry in this table corresponds to the channel of the Amplicon interface card which was used for each unit.

Location	Type	Range	I/O Channel
Evaporator	Landis & Gyr	0–10 barg	4
Heavy Storage	Druck PDCR510	0-15 barg	14
Light Storage	SHAPE SP1080	0–15 bara	15
First condenser	Druck PDCR510	0–35 barg	13
Second condenser	Druck PDCR510	0–35 barg	7

Table D.2: Pressure Transducers Mounted on Pilot Plant

D.3 Other Instrumentation

The other instruments connected to the PC are itemised in the following table, which lists the connection channel numbers for each unit.

Location	Type	Range	I/O Channel
Evaporator	Water thermopile	0–35°	11
Condensers	Water thermopile	0–35°	12
C1 water outlet	control thermocouple	0–100°C	10
Evaporator level	Druck PDCR120W	0–150 mbard	5
Cold water flow	Platon ΔP transmitter	0–150 mbard	0
Hot water flow	Platon ΔP transmitter	0–150 mbard	1
Pump head 1 position	potentiometer	0–100 l/hr	8
Pump head 2 position	potentiometer	0–100 l/hr	9
Compressor speed	driver output signal	0–10V	2

Table D.3: Instrument Connections to PC

D.4 Electronic Circuitry

The circuit diagrams for the instrumentation rack system cards are reproduced: the function of each circuit is explained by the appropriate figure caption

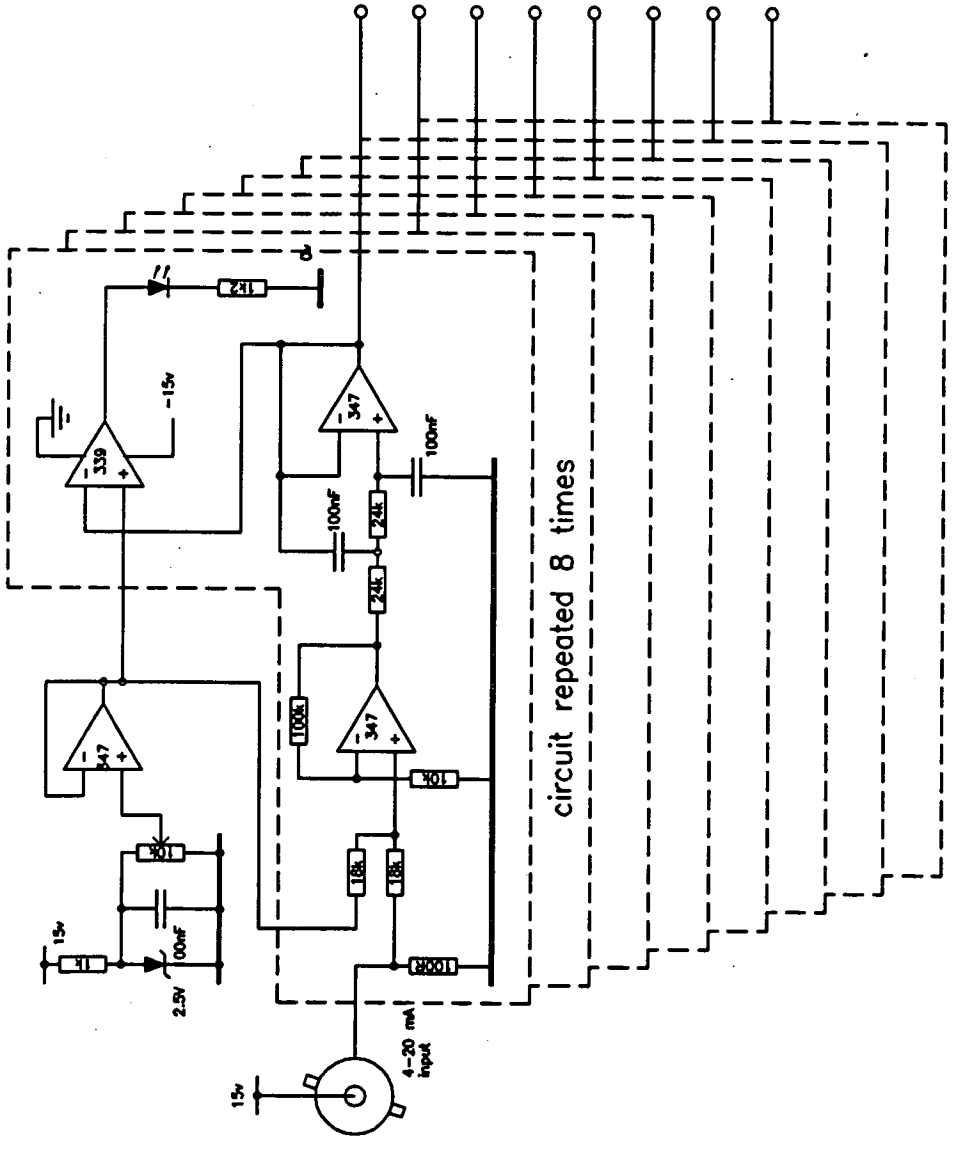

Figure D.1: Analogue Input Card: 8 by 4–20 mA inputs *via* 15V 2–wire connection

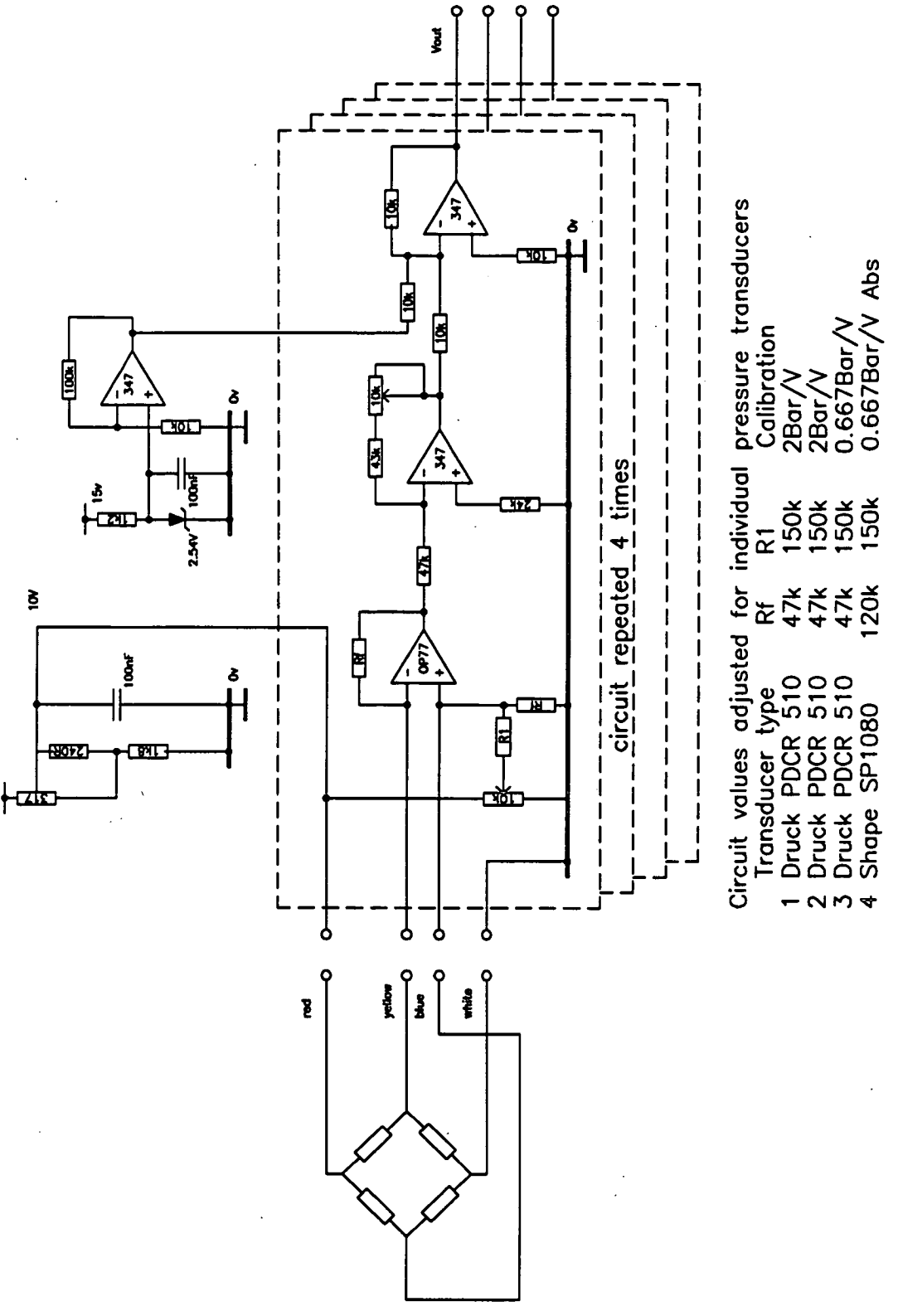

Circuit values adjusted for individual pressure transducers

	Transducer type	Rf	R1	Calibration
1	Druck PDCR 510	47k	150k	2Bar/V
2	Druck PDCR 510	47k	150k	2Bar/V
3	Druck PDCR 510	47k	150k	0.667Bar/V
4	Shape SP1080	120k	150k	0.667Bar/V Abs

Figure D.2: Pressure Transducer Amplifier/Conditioner Card

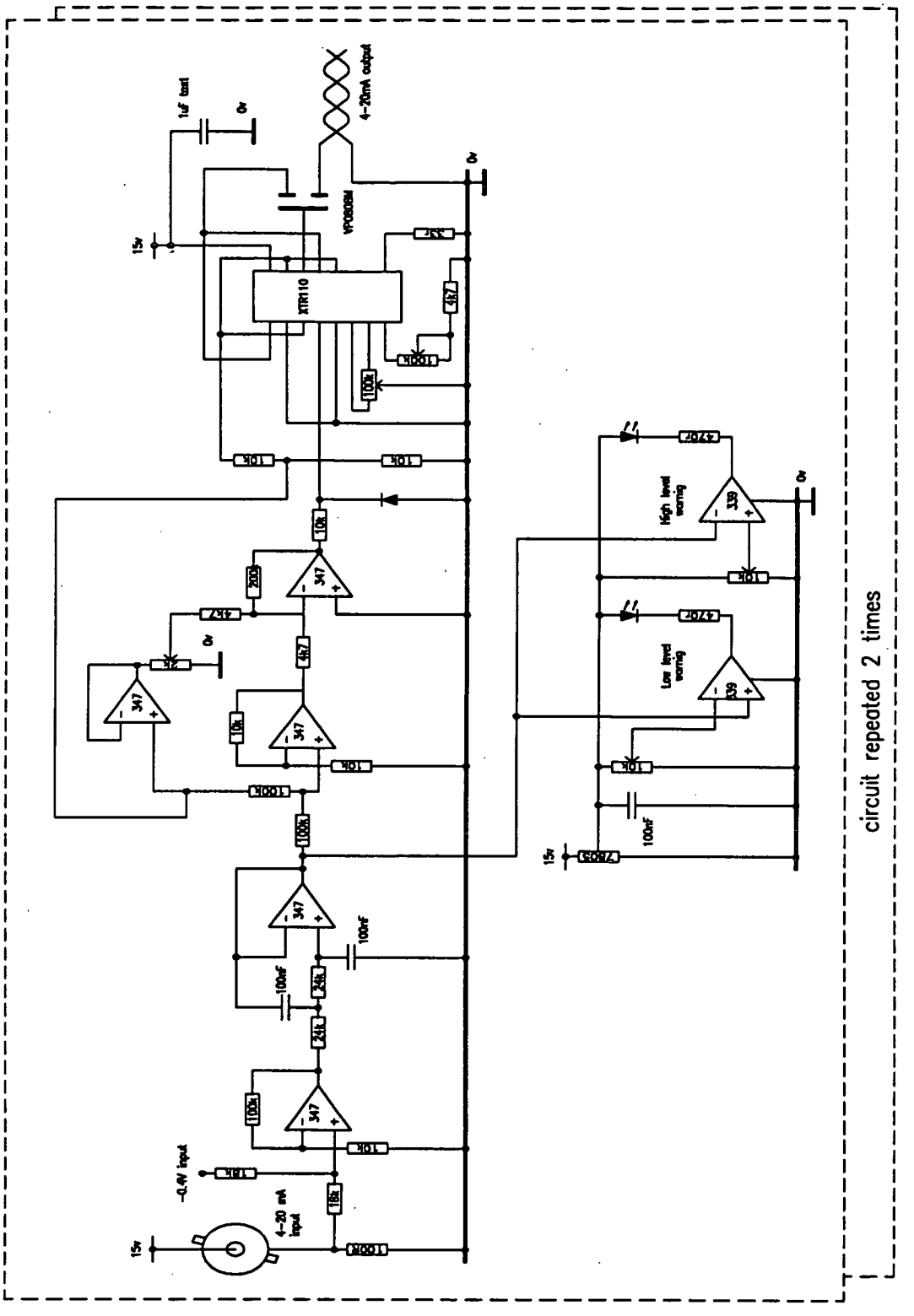

Figure D.3:

Level Controller Card

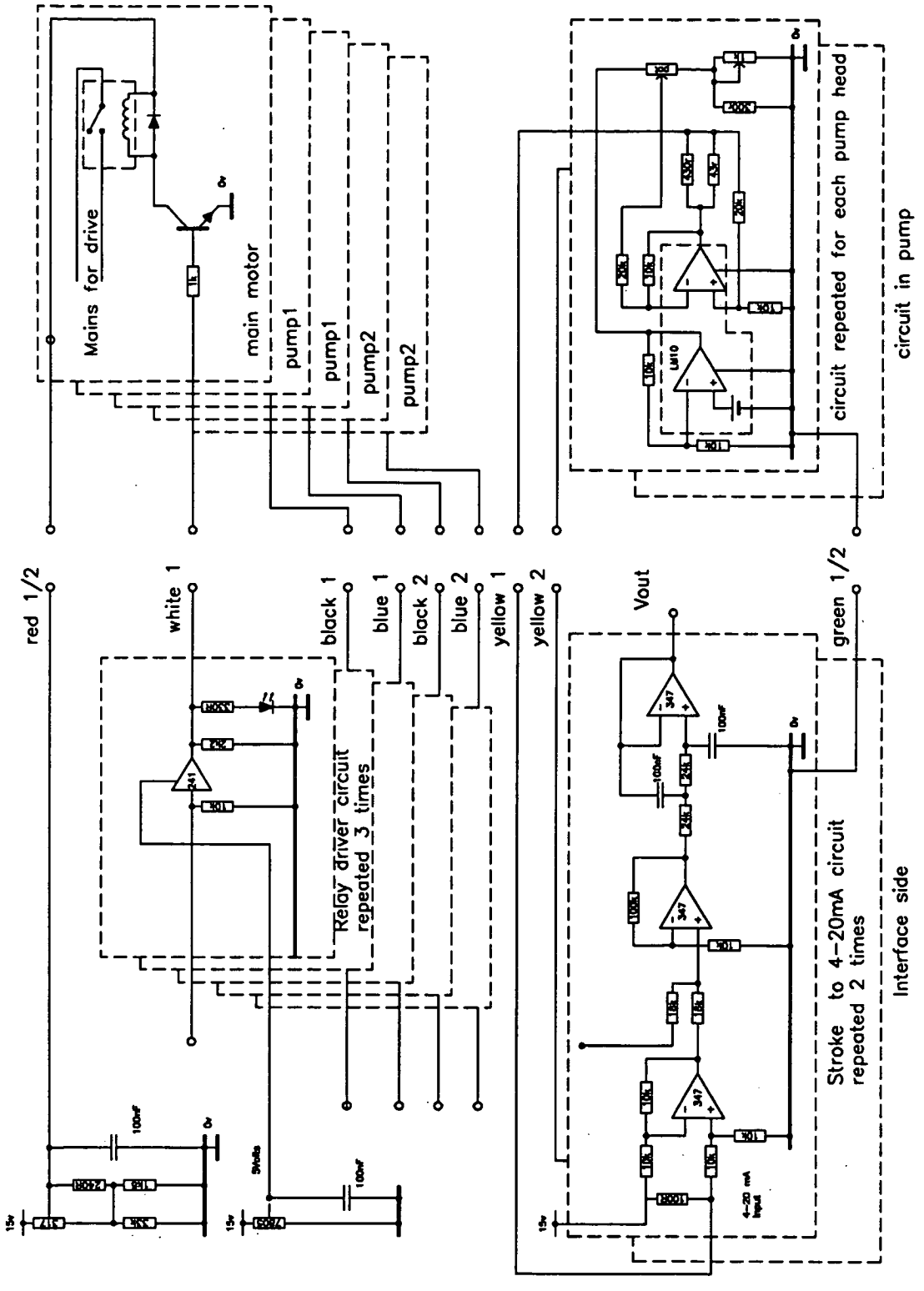

Figure D.4: Metering Pump Controller Card

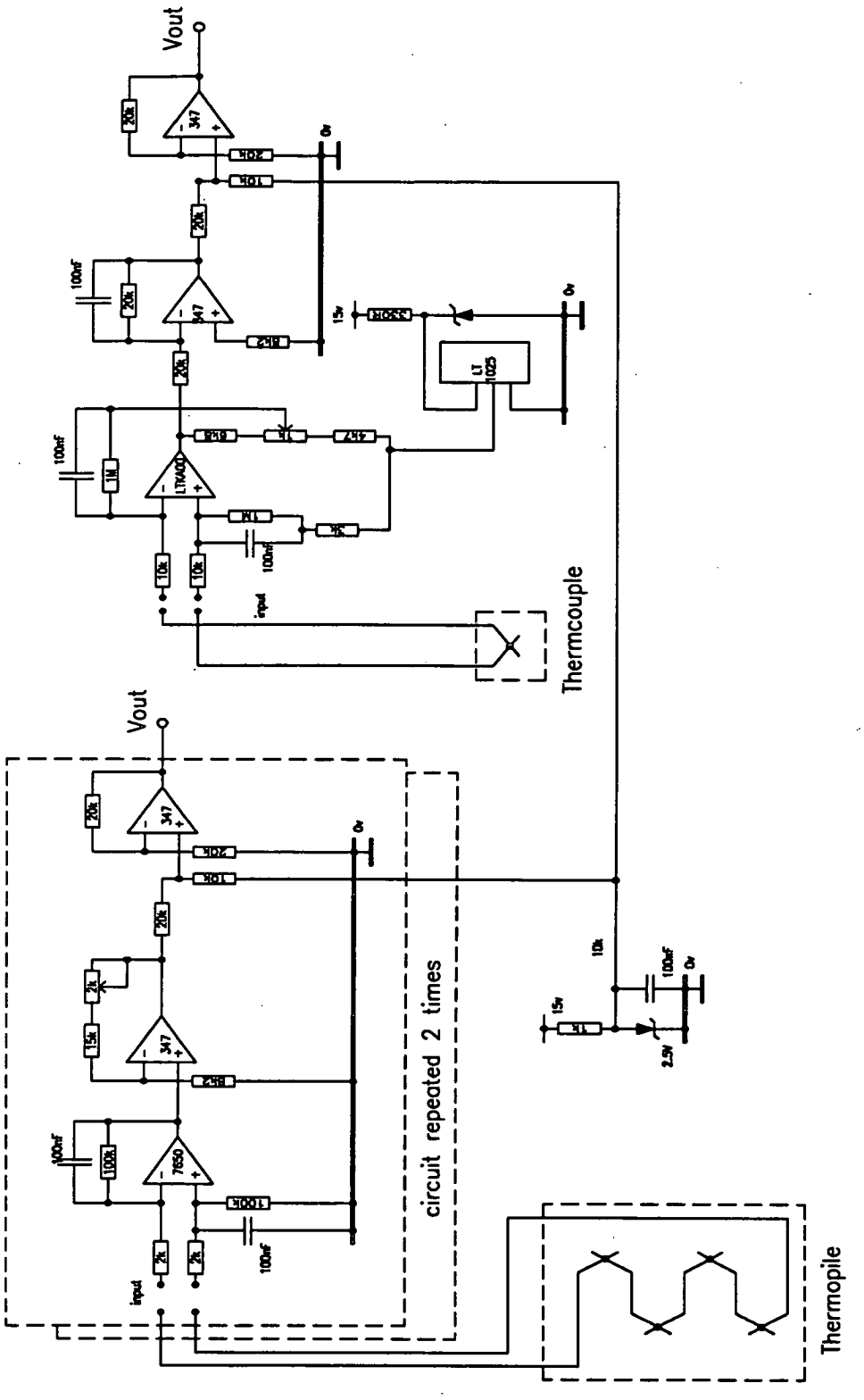

Figure D.5: Thermopile and Thermocouple Conditioner/Amplifier Card

Appendix E

Publications by the Author

This Appendix holds a list of the papers written or co-written by the author during the course of this project. Full details of these papers are given in the Bibliography: the notes here are intended to convey the contents of each paper.

1. *Wave Powered Desalination.* Crerar, Low and Pritchard [18] (1987). A discourse on the potential application of heat pump technology to marry a perceived requirement for new desalination techniques to renewable energy resources.

2. *Techniques for Thermodynamic Property Prediction with Reference to Microcomputer Applications.* Low [58] (1988). An analysis of the performance of the CCOR equation as a predictor of properties of pure halohydrocarbons, including comparison with other property prediction methods.

3. *A Self-Regulating Heat Pump for Systems With Variable Power Input.* Pritchard and Low [90] (1988) Presentation of the design philosophy, plant flowsheet and experimental plan for the project, with economic analysis of the costs of wind and wave power abstraction for heating duties.

4. *A Self-Regulating Heat Pump for Renewable Energy Applications* Pritchard and Low [91] (1990) An update of the plant design, with some experimental data and performance assessments of the pilot plant.

5. *A Self-Regulating heat pump to utilize Wind and Wave energy resources.* Pritchard and Low [93] (1990). A summary of the progress of the experimental programme, indicating the early findings of the work and highlighting some possible modifications to the plant design resulting from the first experiments.

6. *Prediction of Thermodynamic Properties of CFC Mixtures Using the CCOR Equation of State.* Low and Pritchard [59] (1990). A description of the details of implementation of the CCOR equation of state, including auxiliary equations, algorithms and comparison with experimental VLE data.

7. *A Self-Regulating Heat Pump for Systems With Variable Power Input.* Pritchard and Low [92] (1990). Similar content to the Munich paper [91] but with more speculation on future designs.

8. *Thermodynamic Properties of Refrigerant mixtures from the CCOR equation of state.* Low and Pritchard [60] (1990). Further application of the CCOR equation to mixtures: comparison of predictions against data for six binary refrigerant mixtures.